AFWAL-TR-81-2004

AD A103528

EXPENDABLE GASIFIER

TELEDYNE CAE
1330 LASKEY ROAD
TOLEDO, OHIO 43612

MARCH 1981

TECHNICAL REPORT AFWAL-TR-81-2004
Final Report for Period March 1976 through December 1980

AERO PROPULSION LABORATORY
AIR FORCE WRIGHT AERONAUTICAL LABORATORIES
AIR FORCE SYSTEMS COMMAND
WRIGHT-PATTERSON AIR FORCE BASE, OHIO 45433

DTIC FILE COPY

819 01 011

This technical report has been reviewed and is approved for publication.

JOSEPH M. GOTTSCHLICH
Project Engineer
Power Systems Branch
Aerospace Power Division

B. L. MCFADDEN
Technical Area Manager
Power Systems Branch
Aerospace Power Division

FOR THE COMMANDER

JAMES D. REAMS
Chief, Aerospace Power Division
Aero Propulsion Laboratory

REPORT DOCUMENTATION PAGE	READ INSTRUCTIONS BEFORE COMPLETING FORM

1. REPORT NUMBER	2. GOVT ACCESSION NO.	3. RECIPIENT'S CATALOG NUMBER
AFWAL-TR-81-2004	AD-A103 528	

4. TITLE (and Subtitle)	5. TYPE OF REPORT & PERIOD COVERED
EXPENDABLE GASIFIER	Final Report for Period March 1976 — December 1980
	6. PERFORMING ORG. REPORT NUMBER
	1738

7. AUTHOR(s)	8. CONTRACT OR GRANT NUMBER(s)
Al Gabrys Hans Due	F33657-76-C-2055

9. PERFORMING ORGANIZATION NAME AND ADDRESS	10. PROGRAM ELEMENT, PROJECT, TASK AREA & WORK UNIT NUMBERS
Teledyne CAE 1330 Laskey Road Toledo, Ohio 43613	31450132

11. CONTROLLING OFFICE NAME AND ADDRESS	12. REPORT DATE
Aeropropulsion Laboratory Air Force, Wright Aeronatuical Lab., AFSC Wright-Patterson AFB, Ohio 45433	March 1981
	13. NUMBER OF PAGES

14. MONITORING AGENCY NAME & ADDRESS(if different from Controlling Office)	15. SECURITY CLASS. (of this report)
	Unclassified
	15a. DECLASSIFICATION/DOWNGRADING SCHEDULE

16. DISTRIBUTION STATEMENT (of this Report)

Approved for public release; distribution unlimited

17. DISTRIBUTION STATEMENT (of the abstract entered in Block 20, if different from Report)

18. SUPPLEMENTARY NOTES

19. KEY WORDS (Continue on reverse side if necessary and identify by block number)

20. ABSTRACT (Continue on reverse side if necessary and identify by block number)

The expendable gasifier provides, in a single cost-effective configuration, the core for either a jet fuel starter or a thrust engine for remotely piloted vehicles (RPV's). The gasifier is 12.9 inches in diameter, 18.6 inches long, weighs 78 pounds, and consists of a four-stage axial compressor, a reverse-flow annular vaporizer combustor, a single stage axial turbine and a bearing system that supports the main shaft. The expendable gasifier was designed, fabricated and tested during this program. Test

DD FORM 1473 1 JAN 73 EDITION OF 1 NOV 65 IS OBSOLETE

ABSTRACT (Cont'd.)

results verified the viability of the gasifier as a potential core for jet fuel starters or thrust engine for RPV's, and cost analysis shows that, in the jet fuel starter application, the expendable gasifier would substantially reduce the life cycle cost versus conventional jet fuel starters.

Accession For	
NTIS GRA&I	☒
DTIC TAB	☐
Unannounced	☐
Justification	
By	
Distribution/	
Availability Codes	
Dist	Avail and/or Special
A	

DTIC
SELECTED
SEP 1 1981

D

FOREWORD

This final report covers the results of the Expendable Gasifier Program under Contract No. F33657-76-C-0255, Project No. 3145, Task No. 314501, Work Unit No. 31450132, performed by Teledyne CAE, Toledo, Ohio for the United States Air Force Systems Command, Aero Propulsion Laboratory, Wright-Patterson Air Force Base, Ohio.

This program is monitored by Mr. Joe Gottschlich, Aerospace Power Division (AFWAL/POOS-1) and Mr. Steve Kobelak, Special Engine Technology (AFWAL/POTX).

TABLE OF CONTENTS

TABLE OF CONTENTS

LIST OF ILLUSTRATIONS

LIST OF ILLUSTRATIONS

LIST OF ILLUSTRATIONS

ix

LIST OF ILLUSTRATIONS

LIST OF ILLUSTRATIONS

LIST OF ILLUSTRATIONS

LIST OF ILLUSTRATIONS

LIST OF ILLUSTRATIONS

xiv

LIST OF ILLUSTRATIONS

LIST OF ILLUSTRATIONS

LIST OF ILLUSTRATIONS

LIST OF ILLUSTRATIONS

xviii

LIST OF ILLUSTRATIONS

LIST OF ILLUSTRATIONS

LIST OF ILLUSTRATIONS

LIST OF ILLUSTRATIONS

LIST OF ILLUSTRATIONS

LIST OF TABLES

xxiii

LIST OF TABLES

LIST OF TABLES

AR	Area ratio
AS	Aspect ratio $\dfrac{\text{(average height)}}{\text{cord}}$
b	Passage width in meridional plane
B	Fraction of geometric area blocked by boundary layer
B.C.	Backward curvature angle (angle of blade tip relative to radial line through tip)
C	Vane chord length
C_p	Coefficient of static pressure recovery, $(P_2-P_1)/P_{01}-P_1)$
D	Diffusion factor, $(1-V_2/V_1) + (V_1-V_2)/2\ V_1$
i	Incidence, B' -BBL at leading edge
L	Flow length in meridional or radial plane
M, M_N	Mach number, local velocity/local sonic velocity
N_B, N_V	Blade number, vane number
R	Radius
SLIP	Slip factor, $(V_u+V_m\tan(\text{B.C.}))/U_T$
T_m	Maximum thickness
T_n	Thickness normal to blade meanline
U	Blade tangential velocity
V	Flow velocity in the absolute (stationary) frame of reference
W	Flow velocity relative to the rotating blades, diffuser channel width in radial plane
α	Slope angle of flow relative to axial direction in meridional plane
β	Angle of flow or blade relative to the meridional plane
γ	Stagger angle between vane chord line and axial direction
δ	Deviation angle between flow direction and blade trailing edge meanline

ϕ	Camber (vane turning angle)
σ	Solidity (chord length/tangential spacing)
θ	Divergence angle of vane surface from channel meanline
ω	Total pressure loss coefficient, $(P_{01}-P_{02})/(P_{01}-P_1)$
$\Delta P/P$	Pressure difference divided by initial pressure
TSFC	Thrust Specific Fuel Consumption
TRIT	Turbine Rotor Inlet Temperature
pr/t	Hoop Stress - internal pressure times radius divided by thickness
O.D.	Outer Diameter
CDP	Compressor Discharge Pressure
EB	Electron Beam (Weld)
DN	Bearing Diameter times Shaft RPM
RPM	Rotating Shaft Speed, Revolutions per Minute
A	Surface Area, ft.^{2}
T	Temperature, $^{\circ}R$
K	Thermoconductivity BTU/ft^2/ft
X	Distance along wall, ft
W	Flow Rate, lb/sec
C_p	Specific Heat of Constant Pressure, BTU/lb $^{\circ}F$
P	Pressure, psia
t	Thickness, ft
N_{Re}	Reynolds Number
N_{pt}	Prandtl Number
δ	Stefan Boltzman Constant
ϵ	Flame Emissivity
ξ	Effectiveness
α	Wall Absorbtivity

SUBSCRIPTS

1	Inlet station
2	Exit station
H	Hub
m	Mean, meridional plane
P_S	Pressure surface
S	Shroud
ss	Suction surface
T	Tip
t	Throat
u, 0	Tangential direction
A	Air (Outer Annulus Flowpath)
B	Air (Inner Annulus Flowpath)
G	Gas
C	Coolant
FT	Flame
W	Wall

SUPERSCRIPTS

'(apostrophe) Denotes quantity relative to blade

SECTION 1.0

INTRODUCTION

Air Force system requirements in the 1980 time period will require a number of low cost turbine engines to provide economically viable systems. The systems will require jet fuel starters and small turbojet and turbofan engines. Turbine engine cost is highly sensitive to design and fabrication techniques that define the basic labor and material content of the powerplant. Production rates greatly influence engine cost and in most military applications any one system is unable to generate a quantity production rate high enough to materially affect cost. An engine design approach using common components for a number of different powerplants can provide overall cost benefits through increased production rates for the common parts.

The objective of the Expendable Gasifier Program is to provide a single expendable gasifier configuration which will be suitable as the core of either a jet fuel starter or a thrust engine for remotely piloted vehicles (RPV's).

The Expendable Gasifier (EG) design approach consists of using a common gasifier for a jet fuel starter, a turbojet and a turbofan to provide the maximum amount of commonality for a wide range of small powerplants. The gasifier consists of a four-stage axial compressor, a reverse-flow annular vaporizer combustor, a single-stage axial turbine and a bearing system that supports the main shaft.

The gasifier is 12.9 inches in diameter, 18.6 inches long and weighs 78 pounds.

The expendable gasifier is readily adaptable to different power output modules as illustrated in Figure 1.

Jet Fuel Starter: The gasifier attaches to a power output module by a quick disconnect vee band clamp to provide a jet fuel starter. A quick attach fuel control, fuel handling components, and a gasifier starter motor will complete the overall jet fuel starter package. The power turbine module consists of a turbine driving through a reduction gear to a 3600 rpm power output shaft. An exhaust collector and right angle outlet is provided to duct the hot exhaust gases away from the reduction gear. The baseline gasifier is sized by the jet fuel starter requirements of 230 HP on a sea level standard day (59°F).

Turbofan: The gasifier converts to a turbofan by the addition of a low pressure spool, a primary jet nozzle and a bypass duct with an integral jet nozzle. The low pressure spool is simply supported in two bearings and consists of a single stage fan driven by a single stage

1

18.4 IN

12.7 IN

21914
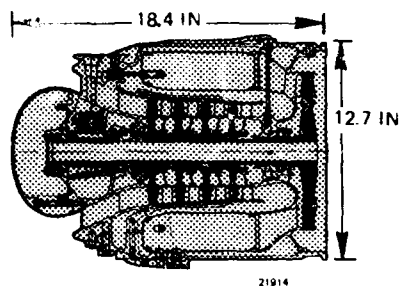
EXPENDABLE
GASIFIER
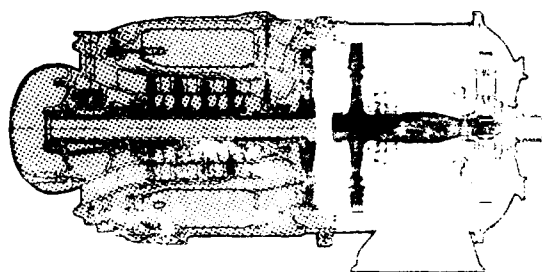
JET FUEL STARTER
130 HORSEPOWER

22364
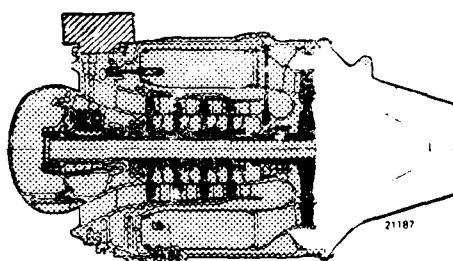
TURBOJET
229 POUNDS THRUST

21187
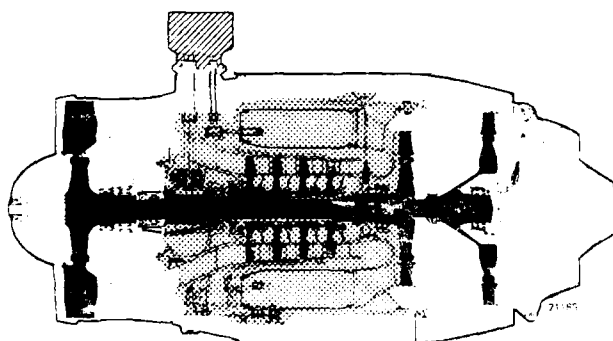
TURBOFAN
500 POUNDS
THRUST

23685

Figure 1.   The Expendable Gasifier Powers Jet Fuel Starter, Turbojet
and Turbofan Engines.

2

fan turbine. The front frame is integral with the stator row, and is attached to the gasifier by radial pins. The fan turbine nozzle and primary exhaust and jet nozzle are attached to the gasifier by a vee band clamp. The turbofan is rated at 500 pounds thrust at a specific fuel consumption of 0.91 pounds per hour per pound.

Turbojet: The gasifier readily converts to a turbojet by attaching a jet nozzle with the quick disconnect clamp and installing the quick-attach fuel handling components, starting and control system to provide the required operational modes. The gasifier operating in the turbojet mode has a thrust of 229 pounds and a specific fuel consumption of 1.56 pounds per hour per pound.

The main emphasis of the program is on very low cost at a pre-selected performance level. The cost goal is an initial price of $8,000 (1976 dollars) for the gasifier. This is being accomplished through the use of innovative design techniques such as: (1) a low speed (33,000 rpm) design with corresponding low stress levels, thus permitting the use of aluminum castings for both rotating and stationary components; (2) an expendable design which eliminates overhaul and maintenance; and (3) the use of radial pin construction which eliminates the requirements for precision threaded fittings and multiple pilot diameters. The final result of this type of design approach will be a single, inexpensive gasifier for a jet fuel starter, turbojet engine, and turbofan engine.

The program consists of four phases as follows: Phase I, definition of the overall system requirements for the gasifier in a jet fuel-starter, turbojet engine, or turbofan engine; Phase II, preliminary design of the gasifier. This included component design and a detailed cost analysis; Phase III, detail design of all components and test rigs. Also the highest risk development item, the combustor, was fabricated and tested to demonstrate structural integrity and performance levels. Phase IV, procurement and testing of the compressor hardware as well as the gasifier in the turbojet engine configuration at sea level static and at altitude conditions.

All phases of the program have been completed. The results have indicated that the cost objective of the gasifier can be met and that the engine hardware can achieve adequate performance for all EG applications.

It is expected that the four-phase approach presented in this report will supply the technology necessary to build a low cost, reliable gas turbine engine which meets future Air Force requirements for jet fuel starters, APU's, and propulsion engines for drones, missiles and RPV's.

3

SECTION 2.0

PROGRAM OVERVIEW

2.1 General

The objective of this program is to demonstrate the technology necessary to provide low cost, reliable gas turbine engines able to be used in a number of economically attractive systems. The broad statement of the main objective leads to a number of secondary objectives as follows:

- To design a single expendable gasifier (EG) suitable for use as the core of a jet fuel starter, turbojet or turbofan to provide a high production rate.

- To show a cost benefit by employing the expendable concept (discarding the EG) to eliminate replaceable parts, overhaul, accountability paperwork and many transportation/shipping costs.

- To establish the gasifier aerothermo cycle to provide low rotor speed, low turbine inlet temperature, and conservative component efficiencies allowing manufacturing methods and materials to be minimum cost.

- To use innovative design features to reduce assembly labor and to design for maximum use of castings and low cost materials.

- To demonstrate the capability to achieve low fabrication cost by producing components using the production processes.

- To demonstrate the performance of the EG in the turbojet version at all operating points in the spectrum of the three applications.

The program consisted of four phases as follows:

```
Phase I    - System Design
Phase II   - Preliminary Gasifier Design
Phase III  - Detail Design and Combustor Test
Phase IV   - Fabrication and Testing
```

5

2.2 Phase I - System Design

A preliminary system design of turboshaft, turbojet and turbofan engine configurations using a common gasifier was performed to establish the detailed design requirements and to determine tradeoffs to achieve maximum commonality. These tasks were completed according to the schedule shown in Figure 2. The expendable gasifier, Figure 3, was the result of the tradeoffs to accommodate the three engine configurations. The EG geometry was defined by sizing the unit to meet the jet fuel starter power requirement of 230 SHP at 59°F, sea level static conditions. The controls package for each of the engine configurations was investigated and defined. The JFS configuration has an inherently simple control system which is self-sufficient and operates automatically. The control scheme devised for the powerplant configurations consists of a single point fuel metering governing valve which depends on external launch equipment for start and acceleration. Installation drawings were prepared for each engine configuration and preliminary analyses conducted to provide the following:

Jet Fuel Starter		Turbojet	Turbofan
SHP - 230	Thrust - lbs.	229	500
BSFC - lbs/hr/HP - 1.43	SFC - lb/hr/lb	1.56	0.91
Airflow - lb/sec - 3.86	Airflow - lb/sec	4.06	16.0

2.3 Phase II - Preliminary Gasifier Design

A preliminary design of the basic gasifier configuration was performed using the detailed gasifier requirements generated in Phase I. The preliminary analyses performed for the Expendable Gasifier Components were conducted per the events scheduled in Figure 4. The level of effort for the preliminary aerodynamic design consisted of definition of the flowpath, number of stators and rotor blades, velocity triangles and efficiencies. Mechanical and thermal stress analyses were conducted of critical components to insure meeting the life requirements of the engine applications. Design layouts were made in detail of the combustor rig and modified as necessary for the EG and other test rig configurations. Cost drawings were prepared showing the necessary detail to define the manufacturing and assembly procedures sufficiently for the detailed cost analysis. The results of this analysis are tabulated as follows:

	Model	Cost **
Expendable Gasifier	506	$ 7,800
Jet Fuel Starter*	206	$18,670
Turbofan*	406	$18,280
Turbojet*	306	$10,900

		MARCH	APRIL	MAY

PHASE I SYSTEM DESIGN
- SIZE EG FOR 230 HP JPS
- DEFINE JFS INTERFACE
- DEFINE T/J INTERFACE
- DEFINE T/F INTERFACE
- DEFINE CONTROLS
- PREPARE INSTALLATION DWGS
- CONDUCT PERFORMANCE ANALYSIS

PHASE I REVIEW
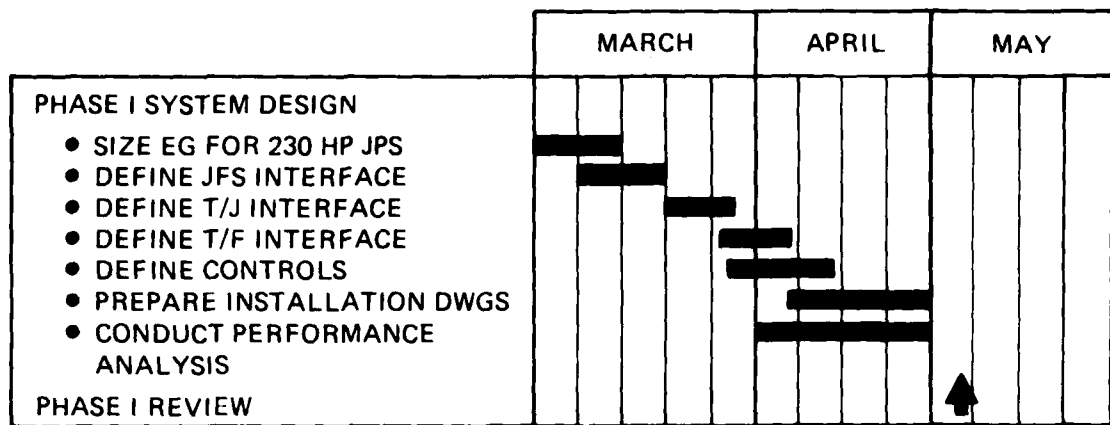
27348

Figure 2.   Phase I Program Schedule.

18.4 IN

12.7 IN
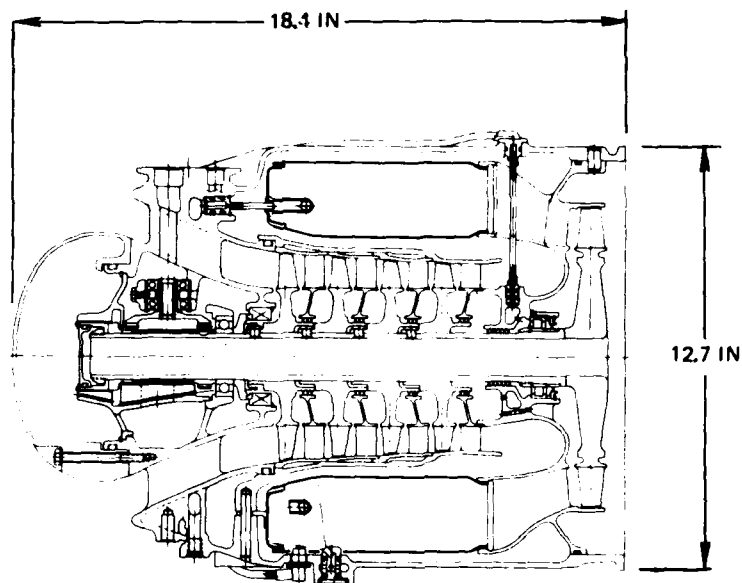
22365

AERODYNAMIC DESIGN POINT (SLS, 59°F)	
Wa = 3.86 LB/SEC	TIT = 1800°F
PR = 2.86	N_G = 33,000 RPM
WT. = 70 LBS	

Figure 3.   Model 506 Expendable Gasifier Cross-Section (Phase I).

7
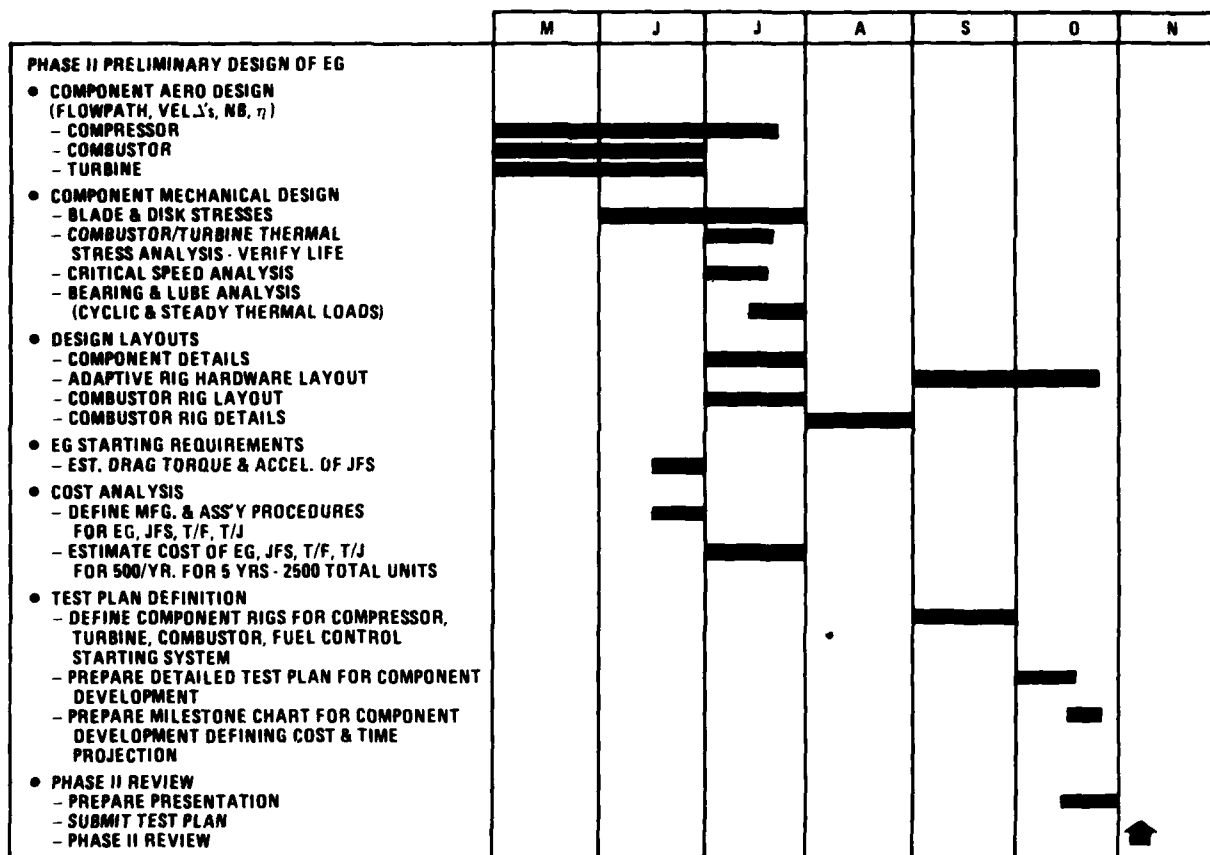
Figure 4. Phase II Program Schedule.

* Includes controls, accessories and expendable gasifier.
** Includes G&A, Profit, Material Handling, Burden, in
1976
dollars.

2.4 Phase III - Detail Design and Combustor Testing

The final design of the expendable gasifier has been
accomplished per the schedule shown in Figure 5. Detailed
aerodynamic, thermodynamic and structural analyses have been
conducted to fully define the EG component hardware. Detail
drawings were made and released to obtain quotes for cost and
delivery times. From these quotes the Phase IV Fabrication Plan
was formulated. The combustor test rig hardware was fabricated and
the combustor was tested per the test plan generated in Phase II.
At design operating conditions, combustion efficiency, heat release
rate and exit temperature distribution factors met or exceeded
design objectives. The values obtained for these and other
parameters are presented in Table 1, a summary of EG combustor test
results. The combustor ignition envelope was defined over a wide
range of inlet conditions and an expendable gasifier starting
envelope approximated in terms of altitude and flight Mach number.

2.5 Phase IV - Fabrication and Testing

The remaining expendable gasifier and test rig components
have been fabricated and tested per the schedule shown in Figure
6. The hardware was to be fabricated per the approved Phase IV
Fabrication Plan generated in Phase III. Procurement of the
compressor rotors through a special casting process was
unsuccessful and necessitated the procurement of conventional
precision cast rotors. To expedite compressor and engine testing,
machined rotors were procured for initial tests to verify
compressor performance. To verify the capability of producing the
low cost cast rotors, these were also procured for subsequent
testing which demonstrated the performance degradation of the
gasifier using these rotors. Although the performance of the
gasifier is less using cast rotors, both the cast and fully
machined rotors have more than adequate performance to satisfy
present day applictions as a jet fuel starter. The performance of
the turbojet version of the expendable gasifier using both
configurations is presented in Table 2. The successful completion
of Phase IV of this program has demonstrated the application of the
technology necessary to build a low cost, reliable gas turbine
engine which meets future Air Force requirements for jet fuel
starters, APU's, and propulsion engines for drones, missiles and
RPV's.

	1976		1977									
	N	D	J	F	M	A	M	J	J	A	S	O
PHASE III DETAILED EG DESIGN & COMBUSTOR TEST												
● DETAIL COMPRESSOR DESIGN												
AERO DESIGN												
– MECHANICAL DESIGN (STRUCTURAL)												
– DETAIL DRAWINGS												
● DETAIL COMBUSTOR DESIGN												
– AERO THERMO DESIGN AS DEEMED NECESSARY FROM RIG DATA ANALYSIS												
– DETAIL DRAWINGS (IF MODIFIED)												
● DETAIL TURBINE DESIGN												
– AERO DESIGN												
– HEAT TRANSFER												
– MECHANICAL DESIGN (STRUCTURAL)												
– DETAIL DRAWINGS												
● ROTOR SYSTEM DYNAMICS ANALYSIS												
– CRITICAL SPEED												
– BLADE RESONANCE												
● TEST RIG DESIGN (COMPRESSOR, TURBINE)												
– DETAIL ADAPTIVE RIG HARDWARE												
– PREPARE PROCUREMENT PLAN FOR RIG HARDWARE												
● SYSTEM SAFETY ANALYSIS												
● FABRICATION ANALYSIS												
– DEFINE MANUFACTURING METHODS FOR EG COMPONENTS												
– ESTIMATE PROTOTYPE & PRODUCTION COST & DELIVERY FOR EG												
● RELIABILITY & MAINTAINABILITY ANALYSIS												
● CONTROL SYSTEM DESIGN												
– ANALYSIS CONTROL SYSTEM REQ'MTS OF EG APPLIED TO TYPICAL (F-15) AIRCRAFT STARTING SYSTEM												
– ESTIMATE SYSTEM COST EFFECTIVENESS OF HYDROMECHANICAL & ELECTRONIC SYSTEMS												
● COMBUSTOR TEST												
PROCURE COMBUSTOR RIG HARDWARE												
– CALIBRATE FUEL NOZZLES												
– CALIBRATE TURBINE INLET NOZZLE												
– ASSEMBLE & INSTRUMENT TEST RIG												
INSTALL IN TEST FACILITY												
– RUN COLD FLOW TESTS												
– DETERMINE LIGHT-OFF & STARTING CHARACTERISTICS												
– DETERMINE DESIGN & OFF-DESIGN PERFORMANCE												
● PHASE III REVIEW												
PREPARE REPORT COVERING PHASES I, II, III												
– PREPARE ORAL PRESENTATION												
– PHASE III PRESENTATION												

27358

Figure 5.   Phase III Program Schedule.

10

TABLE 1

SUMMARY OF EXPENDABLE GASIFIER COMBUSTOR
TEST RESULTS

	GOAL	ACHIEVED
PRESSURE LOSS — PERCENT	10.0	12.3
HEAT RELEASE — $\dfrac{\text{MBTU}}{\text{HR} \cdot \text{FT}^3 \cdot \text{ATM}}$	9.3	9.3
EFFICIENCY — PERCENT	95.0	95.0
EXIT TEMPERATURE — °F	1800	1800
TEMPERATURE RISE — °F	1516	1516
EXIT RADIAL PROFILE	0.07	0.05
EXIT PATTERN FACTOR	0.20	0.154
MAXIMUM LINER TEMPERATURE — °F	1400	< 1500

41285

11

Figure 6. Phase IV Program Schedule.

41274

ITEM

4.1 ● HARDWARE FABRICATION (ORIGINAL PLAN)
PROCURE MACHINED ROTORS*
PROCURE ALTERNATE CASTINGS*
MACHINE ROTOR CASTINGS*

4.2 ● COMPRESSOR COMPONENT TEST
MECHANICAL PROPERTIES OF CASTINGS
ROTOR SPIN TEST
PREPARE FACILITY
RIG ASSEMBLY AND INSTRUMENTATION
COMPRESSOR TESTING
COMPRESSOR DATA ANALYSIS
EVALUATE EFFECT OF PERFORMANCE ON EG
OPERATION

4.3 ● GASIFIER TESTING
MECHANICAL PROPERTIES OF CASTINGS
TURBINE ROTOR SPIN TEST
PREPARE FACILITY ALTITUDE CHAMBER
CHECKOUT FUEL SYSTEM
CHECKOUT STARTING SYSTEM
TURBOJET ASSEMBLY AND INSTRUMENTATION
CELL INSTALLATION AND SYSTEM CHECKOUT
GASIFIER TESTING (MACHINED ROTORS)
DATA ANALYSIS
PRESENTATION — GASIFIER TEST*
PREPARE FACILITY ALTITUDE CHAMBER*
TURBOJET ASSEMBLY AND INSTRUMENTATION*
CELL INSTALLATION AND SYSTEM CHECKOUT*
GASIFIER TESTING (CAST ROTORS)*
DATA ANALYSIS

● REVIEW — DEMONSTRATION TEST

FINAL REPORT DRAFT
FINAL REPRODUCIBLE

*ITEMS ADDED TO ORIGINAL PROGRAM

RECEIVED 6 ROTOR CASTINGS

AIR FORCE REVIEW

AIR FORCE REVIEW

LEGEND

TASK
START   COMPLETE

MAJOR
MILESTONE
(CRITICAL PATH)

SCHEDULE BASELINE PLAN
SCHEDULE COMPLETED AS PLANNED
SLIPPAGE SCHEDULE PLAN
SLIPPAGE SCHEDULE COMPLETE

PLANNED PROGRESS
ACTUAL PROGRESS

EXAMPLES

TASK IN PROGRESS AND ON SCHEDULE
TASK STARTED LATE AND BEHIND SCHEDULE
TASK ON SCHEDULE MAJOR MILESTONE RESCHEDULED

12

TABLE 2

EXPENDABLE GASIFIER
OVERALL PERFORMANCE COMPARISON

		MACHINED COMPRESSOR	CAST * COMPRESSOR	Δ
CORRECTED SPEED	% RP,	100%	100%	+0
THRUST	LBF	184	166	-9.8%
COMPRESSOR EFFICIENCY	%	77.3	75.0	-2.3% PTS.
AIR FLOW	LBS/SEC	4.02	3.79	-5.7%
JET NOZZLE AREA	IN2	17.8	17.8	+0

* First useable article (Not to print).

41263

13

SECTION 3 - SYSTEM DESIGN (PHASE I)

3.1 DEFINITION OF GASIFIER CONFIGURATIONS

The expendable gasifier (Figure 7) was configured to interface with the
jet fuel starter, turbofan and turbojet applications. The initial step was to
define the EG geometry by sizing the unit to meet the jet fuel starter (JFS206)
power requirement of 230 SHP at 59°F, sea level static conditions. Additional
power requirements were imposed on the EG to provide 3 HP for accessories and 7
HP to account for production margins.

The component efficiencies were degraded to account for larger tolerances
on flow surfaces expected when low cost fabrication methods are employed.

The compressor performance was scaled from the Model 469, four stage, axial
compressor previously tested at Teledyne CAE. The low tip speed (900 ft/sec) of
that compressor uniquely qualifies it for the EG by virtue of relatively low stresses
and demonstrated performance. The EG airflow of 3.86 lb/sec set by the JFS design
point requires that the Model 469 compressor be scaled up by a 1.32 linear scale
factor. The table below summarizes the EG compressor requirements compared to the
Model 469.

	JFS 206	Model 469
Airflow, lb/sec	3.862	2.228
Pressure Ratio	2.857	2.857
Adiabatic Efficiency	80.0	82.0
Tip Speed, ft/sec	900.0	900.0
Tip Diameter, in	6.25	4.74
Rotor Speed, RPM	33,000	43,500

The combustor design point requires a combustor efficiency of 95 percent,
a pressure loss of 5 percent with a temperature rise of 1516 degrees. The combus-
tor aerodynamic loading of 2.1 (lb/sec/ft^3/atm^2) is within the demonstrated capa-
bility of Teledyne CAE reverse flow annular combustor technology. The combustor
was tested in Phase III, however, to verify its performance before engine testing.

The turbine design point efficiency was set at 82.5 percent for a referred
work level of 13 BTU/lb. The turbine efficiency expected at that work level based
experimental turbines of similar flow size is 85 percent. The 2.5 efficiency
points deducted from the expected efficiency accounts for potentially higher losses
associated with the manufacturing tradeoffs to achieve low cost such as surface
finish, larger leading and trailing edge radii and running clearances.

The jet fuel starter configuration (Figure 8) consists of the expendable
gasifier rear mounted to the power turbine which drives through a gear reduction
to achieve a maximum output speed of 3600 RPM. The major interface tradeoffs for
the EG in the jet fuel starter application consisted of: the incorporation of a
containment ring surrounding the gasifier and power turbine; locating the turbine
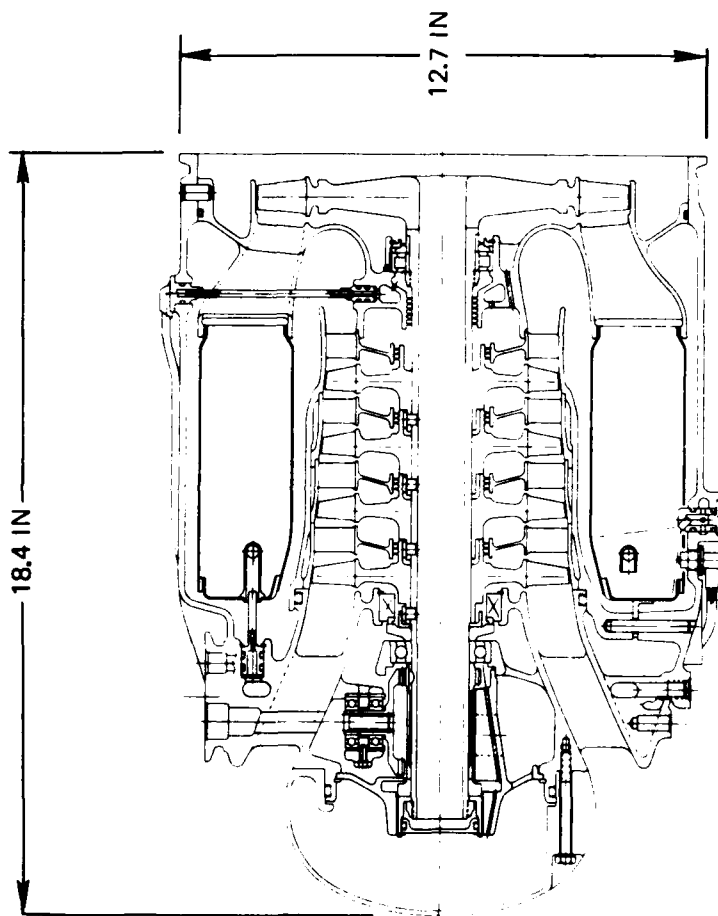
15

AERODYNAMIC DESIGN POINT (SLS, 59°F)	
Wa = 3.86 LB/SEC	TIT = 1800°F
PR = 2.86	N_G = 33,000 RPM
$WT.$ = 70 LBS	

22365

Figure 7 . Model 506 Expendable Gasifier Cross-Section (Phase I).

16

12.7 IN

30.0 IN

22364

21510
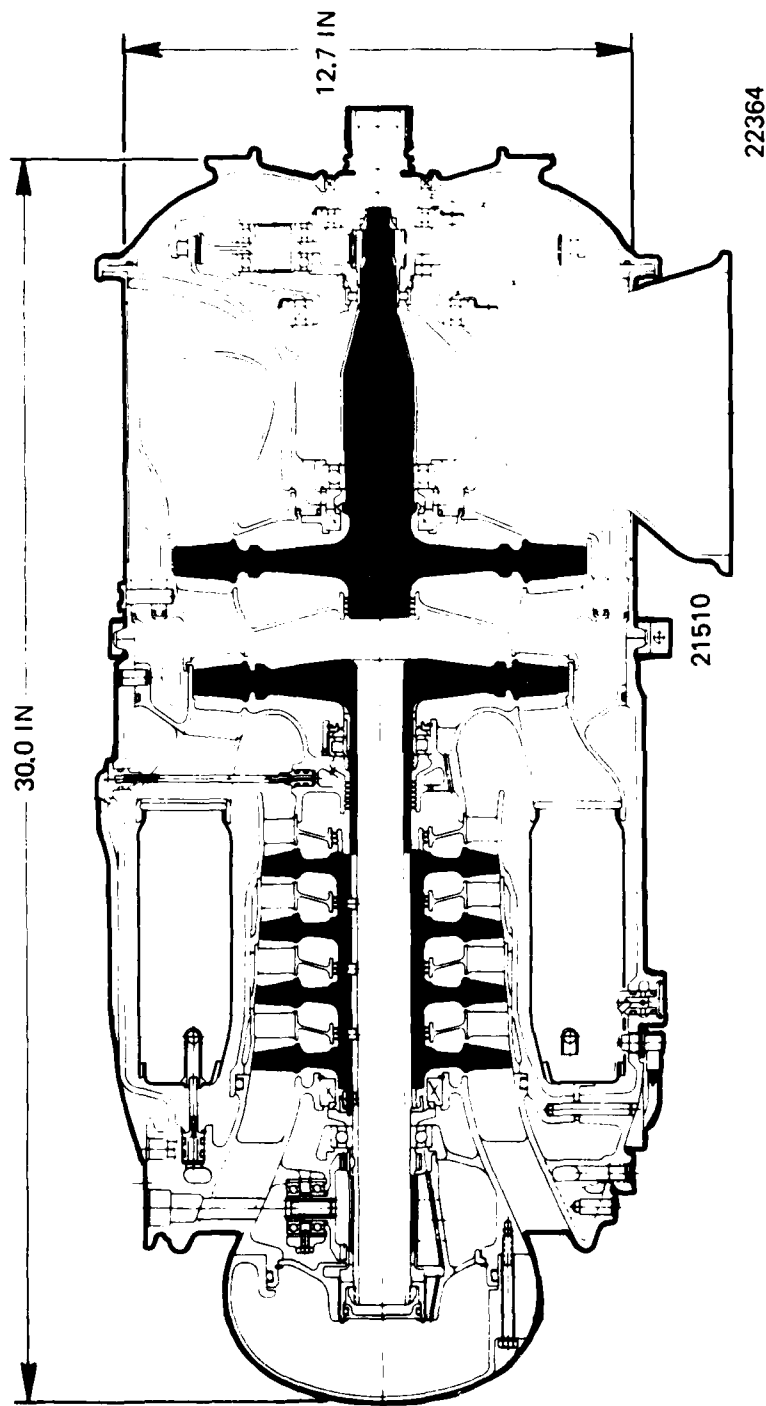
PERFORMANCE (SLS, 59F)			
HORSEPOWER	230	CPR	2.86
SFC	1.43 LB/HR/HP	WEIGHT	150 LBS
AIRFLOW	3.86 LB/SEC	POWER/WEIGHT	1.53 LB/HP
TIT	1800°F	N_{PTO}	3600 RPM

Figure 8 . Model JFS 206 Jet Fuel Starter.

17

bearing in front of the turbine rotor and locating the fuel-air lubrication supply through the turbine inlet vane; providing a hollow shaft for the turbofan, and extending the inlet diameter to form a smooth flowpath for the turbofan configuration.

The containment ring tradeoff required that the EG turbine inlet nozzle be designed to include space for the containment ring since the ring is arranged as a part of the power turbine module.

The overall dimensions of the jet fuel starter package is 30.1 in. long and 12.7 in. diameter. A preliminary weight estimate resulted in a weight of 150 lbs. including the controls.

The life of the EG in the jet fuel starter application will be at least 2000 main engine start cycles under ambient conditions of -65°F to 130°F SLS, each main engine start cycle consisting of a 45 second duration maximum power run.

The EG/JFS arrangement is such that minimum effort will be required to remove and replace the EG in a field operation.

The installation drawing (Figure 9) shows some of the salient features of the JFS. The control package is mounted to the EG by a VEE-band clamp. The ignition exciter is mounted to the VEE-band clamp which holds the EG to the power turbine. For EG removal, only the two VEE-band clamps and two ignitor leads must be removed.

The installation drawing of the turbojet is shown in Figure 10 . It features radial pin mounting at two locations (opposite) and one rear mount. The jet exhaust nozzle is attached at the EG main frame housing with a VEE-band clamp. The accessory package, also attached (for easy removal) with a VEE-band clamp, includes the fuel pump, starting drive gear, governing valve, three-way valve, and quick disconnects to fuel tank and launch control equipment. No significant compromises were necessary to adapt the EG to the turbojet configuration.

The Turbofan Installation (Figure 10) has the accessory mounting arrangement identical to the turbojet. The fan turbine module also connects to the EG module with a VEE-band clamp. No significant compromises were necessary to adapt the EG to the turbofan configuration.

3.2   DEFINITION OF GASIFIER CONTROL REQUIREMENTS

The control package for the JFS consists primarily of a hydraulic motor, fuel pump, alternator, stepper motor metering valve, fuel and system management control (FMSC) and ignition exciter. The start and control system schematic is shown in Figure 12 .

The operation of the control is initiated by a mechanical start command which opens the hydraulic accumulator shut off valve (SOV). The same command opens the electrical interface to the FSMC as a safety feature. The hydraulic motor drives into an overrunning clutch, alternator, fuel pump and tower shaft which drives the EG.
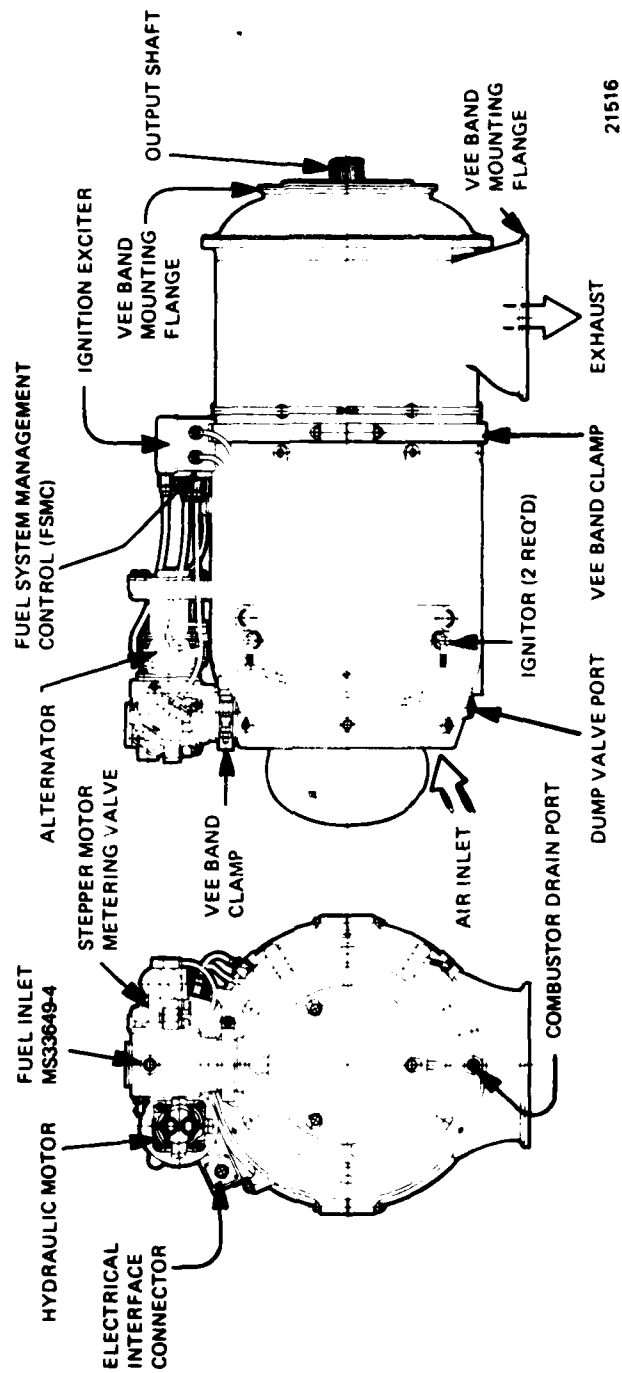
Figure 9 . Model JFS 206 Jet Fuel Starter Installation.

19

PUMP INLET PRESSURE PORT TO AIRFRAME
FLUID QUICK DISCONNECT

PUMP OUTLET PRESSURE
PORT TO AIRFRAME
FLUID QUICK DISCONNECT

FUEL INLET PORT

CDP PORT TO
FUEL TANK

VEE BAND
CLAMP

GOVERNING VALVE

VALVE SIGNAL CONNECTOR TO AIRFRAME
ELECTRICAL QUICK DISCONNECT

SPUR GEAR
STARTING DRIVE

3 WAY VALVE

MAIN FUEL BLEED PORT TO AIRFRAME
FLUID QUICK DISCONNECT

FUEL PUMP

PRIMER FUEL INLET PORT TO AIRFRAME
FLUID QUICK DISCONNECT

IGNITOR LEADS TO AIRFRAME
ELECTRICAL QUICK DISCONNECT

REAR ENGINE MOUNT

ENGINE MOUNT (2)
FOR 0.375 DIA. PIN

20147

Figure 10. Model 306 Turbojet Installation.

VALVE SIGNAL CONNECTOR TO AIRFRAME
ELECTRICAL QUICK DISCONNECT

3 WAY VALVE

MAIN FUEL BLEED PORT TO AIRFRAME
FLUID QUICK DISCONNECT

PRIMER FUEL INLET PORT TO AIRFRAME
FLUID QUICK DISCONNECT

IGNITOR LEADS TO AIRFRAME
ELECTRICAL QUICK DISCONNECT

REAR ENGINE MOUNT

20138

PUMP OUTLET PRESSURE
PORT TO AIRFRAME
FLUID QUICK
DISCONNECT

GOVERNING
VALVE

CDP PORT TO
FUEL TANK

FUEL PUMP

SPUR GEAR
STARTING DRIVE

VEE BAND CLAMP

ENGINE MOUNT (2)

FUEL INLET PORT

PUMP INLET
PRESSURE PORT
TO AIRFRAME
FLUID QUICK
DISCONNECT

Figure 11. Model 406 Turbofan Installation.

21
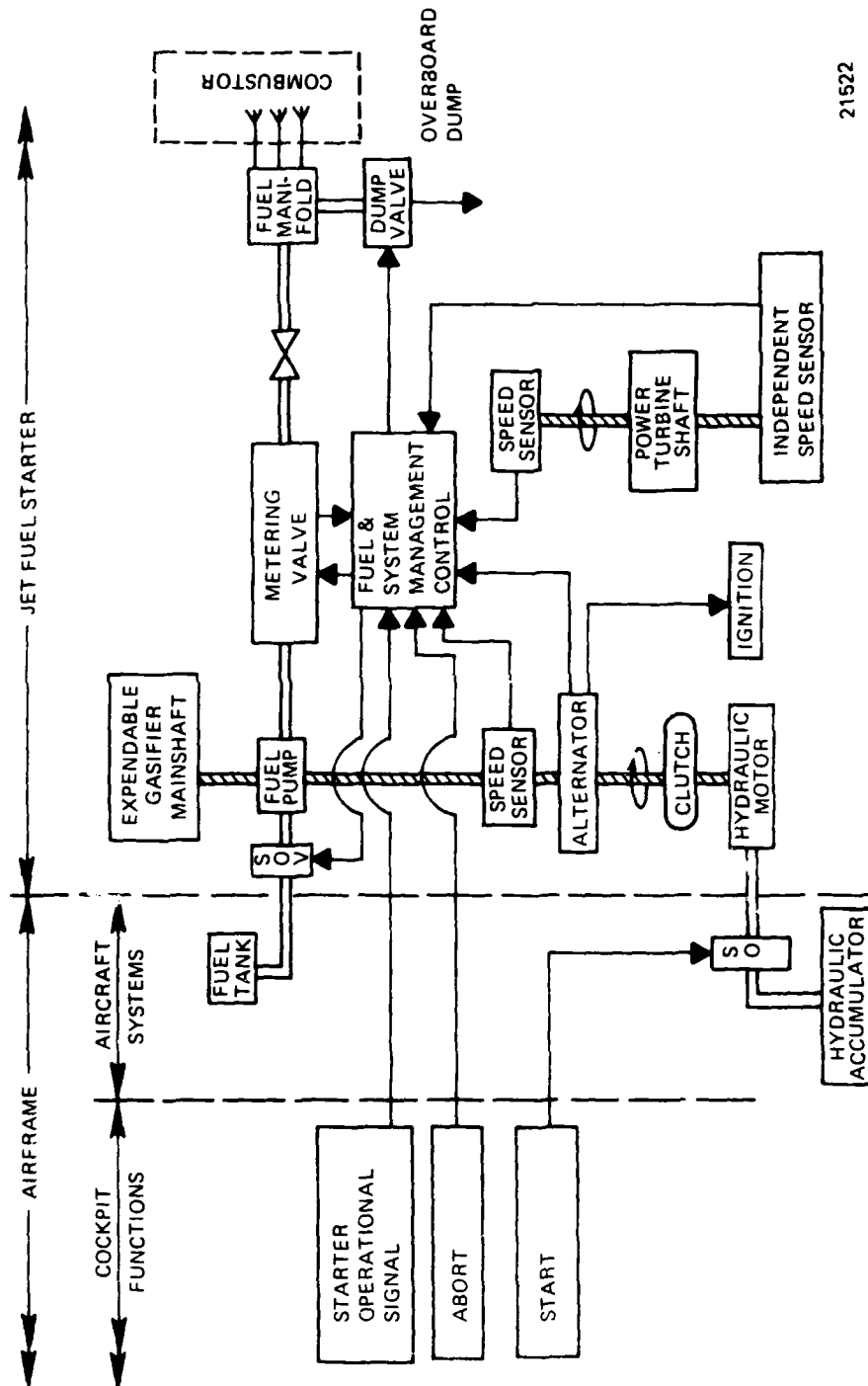
Figure 12 . Jet Fuel Starter Control System.

22

As the motor accelerates, the alternator supplies power to the ignition exciter (AC) and FSMC (DC) and the fuel pump supplies fuel to the fuel primer, fuel to lube the EG turbine bearing and fuel to the EG combustor. The FSMC electronics are programmed to accept inputs from combustor pressure, tower shaft speed (related to EG speed by the gearing ratio), metering valve position and power turbine shaft speed. The fuel tank SOV is actuated open and the stepper motor valve is adjusted according to a pre-programmed fuel flow schedule when power is initially supplied to the FSMC. The pre-programmed fuel flow schedule is a function of EG speed and combustor pressure. Surplus flow is bypassed to the fuel pump inlet. A three-way valve in the fuel primer circuit is actuated by compressor discharge pressure (CDP) and allows CDP air to continually flow through the primer orifices during EG operation.

When the main engine attains a predetermined speed, sensed by the power turbine speed sensor, the FSMC triggers the command to shutdown. Shutdown consists of the closing of the fuel tank SOV and opening the fuel mainfold overboard dump to effect a rapid fuel pressure decay. The final FSMC command resets the start and abort switch to the open position. The overrunning clutch in the power turbine gearbox disengages the power turbine as the main engine accelerates to idle power.

The control scheme devised for the turbojet and turbofan configuration is shown in Figure 13 . It consists primarily of a single point fuel metering governing valve which depends on external launch equipment for start and acceleration.

When the start command is initiated, mechanical power to the fuel pump and engine mainshaft is supplied through the mechanical drive by the launch equipment. The fuel tank receives initial pressurization from the launch equipment, however, as the engine accelerates, compressor discharge pressure is used for pressurization. Fuel leaving the pump discharge flows into the governing valve and to the roller bearing(s). The fuel pump discharge pressure is sensed by the control for an indication of EG rotor speed. The valve plug in the governing valve meters fuel as a function of fuel pump inlet pressure, valve plug area distribution and a predetermined spring load. The metered flow splits at the valve discharge and a portion is directed to the control and the remainder flows to the primary nozzles in the EG combustor. The flow ratio is determined in the control and is based on the logic shown in Figure 14 . The diagram shows that a fuel flow change occurs as a result of the (exhaust gas temperature) error signal. The error signal is obtained by a comparison of the EGT limit (pre-programmed as a function of EG rotor speed) with the measured EGT (part of the launch equipment). As the engine accelerated, the fuel flow to the combustor primary nozzles is continually adjusted by the governing valve to maintain the EGT limit shcedule programmed within the control. The control also supplies fuel to the fuel primer nozzles from the flow which enters the control. The excess is dumped to a fuel accumulator. After acceleration to a predetermined operating point has been achieved, the command to launch is given and the launch equipment is disconnected. The engine control is now governed by only the governing valve which meters fuel as a function of fuel pump discharge pressure. The valve flow area and spring load have been determined to allow single point operation of the engine at a predetermined thrust.

23

LAUNCH EQUIPMENT EXTERNAL TO VEHICLE
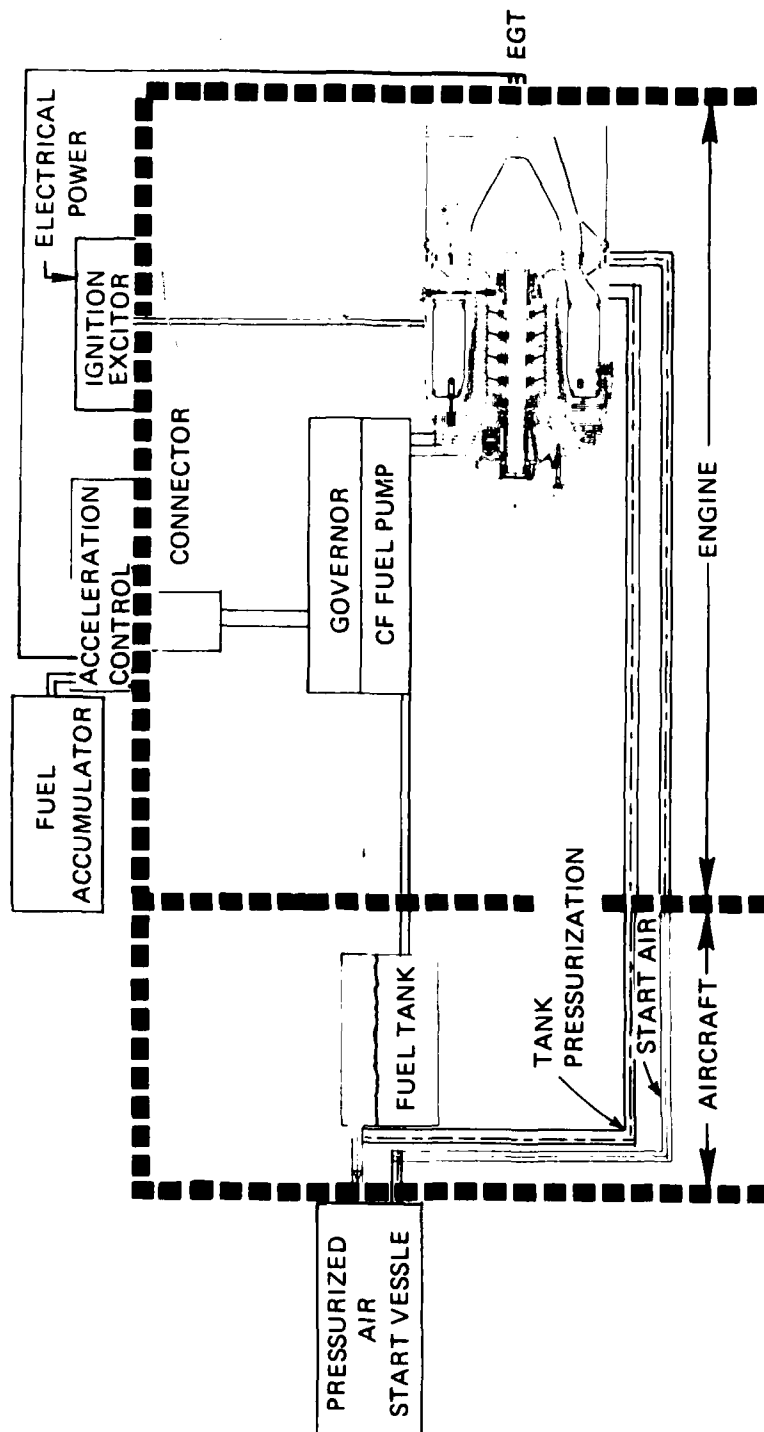
Figure 13. Turbojet and Turbofan Basic Start & Control System.

24
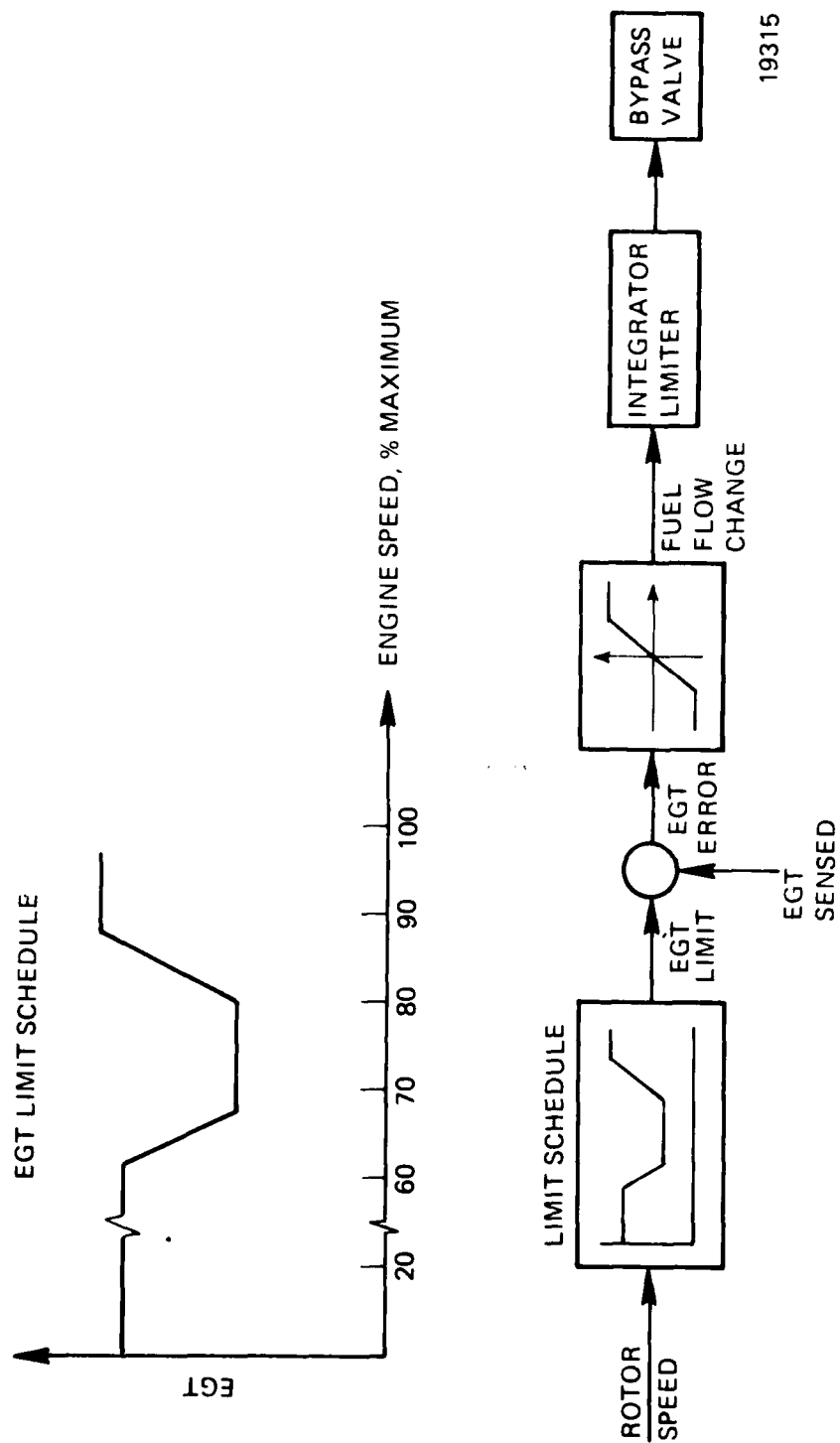
Figure 14. Control Logic for the Turbojet/Turbofan Start and Acceleration.

19315

25

3.3 PRELIMINARY PERFORMANCE ANALYSIS

Preliminary performance estimates were made for the jet fuel starter using a design point, turboshaft, cycle program. The results are shown in Table 3 for -65, 59 and 130°F inlet conditions (SLS). The turbine inlet temperature was constrained at 1800°F and the EG speed at 33,060 RPM to preserve the low stress environment required to incorporate low cost technology. The power lapse with ambient temperature is shown in Figure 15. The variation of output power with inlet temperature is nearly linear over the range of -65 to 130°F. An additional three percent (7 hp) was included in the cycle to account for production variability. Figures 16, 17, and 18 present the thermodynamic state points throughout the EG/JFS flowpath for the three inlet temperature conditions - standard day (59°F), hot day (130°F) and cold day (-65°F) at SLS.

The turbojet and turbofan engines were configured using the EG sized for the JFS operation described previously. A cycle study was performed to provide the greatest usable flight operation envelope (altitude - Mach No) without overspeeding the EG rotor (33,060 RPM maximum) or exceeding the turbine inlet temperature of 1800°F. Several altitudes were investigated over a range of Mach numbers and the condition of 30,000 ft., 0.40 Mach was chosen as the match point for both the turbofan and turbojet cycles.

The turbojet configuration (Figure 10) consists of simply the EG with an exhaust nozzle attached with a VEE-band clamp. The controls are attached with a VEE-band clamp at the tower shaft accessory pad. The turbojet (Figure 19) is 29.0 in. long and 12.7 in. in diameter. It produces 229 lbs. of thrust at SLS, standard day with an SFC of 1.56 lb./hr./lb. The weight including controls was estimated to be 80 lbs. The large volume over the turbine outer shroud is the result of allowing for the containment ring in the JFS application. Figure 20 presents the thermodynamic state points through the engine flowpath at SLS, standard day.

The turbojet analysis yielded a preliminary estimate of the performance over a range of altitude and Mach number conditions. Figure 21 displays a carpet plot of thrust and thrust specific fuel consumption over a range of altitudes from sea level to 40,000 ft. and Mach number from 0 to 1.0.

The turbofan pressure ratio and bypass ratio were investigated over a range of bypass ratios and fan pressure ratios at sea level static inlet conditions, (Figure 22). It was determined from that analysis that the EG core was power limited when designed for a bypass ratio of 3.0. A bypass ratio of 2.0 and a fan pressure ratio of 1.52 was selected as near optimum. It was decided that a single stage fan would provide a low-cost turbofan and the fan performance could be achieved with existing technology. The optimization analysis was performed using 5 HP for accessory power takeoff and yielded a net thrust of 470 lb. at SLS for the selected bypass ratio and fan pressure ratio. It was subsequently assumed that 3 HP would be adequate for accessory power requirements for the turbofan and turbojet configurations and that assumption yielded a net thrust of 500 lb. at SLS conditions.

26
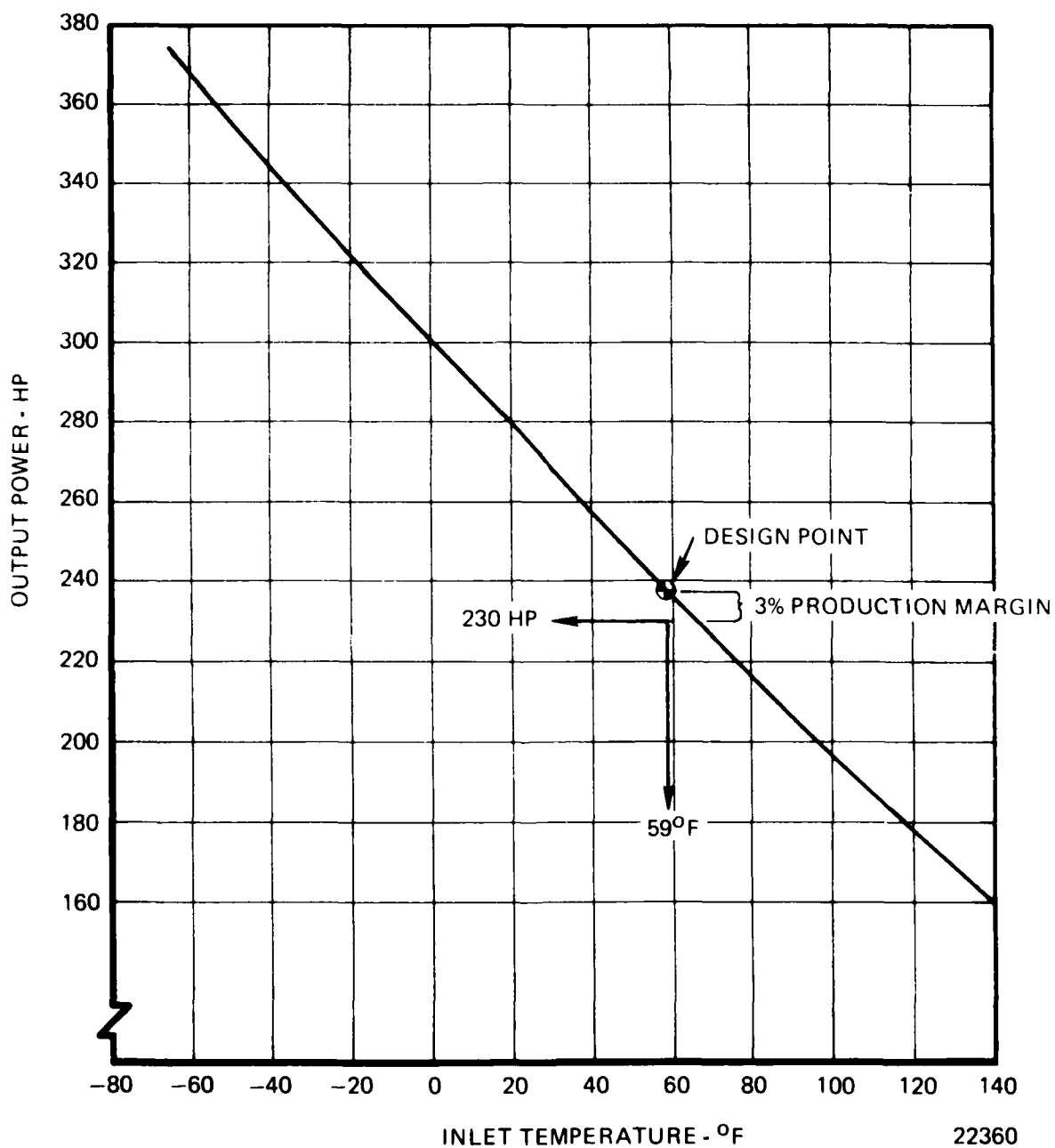
Figure 15. Model JFS 206 Power Lapse with Ambient Inlet Temperature.

27

19720

STANDARD DAY					
	P_T (PSIA)	T_T (F)		P_T (PSIA)	T_T (F)
1	14.7	59.0	5	36.0	1800
2	14.1	59.0	6	24.3	1612
3	40.3	284	7	22.8	1612
4	38.3	1800	8	15.8	1455
			9	14.9	1455
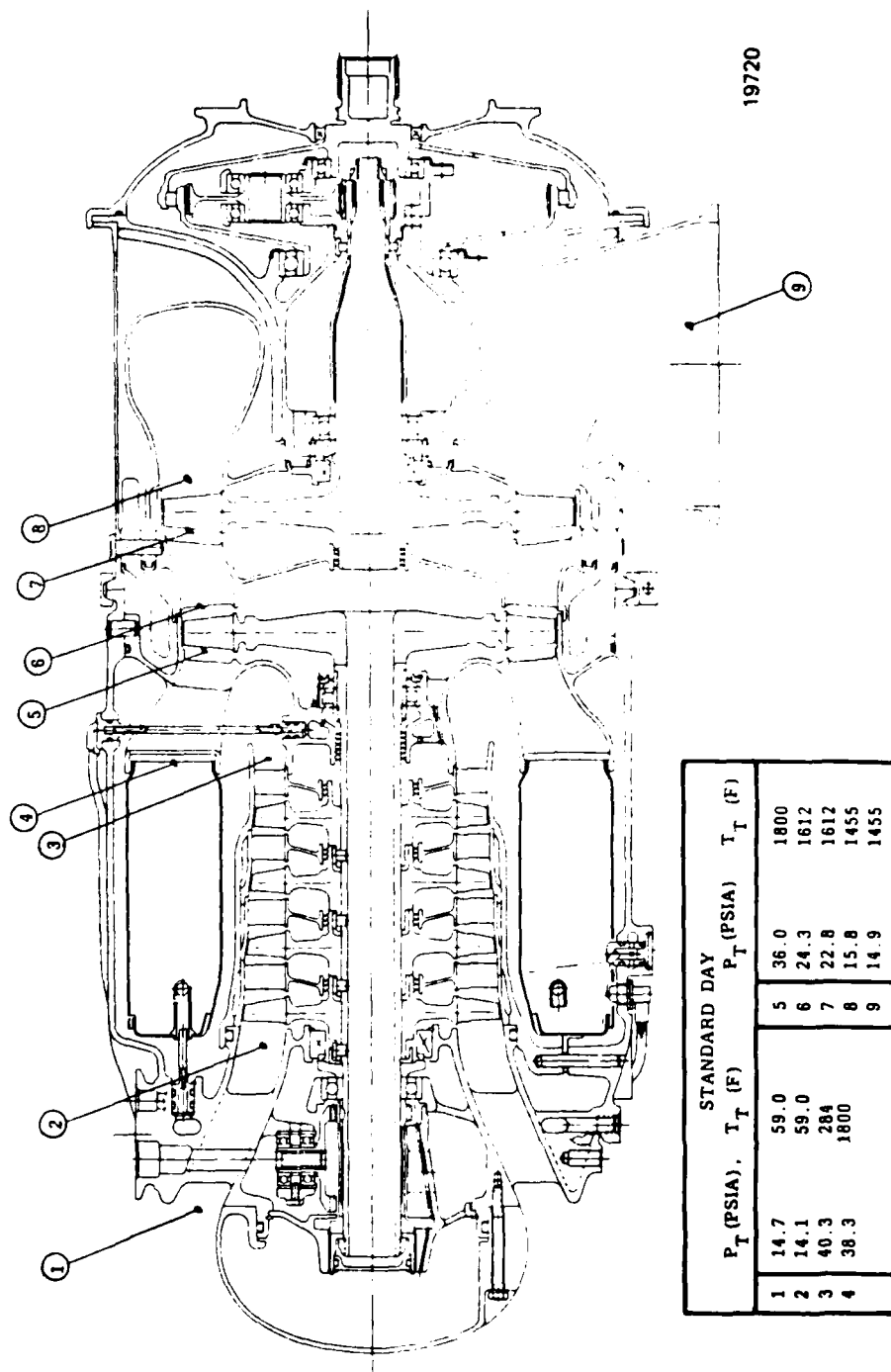
Figure 16 . Model JFS 206 Jet Fuel Starter, SLS, Preliminary Thermodynamic State Points (Standard Day, 59°F).

HOT DAY					
	P_T (PSIA)	T_T (°F)		P_T (PSIA)	T_T (°F)
1.	14.7,	130	5	32.1,	1800
2	14.1,	130	6	21.9,	1616
3	36.0,	349	7	20.6,	1616
4	34.2,	1800	8	15.8,	1496
			9	14.9,	1496
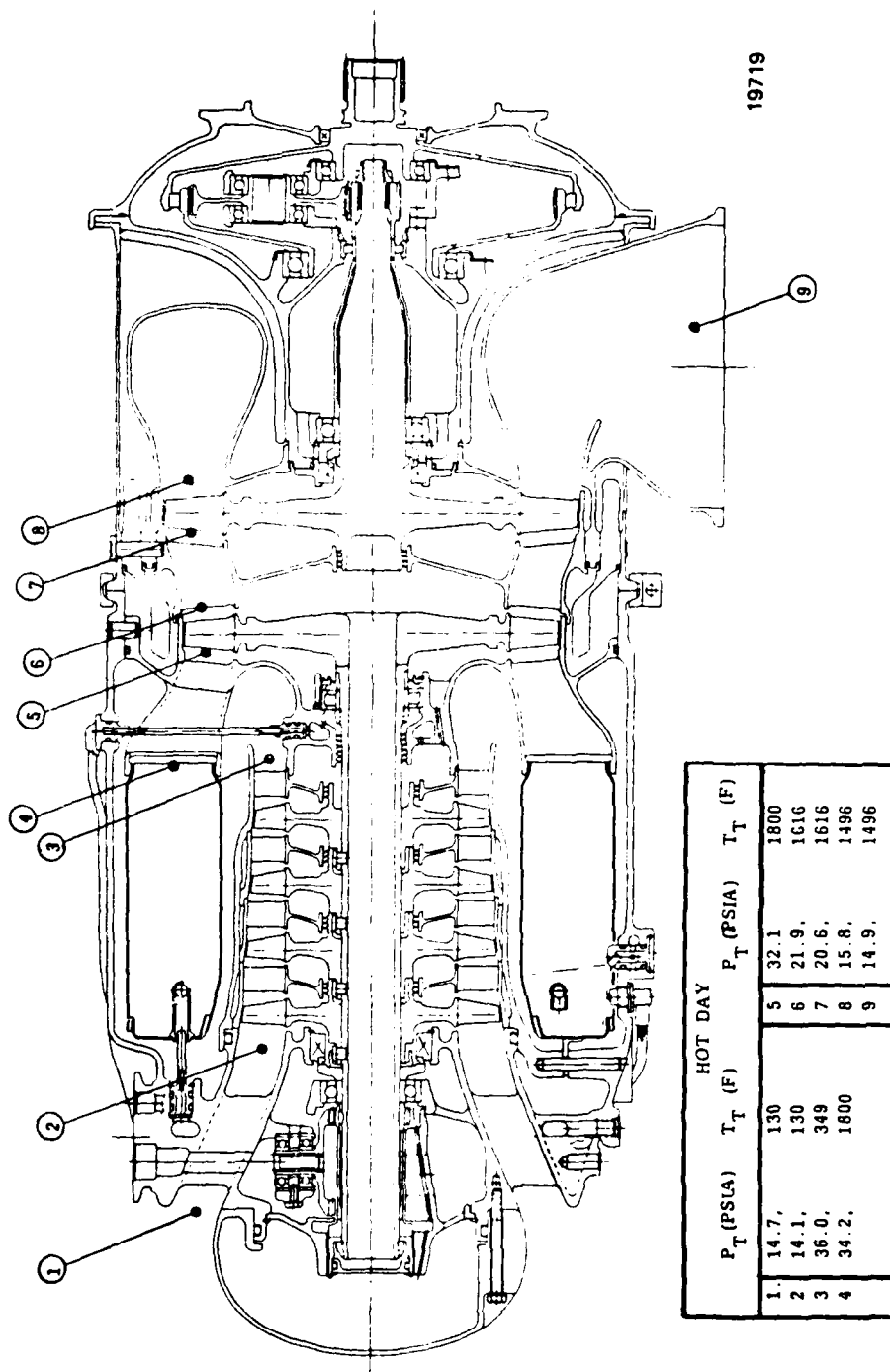
Figure 17 . Model JFS 206 Jet Fuel Starter, SLS, Preliminary Thermodynamic State Points (Hot Day 130°F).

29

22366

COLD DAY					
	P_T(PSIA)	T_T(°F)		P_T(PSIA)	T_T(°F)
1	14.7	−65	5	39.6	1800
2	14.1	−65	6	26.4	1611
3	43.9	164	7	25.1	1611
4	41.7	1800	8	15.8	1426
			9	15.0	1426
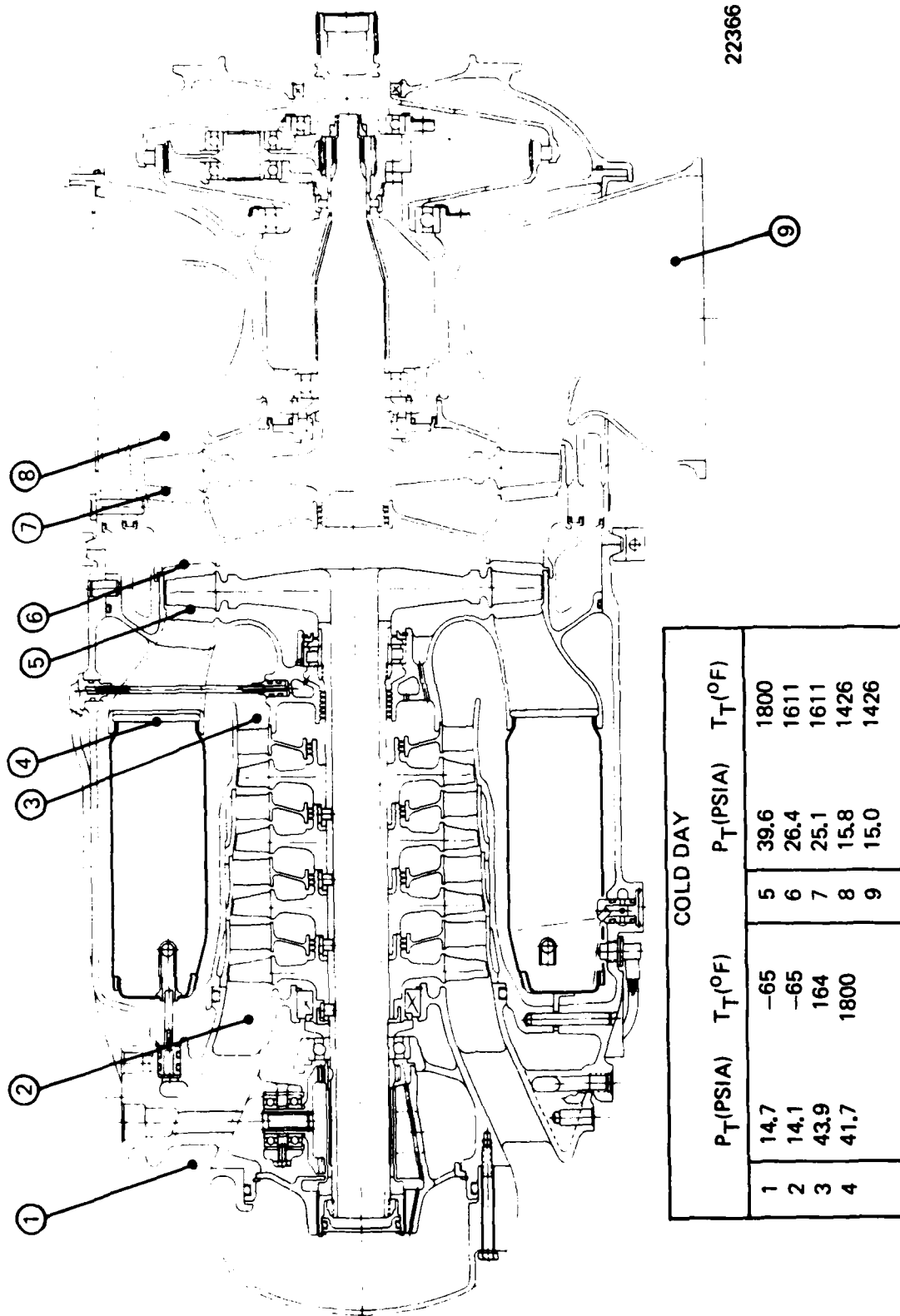
Figure 18 . Model JFS 206 Jet Fuel Starter, SLS, Preliminary Thermodynamic State Points (Cold Day - 65°F).

30

12.7 IN

22367

EXPENDABLE
GASIFIER

JET
NOZZLE

28.0 IN
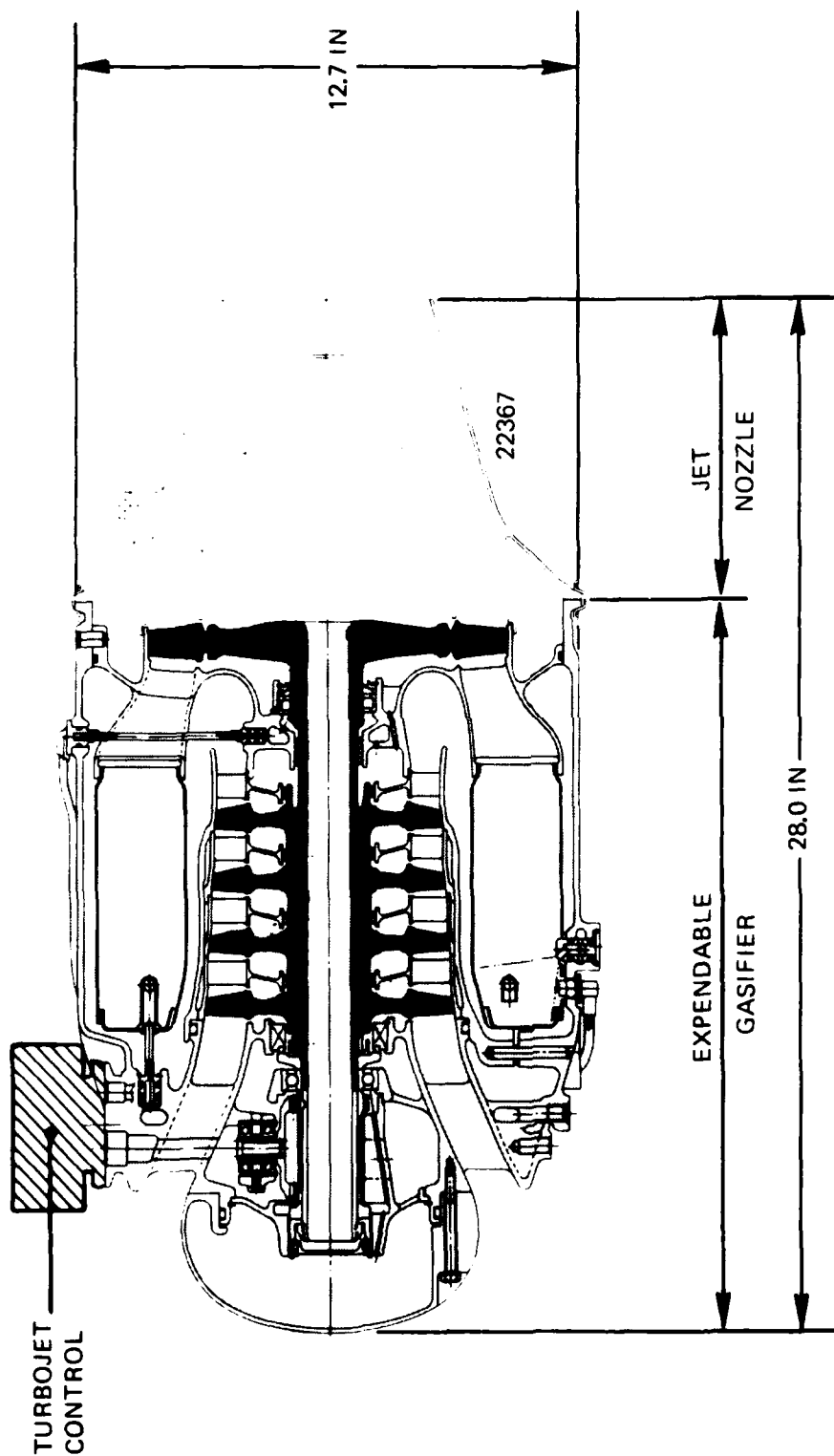
TURBOJET
CONTROL

PERFORMANCE (SLS, 59°F)	
Wa = 4.06 LB/SEC	N_G = 33,000 RPM
PR = 2.67	FN = 229
TIT = 1780°F	SFC = 1.56 LB/HR/LB
AccHP = 3.0 HP	WT = 80 LBS

Figure 19. Turbojet Commonality with Expendable Gasifier.

31
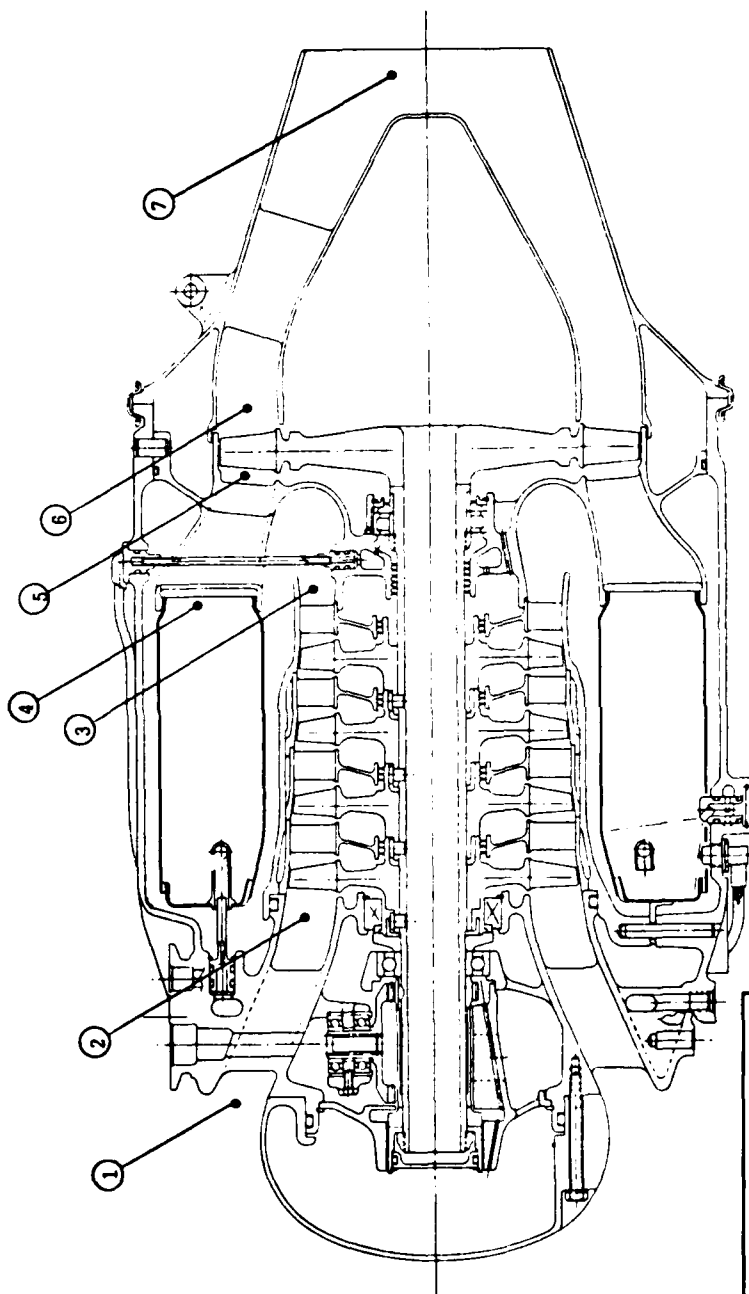
22368

	STANDARD DAY	
	P_T(PSIA)	T_T(°F)
1	14.7	59
2	14.7	59
3	39.3	266
4	37.3	1780
5	35.0	1780
6	24.8	1614
7	23.8	1614

Figure 20 Model 306 Turbojet, SLS, Preliminary Thermodynamic State Points (Standard Day 59°F).
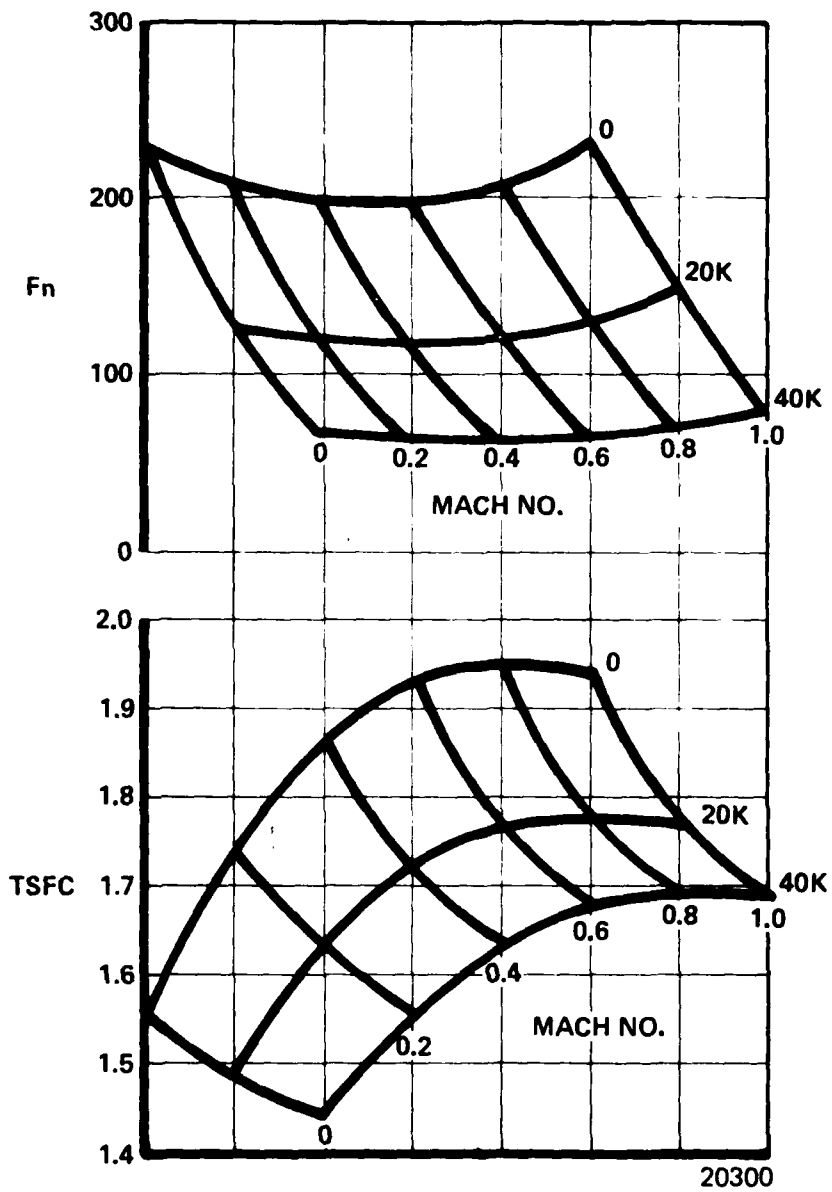
Figure 21 . Variation of Turbojet Performance with Altitude and Mach No.
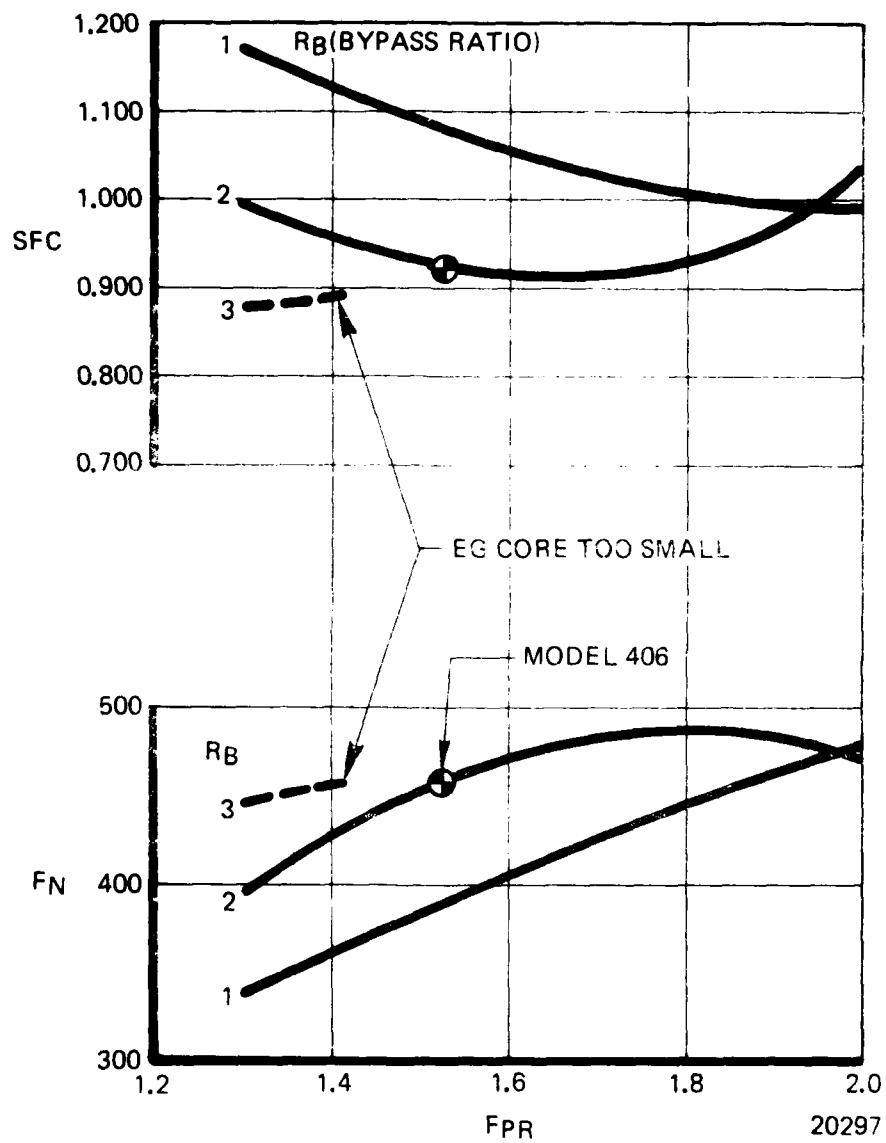
Figure 22. Optimization of Fan Pressure Ratio and Bypass Ratio for the EG/Turbofan Configuration.

34

TABLE 3

MODEL JFS206 JET FUEL STARTER PERFORMANCE

ENGINE PARAMETERS	PERFORMANCE		

INLET CONDITION:
    Ambient temperature (^{O}F)
    Inlet pressure recovery (%)
	59
	96
		130
		96
			-65
			96

COMPRESSOR:
    Pressure ratio
    Adiabatic efficiency (%)
    Airflow (lb/sec)
    Tip diameter (in)
	2.857
	80
	3.862
	6.288
		2.55
		81.8
		3.411
		6.288
			3.11
			66.0
			5.128
			6.288

GAS GENERATOR TURBINE:
    Horsepower extraction
    Turbine inlet temperature (^{O}F)
    Adiabatic efficiency (%)
	3
	1800
	82.5
		3
		1800
		82.5
			3
			1800
			82.5

POWER TURBINE:
    Adiabatic efficiency (%)
    Mechanical efficiency (%)
	80
	96
		80
		96
			80
			96

TOTAL PRESSURE LOSS (%):
    Combustor
    Inter turbine passage
    Exhaust diffuser
	5.0
	1.5
	5.0
		5.0
		1.5
		5.0
			5.0
			1.5
			5.0

SPEED:
    Gas generator (RPM)
    Power turbine (RPM)
	33,060
	24,670
		33,060
		24,670
			33,060
			24,670

OVERALL PERFORMANCE:
    Power turbine output (HP)
    BSFC (lbs/hr-BHP)
    Nozzle pressure ratio
	237
	1.435
	1.02
		160
		1.799
		1.02
			372
			1.305
			1.02

The turbofan cross-section (Figure 23) shows the length at 30.7 in. and diameter at 16.0 in. The weight estimate of 140 lbs. includes the controls. The performance at SLS, standard day shows that a thrust of 500 lbs. is generated at an SFC of 0.91 lb./hr./lb. At the SLS, 59°F condition, the fan is operating at a pressure ratio of 1.53, airflow of 16 lb./sec. and rotor speed of 17,500 rpm. The fan performance requirements can be achieved using the aerodynamic design of a fan recently tested at Teledyne CAE. The efficiency has been degraded, however, to account for the application of low cost manufacturing techniques.

The thermodynamic state points throughout the turbofan flowpath are pre-sented in Figure 24 at SLS standard day conditions.

The turbofan engine performance was then run for a range of altitude and Mach numbers from sea level to 40,000 ft. and 0 to 1.0 Mach number and the re-sulting performance is shown in Figure 25 .

A critical design parameter in the application of the low cost EG design will be the allowable compressor discharge temperature to permit the use of alumi-num in the main frame and compressor components. The variation of CDT over the range of altitudes and Mach numbers in the turbofan application is shown in Figure 26 . The turbofan flight envelope will be limited on one extreme by the turbine inlet temperature of 1800°F and on the other by the maximum compressor discharge temperature which will approach 400°F (Figure 27).

Table 4 summarizes the turbojet and turbofan overall performance together with the component performance used in the preliminary analysis.

Table 5 summarizes the preliminary weight estimates for the JFS, T/J and T/F configurations, including controls.

36

PERFORMANCE (SLS, 59°F)

THRUST	500 LBS	CPR	3.9
SFC	0.91 LB/HR/LB	FPR	1.53
AIRFLOW	16.0 LB/SEC	WEIGHT	140 LBS
TIT	1800°F	T/W	3.57
BPR	1.97		
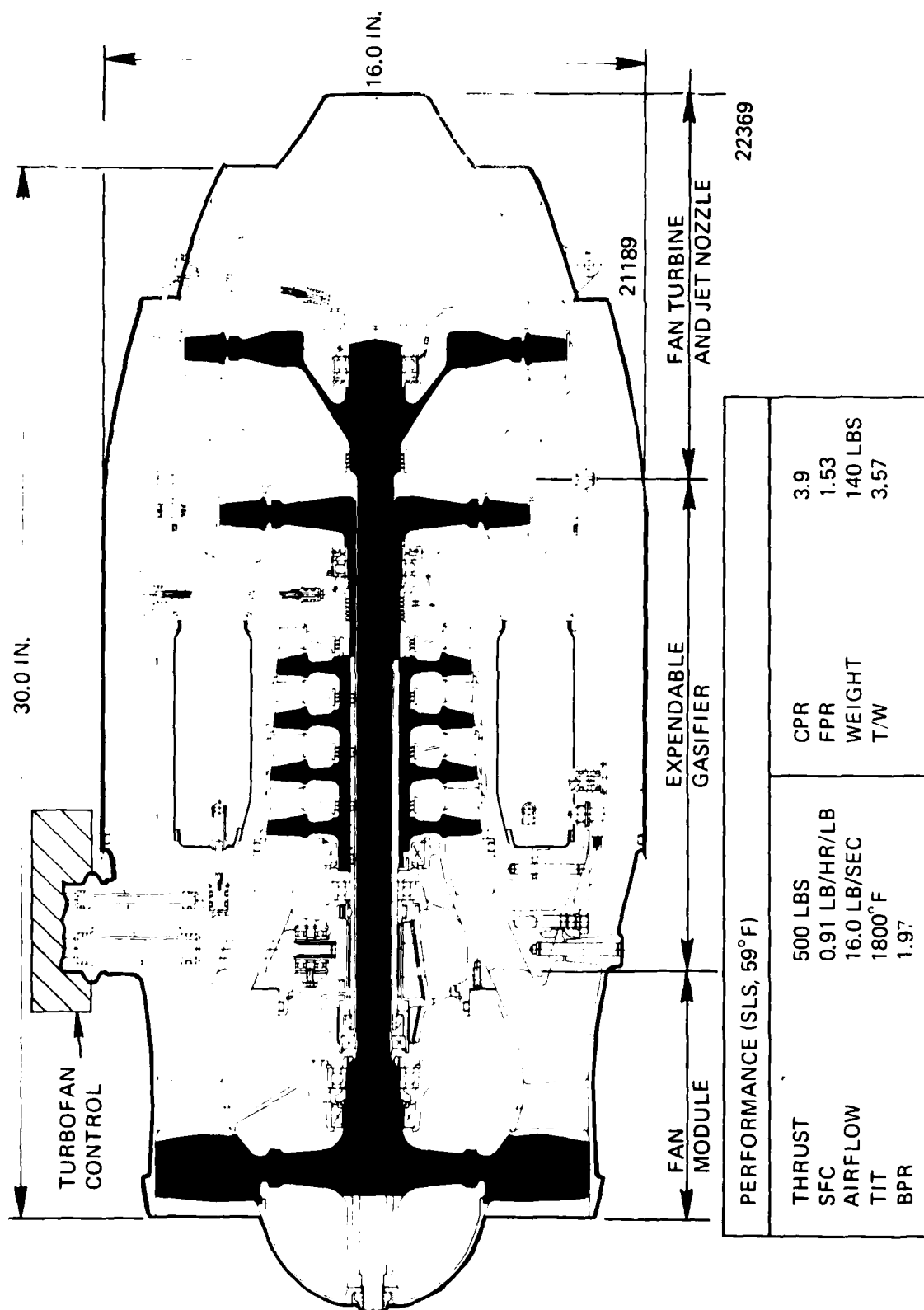
Figure 23 . Model 406 Turbofan.
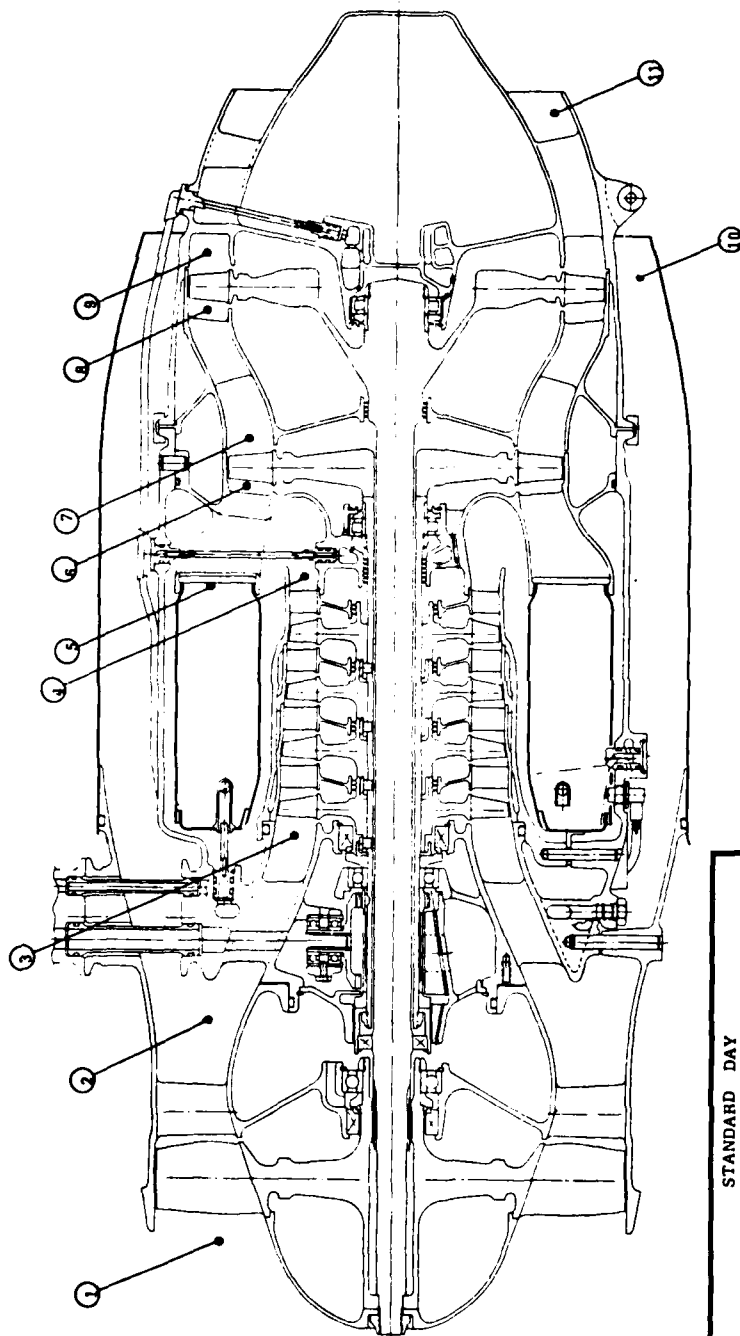
STANDARD DAY					
	P_T (PSIA)	T_T (F)		P_T (PSIA)	T_T (F)
1	14.7	59	6	50.3	1800
2	22.4	140	7	34.5	1628
3	21.8	140	8	31.9	1628
4	56.4	365	9	19.8	1430
5	53.5	1800	10	21.6	140
			11	19.2	1430

19722

Figure 24 . Model 406 Turbofan, SLS, Preliminary Thermodynamic State Points.

38
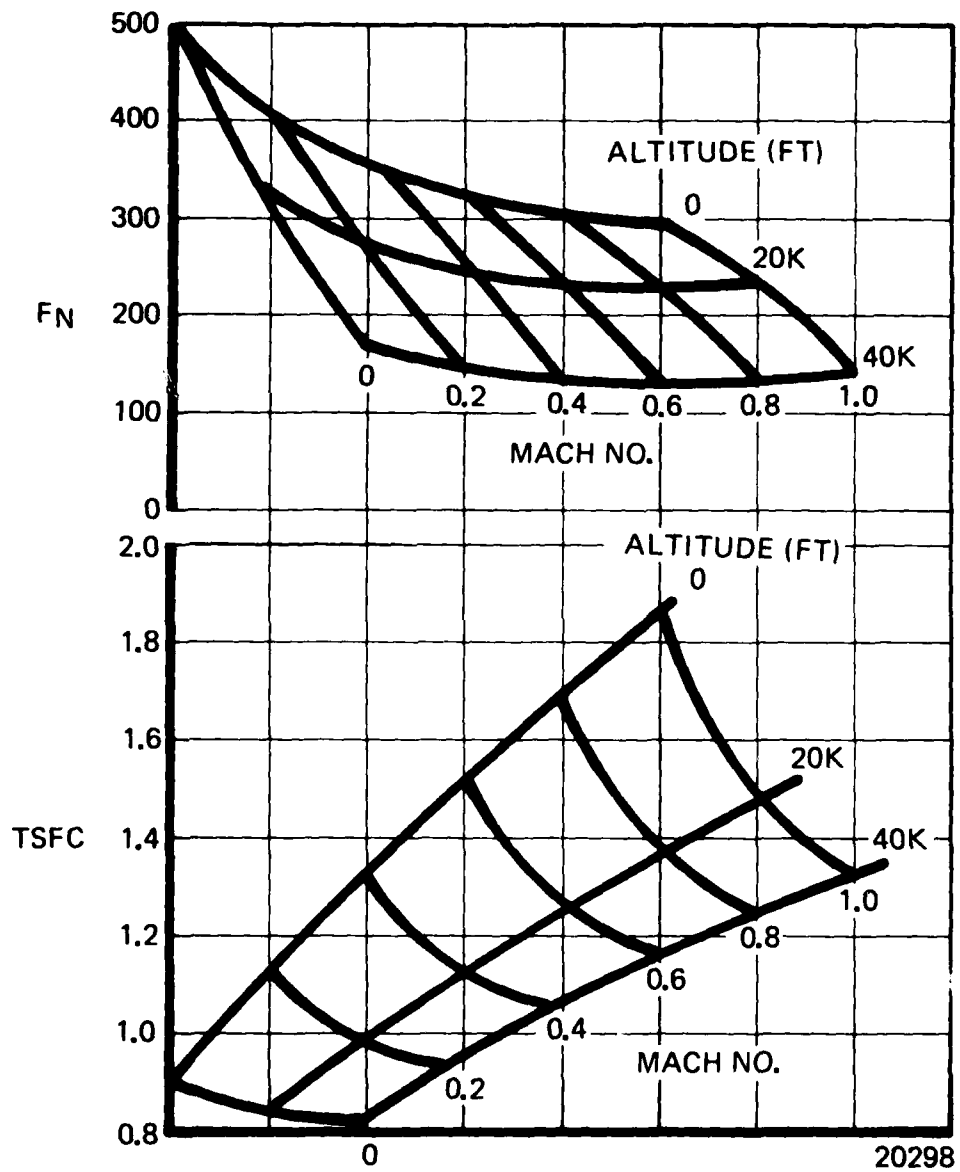
Figure 25 .   Turbofan Performance Using the EG Core.

39
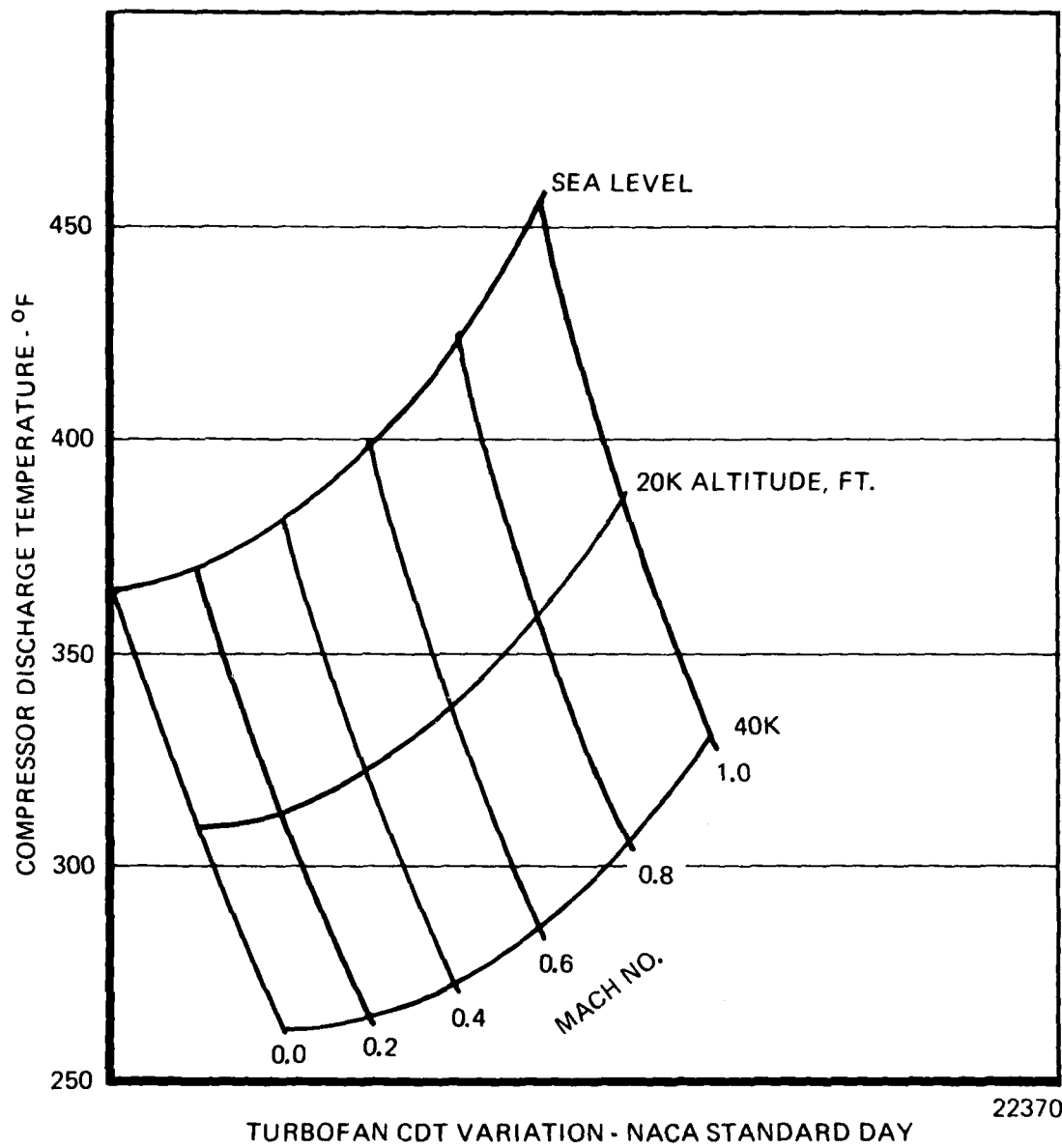
Figure 26 . Preliminary Range of CDT for the Turbofan Configuration.
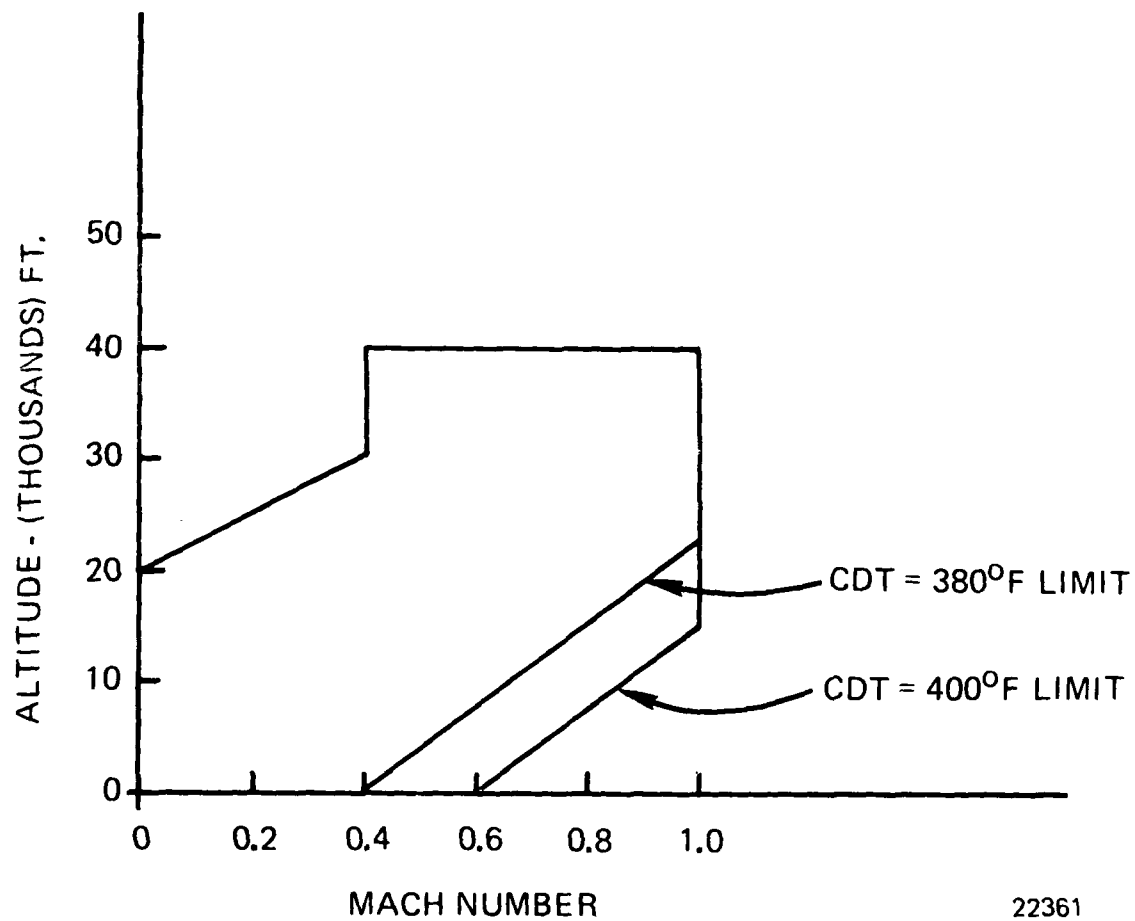
Figure 27 . Turbofan Flight Envelope for Various Maximum CDT Temperatures.

41

TABLE 4

MODEL 306 AND 406 ENGINE PERFORMANCE
SEA LEVEL STATIC
STANDARD DAY

PARAMETERS	ENGINE	
	MODEL 306 TURBOJET	MODEL 406 TURBOFAN
FAN:		
Pressure Ratio	-	1.53
Adiabatic Efficiency (%)	-	81.6
Speed (RPM)	-	17,491
Bypass Ratio	-	1.974
COMPRESSOR:		
Pressure Ratio	2.67	2.54
Adiabatic Efficiency (%)	80.7	80.5
Speed (RPM)	33,055	33,055
HP TURBINE:		
Turbine Inlet Temperature ($^{\circ}$F)	1783	1811
Adiabatic Efficiency (%)	82.3	82.4
Horsepower Extraction	3.0	3.0
$\Delta H/\theta$	11.7	12.6
LP TURBINE:		
Adiabatic Efficiency (%)	-	78.7
$\Delta H/\theta$	-	14.5
OVERALL PERFORMANCE:		
Net Thrust (Lb)	229	500
SFC (Lb/Hr/Lb)	1.563	0.910
Total Airflow (Lb/Sec)	4.06	16.0

TABLE 5

PRELIMINARY WEIGHT ESTIMATES GASIFIER MODEL - 506		
	MATERIAL	WT.
Air Inlet & Accessory Bevel Drive Group		
Nose Cone	C.AL.12	2.39
Support Housing	C.AL.14	1.40
Air Inlet & Combustor Housing (Main Frame)	C.AL.15	21.98
Oil Seals, Spacers, Brgs., Gears, Nuts, Pins		3.20
TOTAL		28.97
Compressor Group		
1st Rotor - Compressor	C.AL.	0.72
2nd Rotor - Compressor	C.AL.	0.70
3rd Rotor - Compressor	C.AL.	0.68
4th Rotor - Compressor	C.AL.	0.66
1st Stator & Shroud	C.AL.	0.76
2nd Stator & Shroud	C.AL.	0.69
3rd Stator & Shroud	C.AL.	0.72
4th Stator & Shroud & Housing	C.AL.	2.05
Pins (12)		0.05
TOTAL		7.03
Combustor & Turbine Group		
Turbine Rotor & Shaft	C.STL	10.20
Nozzle - Turbine Inlet	C.STL	16.50
Combustor Assembly	0.035 STL	7.00
Roller Bearing - Rear		0.30
TOTAL		34.00
TOTAL GASIFIER WEIGHT (LESS CONTROLS)		70.00

43

TABLE 5 (continued)

JET FUEL STARTER MODEL JFS-206		
	MATERIAL	WT.
Gasifier		70.00
Starter Group		
Outer Housing	0.05 STL	5.30
Clamp		2.10
Power Turbine Nozzle	C.STL.08	7.24
Containment Ring	STL	14.6
Exhaust Duct	C.STL.08	10.50
Insulation		2.10
Power Turbine Rotor & Shaft	C.STL	9.62
Reduction Gear Support Housing	C.AL.15	3.52
Reduction Gear Rear Housing	C.AL.15	2.86
Ring Gear	STL	3.18
Clutch		0.60
Idler Gear	STL	0.65
Support Idler Gear Assembly	C.AL.	0.96
Pinion Gear	STL	0.29
Power Gear	STL	3.50
Bearing (6)		2.17
Locks, Seals, Spacers, Pins, Seal Hsg.		1.58
TOTAL		70.77
Controls		
Ignition Coil		0.55
Alternator		0.92
Metering Valve		1.75
Hyd. Motor		1.85
Accy. Drive & Gear, Brgs. Assembly		2.5
Fuel Pump		0.75
Lines, Fitting		0.50
Electronic Control		0.70
Ignitors & Primers		0.15
TOTAL		9.67
TOTAL J.F.S. WEIGHT (LB)		150.44

TABLE 5 (continued)

FAN ENGINE MODEL - 406		
	MATERIAL	WT.
Gasifier		70.00
L.P. Fan Group		
Spinner	C.AL.08	0.55
Transition Duct	C.AL.15	12.9
Fan Rotor	C.AL.	6.17
Brg., Nuts, Seal, Spacer, Pins		1.31
TOTAL		20.93
L.P. Turbine Group		
Exhaust Duct	C.STL.10	14.5
L.P. Turbine Rotor & Shaft	C.STL	15.6
L.P. Turbine Nozzle	C.STL.10	10.2
Fan Duct	AL.04	3.30
Clamp, Brg., Nut, Seals, Pins		2.80
TOTAL		46.40
Controls		
Fuel Pump		0.45
Three-Way Valve		0.25
Valve Act & Housing		1.30
Ignitor, Lines, Fitting, Clamp		0.67
TOTAL		2.67
TOTAL FAN ENGINE WEIGHT (LB)		140.00

TABLE 5 (continued) JET ENGINE MODEL 306		
	MATERIAL	WT.
Gasifier		70.00
Exhaust Duct	C.STL.08	6.53
Clamp - Rear	STL.06	1.20
TOTAL		77.73
Controls		
Fuel Pump		0.45
Three-Way Valve		0.25
Valve Act. & Housing		1.30
Ignitors, Lines, Fitting, Clamp		0.67
TOTAL		2.67
TOTAL JET ENGINE WEIGHT (LB)		80.40

SECTION 4 - PRELIMINARY GASIFIER DESIGN (PHASE II)

4.1   COMPONENT PRELIMINARY AERODYNAMIC DESIGN

Preliminary analyses were performed for the Expendable Gasifier Components including aerodynamic, mechanical and thermal. The components included the compressor, combustor and turbine, both rotating and static structures. More detail was applied to the combustor since that component was released for test hardware at the end of Phase II. The level of effort for the preliminary aerodynamic design consisted of definition of the flowpath, number of stators and rotor blades, velocity triangles and efficiencies.

4.1.1 Compressor Design

Preliminary aerodynamic design of the Expendable Gasifier (EG) four stage axial compressor is based on the sea-level, static, Jet Fuel Starter configuration performance objectives established in Phase I.

The basis of the EG compressor design is a modified upscale of the Teledyne CAE Model 469 compressor (Figure 28) incorporating optimized blading aspect ratios and various design features for low cost manufacture. Most notable of the low cost features is the use of a common rotor casting in all four stages. The low-cost, cast blading will differ from conventional machined blading by having increased edge radii and tolerance band widths, and possible increases in surface roughness and rotor tip clearance.

The use of a common stator was unattractive because of: (1) it did not show a significant cost payoff, (2) it presented a formidable attachment problem to the outer shroud, and (3) it severely compromised the stage aerodynamic performance. The use of individual stator designs makes possible the precise achievement of reference incidence for all blade rows. This approach affords the benefits of: (1) realizing the maximum design point performance potential, and (2) a broader, stable operating range at off-design conditions.

Accomplishments during the preliminary design phase include establishing the feasibility; the definition of preliminary flowpath (Figure 29), velocity triangle data, and blading; and the definition of the procedure for final design.

The compressor is a subsonic, highly loaded, four stage machine derived from an upscale of the Teledyne CAE Model 460 compressor. The design corrected flow of the EG compressor is four percent higher than that which would result from a direct upscale of the Model 469 at the design speed and pressure ratio. The aerodynamic design point is shown below.

EG COMPRESSOR
AERODYNAMIC DESIGN POINT

Corrected Speed, $N/\sqrt{\theta}$ - rpm	33,060
Corrected Flow, $W\sqrt{\theta}/\delta$ - lbm/sec	4.023
Pressure Ratio	2.86
Adiabatic Efficiency - percent	80.0

47

14912
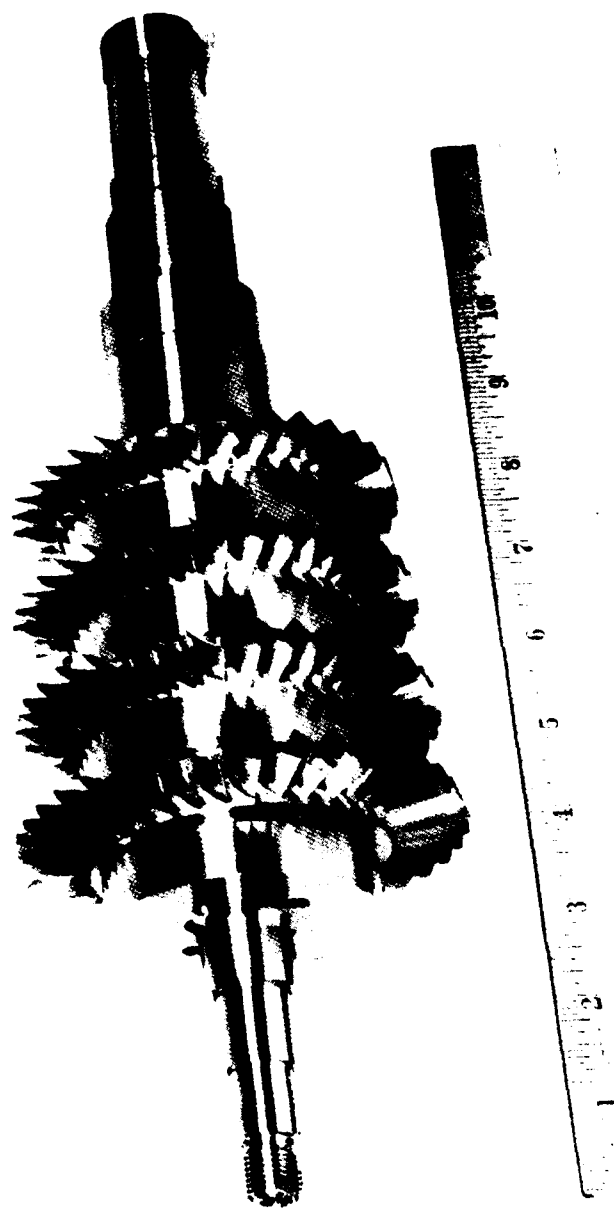
Figure 28 . Four-Stage Model 469 Axial Compressor Rotor.

48

Figure 29. Expendable Gasifier Compressor Preliminary Flowpath.

LOCATION	RH	RT	ZH	ZT	LOCATION	RH	RT	ZH	ZT
R1 IN	2.043	3.118	0.	0.113	R3 OUT	2.043	2.820	3.893	3.810
OUT	2.043	3.033	0.671	0.567	S3 IN	2.043	2.802	4.073	4.073
S1 IN	2.043	2.997	0.851	0.851	OUT	2.043	2.802	4.653	4.653
OUT	2.043	2.997	1.431	1.431	R4 IN	2.043	2.788	4.833	4.911
R2 IN	2.043	2.969	1.611	1.708	OUT	2.043	2.742	5.504	5.431
OUT	2.043	2.914	2.282	2.192	S4 IN	2.043	2.731	5.684	5.684
S2 IN	2.043	2.889	2.462	2.462	OUT	2.043	2.731	6.264	6.264
OUT	2.043	2.889	3.042	3.042	—	1.980	2.790	6.850	6.850
R3 IN	2.043	2.870	3.222	3.310	—	1.860	2.846	7.465	7.465

21909

49

With emphasis on low cost, the principal guideline was the requirement for the use of a common castings in all four stages. Common rotors and stators were considered during the prelim nary design phase. Initially, the possibility of direct adaptation of Model 469 blading was explored with regard to commonality. Model 469 blading metal angles were plotted against radius, (Figures 30 and 31). However, the compromise was not feasible for rotor exit metal angle since there were stage-to-stage variations of as much as eleven degrees at constant radius. Stator metal angles (Figure 32), both inlet and exit - agreed closely from stage-to-stage such that a common stator could be utilized for the Model 469 or a scaled derivative with minimal adverse effect. Since rotor angles could not be satisfied with a common design in all four stages, the adaptation of upscaled Model 469 blading was dropped from consideration. However, an upscale of the Model 469 flowpath was used as the starting point for the EG compressor preliminary design.

The preliminary EG compressor flowpath shown in Figure 29, is upscaled directly from the Model 469, with the scale factor on linear dimensions being 1.3166. Axial dimensions were modified to equalize rotor and stator aspect ratios for each stage on the basis of common rotor and stator blading. Relative to Model 469, rotor aspect ratios were reduced and stator aspect ratios increased, as shown in the following table.

ASPECT RATIO COMPARISON		
Blade Row	EG	469
Rotor 1	1.512	1.560
Stator 1	1.488	1.341
Rotor 2	1.309	1.366
Stator 2	1.320	1.189
Rotor 3	1.172	1.218
Stator 3	1.184	1.067
Rotor 4	1.054	1.098
Stator 4	1.073	0.967

Axial gaps between blade rows were set at 0.180 inch.

The EG Jet Fuel Starter front frame inlet duct flowpath, Figure 33, was defined to allow insertion of flowpath fairings to satisfy turbojet, and turbofan configuration requirements. Four equally spaced struts are included in the inlet duct at an inclination of 10.5 degrees from radial. Maximum strut thickness is 0.80 inch while chord is 3.00 inches. Figure 34 shows inlet duct area distributions for the JFS and a typical turbojet configuration. The preliminary fan configuration of Figure 23 assumes a constant transition duct Mach number and thus would have a nearly constant area. Wall meridional velocity distributions for the JFS baseline configuration are shown in Figure 35.
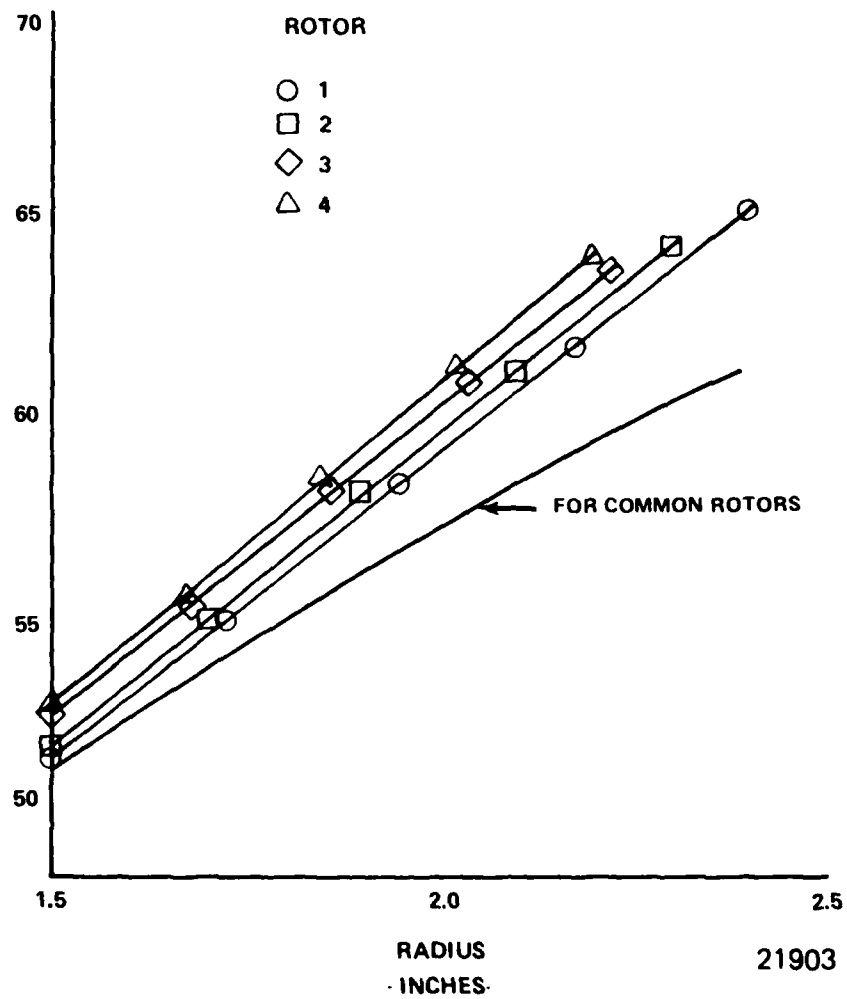
Figure 30 . Model 469 Compressor Rotor Inlet Metal Angle vs. Radius.
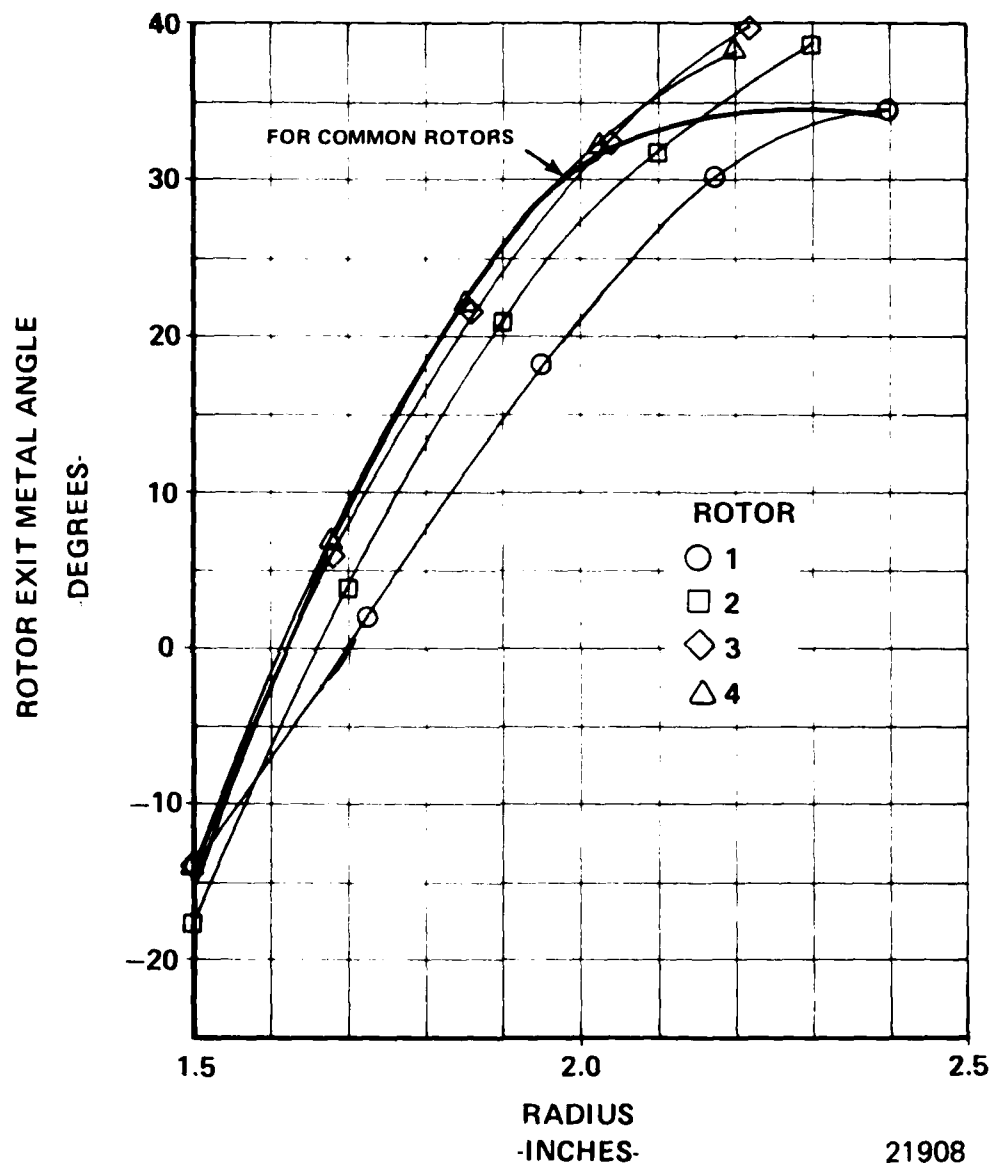
Figure 31 . Model 469 Compressor Rotor Exit Metal Angle vs. Radius.
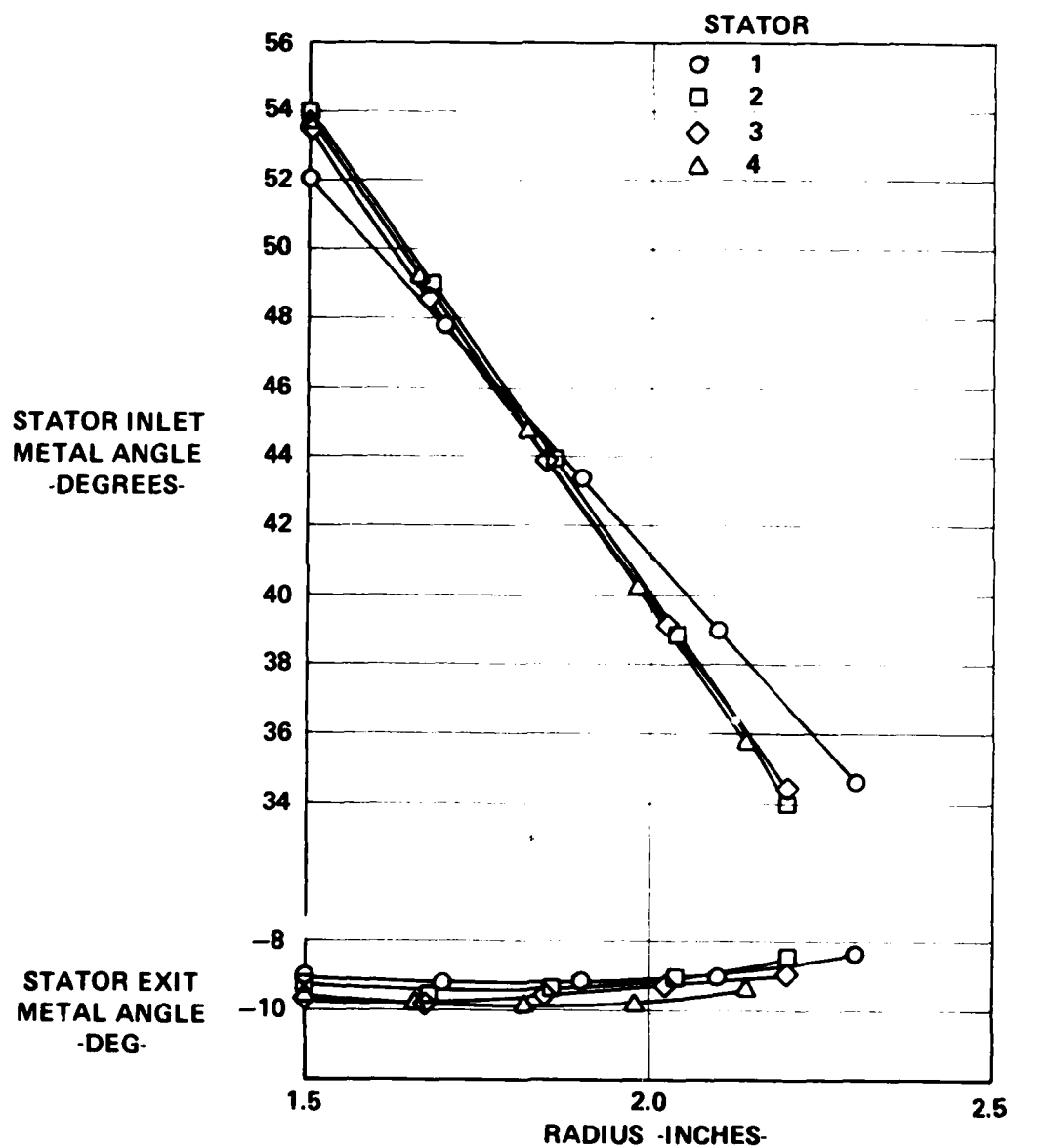
Figure 32 . Model 469 Compressor Stator Metal Angles vs. Radius.

53
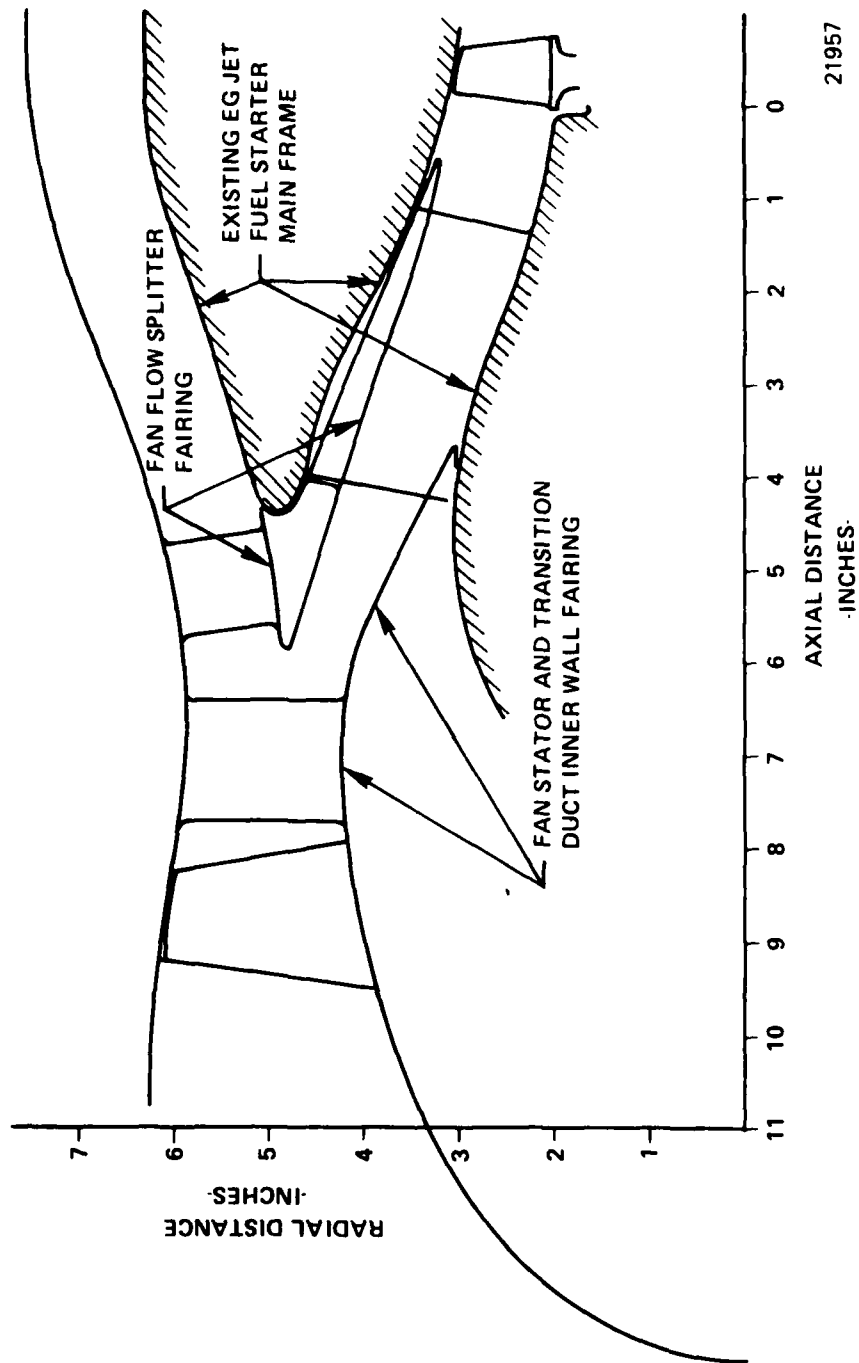
Figure 33 . Expendable Gasifier Preliminary Flowpath for Fan and Associated Ducting Showing Adaptation to Jet Fuel Starter Main Frame.

54

JET FUEL STARTER CONFIGURATION

○ JFS WITH 4 STRUTS; t_{max} = 0.80 in., C = 3.00 in.
◉ JFS WITHOUT STRUTS
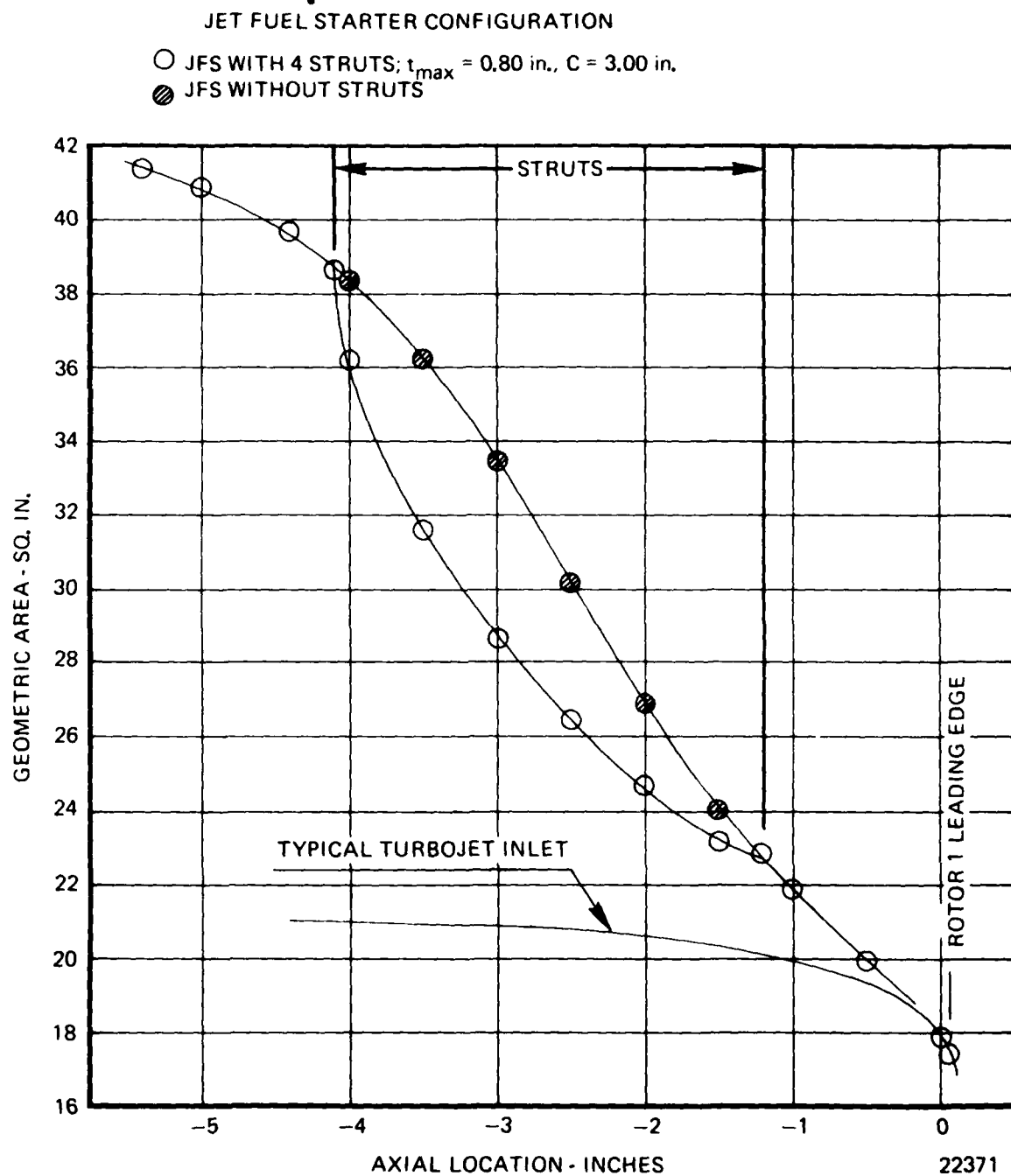
Figure 34 . Expendable Gasifier Compressor Main Frame Inlet Transition Duct
Area Distribution.

55
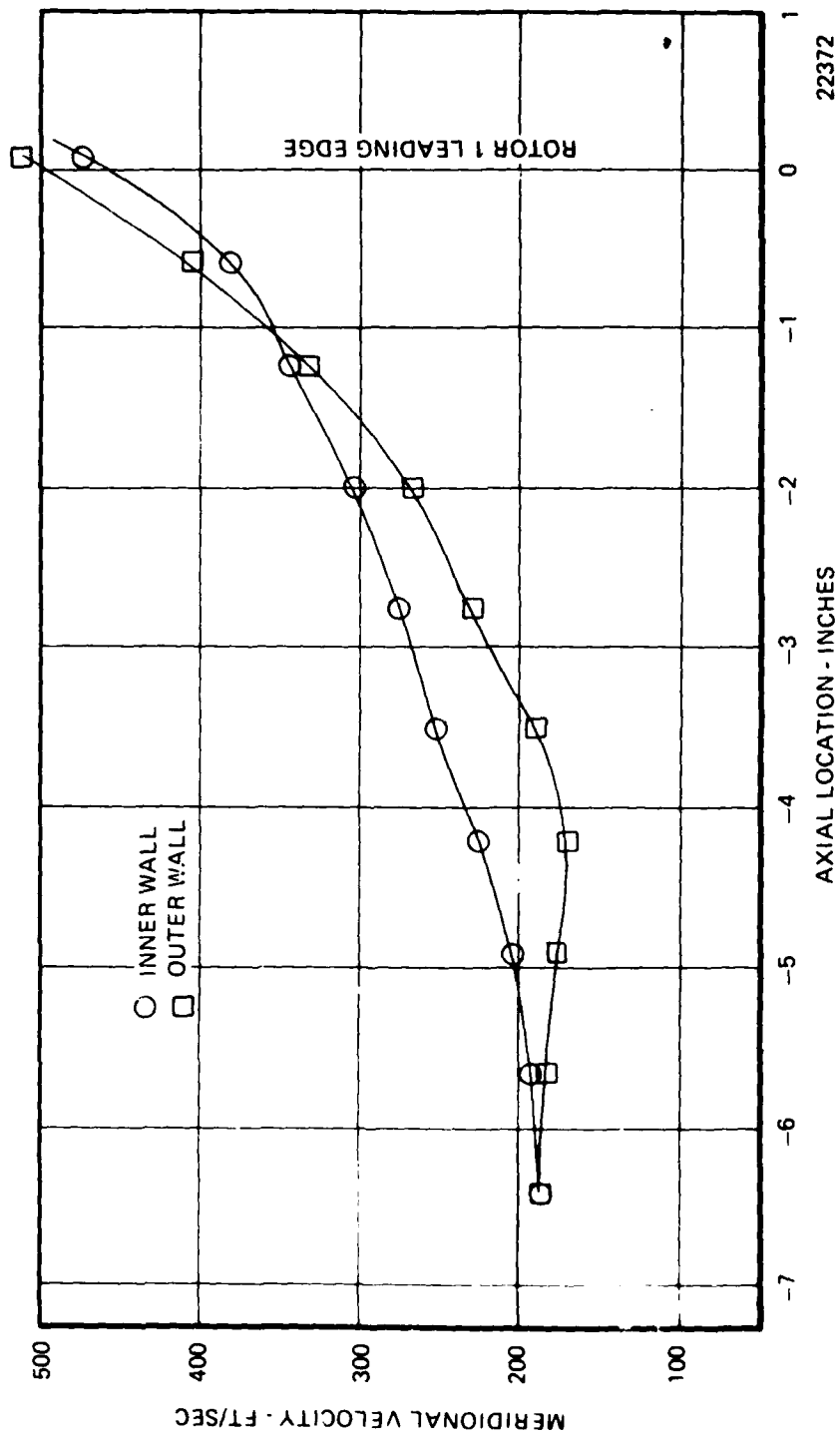
Figure 35. Expendable Gasifier Compressor Main Frame Inlet Transition Duct Wall Meridional Velocity Distribution.

Preliminary design point velocity triangle calculations for the EG compressor were obtained with the use of a computer program. The program performs axial compressor off-design performance calculations with account of variable specific heat and full radial equilibrium, including streamline curvature and radial gradients in total enthalpy and entropy.

As a consequence of using an off-design program, there are significant differences in the procedure and results from those of a conventional design approach, (Figure 36). Most notable is the fact that in the off-design approach, blade geometry details are inseparable from the velocity triangle solution. In addition to input of flowpath, assumed blockage distribution and blading geometry, it is also required to select (1) the means of determining reference incidence, (2) the method of calculating deviation angle, and (3) the appropriate loss parameter vs. diffusion factor tables. During the course of the preliminary design, considerable evolution occurred to satisfy each of these three aspects.

The preliminary design velocity triangle calculation results for the Expendable Gasifier compressor are shown in Table 6. The velocity triangle data are for a configuration having a common rotor in all stages but individual stator designs for each stage. The stator metal angles were not yet optimized to obtain minimum loss incidence for each blade row, and the rotor metal angles were not adjusted to provide exactly the desired overall pressure ratio and flat exit pressure profile. These tasks were accomplished in the final design phase. The feasibility of the design objectives and approach, however, were supported by the fact that the levels of all aerodynamic variables and loading parameters fell within the range of Teledyne CAE previous design experience.

Preliminary rotor and stator airfoil sections were defined graphically at seven radial locations to provide a basis for manufacturing cost estimates. A further iteration was made with minor changes in the blading to obtain aerodynamic parameters from an updated program version. The preliminary stator definition is based on the common stator approach.

The preliminary rotor and stator were generated on conical surfaces that approximate the design streamlines of revolution for the velocity triangle solutions of the first stage. Double circular arc (DCA) airfoil sections (sections having equal inlet and outlet segment turning rates on conical surfaces) were selected for the rotor on the basis of relative inlet Mach numbers ranging from 0.64 to 0.95. The preliminary stator airfoil sections were similar, the exception being the placement of maximum thickness at 40 percent chord to simulate a 65 Series thickness distribution since stator inlet absolute Mach numbers were 0.7 or less.

Certain changes from normal airfoil section definition practice were made for consistency with the casting process anticipated for the manufacture of the rotor and stator. Section edge radii were increased 50 percent for machined blading of this size. Tolerance band width was similarly increased from ±0.002 to ±0.003 inch.

57

NORMAL PROCEDURE   **E.G. (COMMON BLADING) PROCEDURE**
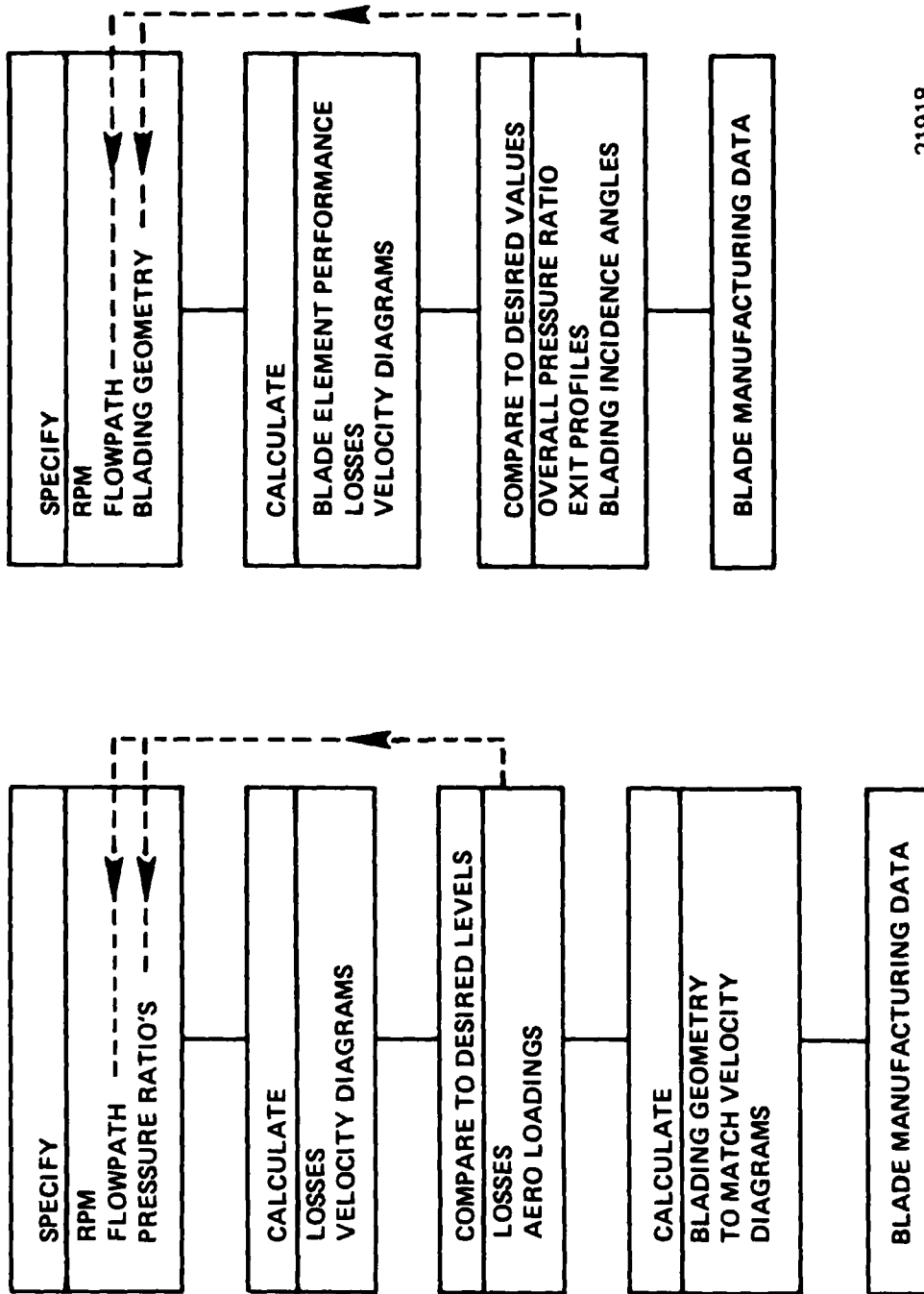
Figure 36. Subsonic Axial Compressor Design Procedure.

58

TABLE 6

EXPENDABLE GASIFIER COMPRESSOR
COMPARISON OF PRELIMINARY DESIGN VELOCITY TRIANGLE SOLUTIONS

VELOCITY TRIANGLE	DESIRED	RUN A	RUN B	FIRST UNCOMMON STATOR RUN
Blading Rotor	-	Common	Common	Common
Stator	-	Common	Common	Individual
Pressure Ratio	2.86	2.813	2.829	2.800
Efficiency	80+	83.1	83.0	81.9*
Exit PT Profile				
Variation From	Flat	+2.43	+1.10	+7.24
Average %	(0%)	-4.40	-1.84	-1.90
Maximum Incidence Angle Variation From Reference Value Degrees				
Rotor	0	+12.4, -1.56	+3.0, -1.57	+4.37, -4.88
Stator	0	+18.27, - 4.5	+15.89, - 2.05	+2.45, -9.20**
Surge Margin	Good	Poor	Poor	Better Good

* LOSS MODEL (IMPROVED; CHANGED) AFTER RUN B SO EFF. OF 81.9°
  IS NOT ONLY A RESULT OF INCIDENCE
** FURTHER REDUCTION IN INCIDENCE WILL PRODUCE GOOD SURGE MARGIN

Current indications are that the cast airfoil surfaces have finishes in the 40-80 microinch range or better. This is comparable to current specification for other compressors having similar sized blading (including machine airfoils, as for Models 471 and 555 compressors). Since these surface finish levels can in fact be achieved (at no cost penalty) there is no appreciable performance decrement for the EG compressor.

The final design procedure to be employed in the EG compressor velocity triangle calculation and airfoil definition is illustrated by the logic path of Figure 37. With the flowpath defined and with the requisite loss, incidence and deviation models established, the successive adjustment of rotor exit metal angle and stator inlet and exit metal angles was performed to satisfy the overall pressure ratio objective with a reasonable flat exit pressure profile.

4.1.2 Combustor Design

The flowpath for the combustor is shown in Figure 38 . The combustor flowpath is of the reverse flow-type, with air outside the liners moving in a direction opposite to that inside the liners. Air from the compressor diffuser enters a small plenum inboard of the expendable gasifier turbine inlet nozzle where approximately one-half of the air is turned 180 degrees to flow forward through the inner annulus formed by the combustor inner liner and the compressor housing. The remaining air flows radially outward through the hollow turbine inlet nozzles (and in the process, regeneratively cools them) into the outer annulus formed by the combustor housing and outer liner. The combustor is fabricated from Haynes 556 sheet metal with punched holes for liner cooling and dilution air.

Figure 38 also shows the preliminary air distribution for the combustor. Seven sets of cooling holes have been estimated for the outer and inner liners perforated sheet requiring about 24 percent of the flow. Thirty-six percent of the air enters the primary zone while about 40 percent is used for dilution flow.

Several combustor parameters calculated during the preliminary design effort are presented below:

Heat Release Rate	- 9.3 MBTU/Hr/Ft^3/ATM
Residence Time	- 9.3 m sec
Reference Velocity	- 57 ft/sec
Pressure Drop	- 10 percent
Temperature Rise	- 1516°F
Combustor Efficiency	- 95 percent

The combustor has a relatively high heat release rate, however, both the relatively low residence time and high reference velocity indicate that the combustor should yield good starting characteristics, design point performance and, fairly uniform temperature distribution factor (TDF) of 0.20 exit temperature distribution. The combustor Mach numbers and local pressures throughout the combustor cavity are shown in Figure 39 . The primary zone is designed to operate at stoichiometric equivalence

60
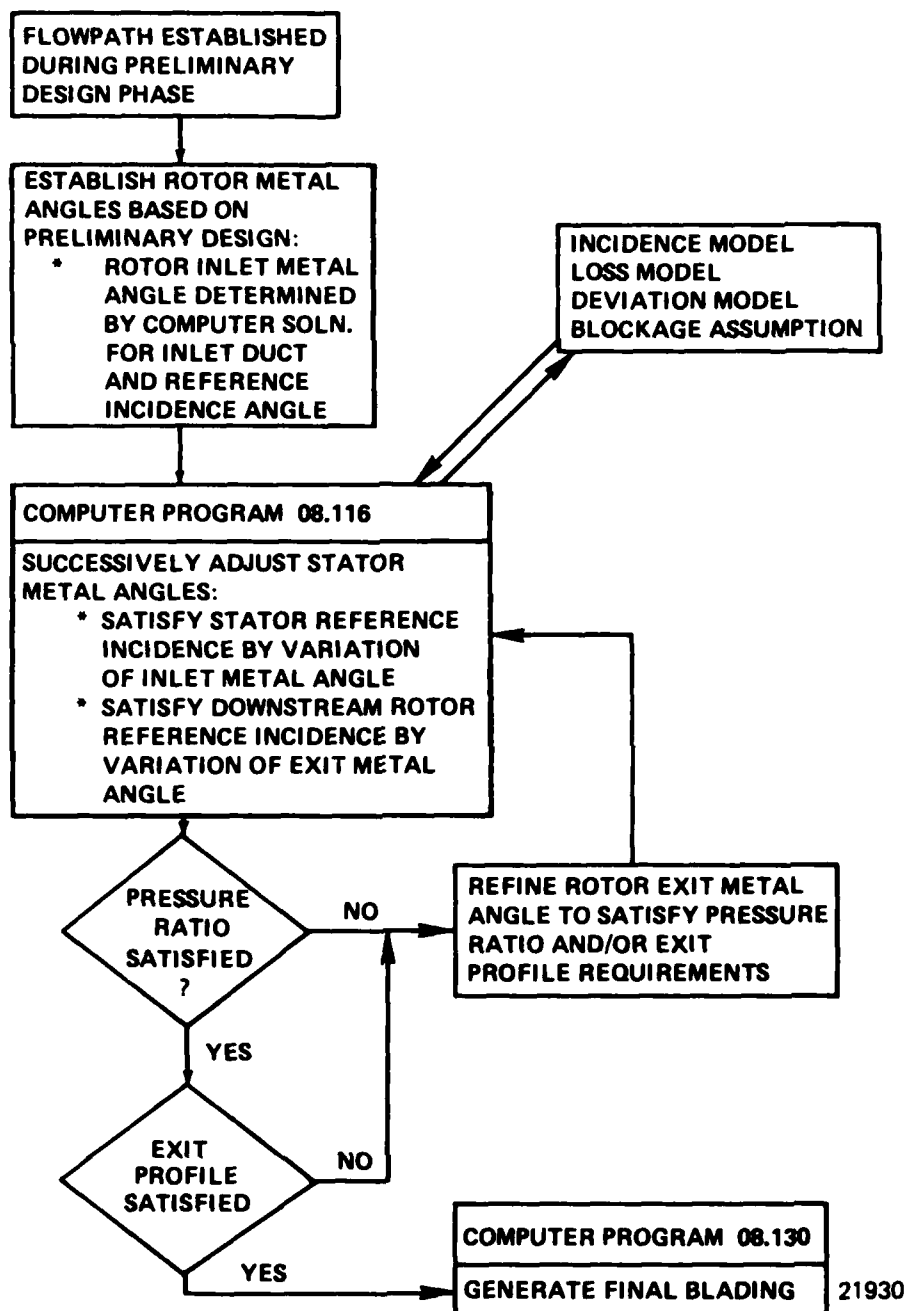
jure 37 . Expendable Gasifier Compressor - Final Design Procedure Logic Path.
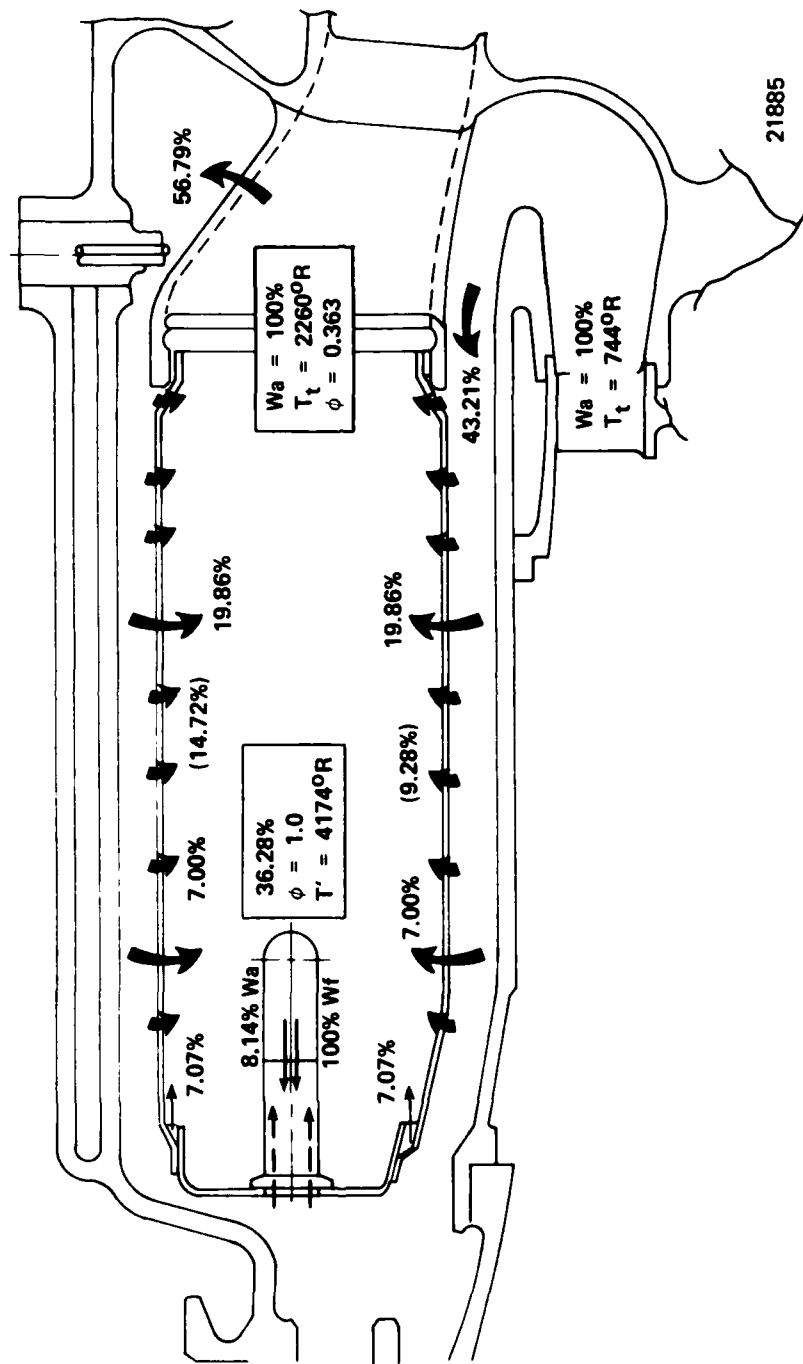
Figure 38 . Combustor Flowpath Showing Estimated Airflow Distribution.

$P_T = 40.07$
$M_N = 0.223$

21883

$P_T = 38.35$
$M_N = 0.128$

$P_T = 36.3$
$M_N = 0.106$

$P_T = 38.42$
$M_N = 0.178$

$P_T = 40.31$
$M_N = 0.324$

$P_S = 36.3$

$P_T = 38.13$
$M_N = 0.058$

$P_T = 38.01$
$M_N = 0.092$

$P_T = 37.83$
$M_N < 0.01$
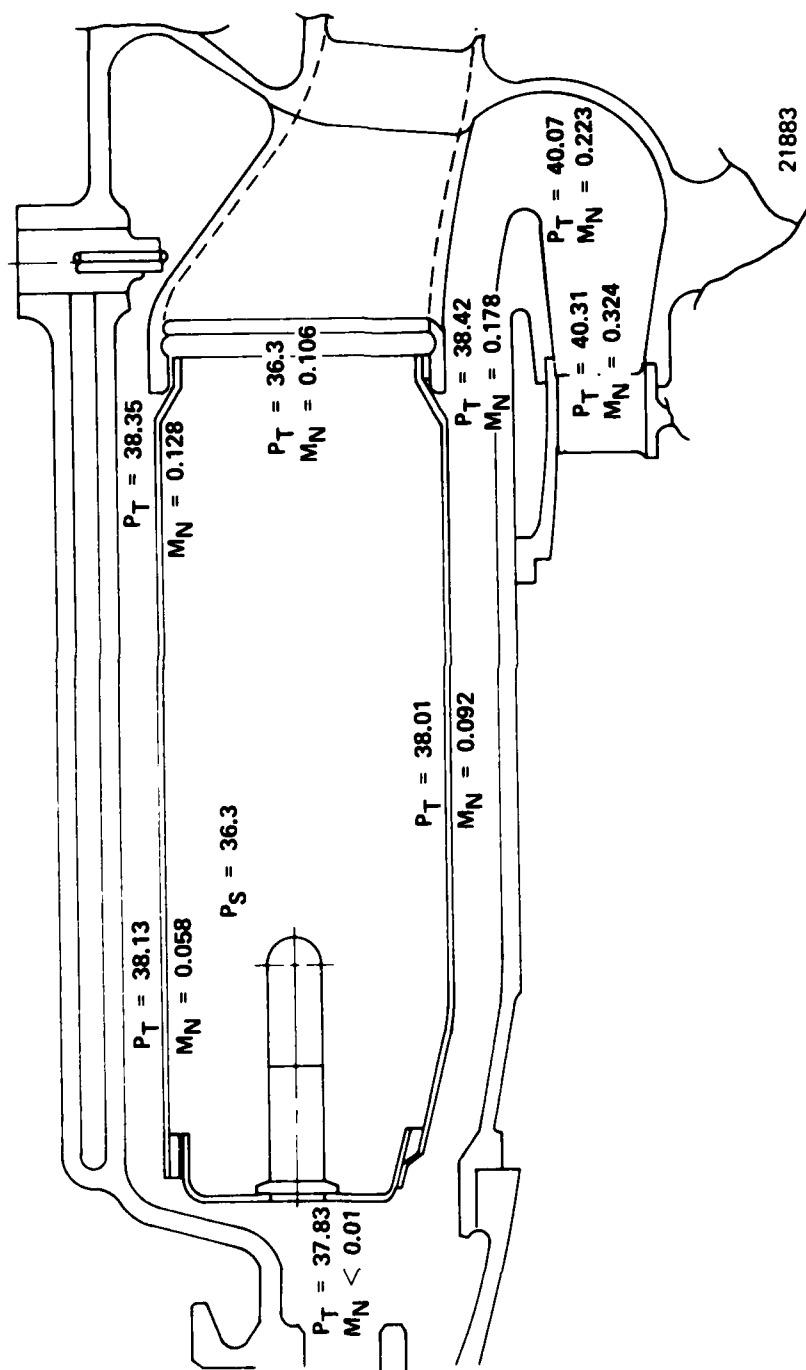
Figure 39. Combustor Flowpath and Pressure Distribution.

63

ratio (ϕ), while the equivalence ratio within the vaporizer pipes is set outside the flammability range at 4.45. Primary holes in the inner and outer liners provide the driving force for recirculation and flame stabilization. Dilution ports are 180 degrees opposed thus providing the strong mixing action necessary for control of the exit temperature profile and achievement of the design TDF of 0.2, (Figure 40).

Estimates of liner metal temperatures based on the film cooling model shown in Figure 41 , indicate maximums below 1400°F (Figure 42), with the cooling hole configuration shown. Should subsequent analysis indicate that this level of liner temperature results in too high a heat input to the combustor housing, dilution air will be traded off for cooling flow and the liner temperature reduced. An alternate double wall liner construction has been devised (Figure 43), in the event that efforts to tradeoff liner cooling and dilution air fail.

During the course of combustor hardware procurement, it was observed that considerable expense is related to the tooling required for punching unique hole patterns in sheet metal. The expense is also compounded by the effort involved when specifying high temperature alloys such as Haynes 556. In order to circumvent the expense, a search was conducted for existing tooling which would meet the hole pattern requirements if not exactly duplicate them. Figure 44 shows the selected (available) pattern compared to that desired during the preliminary design. A comparison of the film coverage indicated that the available pattern would be adequate and yield the same metal temperature distribution as shown in Figure 3-14.

The fuel distribution system employed for the EG combustor is shown in Figure 45 . Fuel enters from the manifold cast integrally in the main frame into each of fourteen injection points. A metering orifice restricts the fuel flow to the desired valve and the fuel flows through the fuel tube into the primary pipe. Inside the primary pipe it mixes with combustor air, vaporizes and flows into the primary zone of the combustor.

The ignition system (Figure 46) consists of two sets of ignitor, primer nozzles placed 90 degrees apart. The primer nozzle receives fuel at the start command initiation from the primer fuel manifold cast integrally in the main frame.

An estimate of the combustor performance is shown in Figure 47 for the three engine applications, JFS, T/J and T/F at selected operating conditions.

A summary of the Combustor Design Parameters is presented in Table 7 .
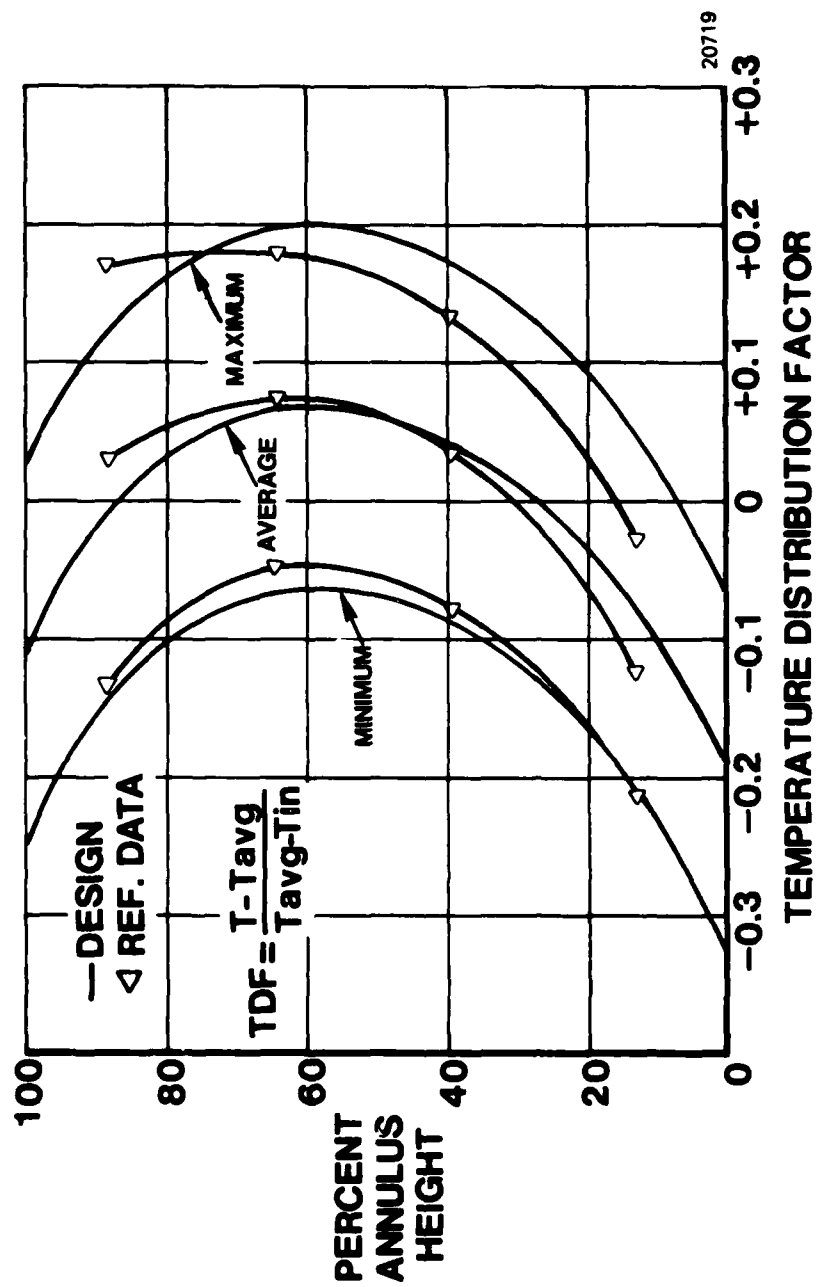
Figure 40 . Radial Temperature Profile Objective.
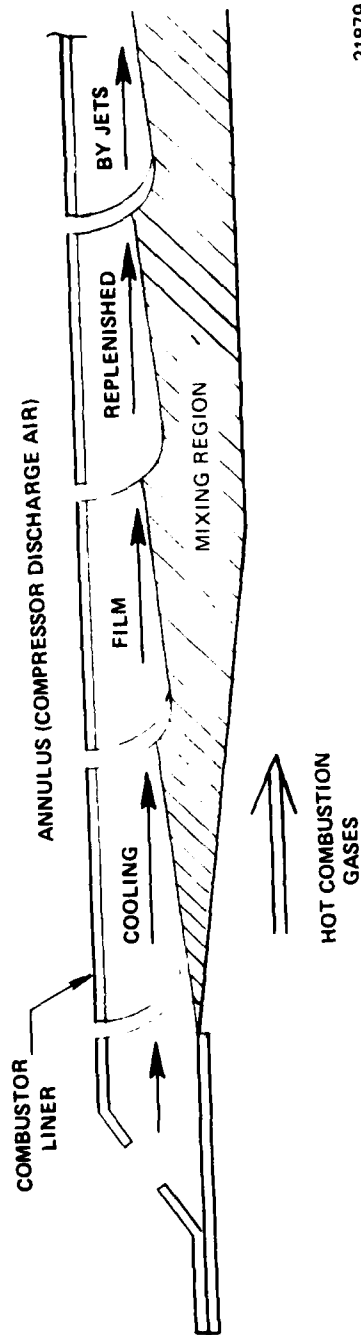
Figure 41 . Schematic of Model for Full Coverage Film Cooling.

66

21847
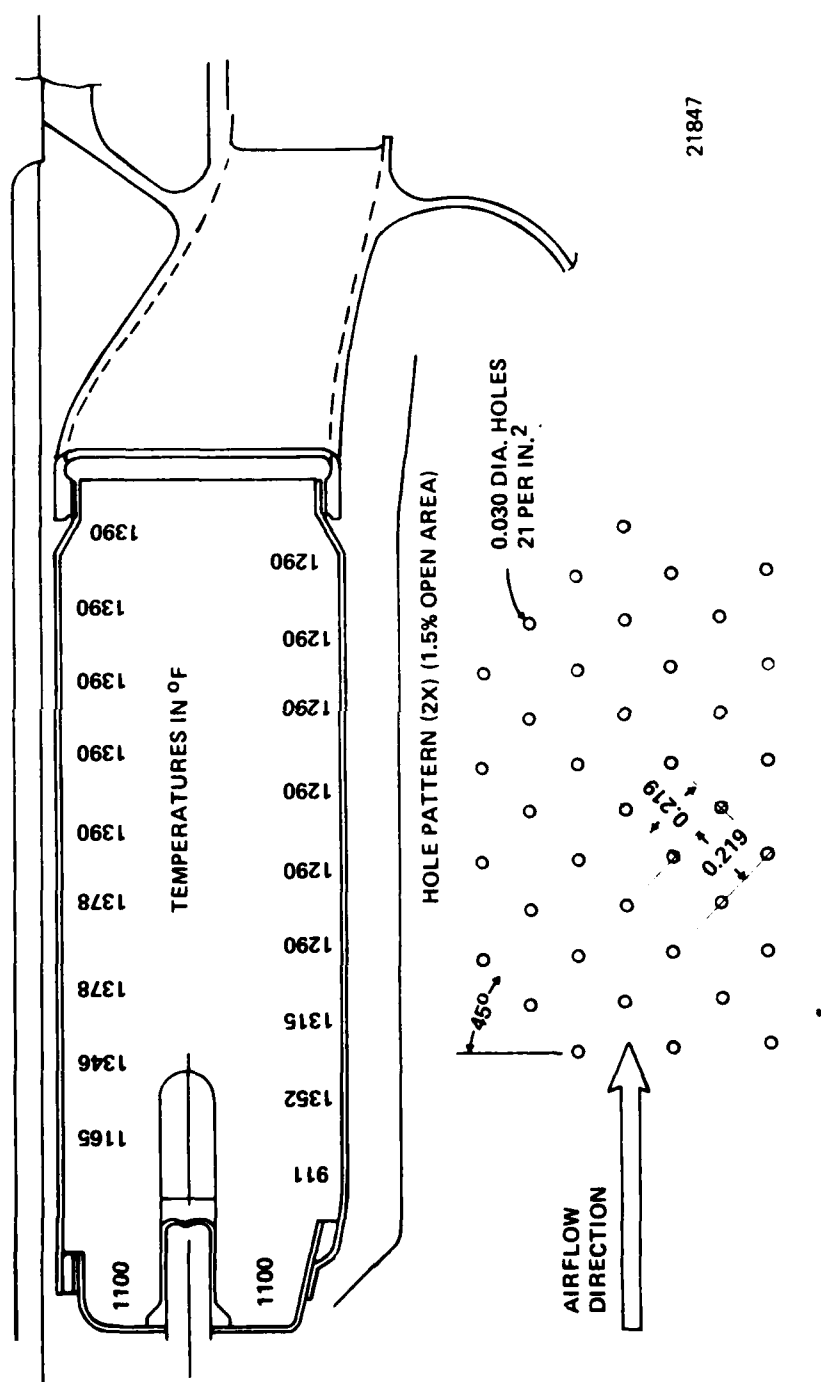
Figure 42. Estimated Liner Metal Temperatures Preliminary Design - SLS Standard Day.

ORIFICE PLATE

OUTER LINER

ORIFICE PLATE
HOLES

LINER HOLES

0.074 DIA.

0.438 0.438

0.438

45° 0.438

0.219
REF
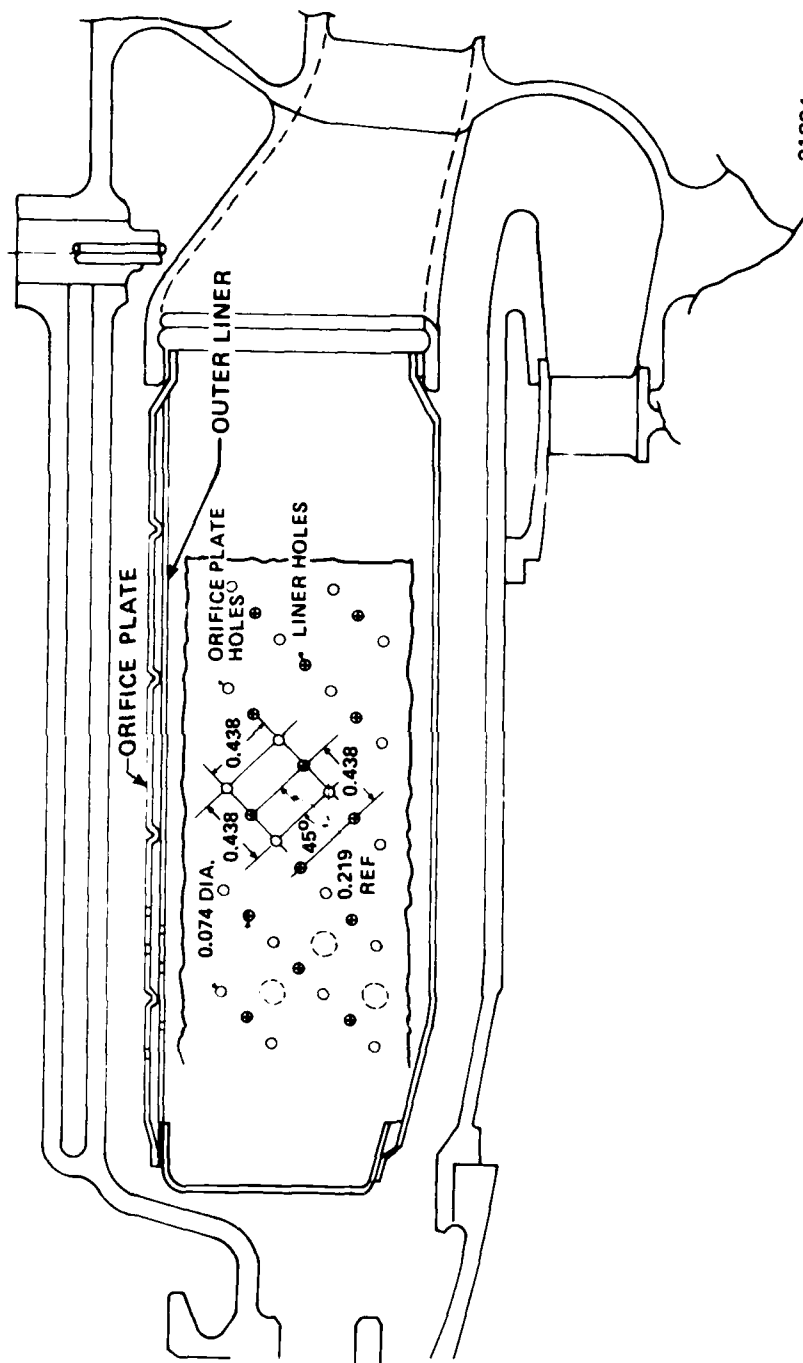
21884

Figure 43 . Alternate Double Wall Liner Construction.
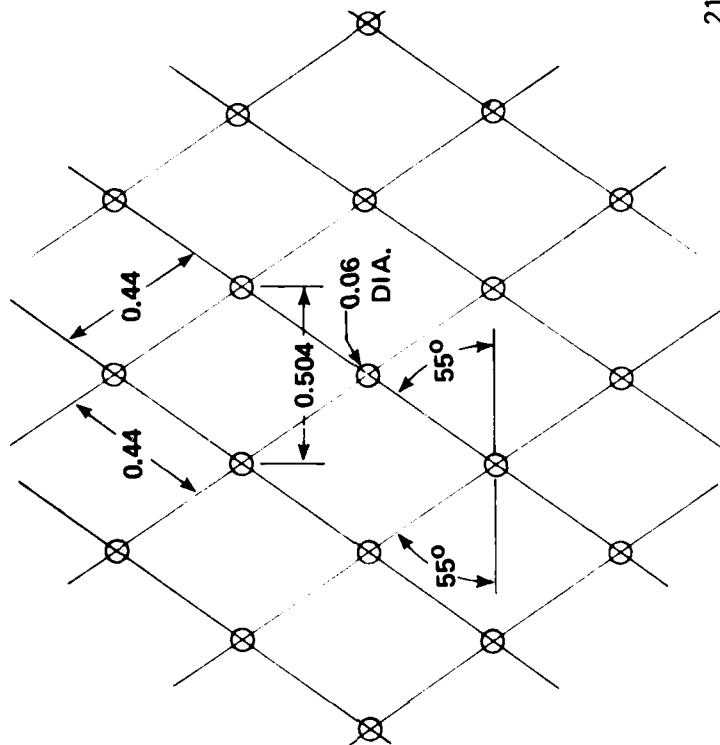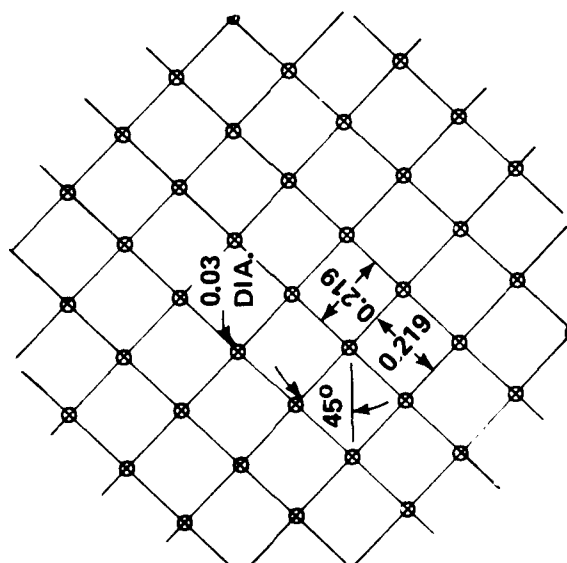
TOOLING AVAILABLE

PRELIMINARY
DESIGN
(NEW TOOLING)

21889

69

21854

PRESSURE DROP

AT START   1 PSI

AT DESIGN   100 PSI

METERING
ORIFICE
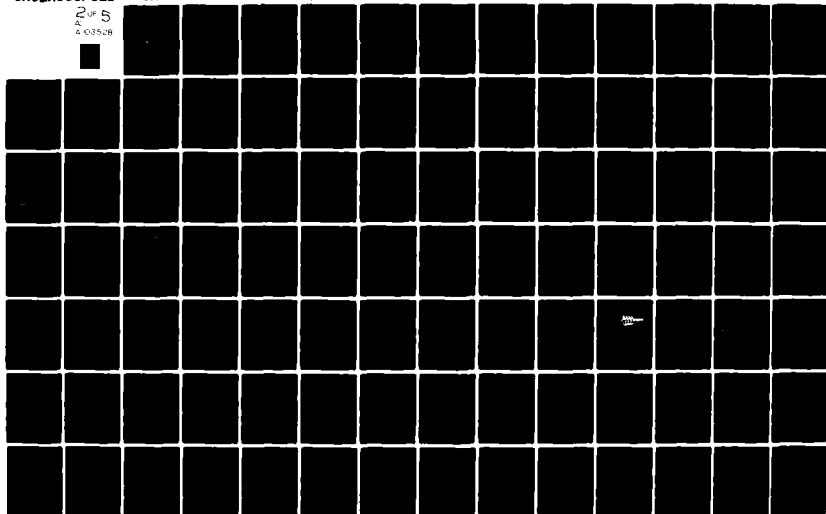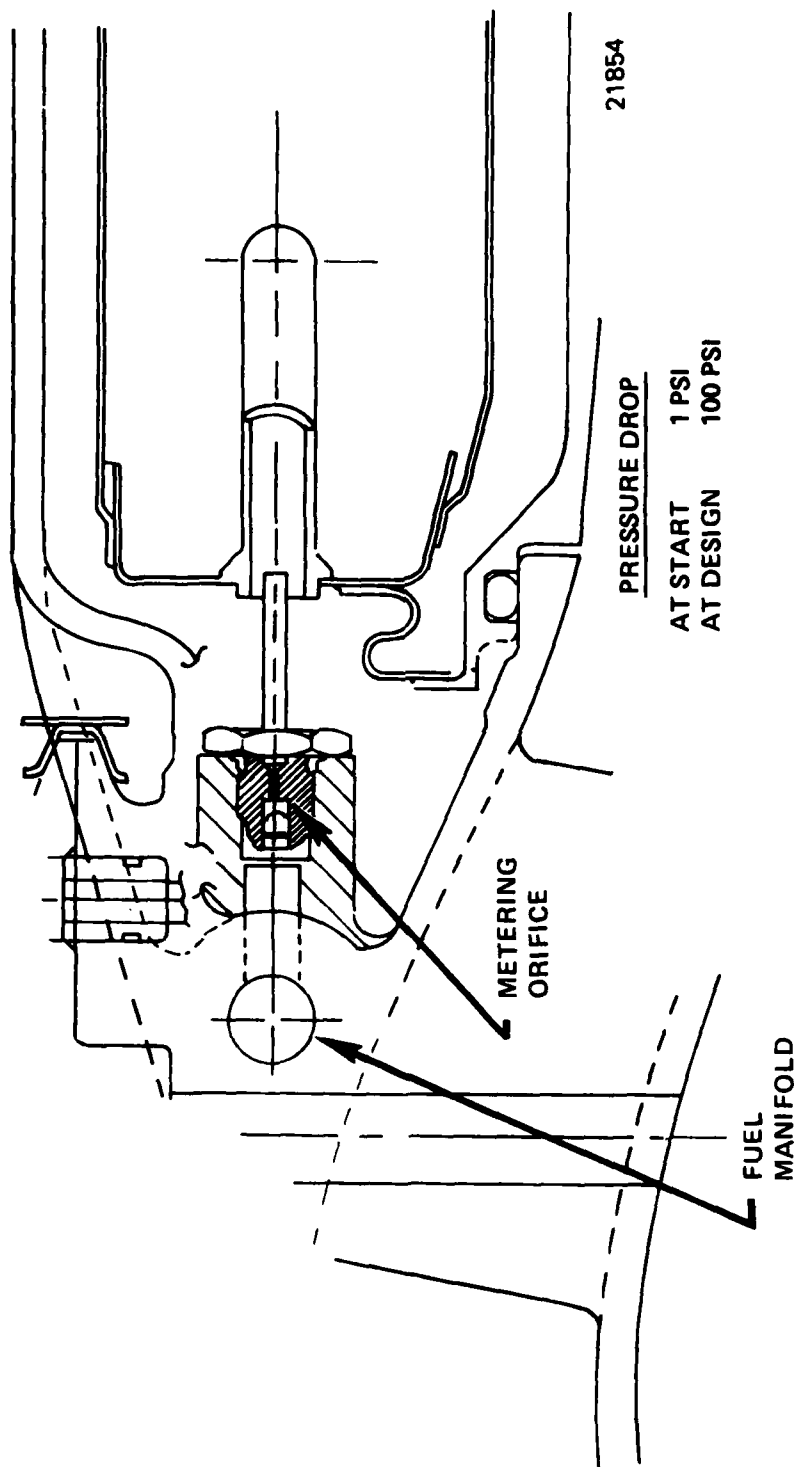
FUEL
MANIFOLD

Figure 45. EG Fuel Distributor System.

70

PRIMER NOZZLE

INTEGRAL LEAD IGNITOR
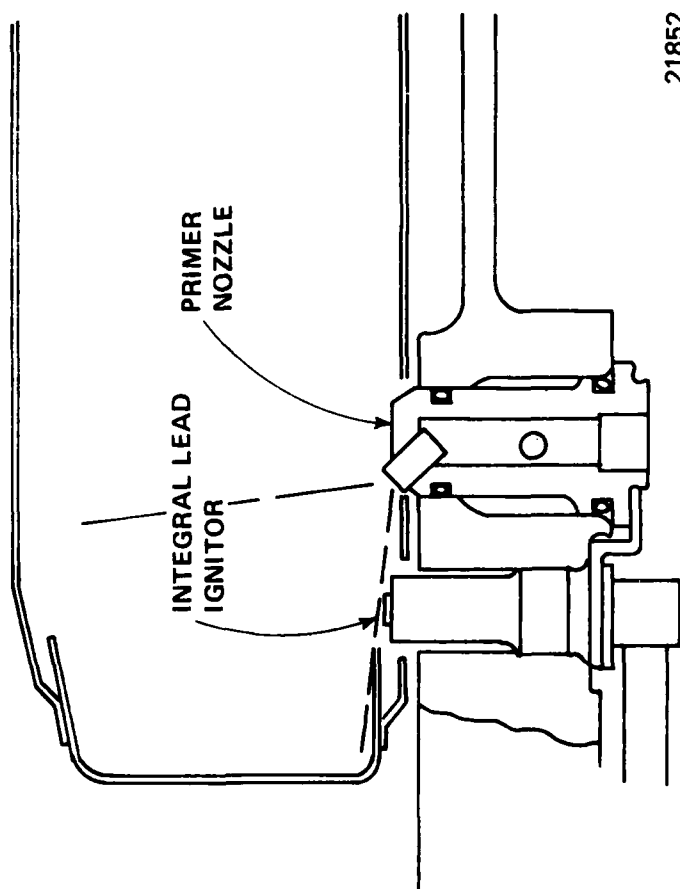
21852

Figure 46 . EG Ignition System.

71
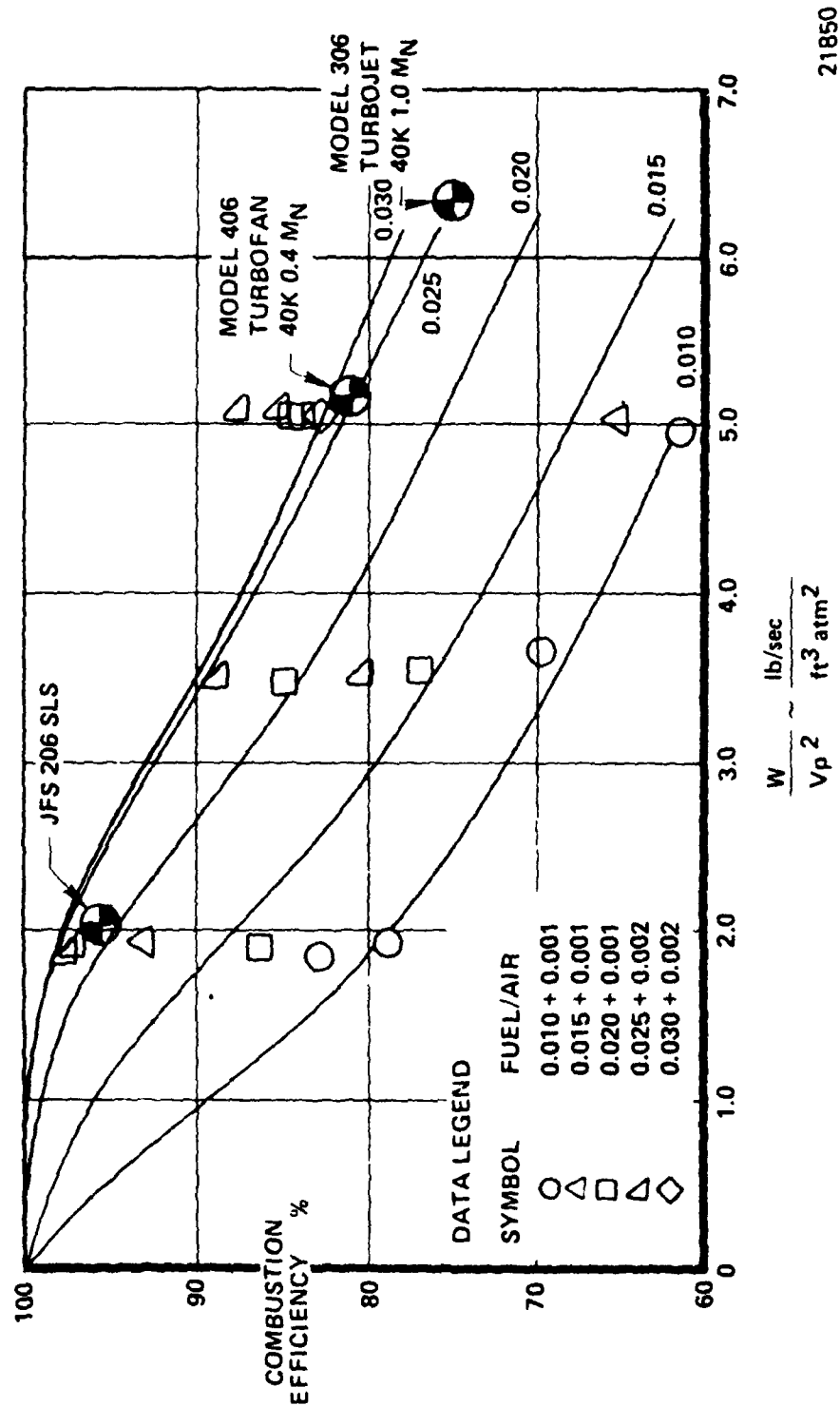
Figure 47. Estimated Combustor Performance.

21850

72

TABLE 7

COMBUSTOR DESIGN PARAMETERS	
Engine Airflow, lb/sec	3.862
Compressor Discharge Pressure, psia	40.31
Compressor Discharge Tempeature, ^{o}F	284
Fuel Flow, lb/hr	341
Fuel - Air Ratio	0.0245
Total Pressure Loss - %	10.0
Average Exit Temperature, ^{o}F	1800
Reference Velocity, ft/sec	45.6
Isothermal Residence Time, Milliseconds	8.88
Aerodynamic Loading, $\dfrac{\text{lb air}}{\text{sec ft}^3\text{atm}^2}$	2.087
Heat Release Rate, $\dfrac{\text{MBTU}}{\text{Hr ft}^3\text{atm}}$	9.30
Combustor Inlet Mach Number	0.324
Reference Area, ft^2	0.608
Combustor Length, ft	0.548
Combustor Annulus Height, ft	0.1796
Combustor Length to Annulus Height Ratio	3.05
Number of Fuel Injection Points	14

4.1.3 Turbine Design

The Expendable Gasifier turbine was designed to satisfy the following performance objectives:

$$\frac{\Delta H}{\theta_{cr}} = 12.9 \ \frac{BTU}{lb}$$

$$\frac{N}{\sqrt{\theta_{cr}}} = 16,080 \ RPM \qquad PR_{T-T} = 1.575$$

$$\eta_{T-T} = 82.5\% \ (minimum)$$

$$\frac{WN\epsilon}{\delta 60} = 871 \ \frac{lb-R_{cv}}{SEC^2} \qquad T_{IN} = 1800^oF$$

At the design point, the turbine rotational speed is 33,060 RPM. The preliminary flowpath (Figure 48) shows that the nozzle has 13 vanes and the rotor 26 blades. Initially twelve nozzle vanes were analyzed, however, the number was changed to thirteen to avoid possible rotor excitations caused by even multiples. The preliminary velocity diagrams are shown in Figure 49 . They show that the design of the turbine is conservative in that the highest Mach number (0.663) occurs at the nozzle tip discharge. In addition, the velocity diagrams show that an average exit swirl of 7 degrees exists at the turbine exit (a level which is deemed acceptable for a gasifier turbine).

The nozzle design (Figure 50) consists of an integral 13 vane casting with generous wall thicknesses and tolerances for ease of castability. The nozzle vane section is of constant profile from hub to tip. A flow analysis on the vane (Figure 51) showed that good acceleration is achieved along the suction and pressure surfaces. A small amount of diffusion on the suction surface near the trailing edge was determined to have negligible effect on the vane performance based on a preliminary boundary layer analysis.

The rotor design performed resulted in a 26 bladed integral casting with the blade stacked on the center of gravity of the sections, (Figure 52). Phase III analysis will investigate whether it will be advantageous to lean the blade to counteract gas bending loads. A flow analysis was performed at the critical aerodynamic section (Figure 53) and the velocity distribution results (Figure 54) indicate that the design is satisfactory for the preliminary blade section.

The flowpath analysis consisted of a streamline analysis which incorporate combustor TDF (Figure 55), radial distribution of stator and rotor losses (Figure 56), and radial work distribution (Figure 57), in order to achieve the most realistic preliminary design and minimize the number of iterations during the Phase III detail design. Some of the salient blade row design parameters are summarized in Table 8.
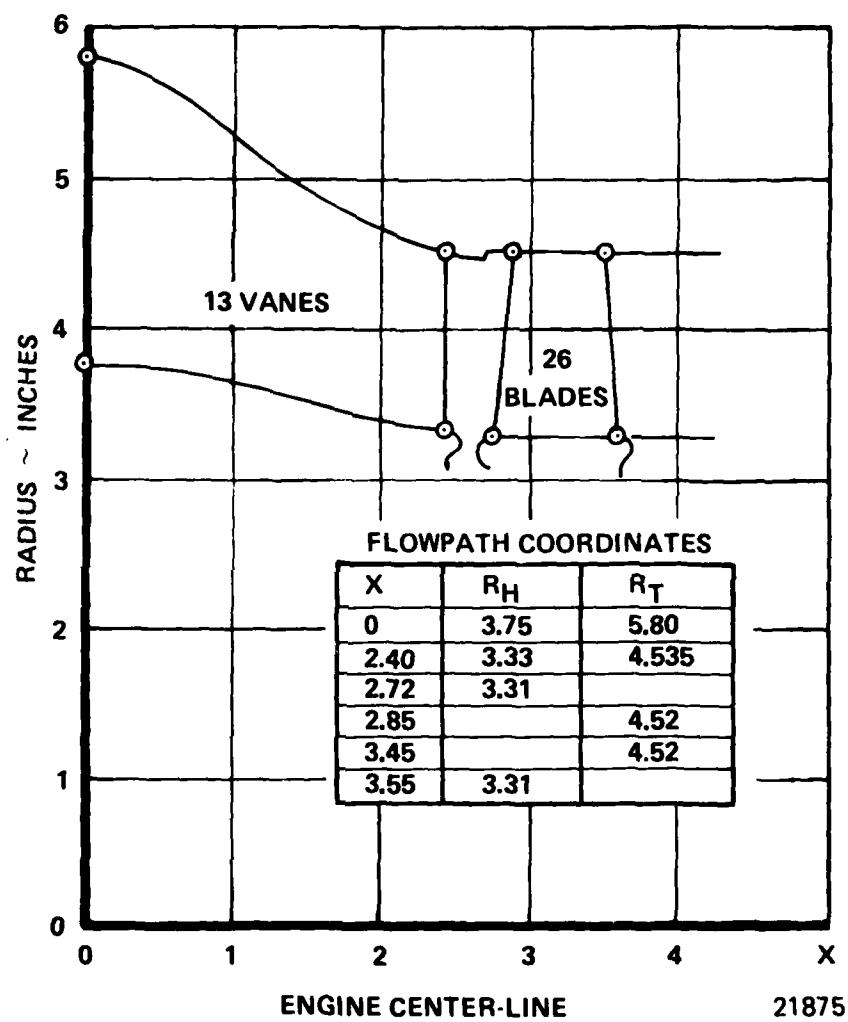
Figure 48 . Preliminary EG Turbine Flowpath.

The figure contains the following flowpath coordinates table:

FLOWPATH COORDINATES

X	R_H	R_T
0	3.75	5.80
2.40	3.33	4.535
2.72	3.31	
2.85		4.52
3.45		4.52
3.55	3.31	

13 VANES

26 BLADES

RADIUS ~ INCHES

ENGINE CENTER-LINE   21875

75
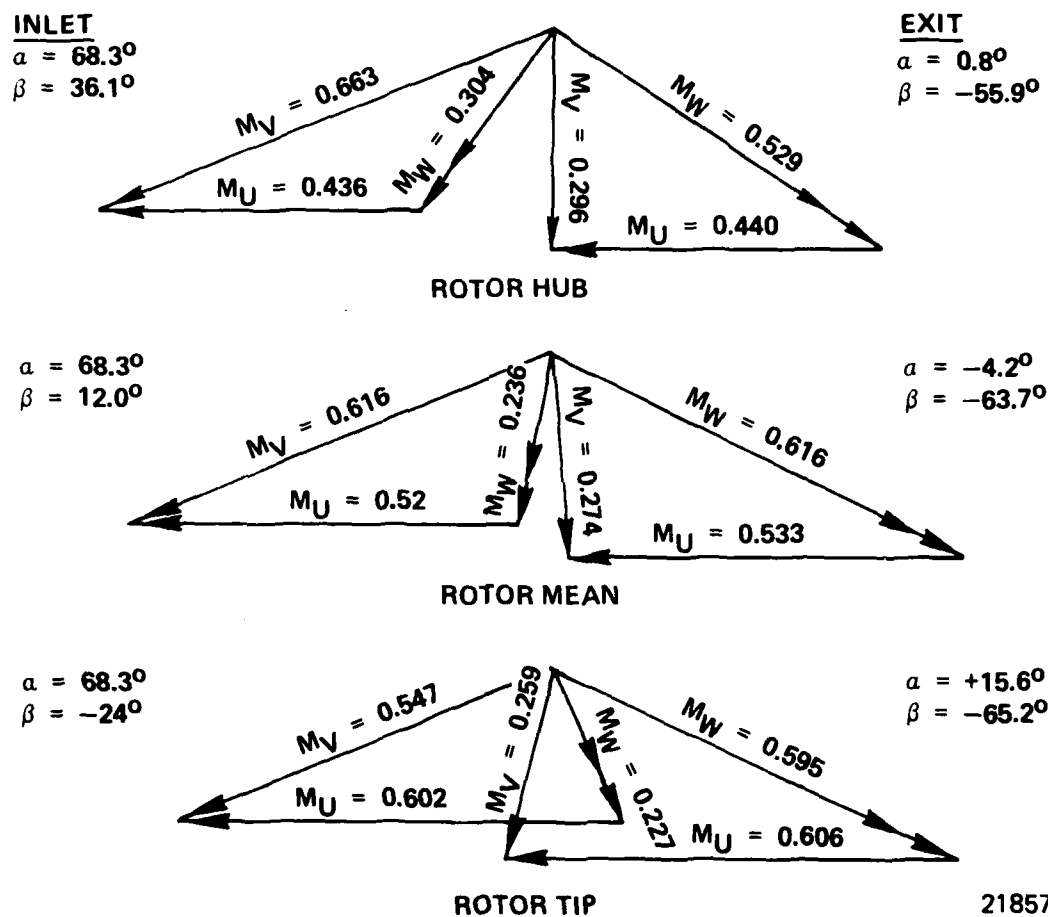
Figure 49 .   Preliminary EG Turbine Velocity Diagrams.

76

WALL THICKNESS
0.030 - 0.050 IN.

PROFILE
TOLERANCE
± 0.010 IN.

21911

52°30'

OPEN AREA
1.02 IN² PER VANE

NOMINAL T.E.T. = 0.048 IN

13 VANES
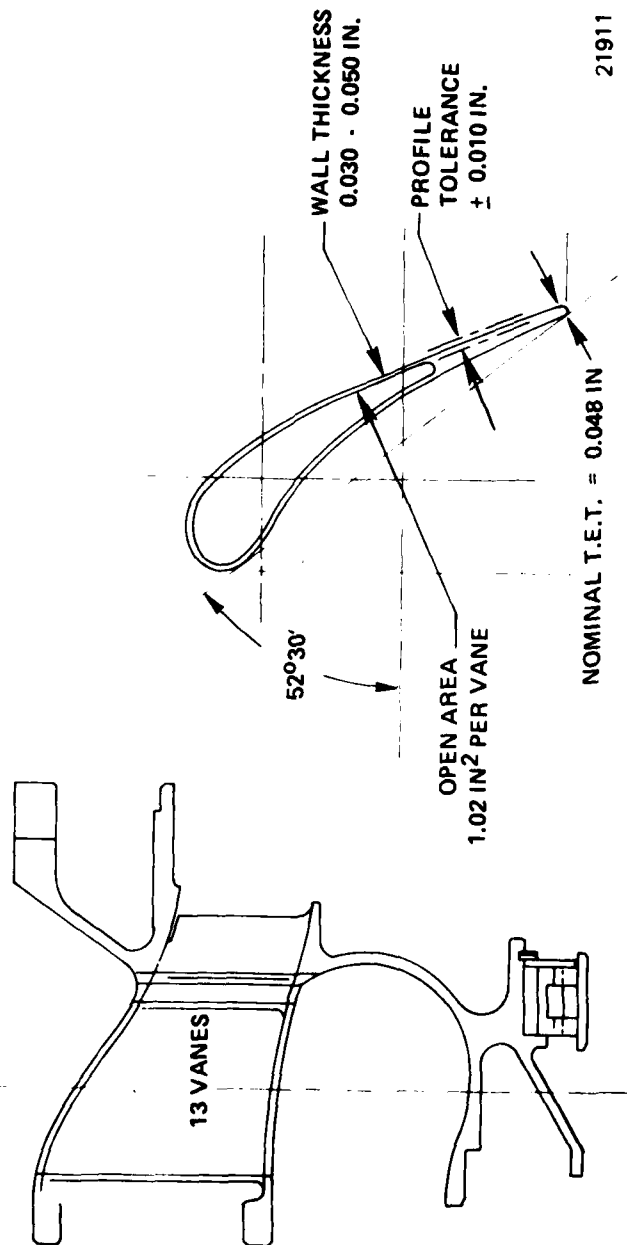
Figure 50 . Nozzle Designed for Ease of Castability.

77
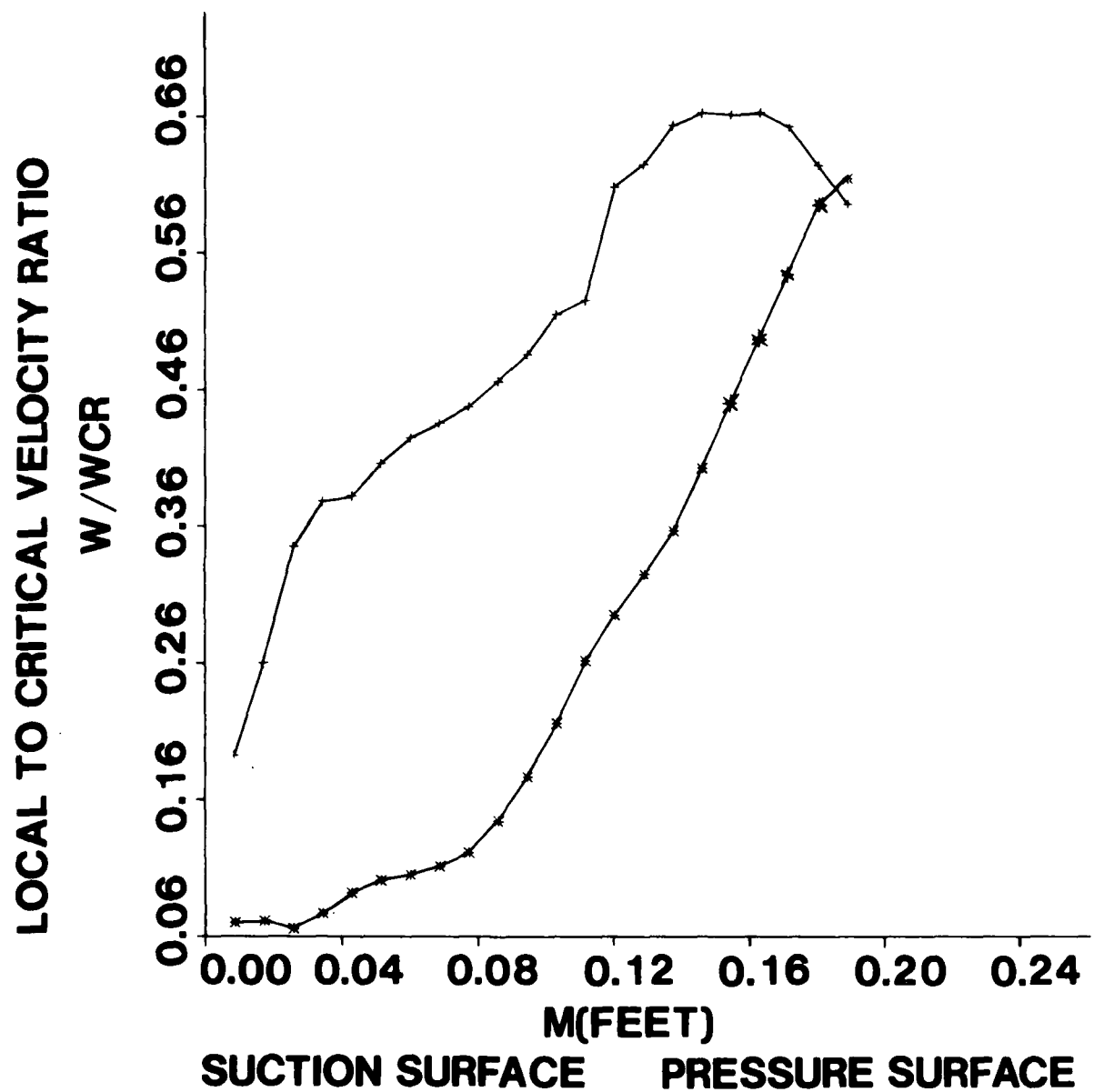
21959

Figure 51 . Critical Velocity Distribution - Preliminary Nozzle Constant Section
Vane Tip Solution.

STACKING POINT

PERCENT
BLADE
HEIGHT

0   HUB
20
40
60
80
100 TIP

0   0.1   0.2   0.3   0.4   0.5   0.6   0.7   0.8   0.9   1.0

SCALE INCHES

21871
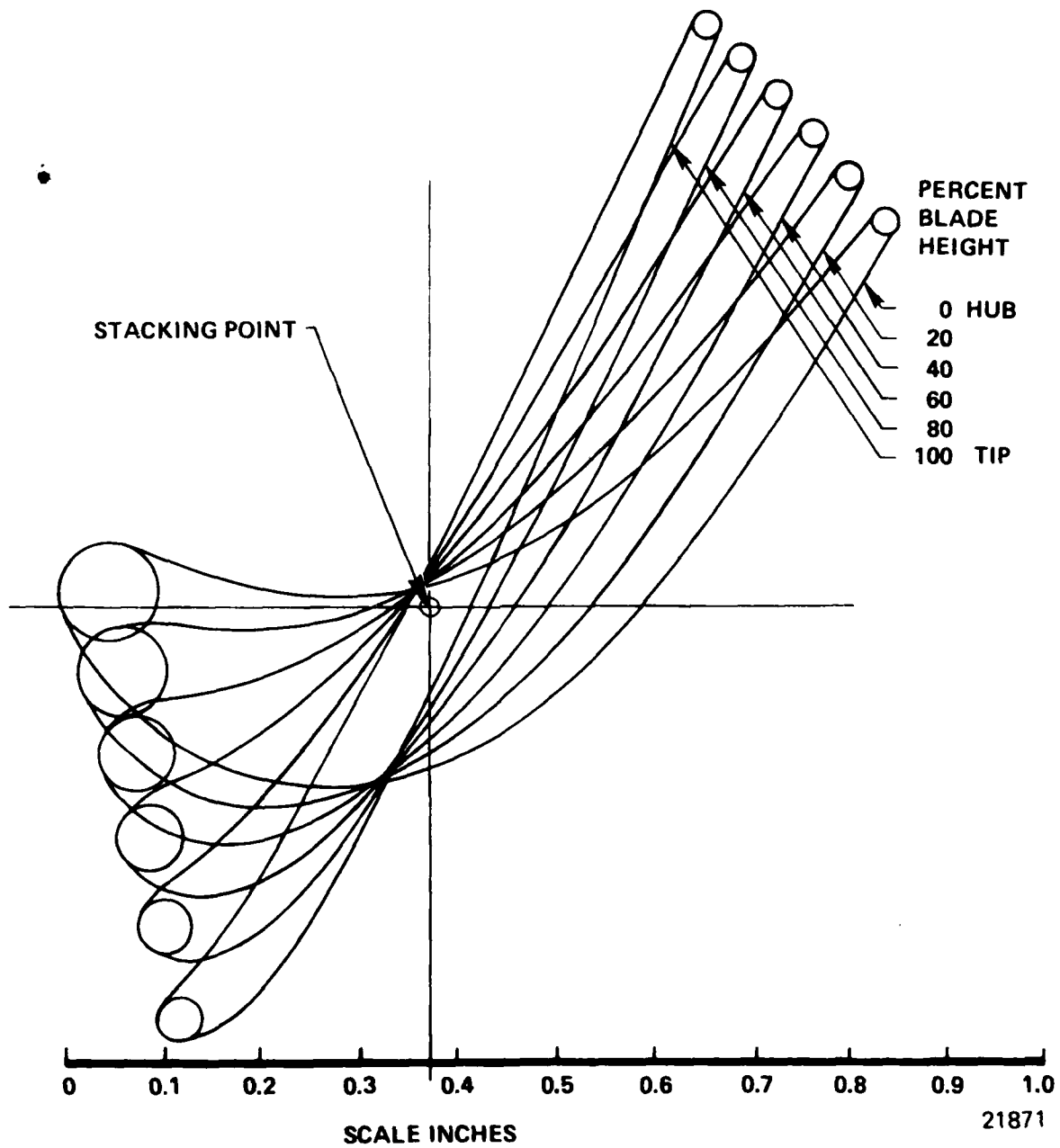
Figure 52 .   Rotor Blade Sections Stacked on Center of Gravity.

79
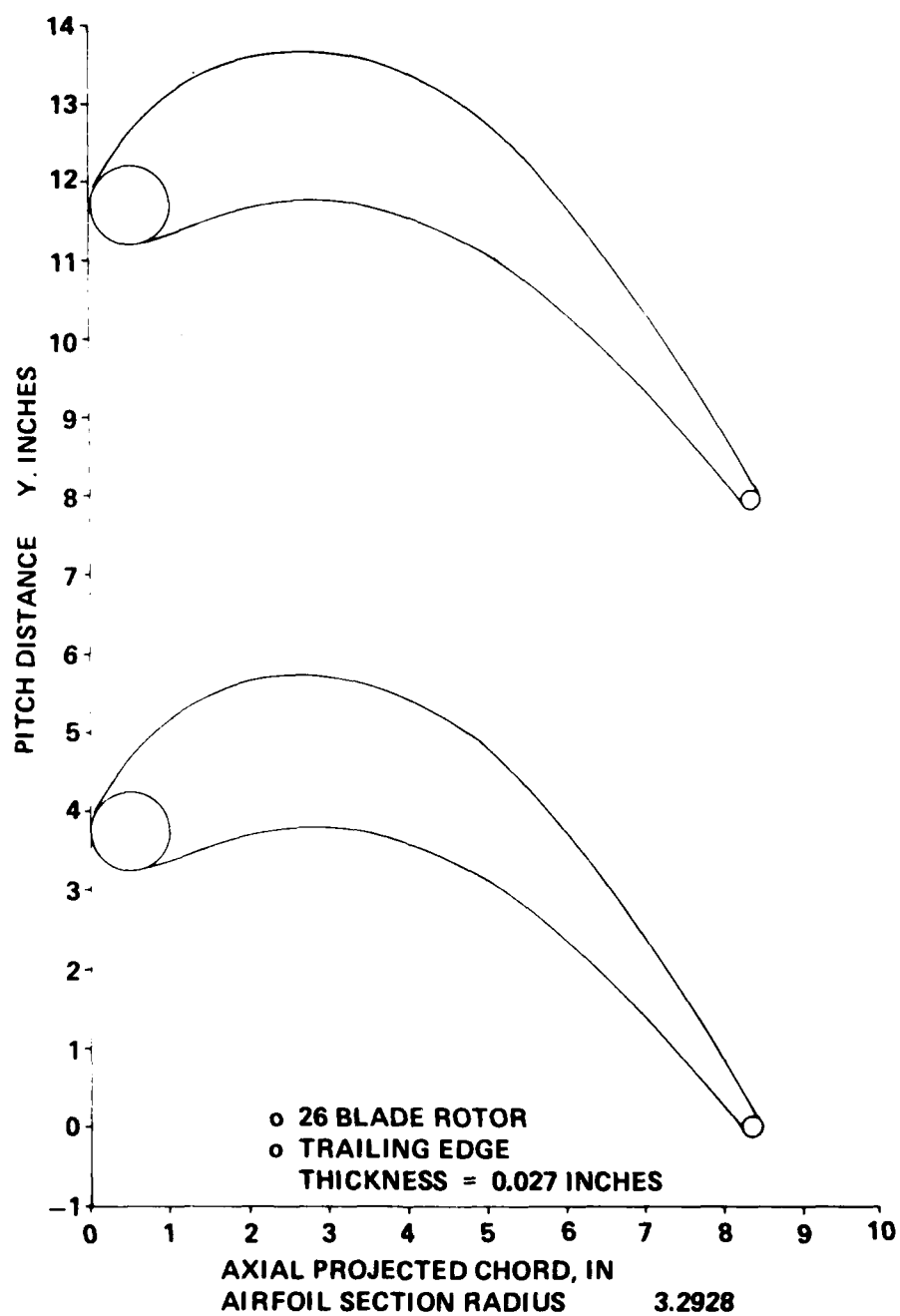
Figure 53. EG Preliminary Rotor Hub Section.
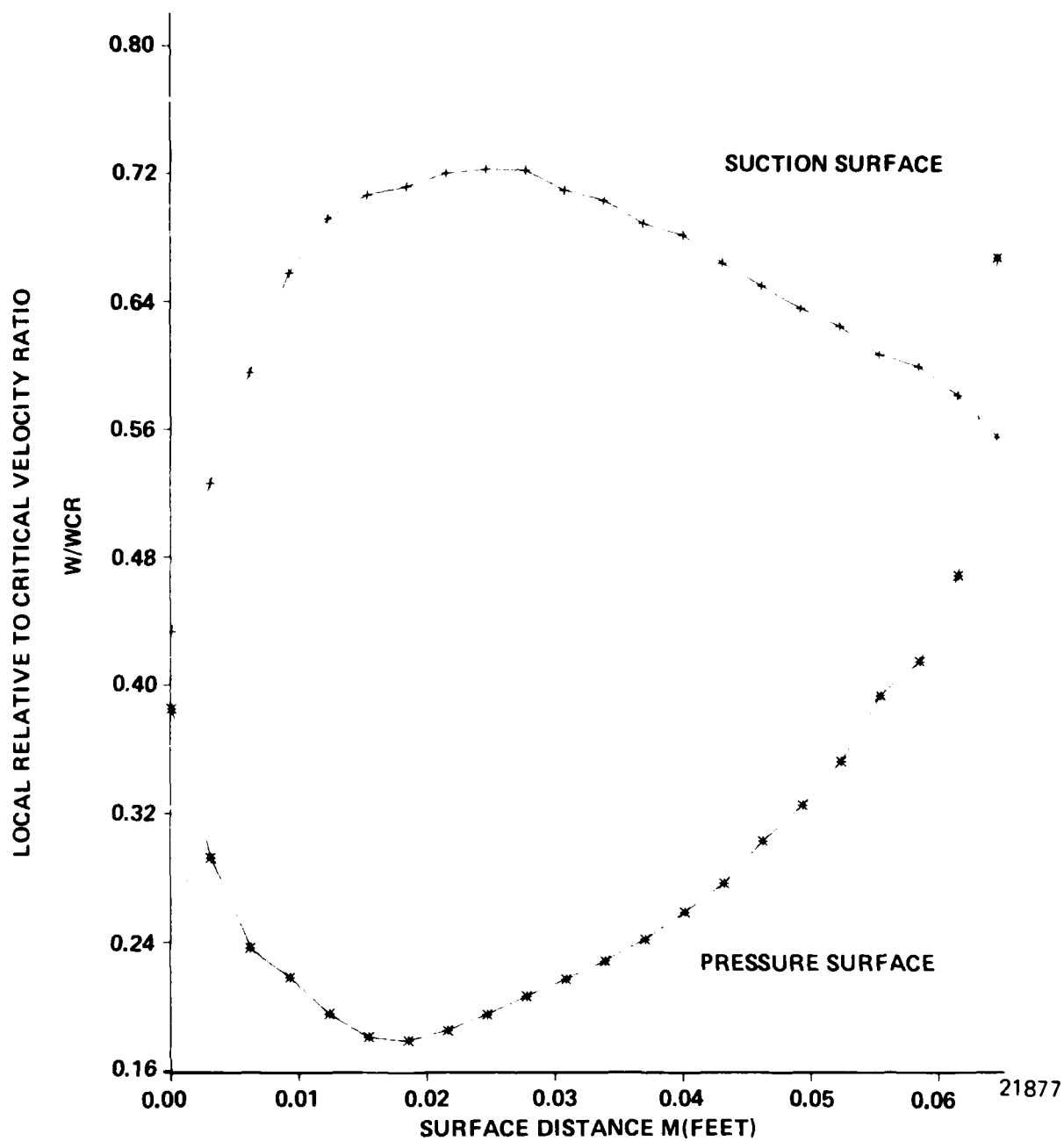
Figure 54 . Compressible Flow Solution for the Rotor Hub Section.
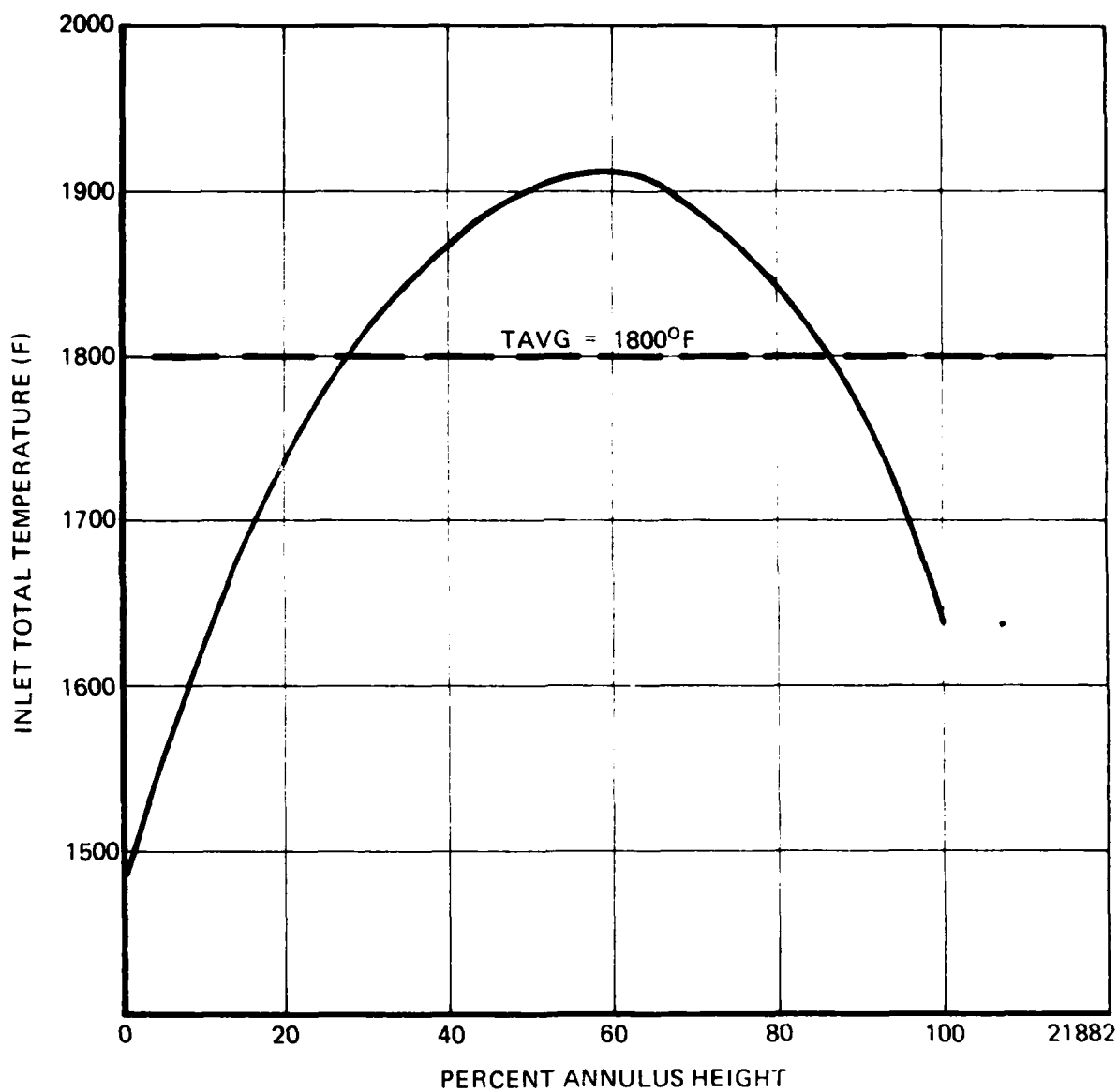
Figure 55. Combustor Exit Temperature Profile Used for Turbine
Design.

ΔP = BLADE ROW TOTAL PRESSURE LOSS
P = STAGNATION PRESSURE
p = STATIC PRESSURE

ROTOR

$$\bar{\omega} = \frac{\Delta P_r^{\,o}}{(P^o_r - p)\ EXIT}$$

NOZZLE

$$\bar{\omega} = \frac{\Delta P^o}{(P^o - ps)\ EXIT}$$

PRESSURE LOSS COEFFICIENT - $\bar{\omega}$

0.4
0.3
0.2
0.1
0.0

0.0   20   40   60   80   100   21880

HUB   PERCENT HEIGHT   TIP
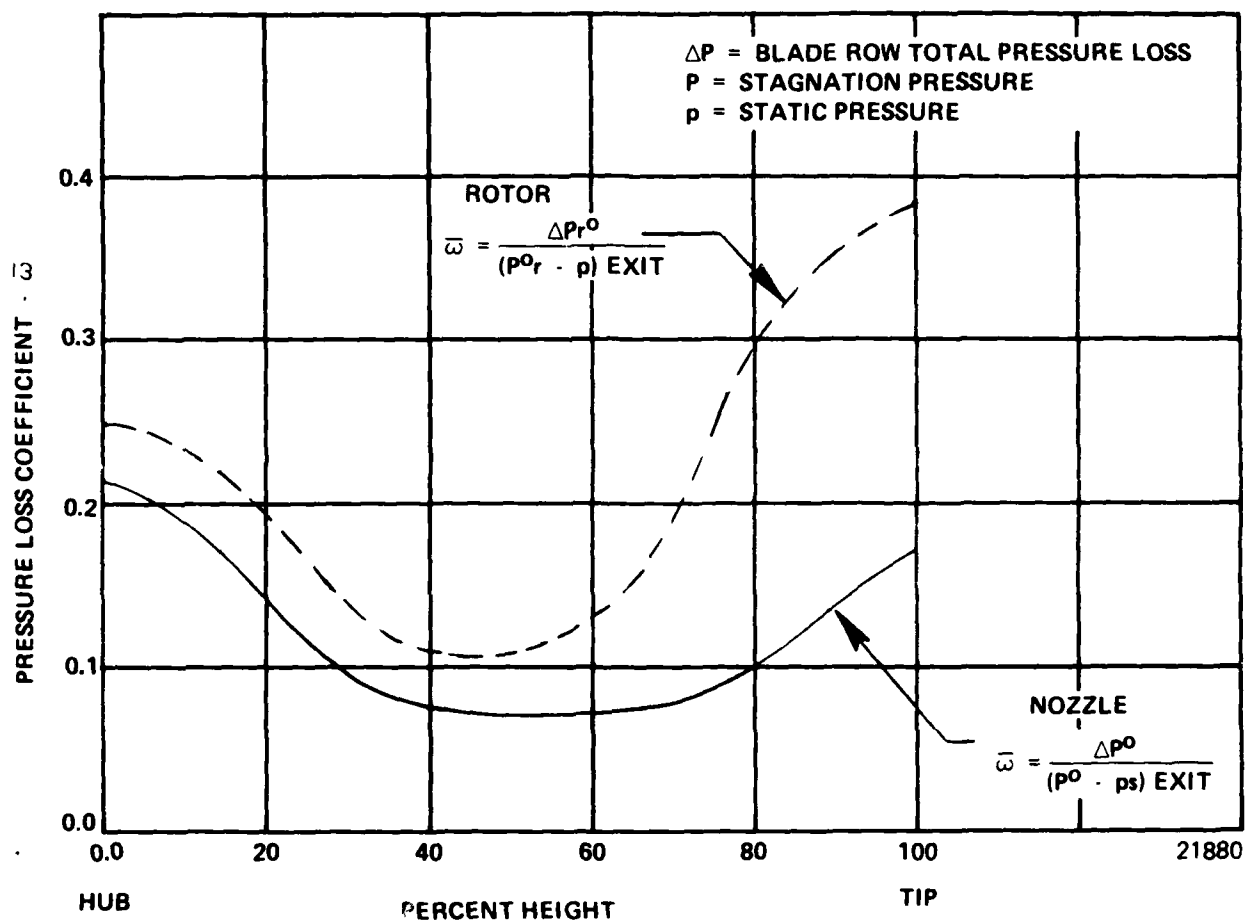
Figure 56. Nozzle and Rotor Loss Coefficients.

83
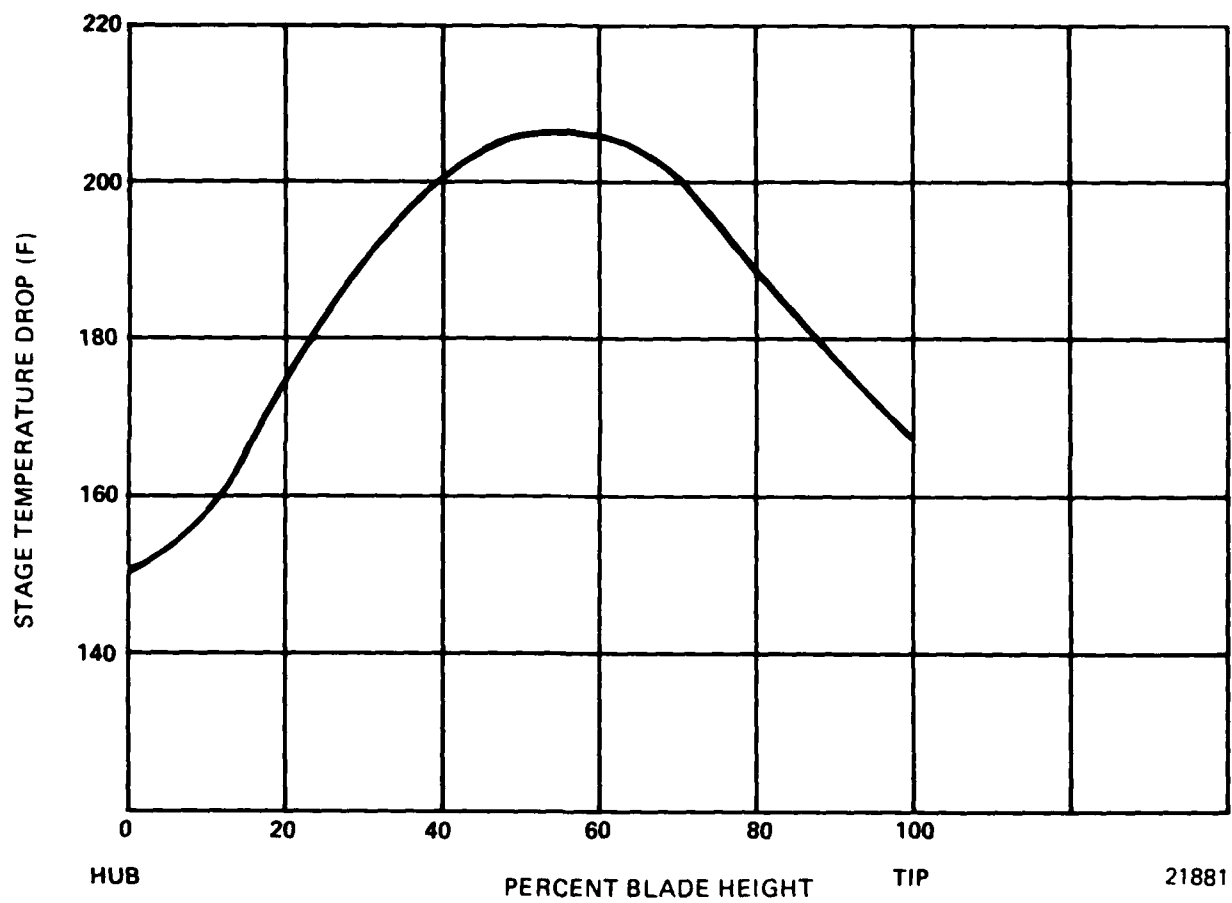
Figure 57. Turbine Radial Work Distribution in Terms of Stage Temperature Drop.

TABLE 8

BLADE ROW DESIGN PARAMETERS

	ROOT	PITCH	TIP
NOZZLE SOLIDITY	2.34	1.89	1.6
ROTOR SOLIDITY	1.184	1.14	1.288
NOZZLE REACTION	5.83	6.44	7.04
ROTOR REACTION	1.784	2.452	2.328
NOZZLE ZWIEFEL COEFFICIENT	0.336	0.398	0.457
ROTOR ZWIEFEL COEFFICIENT	1.042	1.052	0.943

	NOZZLE	ROTOR
TRAILING EDGE THICKNESS	0.048″	0.027″
THICKNESS CHORD RATIO	0.18	0.10
PROFILE LOSS, Y_p	0.05286	0.05052
TRAILING EDGE LOSS, Y_{te}	0.02817	0.02562
INCIDENCE LOSS, Y_i	0.	0.
SECONDARY LOSS, Y_s	0.059308	0.02892
CLEARANCE LOSS, Y_{cl}	0.	0.07302
TOTAL LOSS, Y_{tot}	0.1122	0.1614

22015

85

During the design effort several considerations were examined in regard to the efficiency potential of the EG turbine.

Figure 58 considers only the effect of aerodynamic losses on turbine efficiency and shows that the EG turbine has an efficiency potential of 86.8 percent. The effect of nozzle trailing edge thickness and tip clearance on efficiency (Figure 59) shows that with generous tip clearance (0.027 in.) and trailing edge thickness (0.042 in.) the decrement is less than one percentage point. The summation of all possible efficiency decrements which could occur in a production engine turbine are listed in Figure 60 . The range of efficiency is 85.3 to 82.0 percent resulting in an average of 83.7 percent.

A preliminary off-design turbine performance analysis was performed and produced the map shown in Figure 61 . The efficiency objective of 82.5 percent at design point was used as the baseline for the map generation so the map is a conservative estimate. It does indicate however, that a large limit load capability exists and no efficiency fall off with decreasing power output - a very desirable characteristic for an APU gasifier turbine as well as a JFS turbine.

4.2 COMPONENT PRELIMINARY MECHANICAL DESIGN

The preliminary mechanical design for the compressor, combustor and turbine components of the Expendable Gasifier (EG) consisted of the following items; definition of the blade and disk stresses, rotor dynamic analysis (critical speeds), bearing and lubrication system, accessory systems interfaces, design layout and detail component drawings to determine fabrication costs.

4.2.1 Blade and Disk Preliminary Stress Analysis

The structural design criteria used in sizing the rotors for the EG **are shown** in Table 9 .

The combined gas bending, centrifugal P/A and untwist stresses, based on a tapered twisted beam analysis, are compared to the minimum IN-100, 20 hour stress rupture strengths in Figure 62 . The stress rupture curve is based on an estimated spanwise temperature distribution corresponding to an average turbine inlet temperature of 1800°F. A margin of 12 percent exists at the 50 percent span location and is deemed adequate for the preliminary design.

The life controlling factor in the design of the cast IN-100 turbine disk is the low cycle fatigue (LCF) requirement of 2,000 start-stop cycles. A start gradient assuming a thermal gradient of 1000°F from bore to rim (based on the second stage SLCM type rotor) was used to obtain a preliminary rotor size. The resulting disk shape and the elastically calculated stresses, which ignore the effect of the integral shaft, are shown in Figure 63 . This disk shape satisfies the LCF requirement on a preliminary basis. The turbine blade and disk stresses are summarized in Table 10.
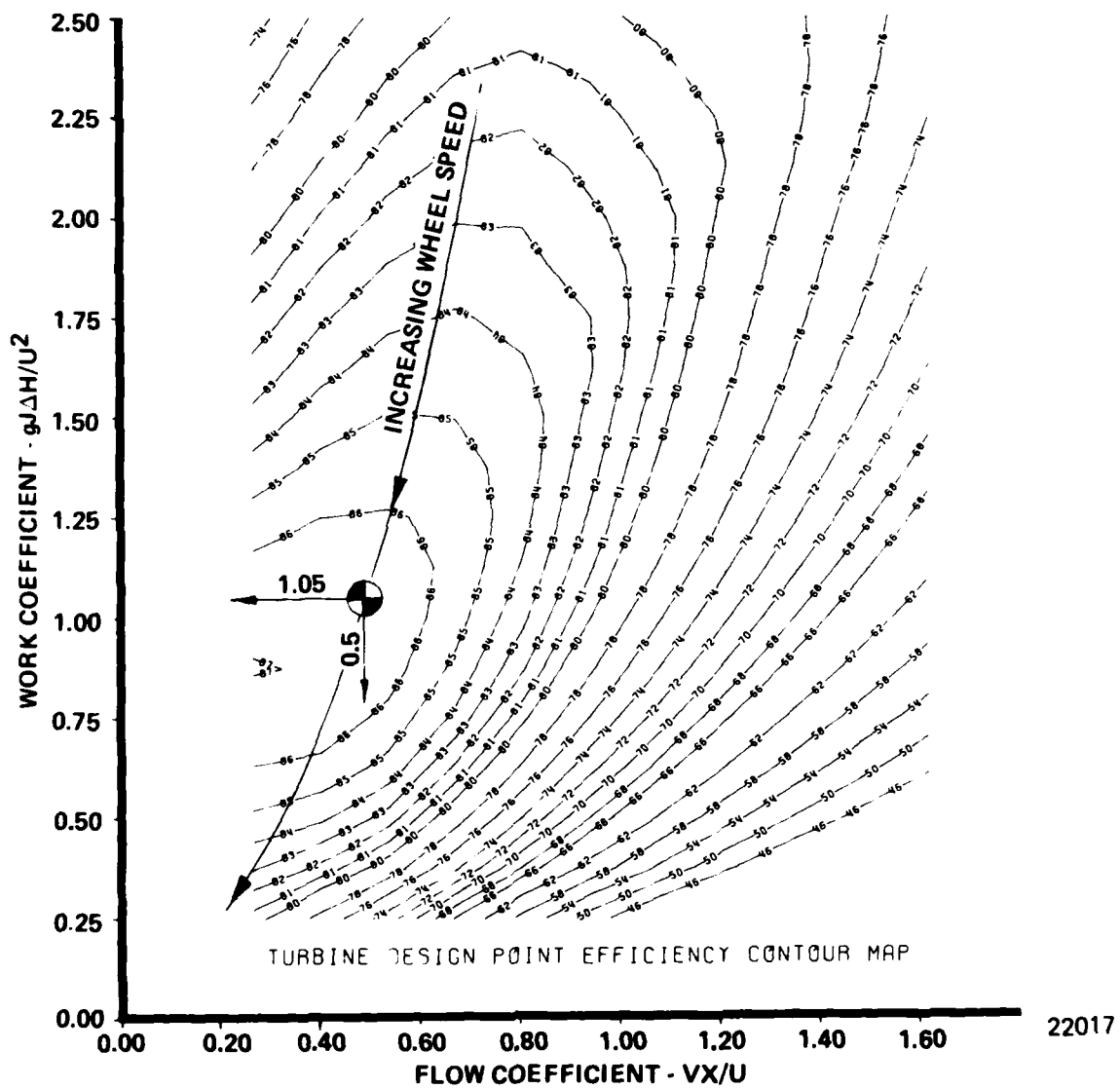
Figure 58. EG Turbine Design Optimization.

87
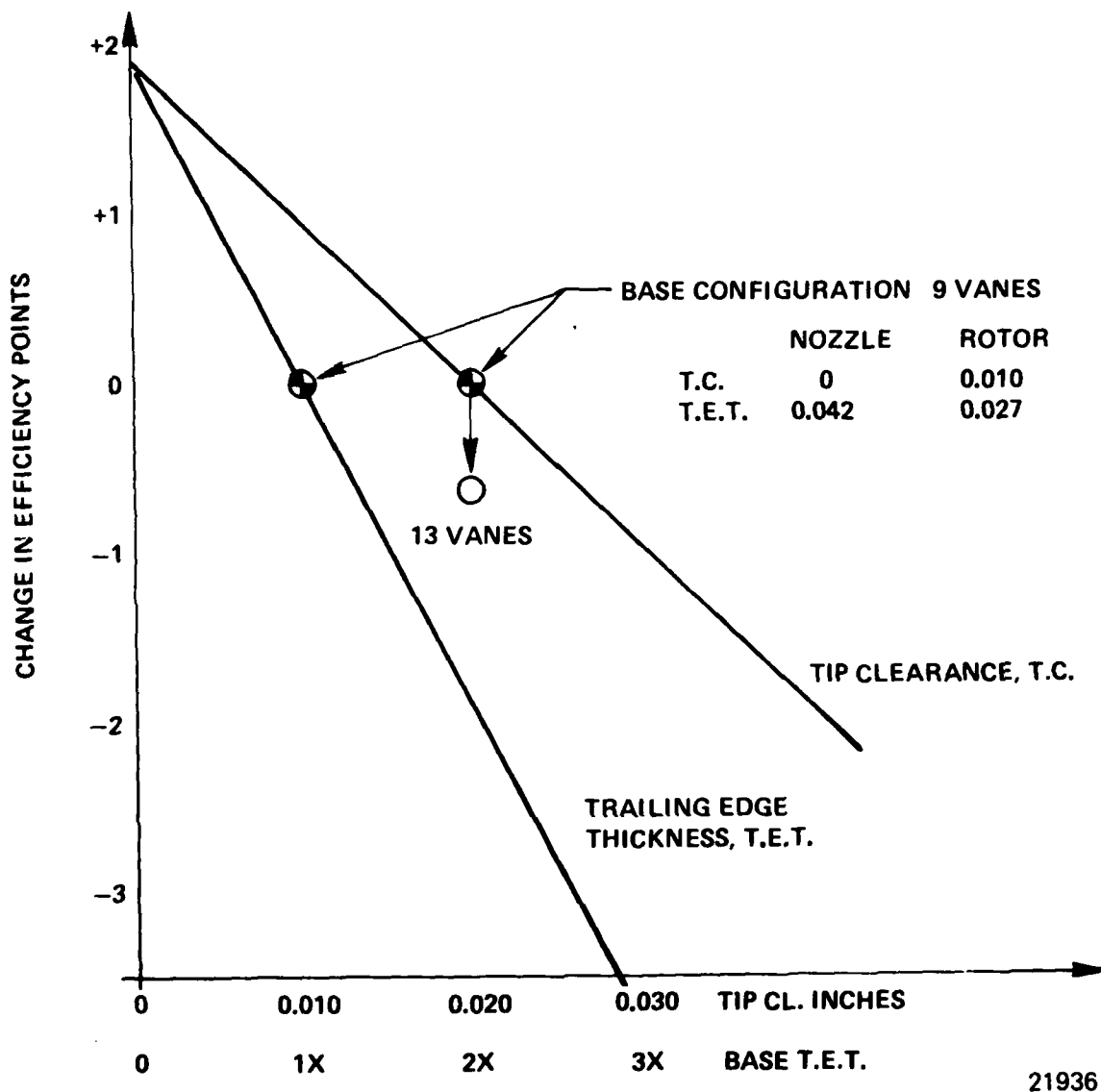
Figure 59 . Expendable Gasifier Turbine Efficiency Variation with Tip-Clearance and Trailing Edge Thickness.

	BASE	PRODUCTION
FLANGE LEAKAGE	0	0.5%
LAB. SEAL TOLERANCE	0	± 0.0015 IN.
LAB. SEAL CLEARANCE	0	0.004 - 0.012
INTER-ROW LEAKAGE	0	0.24 - 0.72%
WINDAGE & BEARINGS	0	(1.7%)
ROTOR RADIAL TOL.	0	0.002 IN.
ROTOR CLEARANCE	0.010	0.028 ± 0.008
CLEARANCE LOSS	—	1.76% - 4.6%
EFFICIENCY	86.8%	85.3 - 82.0%
OBJECTIVE AVG.	82.5%	83.7%
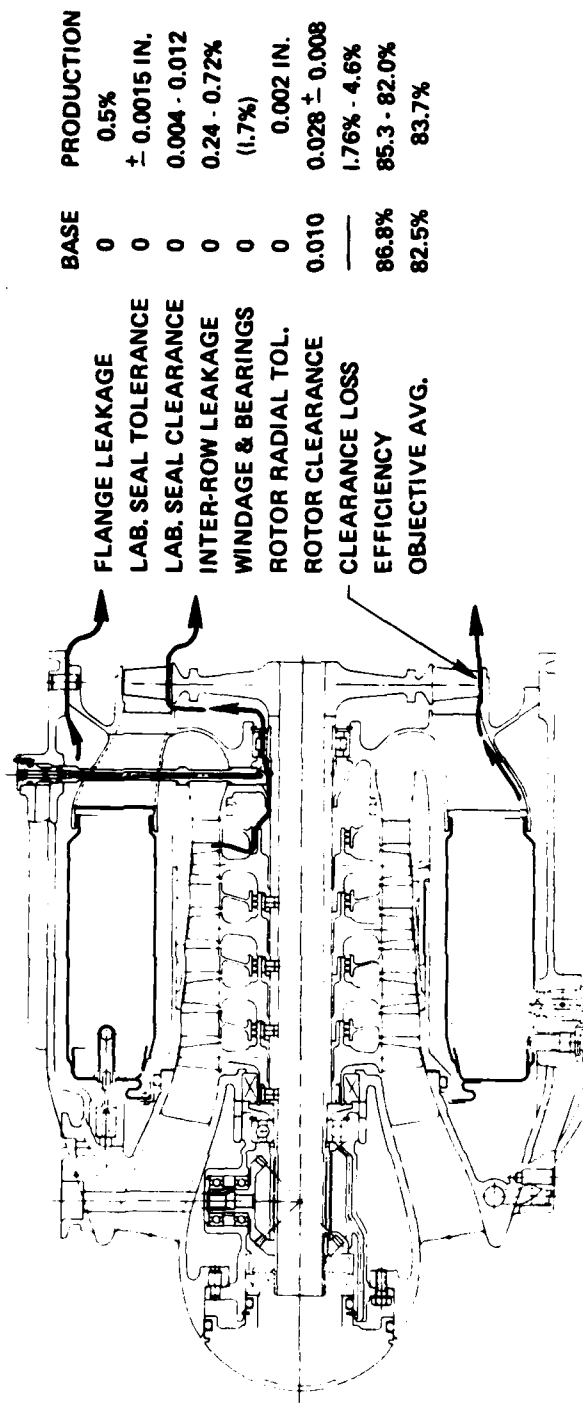
22012

Figure 60 . Turbine Performance Met With Production Tolerances.

89
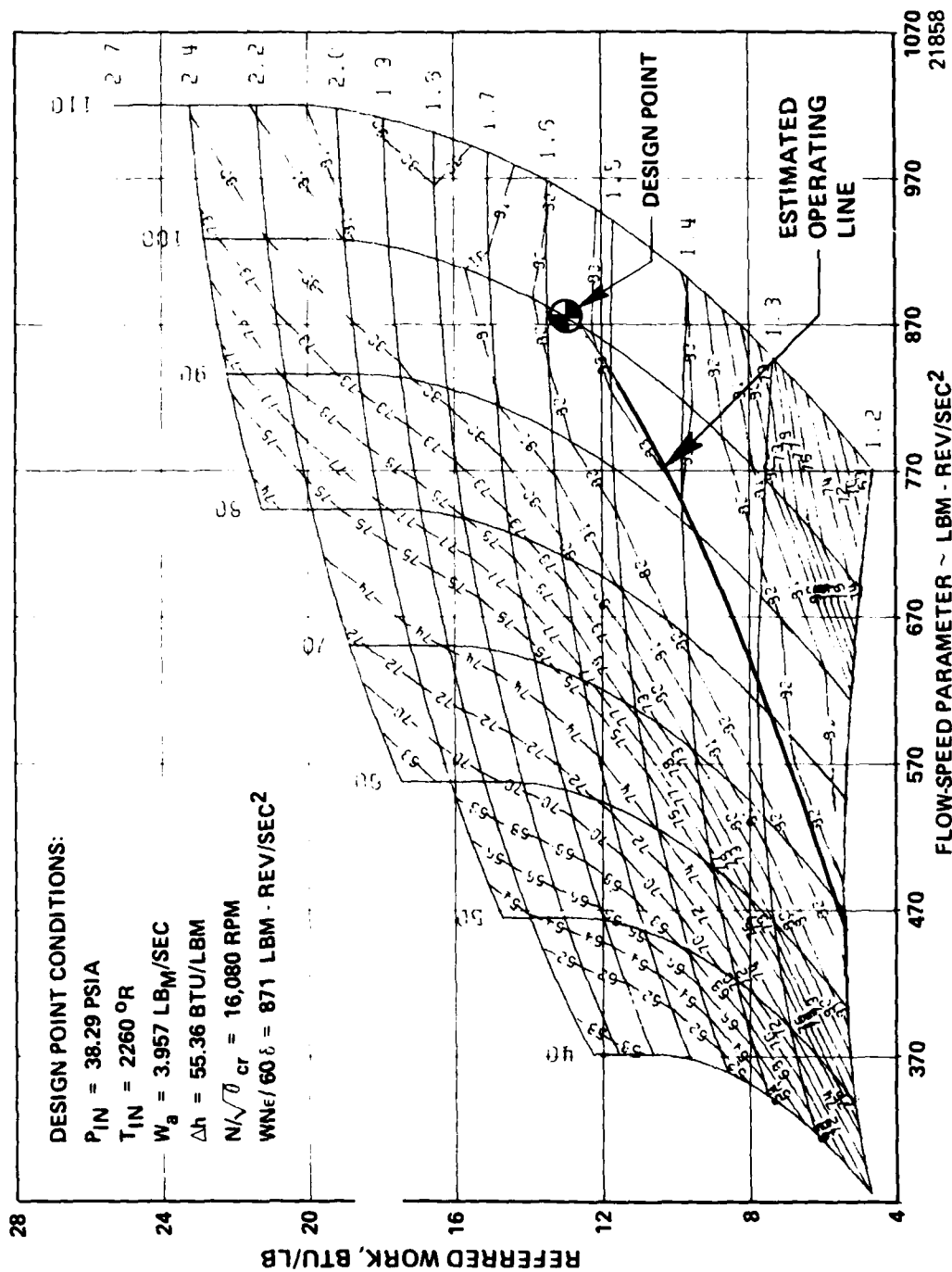
Figure 61. Expendable Gasifier Preliminary Turbine Map.

DESIGN POINT CONDITIONS:

P_{IN} = 38.29 PSIA
T_{IN} = 2260 °R
W_a = 3.957 LB_M/SEC
Δh = 55.36 BTU/LBM
$N/\sqrt{\theta}_{cr}$ = 16,080 RPM
$WN_E/60 \delta$ = 871 LBM · REV/SEC²

REFERRED WORK, BTU/LB

FLOW-SPEED PARAMETER ~ LBM · REV/SEC²

90
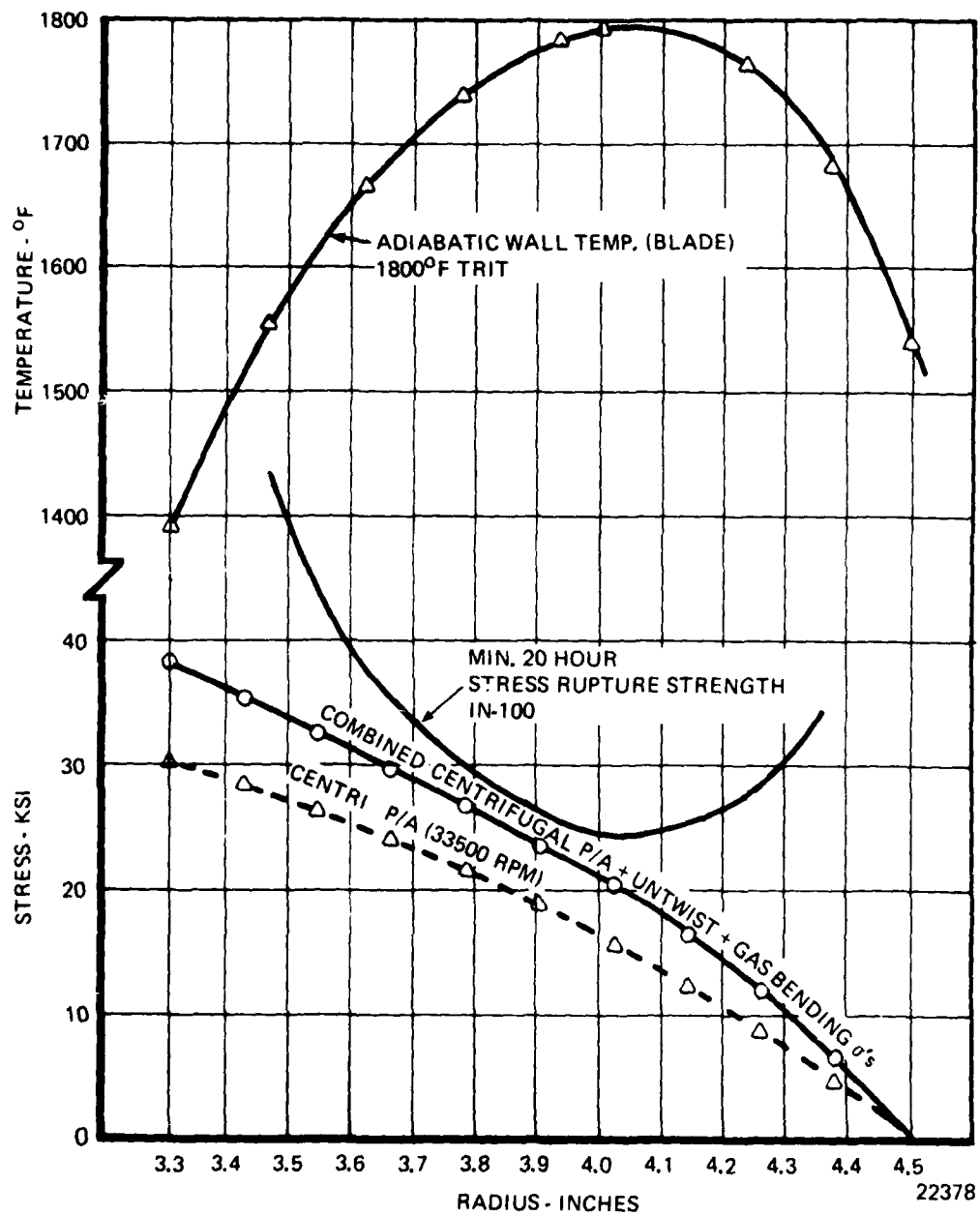
Figure 62. Expendable Gasifier Preliminary Turbine Blade Stresses Compared to Stress Rupture Strength.
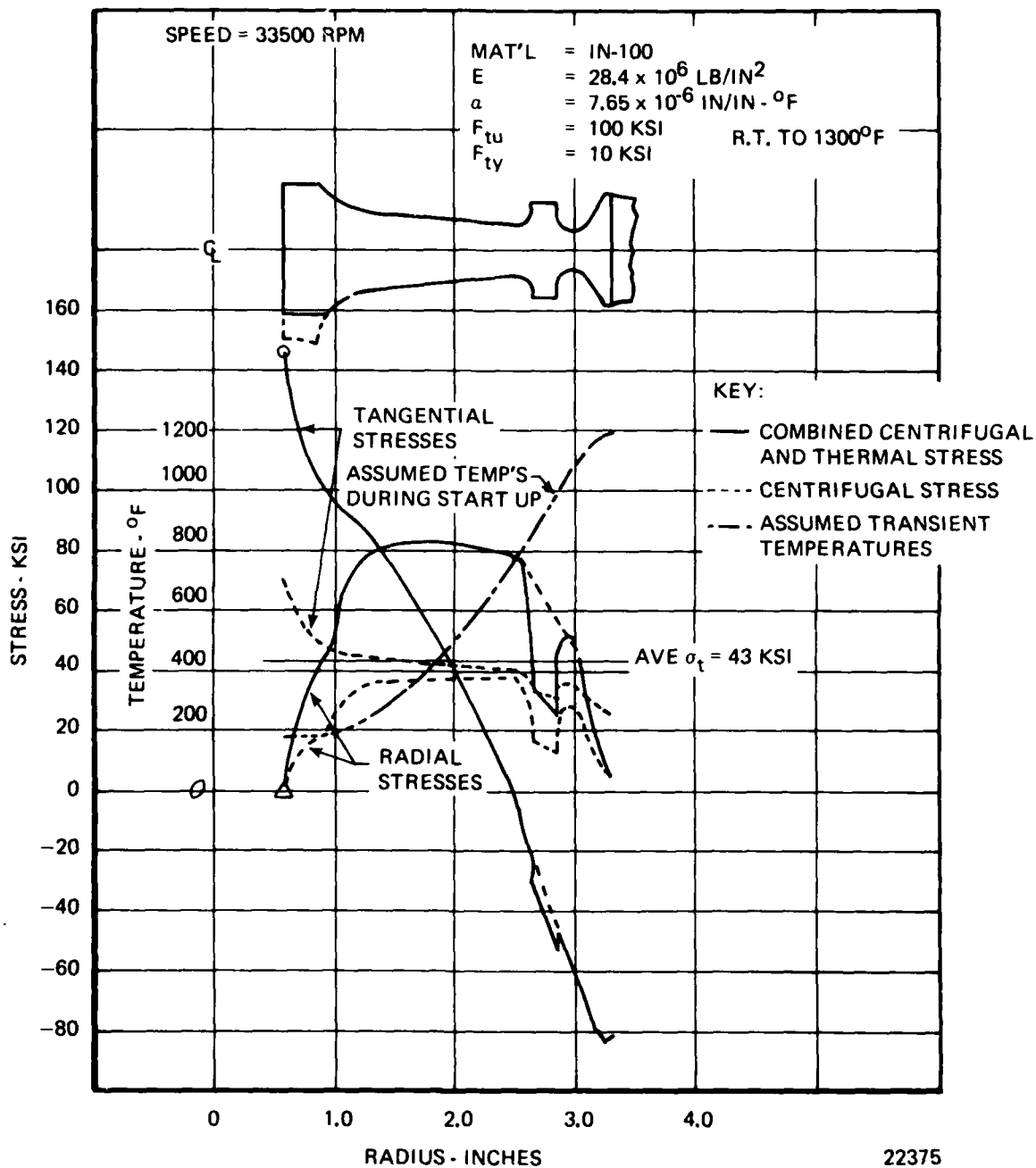
Figure 63. Expendable Gasifier Preliminary Turbine Disk Centrifugal and Transient Thermal Stresses.

TABLE 9

MODEL 506 EXPENDABLE GASIFIER
STRUCTURAL DESIGN CRITERIA SUMMARY

I   Burst Speed-------------------------------------122% of Maximum Steady State Speed

II   Safety Factor on Ultimate Strength

     Primary Stress

          Pressure Casings-----------S.F. 1.5 - Based On Maximum Pressure
          All Other Components-------S.F. 1.5 - Based On Primary Stress at Maximum
                                                 Condition

     Vibratory Stress---------------S.F. 1.5 - On Fatigue Strength as Determined
                                                From Modified Goodman Diagram

III Secondary Stress

     Low Cycle Fatigue Life---------   2000 Start Cycles - Using Combined Effect
                                       Of Cyclic Strain with Superimposed
                                       Steady State

IV   Stress Rupture Life------------   20 Hours - Based on 100% Speed at Maxi-
                                       mum Turbine Inlet Temperature for
                                       Full Time

93

TABLE 10

MODEL 506 TURBINE ROTOR STRESSES
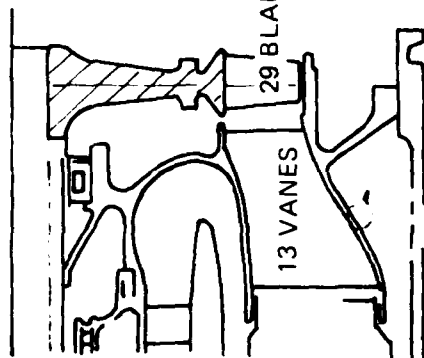
ROTOR MATERIAL: IN-100
SHAFT SPEED: 33,500 RPM (MAX)
T.I.T.: 1800°F

29 BLADES
13 VANES

- SUMMARY OF BLADE STRESSES -

BLADE LOCATION	TEMP. °F	MIN. MATERIAL PROPERTIES, KSI			APPLIED STRESSES, KSI				SAFETY FACTORS		
		Ult.	0.2% Yield	20 Hrs. S.R.	Cent. P/A	Cent. Unt'St	Restored Gas Bending	Max. Comb'e	Ult*	Yield	St.* Rupture
Root (Hub)	1390	108	94	81	30.3	8.8	-0.9	38.2	3.6	2.5	2.7
50 Span	1775	58	45	26.5	18.8	5.5	-0.6	23.7	3.1	1.9	1.4

- SUMMARY OF DISK STRESSES -

CONDITION	TEMP. °F	MINIMUM MATERIAL PROPERTIES, KSI		AVE. ① TANGENT STRESS KSI	MAX. BORE STRESS OR STRAIN ② KSI	BURST SPEED MARGIN	BURST SPEED RPM	NOTES
		ULTIMATE	0.2% YIELD					
Start-Up Transient (1000° ΔT) ③	1800° (Bore)	100	90	---	E = 0.5 ④	---	---	① At Design Speed
Steady State (No ΔT)	1200 °F (Ave)	100	90	43	70	32	44,240	② Calculated elastically
								③ Estimated
								④ LCF Goal: 2000 Start stop cycles

* BASED ON PRIMARY STRESSES (CENTRIFUGAL P/A) ONLY

22377

A simple beam type analysis of the turbine blade indicated a resonance with the originally selected 11 inlet nozzle vanes at 30,000 rpm, as shown in Figure 64 . The margin between the blade frequency and the 11E exictation at maximum speed is about 10 percent. It was desirable that the number of nozzles be increased for the following reasons:

1. To increase the margin between the vane excitation and blade frequency at maximum speed.

2. To reduce the resonance speed of the first bending mode.

3. To eliminate the possibility of reinforcing sources of blade excitations that are multiples of the vane passing frequency subharmonics, by maintaining the number of vanes as a prime number.

The number of vanes was increased to 13 vanes so that criteria above would be satisfied. The margin between the first bending frequency and design point vane excitation for 13 vanes is shown to be 30 percent (Figure 64).

The four compressor blades were checked for centrifugal P/A stresses. Maximum P/A stresses were 6.0 to 4.3 ksi on the first through fourth stages respectively at 33,500 rpm. These stresses result in yield safety factors of 4.7 to 6.3 for aluminum.

Centrifugal stresses were calculated for the first stage rotor disk. The maximum bore stress at 33,500 rpm was 11.8 ksi with an average tangential stress of 8.3 ksi. This results in a burst speed margin of 77 percent using a burst factor of 0.75 for cast C-355-T61 aluminum. The remaining three disks were estimated to have greater margin than the first as shown in summary Table 11.

The integrally cast compressor rotor design shows generous structural margin on the preliminary basis.

4.2.2 Static Structure Combustor Housing

The combustor housing hoop stresses are low for 0.18 inch thickness at sea level static operation conditions. For the jet fuel starter application, the hoop stress is less than one ksi for a 20 hour stress rupture safety factor of more than 20 at 400°F, for C-355-T61 cast aluminum. The hoop stress for the fan engine is 1.5 ksi for a 20 hour stress rupture safety factor at 16 at 400°F.

4.3.3 Rotor Dynamics

The results of the critical speed analysis indicated that an increase in shaft stiffness was necessary to provide an adequate third critical speed margin. The critical speed curves (Figures 65 and 66) are based on a shaft diameter of of 1.56 inch.
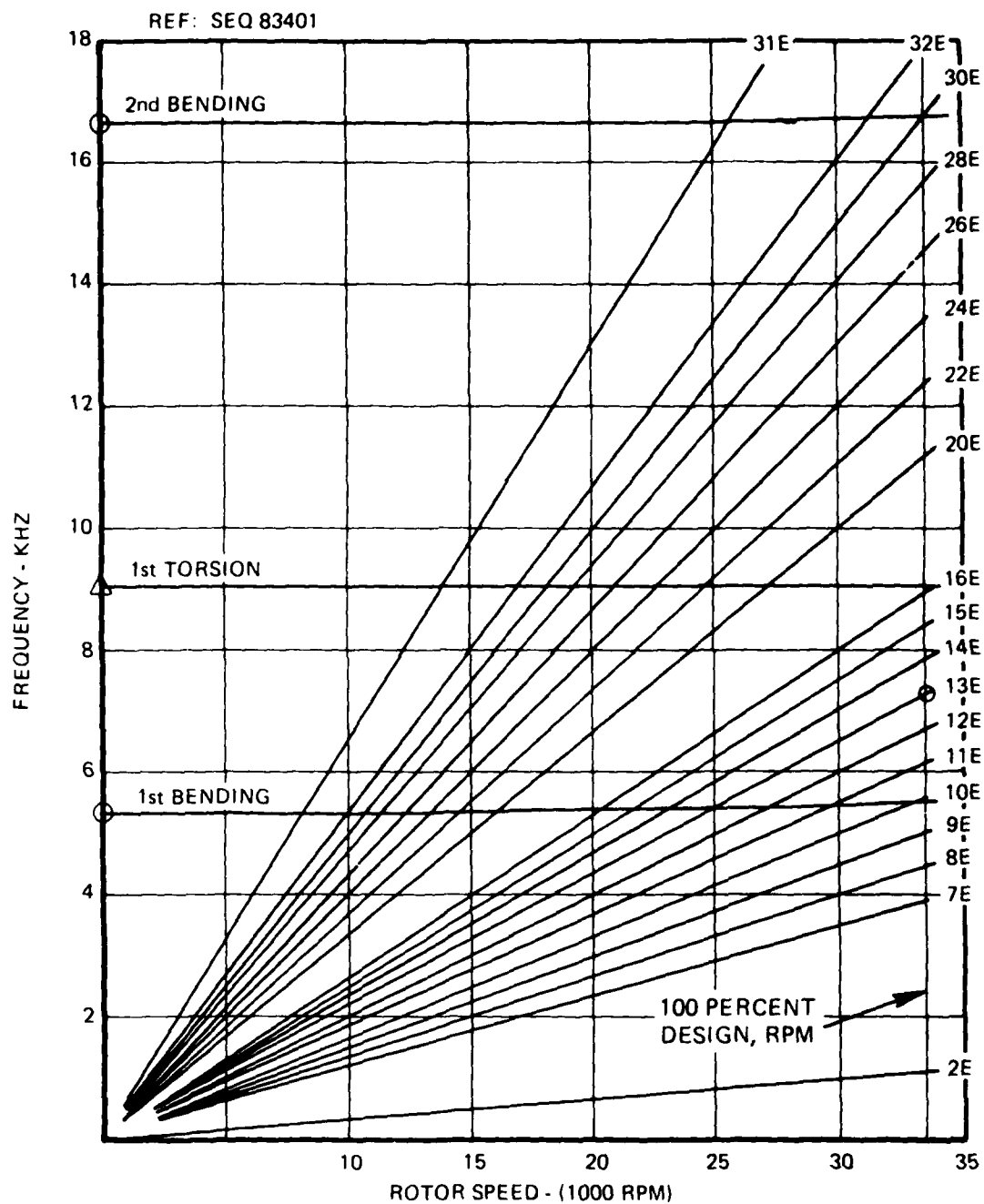
Figure 64. Expendable Gasifier Preliminary Turbine Blade Resonance Diagram.

96

PIN JOINT STIFFNESS
$K_{PR} = (10)^6$
$K_{PM} = 6(10)^5$
SHAFT O.D. = 1.56
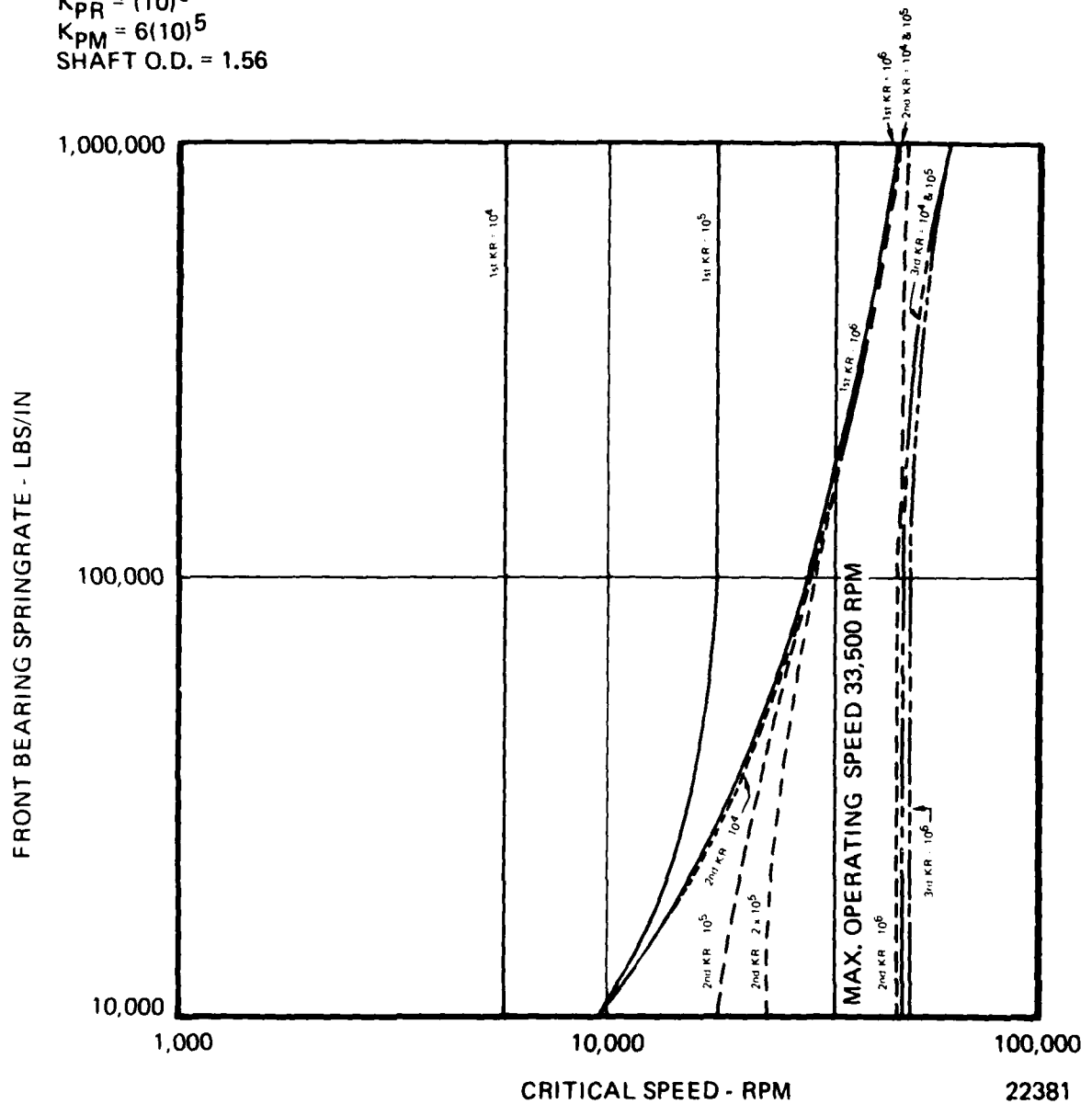
Figure 65. Expendable Gasifier Critical Speeds.

97

PIN JOINT STIFFNESS
$K_{PR} = (10)^5$
$K_{PM} = 6(10)^4$
SHAFT O.D. = 1.56
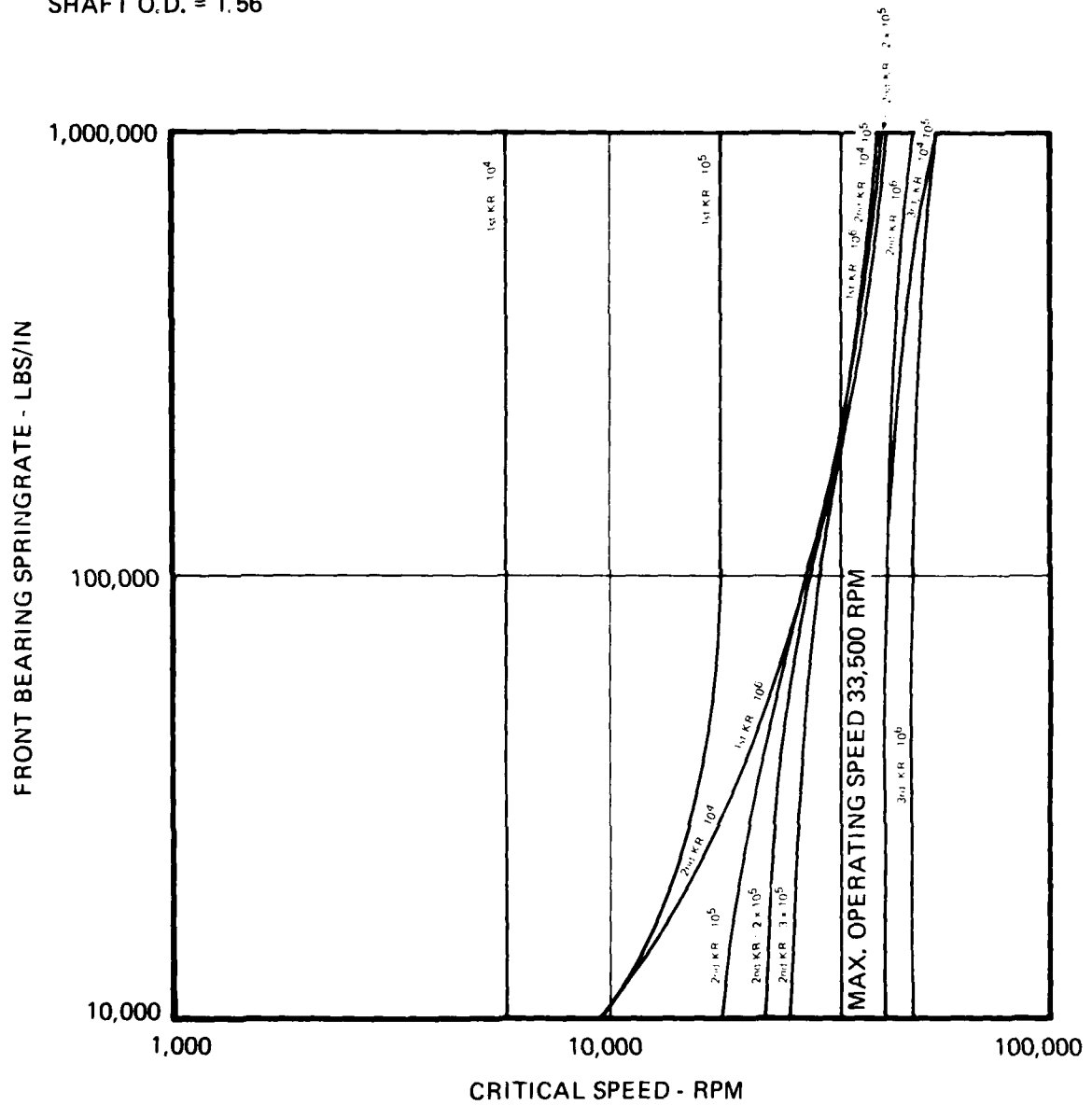
22380

Figure 66 . Expendable Gasifier Critical Speeds.

98

TABLE 11

MODEL 506 AXIAL COMPRESSOR BLADE AND DISK STRESSES
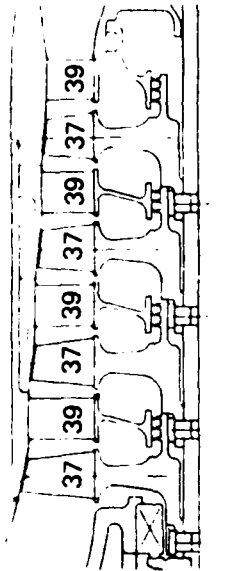
DESIGN SPEED = 33,500 RPM
MATERIAL: C355-T61

BLADE STRESS SUMMARY

ROTOR STAGE	BLADE HUB TEMP °F	MINIMUM MATERIAL PROPERTIES KSI		HUB CENTRIFUGAL STRESS KSI	SAFETY FACTORS	
		ULTIMATE	0.2% YIELD		ULTIMATE	YIELD
1	100	35	28	6.0	5.8	4.7
2	165	33	27.7	5.3	6.2	5.2
3	230	31	27.3	4.7	6.6	5.8
4	295	29	27	4.3	6.7	6.3

DISK STRESS SUMMARY

ROTOR STAGE	TEMPERATURE °F	MINIMIM MATERIAL PROPERTIES KSI		CENTRIFUGAL STRESSES KSI		BURST SPEED MARGIN, %	BURST SPEED RPM
		ULTIMATE	0.2% YIELD	BORE TANGENTIAL	AVERAGE TANGENTIAL		
1	100	35	28	11.?	9.?	77	59,300
2	165	33	27.7	<11.?	<9.3	>77	>59,300
3	230	31	27.?	<11.?	<9.?	>77	>59,300
4	295	29	27	<11.?	<8.3	>77	>59,300

Each of the two critical speed curves presented is based on a specific value of pin joint stiffness, either 1,000,000 lbs/in. radial springrate and 600,000 (lb.-in.)/rad. moment rate, or 100,000 lbs/in radial springrate and 60,000 (lb.-in.) rad. moment rate. The radial and moment springrates are interdependent; their relationship depends primarily on the diameter of the shaft at the pin joint. It is estimated that the actual stiffness will fall between these values; probably closer to the lower springrate.

At the third critical, a margin of 26 percent is obtained with the lower value of joint stiffness, and 43 percent for the higher value. The final design will be analyzed to ensure that the joint spinrgrate is maintained at a sufficiently high level not only to assure that the 26 percent critical speed margin is maintained, but also to assure the critical speed margin is large enough that it does not result in requirements for time consuming balancing procedures, or costly manufacturing tolerances.

To prevent a first or second critical speed from occurring close to the design operating speed of 33,050 rpm, the combined front bearing and support structure springrate must be less than 60,000 lbs. in., while the combined rear bearing and support springrate must be either very stiff (greater than 10^6 lbs./in.) or moderately soft (less than 150,000 lbs./in.). Since it is not practical to obtain a completely rigid combined bearing and support structure springrate (possible thermal radial growth stress problems, inherent bearing springrate, etc.) it is desirable that the rear structure be designed to incorporate the lower springrate.

The front bearing support structure design (Figure 67) was designed to incorporate sufficient flexibility. The final design will be analyzed to ensure that it satisfies the springrate requirements. It is also desirable that the radial springrate of the rear bearing support structure be determined experimentally when the part is fabricated. If the combined bearing and support springrate results in a critical speed problem, additional flexibility can be provided by inserting a flexible ring between the bearing O.D. and the bearing housing, which must be bored out to accept the ring. The housing is designed with sufficient radial thickness to accommodate the additional radial space required by a flexible ring. The results of the critical speed anlaysis are summarized in Table 10.

4.2.4 Bearing and Lubrication System

The Expendable Gasifier bearing and lubrication system consists of a front shaft mounted thrust (ball) bearing with self-contained (pot) lubrication and a rear shaft mounted roller bearing with fuel-air mist lubrication.

The ball bearing was selected on the basis of the lowest cost bearing which would meet the EG requirements. The bearing specifics are given below:

TYPE: BALL
SPECIAL FEATURES: FRACTURED OUTER RING, OUTER RING,
RIDING RETAINER

100

ROTATING MASS

REAR BEARING SUPPORT*

COMPRESSOR ROTOR-TO-SHAFT PIN JOINTS

22386

FRONT BEARING
SUPPORT*

* BOTH SUPPORTS CAN ACCOMMODATE SPRING RINGS IN EVENT THEY ARE
NEEDED TO CONTROL BEARING SUPPORT STRUCTURAL SPRING RATE.
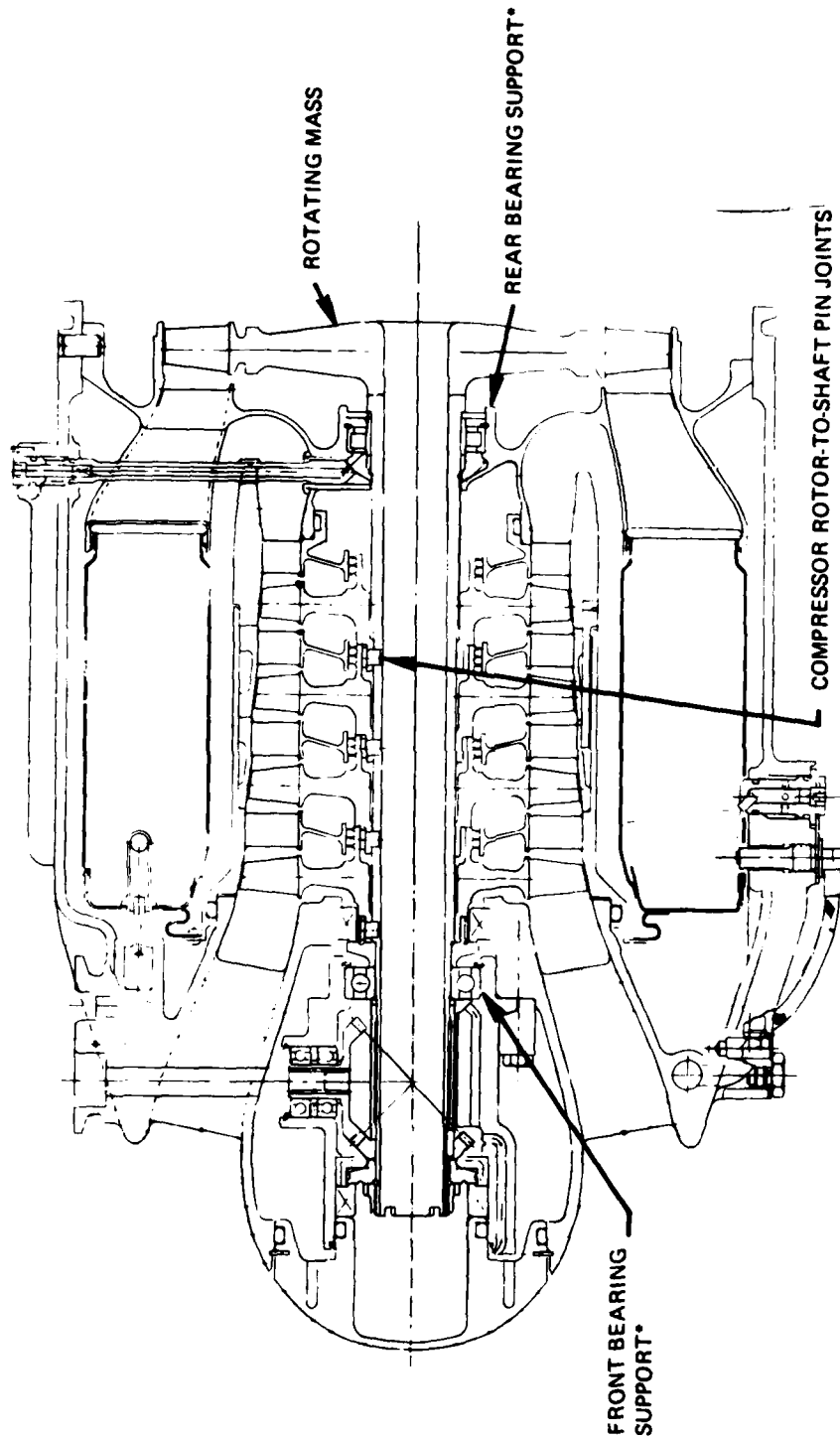
Figure 67 . Model 506 Shaft Dynamics.

101

TABLE 12

MODEL 506 MAIN SHAFT CRITICAL SPEED SUMMARY

SHAFT CRITICAL SPEEDS ARE DEPENDENT ON
COMPRESSOR ROTOR - SHAFT PIN JOINT STIFFNESS

ESTIMATED ROTOR - SHAFT PIN JOINT STIFFNESS

	RADIAL SPRING RATE - LBS/INCH	MOMENT RATE LBS/INCH/RADIAN	① REQ'D FRONT BRG SUPPORT SPRING RATE - LBS/INCH	① REQ'D REAR BRG SUPPORT SPRING RATE - LBS/INCH
HIGHEST ESTIMATE	1,000,000	600,000		
LOWEST ESTIMATE	100,000	60,000	60,000 OR LESS	150,000 OR LESS

① REQUIRED TO ASSURE SAFE OPERATING MARGINS
WITH BOTH 2nd & 3rd CRITICALS

MAIN SHAFT OPERATING CRITICAL SPEED MARGINS

	1,000,000 LBS/IN. PIN RADIAL SPRING RATE			100,000 LBS/IN. PIN RADIAL SPRING RATE		
	FRONT BEARING (60,000 LBS/IN)	REAR BEARING (150,000 LBS/IN)		FRONT BEARING (60,000 LBS/IN)	REAR BEARING (150,000 LBS/IN)	
	CRITICAL SPEED	MARGIN*		CRITICAL SPEED	MARGIN*	
2nd MODE	26,600	19.5%		25,000	24.4%	
3rd MODE	48,200	43.9%		42,000	25.4%	

* BASED ON 33,060 SHAFT RPM
** BASED ON 33,500 SHAFT MAX. RPM.

```
MATERIALS:  INNER AND OUTER RINGS
            SAE 52100 STL (VACUUM DEGASSED)
            HARDNESS:  RC 60 MIN.
            BALLS
            SAE 52100 STL (VACUUM DEGASSED)
            HARDNESS:  RC 60 MIN.
            RETAINER
            AMS 6415 STL, ONE PIECE MACHINED,
            SILVER PLATED
DN:  1.155 x 10⁶
```

DN: 1.155×10^6

BIO LIFE: +10,000 HRS. BASED ON 150 LB. THRUST LOAD AND
            100 LB. RADIAL UNBALANCE

TOLERANCE CLASSIFICATION: ABEC-5

The lubrication scheme selected for the EG shown in Figure 68 is a self-contained (pot-lube) system which is capable of serving not only the JFS and T/C applications but also the T/F application without modification. In operation, the oil is pumped by the accessory drive bevel gear into passages which direct the oil at the bearing inner race. Excellent heat transfer is achieved to cool the oil by the oil contact with the aluminum housing which is cooled by the compressor inlet air. A nose cover of polyether sulfone thermoplastic permits visual inspection of the oil level in the sump to assure a safe level for operation.

The roller bearing was also selected on the basis of lowest cost to achieve adequate operation. The bearing specifics are given below:

TYPE: ROLLER

SPECIAL FEATURES: OUTER RING RIDING RETAINER,
                    EXTENDED INNER RING

MATERIALS: INNER AND OUTER RINGS
            CEVM M-50 TOOL STEEL
            HARDNESS: RC 60 MIN.
            ROLLERS
            CEVM M-50 TOOL STEEL
            HARDNESS: RC 60 MIN.
            RETAINER
            AMS 6414 STL, RC 30-38, ONE
            PIECE MACHINED, SILVER PLATE

DN: 1.32×10^6

BIO LIFE: +10,000 HRS. BASED ON A 100 LB. RADIAL UNBALANCE

TOLERANCE CLASSIFICATION: RBEC-5

The lubrication scheme for the rear bearing was selected based on the successful proven VSTT fuel-air system. In operation, fuel is delivered from the main fuel supply to the fuel transfer tube (Figure 69) and directed through a jet at the roller bearing inner race. A preliminary estimate indicates that two percent (not included in SFC) of the EG fuel flow at the SLS, 59°F JFS design point condition will be required for the rear bearing cooling flow. Upon entering the bearing

103

MIST LUBRICATED

ENGINE ℄

FRONT THRUST BEARING 22387

BEVEL GEAR ACTS
AS CF PUMP FOR
OIL DISTRIBUTION

OIL SUMP

OIL FLOW FOR FAN THRUST BEARING

PLASTIC NOSE CONE FOR OIL LEVEL INDICATION
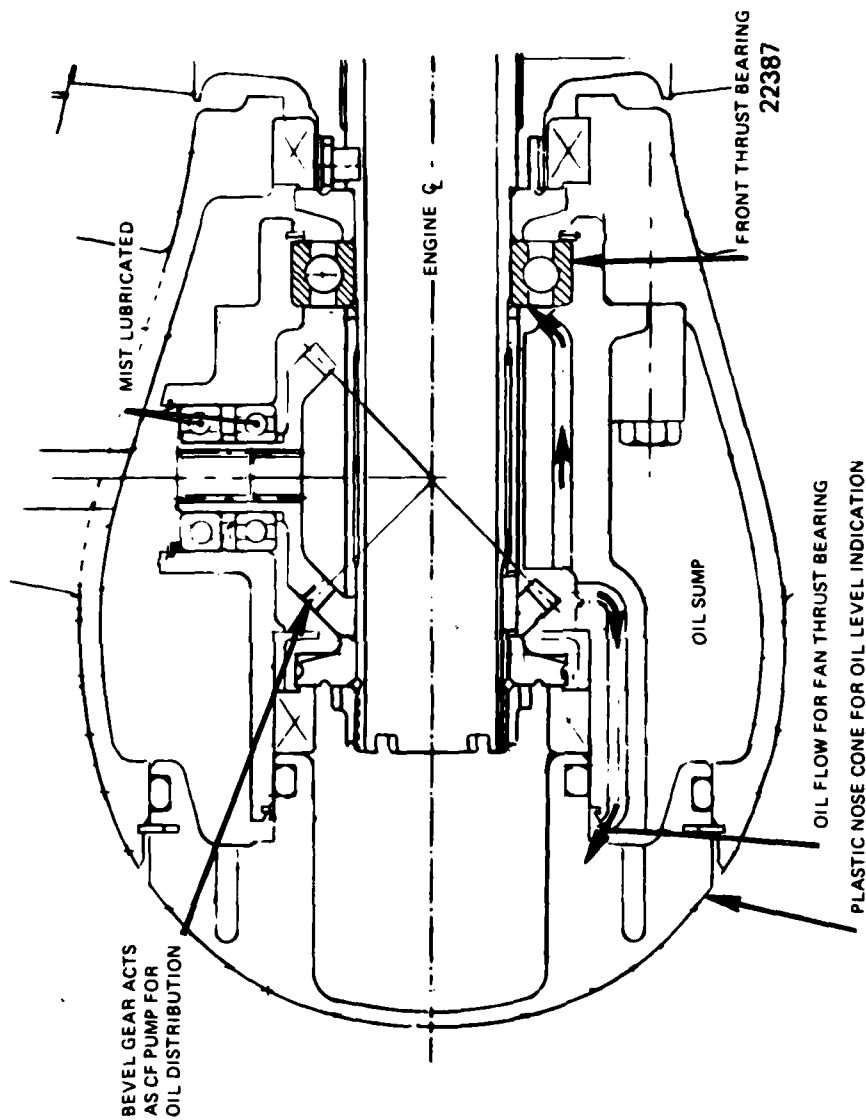
THRUST BEARING LUBRICATION SYSTEM

LUBRICANT: MIL-L-7808

NOTE: BEARING SUMP INITIALLY FILLED TO
ENGINE CENTERLINE QUANTITY OF
OIL APPROX. 548 C.C.'S

Figure 68 . EG Front Bearing and Lubrication System.

FUEL IN

METERING VALVE
AND FILTER

FUEL TRANSFER TUBE

AIRFLOW

EXPENDED
FUEL

BEARING
SHIELD

FUEL JET

REAR BEARING

FUEL FLOW APPROX. 75 C.C./MIN.

22385
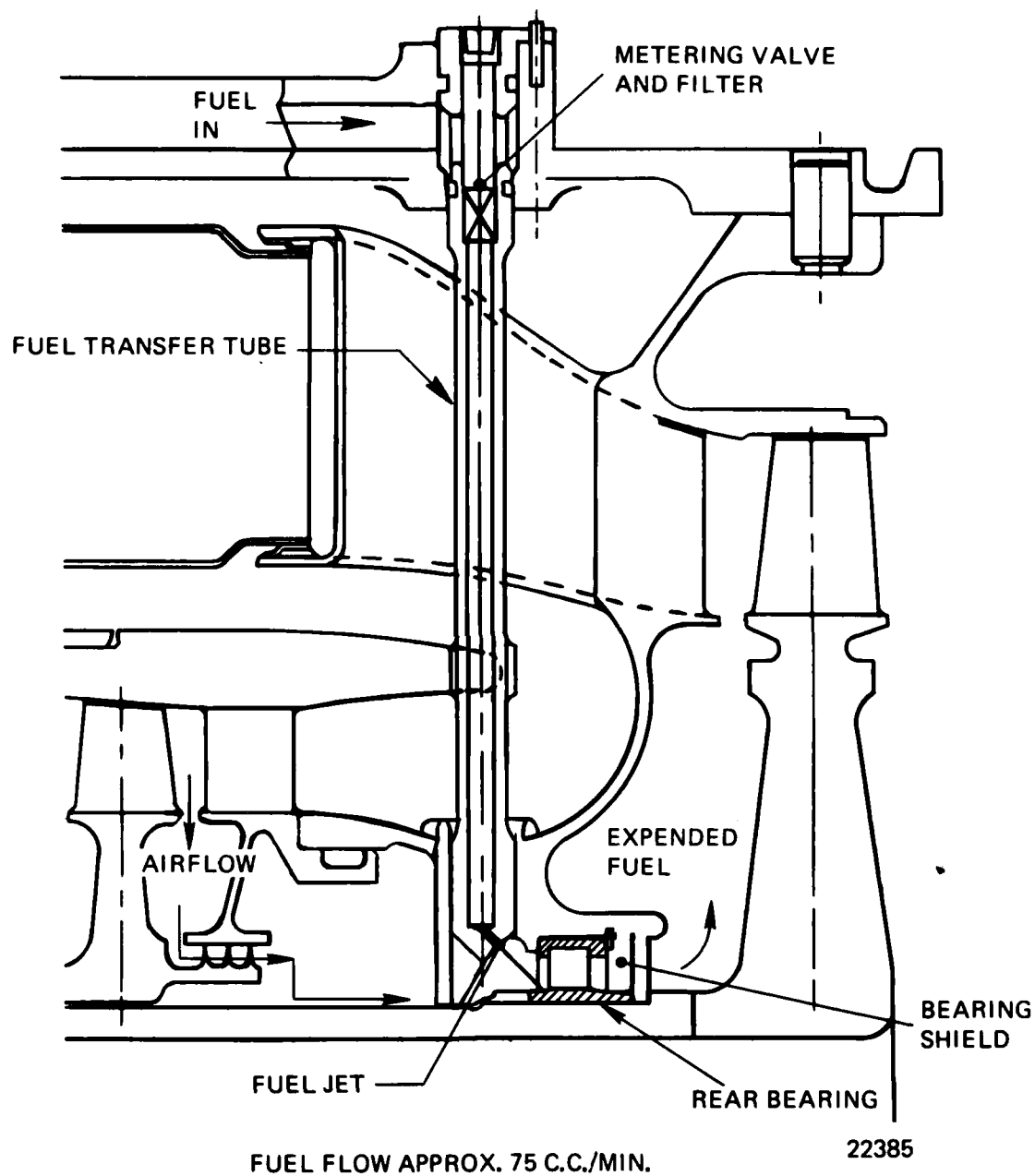
Figure 69 .   EG Rear Bearing and Lube System.

105

cavity the fuel mixes with leakage airflow from the compressor and passes through the bearing. The expended fuel air mixture (outside the limits of ignition) flows into the turbine rotor gas path.

4.2.5 Accessory System Interfaces

The operation of the EG in all applications is dependent on the accessory drive system (Figure 70) consisting of a drive/driven bevel gear set, an accessory bearing set and a full-floating accessory drive shaft. The accessory drive transmits power to the EG main shaft during start and acceleration and from the main shaft to drive the fuel pump and alternator during operation. The design criteria for the drive system is stated below.

1. Starter Output Torque   84 In-Lbs
2. Starter-to-Engine Speed Ratio   0.625
3. Starter Cut-Out Speed   10,000 rpm
      @ Engine Speed   16,000 rpm
4. Continuous Acc'y Drive Load   3 HP
      Fuel Pump Drive   1 HP
      Alternator Drive   2 HP

Gears are designed for unlimited life after applying a misalignment (operating) factor of 1.5 to account for the overhung mounting of the gear set.

Preliminary studies of the overhung bevel gear design (Figure 71) indicate that the mounting is satisfactory for the starting load of 84 in.-lbs. torque at the starter pad up to a starter cutout speed of 10,000 rpm (16,000 engine rpm) and a continuous accessory drive load at maximum engine speed (33,050 rpm) of 3 H.P. The accessory load is comprised of a 1 H.P. fuel pump, and 2 H.P. alternator for electrical power extraction. A misalignment (derating) factor of 1.5 has been used to account for the overhung mounting of the gear set, i.e., the calculated applied gear tooth is increased by 50 percent to account for the over-hung mounting. Under these conditions, the bevel gear set with the specified material, processing, and tolerances will exceed all life requirements.

4.3 ESTIMATE OF STARTING DRAG TORQUE AND ACCELERATION OF THE JFS 206

4.3.1 EG Starting Drag Torque Estimate

The Expendable Gasifier torque characteristics (Figure 72) have been determined by scaling available in-house reference data using the following quantities:

	EG	REF
Wa	4.02	1.75
PR	2.86	3.10
$N/\sqrt{\theta}$	33,060	74,700

106

ACCESSORIES

FULL FLOATING
DRIVE SHAFT

DRIVE BEVEL
GEAR SET

DRIVE GEAR ACTS
AS LUBE PUMP -
ASSURES AMPLE
LUBRICATION

GEAR SET SUPPORT
(HOUSES BOTH GEARS,
BEARINGS, ASSURING
ALIGNMENT)
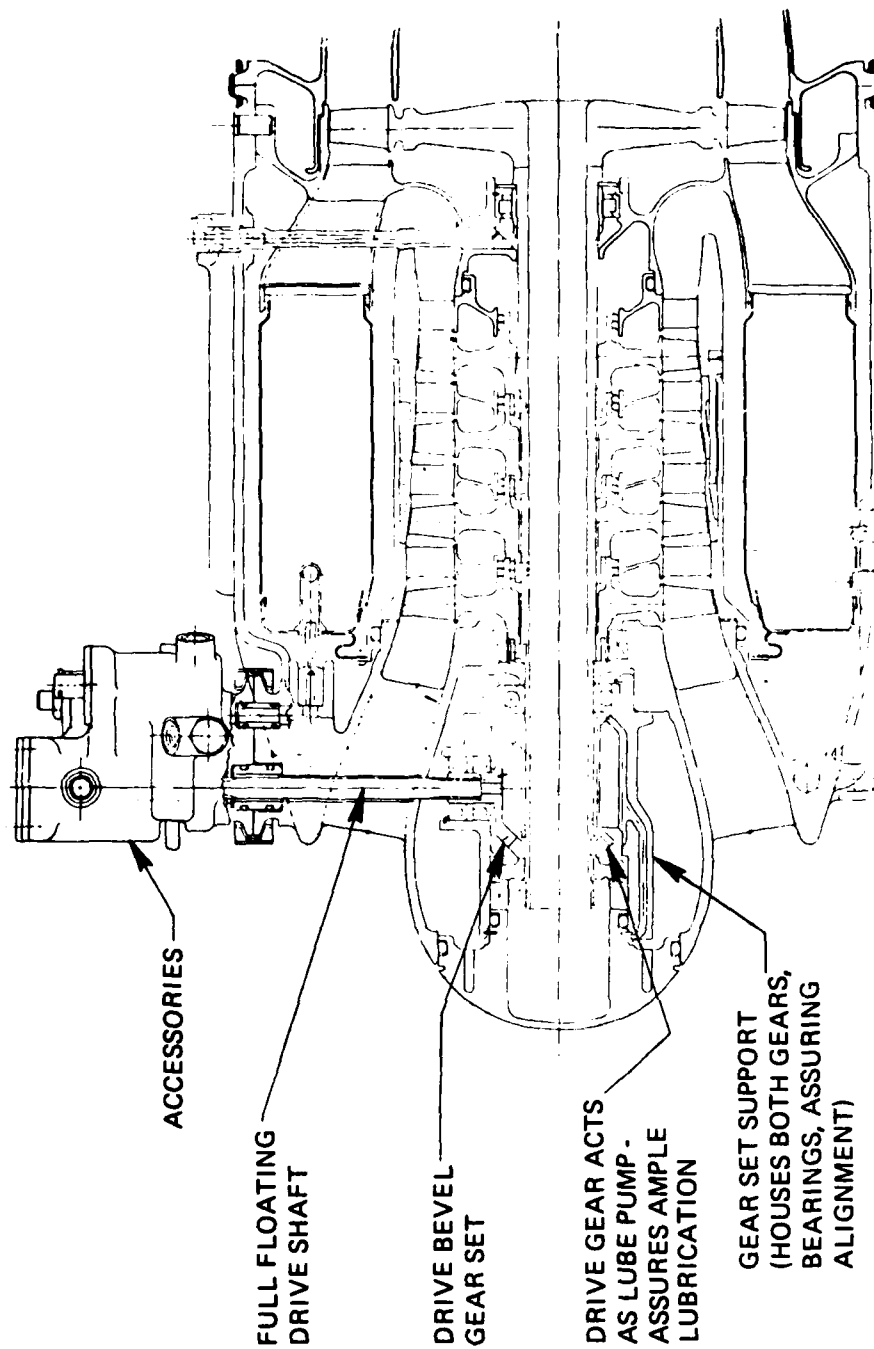
Figure 70 . Model 506 Accessory Drive.

107

N = 31,993 RPM

31 TEETH

30 TEETH

N = 33,060 RPM
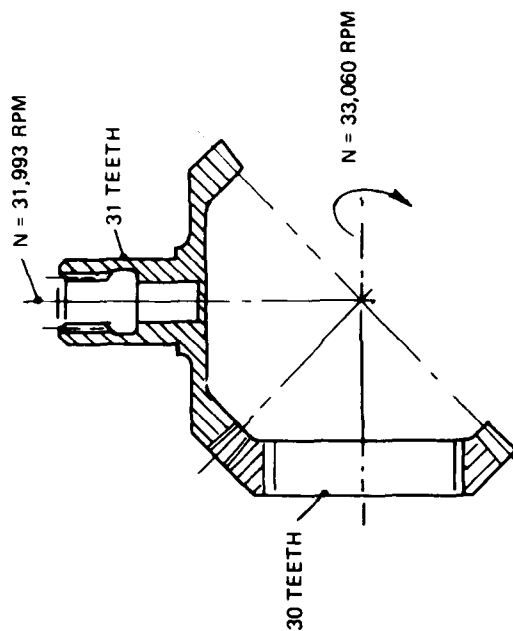
TYPE: CONIFLEX - CARBURIZED TEETH
MATERIAL: AMS 6272 STL
DIAMETRAL PITCH: 14
• STRESS:

MAX. TOOTH ROOT BENDING STRESS •	12,240 PSI
ALLOW STRESS FOR UNLIMITED LIFE (400°F)	21,000 PSI
MAXIMUM HERTZ CONTACT STRESS	145,900 PSI
ALLOW STRESS FOR UNLIMITED LIFE (400°F)	180,000 PSI
SCORING INDEX	
MAX. STARTING LOAD	273°
MAX. CONT. OPERATING LOAD	451°
ALLOW SCORING INDEX	
MIL-L-7808	500°
MIL-L-23699	550°

• NOTE: THE GEAR STRESSES ARE CALCULATED UNDER WORST LOAD CONDITIONS
(STARTING CYCLE);- NORMAL ACCESSORY OPERATING STRESSES ARE
APPROX. 25% OF THESE VALUES

22384

Figure 71 . Accessory Drive Bevel Gear Set - Design Data.
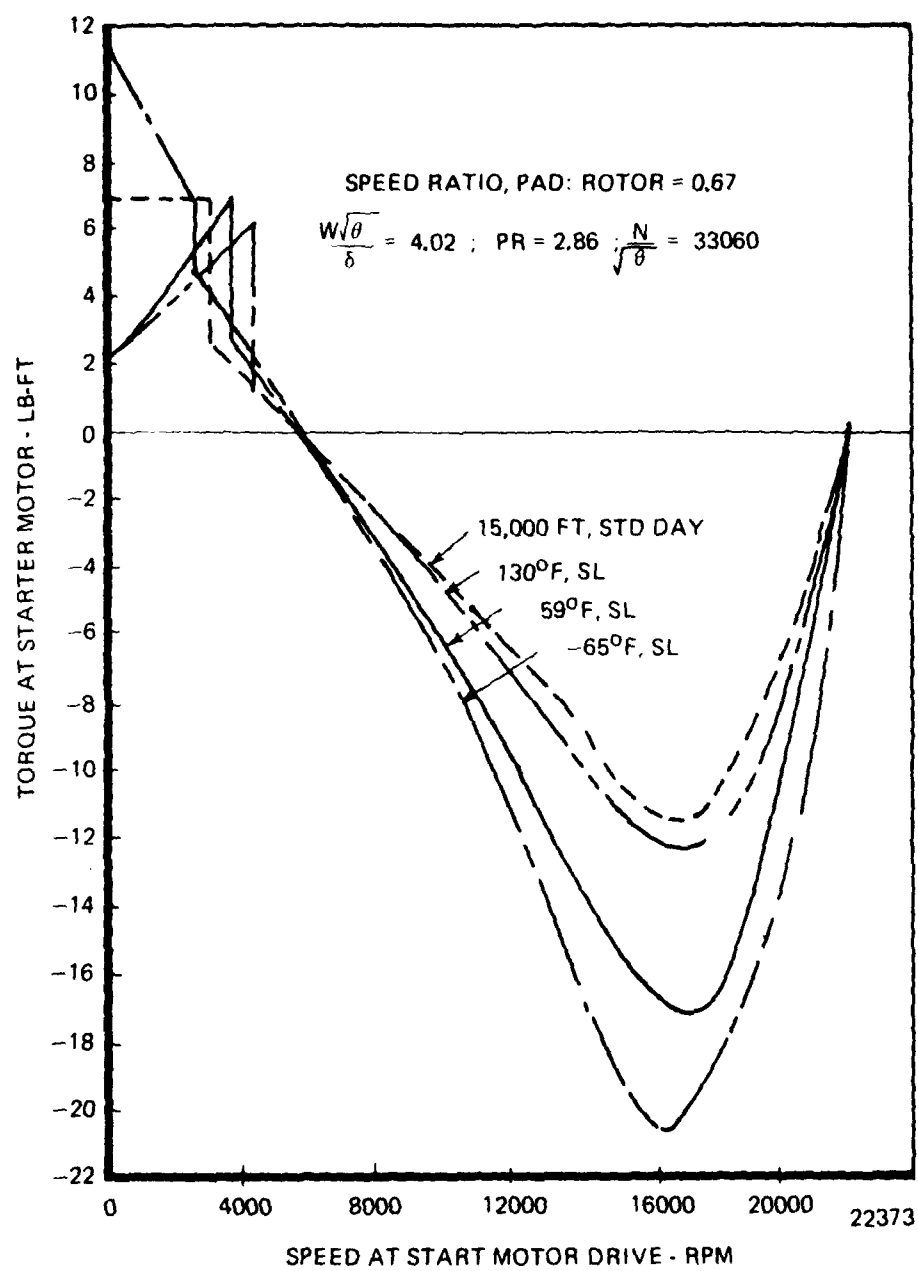
Figure 72. Expendable Gasifier Drag Torque Characteristics During Acceleration.

109

The torque required or developed by the Expendable Gasifier has been taken to vary directly with compressir airflow, (PR) 0.286, and inversely with rotational speed. The ratio of speed at the start motor pad to gas generator speed has been taken to be 0.67. The maximum speed at the start motor pad is 22,100 rpm which corresponds to a gas generator speed of 33,060 rpm. Expendable gasifier ignition occurs in a speed range between 13 and 20 percent of maximum. At speeds less than that at which ignition occurs, a drag torque exists which must be overcome by the starting device.

The shape of the drag torque curve depends on the temperature at tne engine inlet. At standard temperature or higher, engine drag torque increases up to ignition speed. This is due to increasing airflow passing through the engine. However, when the inlet temperature drops to $-65^{\circ}F$, the drag torque becomes maximum at zero speed and then decreases as the engine approaches ignition speed. This characteristic can be attributed to the high viscosity of the bearing and accessory gear train lubricants which exists at these low temperatures. In this sense, the trend of the drag torque at low temperatures is correct but the magnitudes of the torques given may be inaccurate since it is unlikely that these torques will scale according to the procedure given above. The estimate, however, is considered to be reasonably accurate for the preliminary design estimate.

4.3.2   JFS 206 Acceleration Estimate

The JFS 206 starting capability was applied to a typical low bypass ratio turbofan engine in the 25,000 lb. thrust class ($I = 103$ lb-ft^2 at the power take-off PTO).

The start and acceleration control for the JF⌐ 206 was described in Section 2. Basically the control was devised to permit JFS start by pilot command and cut-out automatically after the main engine self-sustains by sensing speed at the P⌐C. The torque and power characteristics ofthe JFS as a function of speed at the PTO is given in Figure 73 for the SLS 59°F condition. Estimates of main engine starting characteristics were made for the SLS condition at two temperatures 59°F and 125°F. The results are shown in Figures 74 and 75 . It can be noted that the lapse in power of the JFS with ambient temperature (230°F to 163 HP) does not impair the starting capability of the JFS since adequate margin exists at the main engine drag torque peak at the 125°F condition. The acceleration transient estimate is shown in Figure 76 as percent shaft speed as a function of time for the EG shaft and the PTO shaft at the SLS 125°F day condition.

4.4   EXPENDABLE GASIFIER COST ANALYSIS

The factors which enter in the total cost of a gas turbine engine can be divided into two categories, acquisition cost and life cycle cost. Acquisition costs are affected by the design of the unit and the production rate over a finite production time frame. Life cycle costs are affected by maintenance, parts replacement, overhaul, and accountability paperwork in addition to acquisition cost.

110
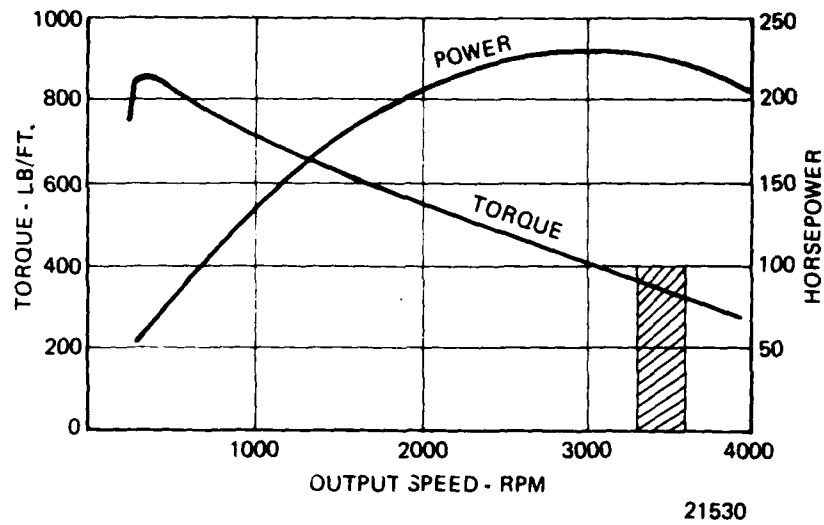
Figure 73 . JFS - Torque and Horsepower Characteristics.
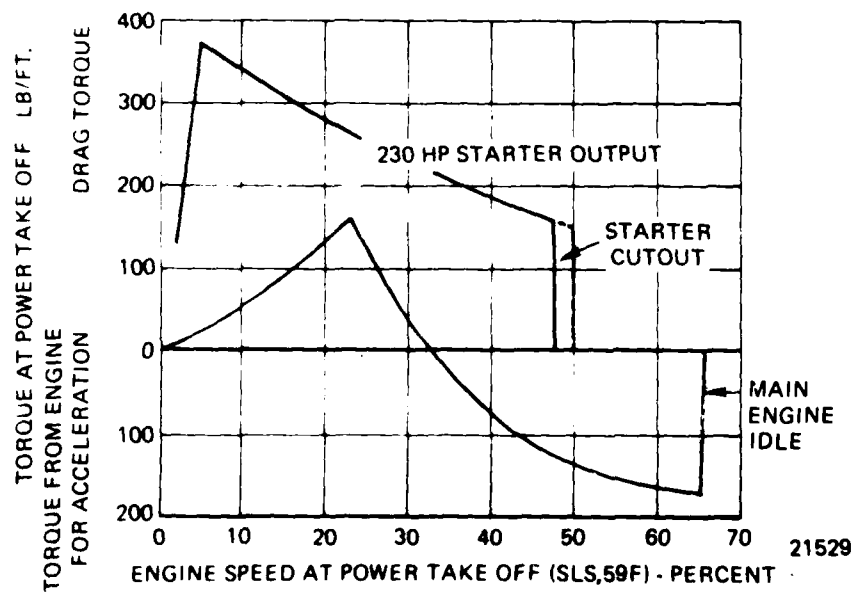
Figure 74 . Engine/Starter Characteristics - SL:59°F.

111
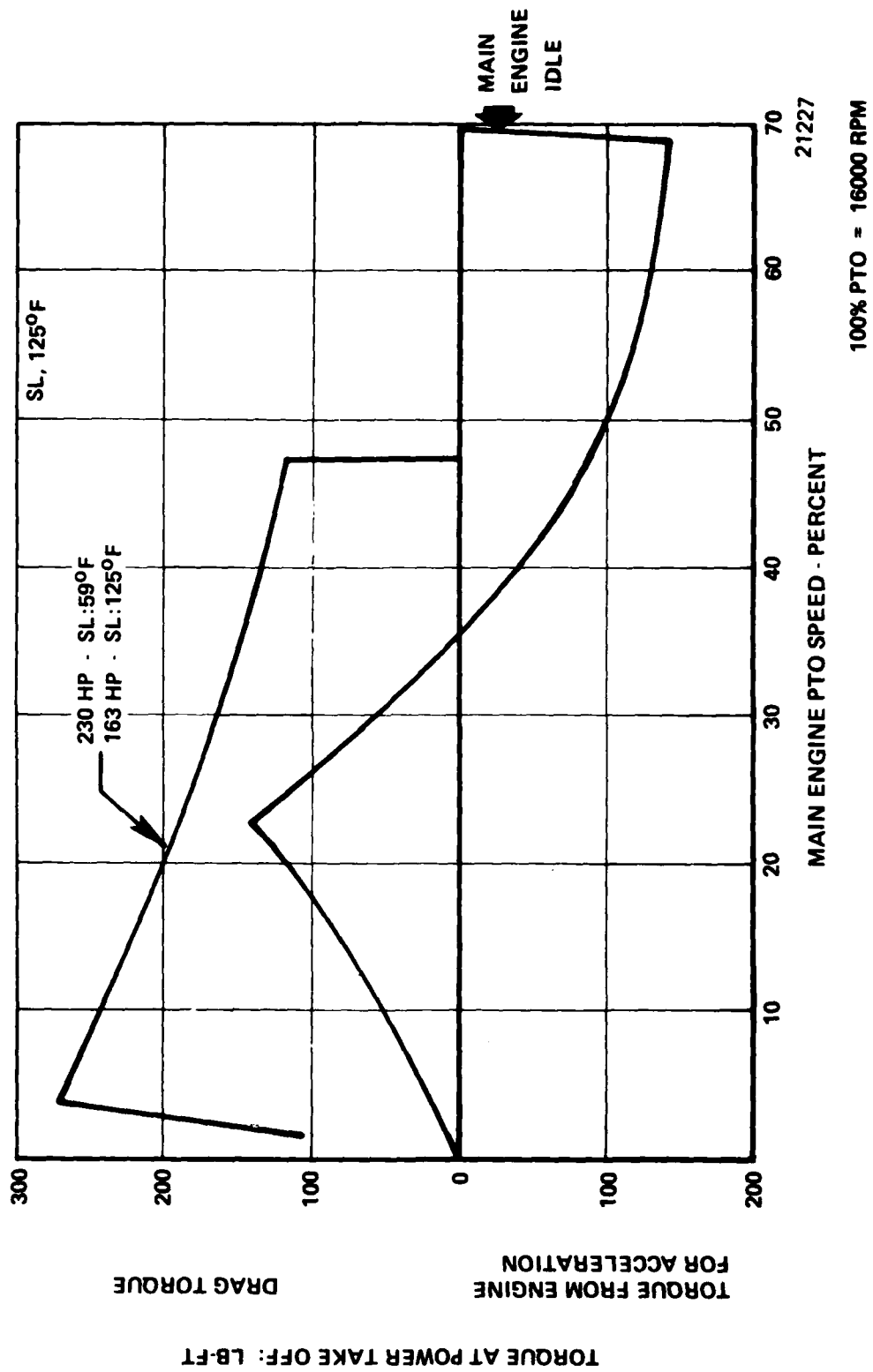
Figure 75 . Engine/Starter Characteristics – SL:125°F.

112
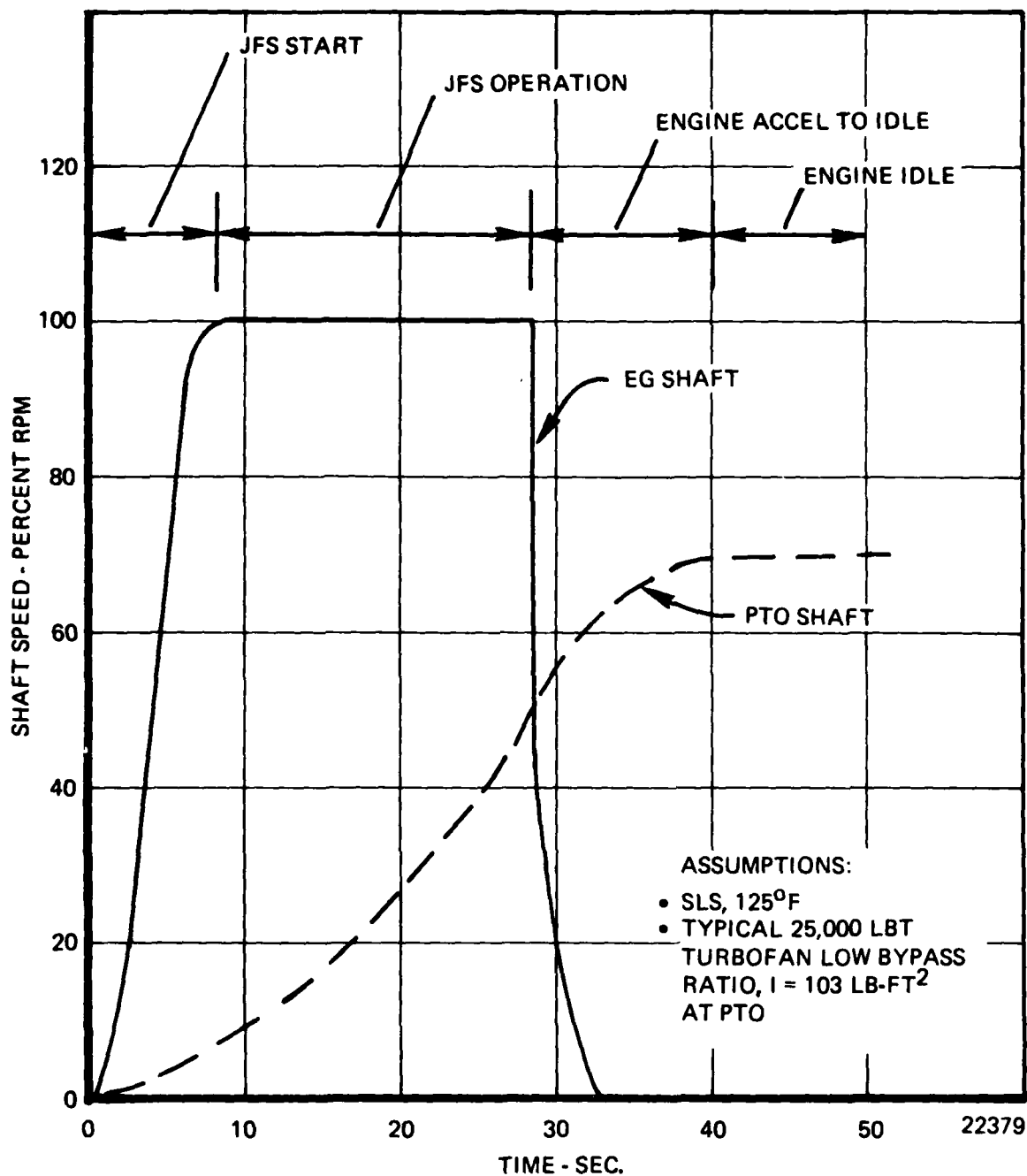
Figure 76 . Estimate of JFS Transient During Starting of Typical Turbofan Engine.

113

To achieve low cost for the expendable gasifier core engine, all of the above-mentioned items are considered. The concept of a throwaway core engine has been the intent of the program since the program start. Life cycle costs are considerably reduced when this concept is applied. It has been observed that the sum of maintenance and overhaul costs of existing JFS systems are nearly equal to the acquisition cost and in many cases those costs are exceeded before the expected time between overhaul (TBO) has been reached. The expendable gasifier core, which is easily replaceable, would be removed after 2000 main engine starts by removing two quick-assembly-disconnect (QAD) VEE-band clamps as shown in Figure 77. A new unit would be installed in its place in a matter of minutes. The power turbine module and the control and accessories have proven to have considerably longer life than the gasifier and are not expendable.

In order to make the throwaway concept pay off, particular attention must be given to acquisition cost. Reference 1 describes the initial conceptual studies which addressed designing a JFS for low cost from the beginning of the design process. During the preliminary cycle analysis low cost is considered by: (1) choosing adequate performance objectives to meet mission requirements; (2) selecting conservative estimates of component efficiencies to permit manufacturing trade-offs and minimize development cost; and (3) selecting a relatively low pressure ratio/low turbine inlet temperature design for minimal use of costly materials.

The preliminary design phase usually has the most critical impact on design-to-cost. During this phase, mechanical, aerothermo, structural, materials and manufacturing engineering must combine talents and work toward minimizing the iterations between flowpath engineering, construction and assembly techniques to meet mission requirements. A few of the low cost design features of the expendable gasifier derived during the Phase I process are:

1. Extensive use of aluminum castings (low cost, lightweight).

2. Identical rotor castings for all four compressor stages with the tip diameters machined to form the individual rotors.

3. Pot-lube front bearing and fuel lubricated rear bearing (no maintenance required - completely self-contained).

4. Main frame casting containing fuel passages for primer fuel, main fuel and rear bearing lube (no external tubing required), Figure 78.

5. Radial pin construction to reduce piloting requirements.

6. Relaxed requirements on surface finish, flow surface tolerances and airfoil thickness to ease casting difficulties.

7. Accessory drive bevel gear set: conventional hardened gear, not ground.

8. Perforated sheet metal combustor shell.

114

ELECTRICAL
CONNECTOR

CONTAINMENT RING

POWER OUTPUT
MODULE

21517

QAD
RING

EXPENDABLE
GASIFIER

FUEL HANDLING
STARTING
CONTROL
MODULE

QAD
RING
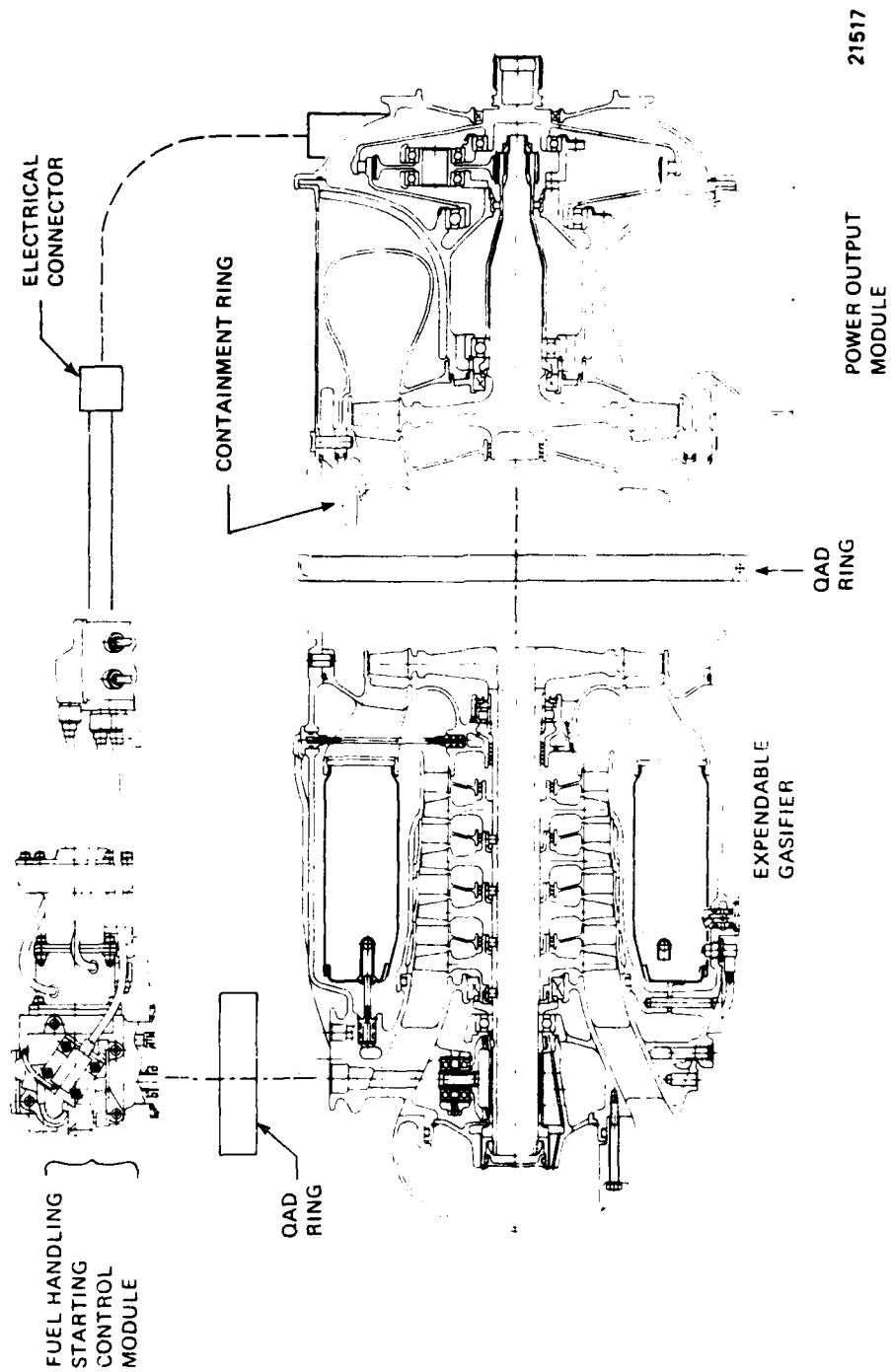
Figure 77 . Jet Fuel Starter Modular Construction.

115
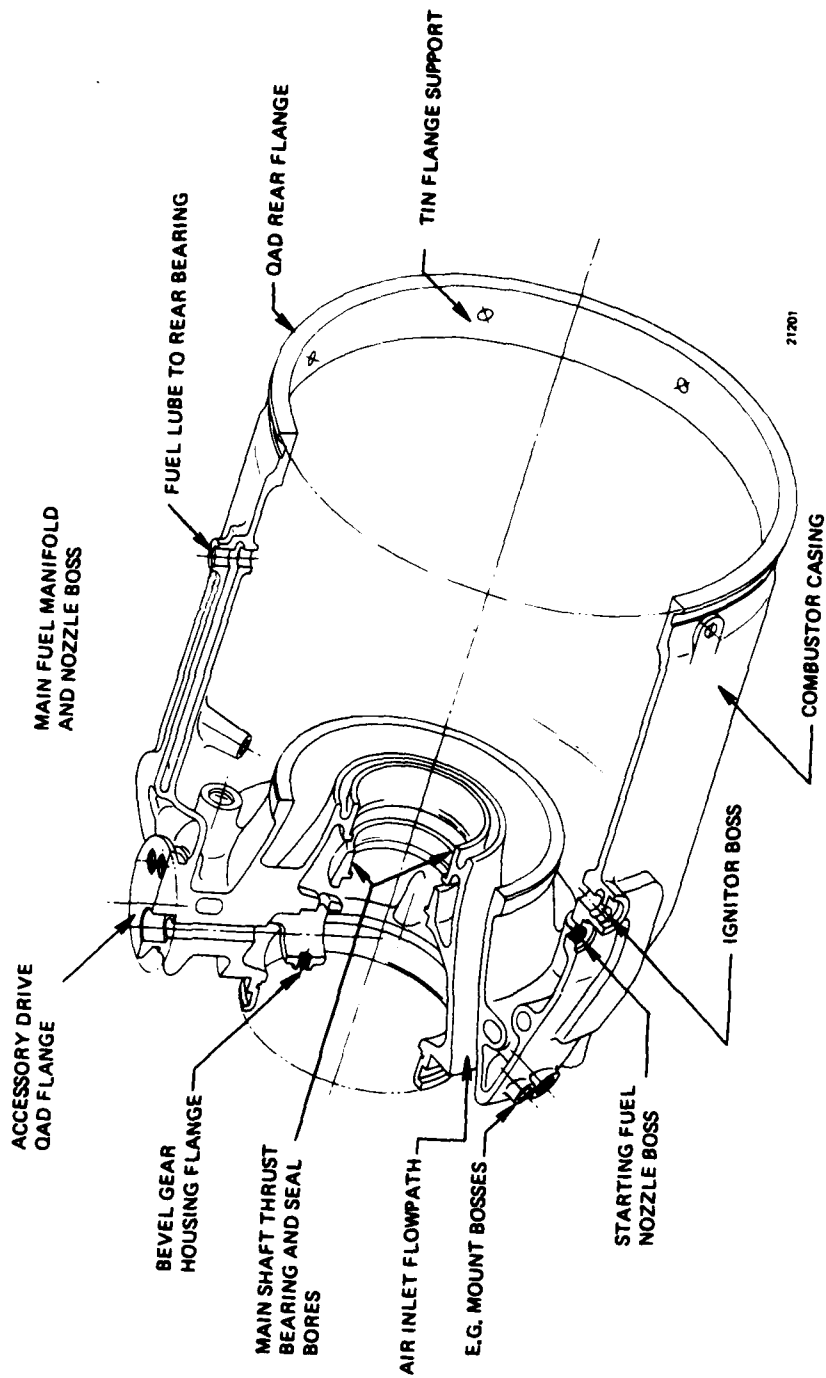
Figure 78 . Main Frame Isometric/Aluminum Casting (C355) Multiple Functions Integral to Reduce Number of Parts.

116

9. Turbine inlet nozzle: monolithic casting with hollow air cooled vanes.

10. Turbine rotor cast to net shape and EB welded to shaft.

11. QAD flanges: permits quick assembly of gearbox and derivative modules.

12. A low rotor speed (33,000 RPM) allows the use of cast aluminum for the compressor rotors.

Some of the low cost features and materials mentioned above are shown in Figure 79 . Detail cost estimate drawings of the individual gasifier parts were prepared and distributed to vendors. Several quotes were obtained on each part and the lowest quote was chosen for the cost estimate. The quotes were based on production quantities of 500 units per year for 5 years for a total of 2,500 units.

Production rate has the greatest influence on unit cost of any product. Typically, automotive type production rates achieve the lowest possible costs. Part of the expendable gasifier intent is to achieve the highest possible production rate by having a common core for jet fuel starters, turbofans, turbojets. Even with those applications, the total estimated production quantity doesn't come close to automotive type of production units. The relatively low level of production rate experienced by the gas turbine manufacturer restricts the dollar investment in automation and tooling which would contribute to lower unit cost. Reference 2 shows that the cost reduction with increasing production rates can be as much as 10 to 1 for a rate of 2,500 parts per year. However, for 500 parts per year, the cost reduction is only two to one.

Cost data received from vendors on the expendable gasifier parts (Figure 80) have indicated a 50 percent reduction for 2,500 units on a 500/year basis which is in fair agreement with Reference 2. However, if all 2,500 engines were produced in one year, the cost reduction could be expected to be tenfold.

Production cost has been subdivided into various categories by Design-to-cost analysis. Figure 81 shows a breakdown of costs in the form of the engine cost "tree" (Reference 3).

The cost of producing the specific parts of an engine are compiled into cost summaries for engine groups and for the total engine. This cost summary is then evaluated with respect to the initial cost objectives and commitments and also serves as an iterative cost model.

The method is based on: (1) identifying the elements of engine cost, at the part design level; (2) providing the designer with "real time" knowledge of the cost consequence of his design decisions; and (3) providing program management visibility of on-going success in achieving cost targets. Other constraints and considerations addressed, in the development of this method, are:

117

C355 SAND CAST CAST ALUMINUM MAIN FRAME CONTAINS FUEL PASSAGES FOR
PRIMER, MAIN FUEL NOZZLES, REAR BEARING LUBRICATION

INVESTMENT CAST N-155 VAPORIZER TUBE

INVESTMENT CAST N-155 TURBINE INLET NOZZLE

INVESTMENT CAST IN-100 TURBINE ROTOR

17-4PH STEEL SHAFT (TUBING) EB WELDED TO ROTOR

PERFORATED SHEET METAL COMBUSTOR MATERIAL: HAYNES 556

22383

C355 SAND OR PLASTER MOLD CAST ALUMINUM FRONT BEARING HOUSING

8617 CARBURIZING STEEL GEARS

INJECTION MOLDED POLYETHERSULFONE TRANSLUCENT PLASTIC FRONT HUB

C355 INVESTMENT CAST ALUMINUM ROTORS AND STATORS

Figure 79 . Low Cost Features of EG.

118
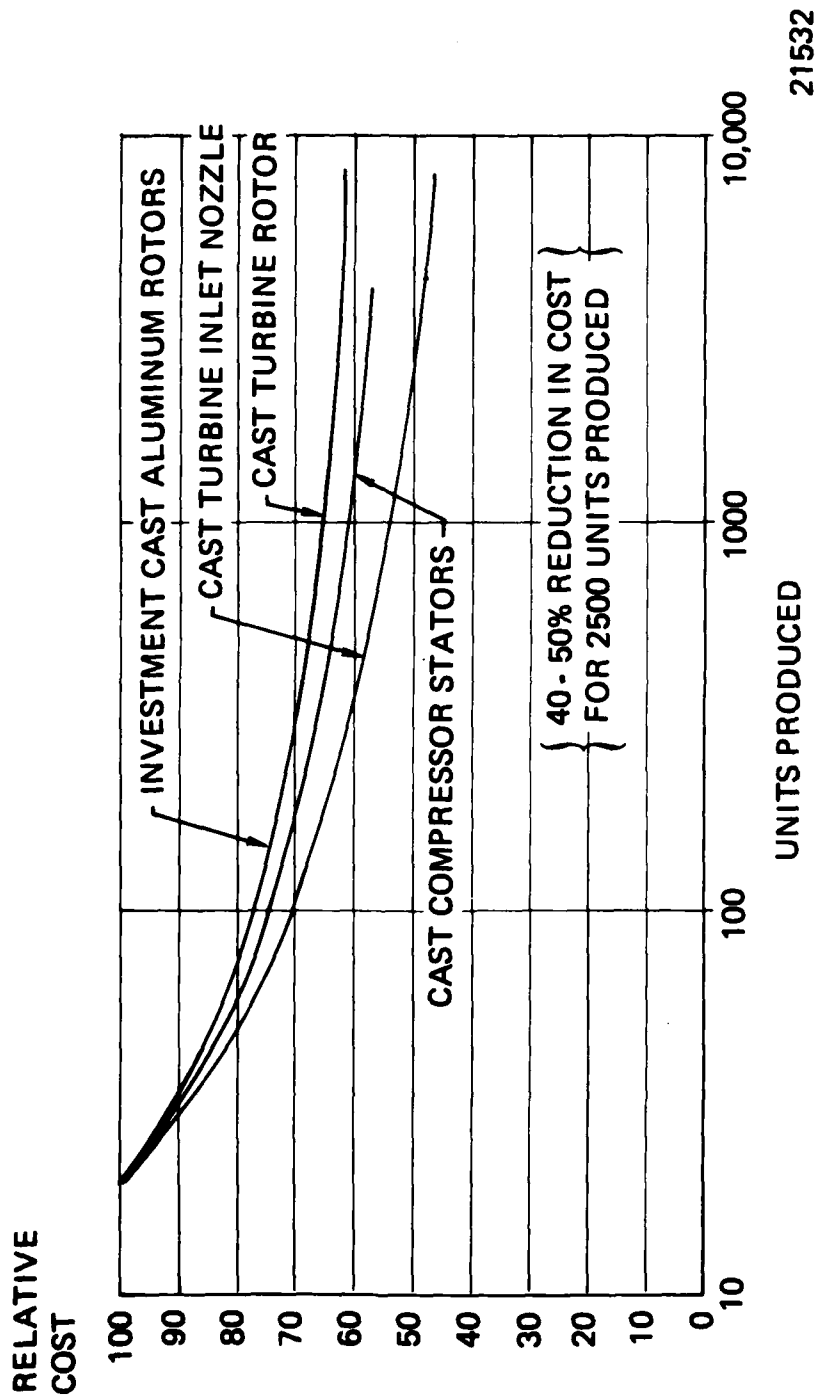
Figure 80 - Effect of Production Units on Unit Cost.

119
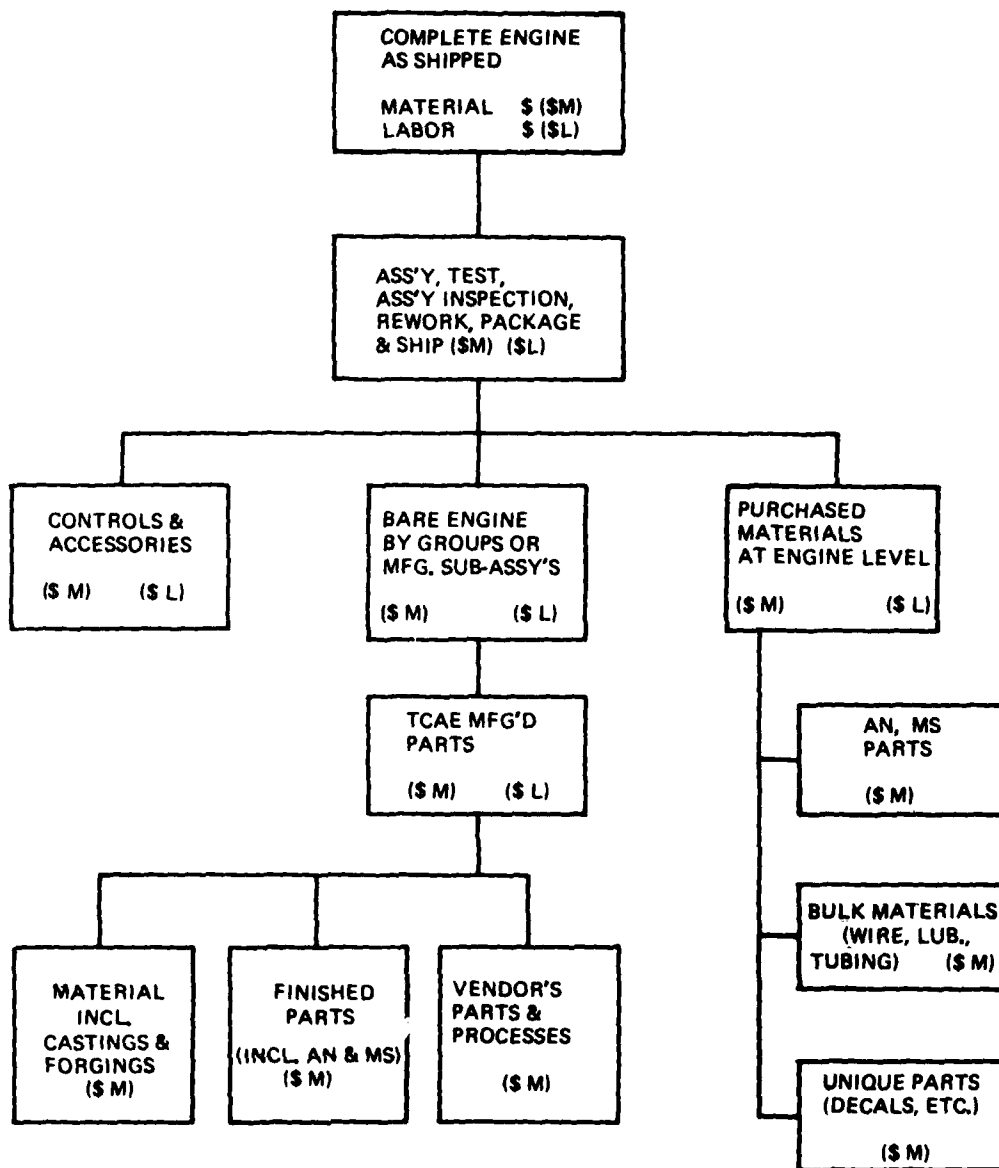
Figure 81 . Engine Cost Tree: A Methodical Approach to Engine Cost Analysis.

1. It must provide sufficient detail to be useful for
    the appropriate phase of design.

2. The method should be compatible with manual as well
    as data processing compilation procedures (Reference 2).

3. The approach must provide the manufacturing engineering
    activity with sufficient information to critique the de-
    sign intent and contribute to achieving the cost objective.

The approach applies the cost-tree procedure to allocate initial cost
objectives and commitments to engine groups, parts and controls/accessories.

During the design process, the cost of manufacturing (or acquiring) each
part is compiled by finite elements. The elements include the manhours for indivi-
dual manufacturing operations, the material costs and the support costs (in man-
hours and materials) of inspection, tool support and applicable overhead opera-
tions. Manhour and material costs are entered at "burdened" values and performance
indices and antiticpated scrap rates are included for each operation, or summarized
for each part.

The method facilitates evaluating the cost consequence of a change in design
and/or manufacturing operations. It also allows for estimating or specifying cost
objectives as a function of production quantitites and delivery rates. (Burdened
rates are used for material and labor but the burden (overhead and material handling
costs) may vary as a function of the production quantity being estimated.

The EG cross-section shown in Figure 82 identifies the major parts and
subassemblies which evolved from the Phase II preliminary design. The turbojet,
turbofan and jet fuel starter unit costs were estimated from the cross-sections
without preparation of detail component drawings. The JFS, T/J and T/F assembly
drawings are shown in Figures 83`, 84 , 85 respectively.

The primary items which effect production unit cost have been identified
as:

1. Raw material and vendor costs
2. Manufacturing operations
3. Assembly
4. Test
5. Shipping

Item 1, raw material and vendor costs were obtained for all of the parts
procured as vendor supplied parts. At least three quotes for each major item were
obtained to get a representative estimate. As those parts are received by Teledyne
CAE receiving/inspection, they are sent through the various manufacturing processes
necessary to produce finished parts for engine assembly.

121
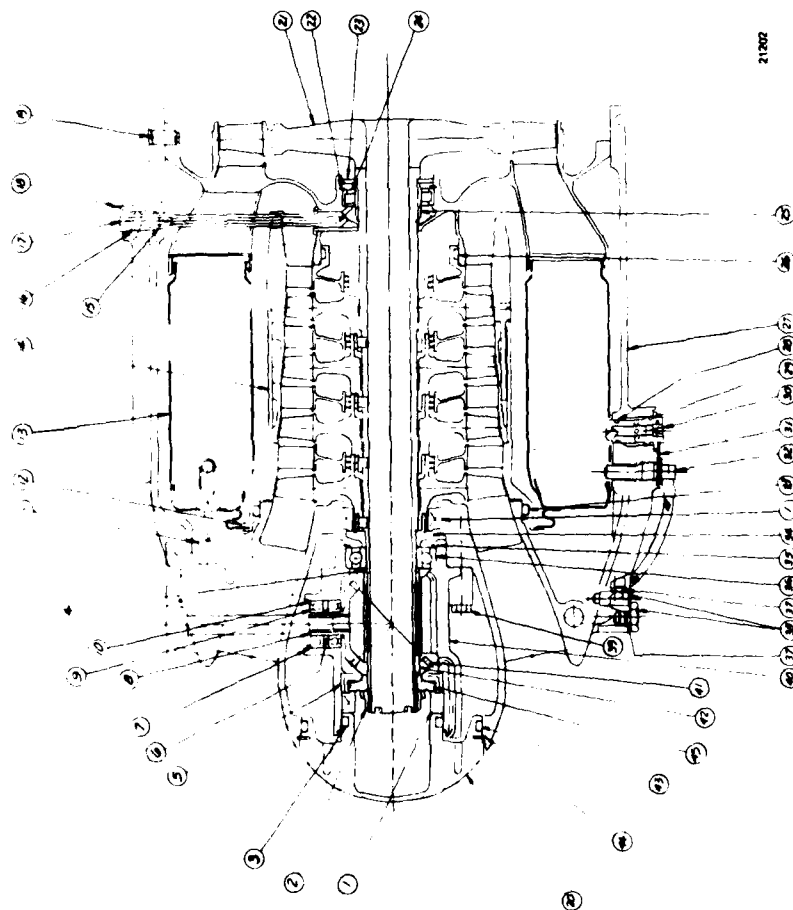
Figure 82 . Expendable Gasifier Assembly and Parts List.

122
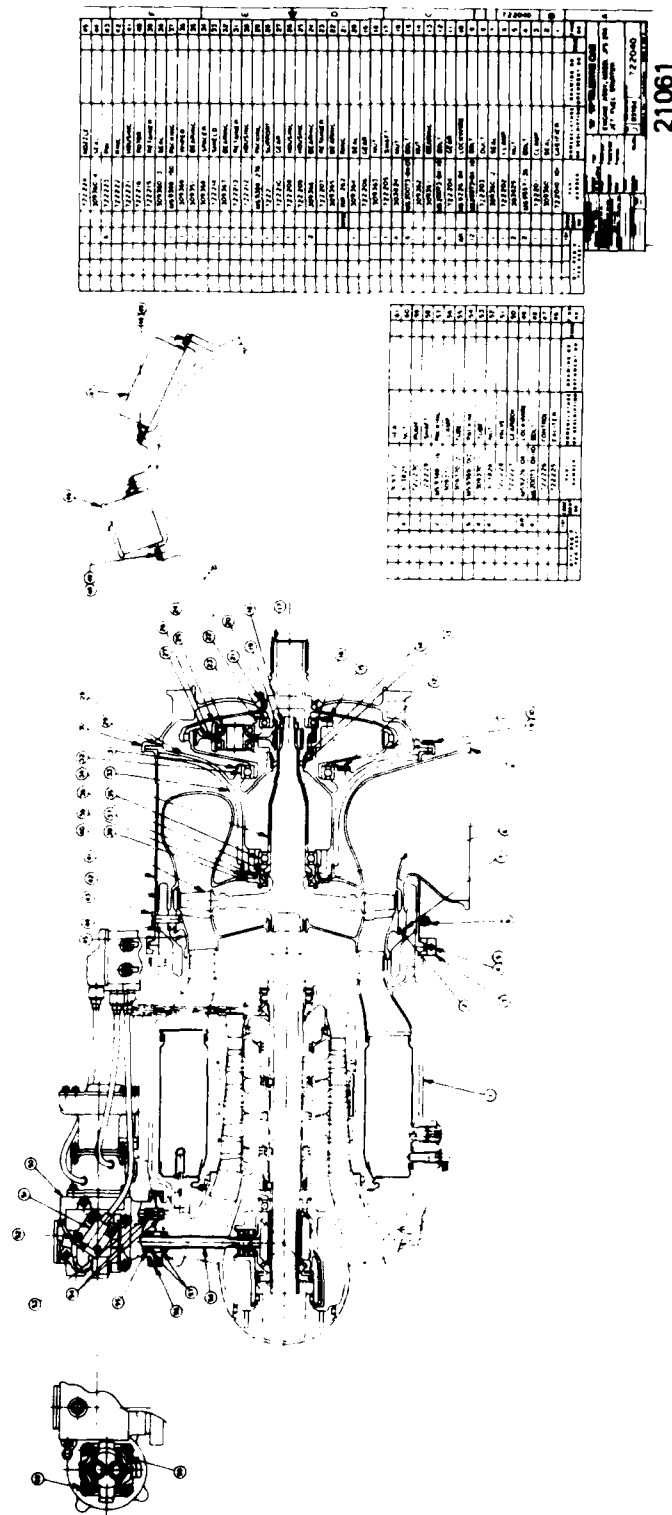
Figure 83 . JFS Assembly and Parts List.

21061

123

Figure 84. Turbojet Assembly and Parts List.

Figure 85 . Turbofan Assembly and Parts List.

The expendable gasifier estimate shown in Table 13 indicates that all vendor supplied (castings, fabrications and finished parts) will cost $3168. ($3900 including handling), in 1976 dollars.

The manufacturing cost analysis performed on the EG included the cost increments of manufacturing operations (machining time, set-up, tool support, inspection, scrap and rework, wash and degrease, manufacturing efficiency, nonrecurring tooling), assembly, test rework and shipping. The analysis indicated that approximately 132 hours will be required based on the 400th production engine. The variation of manufacturing hours required per engine over a production run of 2,500 engines was determined by applying an eighty percent improvement curve to all engines before the 400th engine and a 95 percent learning curve for all engines after the 400th. The average number of hours per engine is approximately 134 over the entire production run of 2,500 engines. Based on that analysis, it is estimated that all manufacturing costs will be approximately $3900 for a resulting total gasifier cost of $7800 not including cost of tooling. The cost of nonrecurring tooling for the gasifier is estimated to be approximately one million dollars. All cost analysis data is based on 1976 dollars.

The cost of the jet fuel starter (Model 206), turbofan (Model 406) and turbojet (Model 306) were determined by estimating the material and manufacturing labor required for the parts associated with each of the models and adding in the gasifier cost. The various models were estimated from the cross-section layouts on the basis of "similar to" parts from existing hardware prices converted to 1976 dollars using the appropriate escalation factor. The results of those analyses are shown in Tables 14, 15 and 16.

The cost of the various engine configurations are tabulated below:

	Model	Cost**
Expendable Gasifier	506	$ 7,800
Jet Fuel Starter*	206	$18,670
Turbofan*	406	$18,280
Turbojet*	306	$10,900

  * Includes controls, accessories and expendable gasifier.
** Includes G&A, Profit, Material Handling, Burden, in 1976 dollars.

TABLE 13

LABOR & MATERIAL FOR MODEL 506 EXPENDABLE GASIFIER
PART NO. 722010-102

Part Number	Part or Operation	Material Cost	Standard Labor hours
722010-102	Engine Assembly	---	8.35
722131-101	Shaft Balancing Assembly	---	2.85
722126-101	Shaft, Complete - Turbine	---	3.30
722127	Rotor, Turbine, H.P.	---	1.51
C722116	Rotor, Casting - Turbine	290	
722126-2	Shaft, H.P. Turbine	31	3.70
C722107	Rotor Casting, Axial Compressor (4 Required/Engine)	320 (Total)	
721131-1, 2, 3, 4	Rotors, Axial Stages (4 Required)	12 (Total)	5.44 (Total)
722176	Pin (12 Required)	6 (Total)	.11
722180	Baffle, Turbine Shaft		---
309349	Bearing, Roller	91.37	
309352	Seal, Oil (2 Required)	53.50 (Total)	
309350	Wiper, Oil Seal	13.75	
309351	Bearing, Ball	21.76	
309358	Wiper, Oil Seal	13.60	
309353	Nut	16.41	
722182-101	Stator Assembly, Axial Comp.	---	2.55
722183	Stator, 1st Stage	---	2.15
C722117	Stator, 1st Stage Casting	125	---
722184	Stator, 2nd Stage	---	1.48
C722118	Stator, 2nd Stage Casting	79	---
722185	Stator, 3rd Stage	---	1.58
C722119	Stator, 3rd Stage Casting	79	---
722186	Stator, 4th Stage	---	2.30
C722120	Stator, 4th Stage Casting	84	---
722159-101	Shell - Complete Combustor	212.50	---
722159-116	Shell - Combustor Components	50	---
C722158	Tube - Vaporizer Casting (14 Required)	68	---
722188	Nozzle - Fuel Inlet (14 Required)	1.50	---
722195	Main Frame & T.I.N. Assembly	---	1.45

TABLE 13 (continued)

LABOR & MATERIAL FOR MODEL 506 EXPENDABLE GASIFIER
(PART NO. 722010-102)

Part Number	Part or Operation	Material Cost	Standard Labor Hours
722105	Main Frame	------	3.79
C722104	Main Frame Casting	580	----
722103	Nozzle – Turbine Inlet	------	4.80
C722103	Nozzle – Turbine Inlet Casting	553	----
722189	Primer – Fuel	40	----
	(2 Required)	(Total)	
722191	Igniter (2 Required)	40	----
		(Total)	
722192-101	Tube Assembly – Fuel Lube	72.50	----
C722193	Tube – Fuel Lube Casting	7.50	----
722129	Housing – Front Bearing	------	2.11
C722128	Housing – Front Bearing Casting	28.80	----
722196	Gear Set – Bevel	170	----
308834	Bearing – Ball (2 Required)	30.40	----
		(Total)	
MS9388-428	"O" Ring	10	----
722200	Cover – Nose	5.20	----
Miscellaneous	Pins, Keys, Shims, "O" Rings, Fasteners, Spacers, Plugs, Etc.	63	1.95
	TOTAL	3168.0	48.42

128

TABLE 14

LABOR & MATERIAL FOR MODEL JFS 206 JET FUEL STARTER
(PART NO. 722040)

Part Number	Part or Operation	Material Cost	Standard Hours
722010-101	Gasifier Assembly	3168.0	48.42
722201	Clamp	9.0	
722202	Clamp	10.0	
309360-1 & 2	Seal	5.0	
722203	Duct	300.0	
722204	Gear	275.0	
309361	Bearing	15.0	
309362	Nut	8.0	
309363	Nut	5.0	
722205	Shaft	200.0	
722206	Gear	35.0	
309364	Seal	10.0	
309365	Bearing	75.0	
309366	Bearing (2 Required)	30.0	
722208	Housing	50.0	
722209	Housing	50.0	
722210	Gear	75.0	
722211	Support	300.0	
722212	Housing	150.0	
722214	Shield	75.0	
309367	Bearing	150.0	
309368	Spacer	50.0	
309351	Bearing	100.0	
309369	Wiper	50.0	
309360 (1 thru 4)	Seal (4 Total)	10.0	
722215	Retainer	30.0	
722216	Rotor	350.0	11.0

129

TABLE 14 (continued)

LABOR & MATERIAL FOR MODEL JFS 206 JET FUEL STARTER
(PART NO. 722040)

Part Number	Part or Operation	Material Cost	Standard Hours
722221	Housing	400.0	
722222	Ring	125.0	
722223	Pin (6 Required)	12.0	
722224	Nozzle	475.0	4.80
722225	Exciter	75.0	
722226	Control	1965.0	1.00
722227	Gearbox	250.0	
722228	Valve	50.0	
722229	Shaft	100.0	
722230	Pump	350.0	.50
309370-1 & 2	Tubes	20.0	
309372	Seal	20.0	
Miscellaneous	Clamps, Spacers, Fasteners, "O" Rings, Seals, Etc.	110.0	
	TOTAL	9453.0	65.72

130

TABLE 15

LABOR & MATERIAL FOR MODEL 306 TURBOJET
(PART NO. 722030)

Part Number	Part or Operation	Material Cost	Standard Labor Hours
722010-102	Gasifier Assembly	3168.0	48.42
722160	Shaft	60.0	
722163	Pump and Control	800.0	.5
722165	Clamp Assembly	9.0	
722166	Duct, Exhaust	250.0	16.5
Misc.	Clamps, Adapters, "O" Rings	18.0	
	TOTAL	4305.0	65.42

TABLE 16

LABOR & MATERIAL FOR MODEL 406 TURBOFAN
(PART NO. 722020)

Part Number	Part or Operation	Material Cost	Standard Labor Hours
722101-103	Gasifier Assembly	3168.0	48.42
722201	Clamp	9.0	
722236	Tube Assembly	75.0	
722237	Nozzle	553.0	4.80
722238	Duct	400.0	
722289	Shaft	700.0	11.00
722290	Duct	550.0	4.80
309386	Retainer	7.0	
309387	Bearing	100.0	
309389	Seal	45.0	
309390	Nut	15.0	
309391	Bearing	100.0	
309392	Wiper	50.0	
309352	Seal	45.0	
309388	Pin (6 Required)	12.0	
		(Total)	
722292	Rotor	300.0	9.00
722293	Housing	400.0	4.50
722294	Nose Cone	25.0	.50
722295	Gearbox	500.0	
722296	Tube Assembly	25.0	
722297	Shaft	100.0	
309393	Nut	15.0	
309370-3	Tube	75.0	
309370-4	Tube (4 Required)	140.0	
		(Total)	
	TOTAL	7409.0	83.02

SECTION 5.0 - DETAIL COMPONENT DESIGN

5.1 Compressor Design

5.1.1 Aerodynamic Design

The design point of the Expendable Gasifier (E.G.) four stage compressor is based on the sea level static jet fuel starter configuration performance objectives established in Phase I. The design goals as established in Phase I are shown in Table 17. The predicted performance of the final design hardware is also shown on this table. The compressor is predicted to achieve its flow goal and be within one percent of the pressure ratio and efficiency goals. The progression of the predicted performance from loop to loop in the iterative design procedure indicated that the design goals could be achieved with several more passes through the design process. However, due to the complexity of the design process, the time and effort required, and since the design was within one percent of all of its design goals it was frozen at this point. The deviation from the performance goals is probably within the tolerance of the design system.

TABLE 17

EXPENDABLE GASIFIER COMPRESSOR AERODYNAMIC DESIGN PERFORMANCE		
	Design Goal	Design Prediction After Phase III
Corrected Speed ($N/\sqrt{\theta}$) - RPM	33,060	33,060
Corrected Flow ($W\sqrt{\theta}/\delta$) - LBM/SEC	4.023	4.023
Pressure Ratio	2.86:1	2.83:1
Adiabatic Efficiency - %	80.0	79.2
Corrected Tip Speed - FT/SEC	900	900

27245

The compressor is a subsonic, highly loaded, four-stage axial machine derived from an upscale of the Teledyne CAE Model 469 compressor. The compressor has a very low tip speed (900 ft/sec), for its pressure ratio, such that stresses are minimized and the blading can be cast in aluminum. The high loading minimizes the number of stages and thus minimize parts and cost. The Model 469 rotor is shown in Figure 86.

The most notable of the low cost features is the use of a common rotor casting for all four stages. The casting is just machined to different outer diameters for each stage. This feature has been used by Teledyne CAE in the past very successfully on the Model 471 axial compressor (SCAD). Teledyne CAE also holds a patent on the common blading compressor design.

133
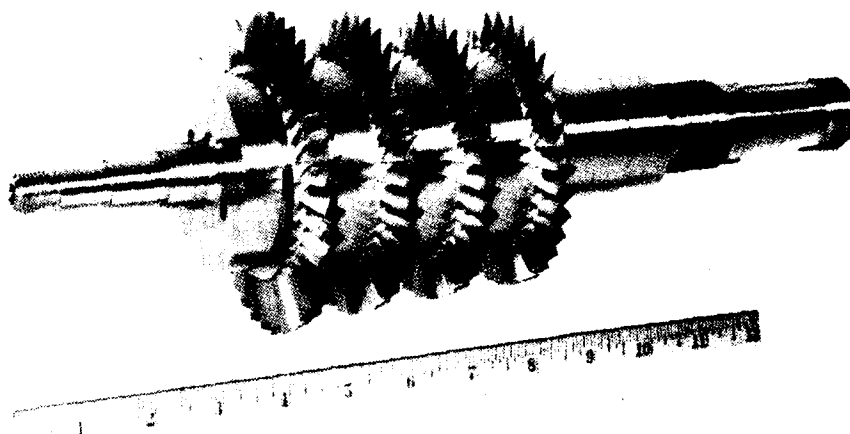
Figure 86.   Four-Stage Model 469 Axial Compressor Rotor.

The final E.G. compressor flowpath is shown in Figure 87. This flowpath was established in the Phase I preliminary design portion of this program and was unchanged in the final design. The radial dimensions are upscaled directly from the Model 469 compressor using a linear scale factor of 1.3166. The axial dimensions were modified to equalize the rotor and stator aspect ratios in each stage. Relative to the Model 469, rotor aspect ratios have been reduced and stator aspect ratios were increased as shown in the following table.

ASPECT RATIO COMPARISON

BLADE ROW	E.G.	MODEL 469
Rotor - 1	1.512	1.560
Stator - 2	1.514	1.341
Rotor - 2	1.315	1.366
Stator - 2	1.341	1.189
Rotor - 3	1.175	1.218
Stator - 3	1.201	1.067
Rotor - 4	1.059	1.098
Stator - 4	1.097	0.967

134

LOCATION	RH	RT	ZH	ZT	LOCATION	RH	RT	ZH	ZT
R1 IN	2.043	3.118	0.	0.113	R3 OUT	2.043	2.820	3.893	3.810
OUT	2.043	3.033	0.671	0.567	S3 IN	2.043	2.802	4.073	4.073
S IN	2.043	2.997	0.851	0.851	OUT	2.043	2.802	4.653	4.653
OUT	2.043	2.997	1.431	1.431	R4 IN	2.043	2.788	4.833	4.911
R2 IN	2.043	2.969	1.611	1.708	OUT	2.043	2.742	5.504	5.431
OUT	2.043	2.914	2.282	2.192	S4 IN	2.043	2.731	5.684	5.684
S2 IN	2.043	2.889	2.462	2.462	OUT	2.043	2.731	6.264	6.264
OUT	2.043	2.889	3.042	3.042	—	1.980	2.790	6.850	6.850
R3 IN	2.043	2.870	3.222	3.310	—	1.860	2.846	7.465	7.465

21909

Figure 87. Expendable Gasifier Compressor Flowpath.

The common rotor blading design requirement altered the aero design procedure from that normally used for subsonic axial compressors. The E.G. design method is compared to the normal design procedure in Figure 88. The usual procedure is to specify an RPM, flowpath geometry and pressure ratio requirements. The design program then calculates the resulting losses and velocity diagrams. The flowpath and specified pressure ratio distributions are then altered to achieve the desired efficiency and blade aerodynamic loading levels. When satisfactory velocity diagrams have been obtained, blading is designed to match those velocity diagrams.

To achieve a single rotor design for all four stages required the compressor to be designed with an off-design compressor performance program such that the blading could be specified first. In the method employed, the RPM, flowpath geometry and blading geometry were specified. The blading geometry definition included the number of airfoils in each blade row plus specification of chords and inlet and exit blade metal angle distributions versus radius for each blade and vane row. The off-design computer program then predicted the blade element losses and pressure ratios plus the velocity diagrams produced by that blading. The resulting pressure ratio, efficiency, and exit velocity profile are compared to the goals and the flowpath and/or blading geometry altered to achieve the desired results because a change in geometry in one of the front stages affects the performance of all the downstream blade rows. A detailed final design procedure logic path is shown in Figure 89.

135

NORMAL PROCEDURE   E.G. (COMMON BLADING) PROCEDURE

SPECIFY

RPM
FLOWPATH - - - -
PRESSURE RATIO'S - - -

CALCULATE

LOSSES
VELOCITY DIAGRAMS

COMPARE TO DESIRED LEVELS

LOSSES
AERO LOADINGS

CALCULATE

BLADING GEOMETRY
TO MATCH VELOCITY
DIAGRAMS

BLADE MANUFACTURING DATA

SPECIFY

RPM
FLOWPATH - - - -
BLADING GEOMETRY - - -

CALCULATE

BLADE ELEMENT PERFORMANCE
LOSSES
VELOCITY DIAGRAMS

COMPARE TO DESIRED VALUES

OVERALL PRESSURE RATIO
EXIT PROFILES
BLADING INCIDENCE ANGLES

BLADE MANUFACTURING DATA

21918

Figure 88. Subsonic Axial Compressor Design Procedure.

136

```
┌─────────────────────┐
│ FLOWPATH ESTABLISHED│
│ DURING PRELIMINARY  │
│ DESIGN PHASE        │
└─────────────────────┘
          │
          ▼
┌─────────────────────┐                      ┌──────────────────────┐
│ ESTABLISH ROTOR METAL│                     │ INCIDENCE MODEL      │
│ ANGLES BASED ON     │                      │ LOSS MODEL           │
│ PRELIMINARY DESIGN: │                      │ DEVIATION MODEL      │
│   *  ROTOR INLET METAL│                    │ BLOCKAGE ASSUMPTION  │
│      ANGLE DETERMINED│                      └──────────────────────┘
│      BY COMPUTER SOLN.│
│      FOR INLET DUCT │
│      AND REFERENCE  │
│      INCIDENCE ANGLE │
└─────────────────────┘
          │
          ▼
┌─────────────────────────┐
│ COMPUTER PROGRAM  08.116 │
├─────────────────────────┤
│ SUCCESSIVELY ADJUST STATOR│
│ METAL ANGLES:           │
│    * SATISFY STATOR REFERENCE│
│      INCIDENCE BY VARIATION│
│      OF INLET METAL ANGLE│
│    * SATISFY DOWNSTREAM ROTOR│
│      REFERENCE INCIDENCE BY│
│      VARIATION OF EXIT METAL│
│      ANGLE              │
└─────────────────────────┘
```

Figure 89.   Expendable Gasifier Compressor - Detail Design Procedure Logic Path.

137

The velocity diagram solutions were obtained through the use of Teledyne CAE's computer program 08.116. This program performs axial compressor off-design performance calculations, solving the full radial equilibrium equation, including the effects of streamline curvature and radial gradients in enthalpy and entropy. Details of the basic program are given in Reference 4.

The use of a compressor off-design performance program requires the following variables of the basic flow model to be specified:

1. Aerodynamic blockage at each computing station
2. A loss model
3. Reference or minimum loss incidence angles
4. A reference deviation angle model or rule

The models used for the above variables for this design are as follows:

Blockage factor is an allowance in the velocity diagram solution to account for the flow area blocked by blade or vane wakes as well as due to end wall boundary layers.

The aerodynamic blockage factors used for this design are shown in Figure 90. Blockage factor is the unblocked annulus area divided by the total area. The blockages used increase by three percent across each rotor and decrease by 1-1/4 percent across each stator. These magnitudes are a result of a number of Teledyne CAE tests of 3 to 5 lbm/sec axial flow compressors which have shown that small compressors have rather large blockages at rotor exits with a decrease in blockages through stator rows.

The small size and high aerodynamic loadings of this design have ruled out the use of Teledyne CAE's conventional large size compressor loss correlation. For this design, several sources from the recent literature, References 5 and 6, were surveyed to determine the applicability of various loss parameter-diffusion factor correlations used in similar designs. The loss correlations which were derived from this data and used in this design are shown in Figures 91 and 92. These correlations were input to the velocity diagram program such that the program could iterate on blade element losses. The final values of total pressure loss coefficient and diffusion factors are shown in Figures 93 through 96 for the rotors and 97 through 100 for the stators.

Reference or minimum loss incidence angles must be specified for each blade row since an off-design compressor performance program was used for this design. This is required such that when the blading incidence angles are at non-optimum (or reference) values, the calculated losses will be increased from those calculated from the loss correlation curves, and blade element turning or deviation angles can be adjusted from the reference values.

BLOCKAGE FACTOR

0.97
0.96
0.95
0.94
0.93
0.92
0.91
0.90
0.89
0.88

ROTOR 1
INLET

ROTOR 1
EXIT

STATOR 1
EXIT

ROTOR 2
EXIT

STATOR 2
EXIT

ROTOR 3
EXIT

STATOR 3
EXIT

ROTOR 4
EXIT

STATOR 4
EXIT

STATION

27247
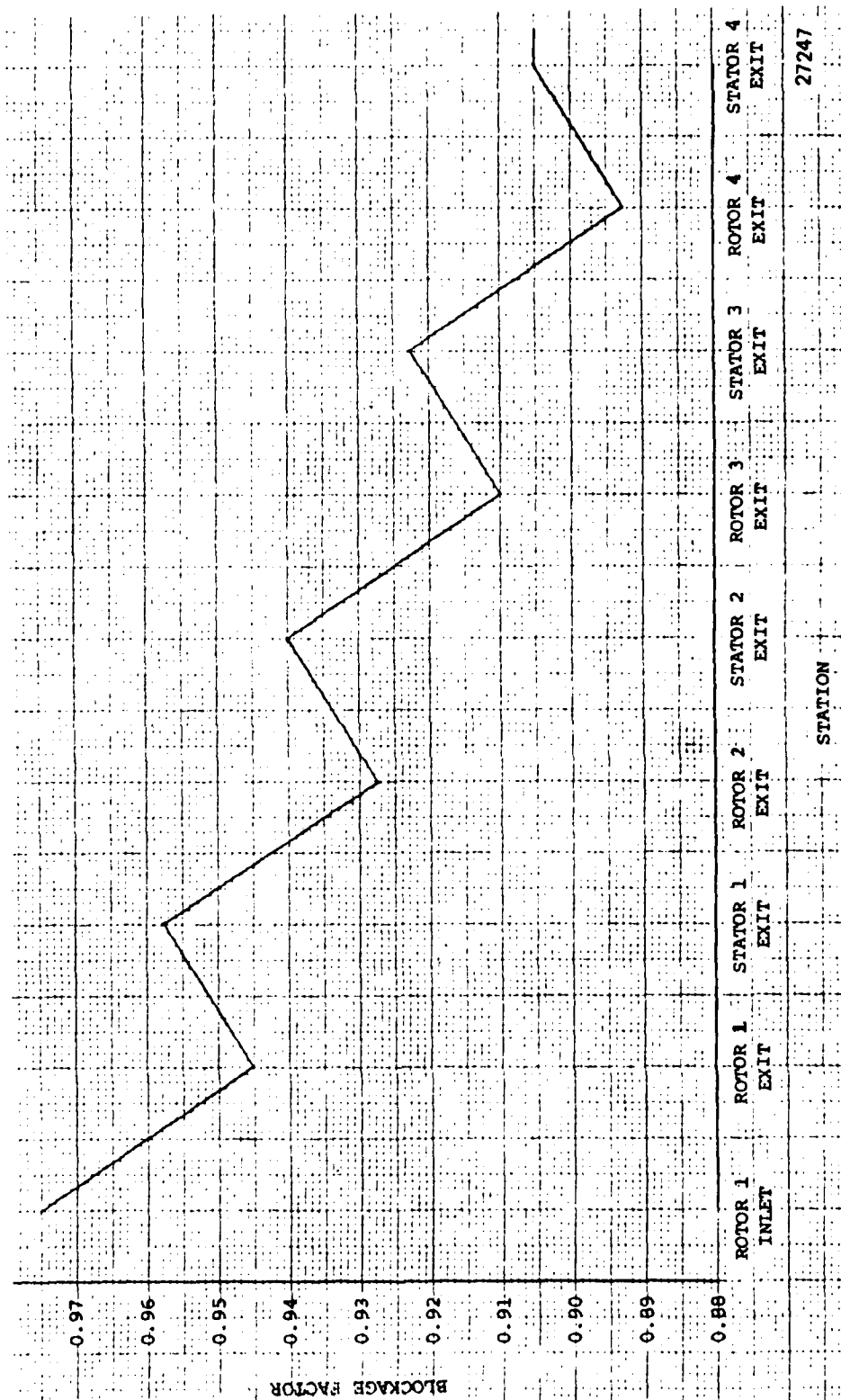
Figure 90. Expendable Gasifier Compressor Design Blockage Distribution.

139
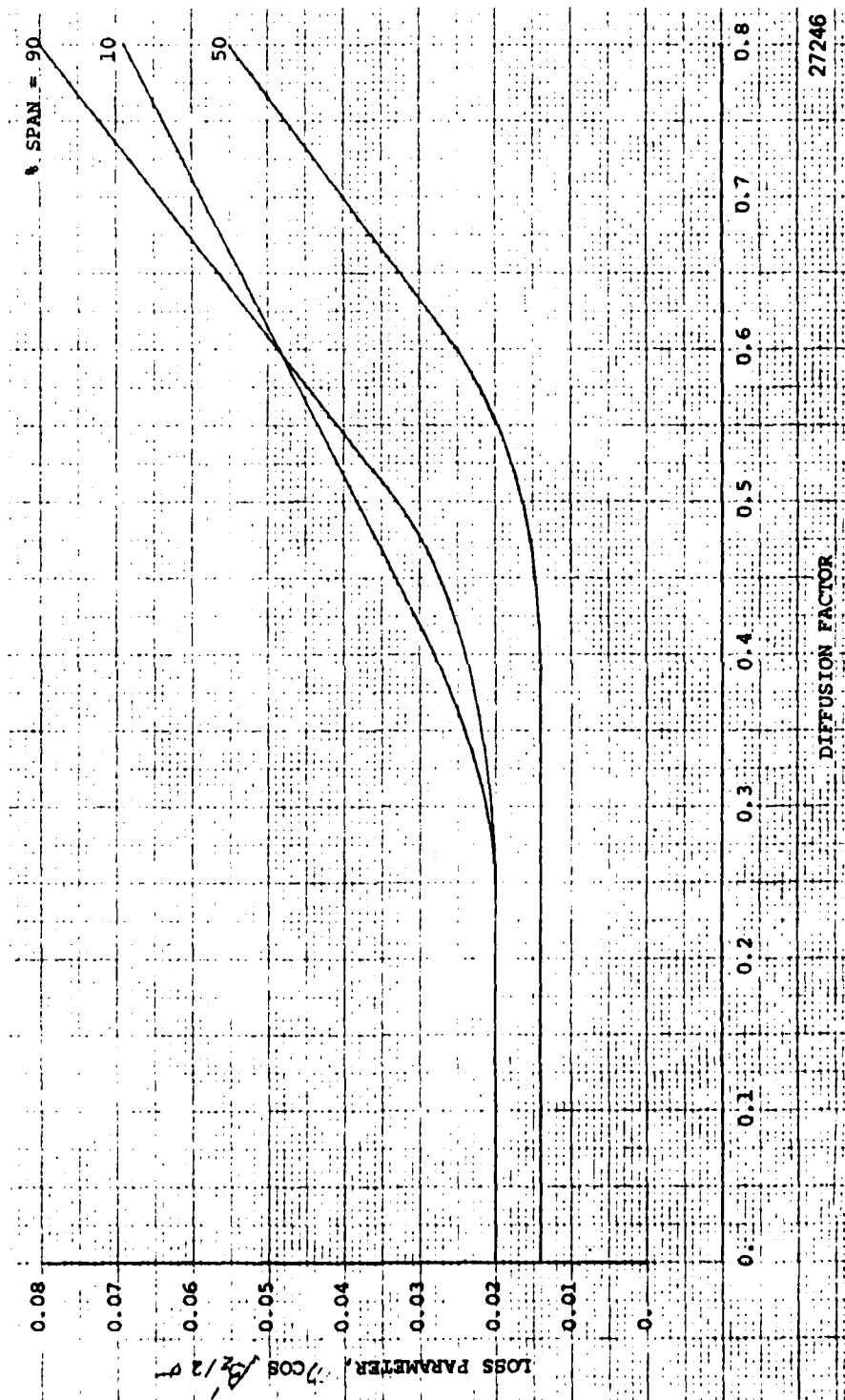
Figure 91. Expendable Gasifier Compressor Design Loss Parameter vs. Diffusion Factor Rotors.

140
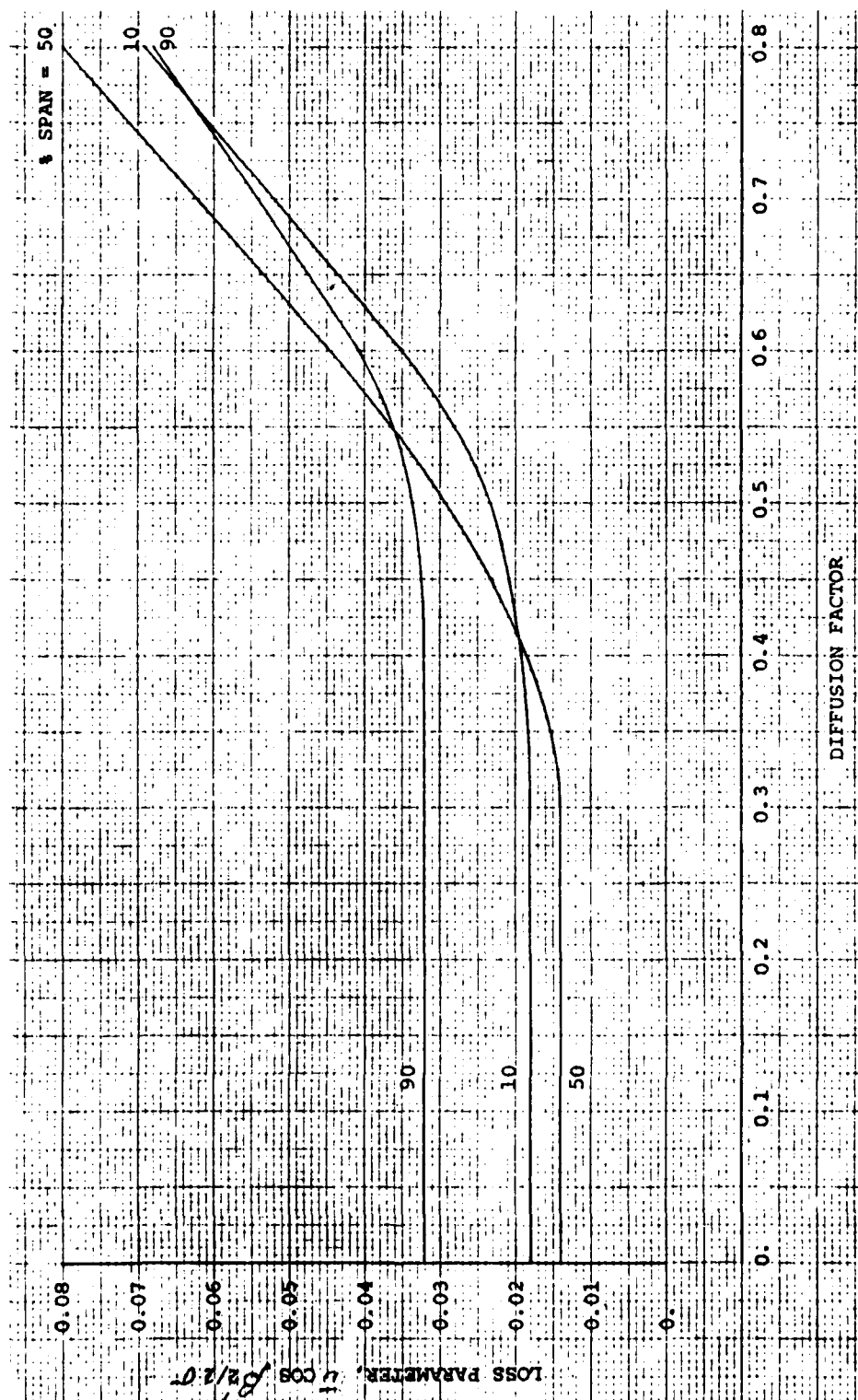
Figure 92. Expendable Gasifier Compressor Design Loss Parameter vs. Diffusion Factor Stators.
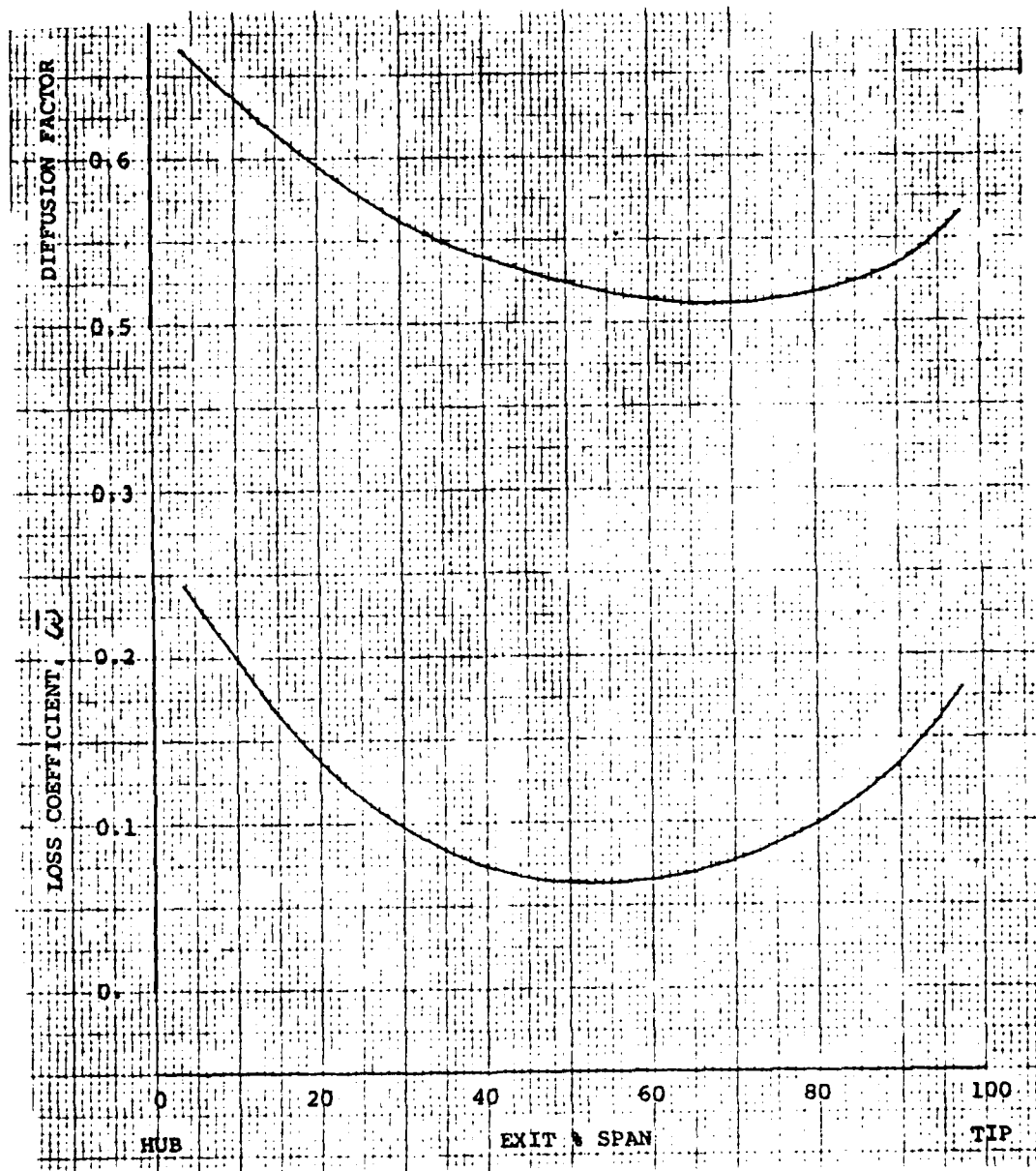
141

Figure 93. Expendable Gasifier Compressor Loss Coefficient and Diffusion Factor
Profiles First Stage Rotor.
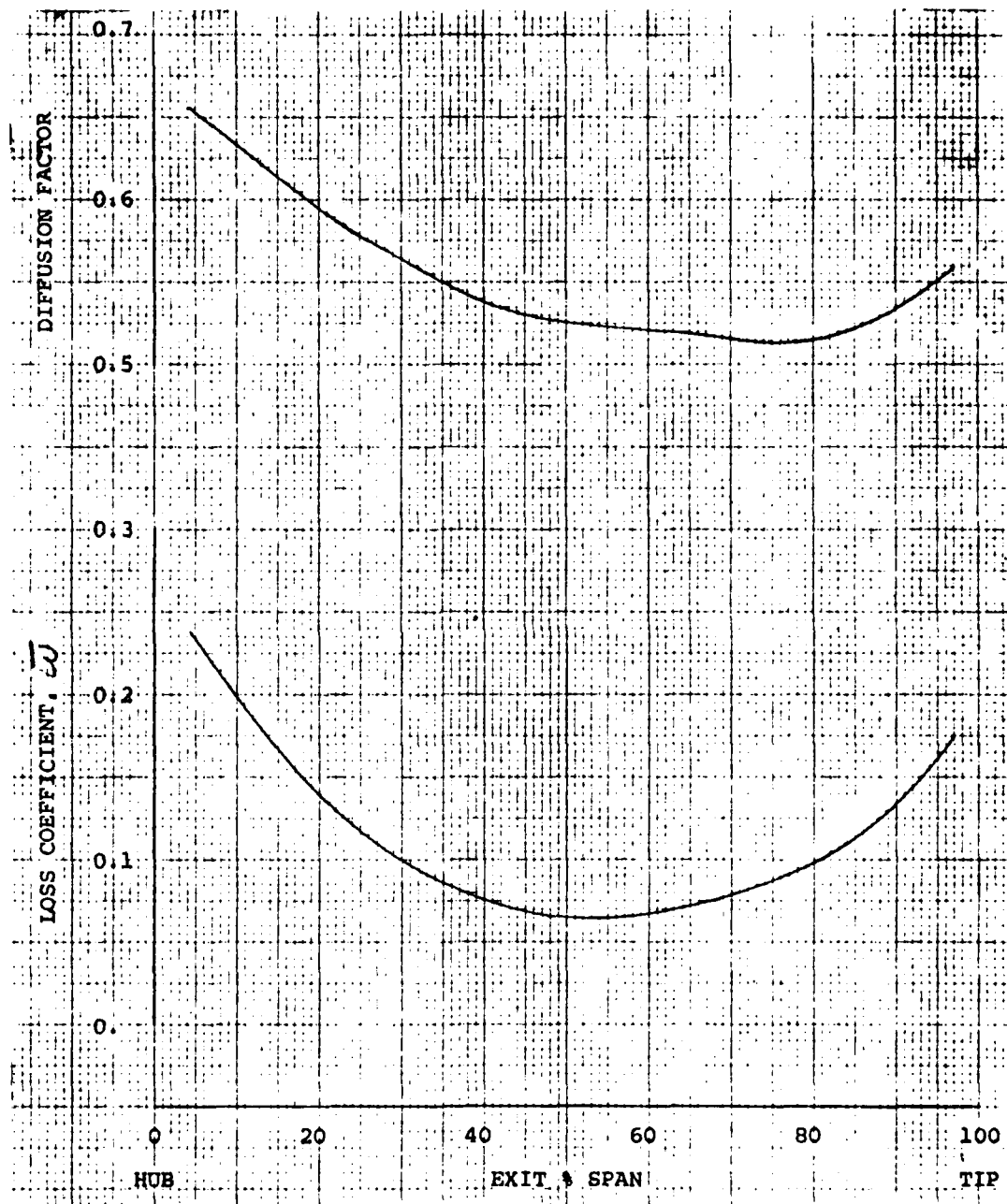
Figure 94. Expendable Gasifier Compressor Loss Coefficient and Diffusion Factor
Profiles Second Stage Rotor.

143
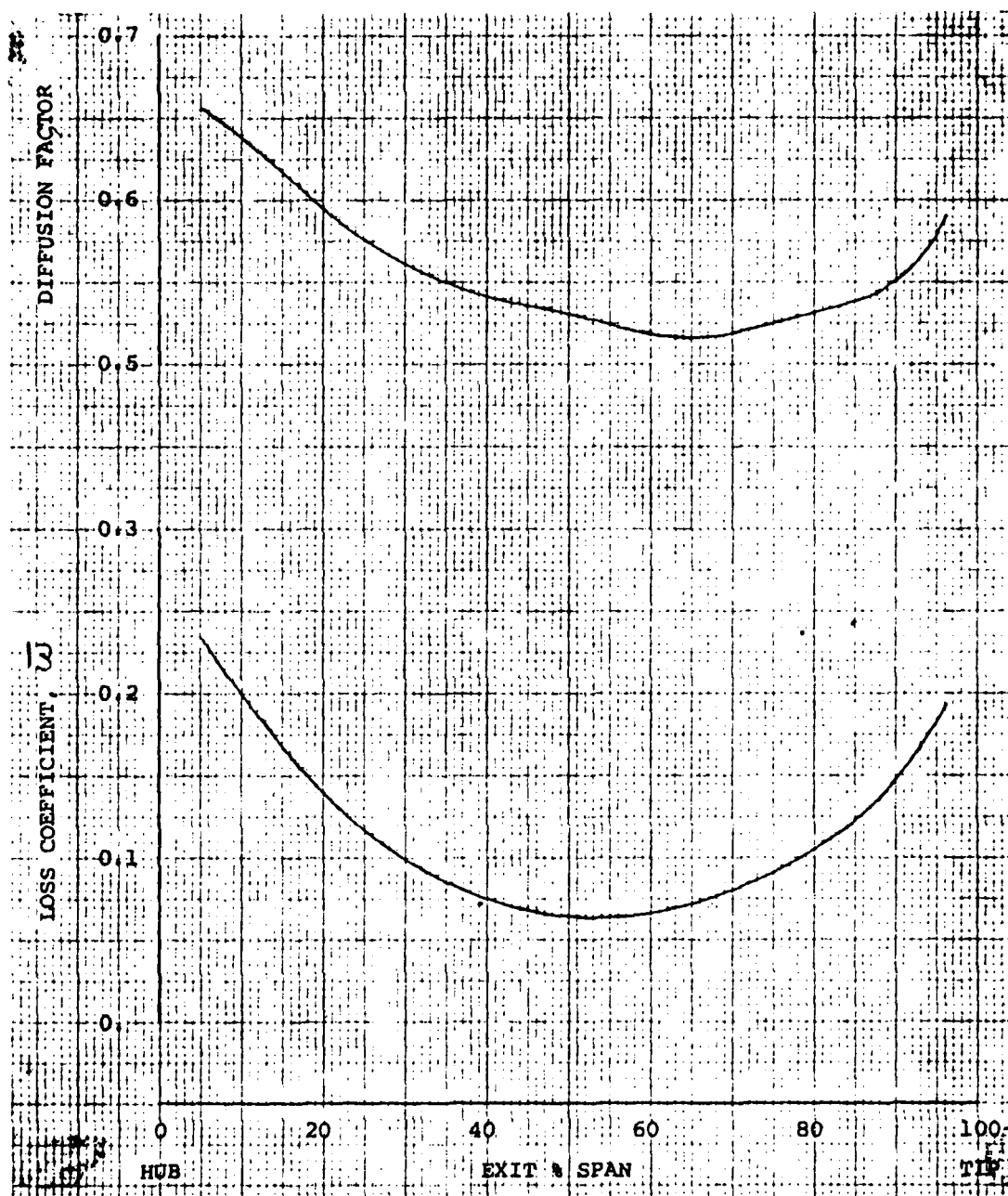
Figure 95. Expendable Gasifier Compressor Loss Coefficient and Diffusion Factor Profiles Third Stage Rotor.

144
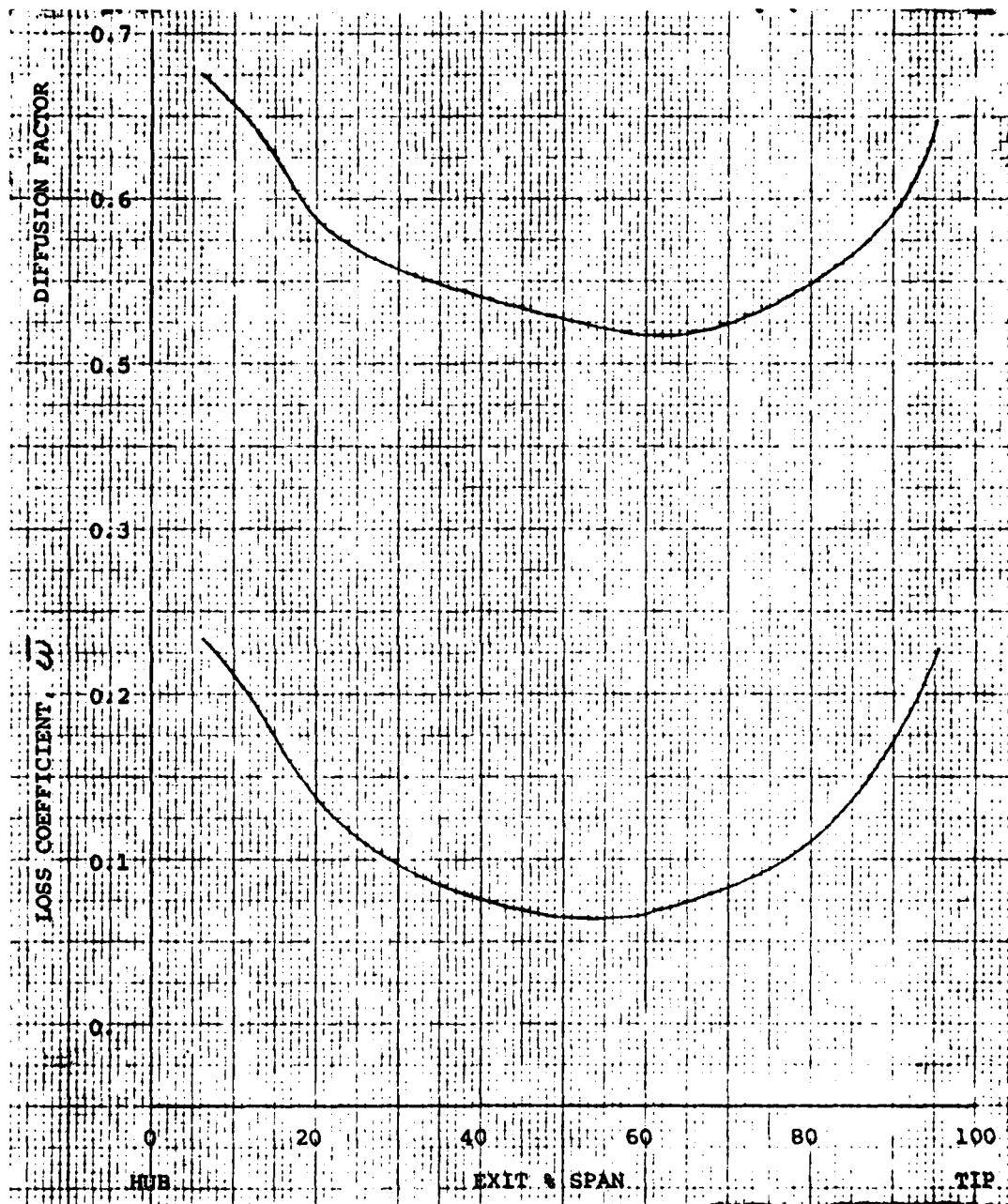
27269

Figure 96. Expendable Gasifier Compressor Loss Coefficient and Diffusion Factor Profiles Fourth Stage Rotor.

145

27250
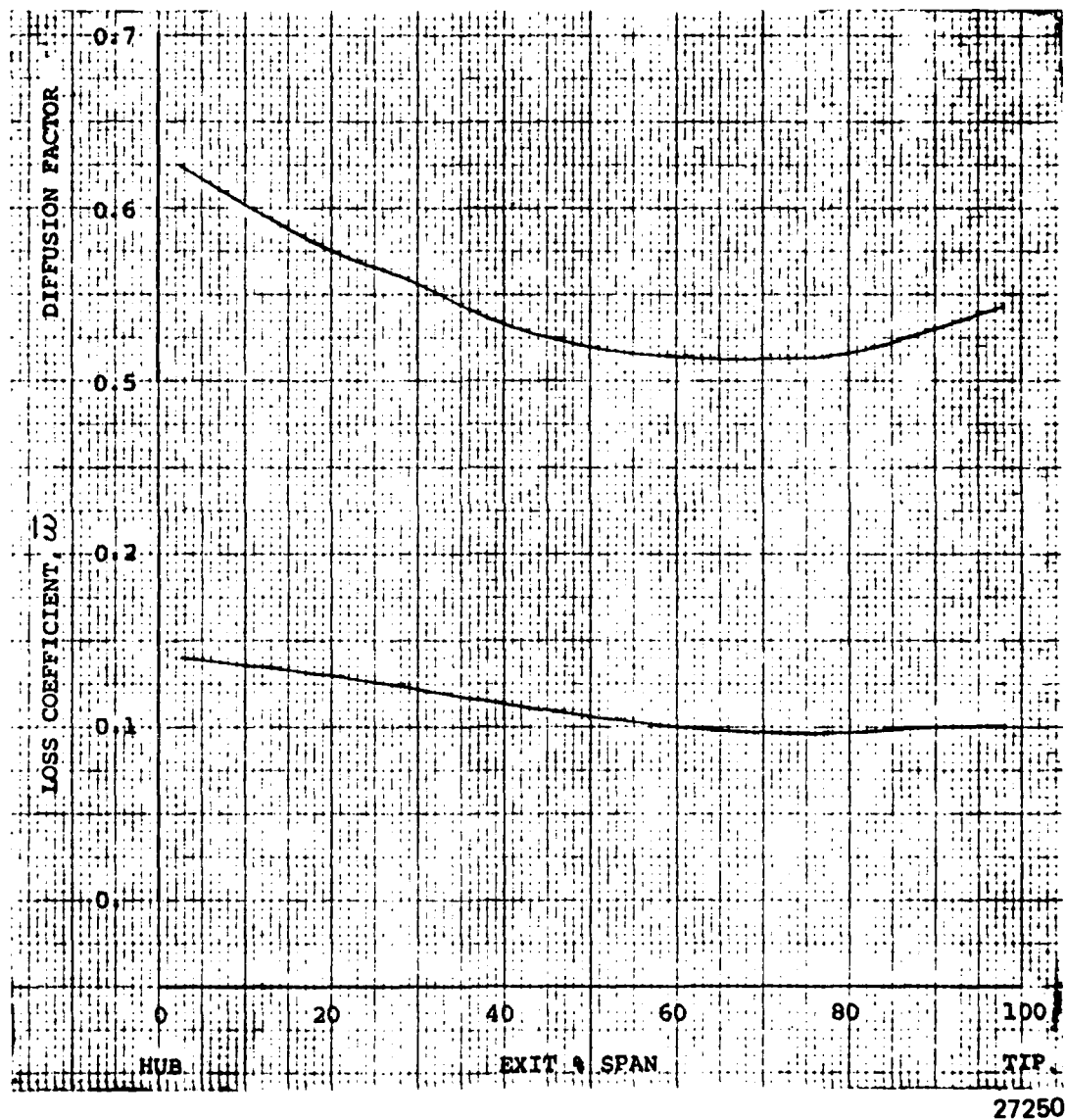
Figure 97. Expendable Gasifier Compressor Loss Coefficient and Diffusion Factor Profiles First Stage Stator.
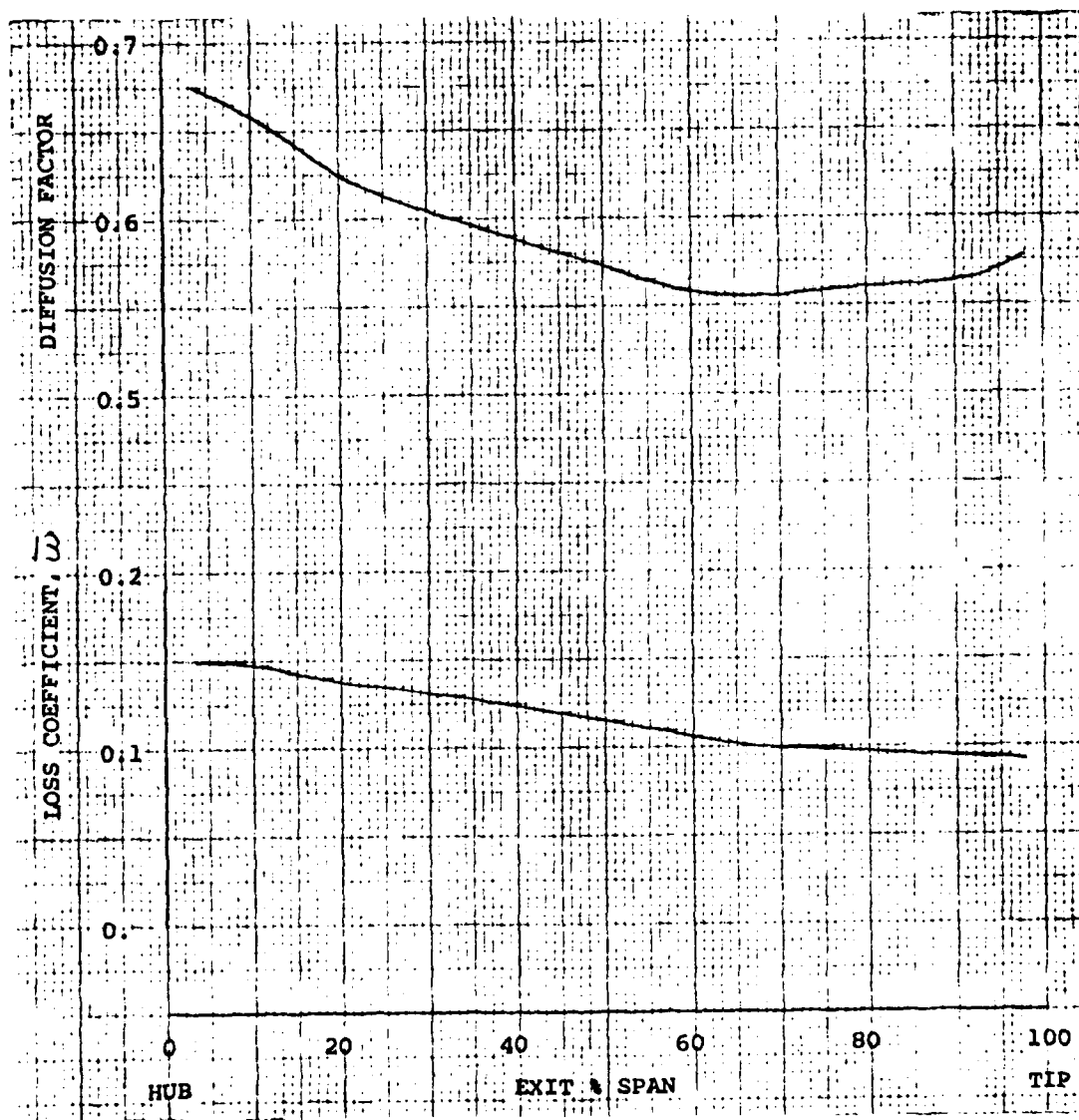
27270

Figure 98. Expendable Gasifier Compressor Loss Coefficient and Diffusion Factor Profiles Second Stage Stator.

147
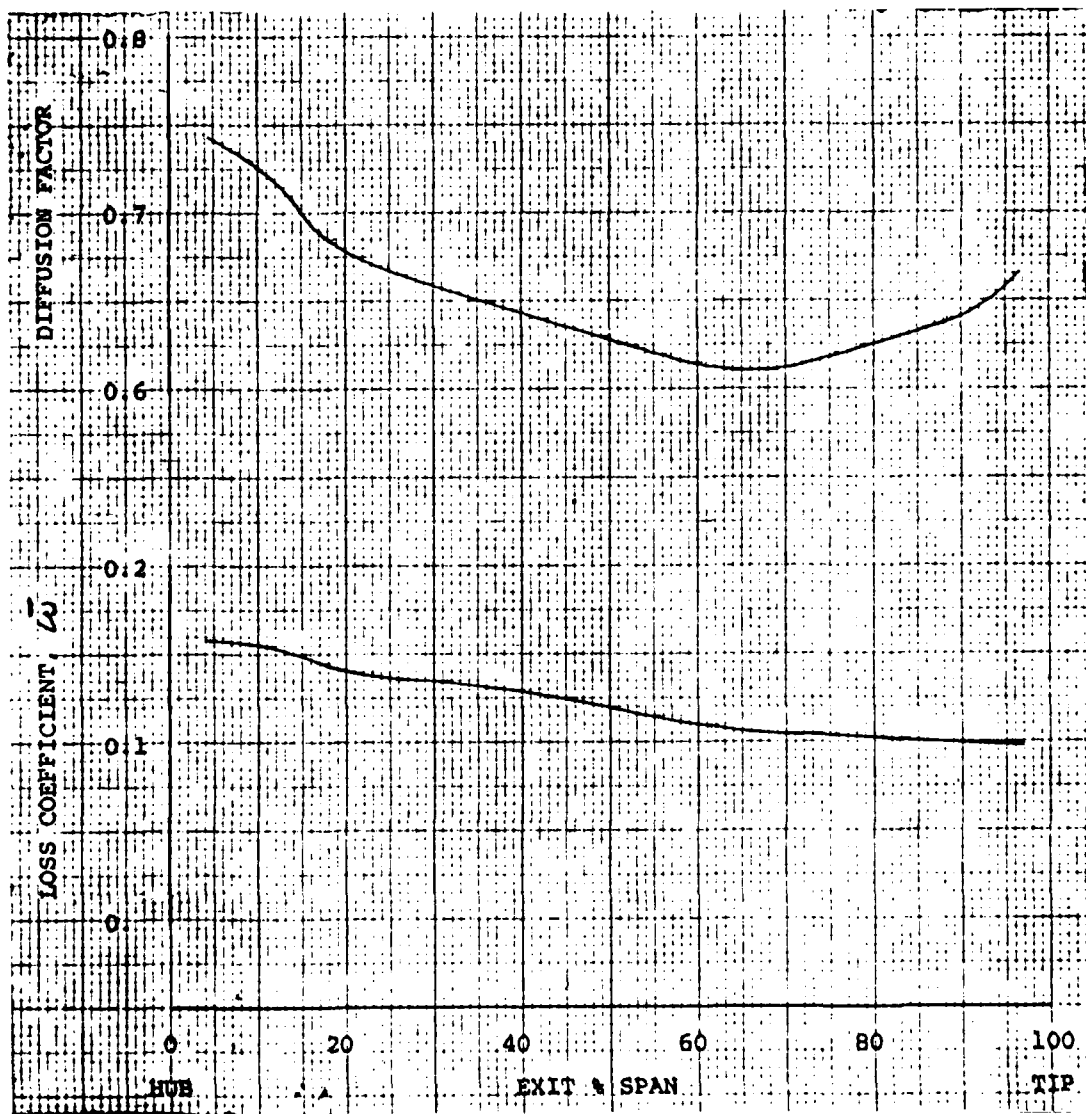
27248

Figure 99. Expendable Gasifier Compressor Loss Coefficient and Diffusion Factor Profiles Third Stage Stator.
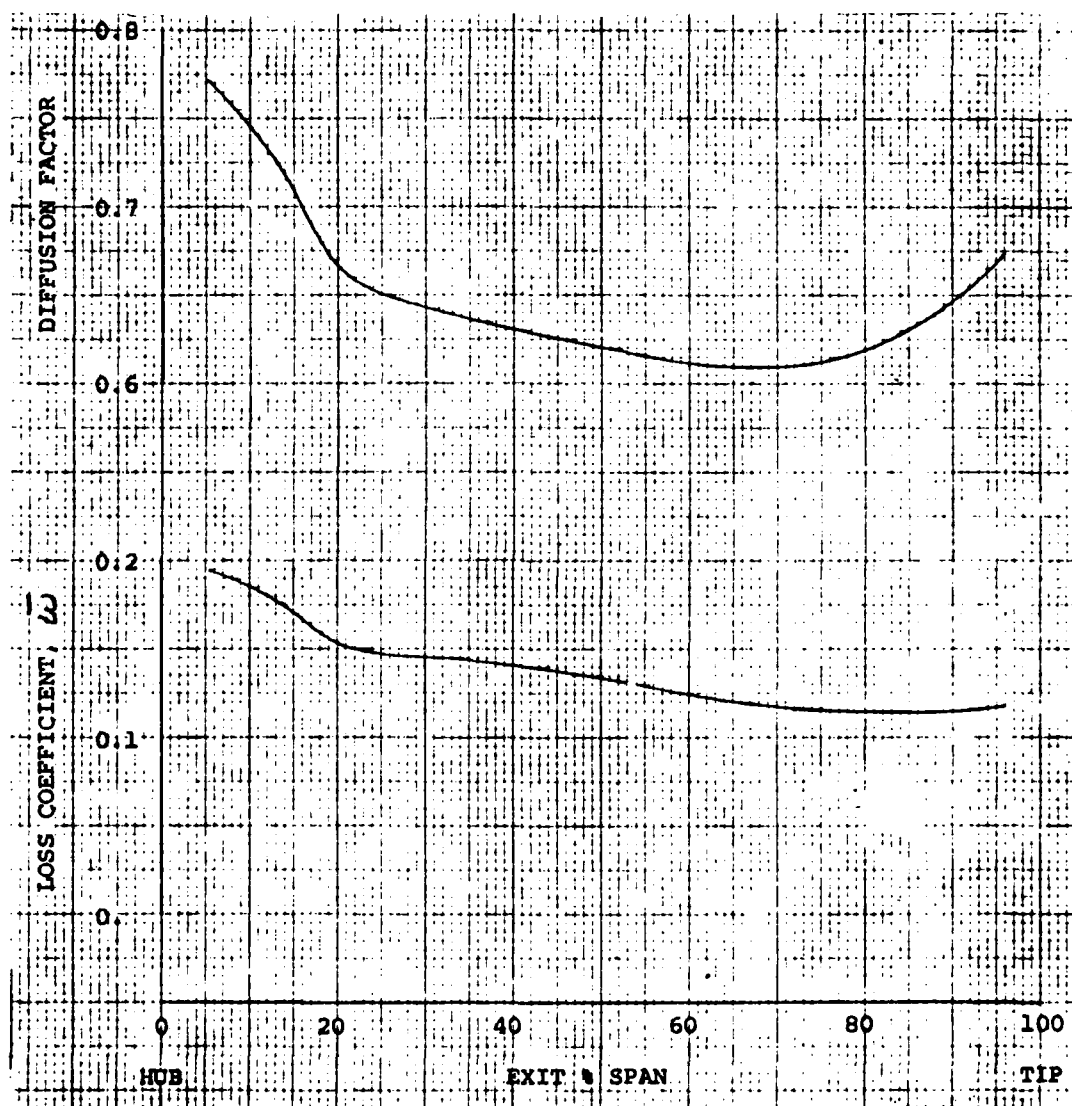
Figure 100. Expendable Gasifier Compressor Loss Coefficient and Diffusion Factor Profiles Fourth Stage Stator.

149

Reference incidence for both rotors and stators was initially set at levels based on the design selection for the Teledyne CAE Model 555 redesigned third stage blading. However, as shown in Figure 101, the first stage rotor incidence profiles were found to be very close to those resulting from the NASA 2-D incidence rule, Equation 286 of Reference 7, with the correction for relative inlet Mach number omitted. Thus, the NASA 2-D rule was selected for the definition of rotor reference incidence in the final design. The original assumption of Model 555 incidence for the stator was retained for the final design.

The blade element deviation angles are composed of a reference or design deviation angle plus a correction to account for any off reference incidence condition. The reference deviation angle rule used for this design is a modified form of Carter's rule plus an empirical deviation angle increment. This deviation angle rule has been used at Teledyne CAE very successfully on many recent designs.

The final results of running the velocity diagram program are summarized in Table 18.. The most notable items on this table are the diffusion factors, which in an aerodynamic loading factor; these values are high however, since they have been accounted for in the loss calculations they should present no problems.

Figure 102 shows the stage exit total pressure profiles. Normal design practice is to design each stage for a flat profile. The common blading technique doesn't allow this. In this design, the final rotor blade design results in excessive tip work in the front stages to minimize the profiles in the rear stages where normally an even higher tip work would be employed. However, the final design does result in very acceptable velocity gradients throughout the compressor which can be seen in axial velocity profiles shown in Figures 103 through 106. The compressor exit velocity profile is only 70 feet per second.

The air angles through the compressor are shown in Figures 107 through 110. The stator leading edge air angles are relatively high due to the high diffusion factors; however, stator camber angles are sufficiently high to achieve the desired air turning.

The detailed blading geometry is developed in the velocity diagram solution, whereas the actual blading coordinates and manufacturing sections are generated in program 08.130 (Reference 8). The blading is generated on conical approximations of the design streamlines. Manufacturing sections are then interpolated from these data by taking planar slices through the blade at a number of radial positions. The rotor blade uses double circular arc blade profiles. The stators, since they are at lower Mach numbers, use a circular arc mean line with the maximum thickness moved forward to 40 percent chord for lower losses and more flow range.

150
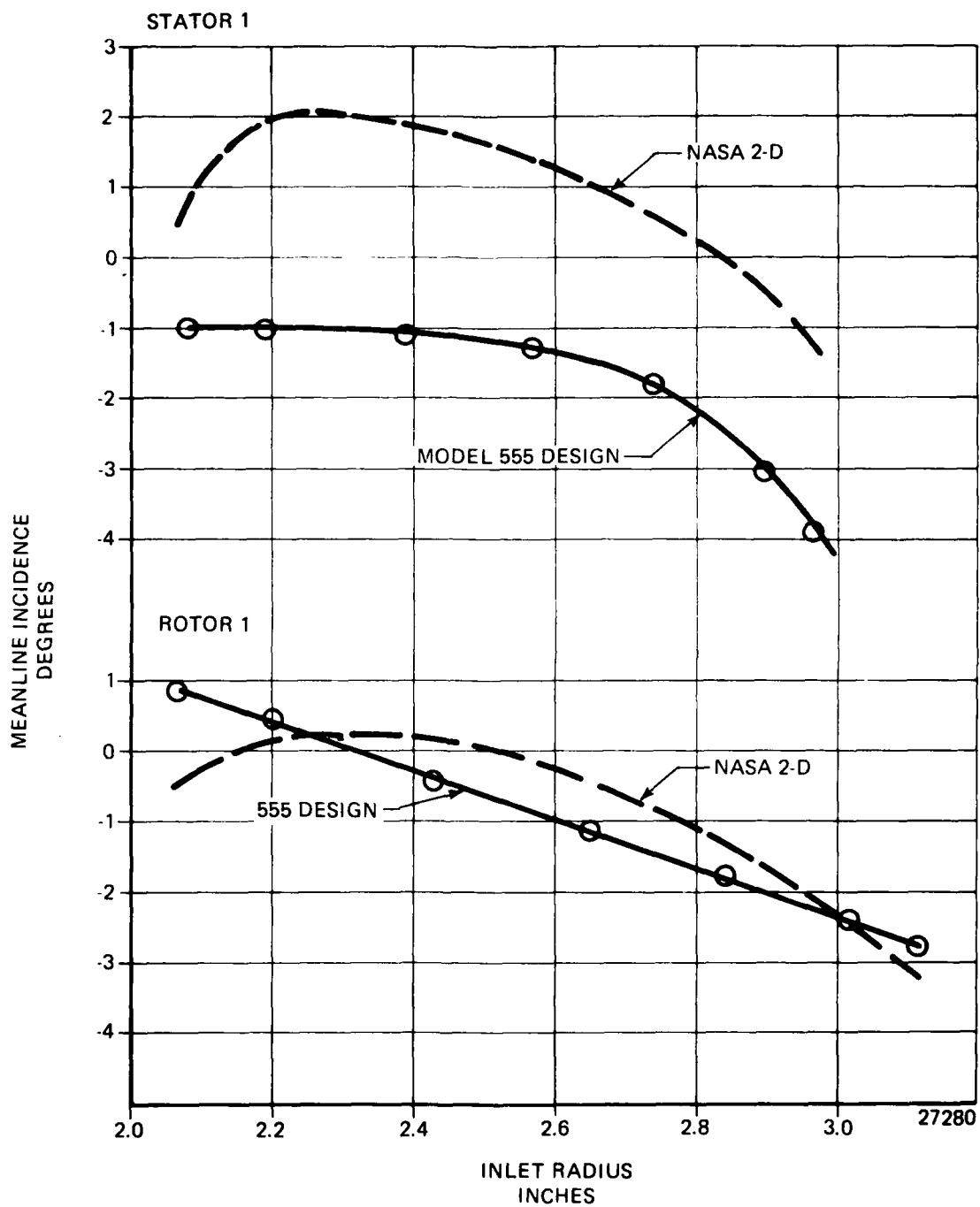
Figure 101. Expendable Gasifier Compressor First Stage Reference Rotor and Stator Incidence.

TABLE 18

EXPENDABLE GASIFIER COMPRESSOR
AERODYNAMIC DESIGN SUMMARY

Corrected Speed, rpm	33,055
Corrected Flow, lbm/sec	4.023
Pressure Ratio	2.827
Adiabatic Efficiency, percent	79.2
First Rotor Inlet Tip Speed, ft/sec	899.1
First Rotor Inlet Tip Radius, in.	3.117

		STAGE			
		1	2	3	4
Mass Averaged Stage Pressure Ratio		1.361	1.308	1.273	1.247
Mass Averaged Stage Adiabatic Efficiency		81.6	81.6	81.5	80.6
Rotor Inlet	Hub	2.5	2.9	3.6	4.5
Percent Radial Height	Mean	46.2	45.6	45.6	45.1
	Tip	98.3	98.0	97.5	96.7
	Hub	1.94	1.94	1.94	1.94
Rotor Solidity	Mean	1.60	1.65	1.68	1.71
	Tip	1.32	1.38	1.43	1.48
	Hub	1.98	1.69	1.40	1.58
Stator Solidity	Mean	1.65	1.45	1.22	1.40
	Tip	1.38	1.23	1.05	1.22
Rotor Aspect Ratio $\frac{\text{Average Height}}{\text{Chord}}$		1.512	1.315	1.175	1.059
Stator Aspect Ratio		1.514	1.341	1.201	1.097
Rotor Inlet Hub-Tip Ratio		0.655	0.688	0.711	0.733
Stator Inlet Hub-Tip Ratio		0.682	0.707	0.729	0.748
	Hub	0.665	0.656	0.656	0.674
Rotor Diffusion Factor	Mean	0.527	0.528	0.535	0.532
	Tip	0.566	0.558	0.590	0.648
	Hub	0.625	0.664	0.743	0.756
Stator Diffusion Factor	Mean	0.530	0.577	0.635	0.621
	Tip	0.555	0.578	0.661	0.672

27268

Figure 102. Expendable Gasifier Compressor Stage Exit Total Pressure Profiles.

Figure 103. Expendable Gasifier Compressor First Stage Axial Velocity Profiles.

154
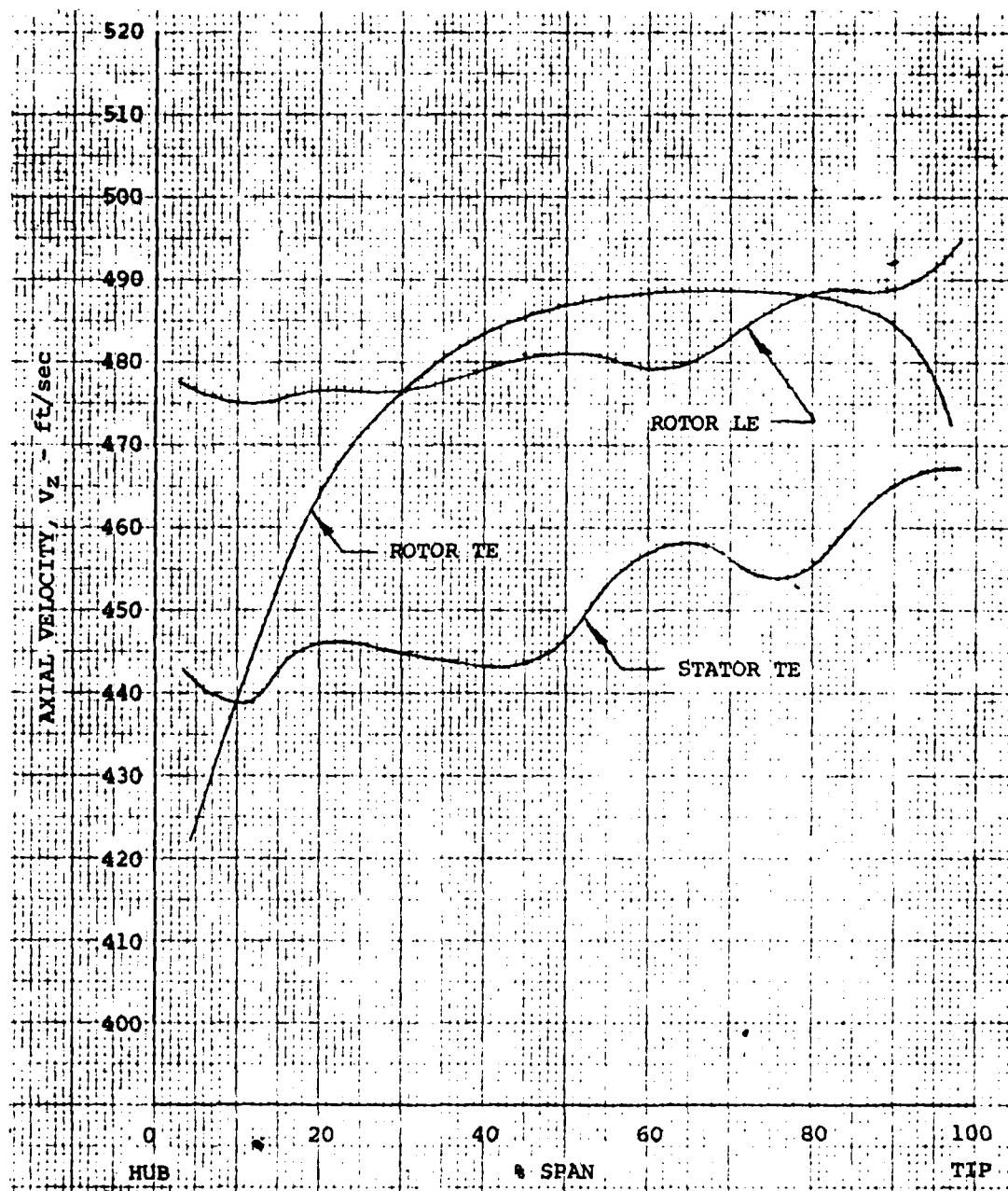
Figure 104. Expendable Gasifier Compressor Second Stage Axial Velocity Profiles.

155
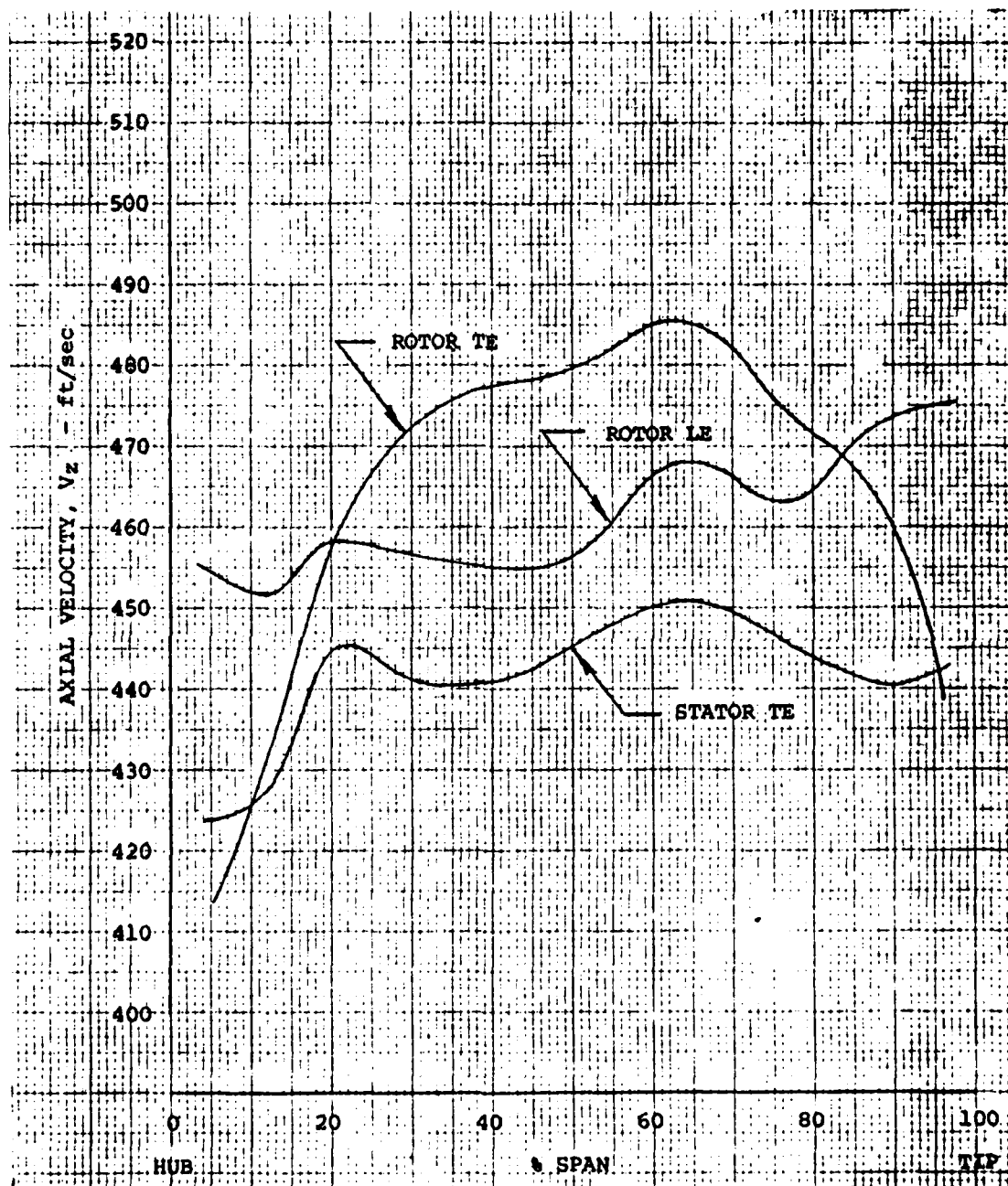
Figure 105. Expendable Gasifier Compressor Third Stage Axial Velocity Profiles.

156
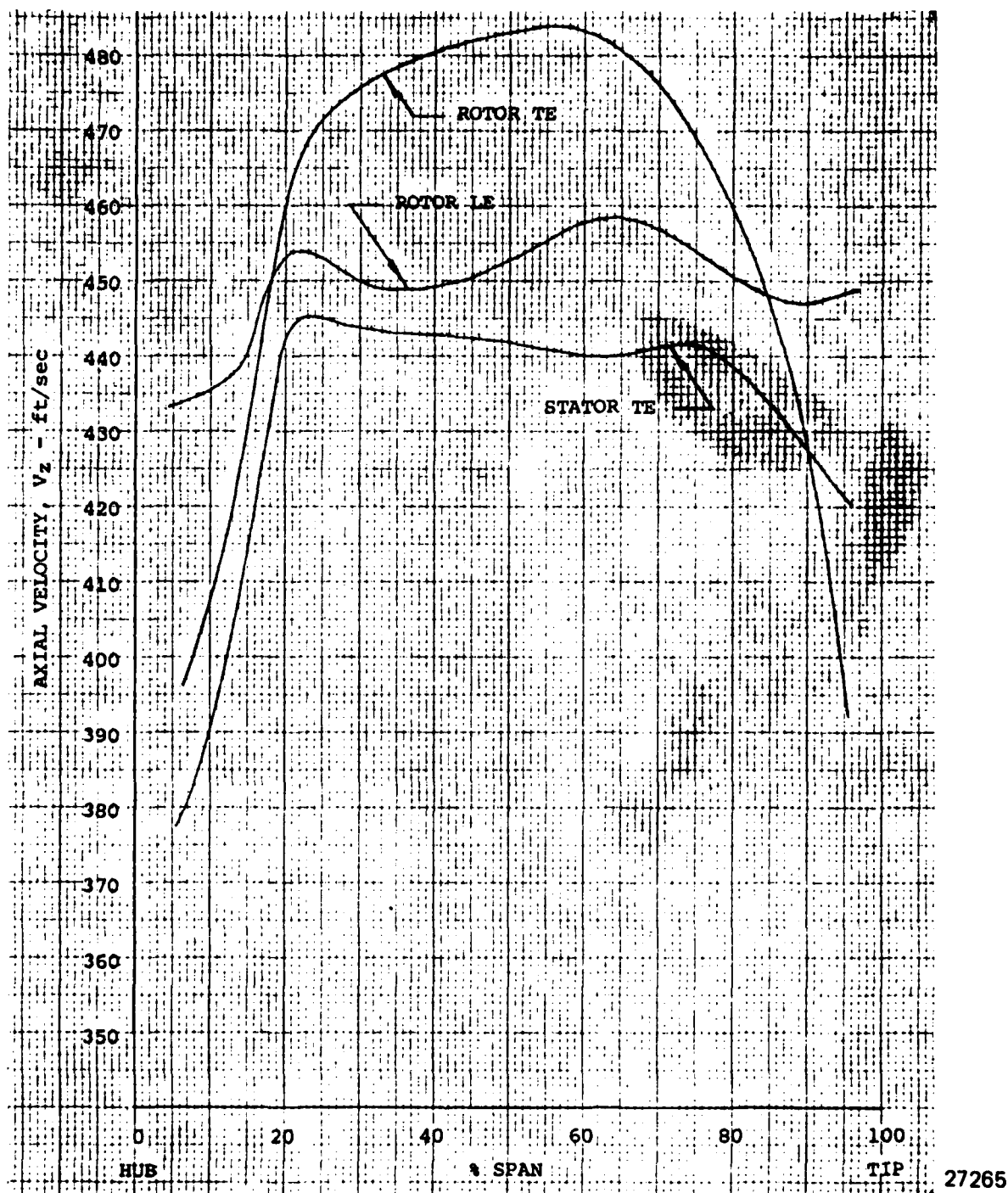
Figure 106. Expendable Gasifier Compressor Fourth Stage Axial Velocity Profiles.

157
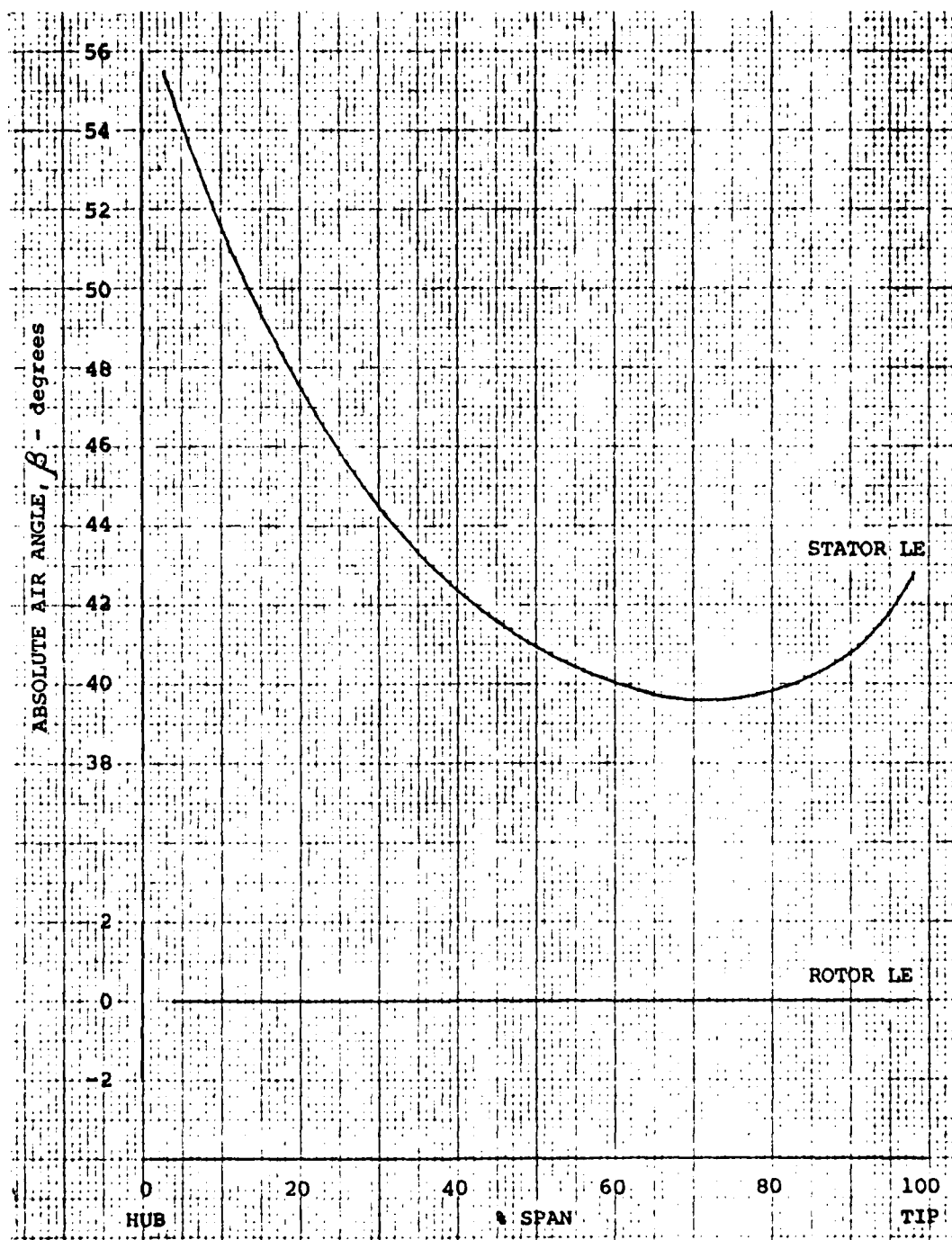
Figure 107. Expendable Gasifier Compressor First Stage Absolute Air Angle Profiles.

158
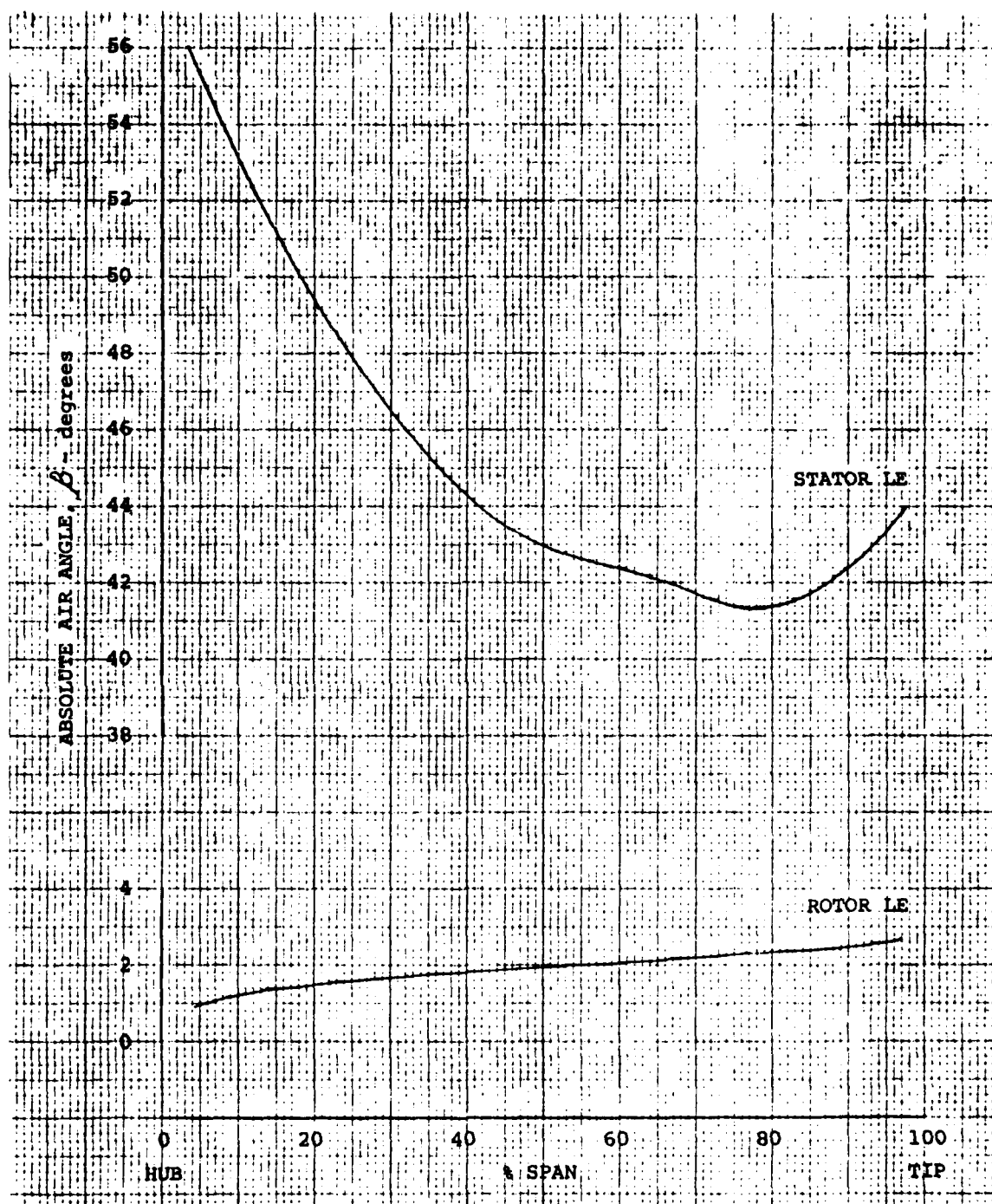
Figure 108. Expendable Gasifier Compressor Second Stage Absolute Air Angle Profiles.

159
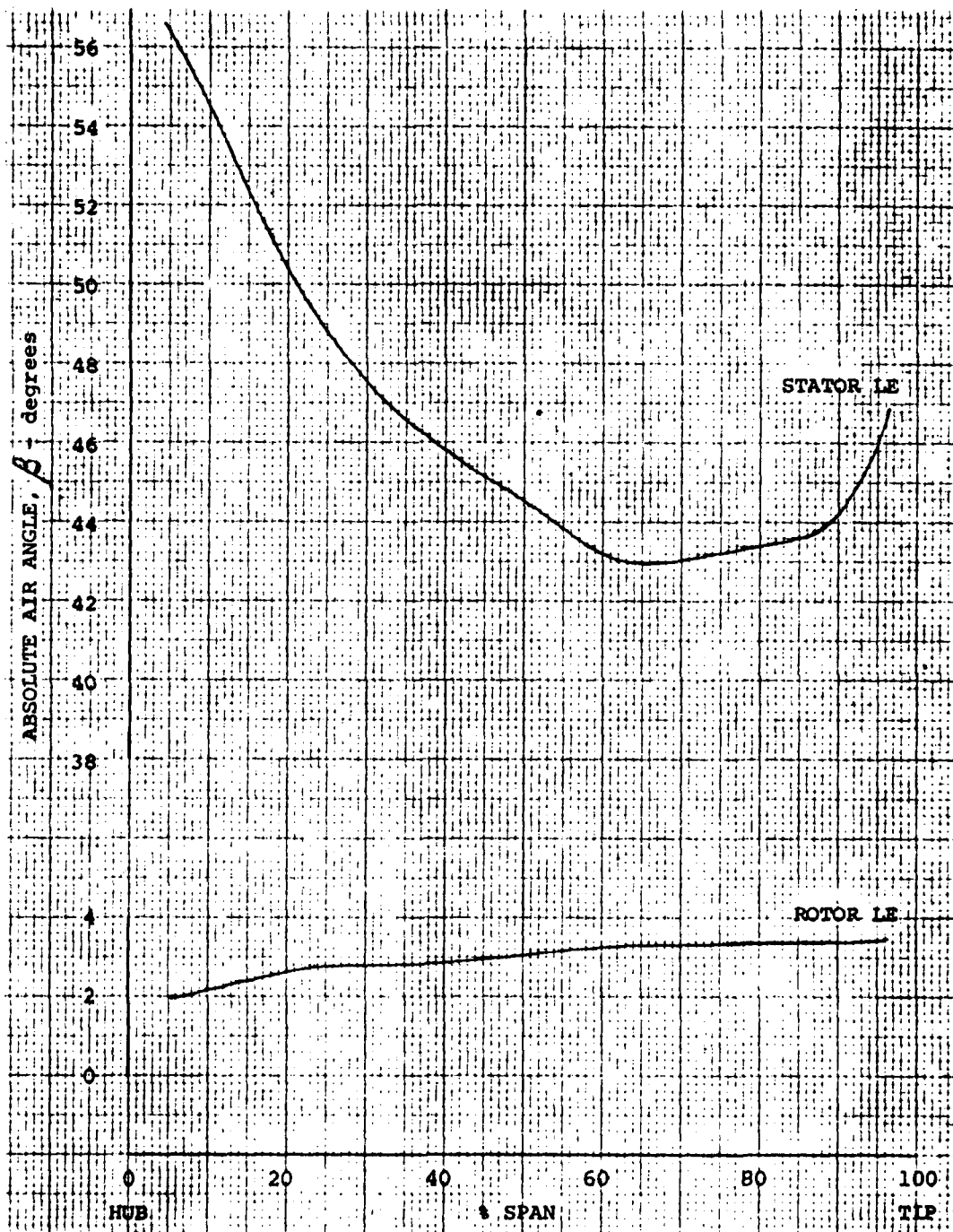
Figure 109. Expendable Gasifier Compressor Third Stage Absolute Air Angle Profiles.
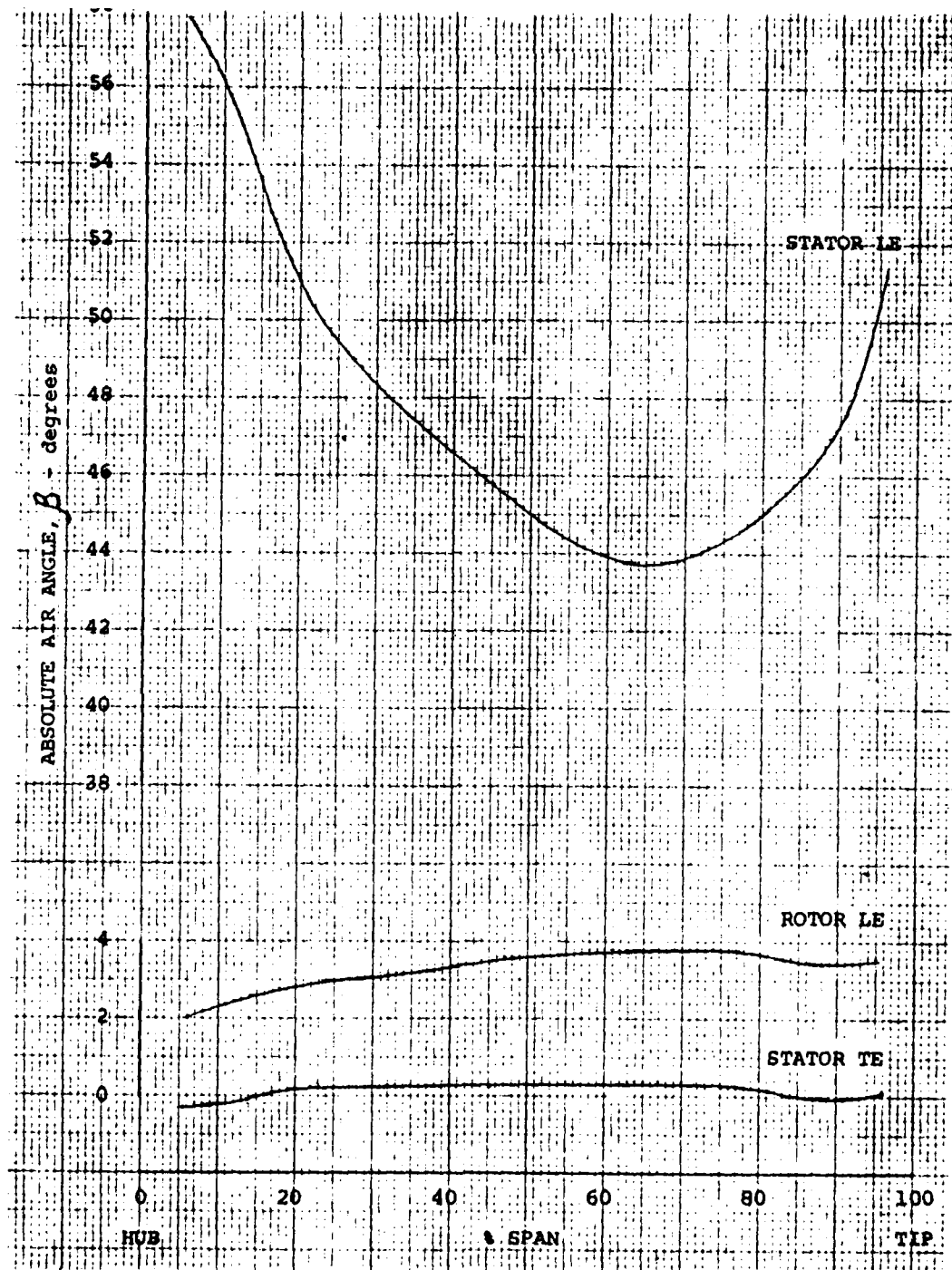
Figure 110. Expendable Gasifier Compressor Fourth Stage Absolute Air Angle Profiles.

161

The rotor camber, or blade metal turning, distribution is shown in Figure 111. The rotor incidence and deviation angles are shown in Figures 112 through 115. The rotor incidence and deviation angles in the four stages will vary slightly due to the differences in air angles the blading is identical. The differences in incidence and deviation angles shown on the figures between the 08.116 (velocity diagram) solution and 08.130 (blading) program are due to the fact that 08.130 translates the velocity diagrams to the actual blade edges from the velocity diagram calculating planes.

The stator camber distributions are shown in Figure 116. As stated previously, the stator cambers are high to achieve the high air turnings required because of the high aerodynamic loadings. Stator incidence and deviation angles are shown in **Figures 117 through 120.**

Certain changes from normal airfoil section definition practice were made for consistency with the casting process anticipated for the manufacture of the rotor and stator. Section edge radii were increased 50 percent to 0.007 for rotors and 0.006 inch for stators, from the size that would normally be specified for machined blading of this size. Tolerance band width was similarly increased from ± 0.002 to ± 0.003 inch.

To improve blade resonance margins between potential excitation sources and the design point operating speed, several modifications were made to the compressor.

Figure 121 shows the various rotor thickness distributions which were evaluated to achieve the desired structural results. Figures 122 through 124 show the effects of the thickness variations on deviation angle, incidence angle and A/A* or choke margin. Because the effects on these dependent variables were small, it was not necessary to modify the aero design or other blading geometry.

The number of vanes in the first and third stages were also changed. Stator one was changed from 39 to 41 vanes and required no other blade or vane geometry changes. Stator three was changed from 34 to 29 vanes. The change in vane row solidity increased the deviation angle enough to require a new stator design. No changes were required in the blading downstream of this blade row due to these changes.

To further increase vibratory interference margin, if preliminary testing proves it necessary, two alternate rotor configurations were considered. Aerodynamic analyses were conducted for both configurations to obtain a comparison of their overall and blade element performance with that of the original, 37-blade common rotor design. As a ground rule, rotor airfoil section geometry was to remain unchanged with only the number of blades varying.

For the initial configuration, the number of rotor blades was increased to 39 only in the third and fourth stage rotors. The velocity vector diagram solution indicated no appreciable change in overall performance and showed only small

162
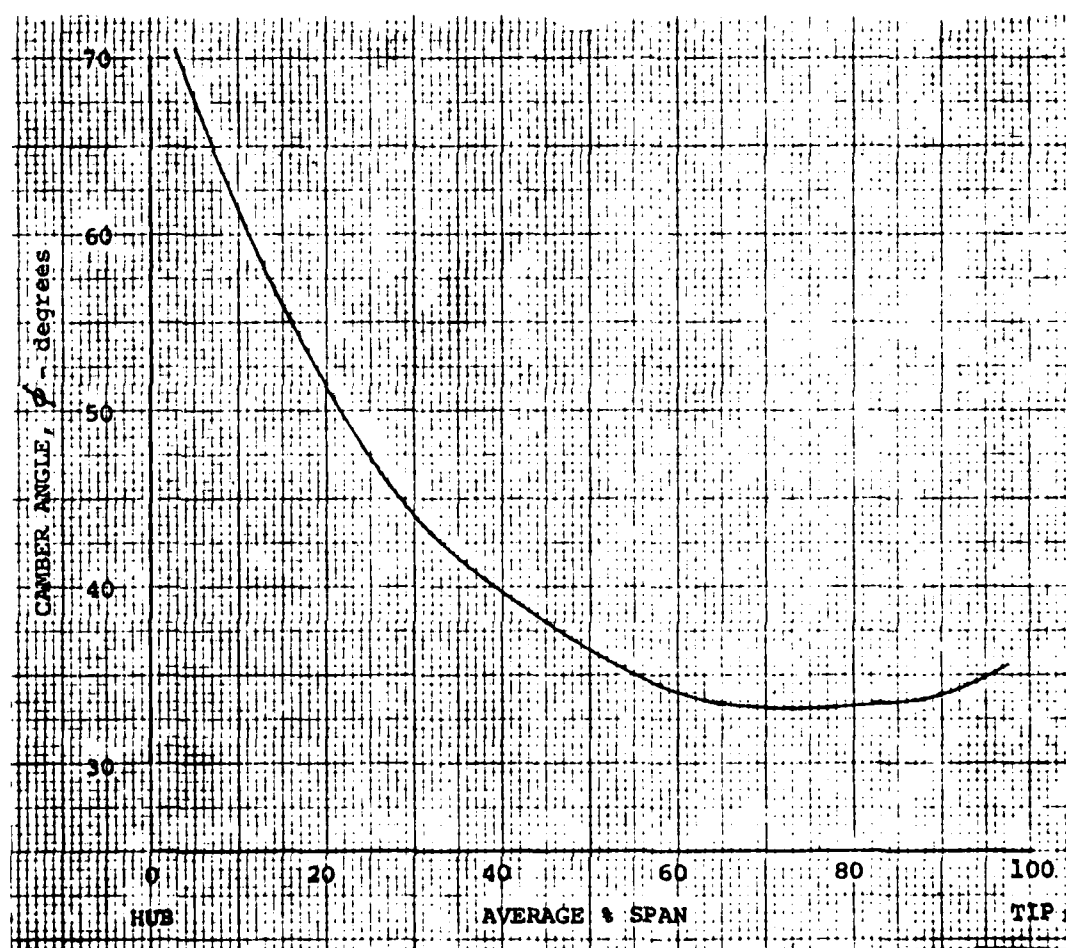
27254

Figure 111. Expendable Gasifier Compressor Rotor Camber Distribution.

163
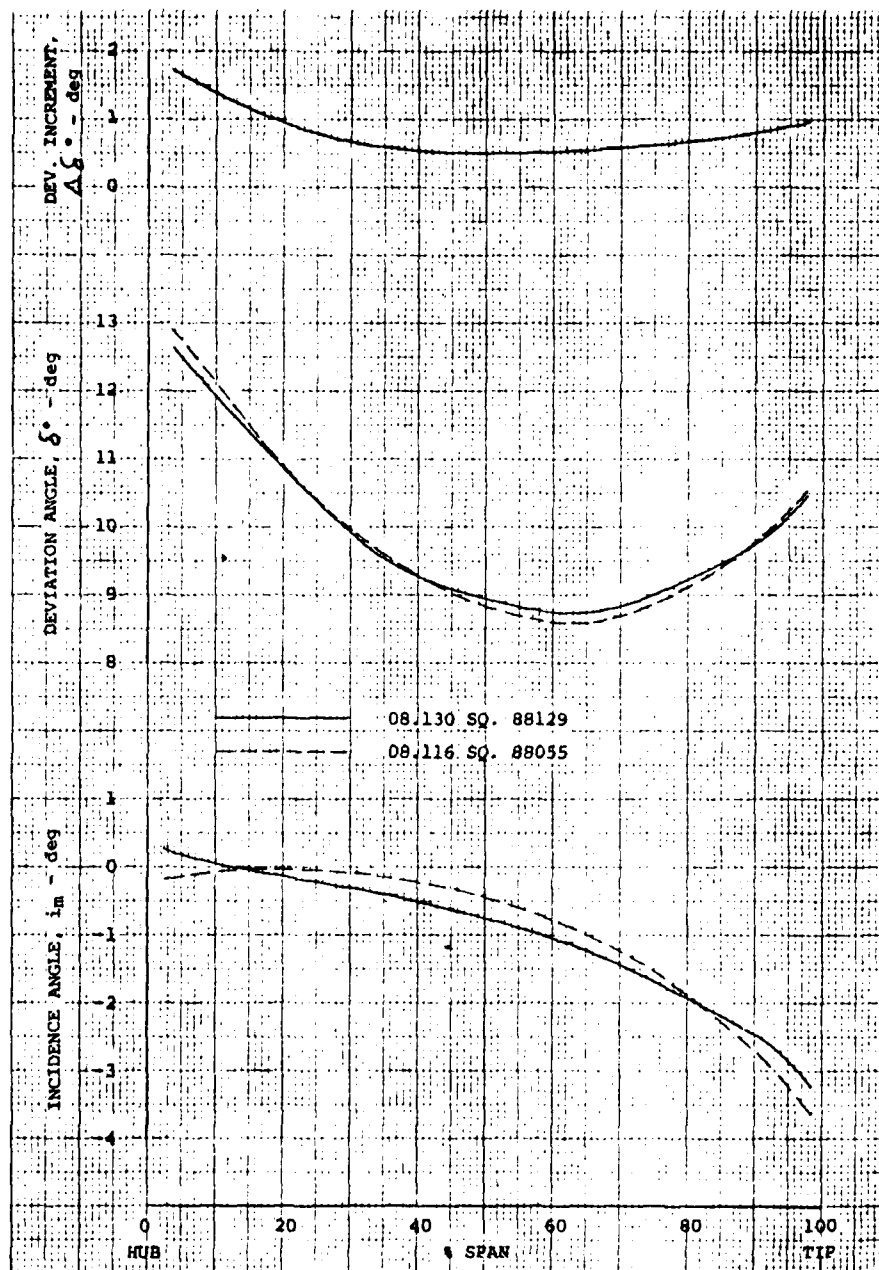
27281

Figure 112. Expendable Gasifier Compressor First Stage Rotor Incidence and Deviation.
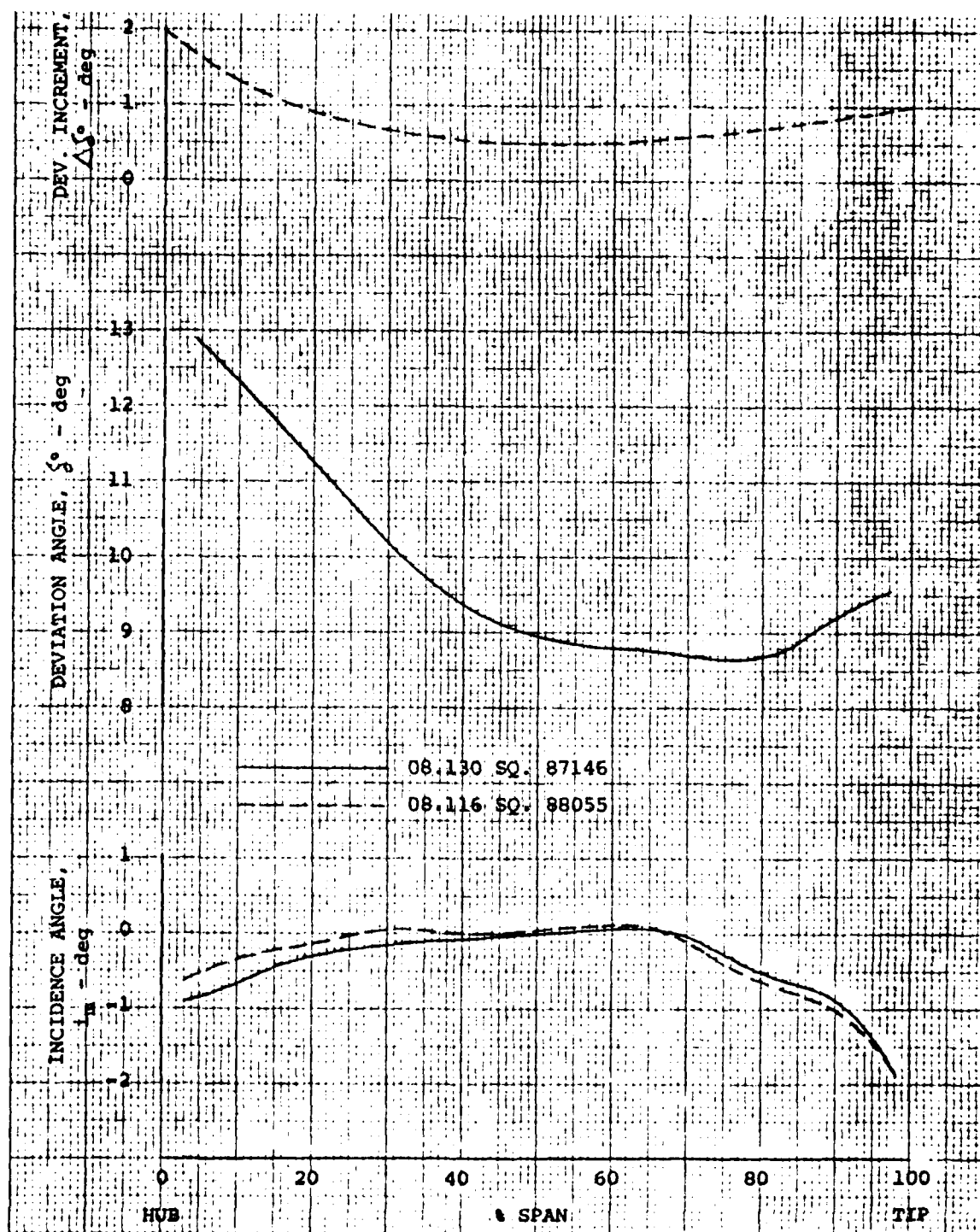
Figure 113. Expendable Gasifier Compressor Second Stage Rotor Incidence and 27282 Deviation.

165
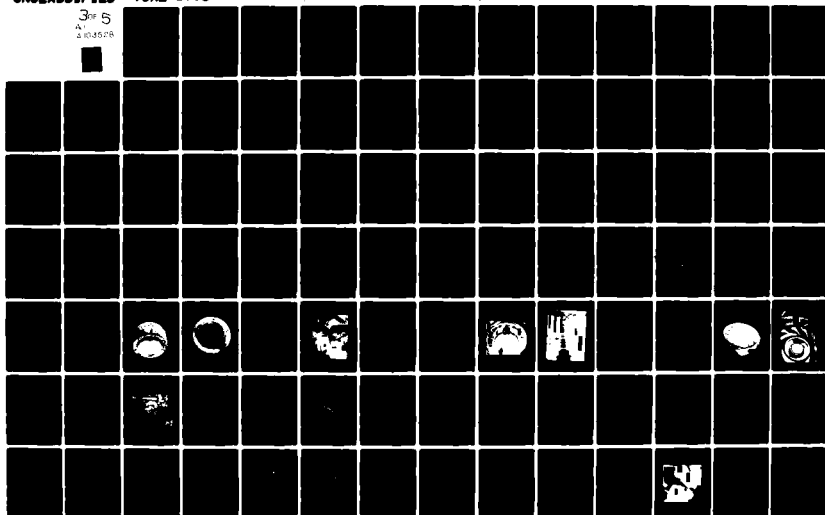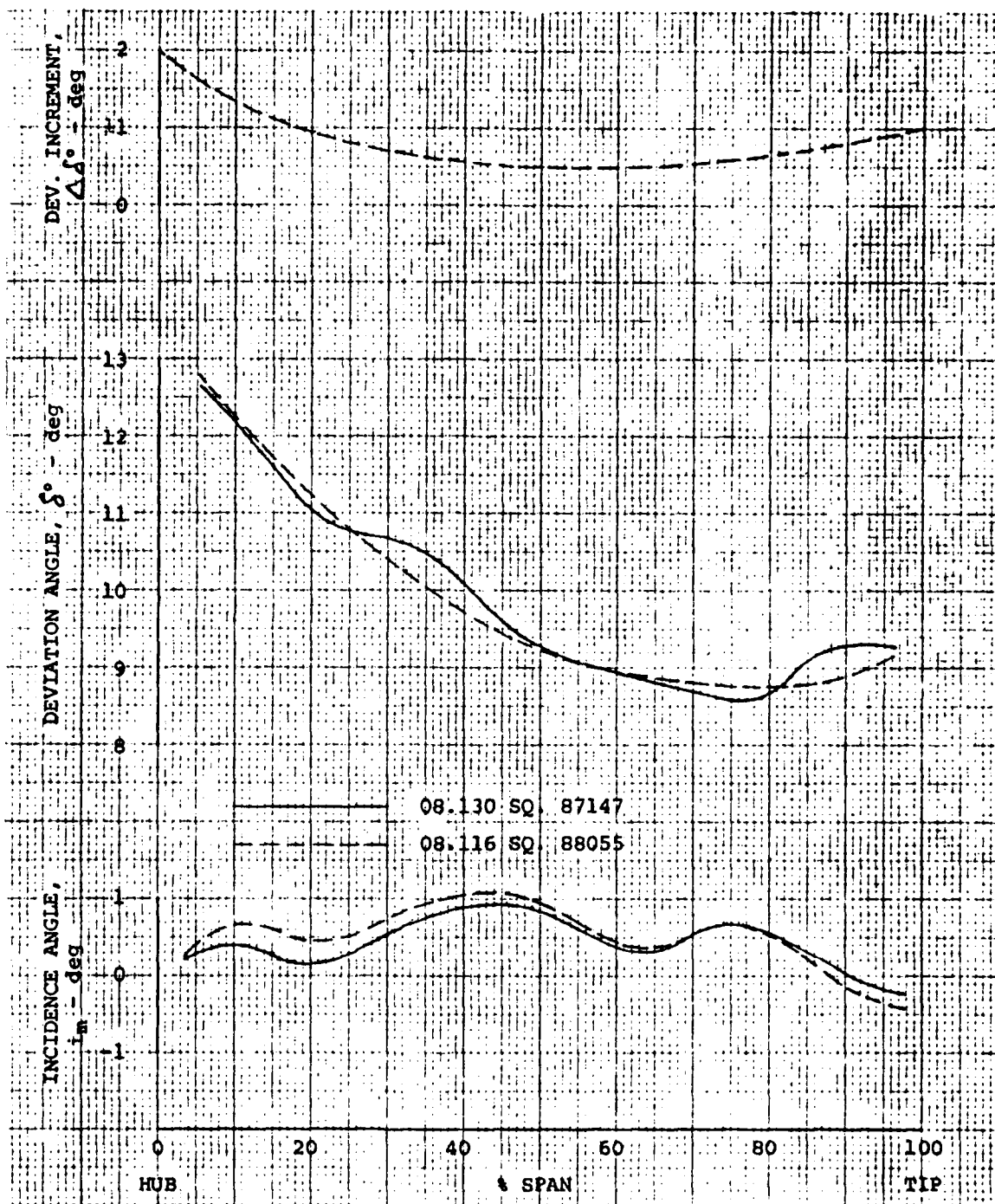
27283

Figure 114 . Expendable Gasifier Compressor Third Stage Rotor Incidence and
Deviation.

166
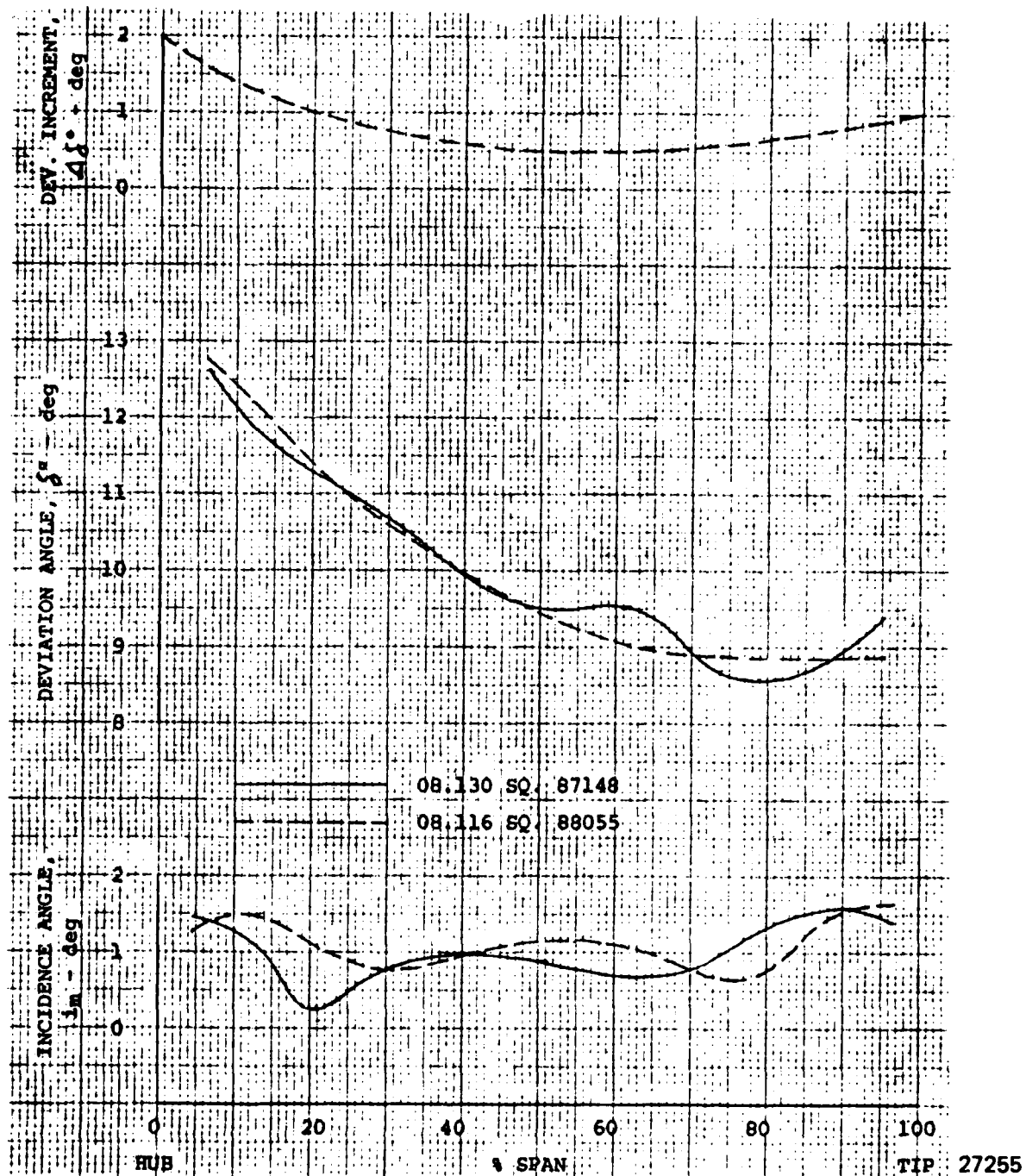
Figure 115. Expendable Gasifier Compressor Fourth Stage Rotor Incidence and Deviation.

167
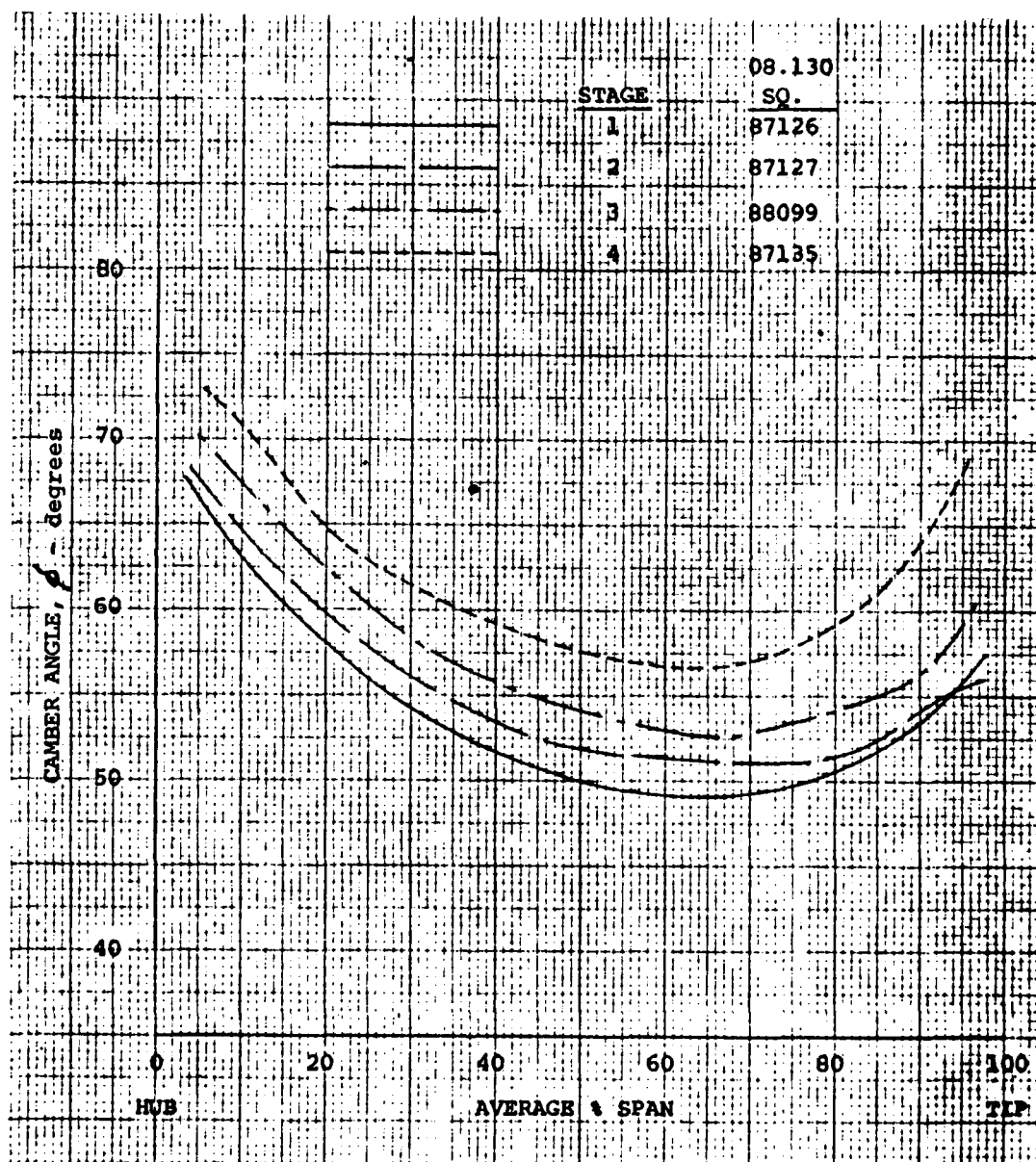
Figure 116. Expendable Gasifier Compressor Stator Camber Distribution.

168
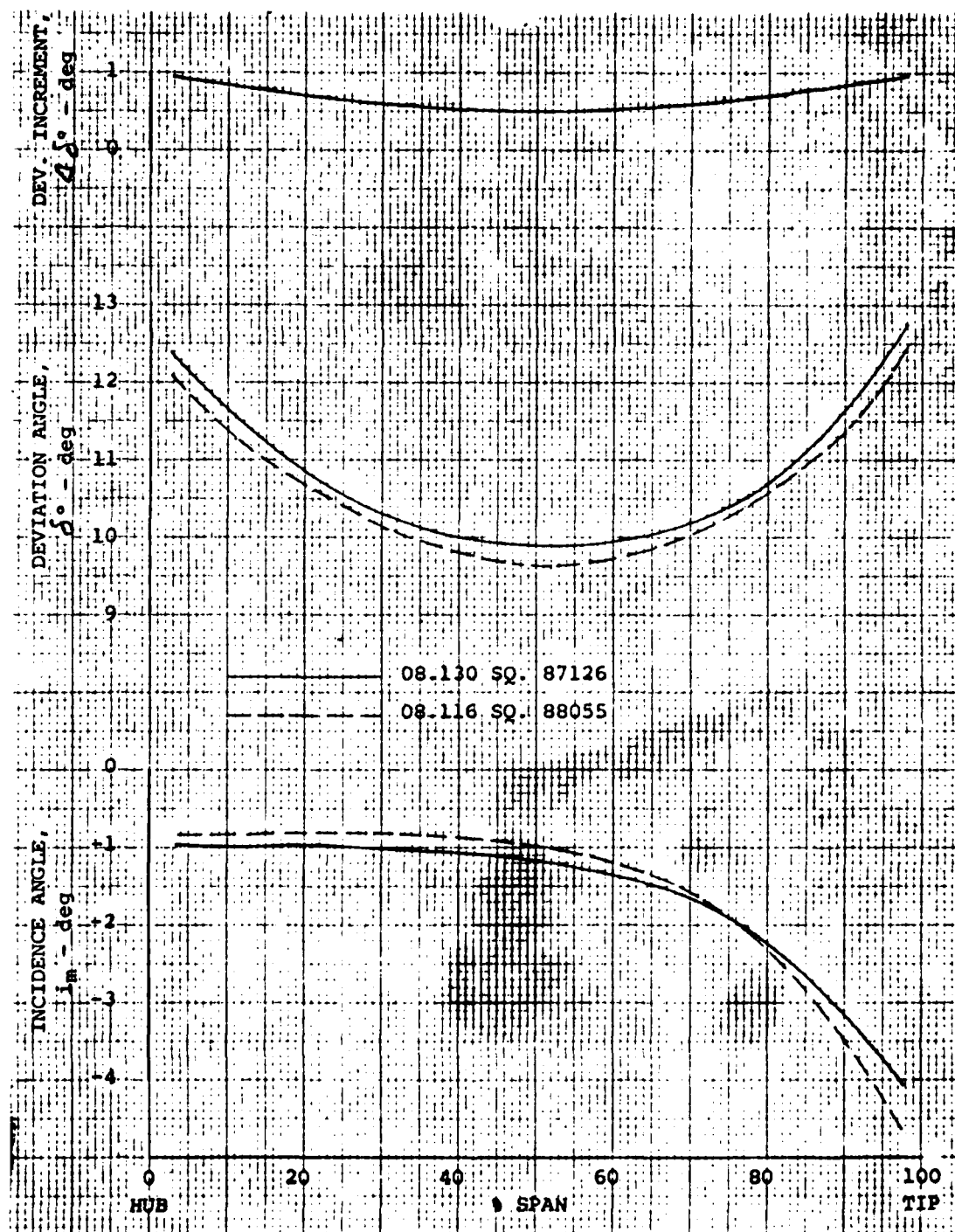
Figure 117. Expendable Gasifier Compressor First Stage Stator Incidence and Deviation.

169

27257
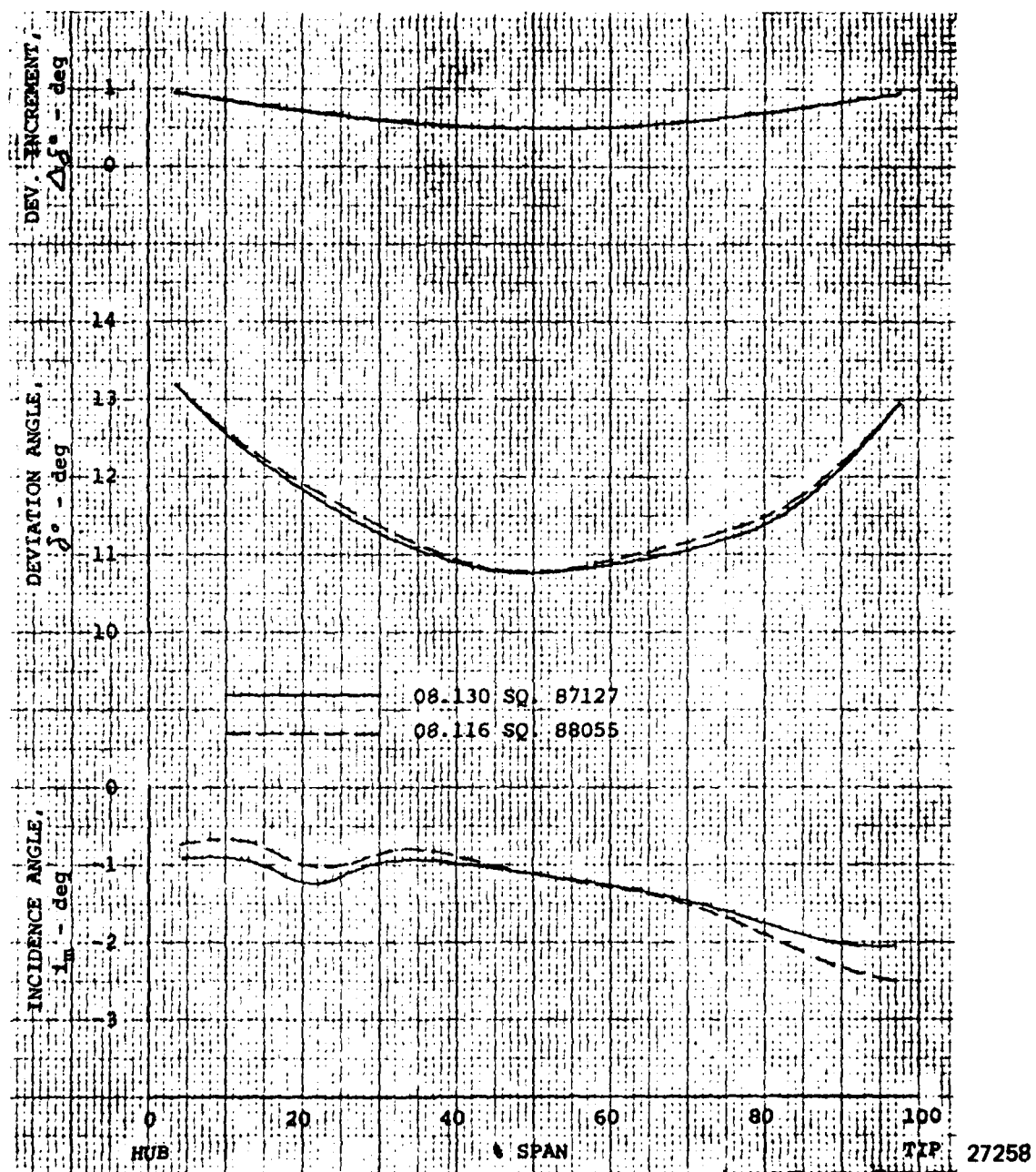
Figure 118. Expendable Gasifier Compressor Second Stage Stator Incidence and Deviation.

170
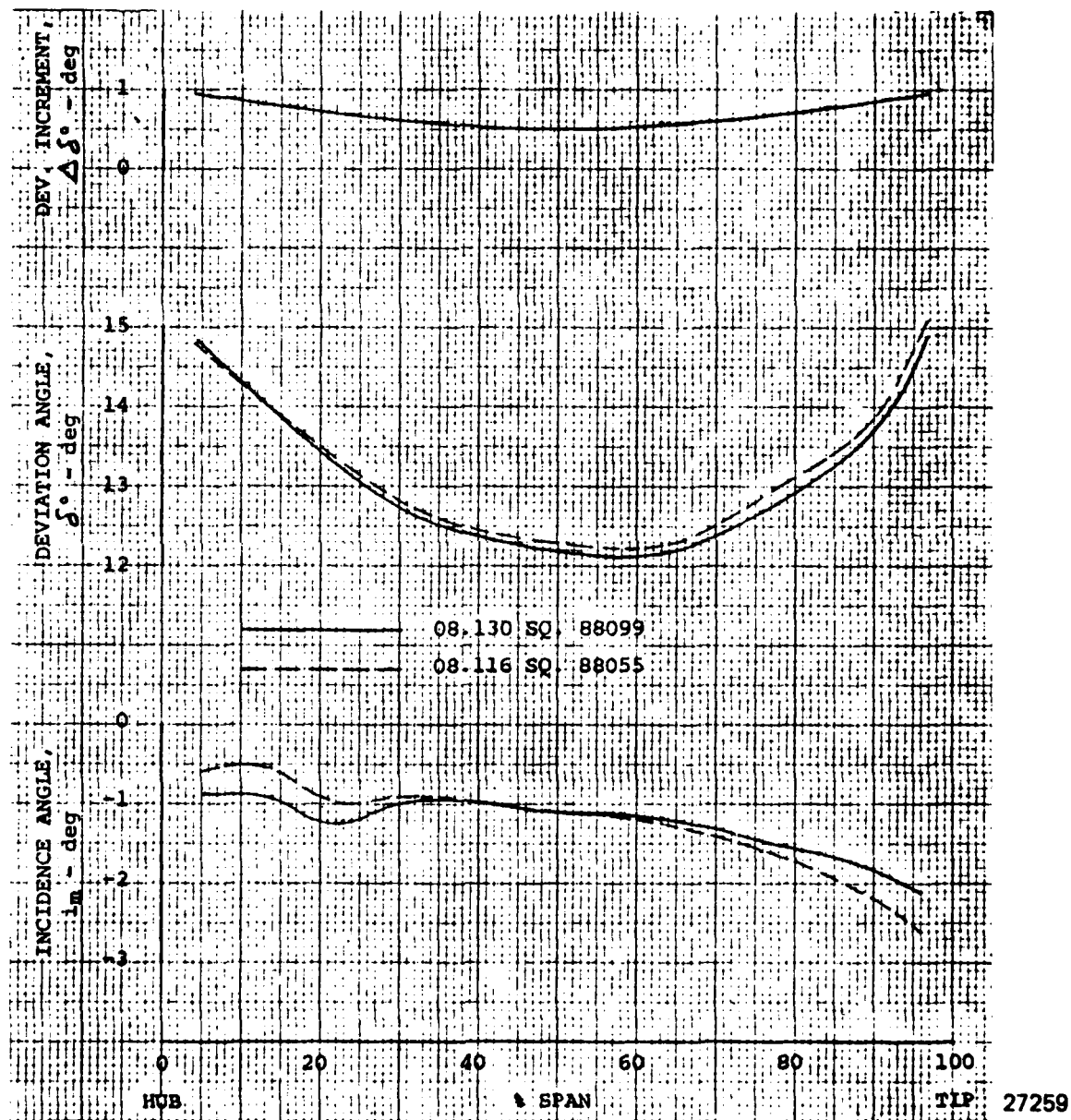
Figure 119. Expendable Gasifier Compressor Third Stage Stator Incidence and Deviation.

171
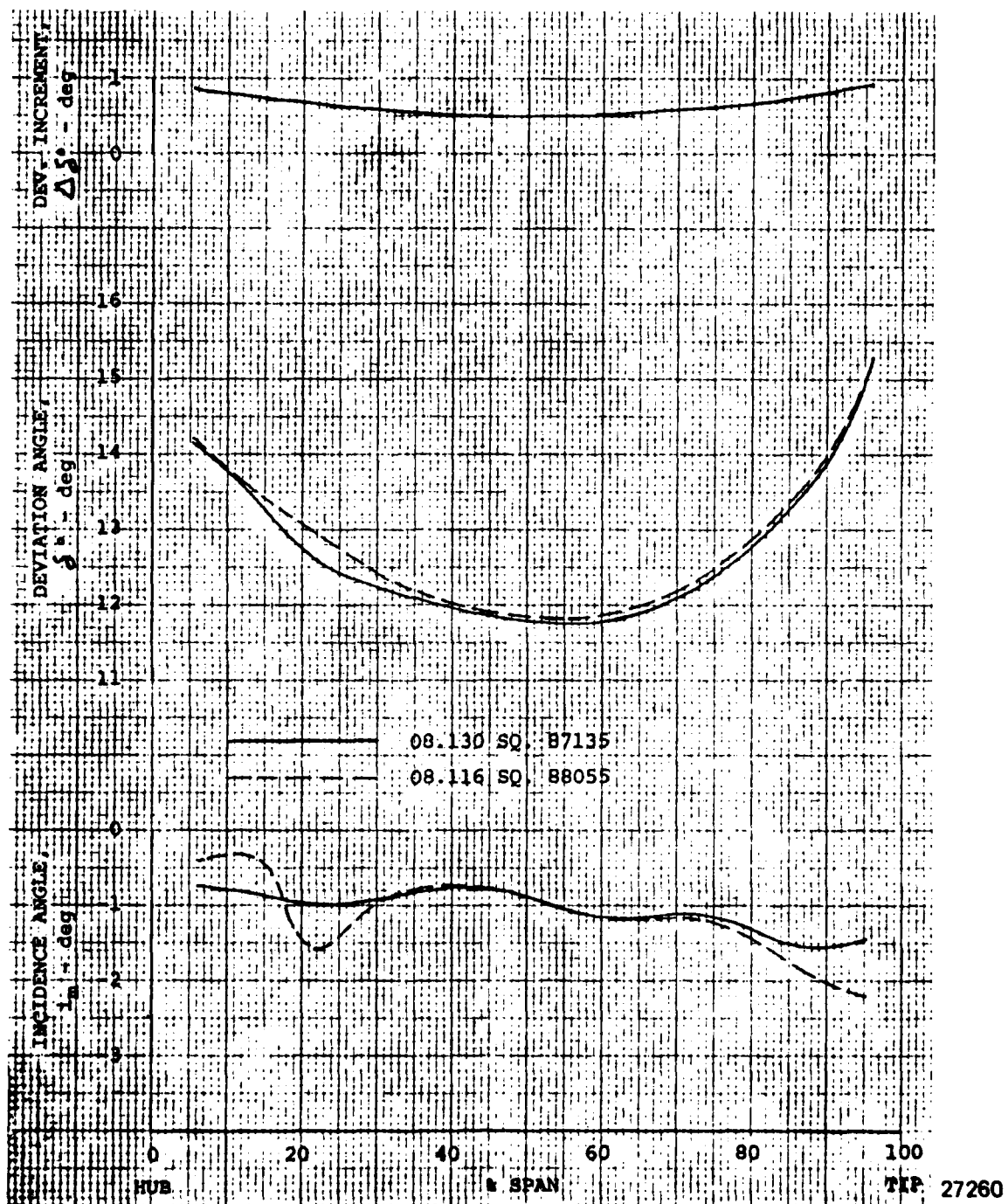
Figure 120. Expendable Gasifier Compressor Fourth Stage Stator Incidence and Deviation.

172
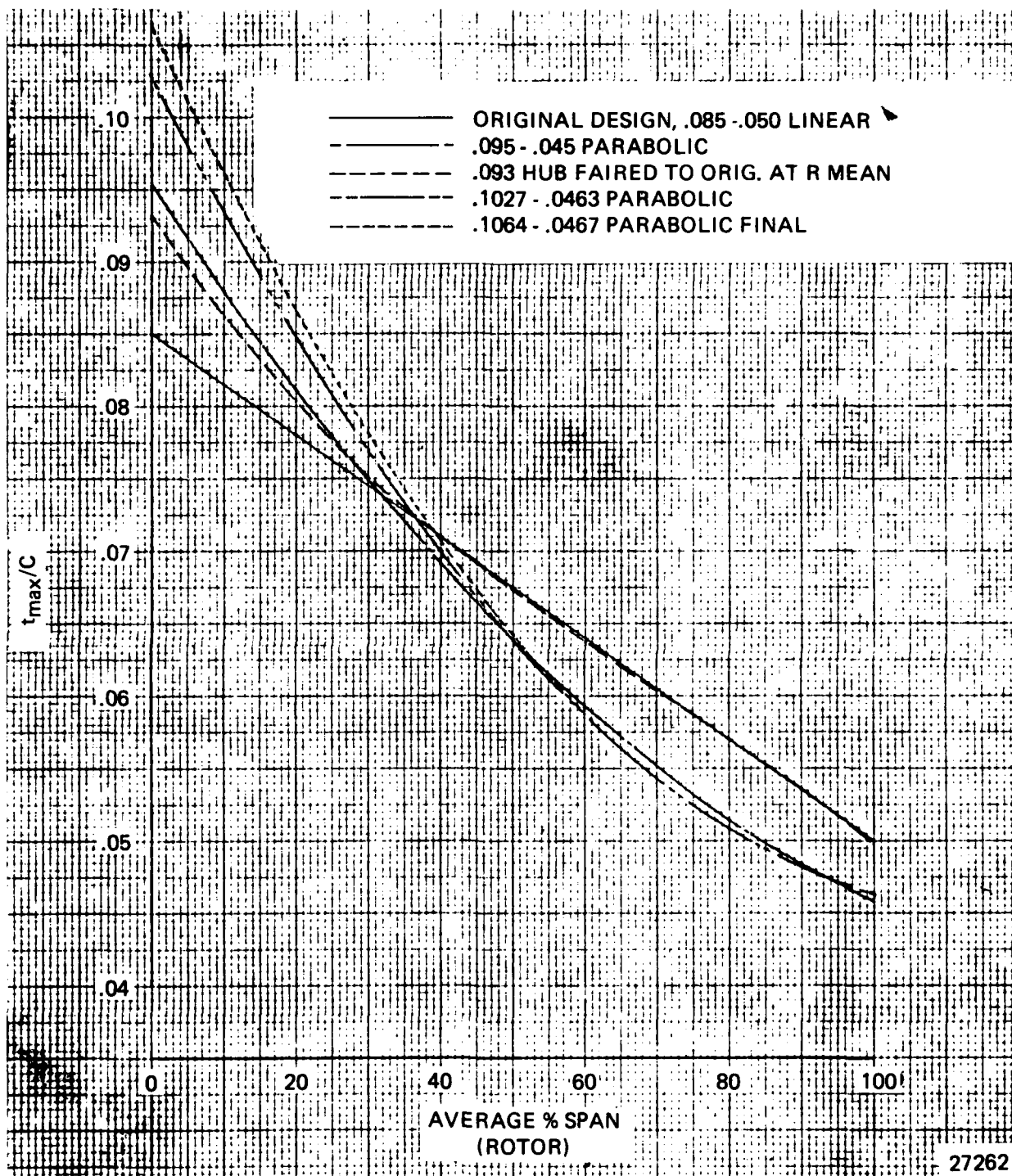
Figure 121. Expendable Gasifier Compressor Rotor T/C Distribution Study for Stress.

173
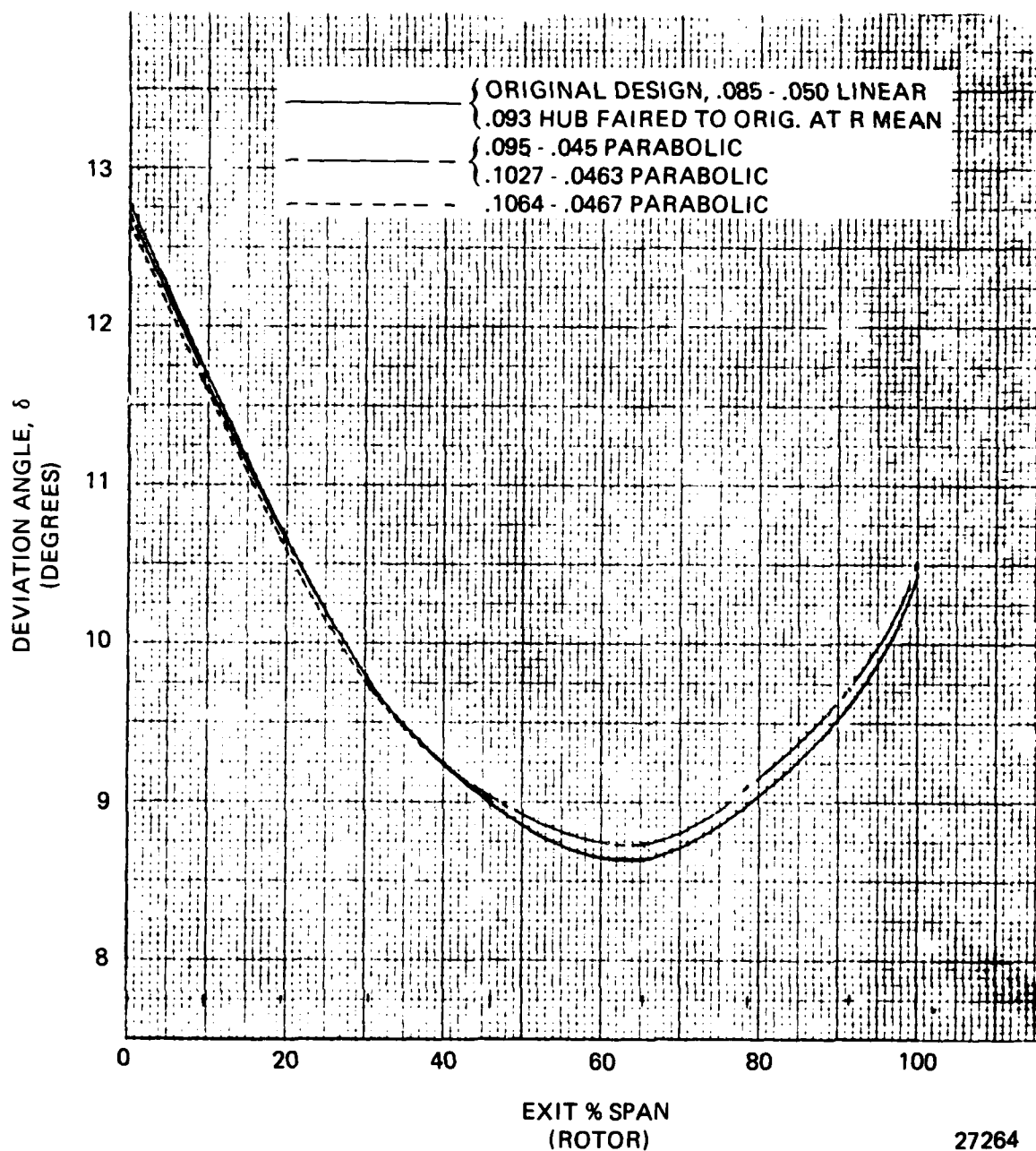
Figure 122. Expendable Gasifier Compressor Rotor T/C Distribution Study for Stress Deviation Angle.

174
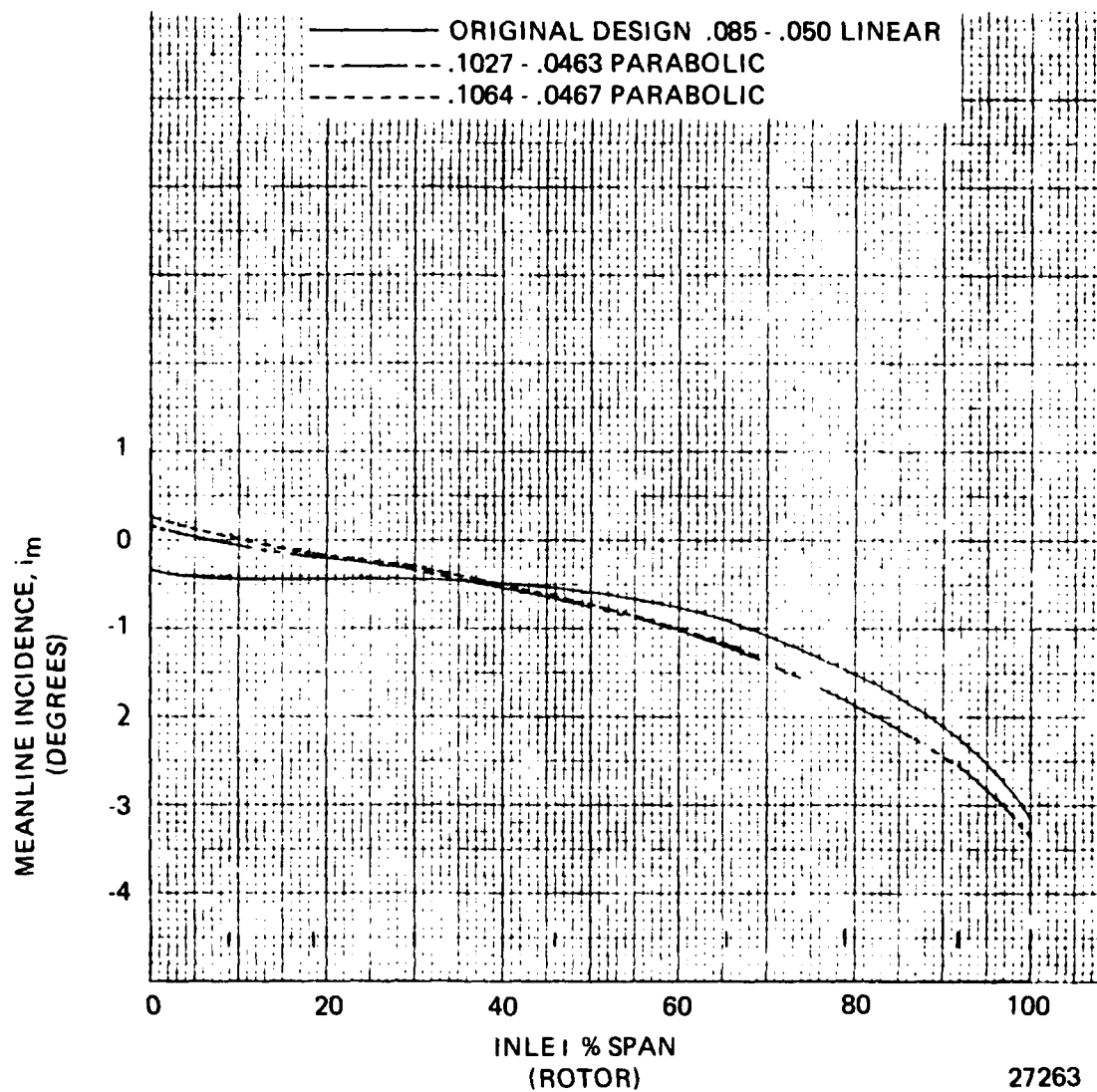
Figure 123. Expendable Gasifier Compressor Rotor T/C Distribution Study for Stress Incidence.

175
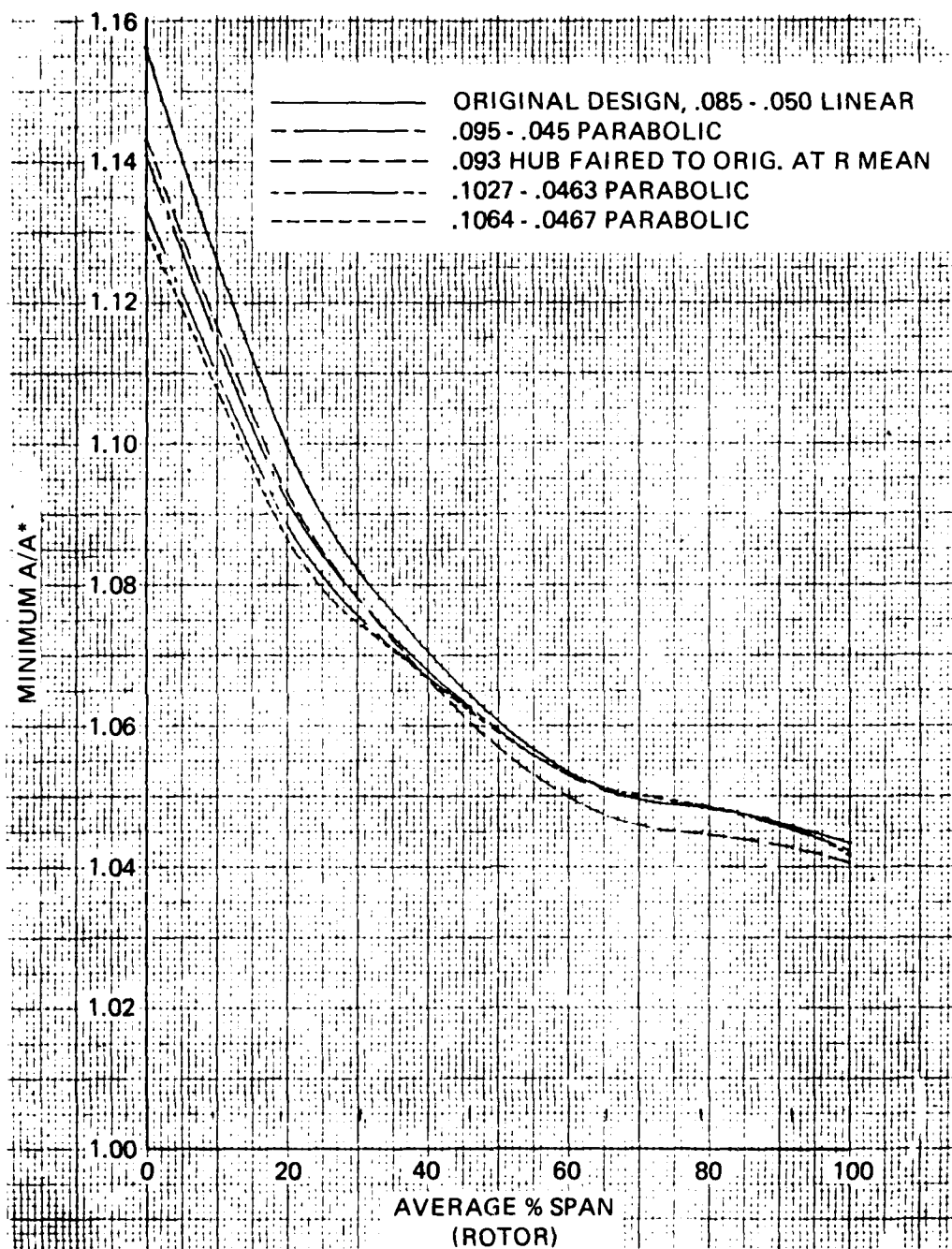
Figure 124. Expendable Gasifier Compressor Rotor T/C Distribution Study for Stress Choke Margin.

176

variations from the original design incidence, loading levels and compressor discharge pressure and velocity profiles. The choke margins of the third and fourth stage rotor blading were sufficient to allow the addition of two blades in each row. This configuration satisfied the vibratory requirement with little or no indication of an aerodynamic performance penalty.

The second configuration had 39-blade rotors in all four stages in the interest of retaining the common rotor concept. The streamline solution indicated the existence of a hub stall problem in the rear stages, with incidence levels as much as eleven degrees above original design reference values. The associated high loss levels in the hub region were evident in corresponding sharp fall-offs of total pressure and axial velocity at the compressor exit station. These factors, combined with an unacceptable choke margin reduction in the first stage rotor, indicated that additional redesign effort would be necessary to make a 39-blade, common rotor configuration feasible.

Comparisons of important variables are shown on Table 19 (incidence), Table 20 (diffusion factor) and Figure 125 (exit total pressure and axial velocity).

5.1.2 Mechanical Design

The criterion of low acquisition costs dictated the material selection and method of fabrication of the compressor and stators. Aluminum with its lower cost ratio of two or three to one over steel was the natural material choice. Following the extensive experience of our production Harpoon engine, C 355 aluminum was selected for both the rotors and stators. This material has gained acceptance in gas turbines for its good elevated temperature properties after heat treat, ease of weld repair and excellent castability required to assure casting fill of the relatively thin airfoils. Both rotors and stators are precision cast, requiring a minimum of machining.

The aluminum compressor thermal expansion and centrifugal strain growth over the shaft are accommodated by employing three radial dowel pins in each rotor. This three-pin complement assures uniform radial growth of the rotor bore, precluding mass center shift. Aerodynamic torque of the stators is transferred to the fourth stage stator through a common axial key and reacted by the rear bearing fuel tube.

The compressor tip and interstage labyrinth seals assembly clearances are shown in Figure 126. The rotor's tip clearances for the first and fourth stages at running conditions were calculated as follows:

Table 19

		CONFIGURATION		
Blade Row	Location	37 Blades All Rotors	37, 37, 39, 39	39 Blades All Rotors

EXPENDABLE GASIFIER COMPRESSOR
INCIDENCE ANGLE COMPARISON
$(i_m - i_m, ref)$*

Blade Row	Location	37 Blades All Rotors	37, 37, 39, 39	39 Blades All Rotors
Rotor 1	Hub	.01	.01	.01
	Mean	-.03	-.03	-.03
	Tip	-.07	-.07	-.07
Stator 1	Hub	.03	.17	.55
	Mean	.03	.21	.27
	Tip	-.18	-.78	-.37
Rotor 2	Hub	.26	.30	.99
	Mean	.03	.09	.03
	Tip	-.21	-.18	-.25
Stator 2	Hub	.07	.39	1.65
	Mean	.01	.07	.02
	Tip	.65	.21	.37
Rotor 3	Hub	.32	.54	3.04
	Mean	-.03	-.03	-.21
	Tip	-.12	-.12	-.22
Stator 3	Hub	.41	1.00	4.39
	Mean	-.02	.0	-.36
	Tip	.70	-.20	-.79
Rotor 4	Hub	.49	1.47	6.97
	Mean	-.02	-.10	-.48
	Tip	-.19	-.19	-.38
Stator 4	Hub	.27	2.12	11.32
	Mean	.27	.17	-.58
	Tip	.22	.19	-1.63

27251

* $(i_m - i_m, ref)$ = difference between operating incidence and minimum loss
or reference incidence (meanline basis), degrees.

178

TABLE 20

EXPENDABLE GASIFIER COMPRESSOR
DIFFUSION FACTOR COMPARISON

BLADE ROW	LOCATION	CONFIGURATION		
		37 BLADE ALL ROTORS	37, 37, 39, 39	39 BLADES ALL ROTORS
Rotor 1	Hub Mean Tip	.665 .527 .566	.665 .527 .566	.662 .519 .563
Stator 1	Hub Mean Tip	.625 .530 .555	.624 .525 .544	.639 .526 .546
Rotor 2	Hub Mean Tip	.656 .528 .558	.660 .529 .559	.674 .519 .553
Stator 2	Hub Mean Tip	.664 .577 .578	.678 .580 .577	.725 .577 .577
Rotor 3	Hub Mean Tip	.656 .535 .590	.656 .526 .589	.726 .519 .580
Stator 3	Hub Mean Tip	.743 .635 .661	.762 .635 .665	.859 .625 .657
Rotor 4	Hub Mean Tip	.674 .532 .648	.692 .521 .650	.876 .505 .622
Stator 4	Hub Mean Tip	.756 .621 .672	.819 .621 .677	1.127 .588 .650

27272

179

Figure 125. Expendable Gasifier Compressor Stator 4 Exit Total Pressure and Axial Velocity vs Radius.

180
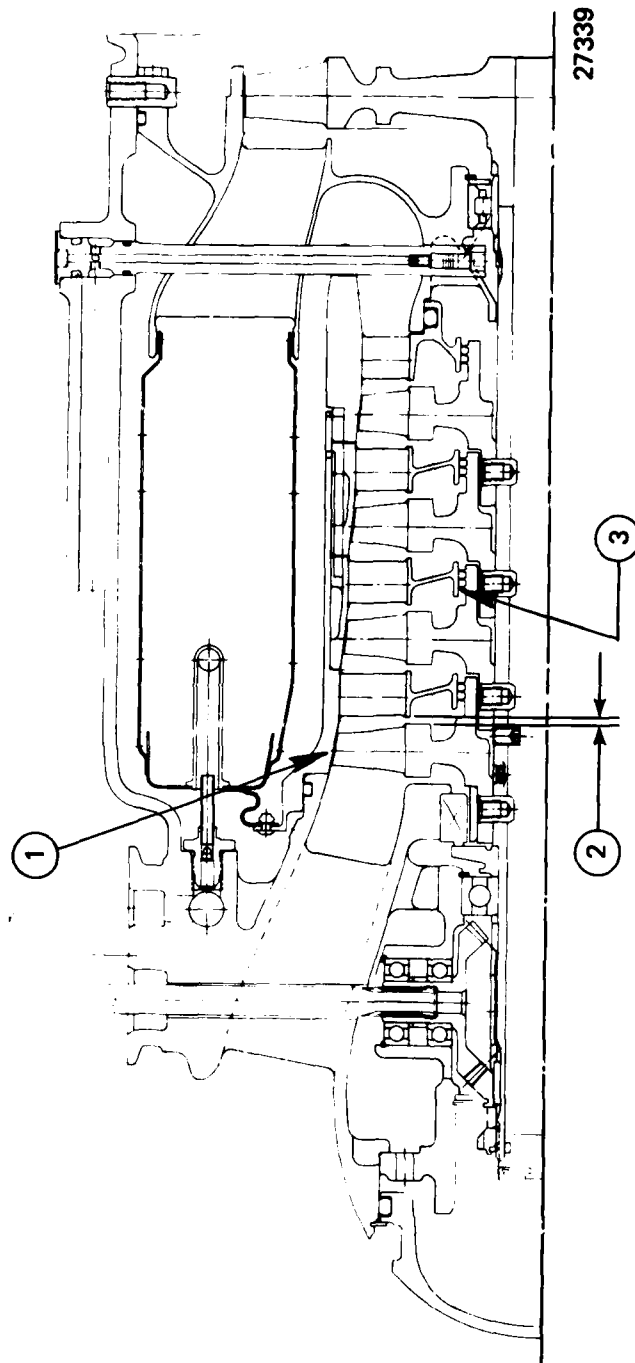
1. COMPRESSOR TIP   .012 ± 0.003 (ALL FOUR STAGES)
2. COMPRESSOR TO STATORS   .092 ± 0.050 @ 1ST STAGE
   AXIAL CLEARANCE   0.102 ± 0.064 & 4TH STAGE
3. COMPRESSOR   0.006 ± 0.003 (ALL FOUR STAGES)
   LABYRINTH SEALS

Figure 126. Compressor Tip and Interstage Labyrinth Seals Clearances (at Cold
Static Conditions).

181

E G Compressor Tip Clearances (Radial)
(At 100% Shaft Speed - Steady State)

1st Stage:

.012 Mean Build Clearance
+.0036 Shroud Thermal Growth
-.0025 Compr. Total Growth
.0131 Mean Tip Clearance

(The first and fourth stages
clearances represent the
maximum and minimum values,
respectively; the second
and third stage clearances
fall between the two limits.)

4th Stage:

.012 Mean Build Clearance
+.008 Shroud Thermal Growth
-.0084 Compr. Total Growth
.0116 Mean Tip Clearance

The compressor rotor consists of four axial stages with identical disk and blade shapes except that the blade tips are machined at different heights. Blade natural frequencies were calculated using NASTRAN finite element models consisting of four node quadrilateral plate elements. The Normal Modes rigid format of NASTRAN was used for zero speed frequencies while the maximum speed frequencies were calculated using the Normal Modes With Differential Stiffness rigid format. Since all four stages are identical except for blade length, a common model was used for all four stages. The decrease in blade height from the first through fourth stages was obtained by removing a row of elements from the tip of the first stage model for each of the second through fourth stage blades. Therefore, the first stage blade consisted of 108 elements, the second 99, and third 90 and the fourth stage 81 elements. The first stage model is shown in Figure 127 with the tip outlines indicated for the other three stages.

The results of the vibration analysis indicated that all of the stages were free of resonances with the stator vane upstream flow blockages at maximum steady state speed. However, the margin between the 4E excitation of the inlet struts and the first stage first bending mode was only 7 percent, where frequency margin is expressed as 1 - excitation freq.
natural freq.

Also a low margin (-2 percent) between the 39 first stage stators excitation and the second stage blade fifth mode was indicated. Thickening the airfoil root resulted in a 4E margin of 16 percent on the first stage blade. This was not considered sufficient margin for the first mode of a cast aluminum blade and since further airfoil changes would have impacted the aerodynamic performance, it was decided to change the number of inlet struts from 4 to 3. The resulting 3E margin was calculated to be 37 percent for the first stage blade first mode. The NASTRAN analysis indicated that the redesigned second stage blade still had a low 39E fifth mode margin (-9 percent). Therefore, the number of first stage stators was changed from 39 to 41 which resulted in a margin of -14 percent between the fifth mode and the first stage stator excitation.

182

UNDEFLECTED

1ST STAGE TIP

2ND STAGE TIP

DEFLECTED IN
FIRST BENDING
MODE

3RD STAGE TIP

4TH STAGE TIP

27291
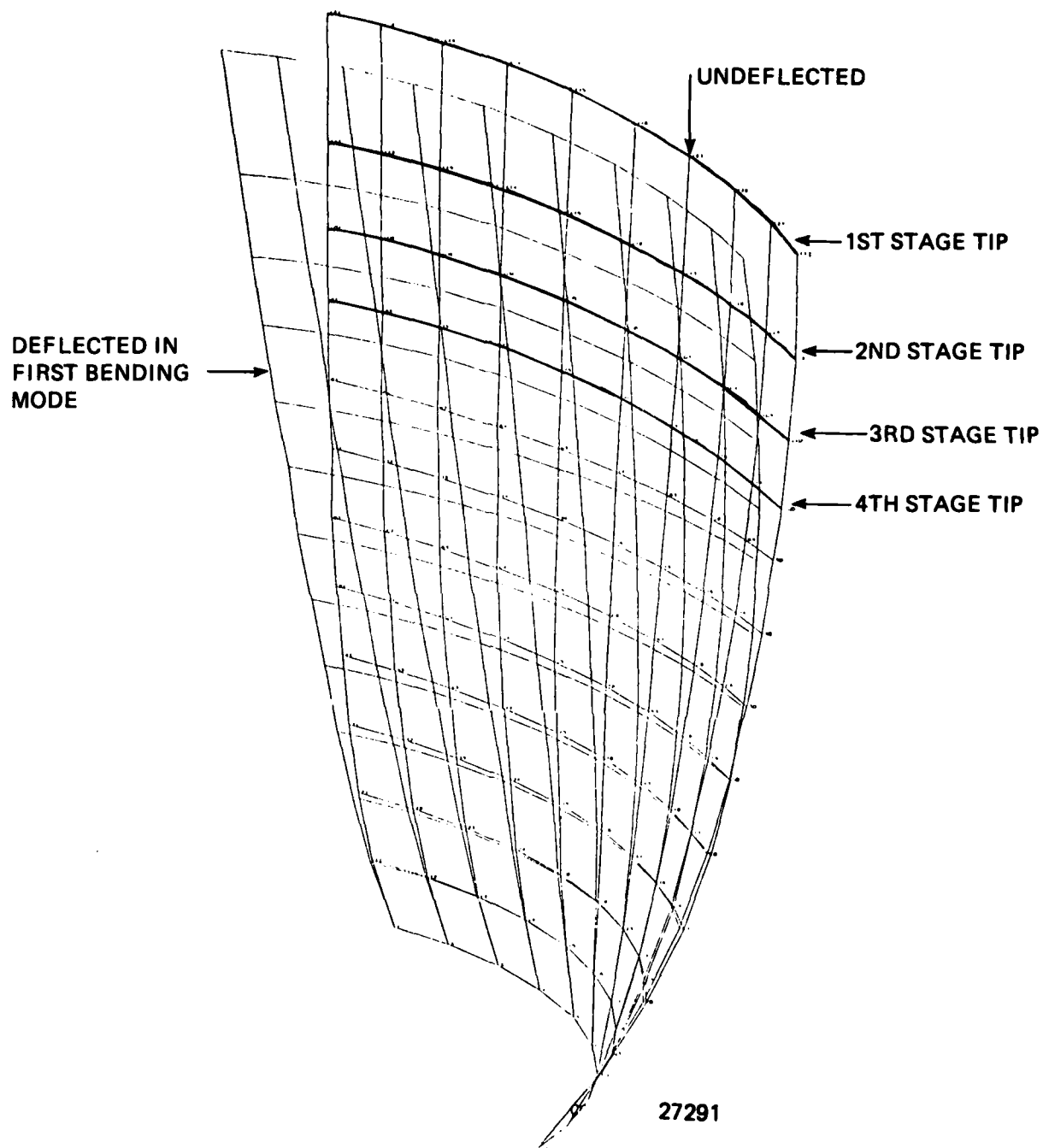
Figure 127.   NASTRAN Model of EG First Compressor Rotor Blade.

A discussion of the various thickness distribution changes which were evaluated to obtain the final blade shape were previously discussed. The various thickness distributions are presented in Figure 121. The blade resonance diagrams resulting from the NASTRAN frequency solutions are presented in Figures 128 through 131 for the first through fourth stage blades respectively. Adequate margins are indicated for all four stages between the blade natural frequencies and upstream flow blockages. The mode shapes for the first six modes of the first stage blade are presented in Figure 132 through 137. The mode shapes of the other three stages are similar.

Restored gas bending and centrifugal stresses were calculated for the blades using tapered twisted beam finite difference models. Calculated ultimate and yield safety factors were at least 6 and 4.5 respectively, as indicated in Figure 138. The blade stresses are shown on a modified Goodman diagram in Figure 139 where the vibratory stress is assumed to be equal to the gas bending stress. High vibratory stress margins are indicated on all four stages.

The compressor rotor disks were analyzed using a conventional disk finite difference model. The blade centrifugal loads were simulated as an evenly distributed rim radial stress. Stresses were purposely kept very low so that burst speed margins of 67 percent or more were calculated. The calculated centrifugal stresses are shown in Figure 138.

The compressor stators which we cast in C355-T61 aluminum alloy were modeled using NASTRAN quadrilateral four node plate elements. The stator airfoils were modeled using 56 elements. The stator was fixed at the integral outer shroud. A one vane pitch segment of the inner shroud was modeled with plates and connected to the inside diameter of the stator with MPC (multi point constraint) relationships. The normal modes with cyclic symmetry rig format of NASTRAN were used to determine the vane natural frequencies coupled to the inner shroud. The natural frequencies for a harmonic index of zero are presented on resonance diagrams in Figures 140 through 143 for the first through fourth stages respectively. The first and second stages appear free of any harmful resonances with the blade passing excitation frequency (37E). However, the third stage has a vane bending mode near 37E at the maximum operating speed and the fourth stage has a vane torsion mode near 37E at maximum speed. Although the excitation is only three percent above the calculated vane frequencies at maximum speed, a decision was made to proceed with the design and fabrication and to determine the resonance speeds experimentally. This decision was made because the accuracy of the NASTRAN vane models was unknown. The vane frequencies were determined experimentally using holographic methods and strain gaged for initial engine testing to determine dynamic strain. For high dynamic stress indications, a change in the number of third and fourth stage blades or a change in the third and fourth stage design or materials will be initiated. The calculated vane mode shapes are presented for the natural frequencies nearest to the 37E excitation in Figures 144 through 147 for the first through fourth stages respectively.

184
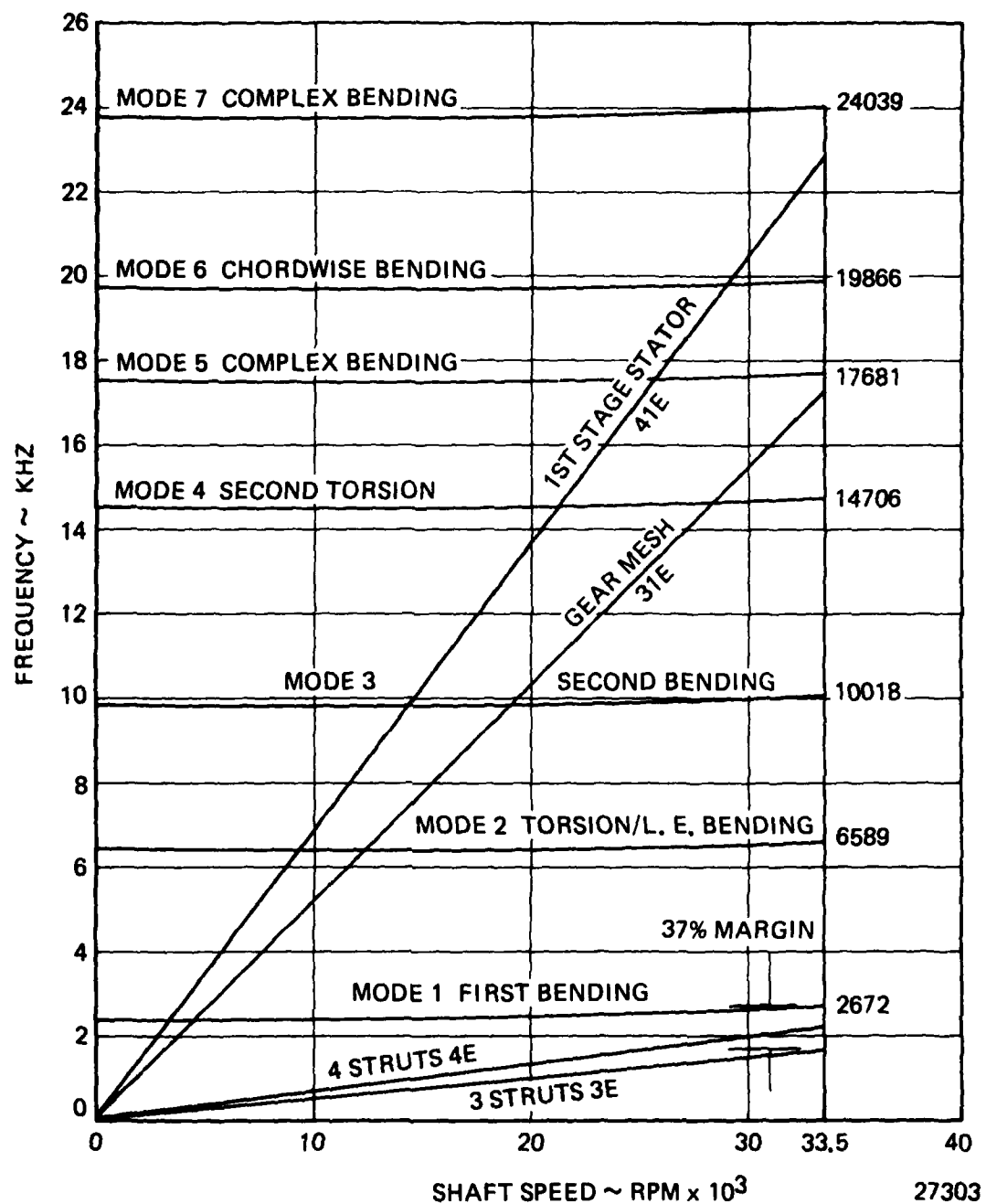
Figure 128 . E.G. First Stage Compressor Blade Interference Diagram.

185
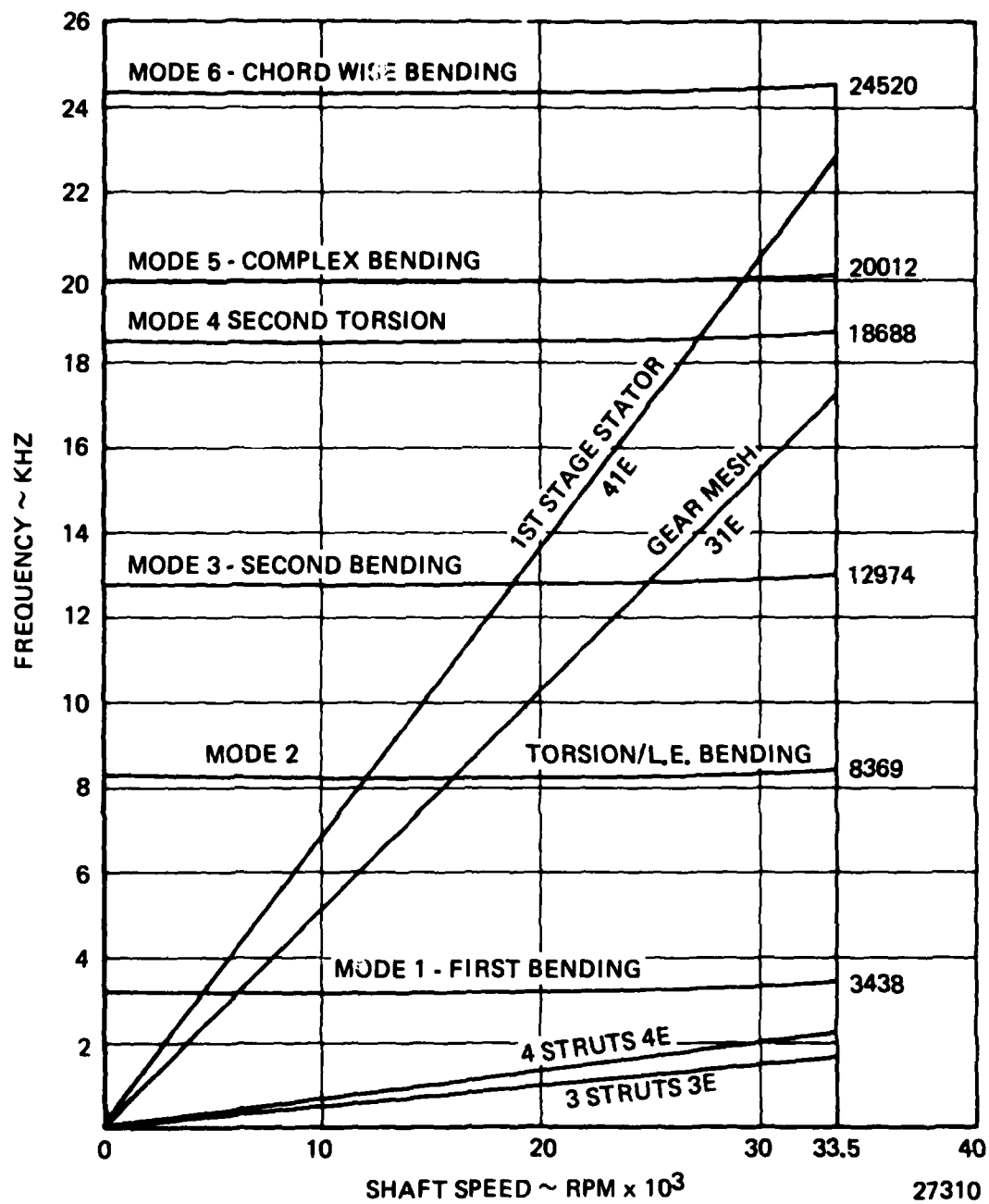
Figure 129 . E.G. Second Stage Compressor Blade Interference Diagram.
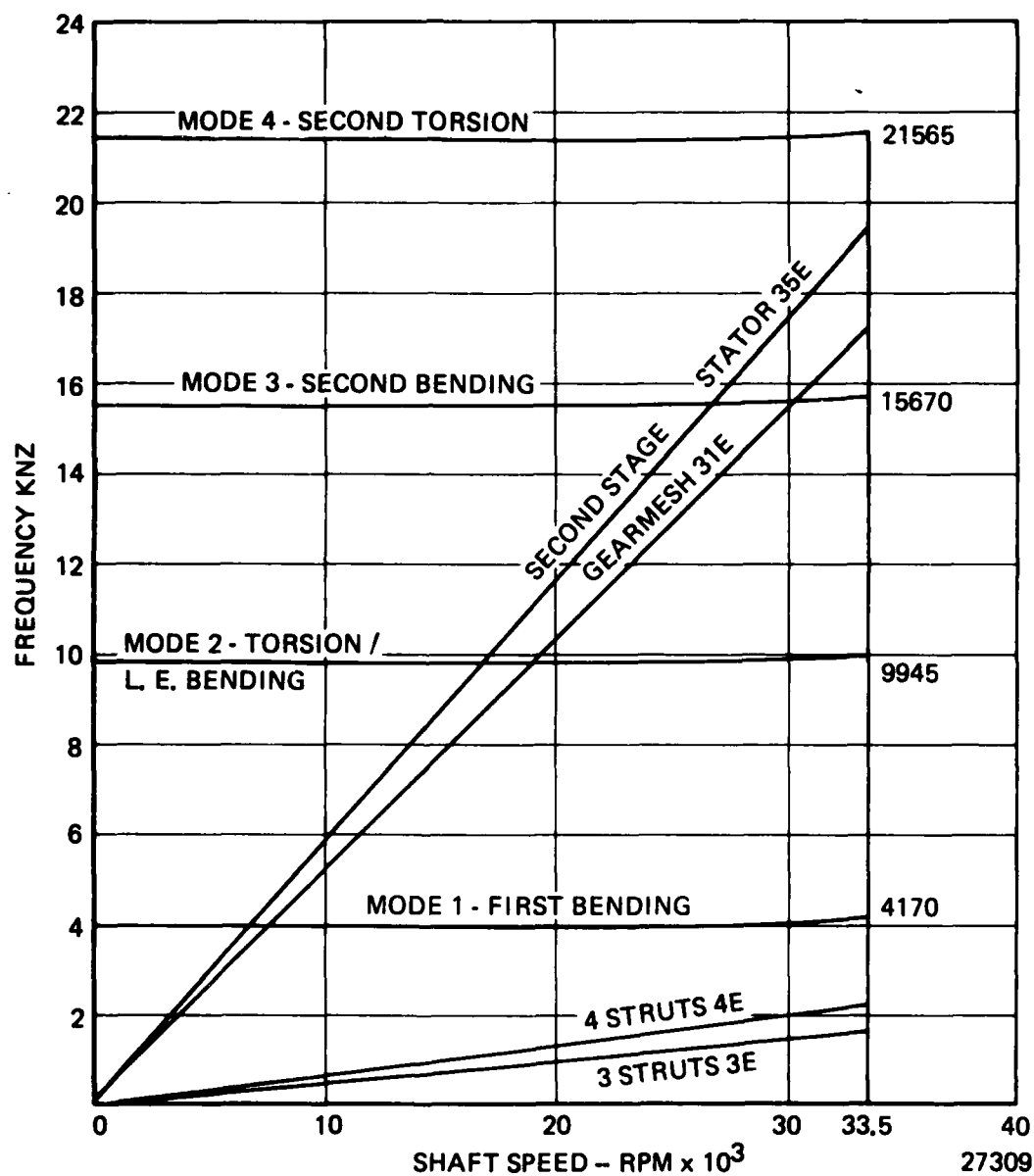
Figure 130 . E.G. Third Stage Compressor Blade Interference Diagram.
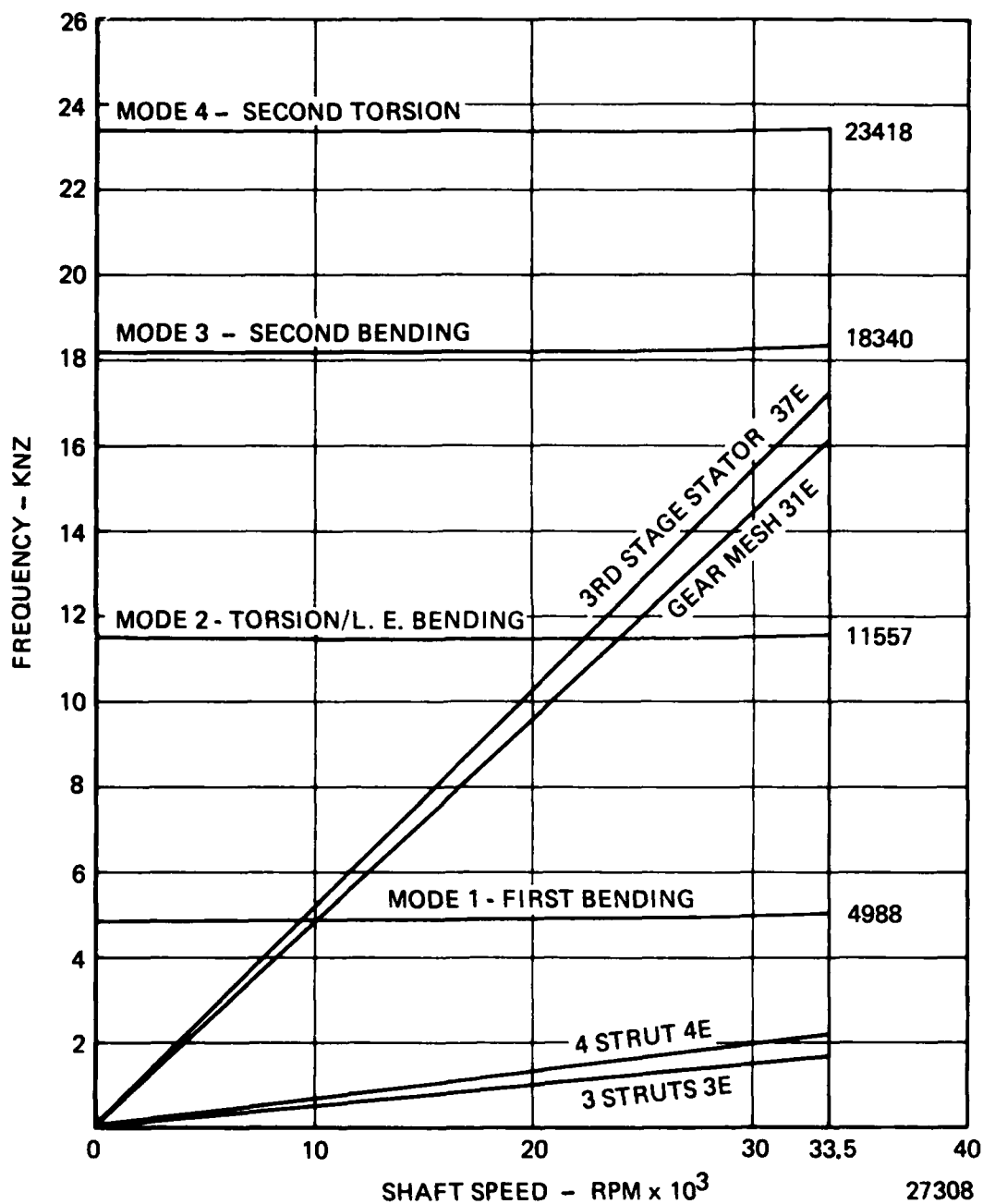
Figure 131 . E.G. Fourth Stage Compressor Blade Interference Diagram.

188

UNDEFLECTED

DEFLECTED→

27290
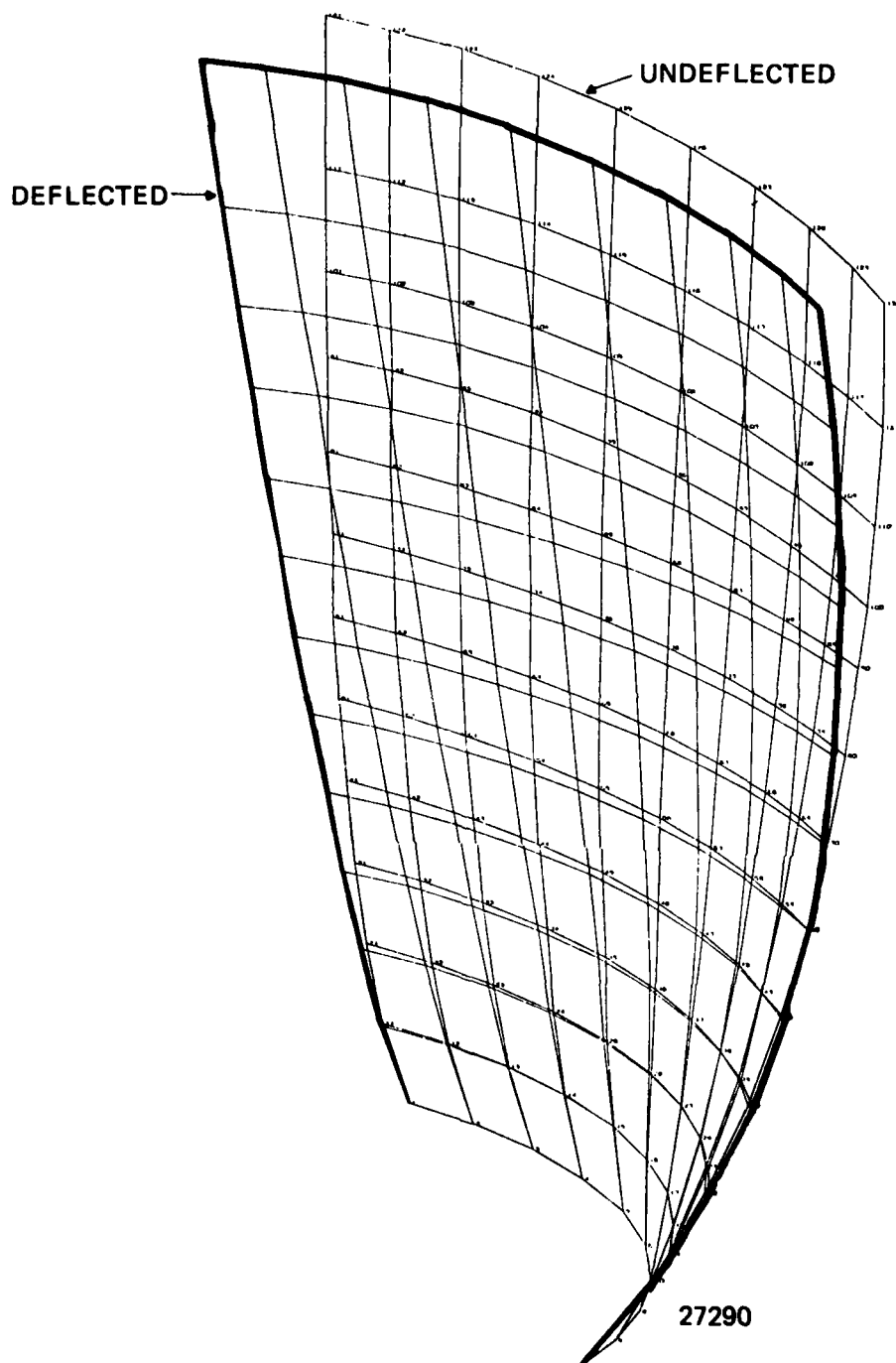
Figure 132. E.G. First Stage Compressor Blade Mode 1 Deflected Shape.
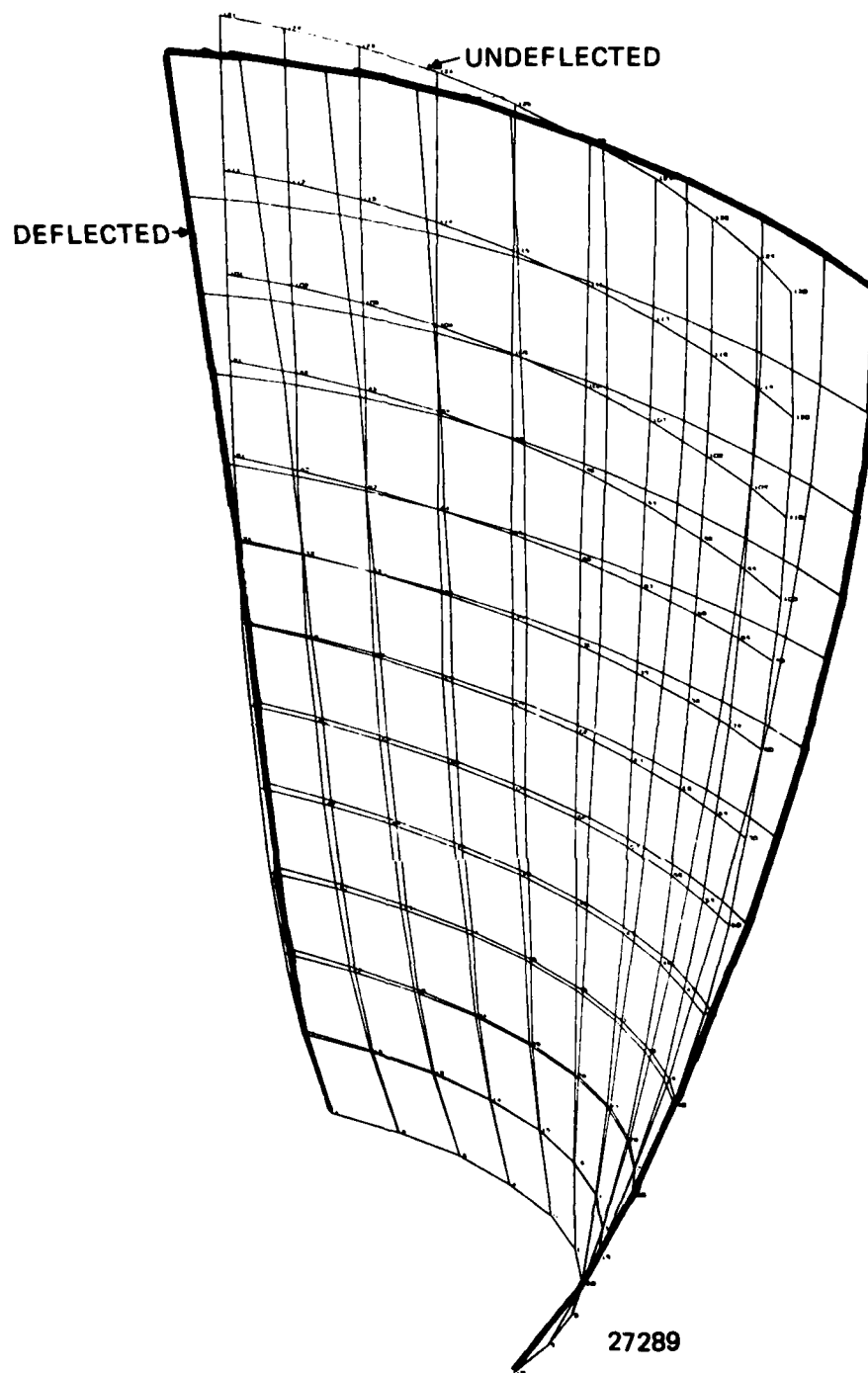
Figure 133. E.G. First Stage Compressor Blade Mode 2 Deflected Shape.

UNDEFLECTED

DEFLECTED

27287
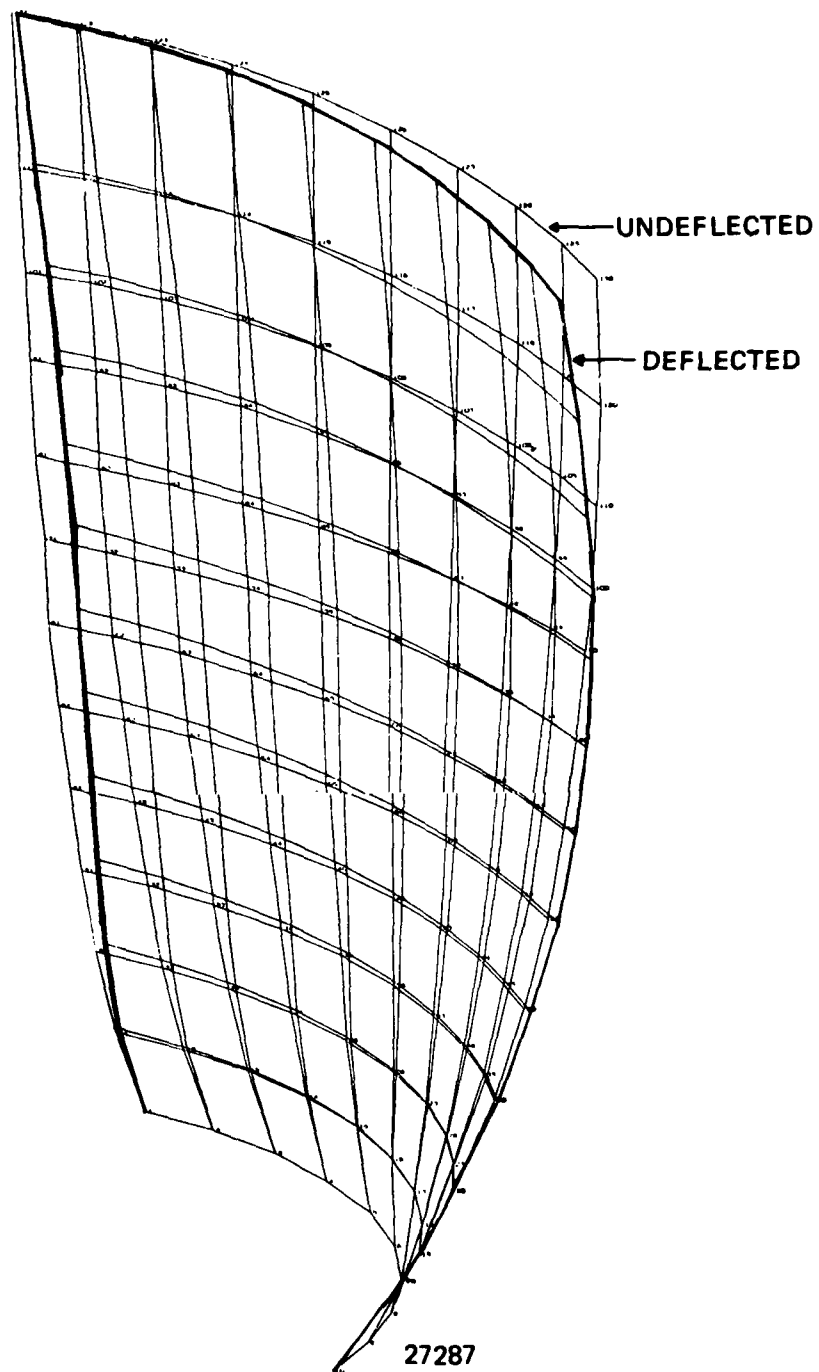
Figure 134. E.G. First Stage Compressor Blade Mode 3 Deflected Shape.

191

DEFLECTED

UNDEFLECTED

27288
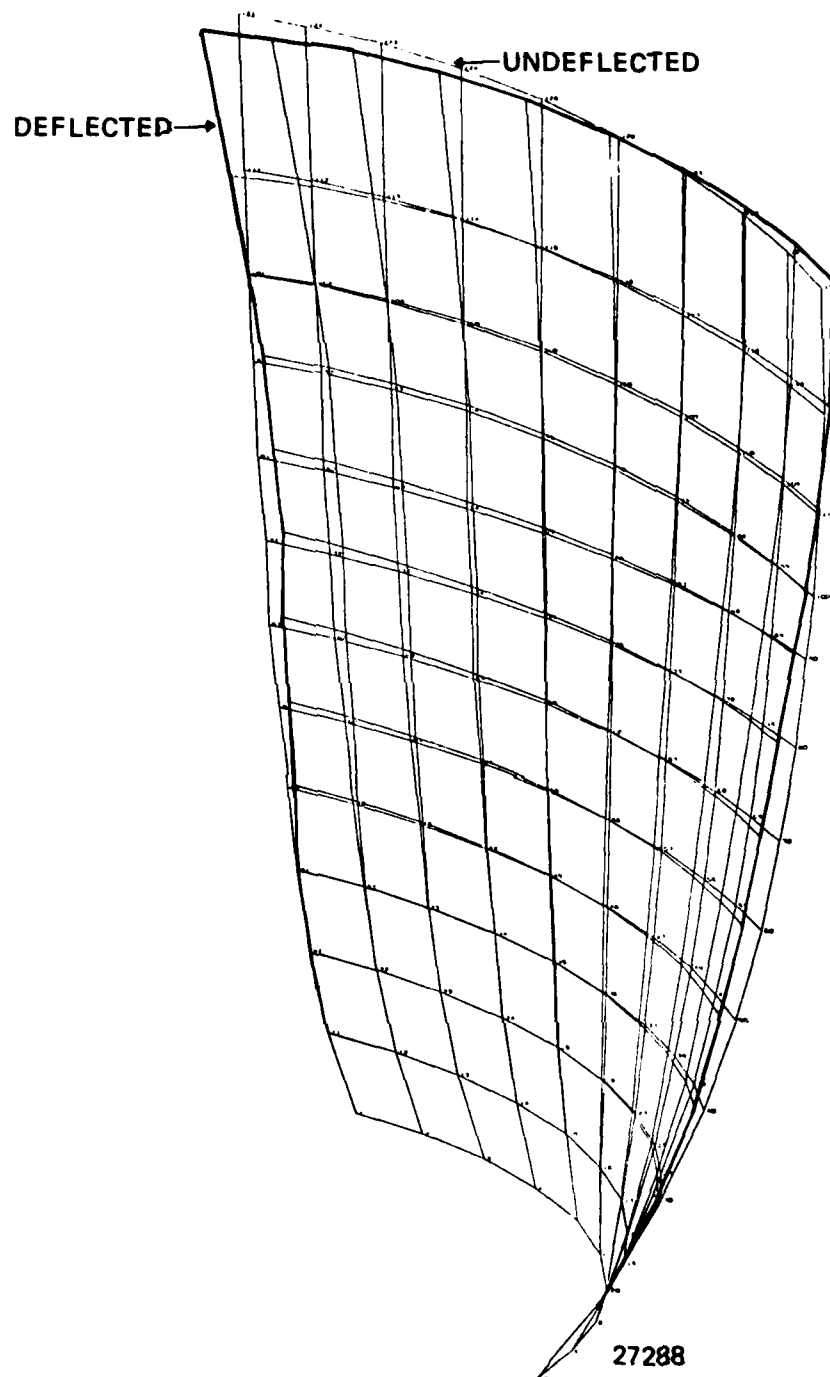
Figure 135 . E.G. First Stage Compressor Blade Mode 4 Deflected Shape.

UNDEFLECTED

DEFLECTED

27286
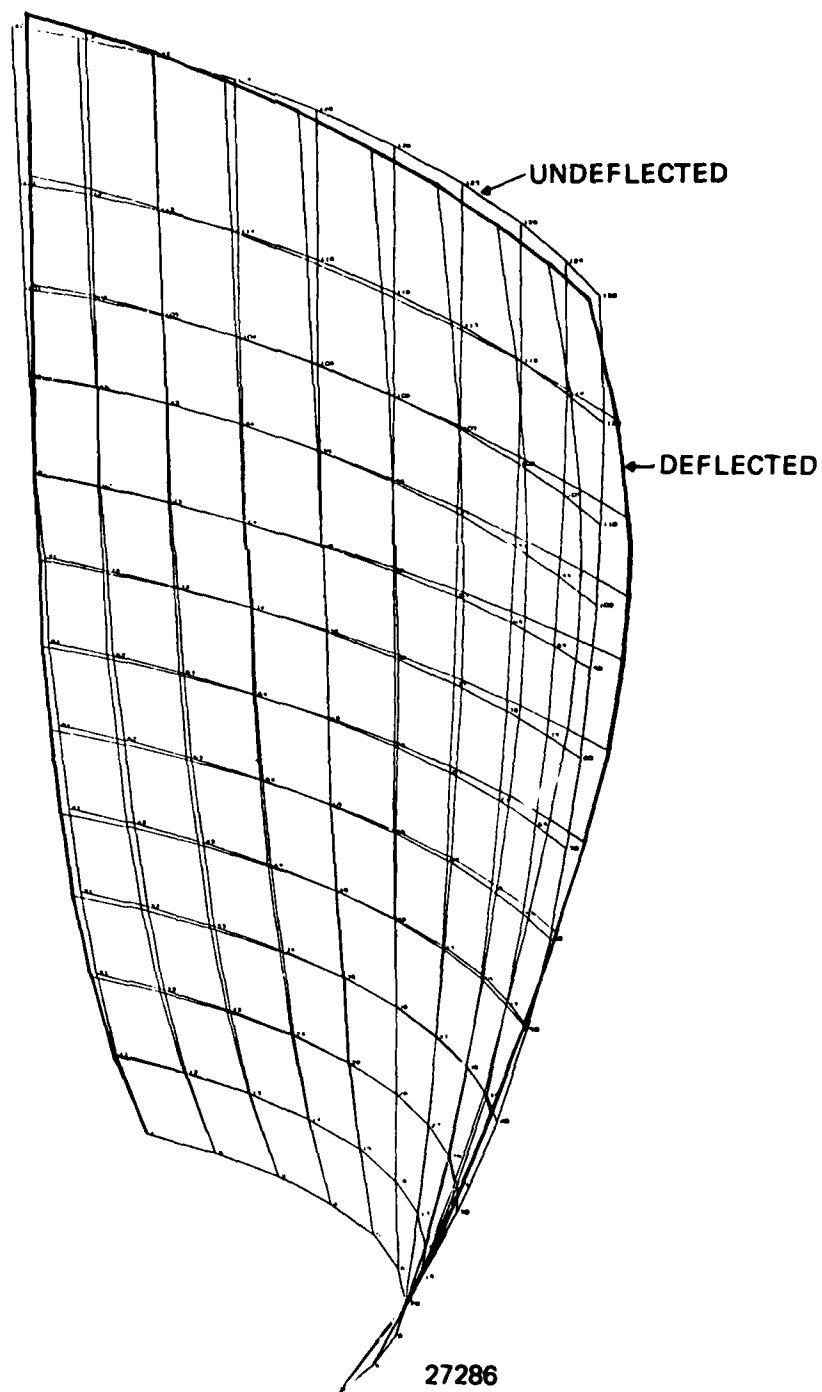
Figure 136. E.G. First Stage Compressor Blade Mode 5 Deflected Shape.

UNDEFLECTED

DEFLECTED

27285
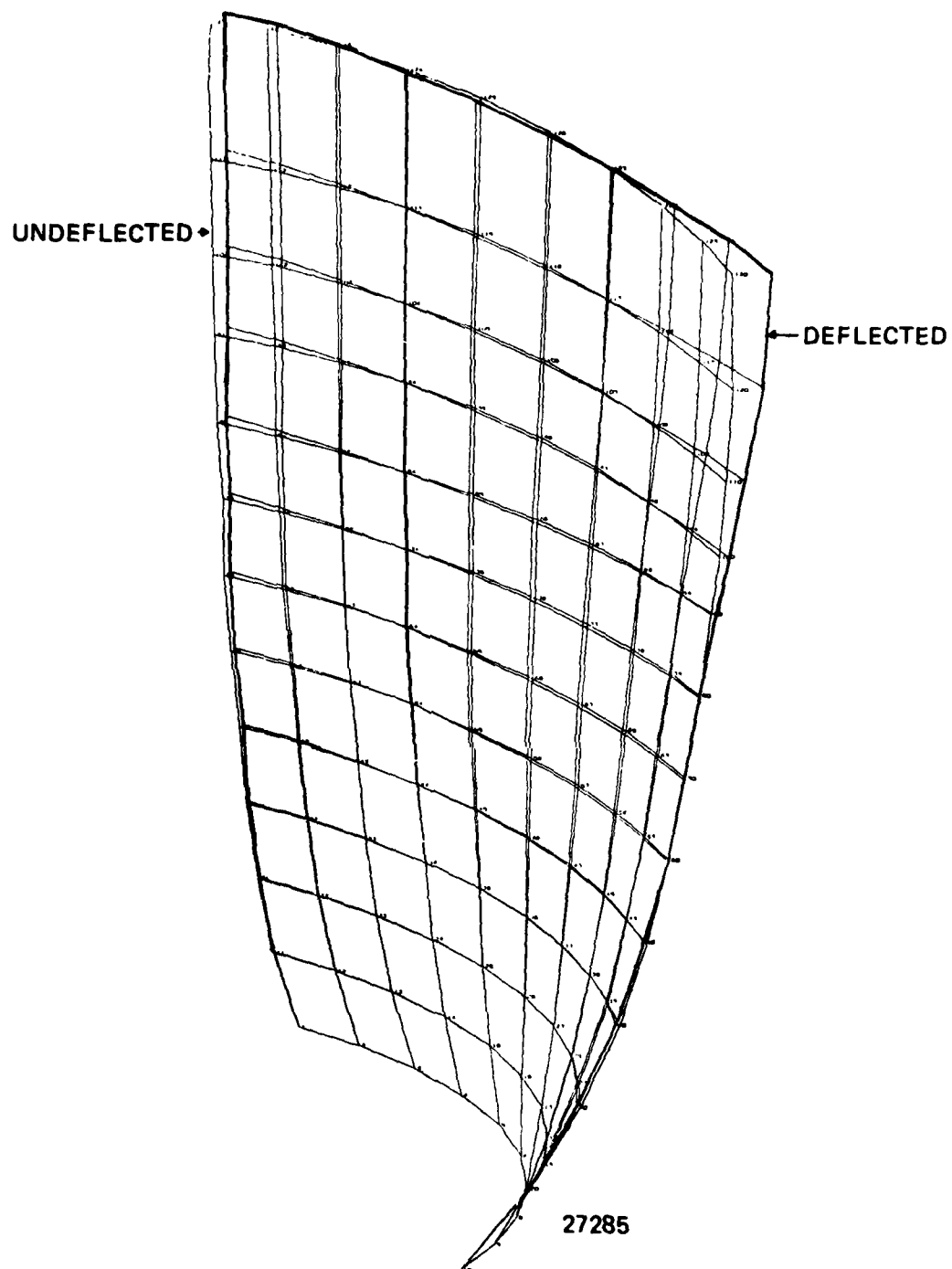
Figure 137. E G First Stage Compressor Blade Mode 6 Deflected Shape.
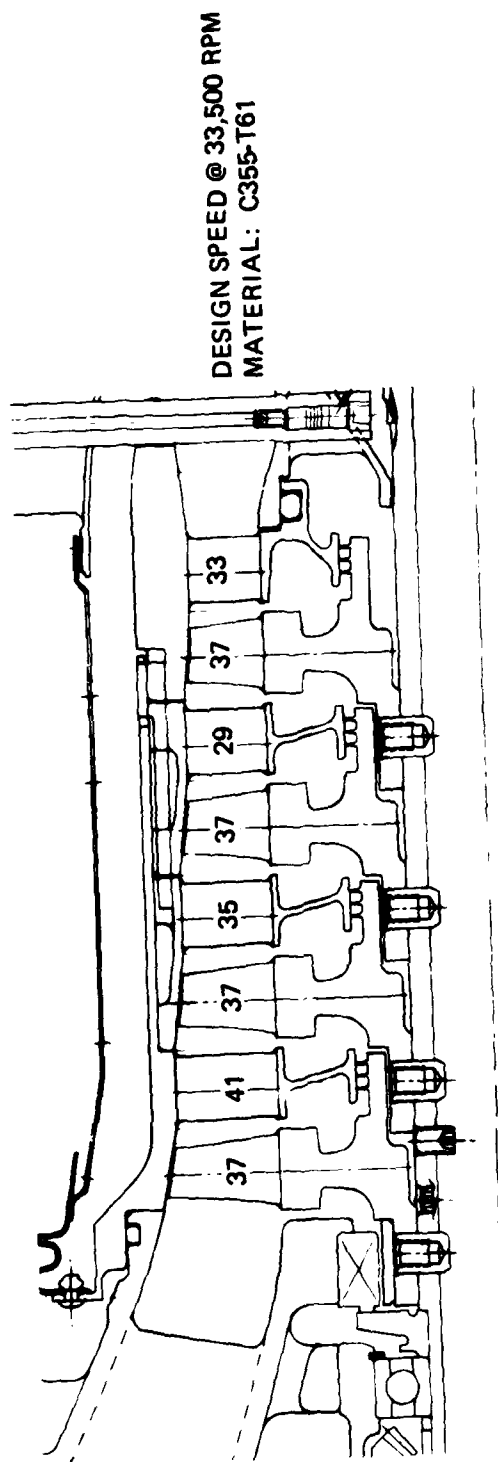
DESIGN SPEED @ 33,500 RPM
MATERIAL: C355-T61

BLADE STRESS SUMMARY

ROTOR STAGE	BLADE HUB TEMP. °F	MINIMUM MATERIAL PROPERTIES - KSI		HUB CENTRIFUGAL STRESS - KSI	HUB G/B STRESS (T.E.) - KSI	SAFETY FACTORS	
		Ultimate	.2% Yield			Ultimate	Yield
1	84	44	33	5.2	2.1	6.0	4.5
2	148	43	32.7	4.6	1.9	6.6	5.0
3	212	41	32.4	4.2	1.7	6.9	5.5
4	275	40	32.1	3.8	1.6	7.4	5.9

DISK STRESS SUMMARY

ROTOR STAGE	TEMP. °F	MINIMUM MATERIAL PROPERTIES - KSI		CENTRIFUGAL STRESSES KSI		BURST SPEED MARGIN, %	BURST SPEED RPM
		Ultimate	.2% Yield	Bore Tangential	Average Tangential		
1	84	44	33	12.7	8.3	71	57300
2	148	43	32.7	≈12.5	≈8.2	≈70	≈56950
3	212	41	32.4	≈12.3	≈8.0	≈68	≈56280
4	275	40	32.1	12.1	7.9	67	55950

27341

Figure 138. Summary of E.G. Compressor Blade and Disk Stresses.

195

	1ST STAGE	2ND STAGE	3RD STAGE	4TH STAGE
αA	= 2282 psi	= 1978 psi	= 1800 psi	= 1639 psi
αEAL	= 10000 psi	= 9714 psi	= 9142 psi	= 8571 psi
αM	= 6083 psi	= 5196 psi	= 4818 psi	= 4402 psi
αRAL	= 35000 psi	= 34000 psi	= 32000 psi	= 30000 psi

*αEAL @ TEMPS = .24αRAL

αA	--	Applied Vibratory Stress
αEAL	--	Endurance Limit
αM	--	Applied Steady Stress
αRAL	--	Ultimate Stress

27325
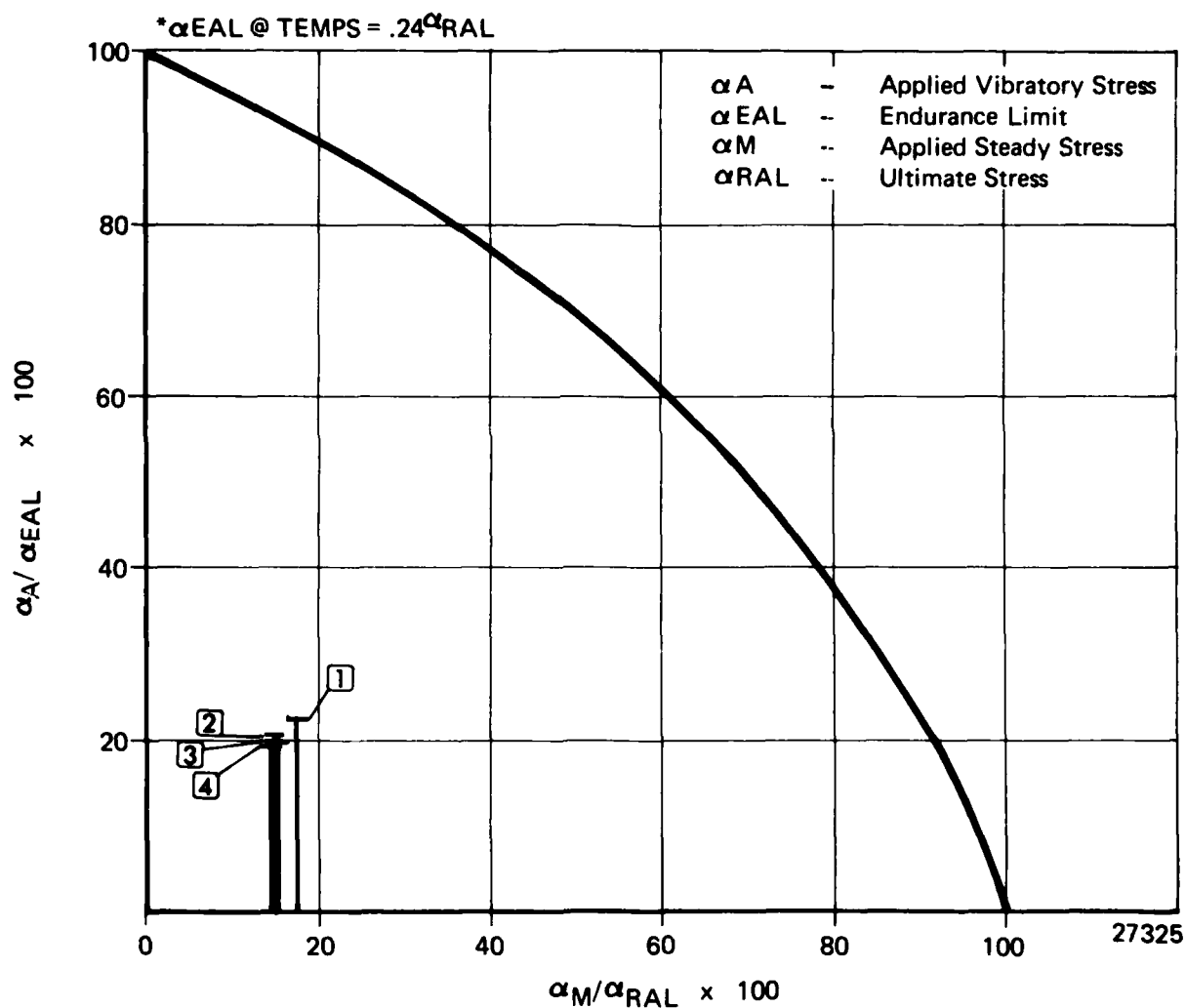
Figure 139. Expendable Gasifier Compressor Blades Four Stages, Material C-355A.

196
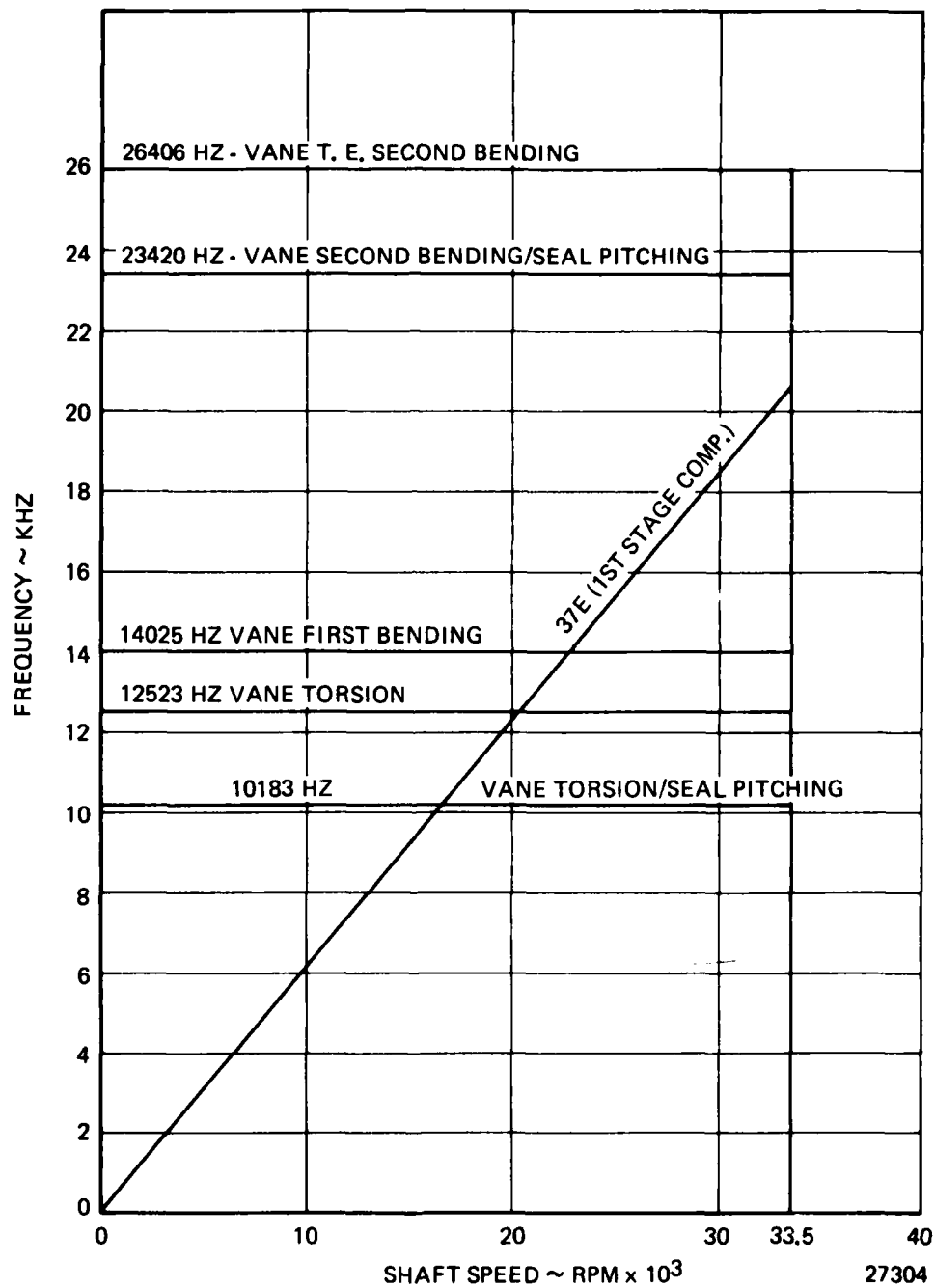
Figure 140. E.G. First Stage Compressor Stator Vanes Interference Diagram.

197
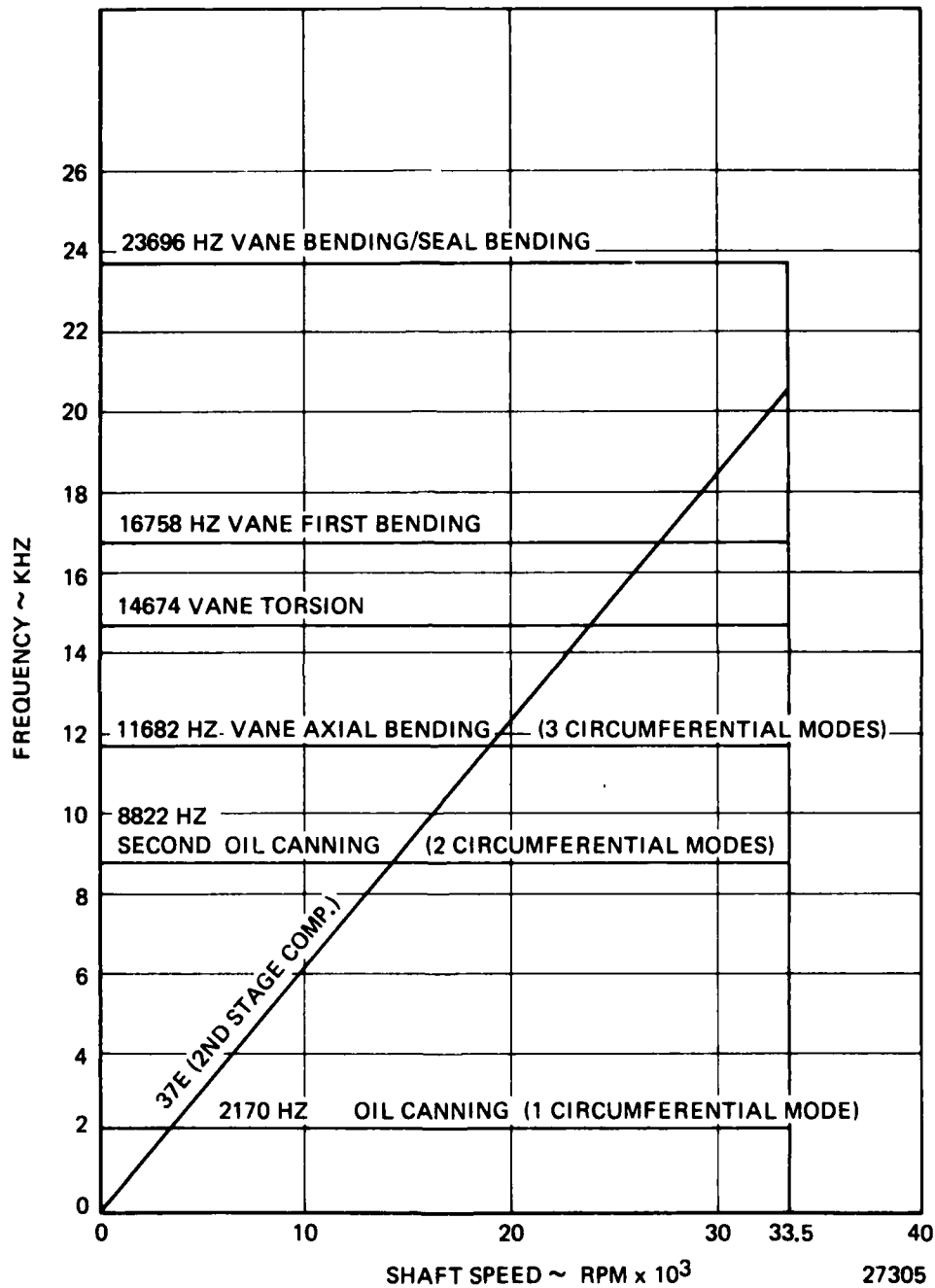
Figure 141. E.G. Second Stage Compressor Stator Vanes Interference Diagram.
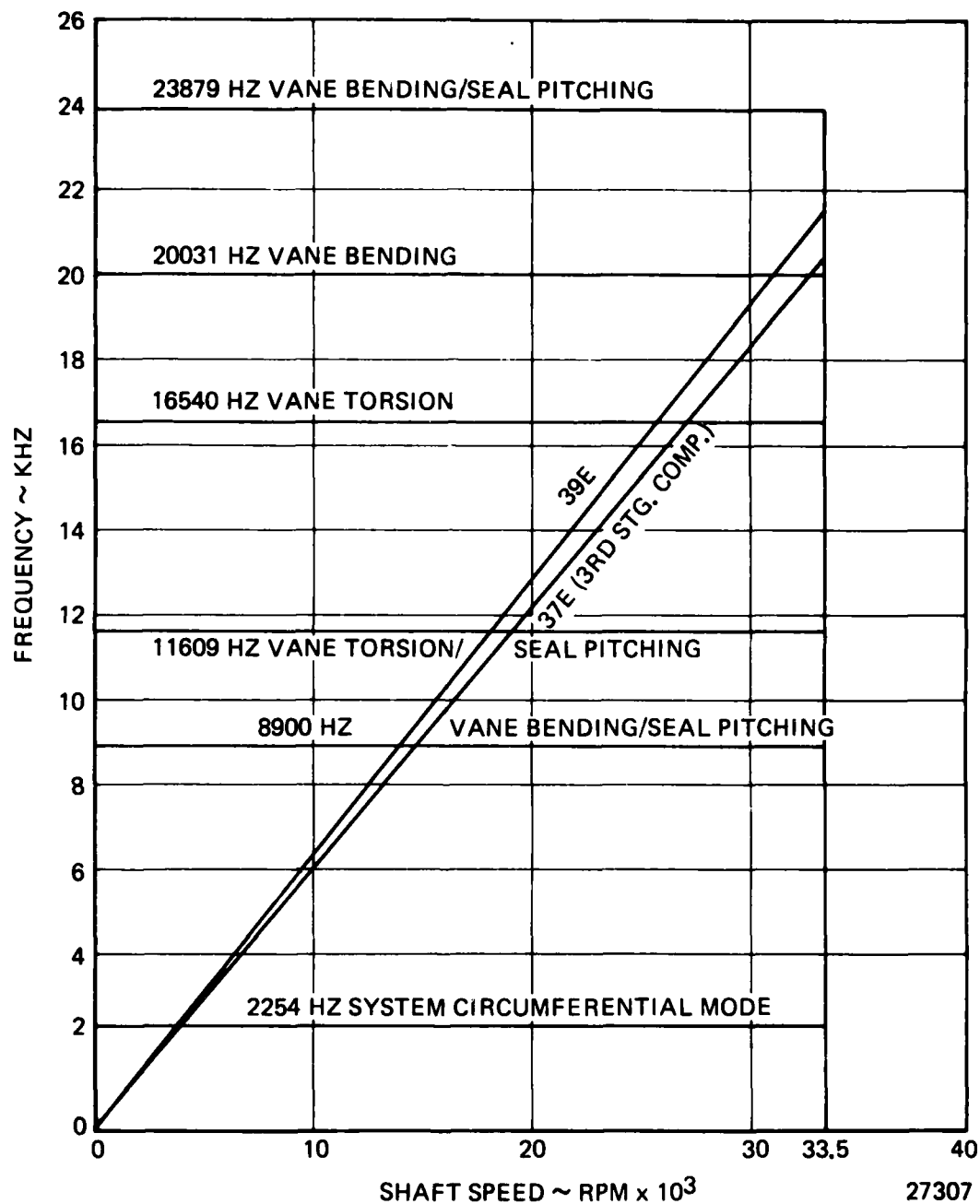
Figure 142. E.G. Third Stage Compressor Stator Vanes Interference Diagram.

199
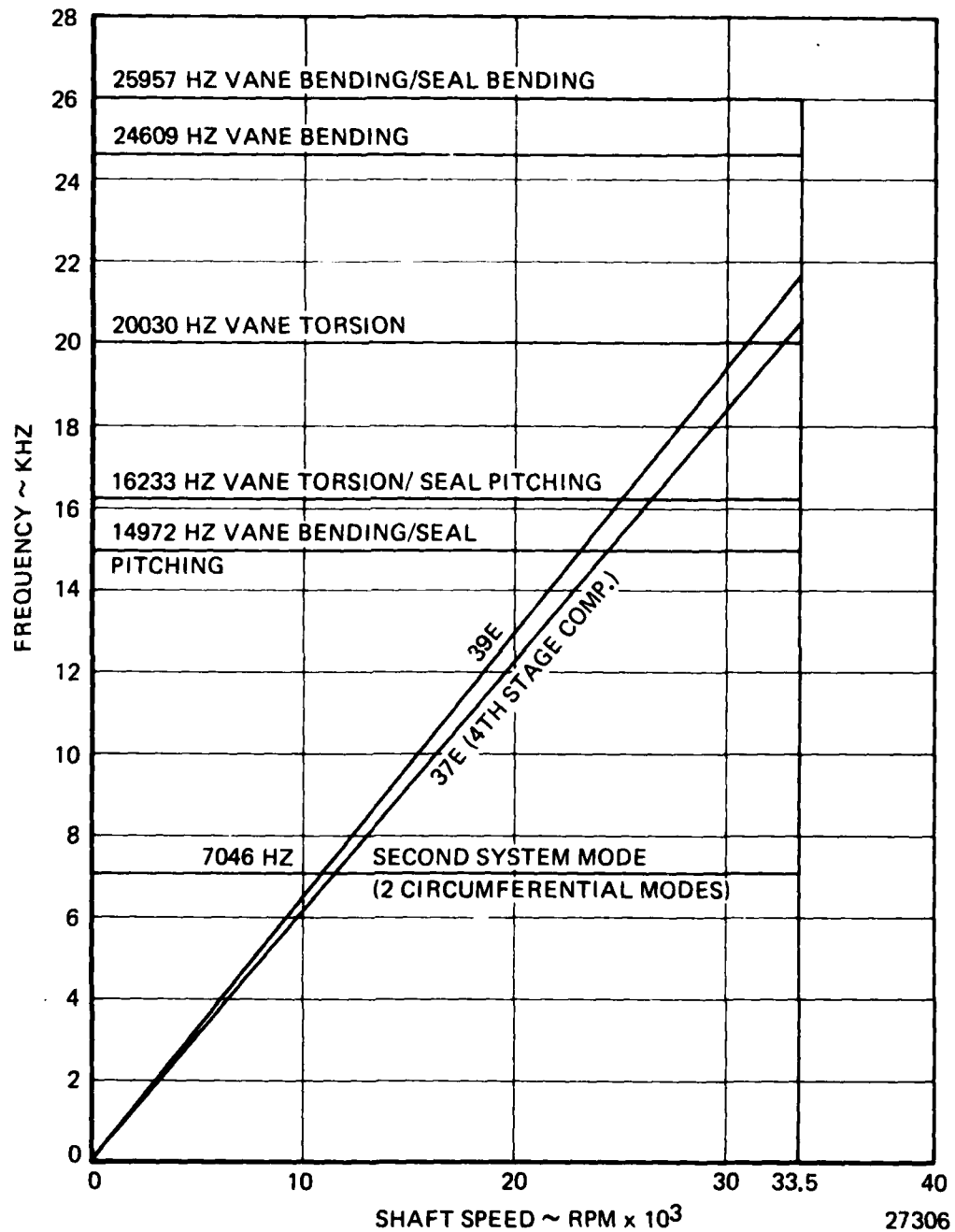
Figure 143. E.G. Fourth Stage Compressor Stator Vanes Interference Diagram.

200
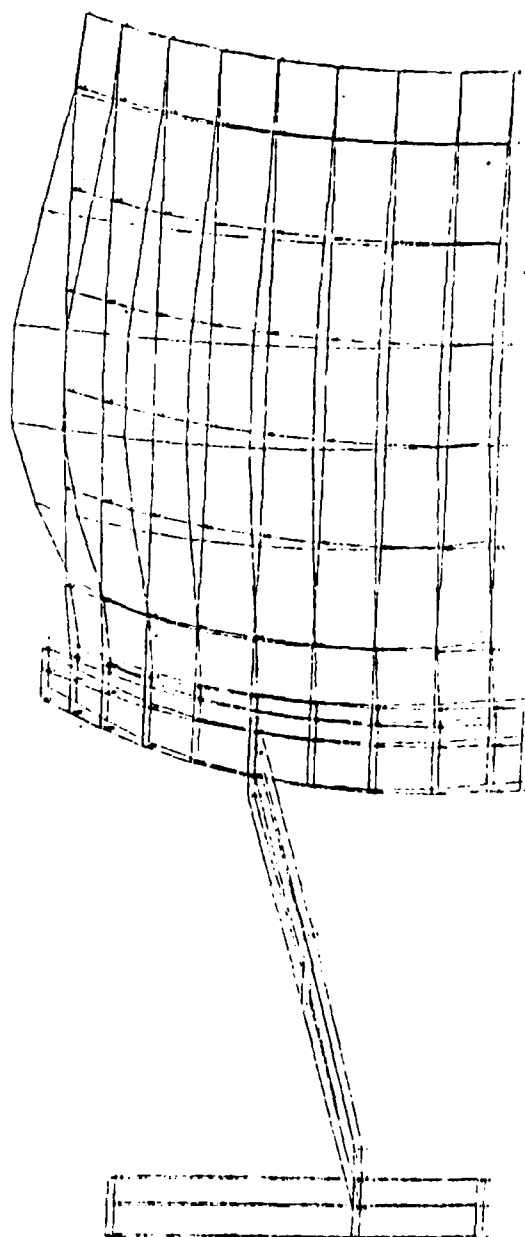
27295

Figure 144. E.G. First Stage Stator Finite Element Model - Mode at 14,024 cps.
(Tangential View).

27294
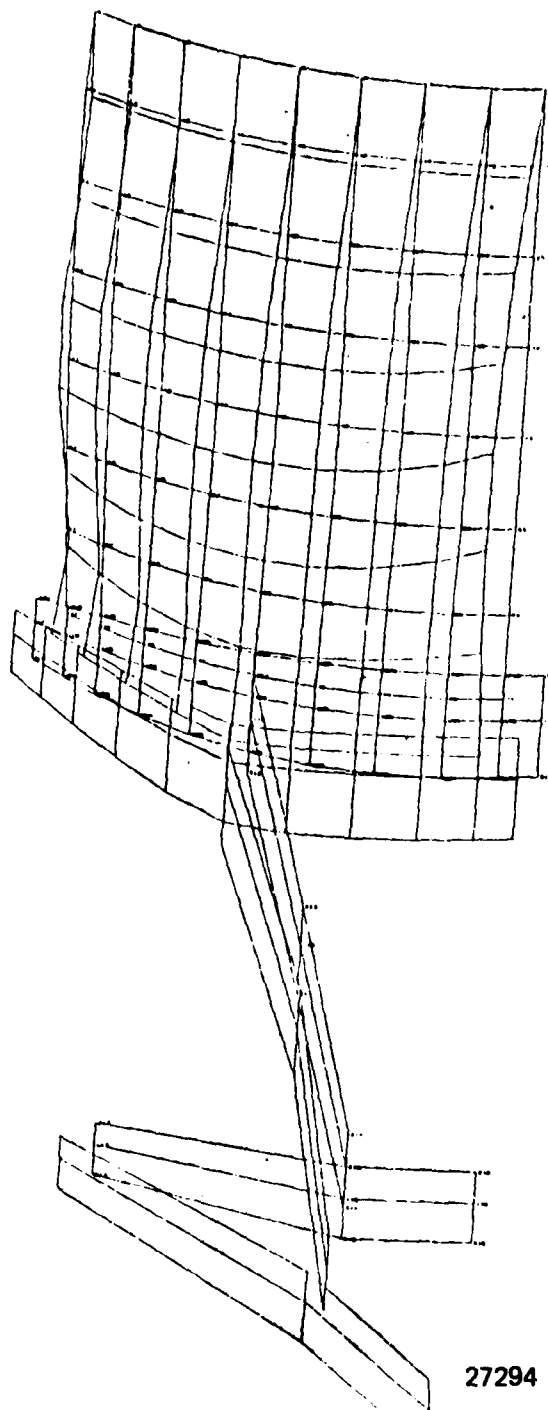
Figure 145. E.G. Second Stage Stator Finite Element Model - Mode Shape at 23,706 cps. (Tangential View).

27292
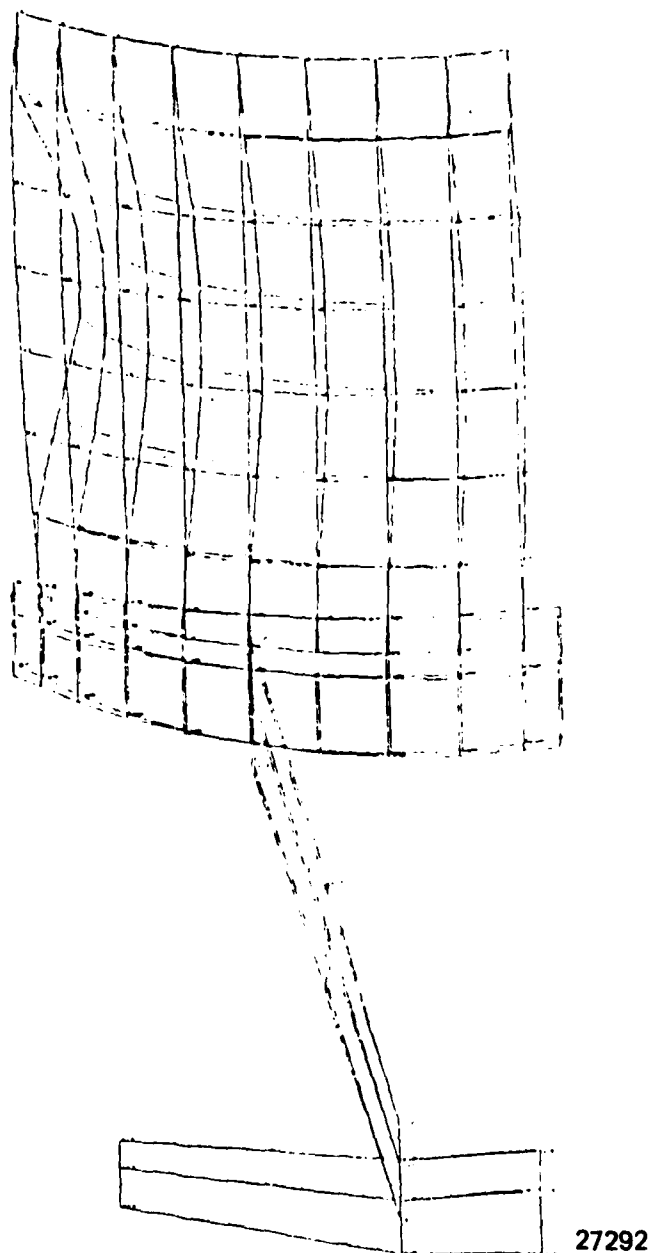
Figure 146. E.G. Third Stage Stator Finite Element Model - Mode Shape at
20,031 cps. (Tangential View).

27293
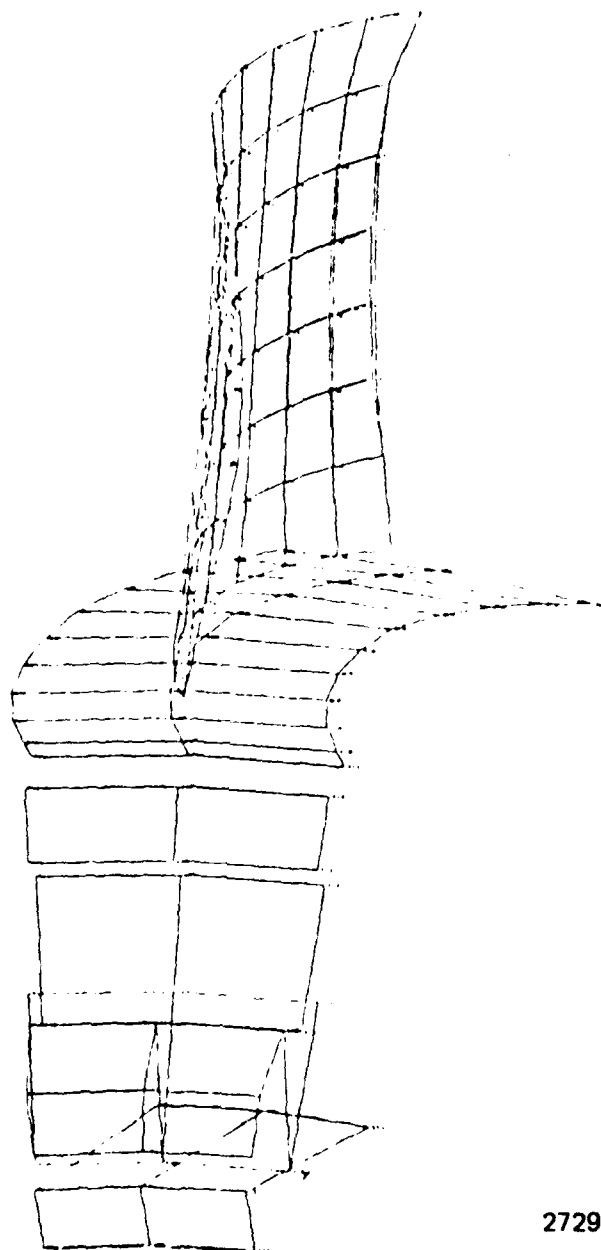
Figure 147. E.G. Fourth Stage Stator Finite Element Model - Mode Shape at 20,039 cps. (Axial View).

The stator vane gas bending stresses were calculated using guided cantilevered twisted beam models. Axial loads from the seal diaphram pressure loads were applied to the vane inner diameters. Calculated stresses were no higher than 3.2 ksi which resulted in very high safety factors, as shown in Figure 148. The vane stresses are shown on a modified Goodman diagram on Figure 149 where the vibratory stresses are assumed to be equal to the vane gas bending stresses. High vibratory stress margins are indicated.

5.1.3 Compressor Test Program

The testing of the expendable gasifier compressor consisted of the determination of material properties and spin pit testing and a rig test evaluation of its aerothermodynamic performance.

Material properties and spin pit testing were done prior to rig testing to assure the structural integrity of rotating components. The blade and vane natural frequencies were determined from the full-scale components and compared to excitation frequencies to determine if resonances would occur in the compressor rig testing or on the subsequent gasifier engine test. Possible resonance problems were indicated and the magnitude of the problem was assessed and corrective action was taken before proceeding to the rotating tests.

The purpose of the aerodynamic rig testing was to:

1. Determine the compressor aero performance
2. Investigate problem areas
3. Modify the blading if necessary, to provide adequate performance for engine operation.

The test rig is shown in Figure 150. The rig makes maximum use of engine hardware. The cross hatched hardware shown on the figure is adaptive facility hardware.

The compressor performance was determined at 40, 50, 60, 70, 80, 90, 100 and 110 percent of design speed. A complete map was obtained and the surge line indicated.

On-line data processing was used during testing to provide continuous print-outs of:

Corrected Speed
Corrected Airflow
Pressure Ratio
Adiabatic Efficiency
Bearing Temperatures

205
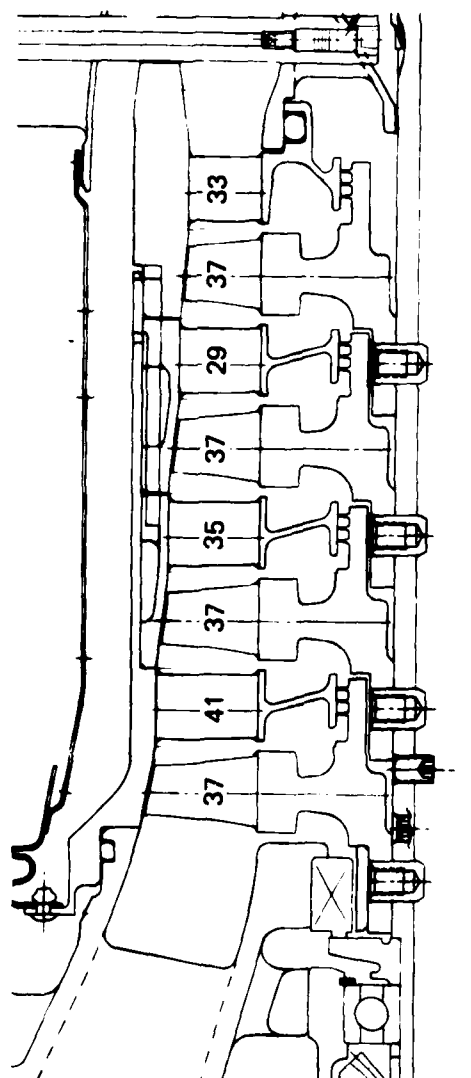
MATERIAL: C355-T61

STATOR VANES STRESS SUMMARY

Stator	Vane Temperature °F	Minimum Material Properties - KSI		Vane Gas Bending Stress (T.E.) - KSI	Safety Factors	
		Ultimate	.2% Yield		Ultimate	Yield
1	127	42	33	3.2	10	10
2	188	40	32	3.1	10	10
3	248	38	32	3.4	10	9.4
4	310	36	32	2.4	10	10

27340

Figure 148. Summary of E.G. Stator Vane Stresses.

The stator vane gas bending stresses were calculated using guided canti-
levered twisted beam models. Axial loads from the seal diaphram pressure loads
were applied to the vane inner diameters. Calculated stresses were no higher
than 3.2 ksi which resulted in very high safety factors, as shown in Figure 148.
The vane stresses are shown on a modified Goodman diagram on Figure 149 where
the vibratory stresses are assumed to be equal to the vane gas bending stresses.
High vibratory stress margins are indicated.

COMPRESSOR TEST PROGRAM

The testing of the expendable gasifier compressor will consist of the
determination of material properties and spin pit testing and a rig test evalua-
tion of its aerothermodynamic performance.

Materials Characterization and Spin Pit Testing

Material properties and spin pit testing will be done prior to rig test-
ing to assure the structural integrity of rotating components. The blade and
vane natural frequencies will be determined from the full-scale components and
compared to excitation frequencies to determine if resonances will occur in the
compressor rig testing or on the subsequent gasifier engine test. If resonance
problems are indicated, the magnitude of the problem will be assessed and correc-
tive action will be taken before proceeding to the rotating tests.

Rig Testing

The purpose of the aerodynamic rig testing is to:

1. Determine the compressor aero performance
2. Investigate problem areas
3. Modify the blading if necessary, to provide adequate
   performance for engine operation

The test rig is shown in Figure 150. The rig makes maximum use of engine
hardware. The cross hatched hardware shown on the figure is adaptive facility
hardware.

The compressor performance will be determined at 40, 50, 60, 70, 80, 90,
100 and 110 percent of design speed. A complete map will be obtained and the
surge line will be indicated.

Data Processing

On-line data processing will be used during testing to provide continuous
print-outs of: Corrected Speed
                 Corrected Airflow
                 Pressure Ratio
                 Adiabatic Efficiency
                 Bearing Temperatures

1st Stage	2nd Stage	3rd Stage	4th Stage
σA = 3173 psi	= 2731 psi (t.e.)	= 2493 psi (t.e.)	= 2245 psi (t.e.)
μEAL= 12180 psi	= 11060 psi	= 11020 psi	= 10440 psi
σM = 2651 psi	= 3135 psi (t.e.)	= 3402 psi (t.e.)	= 2389 psi (t.e.)
σRAL = 42000 psi	= 40000 psi	= 38000 psi	= 36000 psi

σ EAL = .29 σRAL

σA	– Applied Vibratory Stress
σEAL	Endurance Limit
σM	Applied Steady Stress
σRAL	Ultimate Stress

27327
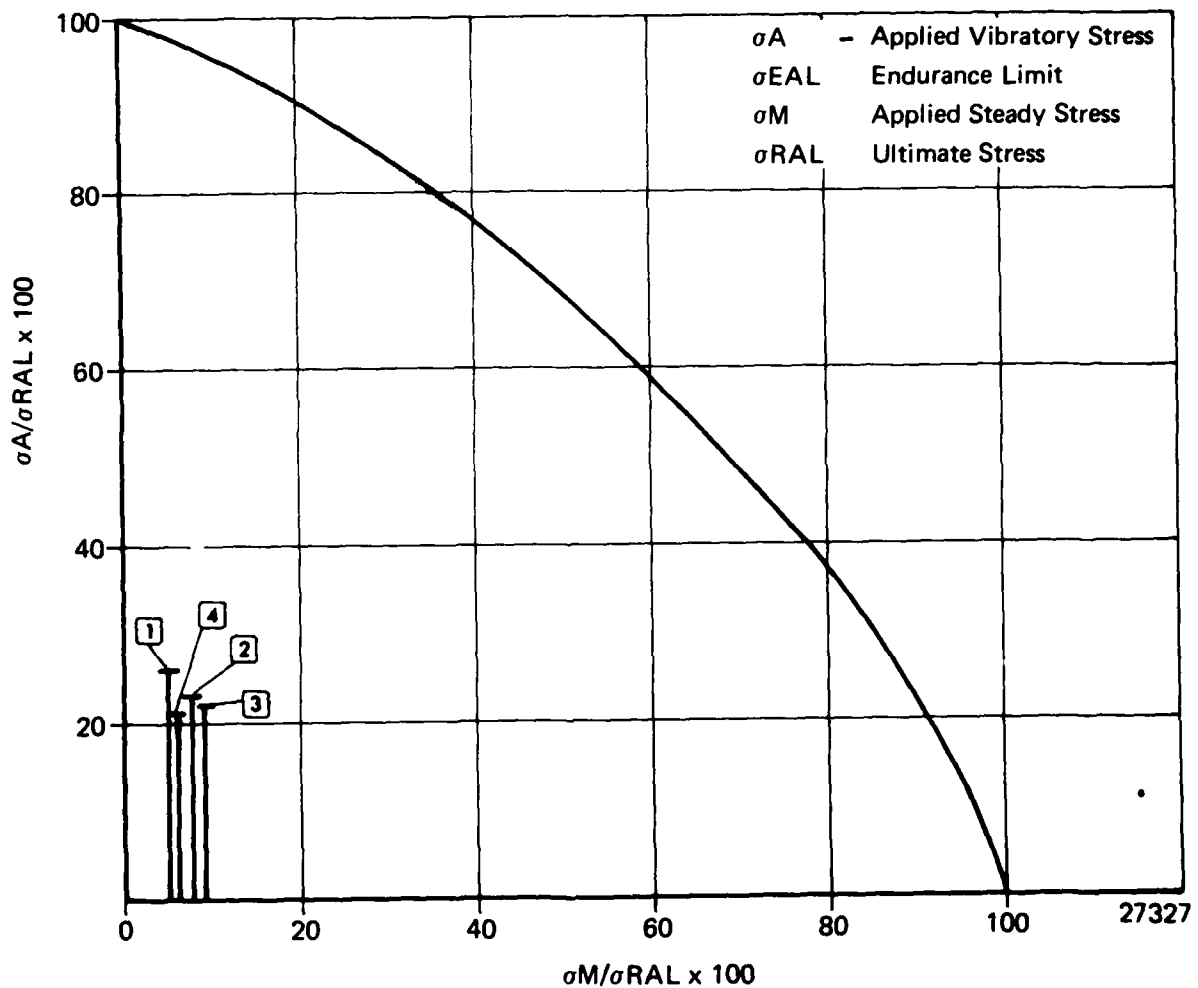
Figure 149. Modified Goodman Diagram Expendable Gasifier Stator Vanes, Four Stages, Material C-355 T-61.

3 - TOTAL PRESSURE RAKES
3 - TOTAL TEMPERATURE RAKES
1 - P_T, Y_{AW} SURVEY PROBE

2 - TOTAL PRESSURE RAKES
2 - TOTAL TEMPERATURE RAKES

● - WALL STATIC PRESSURE TAPS

▨ - COMPONENTS UNIQUE TO THIS TEST RIG

25976
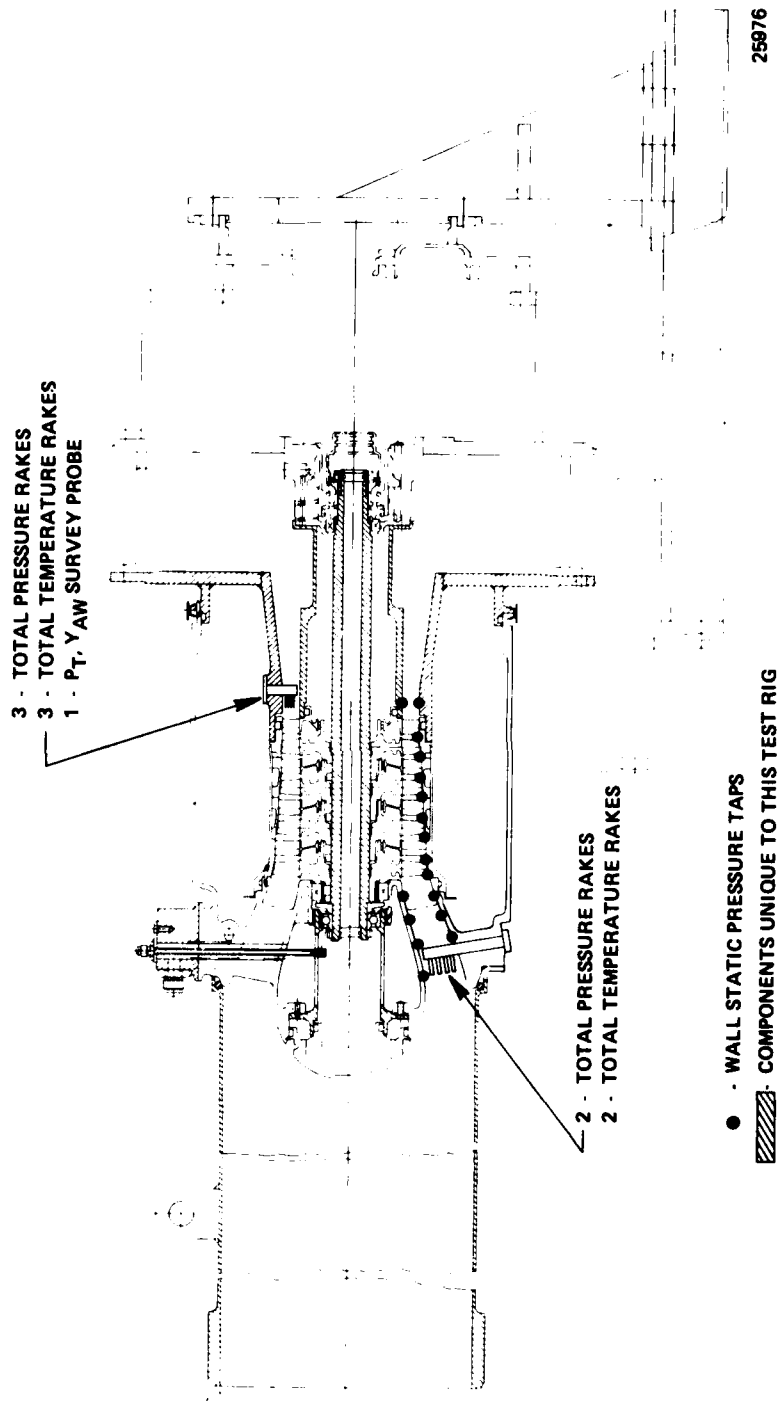
Figure 150. Expendable Gasifier Compressor Test Rig.

208

The individual values of all measured pressures and temperatures were also available on an "as demanded" basis during testing to check data validity to obtain more detailed performance analyses which would be required if performance was low.

Rig instrumentation (Figure 150) consists of inlet and exit pressure and temperature rakes for overall performance calculations, plus wall static pressures to assist in performance analysis. The rakes are the same as those to be used to monitor compressor performance in the demonstrator engine. A cobra probe is used at the compressor exit to measure total pressure and angle. An ASME nozzle is employed upstream of the rig to measure airflow, and an electric counter is used for speed.

Prior to testing, the temperature rakes were calibrated for Mach number effects.

The aero test program consisted of obtaining 5 to 8 data points per speed line from 40 to 110 percent of design speed. After mapping the compressor at selected data points on the engine operating line, the compressor exit was surveyed to obtain angle and total pressure profiles for combustor studies.

A map is generated similar to that shown in Figure 151. Plots of exit total pressure and air angle versus exit radius are made for the exit survey data points.

If a performance deficiency exists, the wall static pressures are used to identify the problem area.

Figure 152 shows the interaction of events planned during the compressor test period. One modification has been included to acknowledge the possibility of a performance deficiency within the rotor or stator blading. Since the compressor design is a modified upscale of an existing compressor (Model 469) which demonstrated higher efficiency than required of the Model 506 (Expendable Gasifier), only slight adjustment of the rotor blading (by bending) was considered necessary to achieve the desired performance.
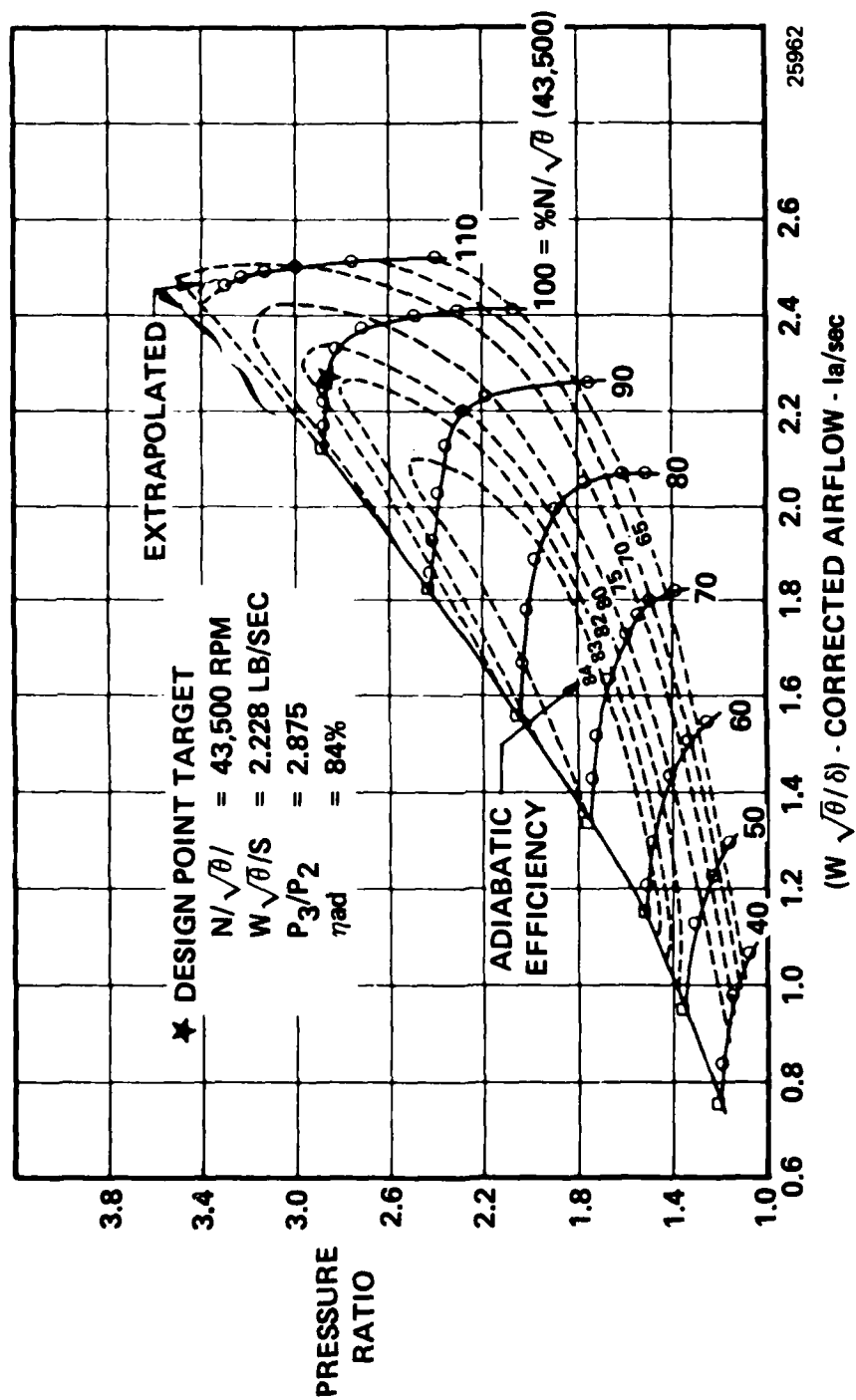
Figure 151.   Model 469 Four-Stage Compressor Performance.

Figure 152. Planned Phase IV Compressor Test Events.

211

5.2   COMBUSTOR DESIGN

5.2.1   Design Objectives

In keeping with the multi-application, Expendable Gasifier concept, a prime design objective for the combustor was to achieve the minimum fabrication and/or acquisition costs commensurate with life, cyclic and performance requirements. Three applications were considered: a Jet Fuel Starter (JFS), a Turbojet and a Turbofan. Their design requirements are listed in Table 21. Of these, the cyclic requirement for the JFS was the most severe and required that liner temperatures and thermal gradients be closely controlled to prevent premature failure through low cycle fatigue and/or oxidation.

TABLE 21

DESIGN REQUIREMENTS			
	Jet Fuel Starter	Turbojet	Turbofan
Thrust/HP	230 HP	230 LBS	500 LBS
Life at Maximum Thrust	--	20 HRS	20 HRS
Start Cycles (45 Seconds Each)	2000	--	--
Operational Altitude	Sea Level Std. Day 59°F Cold Day -65°F Hot Day 130°F	36,000 FT	36,000 FT

The physical envelope requirements of the Expendable Gasifier made the selection of a full annular, reverse flow combustor mandatory. The simplicity and low fuel pressure characteristics of the vaporizer combustor blend well with the low cost objective. Specific combustor performance goals (Table 22) are within Teledyne CAE's experience with annular, reverse flow, vaporizer combustors.

5.2.2   Design Parameters

The combustor design flowpath, airflow distribution, and local equivalence ratios are shown in Figure 153. Several combustor aerothermodynamic and geometric design parameters are summarized in Table 23. Fuel is introduced from an integrally cast manifold in the front frame (Figure 154) through low pressure drop orifices into fuel tubes that subsequently feed 14 vaporizer pipes penetrating into the primary combustion zone. The fuel is mixed with air in the vaporizer pipe

TABLE 22

PERFORMANCE GOALS
(SLS, STANDARD DAY)

PRESSURE LOSS	10.0%	
HEAT RELEASE	9.3	$\dfrac{\text{MBTU}}{\text{HR} * \text{FT}^3 * \text{ATM}}$
EFFICIENCY	95.0%	
EXIT TEMPERATURE DISTRIBUTION FACTOR	0.2	
RADIAL TEMPERATURE PROFILE FACTOR	0.075	

27374
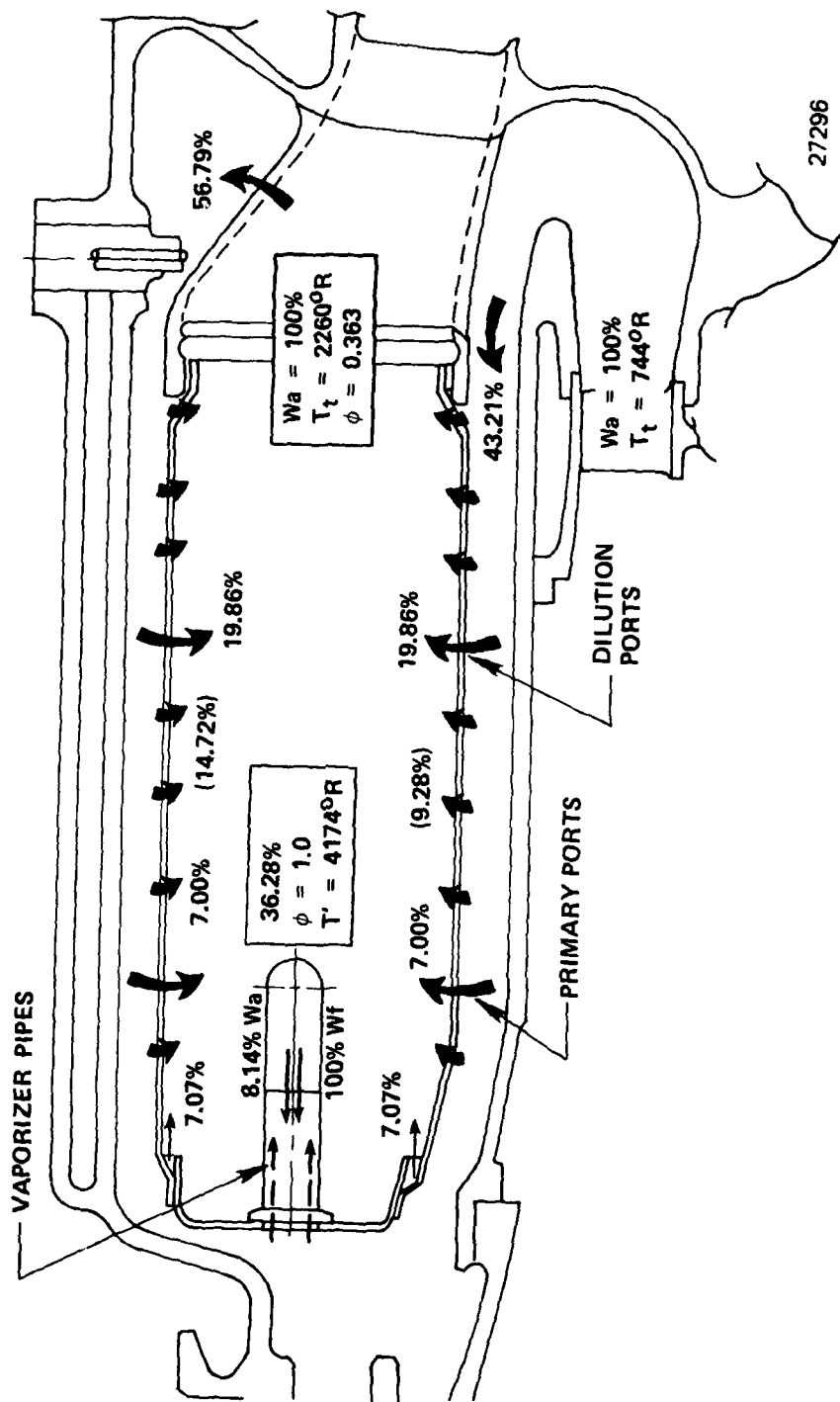
Figure 153. Combustor Airflow Distribution.

214

TABLE 23

COMBUSTOR DESIGN PARAMETERS	
Engine Airflow, lb/sec	3.862
Compressor Discharge Pressure, psia	40.31
Compressor Discharge Tempeature, °F	284
Fuel Flow, lb/hr	341
Fuel - Air Ratio	0.0245
Total Pressure Loss - %	10.0
Average Exit Temperature, °F	1800
Reference Velocity, ft/sec	45.6
Isothermal Residence Time, Milliseconds	8.88
Aerodynamic Loading, $\dfrac{\text{lb air}}{\text{sec ft}^3\text{atm}^2}$	2.087
Heat Release Rate, $\dfrac{\text{MBTU}}{\text{Hr ft}^3\text{atm}}$	9.30
Combustor Inlet Mach Number	0.324
Reference Area, ft^2	0.608
Combustor Length, ft	0.548
Combustor Annulus Height, ft	0.1796
Combustor Length to Annulus Height Ratio	3.05
Number of Fuel Injection Points	14

PRESSURE DROP

AT START   1 PSI
AT DESIGN   100 PSI

METERING
ORIFICE

FUEL
MANIFOLD

21854

Figure 154. Fuel Distributor System.

(at an equivalence ratio of 4.46) partially vaporized, and discharged forward onto the baseplate. Here the fuel-rich mixture distributes both radially and circumferentially and mixes with the remaining combustion air at an overall primary zone equivalence ratio of 1.0. The forward efflux from the vaporizer pipes combines with the radial penetration of the primary jets to generate both a strong recirculation zone and the flame stabilization necessary for good combustion. Diametrically opposed dilution ports provide the turbulent mixing required to tailor exit temperature profiles.

The outer and inner liners are formed from perforated plate that provides full coverage film cooling for these components. While this form of cooling consists of discrete point injection of the cooling air (Figure 155) full coverage is afforded by lateral spreading and axial replenishment prior to destruction of the film by mixing with the hot gases. The design hole pattern of the perforated plate is shown in Figure 156 along with predicted liner temperatures for this cooling hole configuration.

During the procurement stage for the combustor development test hardware, it was found that tooling for this hole size/configuration was not commercially available. Consequently, the available hole pattern shown on the right of Figure 157 was selected as a substitute. This configuration has geometry similar to the design as shown on the left of Figure 157. However, both hole spacing and size have been increased proportionately to maintain the effective open area at the design value of 1.5 percent. Consequently, the cooling air flow per unit area of the liners and liner temperatures were retained at design levels.

Figures 158 and 159 are photographs of the combustion liner ready for test and already shows the perforated plate construction, the orientation of the primary pipes and one pair of the ignition system access holes.

Combustor ignition is achieved by dual spark ignitor/primer fuel nozzle pairs, Figures 160 and 161, located 90° apart on the left side of the gasifier. The primer fuel nozzle is of the simplex, pressure atomizing type operating at a nominal flowrate of five pounds per hour at 50 psi differential. The spark ignitor was designed for 3 to 5 sparks per second with a nominal one joule stored energy

5.2.3 Development Tests

In order to ensure trouble free performance of the combustor when installed in the expendable gasifier, it was necessary to first define and then correct any performance and/or structural deficiencies. This was accomplished using a combustor test rig adapted to accept the combustor flowpath of the expendable gasifier, Figure 162. The rig incorporated as much of the expendable gasifier hardware as possible. These components included the front frame containing the integrally cast main and starting fuel manifolds; the cast turbine inlet nozzle with hollow vanes for supplying air to the outer combustor annulus; the combustor liner; the main fuel tubes; and the dual spark ignitor/starting fuel nozzle pairs.
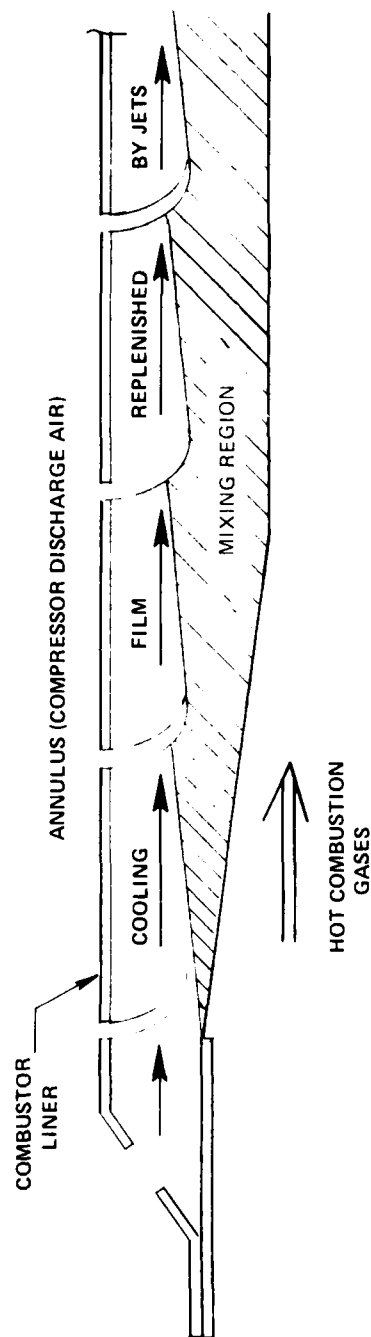
Figure 155. Schematic of Full Coverage Film Cooling.

218

Figure 156. Liner Metal Temperatures Preliminary Design - SLS Standard Day.

21847

0.44

0.504

0.06
DIA.

0.44

55°

55°
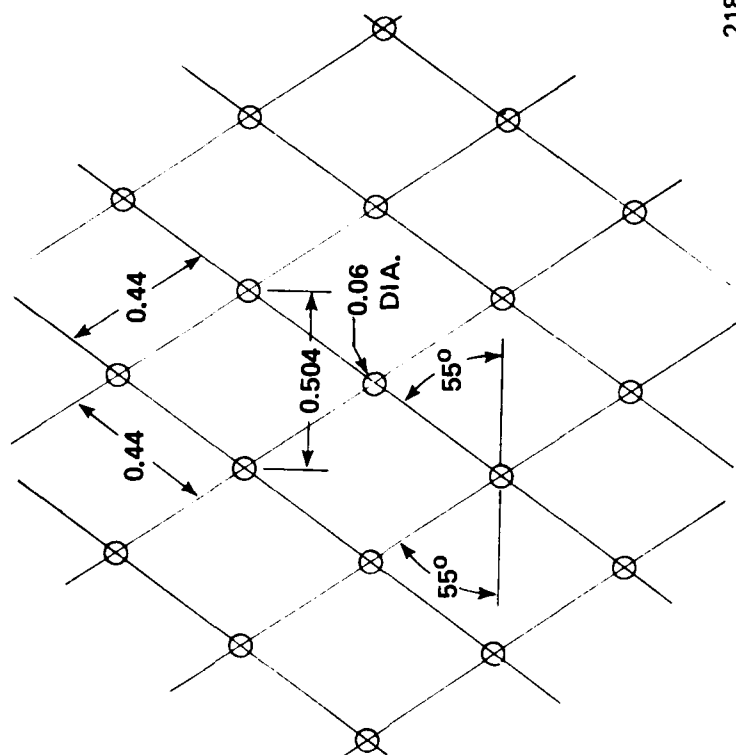
21889

TOOLING AVAILABLE

0.03
DIA.

0.219

0.219

45°
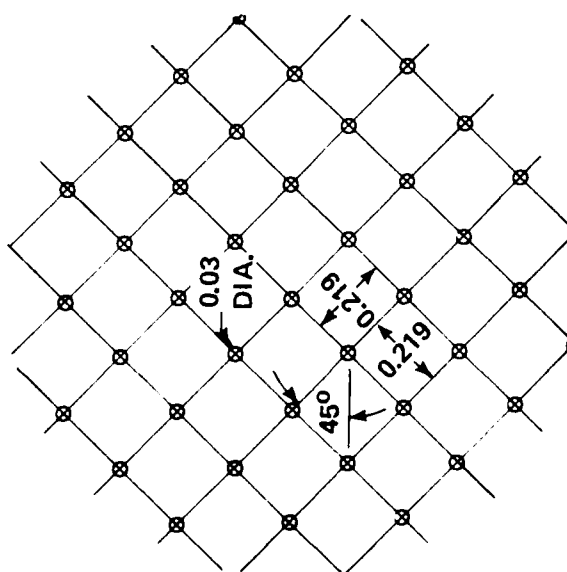
PRELIMINARY
DESIGN
(NEW TOOLING)

Figure 157. Perforated Plate Hole Patterns.

220
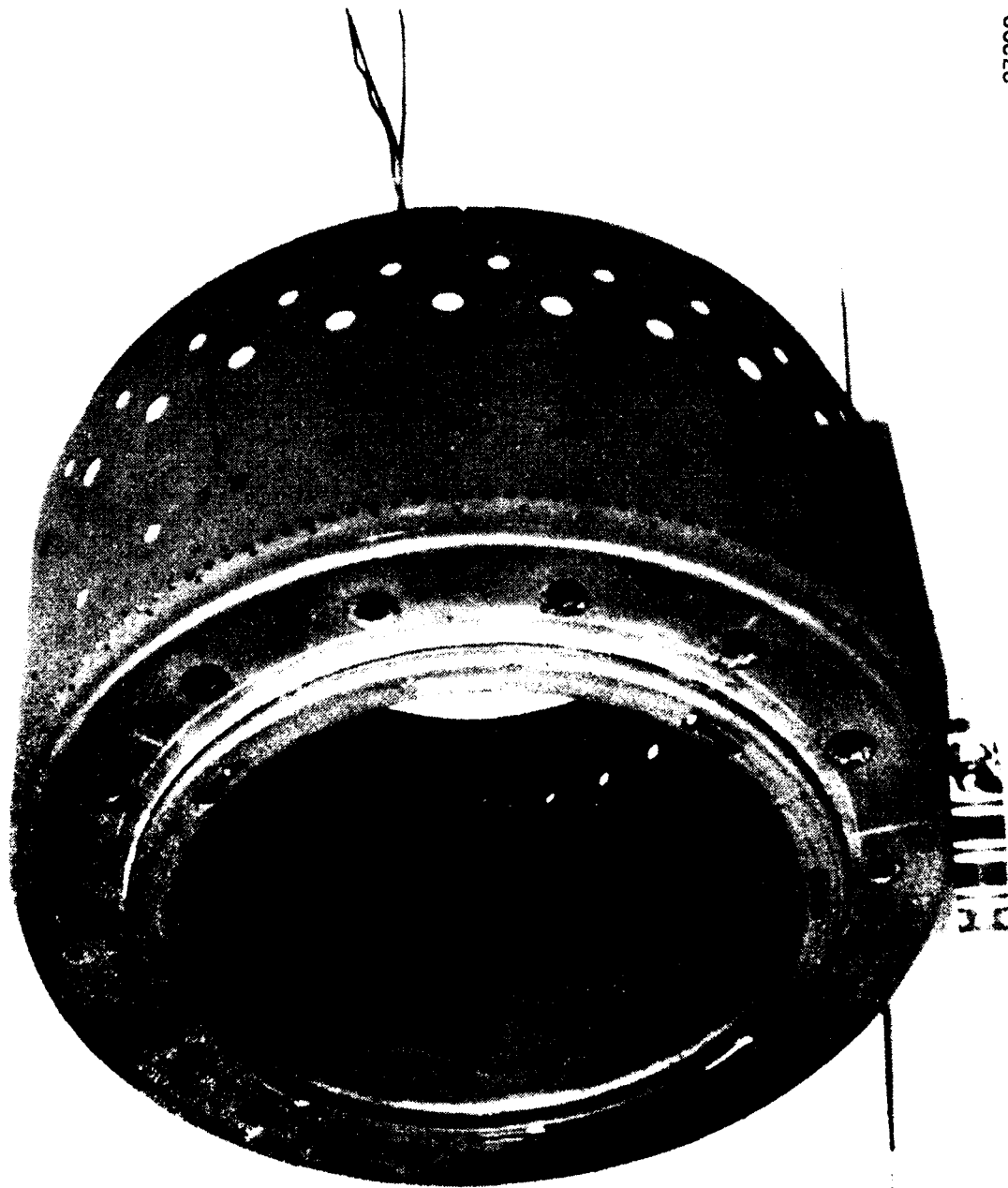
27398

Figure 158. Expendable Gasifier Combustor as Received for Rig Test.
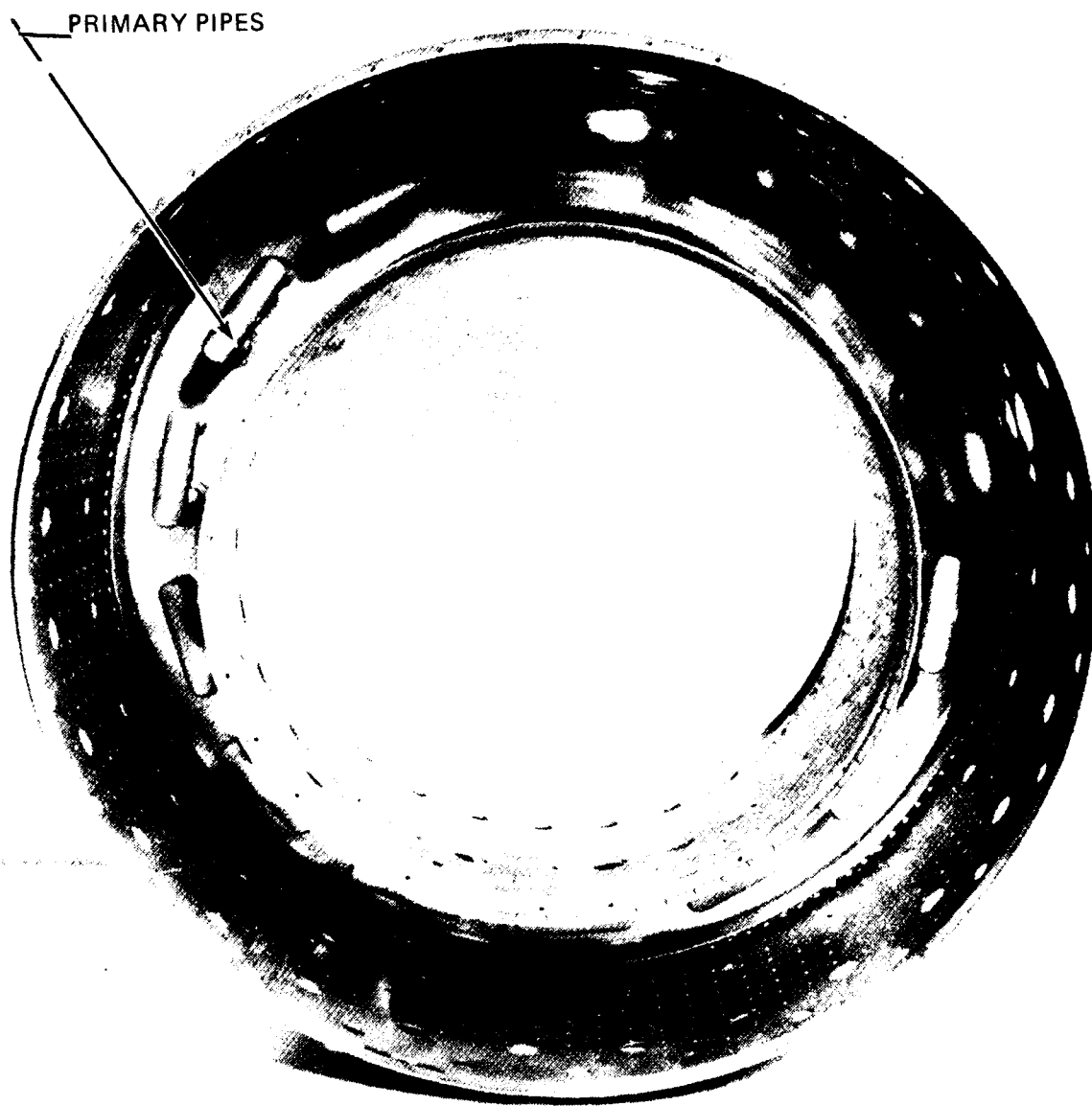
PRIMARY PIPES

27338

Figure 159. Gasifier Combustor Primary Pipes.

PRIMER NOZZLE

INTEGRAL LEAD IGNITOR
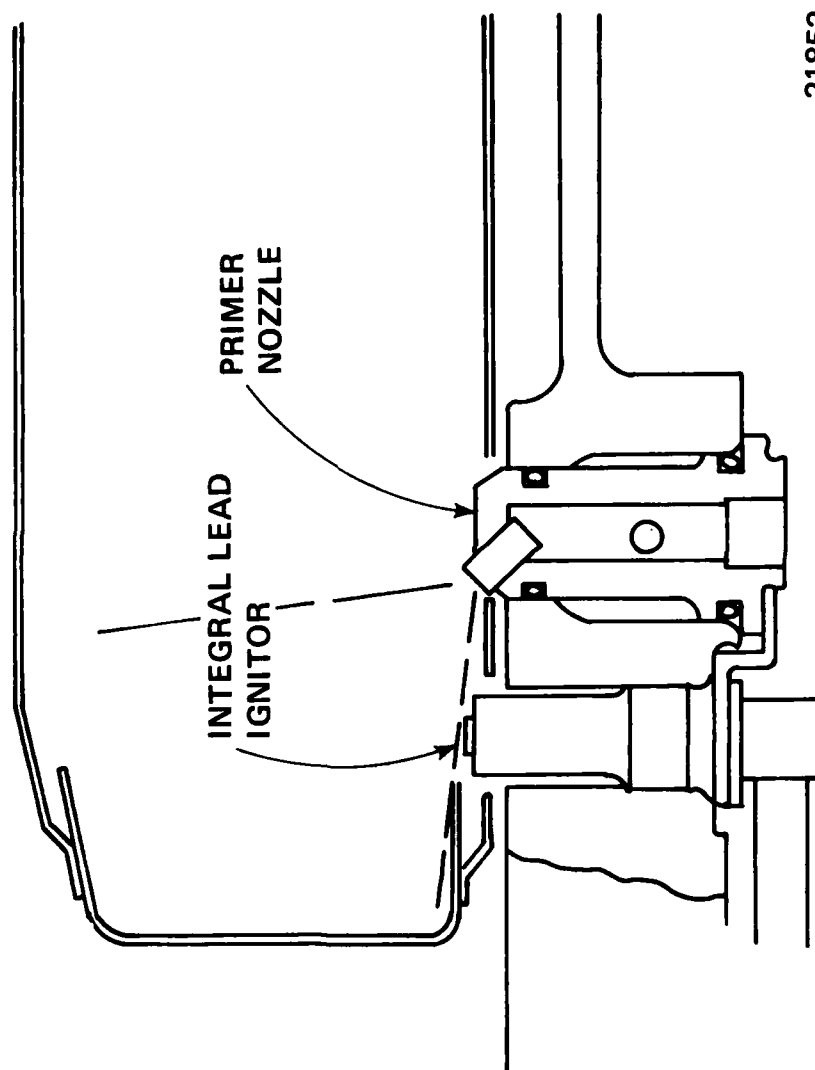
21852

Figure 160. Ignition System.

223
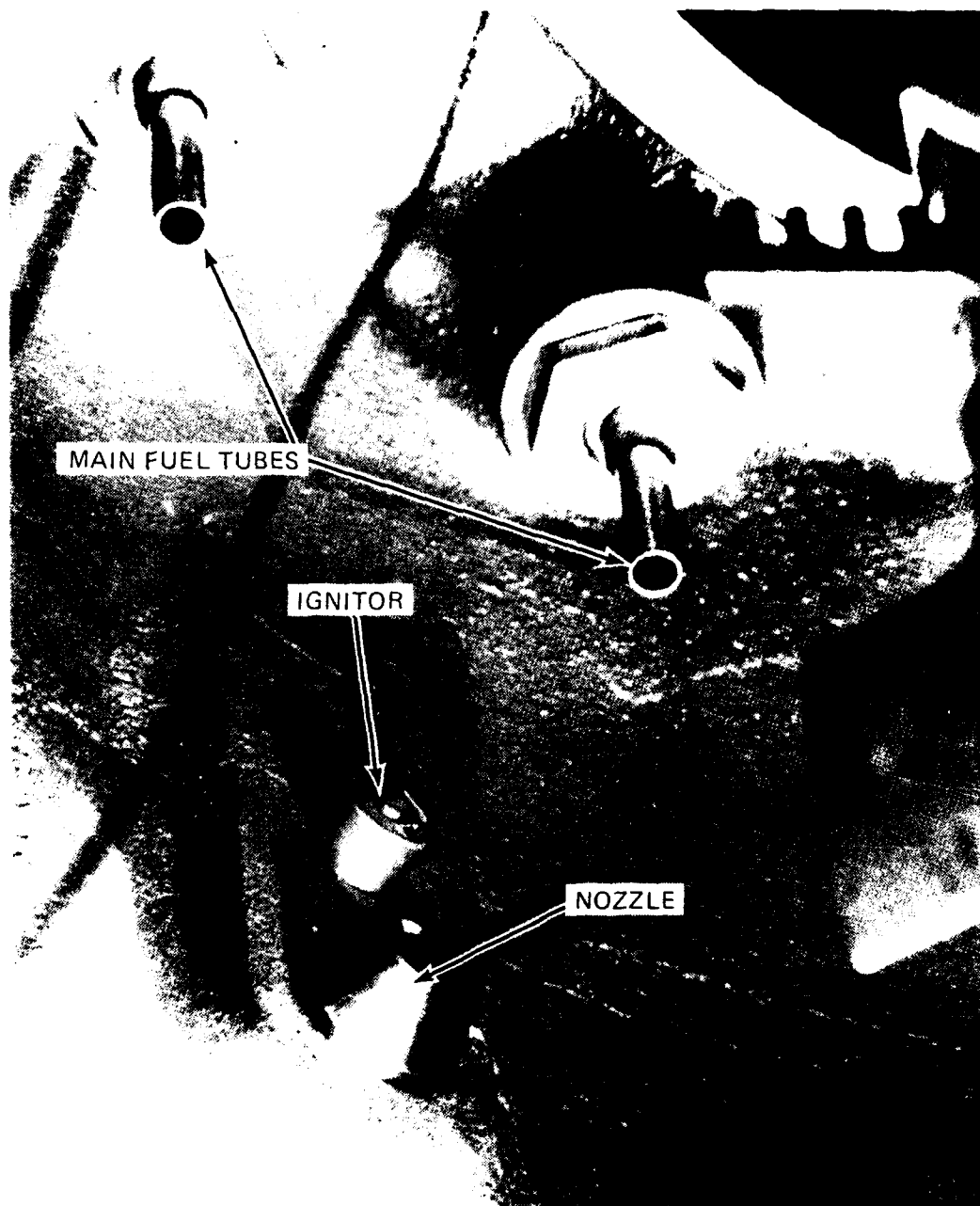
Figure 161. Ignitor/Starting Fuel Nozzle Pair.

224
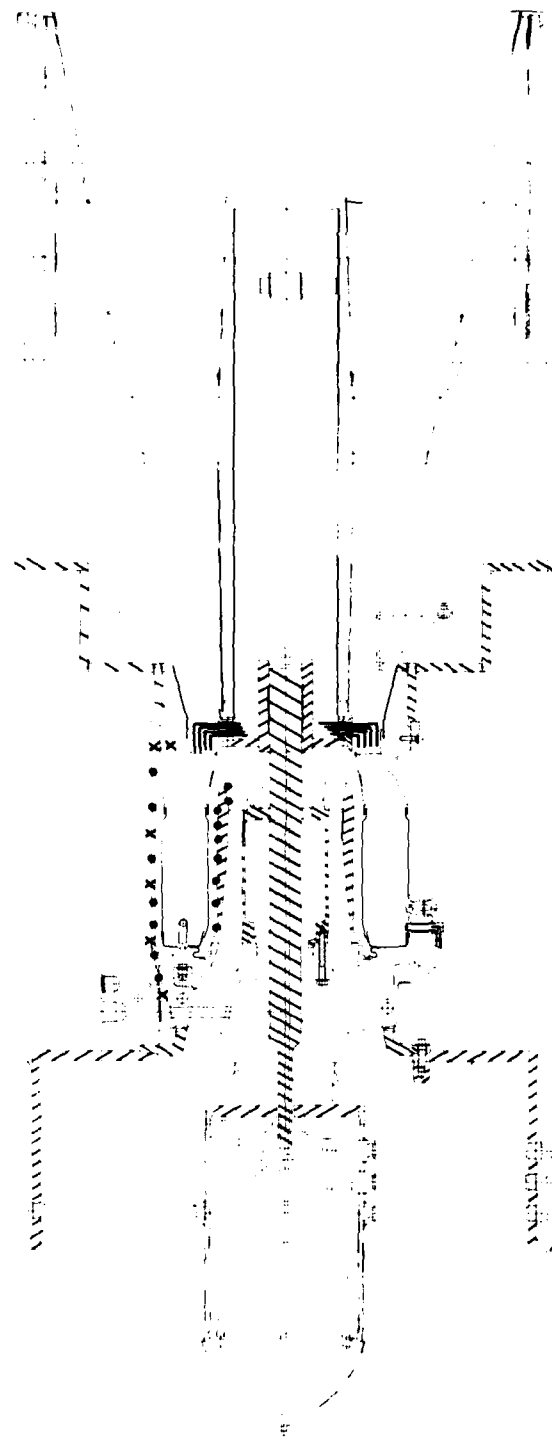
NEW (ADAPTIVE) HARDWARE

• Ps TAPS

X Tc'S

21919

Figure 162. Expendable Gasifier Combustor Rig Cross Section.

225

A detailed discussion of the test program, procedures, test points and rig instrumentation may be found in the Expendable Gasifier Component Development Test Plan for Combustor Test, dated 29 October 1976. However, a few details are summarized below for convenience.

The rig instrumentation included measurement of airflow, fuel flow, inlet and exit gas pressures and temperatures, static pressures throughout the combustor flowpath, and metal temperatures of the front frame and simulated compressor flowpath wall. The combustor exit temperature and pressure rate, Figure 163, were located downstream of the turbine inlet nozzle and were traversed circumferentially to provide a complete temperature and pressure map of the hot gases entering the turbine. The six element temperature rake shown was replaced with a five element rake early in the test program when it was found structurally inadequate.

The test program consisted of four tasks:

1. Cold flow tests to evaluate pressure loss and airflow distribution
2. Calibration of the fuel system to determine the uniformity of fuel distribution through the fourteen fuel injection points
3. Performance evaluation to map efficiency, pressure loss and exit temperature profiles over as much of the operating envelope of the expendable gasifier as facilities permitted
4. Determination of the combustor ignition envelope and correlation with expendable gasifier starting requirements

Figure 164 is a photograph of the expendable gasifier combustor rig ready for testing.

The initial cold flow test (baseline) of the combustor indicated that pressure loss was excessive (Figure 165). Data analysis indicated that this was the result of excessive turning losses at the combustor entrance combined with entrance losses into the cross-flowpath of the hollow turbine inlet nozzle vanes. Figure 166 is a schematic of the flow field in the turning duct at the combustor entrance and illustrates the diffuser separation and resulting high velocity high loss turn. Cutting back the diffuser (by 0.56 inch) for Build 2 reduced the area of separation and turning velocity, and consequently the turning losses.

The as-cast turbine inlet nozzle (Figure 167) also contributed to the high pressure loss because of the protruding, rough-edged entrance to the outer annulus flowpath through the hollow vanes. These edges were subsequently rounded to provide a smooth entrance (Figure 168). The impact of these modifications on pressure loss is also shown in Figure 165 as Build 2 where the pressure loss approaches the design value of 10.0 percent.

Figure 169 illustrates the design values and the variation in combustor airflow distribution to the inner and outer annuli resulting from these modifications. Since Build 2 pressure loss and airflow distribution were near design values, the performance evaluation phase was initiated with the fuel system calibration.
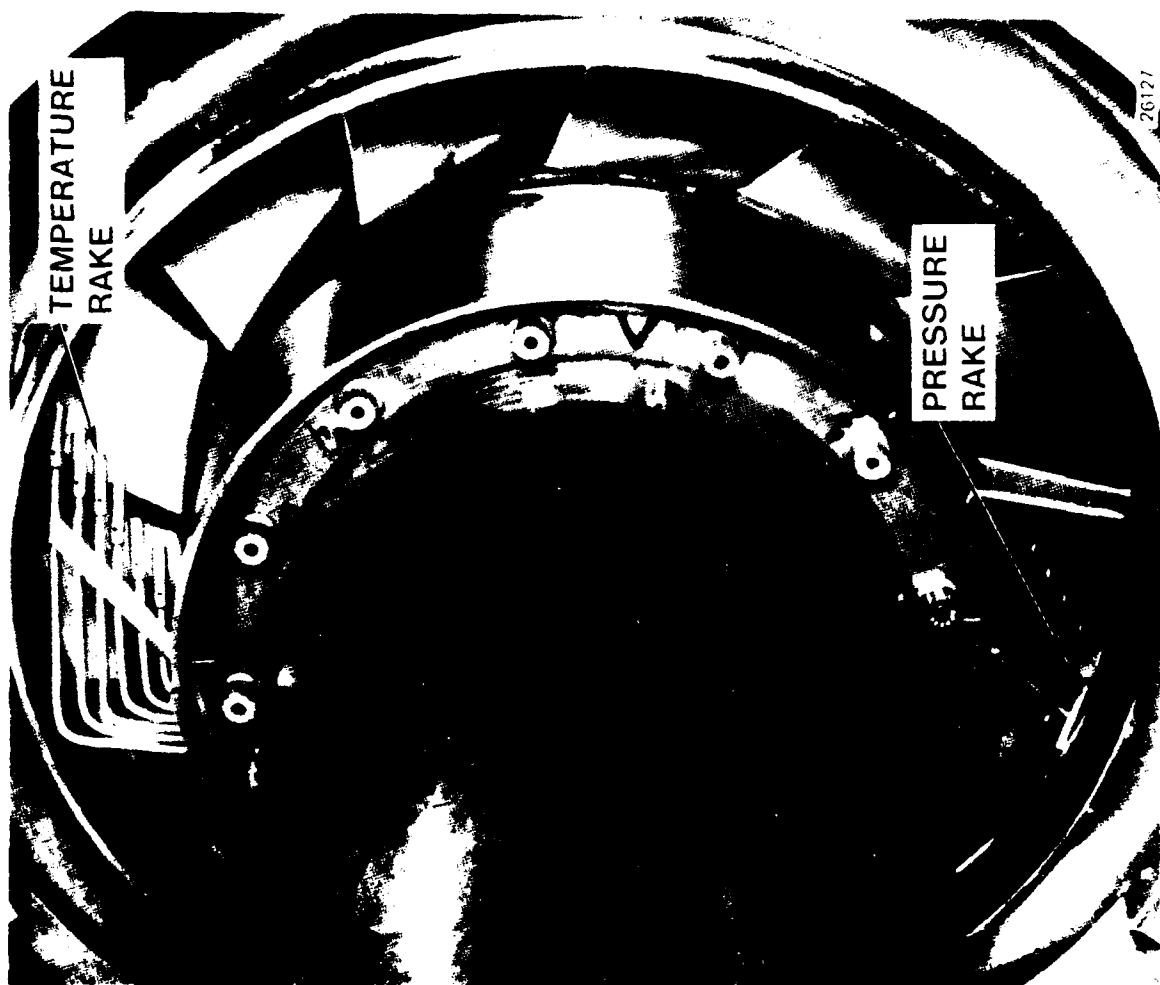
Figure 163 EG Combustor Rig Exhaust Gas Instrumentation.

FUEL INLET BOSS

HOUSING TEMPERATURES

STATIC PRESSURE TAPS

QUICK CONNECT COUPLING

26124

Figure 1-1. FG Combustor Rig.

228
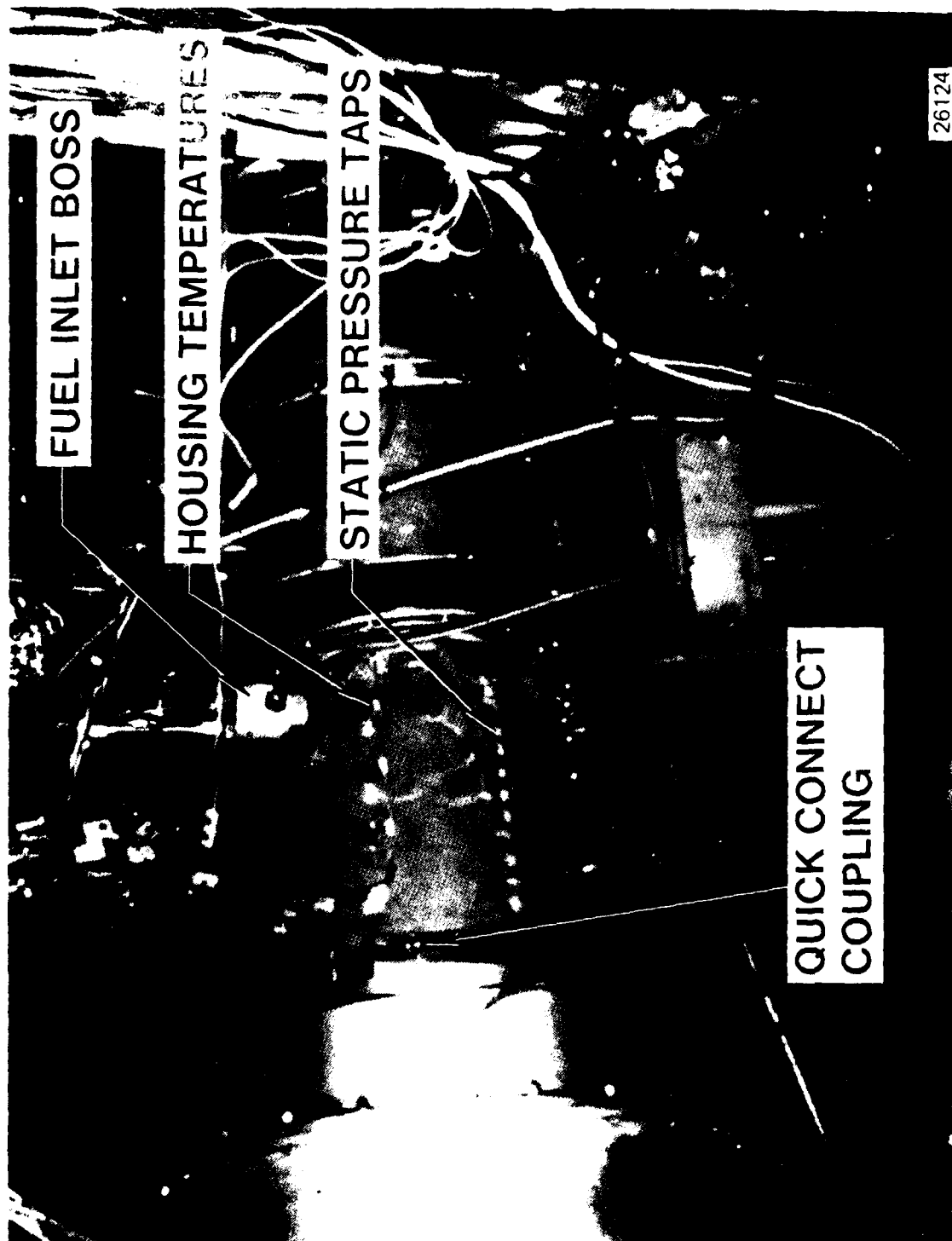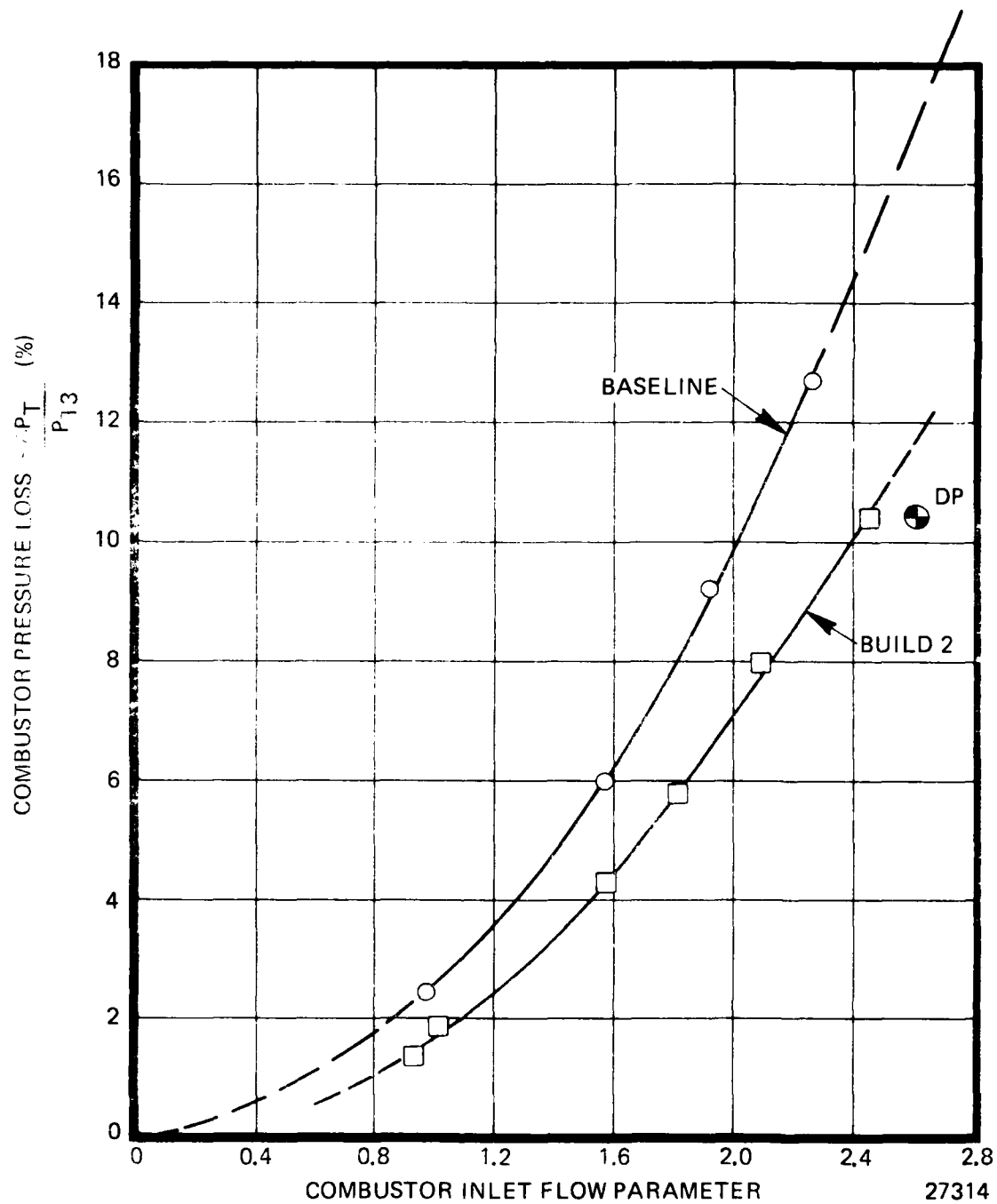
Figure 165. Expendable Gasifier Combustor Cold Flow Pressure Loss.

229

27300

BUILD 1

BASELINE

BUILD 2

CUTBACK DIFFUSER
& ROUNDED NOZZLE

230
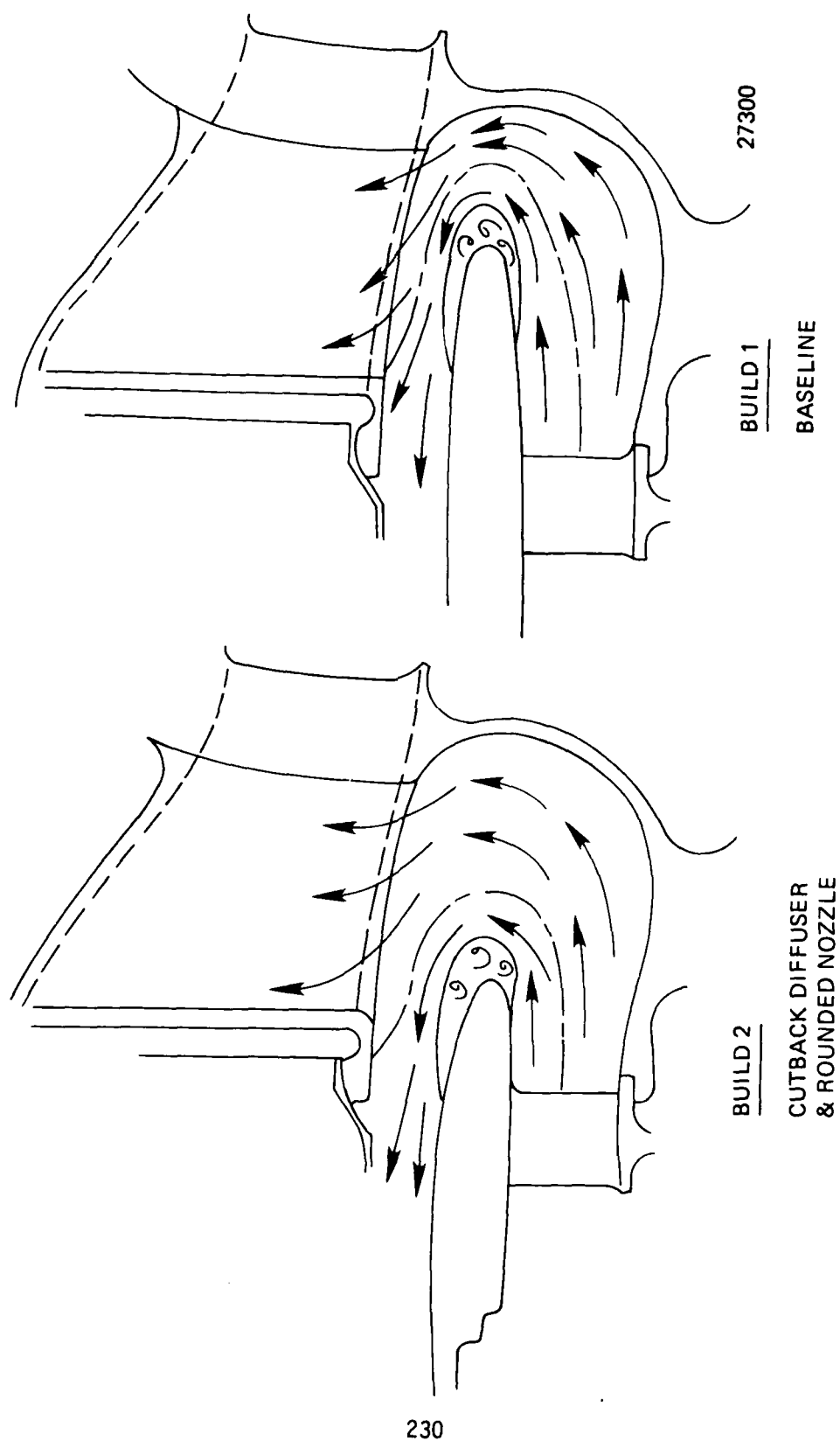
Figure 166. Schematic of the Flow Field at Combustor Entrance.

ROUGH EDGE
ENTRANCE

26122
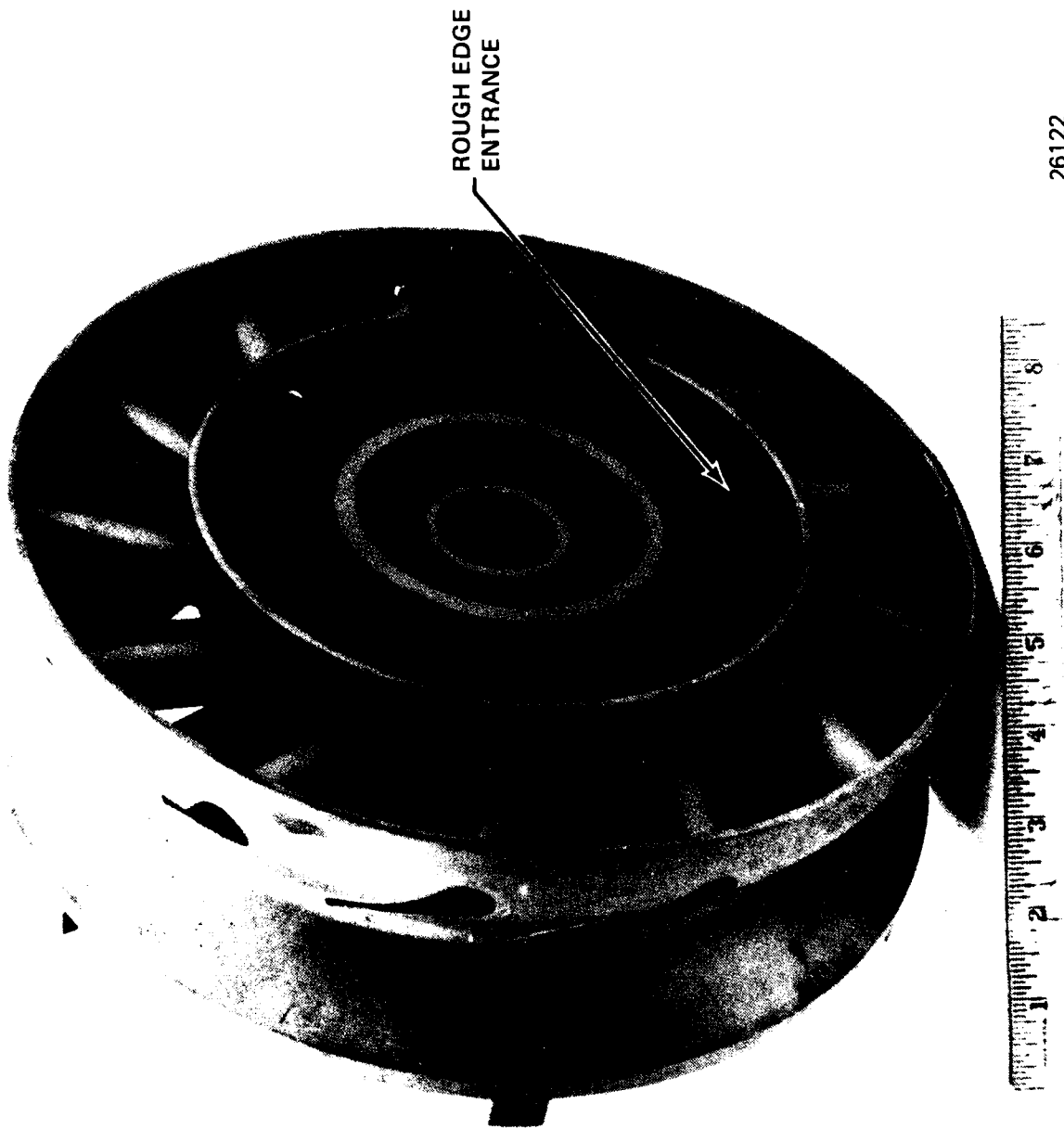
Figure 167   Expendable Gasifier Turbine Inlet Nozzle as Received.

231

ROUNDED ENTRANCE
NOZZLE FLOWPATH

232

Figure 168 Modification to Turbine Inlet Nozzle.
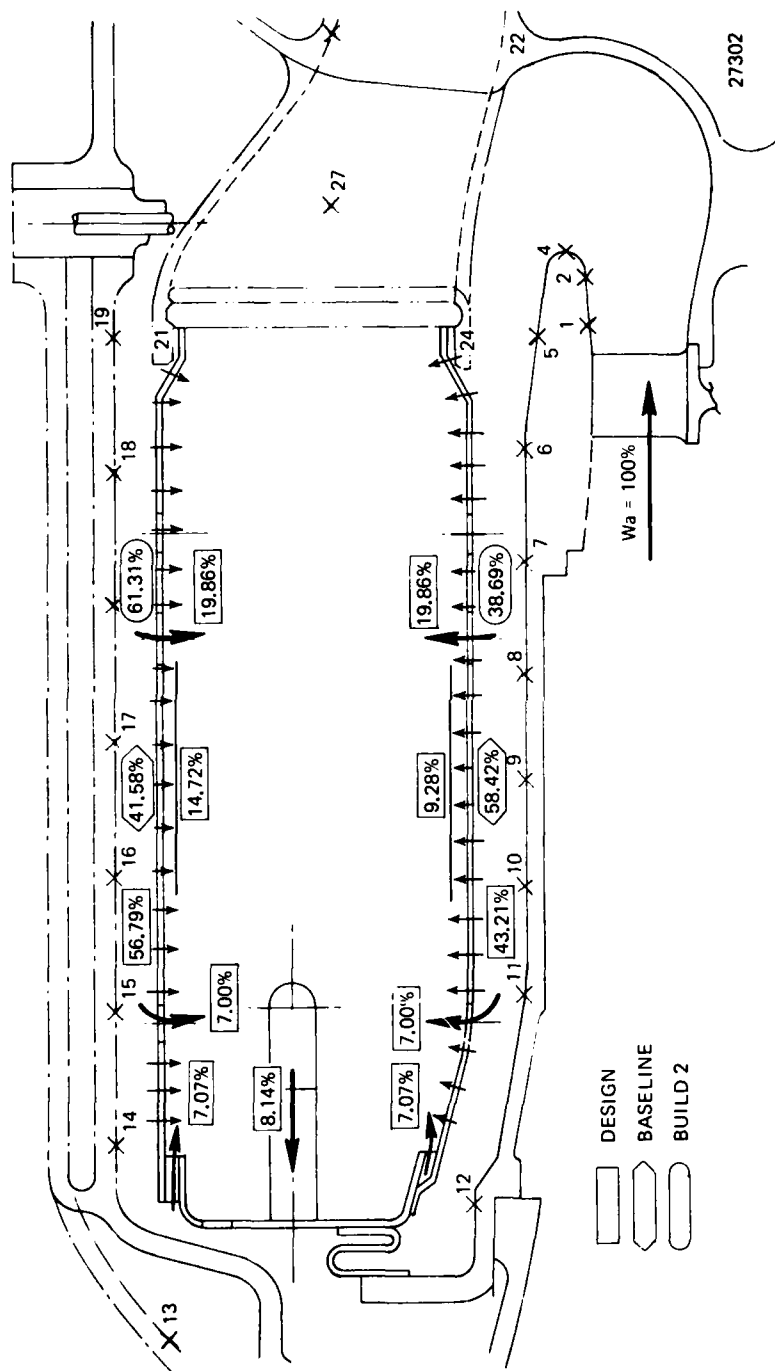
Figure 169   Expendable Gasifier Airflow Distribution.

233

The initial fuel system calibration set-up is shown in Figure 170 with the main (or front) frame mounted vertically. Subsequent calibrations were performed with the front frame mounted horizontally in the rig. Each of the 14 fuel tubes drained (through large diameter flexible tubing) into a graduated beaker. Comparison of the fuel level in the beakers provided calibration uniformity, while the total flowrate (as measured by a turbine flow meter) and the manifold pressure provided the pressure drop flow characteristics. Table 24 is the post performance test calibration and is typical. Variations from the set average were held within ± 5 percent by exchanging the fuel tube/orifice assemblies as required.

Four combustor modifications (in addition to those discussed above) resulted from the ambient pressure performance evaluation tests. Test configuration, summarized in Table 25, were primarily aimed at tailoring the combustor exit radial temperature profile.

The radial temperature profile achieved during Mod 1 testing was very positive (peaked at the O.D.) and is identified as curve 1 on Figures 171 and 172. Figure 171 is a non-dimensionalized combustor exit radial temperature profile and is useful for comparison purposes. Figure 171 is independent of the absolute temperature level seen in Figure 172. Therefore, the combustor need not be operated at design temperature levels for a comparison with the design profile. Because peak local gas temperatures in excess of 2000°F were experienced with the Mod 1 configuration at a fuel-air ratio of 0.02 (design fuel-air ratio is 0.0245), the exit temperature rake was damaged, and testing was halted. The combustor was subsequently modified to the Mod 2 configuration. However, the R_5 element of the temperature rake was not repairable, and testing of Mod 2 was done without this element.

Mod 2 added 60, 0.156 diameter holes to the baseplate near the outer diameter to reduce the local fuel-air ratio in this area, thereby reducing the local temperature level. This was only marginally successful as seen by Curve 2 of Figures 171 and 172. Again, because of the high local temperatures experienced, the six element exit temperature rake was damaged and Mod 2 testing was limited to a fuel-air ratio of 0.0175. Because of the continuing damage to the exit temperature rake, a new five element rake with heavier elements (0.125 instead of 0.090 sheath diameter) was procured and used without problem on subsequent tests.

The combustor was modified to the Mod 3 configuration by closing off 28, 0.30 diameter dilution ports on the inner liner, thereby reducing the airflow through the inner liner while increasing the flow through the outer liner. This modification significantly impacted the radial profile as seen by Curve 3 on Figures 171 and 172.

Mod 4 opened the baseplate holes from 0.156 diameter to 0.25 diameter to introduce additional air to the outer region of the primary zone to further reduce the local fuel-air ratio. While this further reduced the positive gradient, as evidence by Curve 4 of Figures 171 and 172, the profile was not suitable for gasifier testing and a further modification was necessary.

234

MAIN FRAME
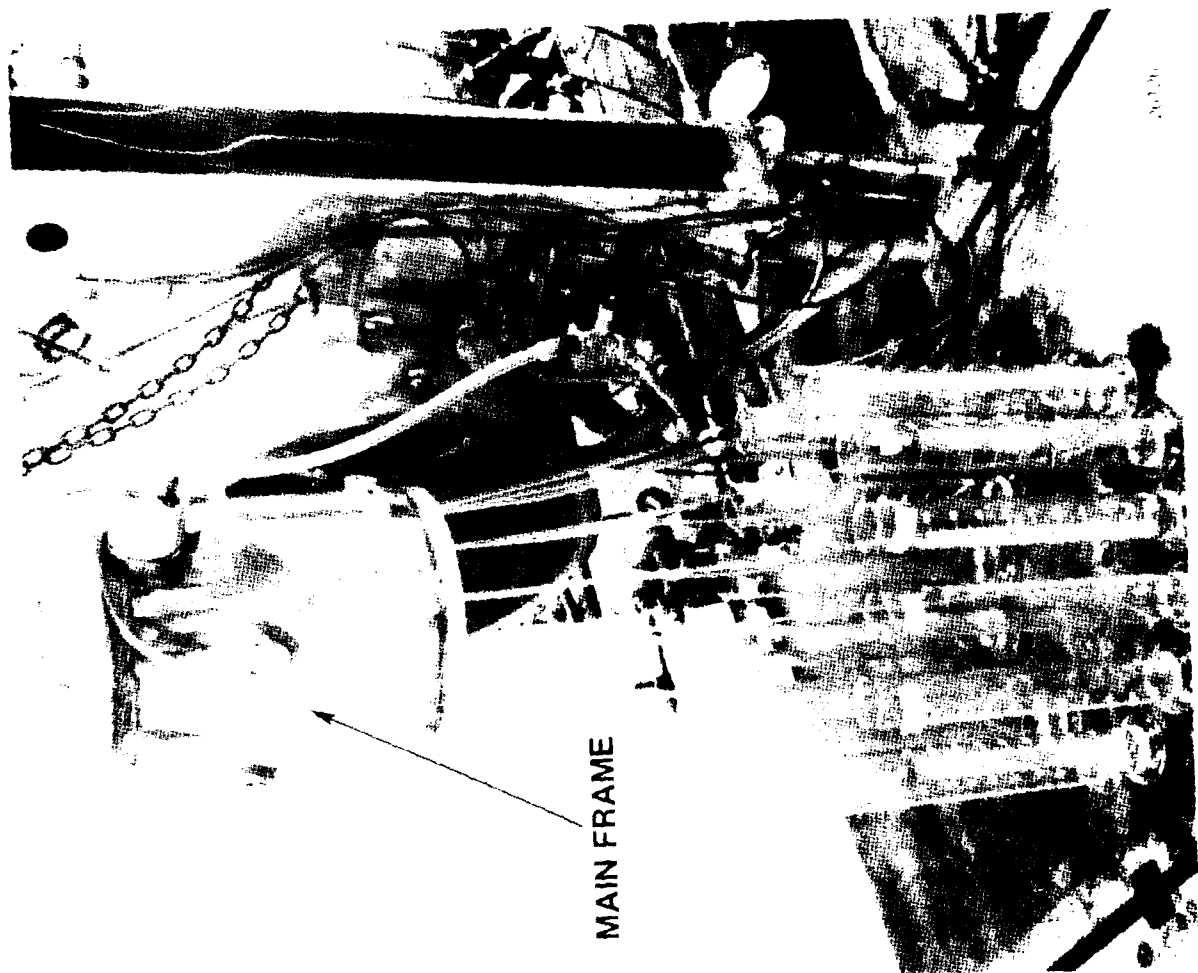
Figure 170   Fuel Manifold Calibration.

TABLE 24

	FLOW		FLOW		FLOW	
NOZZLE S/N	cc/	Variation From Set Average	cc/	Variation From Set Average	cc/	Variation From Set Average
1	1068	+2.75%	716	+2.67%	291	
2	1042		707		290	
3	1028		687	-1.49%	286	
4	1031		689		288	
5	1030		697		290	
6	1039		688		278	-4.07%
7	1032		703		289	
8	1028		688		285	
9	1032		698		295	
10	1062		707		294	
11	1058		707		292	
12	1045		690		290	
13	1026	-1.3%	688		294	
14	1031		698		296	+2.14%
Set Average	1039.4		697.4		289.8	
Manifold Pressure	71		31		6	
Total Flow	FLOW cps lb/hr		FLOW cps lb/hr		FLOW cps lb/hr	
	773 294		517 196.7		210 79.9	
REMARKS:	Fuel Temperature = 70°F				Fuel Temperature = 69°F	

TABLE 25

TEST PROGRAM CONFIGURATIONS

CONFIGURATION	DESCRIPTION
BASELINE	AS DESIGNED
MOD 1	SHORTENED DIFFUSER ROUNDED ID OF TIN VANES
MOD 2	ADDED 60 0.156 DIA. BASEPLATE HOLES
MOD 3	CLOSED-OFF 28 0.30 DIA. DILUTION PORTS ON INNER LINER
MOD 4	OPENED BASEPLATE HOLES TO 0.25 DIA.
MOD 5	ADDED 56 0.262 DIA. HOLES TO OUTER LINER 28 0.262 DIA. HOLES TO INNER & REOPENED 28 0.30 DIA. HOLES ON INNER LINER
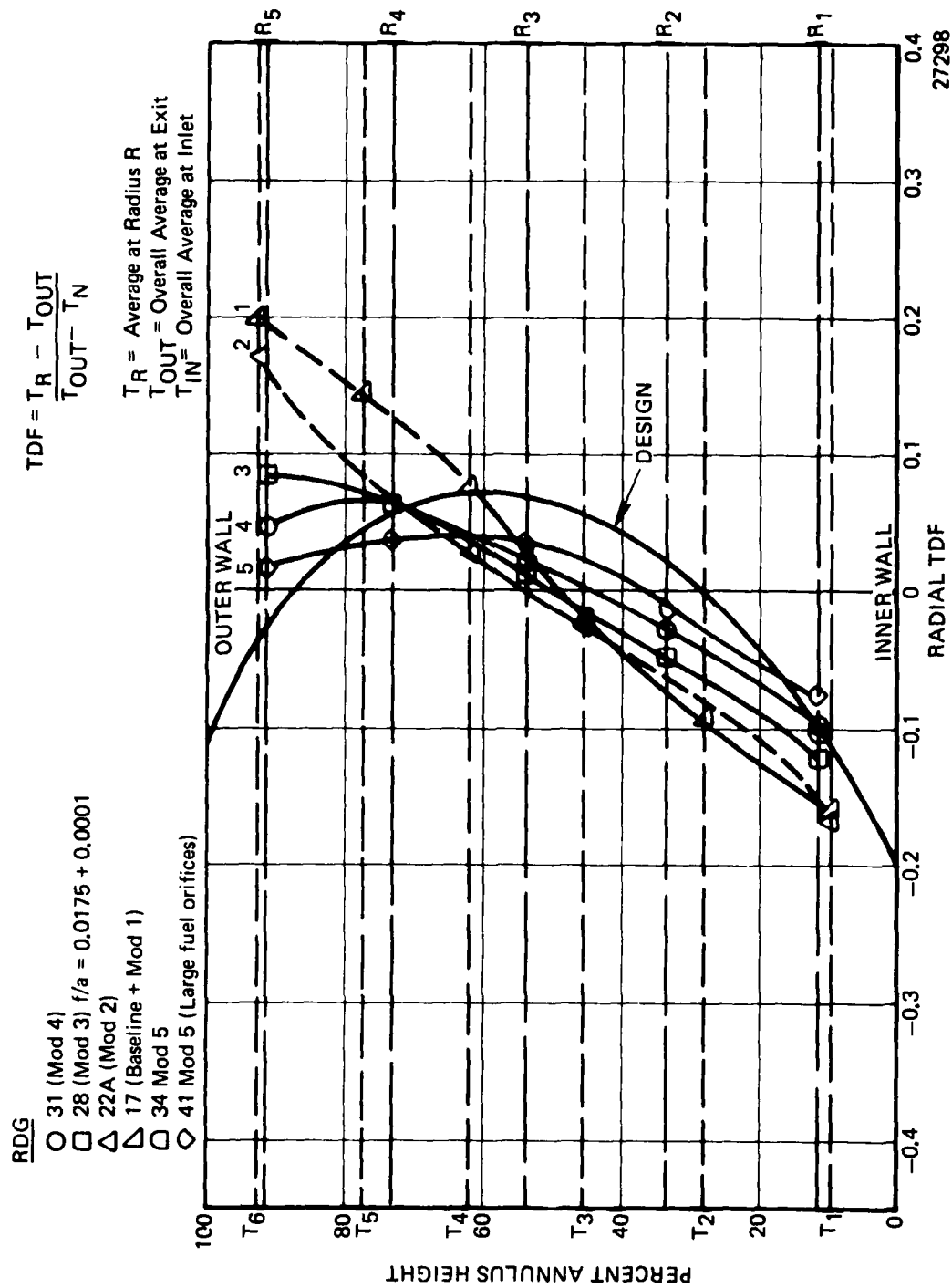
Figure 171. Non-Dimensionalized Radial Temperature Profile.

238
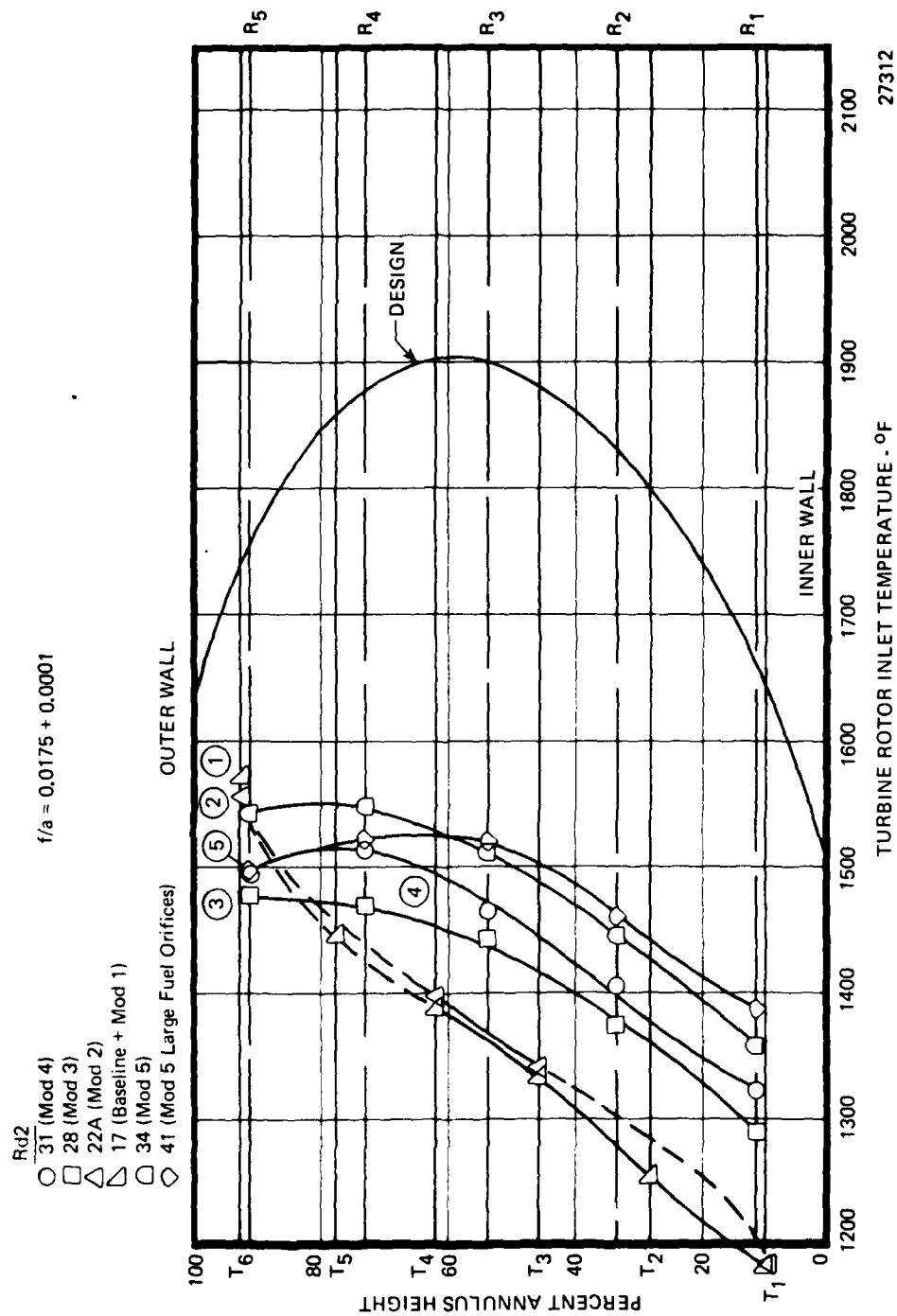
Figure 172. Radial Temperature Profile.

239

The final modification (Mod 5) added 56, 0.262 diameter holes to the dilution zone of the outer liner and 28, 0.262 diameter holes to the dilution zone of the inner liner. In addition, the 28, 0.30 diameter inner liner dilution ports that were closed off by Mod 3 were reopened. This modification had the effect of increasing the effective open area of the combustor liner by 21.3 percent over the Mod 4 configuration and by 18.5 percent over the baseline configuration.

Equally important, it rebalanced the airflow distribution of the combustor, forced more air through the outer liner dilution ports and brought the radial temperature profile into line as evidenced by Curve 5 of Figures 171 and 172.

The combustor airflow distribution for Mod 5 is shown on Figure 173. Twenty-four percent of the air flows through the outer liner dilution ports compared to 18 percent for the inner liner dilution ports. The overall flow split between the inner and outer flowpaths is 36.3 percent and 63.7 percent respectively. This is a 19 percent and 29.7 percent reduction from the design values, and reflects the increase in overall effective open area of the combustor incurred via the modifications.

Since the above comparison of radial temperature profile were made at a fuel-air of 0.0175 instead of the design 0.0245 (to minimize damage to the exit instrumentation) it was necessary to evaluate the variation in radial profile with increased fuel-air ratios. The result is shown in Figure 174 where the radial profile is seen to become increasingly positive with increasing fuel-air ratio. The radial profile at design fuel-air ratio was considered adequately close to design for gasifier test. The combustor was subsequently subjected to performance evaluation at increased inlet pressure, per the combustor component test plan. Actual combustor inlet test conditions for this test series are tabulated in Table 26. Data Point 56 is very near the design operating conditions and the combustor exit temperature distribution for this data point is compared to design in Figure 175 and 176. The average radial temperature profile is close to design and is adequate for gasifier testing. The maximum measured local gas temperature is below the design value and thereby represents a less severe operating condition for the hot end stationary structure. Figure 177 is a non-dimensionalized circumferential temperature profile that immediately identifies where the peaks and/or valleys in temperature level occur. Figure 178 is an isotherm plot of the gas temperatures at the combustor exit annulus and in combination with Figure 177 identifies the extent of hot and/or cold streaks.

The combustor total-to-total pressure loss exceeds the design value of 10.0 percent by about 2.3 points as shown by Figure 179. Although the combustor liner effective open area was increased by 18.5 percent over the Mod 1 configuration (the liner effective open area was unchanged from the baseline to the Mod 1 configuration), the overall pressure loss is essentially unchanged (Figure 179). This may be explained by consideration of Figures 180 through 183. Figures 180 and 181 are based on the inlet total to annulus static pressure loss for the outer and inner flowpaths respectively. While the pressure loss to the outer annulus shows an increase that reflects the increased airflow to this area. The inner annulus pressure loss is essentially unchanged, indicating that the reduced airflow to this region had little, if any, impact on pressure loss. Figure 182

240
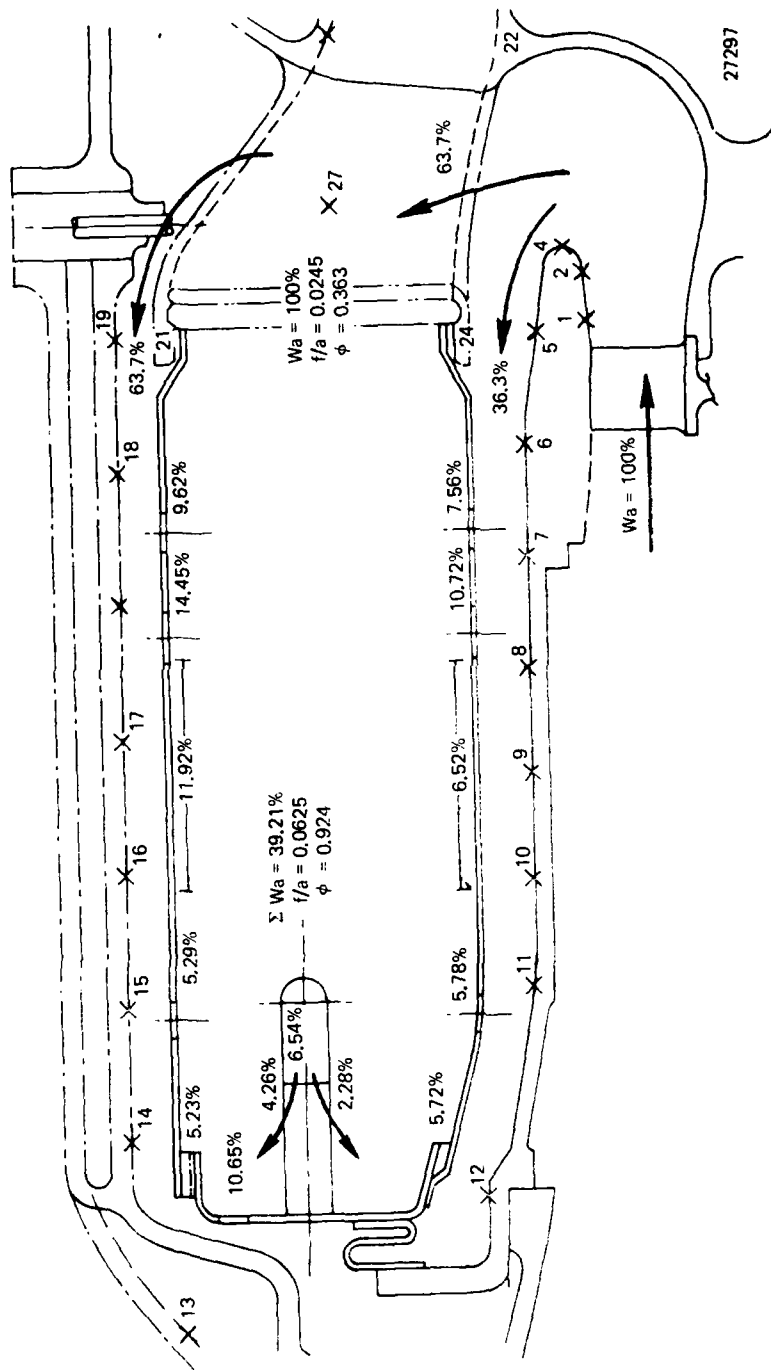
Figure 173. Expendable Gasifier Combustor Airflow Distribution (Mod 5).

241
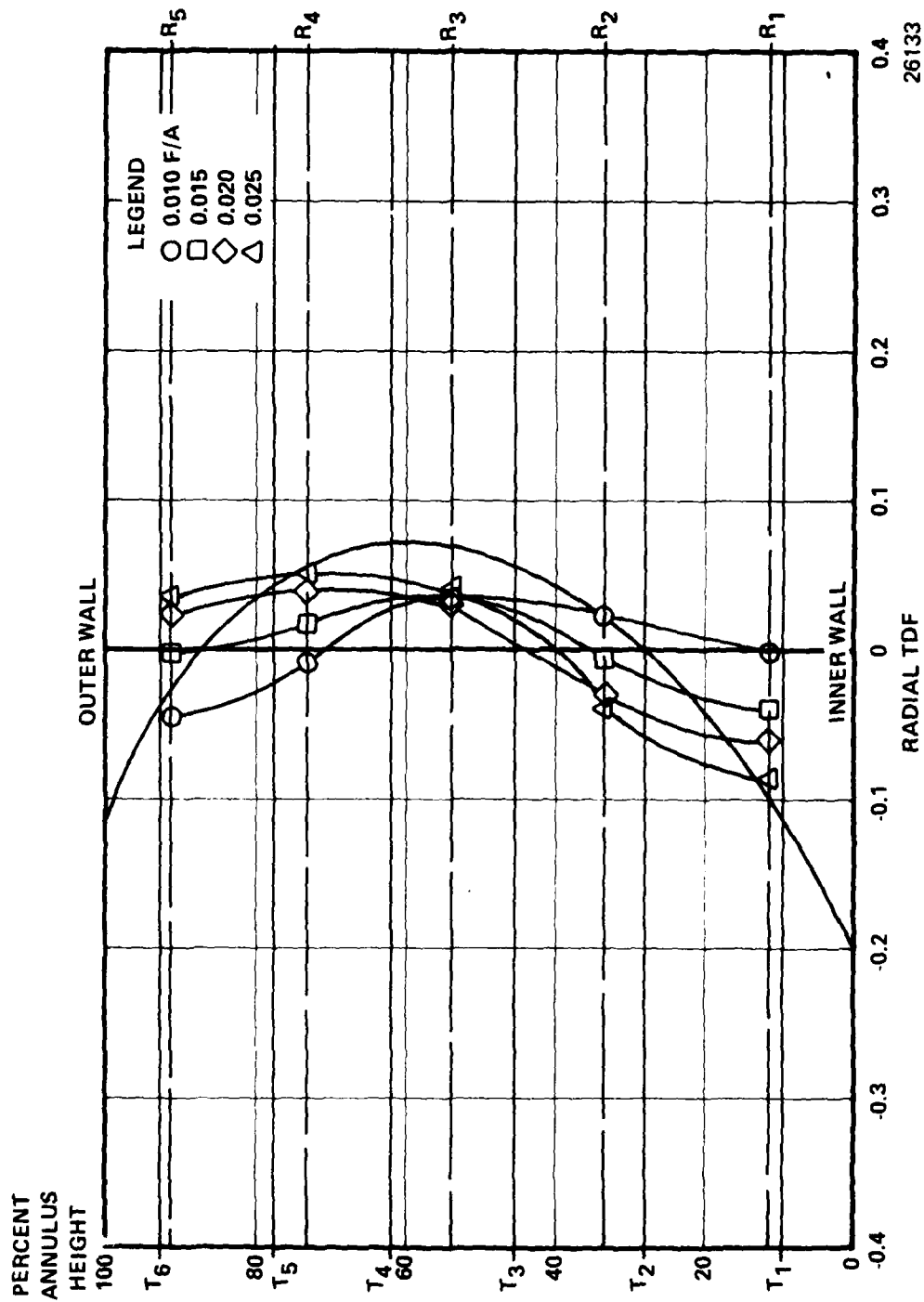
Figure 174. Variation in Radial Profile With Fuel-Air Ratio (Mod 5).

26133

242

TABLE 26

	COMBUSTOR OPERATING CONDITIONS				
READING	CDP "HgA	CDT °F	Wa Lb/Sec	Wf Lb/Hr	F/A
45	50.39	282	2.774	103.8	.010
46	54.62	286	2.898	155.7	.015
47	53.10	287	2.785	154.6	.015
48	55.50	286	2.772	204.6	.020
49	58.03	284	2.794	250.1	.026
50	64.80	283	3.764	142.3	.010
51	68.65	283	3.726	213.2	.016
52	72.92	283	3.730	283.6	.021
53	26.38	279	1.207	68.4	.016
54	26.64	281	1.207	81.2	.021
55	26.71	281	1.217	112.5	.026
56	77.54	279	2.789	357.4	.026
57	73.29	280	3.788	283.6	.021
DP	82.08	284	3.86	341.0	.0245
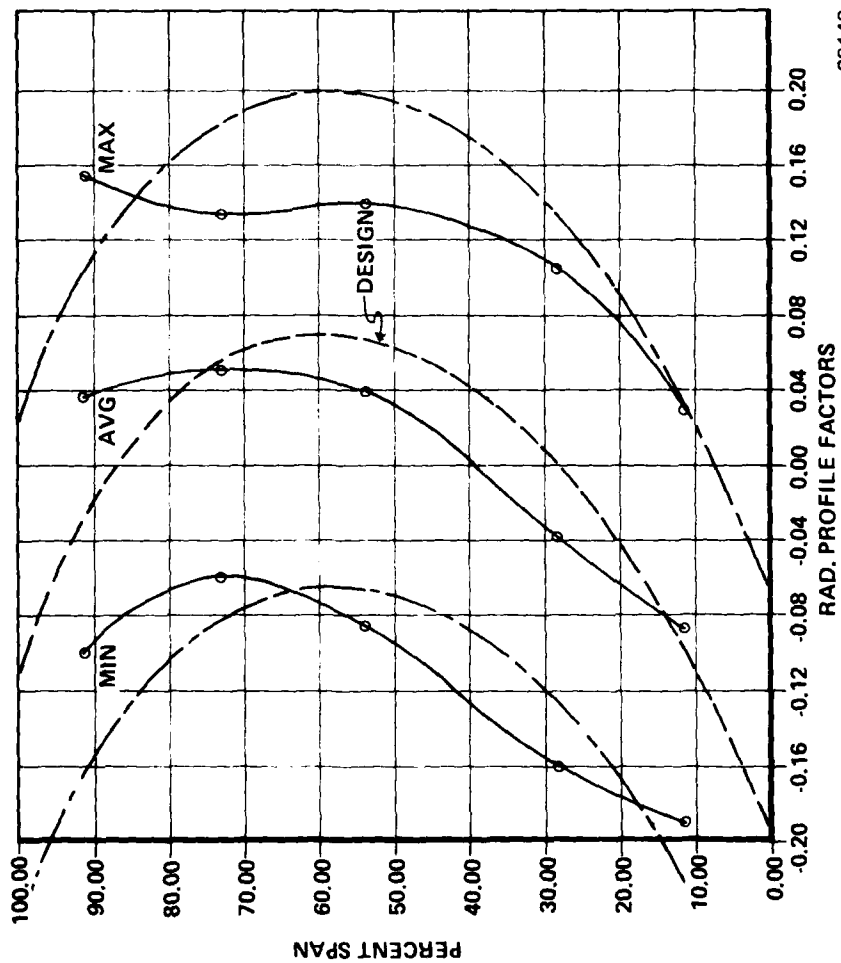
$$FACTOR = \frac{T - \bar{T}_{OUT}}{\bar{T}_{OUT} - \bar{T}_{IN}}$$

WHERE TEMPERATURE (T)

T = MAXIMUM LOCAL
= RADIAL AVERAGE
= MINIMUM LOCAL

AT EACH CIRCUMFERENTIAL POSITION

$\bar{T}_{OUT}$ = AVERAGE TEMPERATURE
AT COMBUSTOR EXIT

$\bar{T}_{IN}$ = AVERAGE TEMPERATURE
AT COMBUSTOR INLET

26143

Figure 175. Expendable Gasifier Data Point 56 Exit Temperature Profile.

244
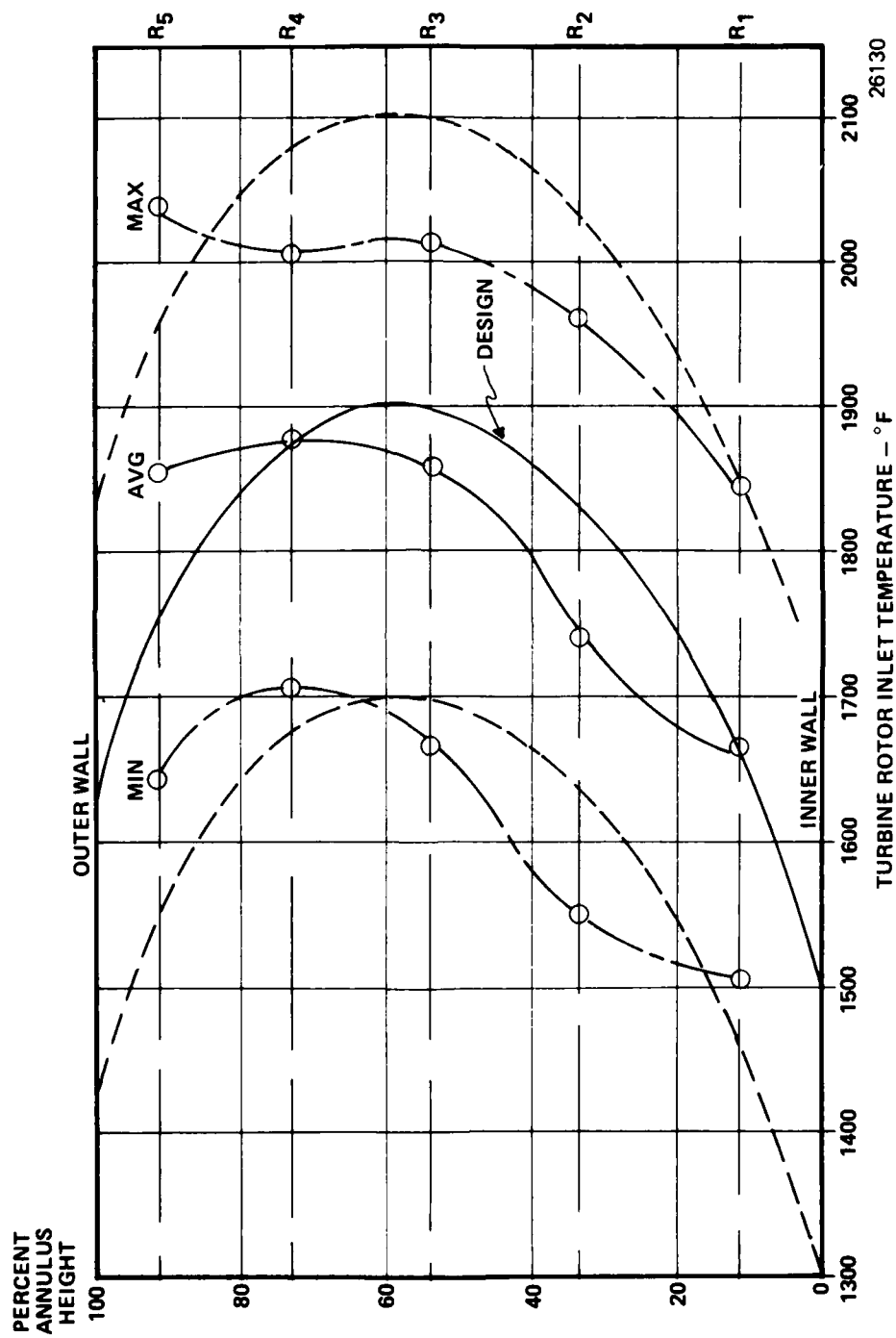
Figure 176. Expendable Gasifier Combustor Exit Temperature Profile Data Point 56.

245
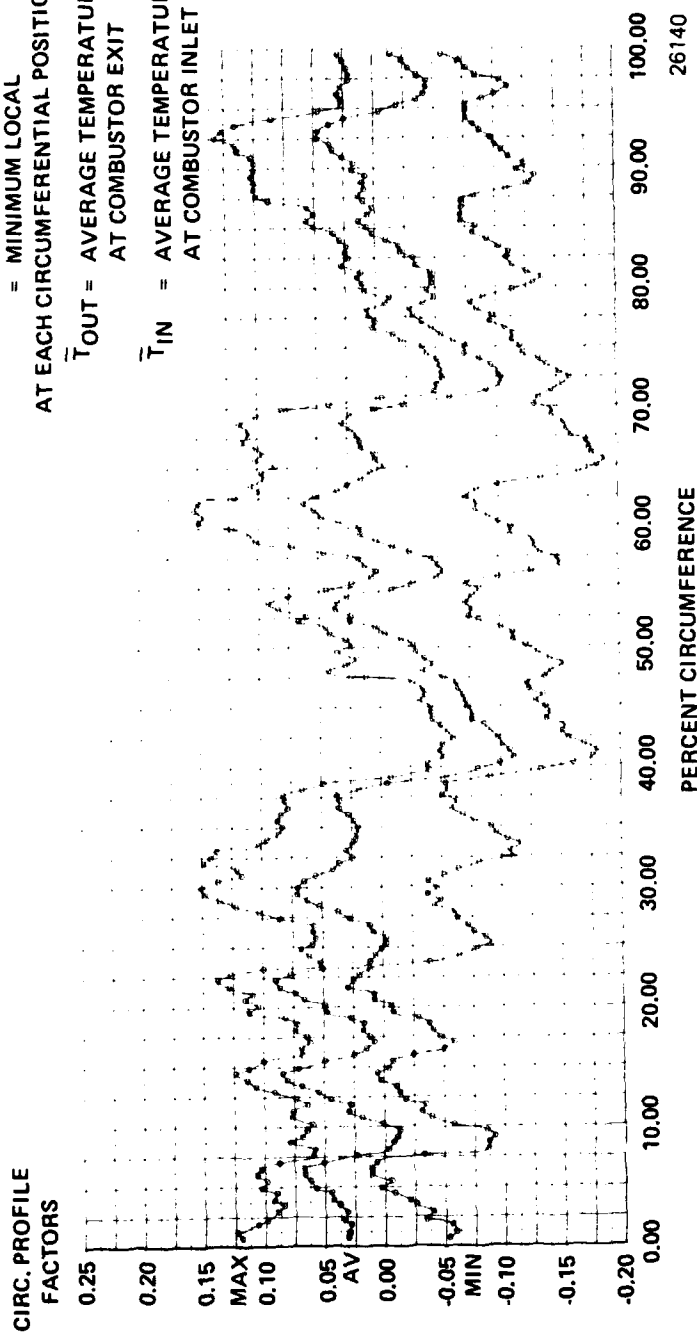
Figure 177. Combustor Exit Circumferential Temperature Profile Expendable Gasifier Data Point 56.

246

ISO-LINE NO.	ISO-QUANTITY VALUE
1	900.0000
2	950.000
3	1000.0000
4	1050.0000
5	1100.0000
6	1150.0000
7	1200.0000
8	1250.0000
9	1300.0000
10	1350.0000
11	1400.0000
12	1450.0000
13	1500.0000
14	1550.0000
15	1600.0000
16	1650.0000
17	1700.0000
18	1750.0000
19	1800.0000
20	1850.0000
21	1900.0000
22	1950.0000
23	2000.0000
24	2050.0000
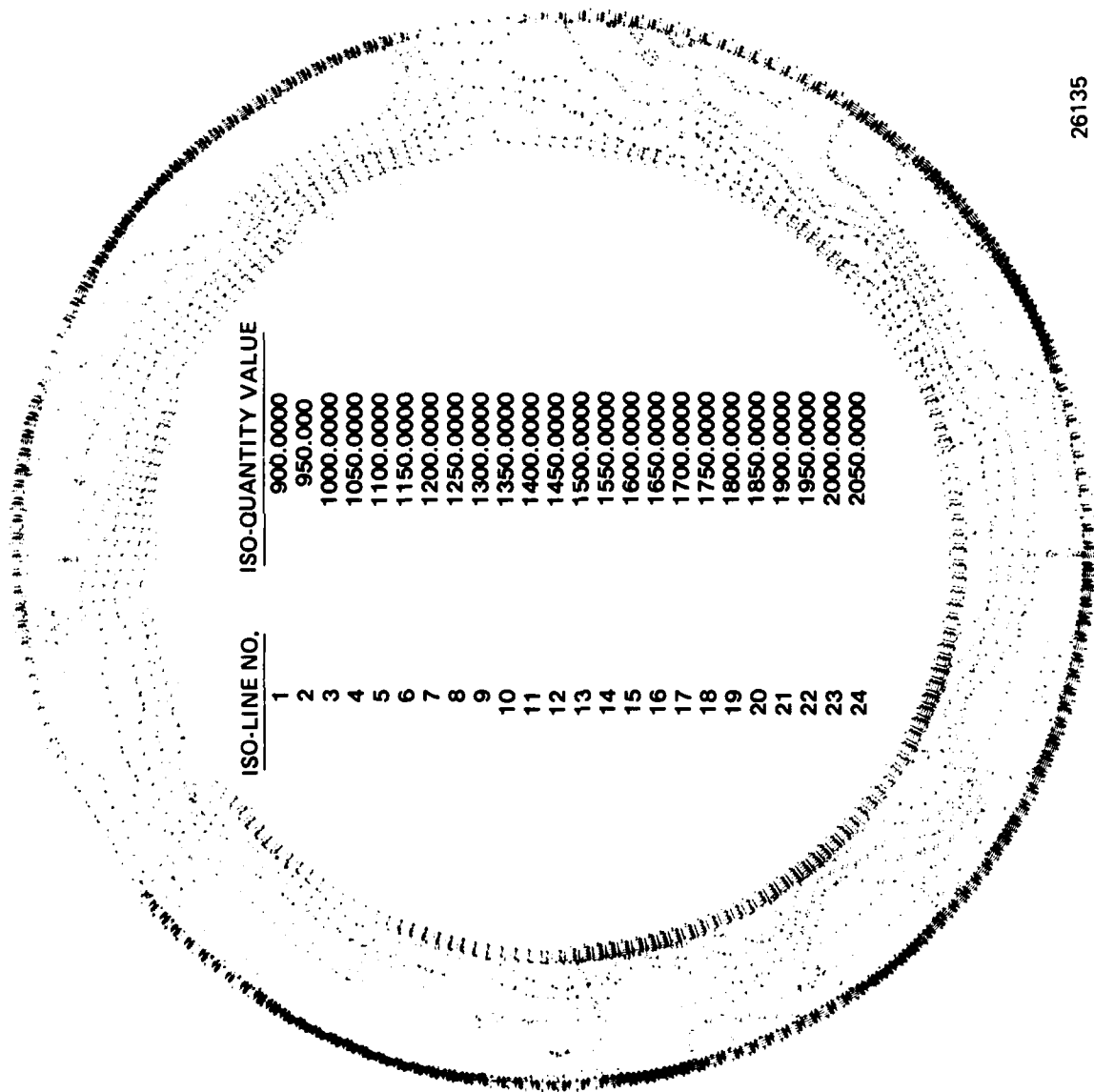
26135

Figure 178. Combustor Exit Gas Isotherms Reading Number 56.
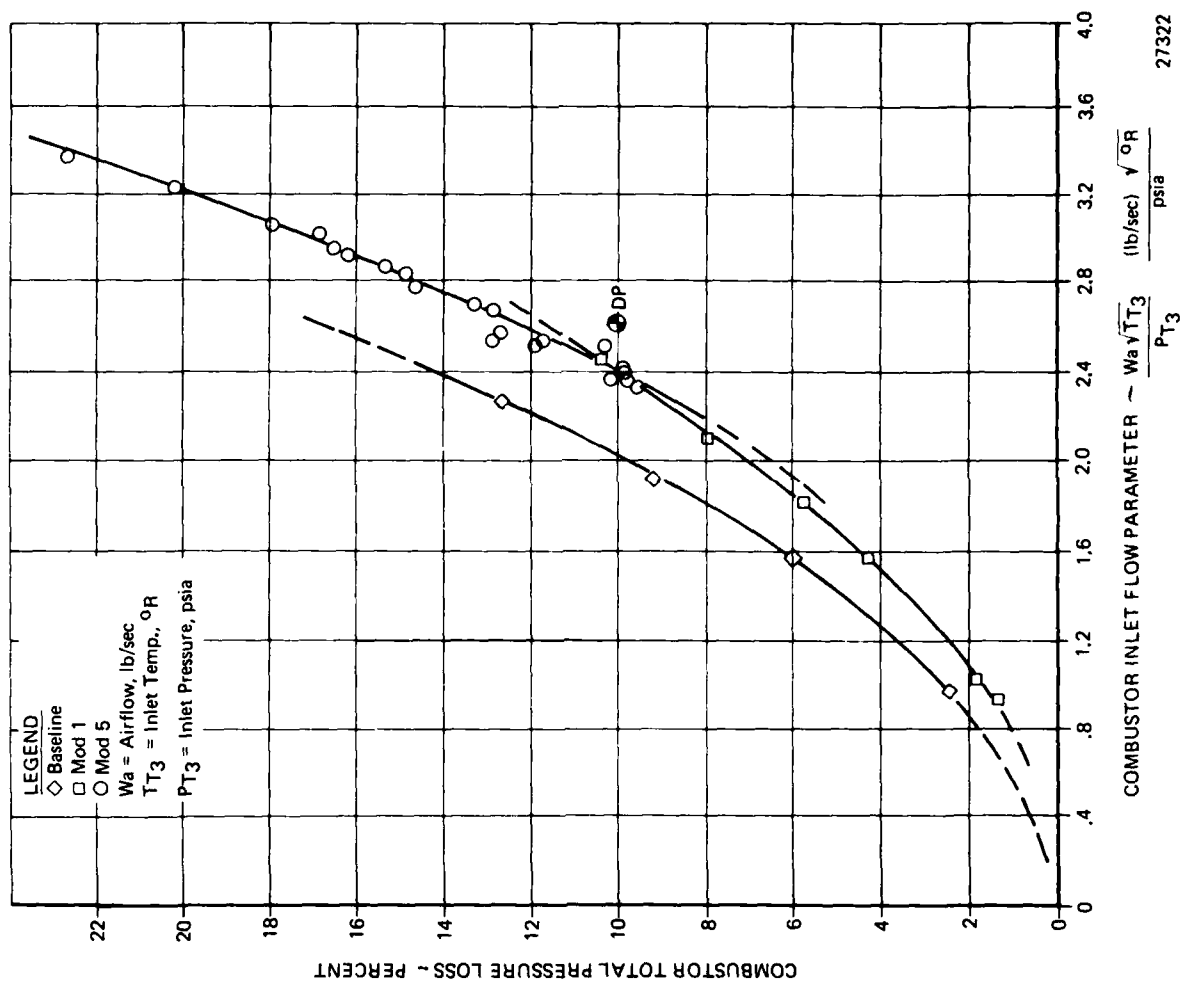
Figure 179. Expendable Gasifier Combustor Pressure Loss Hot Conditions.

248
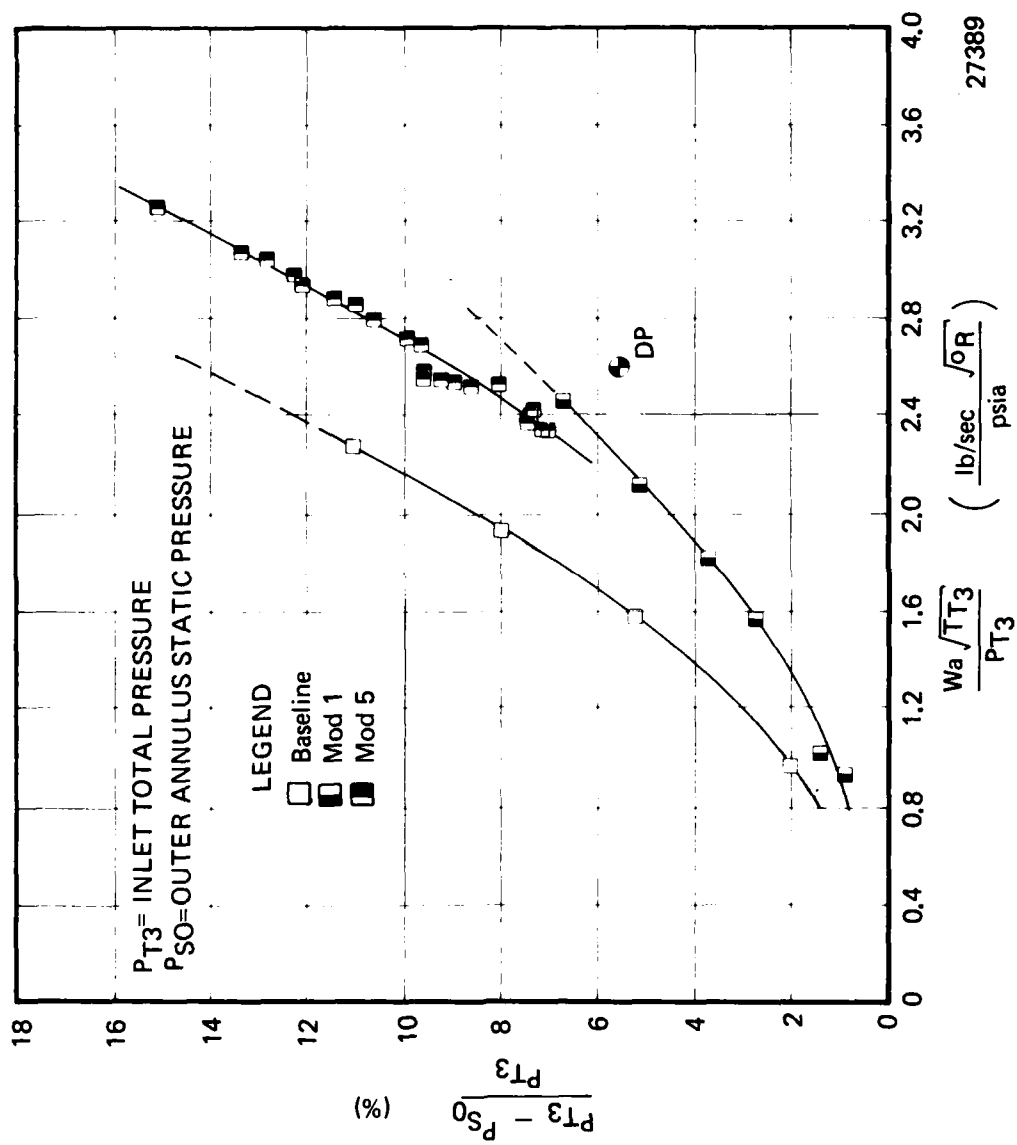
Figure 180. Expendable Gasifier Combustor Pressure Loss to Outer Annulus.
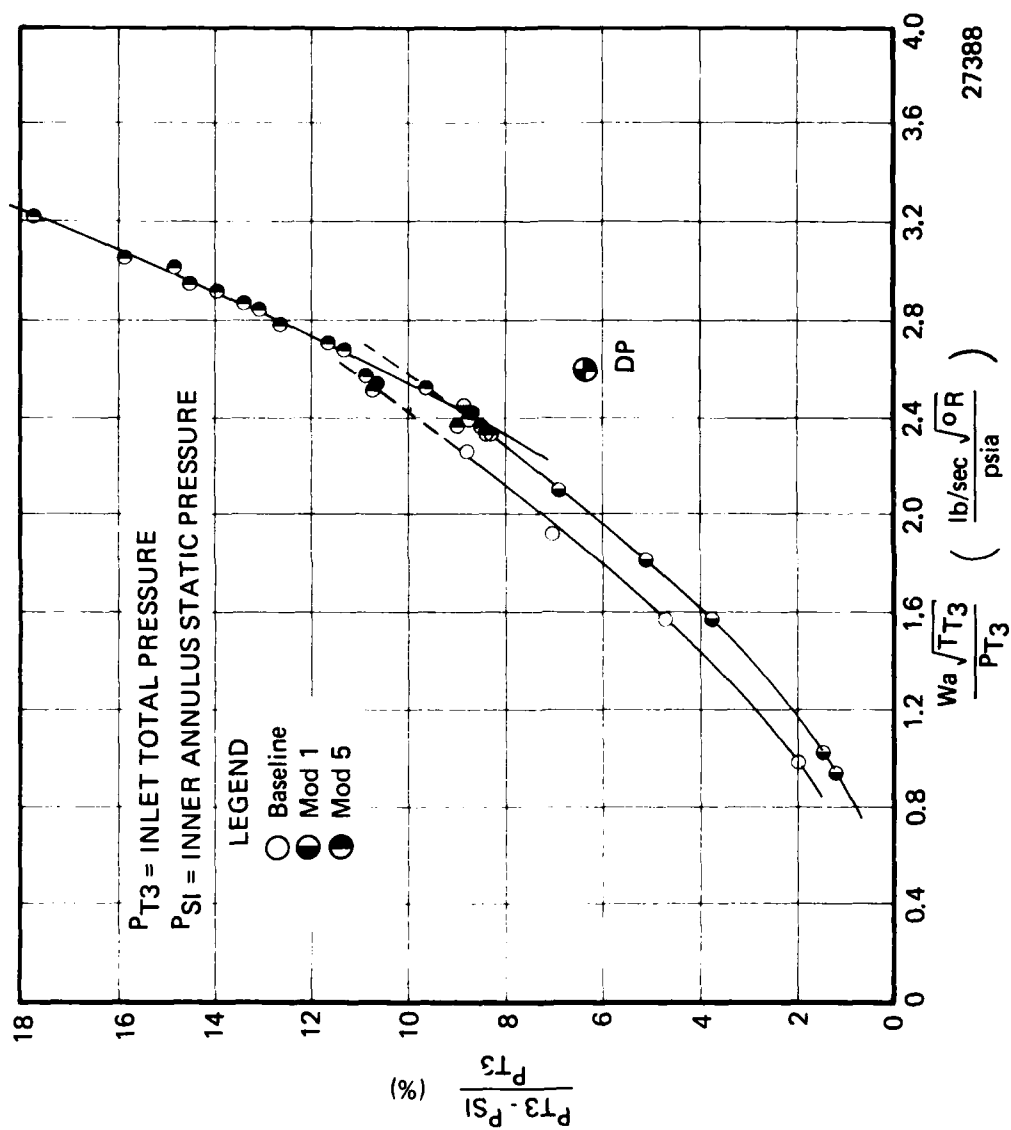
Figure 181. Expendable Gasifier Combustor Pressure Loss to Inner Annulus.
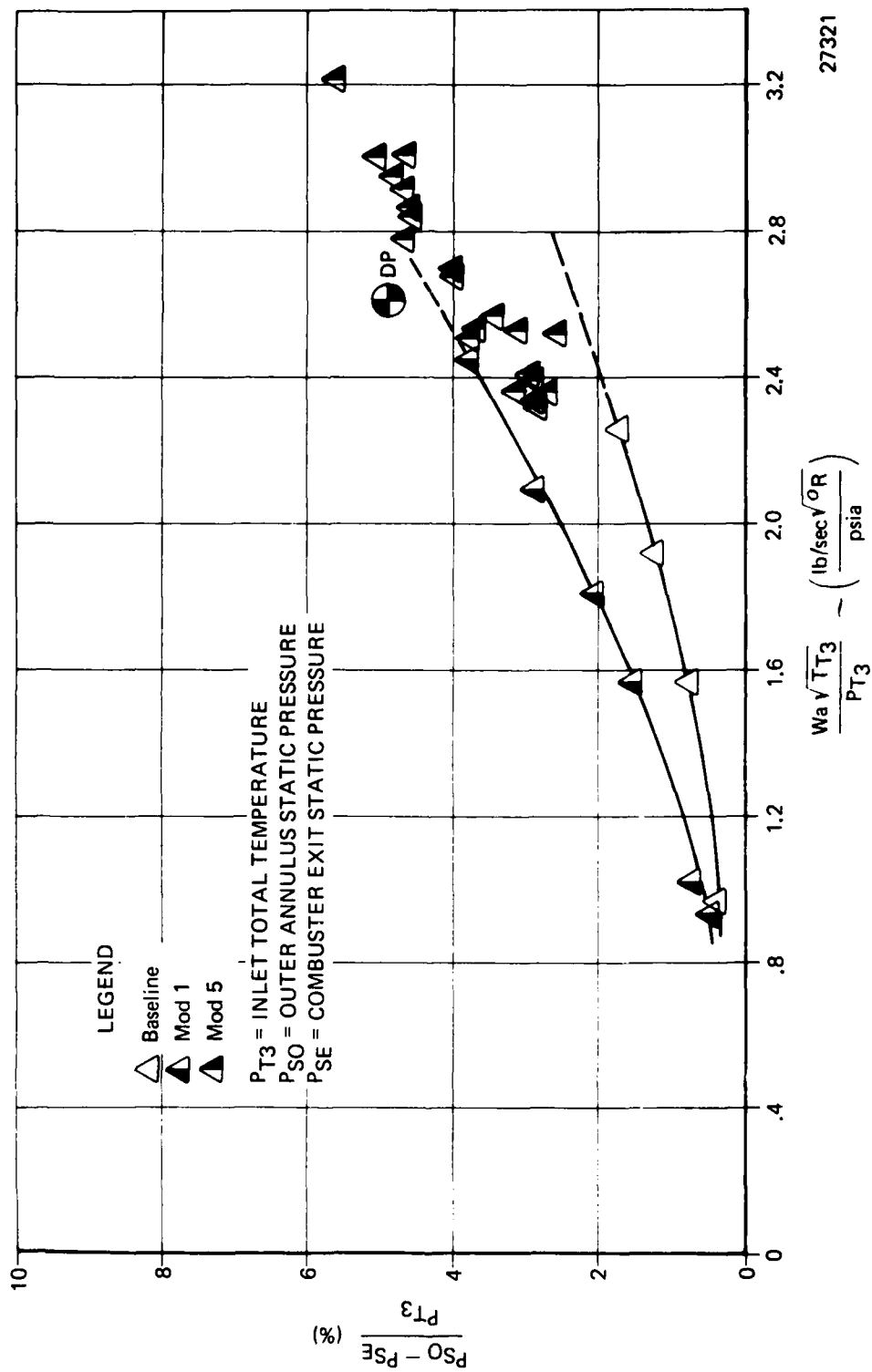
Figure 182. Expendable Gasifier Combustor Pressure Loss Across Outer Liner.

251
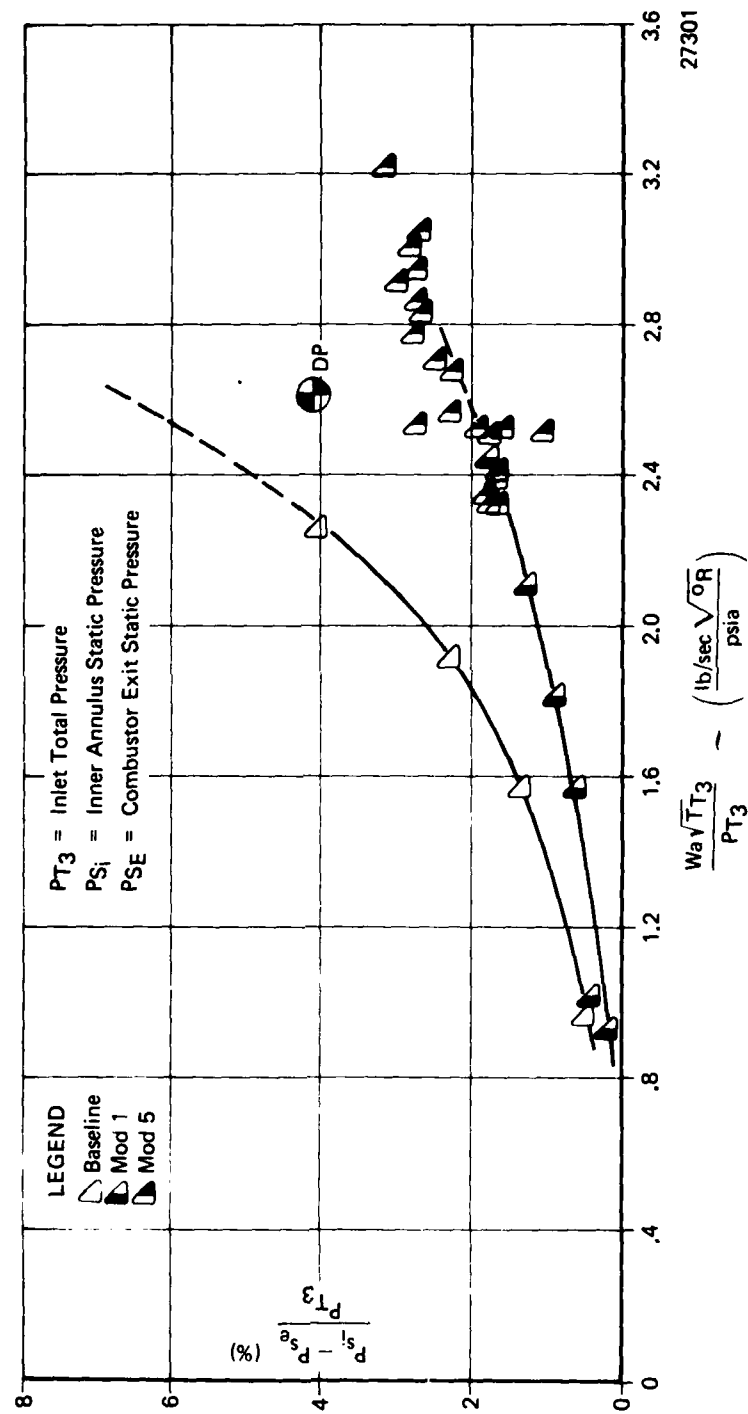
Figure 183. Expendable Gasifier Combustor Pressure Loss Across Inner Liner.

252

indicates an increased pressure loss across the outer liner (despite the increase in effective open area), again reflecting the increased airflow combined with the increased pressure loss to the outer annulus. However, Figure 183 indicates no change in pressure loss across the inner liner although airflow was reduced and effective open area increased. These factors indicate that variations in combustor liner effective open area have only limited impact on overall combustor pressure loss in the expendable gasifier configuration. Consequently, the net effect of Mods 2 through 5 was essentially that there was no change in total-to-total pressure loss.

Combustion efficiency was calculated as the ratio of the actual temperature rise to the theoretical temperature rise. The actual temperature rise was measured as the difference between the average of three, four-element rakes at the inlet and the average exit temperature as measured during the circumferential traverse of the five-element exit temperature rake. Approximately 200, five-point radial profiles were attained during each traverse, providing a complete temperature map of the combustor exit.

Attempts to correlate combustion efficiency against various loading parameters (Figures 184 and 185) indicated a significant amount of scatter in the data. However, the correlation of Figure 185 allowed trends to be established and indicated that the design efficiency of 95 percent had been achieved.

Combustor liner metal temperatures were monitored with surface thermocouples and thermindex OG-6 temperature indicating paint. The thermocouple data for Mod 5 are plotted against combustor exit average temperature in Figure 186 and indicate a peak liner temperature of 1157°F. However, the OG-6 paint indicated local temperatures approaching 1500°F in areas away from the thermocouples and are believed to be a better indication of the peak liner temperatures.

Following the above performance evaluation, the ignition envelope of the combustor was evaluated at simulated altitudes from sea level to 20,000 feet. The range of combustor inlet airflows, pressures and temperatures evaluated is shown in Table 27.

The ignition system consisted of dual spark ignitor/starting fuel nozzle pairs located 90 degrees apart on the left side of the gasifier. The starting fuel nozzles are of the simplex, pressure atomizing type fed from an integrally-cast manifold in the main frame. Starting nozzle fuel pressure was held constant at 50 psid. Figure 187 is a photograph of the nozzle spray and also shows the relative orientation of the ignitor/nozzle pair. The combustor liner was removed for clarity.

The ignition tests consisted of setting combustor inlet airflow, pressure and temperature, then holding these parameters constant while fuel flow was varied in small increments to define the lean and rich ignition limits. For the expendable gasifier combustor, temperature limitations prohibited definition of the rich limit; however, the lean limit is well defined as shown in Figure 188, where primary combustion zone equivalence ratio is plotted against a combustion stability parameter relating reference velocity, inlet pressure and temperature, and laminar

253
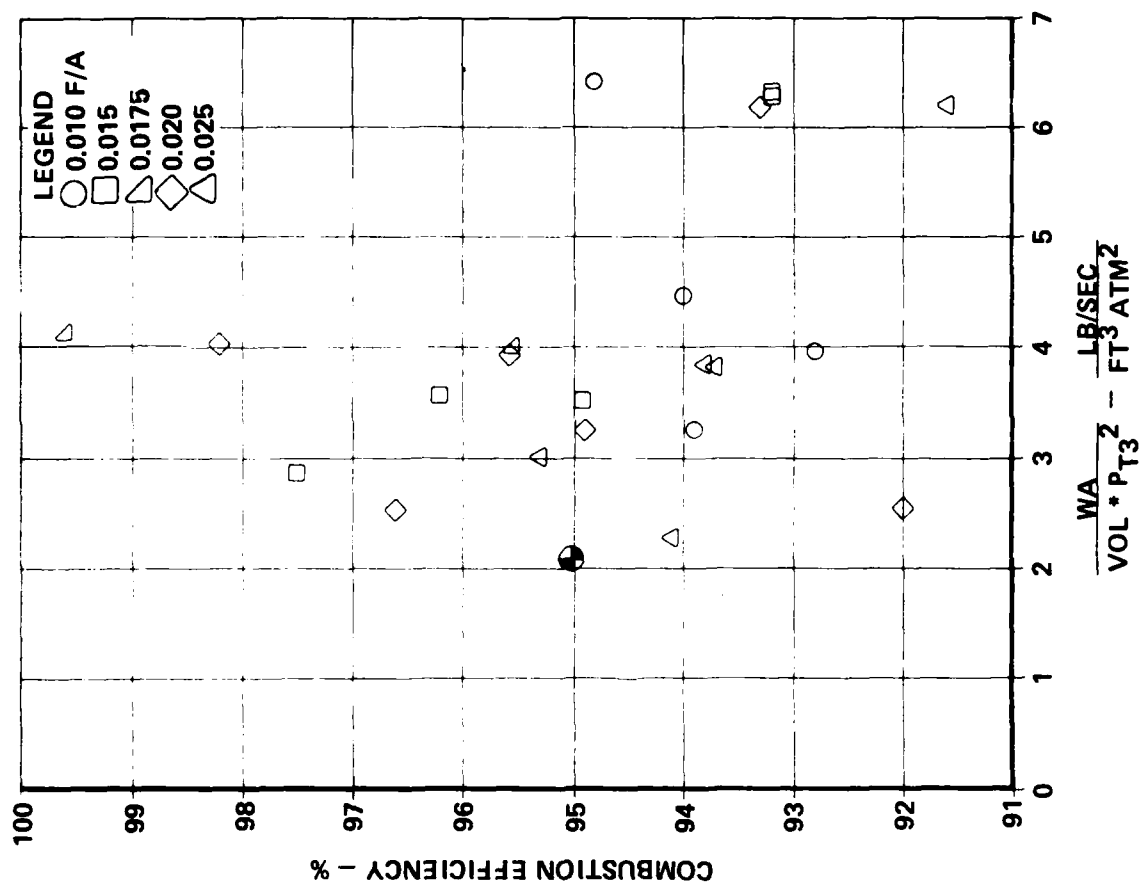
Figure 184. Expendable Gasifier Combustor Performance (Mod 5).

26142

254

COMBUSTION EFFICIENCY – %
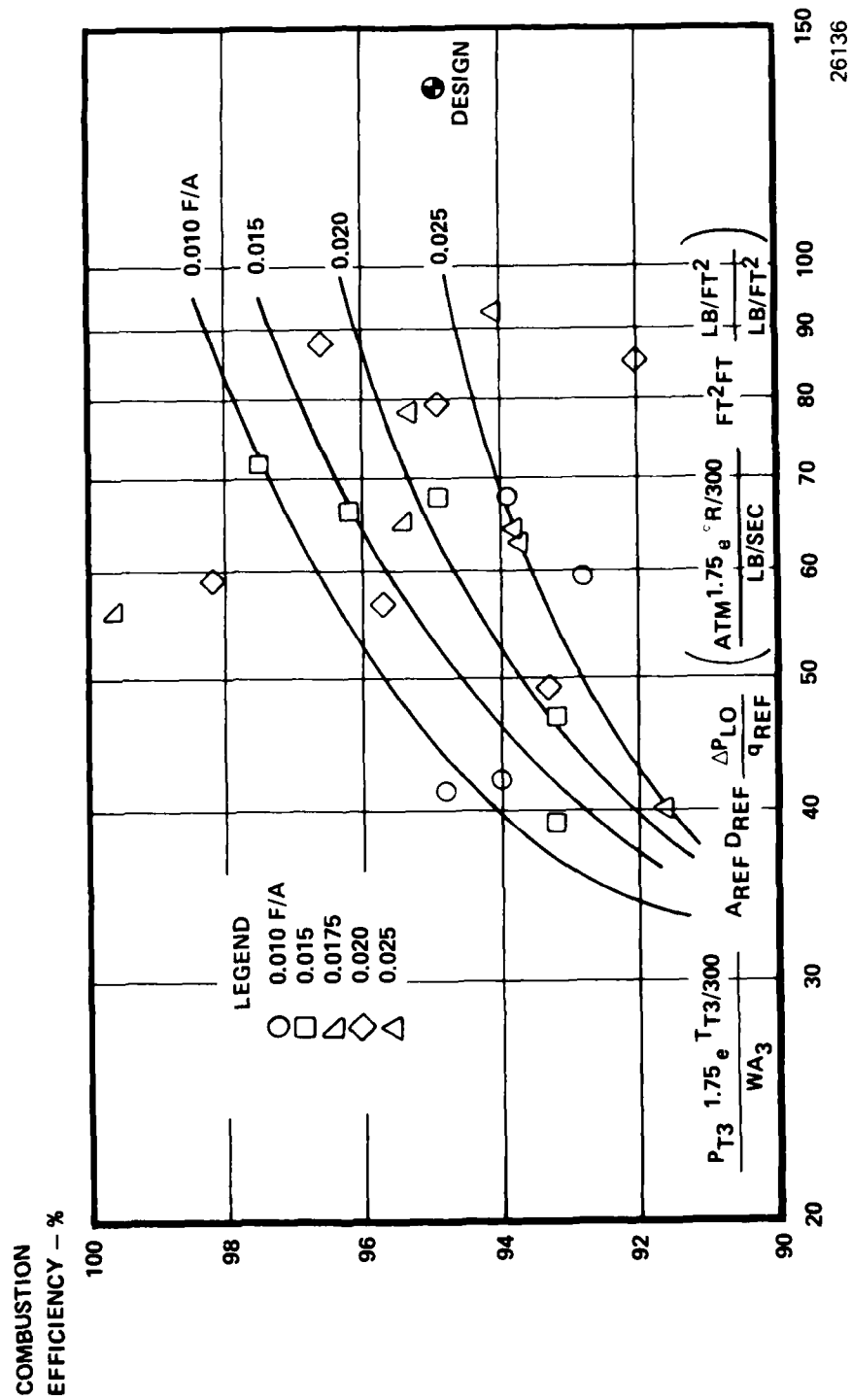
Figure 185. Expendable Gasifier Combustor Performance (Mod 5).

255

26136
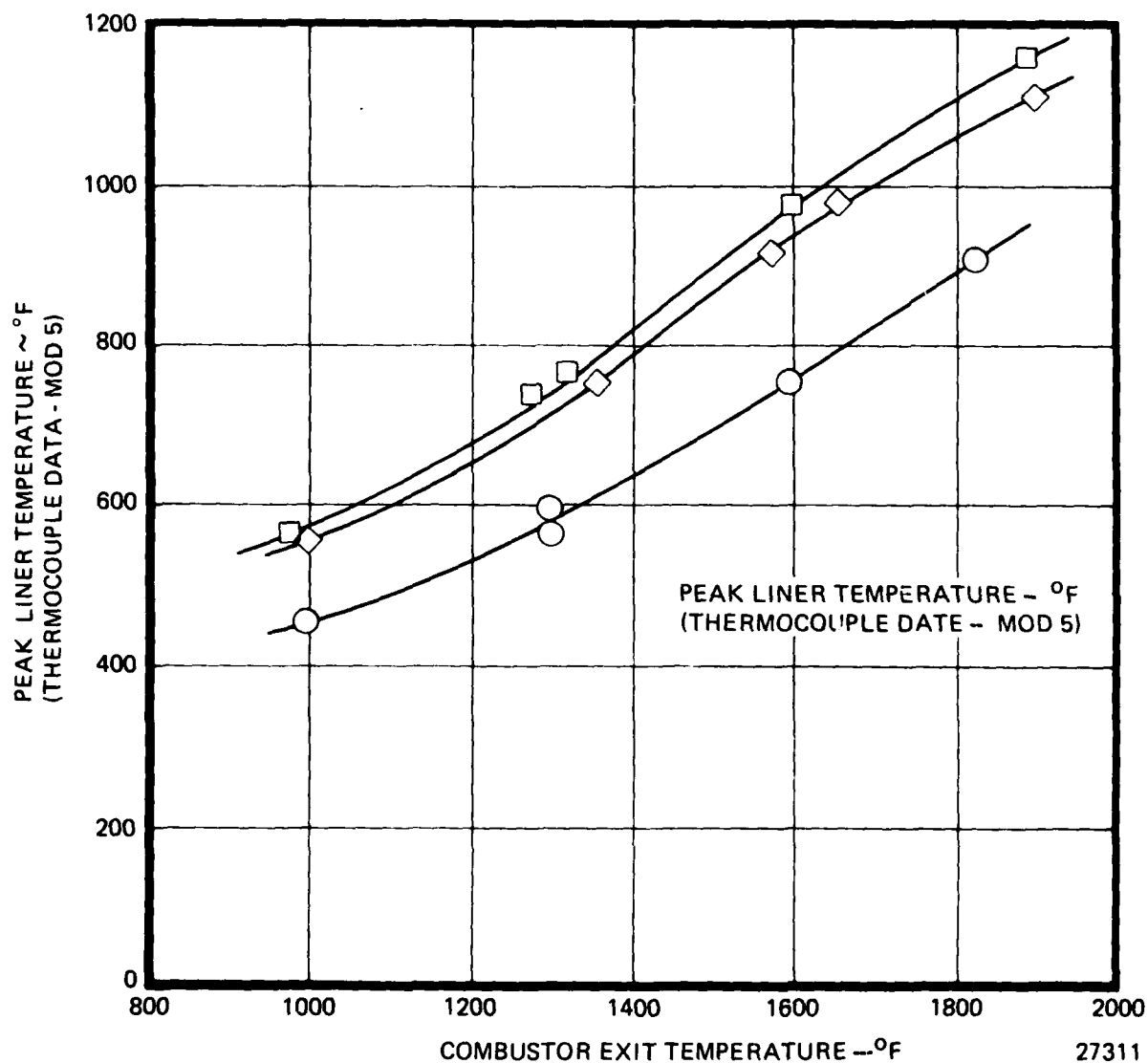
Figure 186. Expendable Gasifier Combustor Liner Thermocouple Measurements.

TABLE 27

RANGE OF IGNITION TEST
PARAMETERS

	MINIMUM	MAXIMUM
Airflow, lb/sec	0.45	1.95
Inlet Pressure, "HgA	13.7	33.4
Inlet Air Temperature, °F	-20	62
Main Fuel Temperature, °F	-22	76
Starting Fuel Temperature, °F	-5	74

27328

257

PRIMARY FUEL TUBE

STARTING FUEL NOZZLE

SPARK IGNITOR

26125
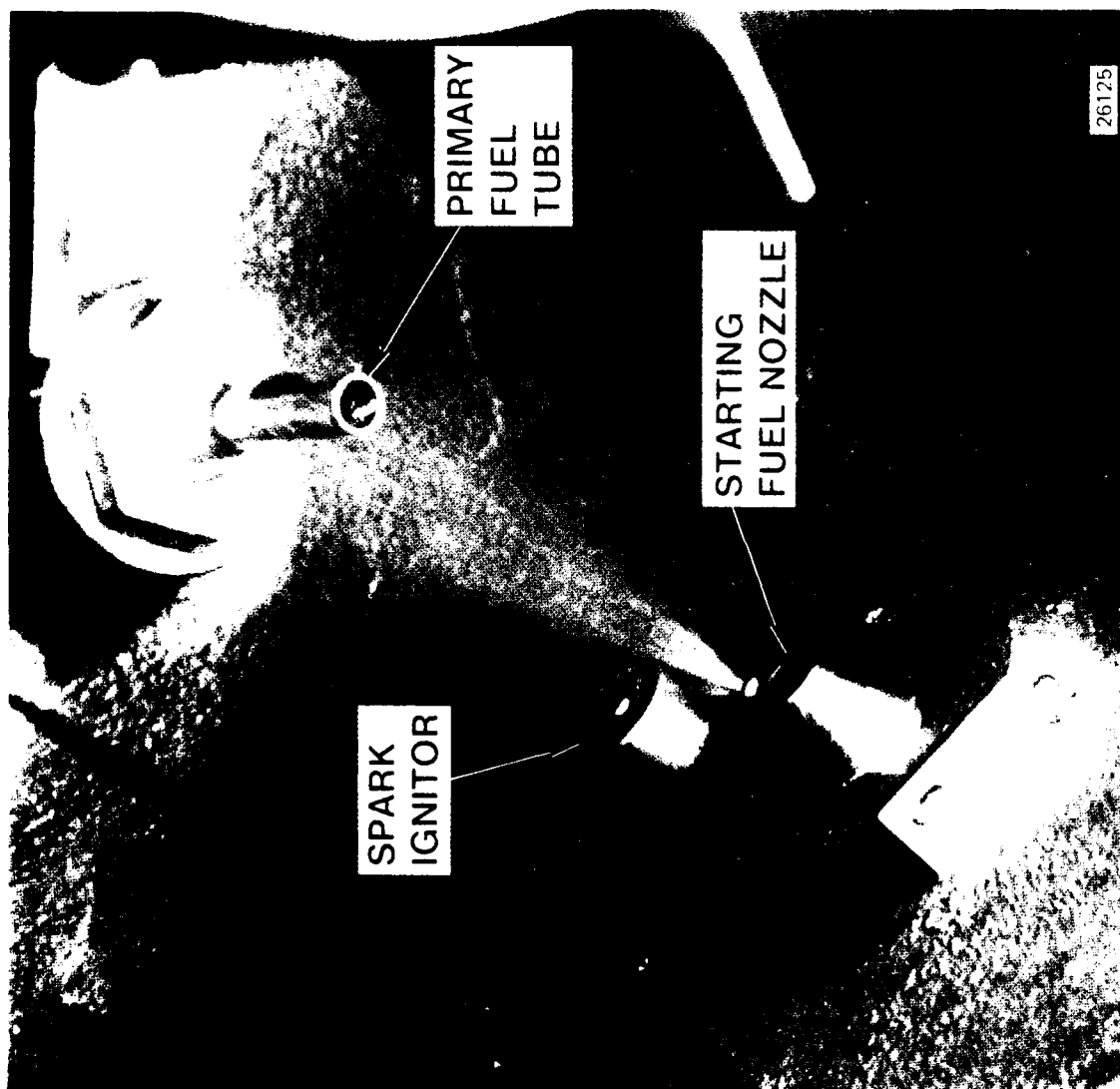
Figure 187. FG Combustor Starting System.

258
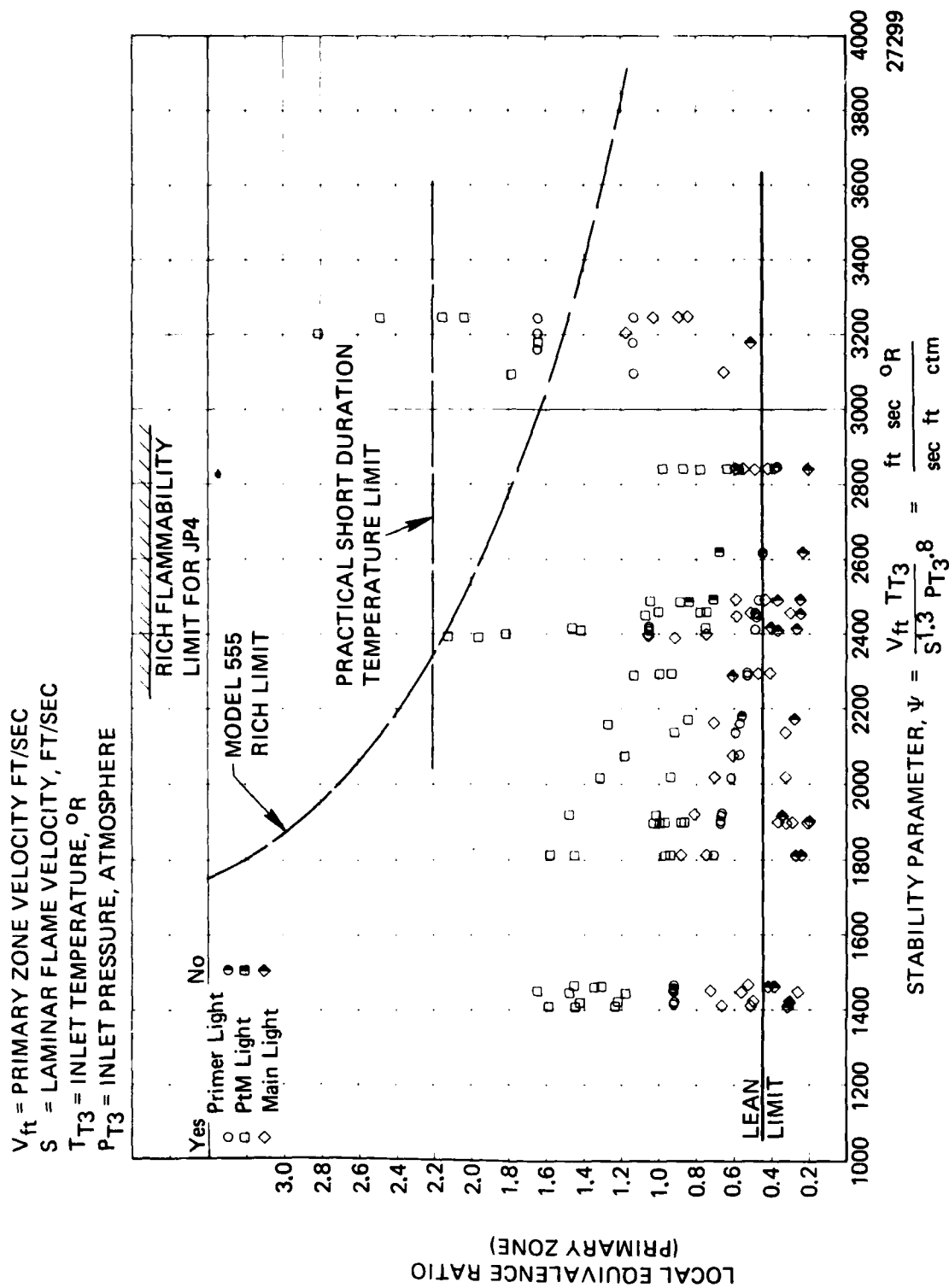
Figure 188. Expendable Gasifier Combustor Ignition Characteristics.

259

flame velocity. While the rich limit was not defined for the expendable gasifier, the shape of the curve is known and its position approximated from tests of similar combustors such as the Teledyne CAE Model 555 shown. Increasing severity of ignition occurs to the right with increasing values of ψ, with the nose of the ignition loop occurring near an equivalence ratio of 1.0. The practical short duration temperature limit shown is an arbitrary limit based on experience with the low speed temperature capabilities of similar axial flow turbines.

The starting conditions of the expendable gasifier were approximated over a range of altitudes from sea level to 30,000 feet and flight Mach numbers from 0 to 0.90. These conditions were then plotted on the ignition envelope of Figure 188 as shown in Figure 189. Where the test points and approximate rich limit have been removed for clarity. The starting points cross the temperature limit in the 25,000 to 30,000 feet altitude and 0.25 to 0.5 Mach number range. This provides the upper limit for a constant starting fuel nozzle flow rate.

Replotting the starting conditions falling within the ignition envelope in terms of altitude and flight Mach number resulted in Figure 190 and provides an estimated expendable gasifier starting envelope.

Table 28 summarizes the combustor test results and shows that with the exception of pressure loss and liner temperature, all performance goals were met or bettered. Consequently, a combustor with well defined performance is available for expendable gasifier demonstration tests.
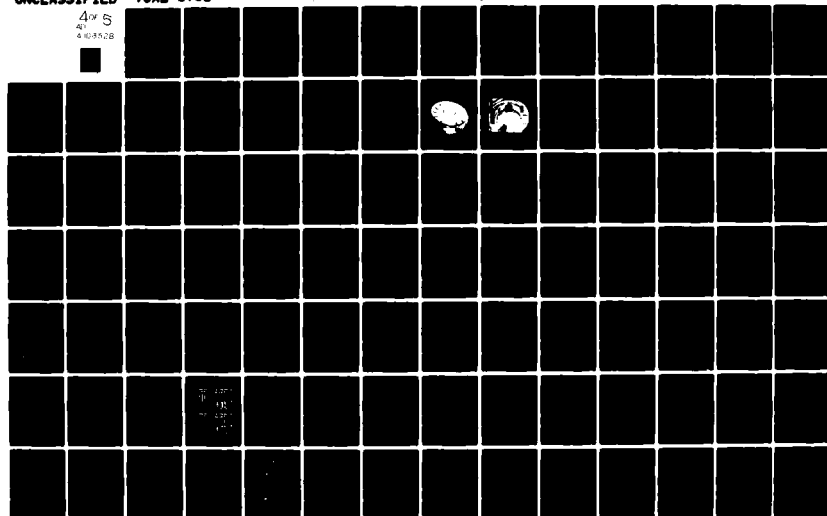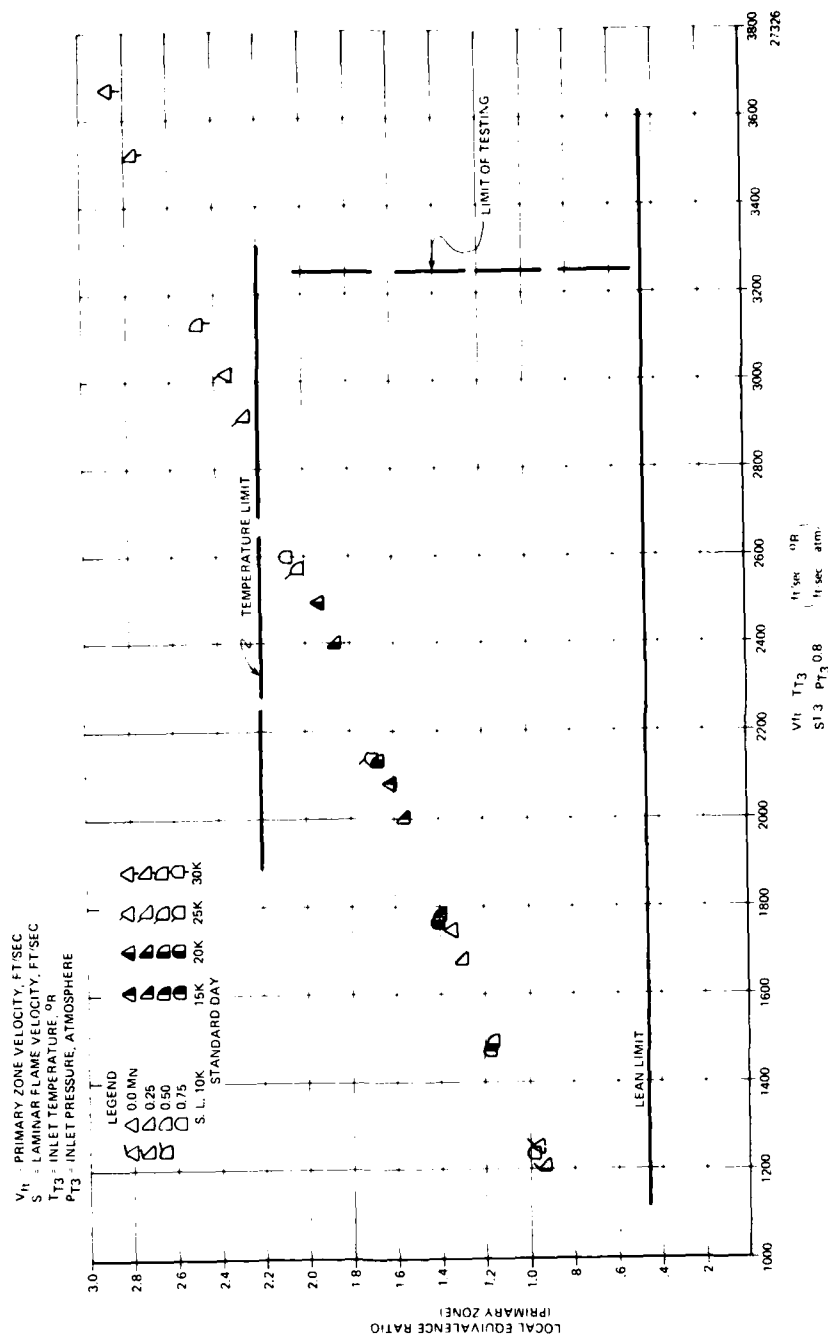
Figure 189. Expendable Gasifier Starting Condtion Plotted in Terms of Combustor Stability Parameter.
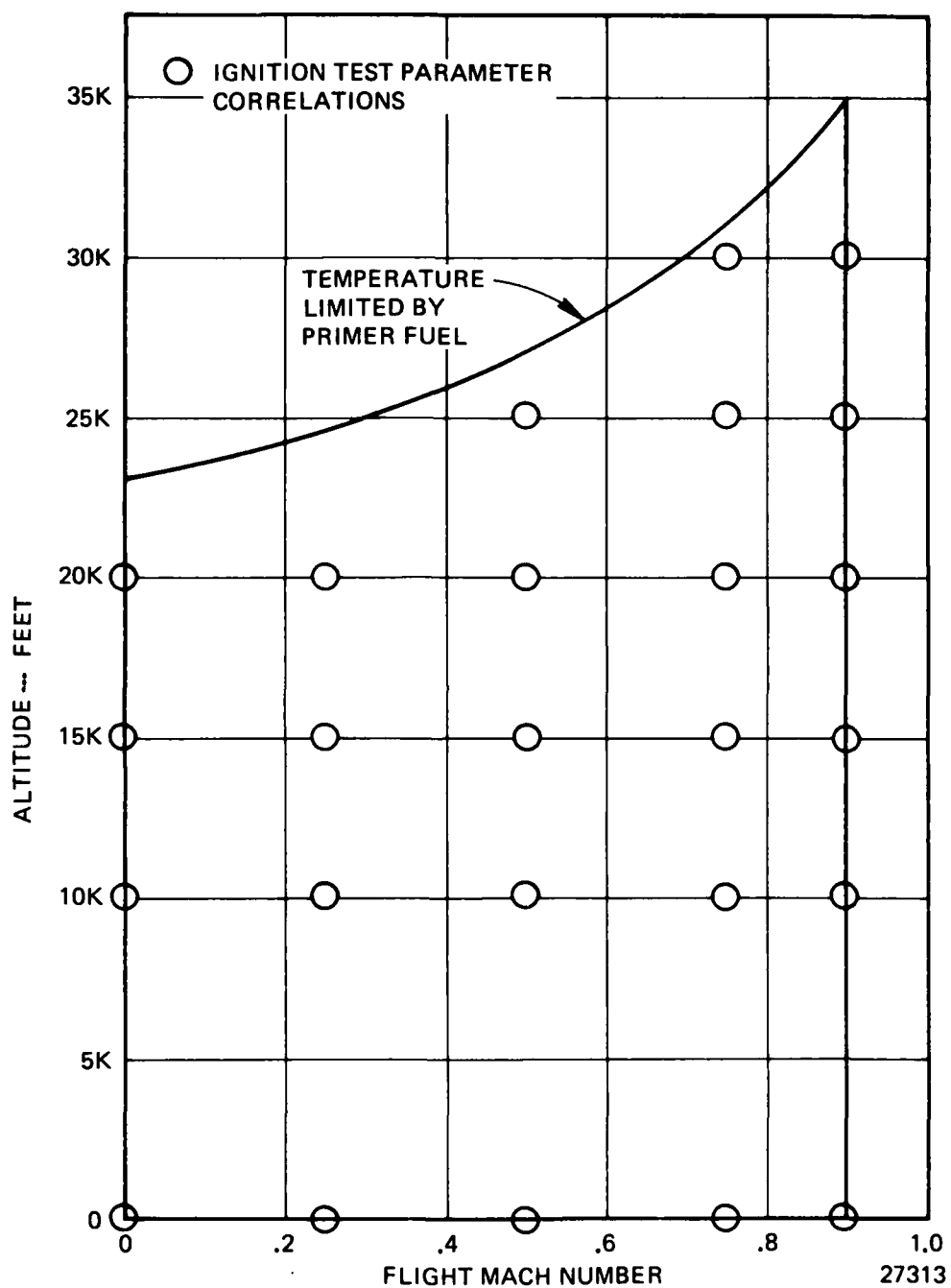
Figure 190. Expendable Gasifier Start Envelope (Standard Day)

262

TABLE 28

SUMMARY OF EXPENDABLE GASIFIER COMBUSTOR TEST RESULTS		
	GOAL	ACHIEVED
Pressure Loss - Percent	10.0	12.3
Heat Realease - $\dfrac{MBTU}{Hr \cdot Ft^3 \cdot ATM}$	9.3	9.3
Efficiency - Percent	95.0	95.0
Exit Temperature - °F	1800	1800
Temperature Rise - °F	1516	1516
Exit Radial Profile	0.07	0.05
Exit Pattern Factor	0.20	0.154
Maximum Liner Temperature - °F	1400	< 1500

27329

5.3   TURBINE DESIGN

5.3.1   Design Objectives

The base HP turbine has as its design objectives the accomplishment of the following:

1. Adaptability
2. Low Cost
3. Good Performance and Flexibility
4. Ease of Development

5.3.2   Design Requirements

Design requirements for the expendable gasifier turbine were established to provide low cost, as exemplified by casting techniques, simple blading design and moderate performance requirements, providing for a wide variety of operating conditions as demanded by various engine development considerations.

The gasifier turbine inlet conditions at design point are:

Inlet Temperature - $^{\circ}R$	=	2260
Inlet Pressure - psia	=	38.29
Inlet Swirl - degrees	=	0
Mass Flow - lb_m/sec	=	3.957

The turbine design requirements at these conditions are given in Table 29.

TABLE   29

EXPENDABLE GASIFIER TURBINE DESIGN REQUIREMENTS	
Referred Work - Btu/lb_m	$\dfrac{\Delta H}{\theta cr} = 12.9$
Absolute Work - Btu/lb_m	$\Delta H = 55.4$
Referred Speed - rpm	$\dfrac{N}{\sqrt{\theta cr}} = 16080$
Referred Flow - Speed Parameter - lb. rev/sec^2	$\dfrac{WN}{60\delta}\varepsilon = 871$
Referred Flow - lb_m/sec	$\dfrac{W\sqrt{\theta cr}}{\delta} = 3.25$
Total-To-Total Efficiency (Minimum) - Percent	$\eta = 82.5$

27336

264

These moderate performance requirements result in hardware that is more adaptable to a variety of engine configurations for optimum performance at low cost.

5.3.3 Aerodynamic Design Approach

The turbine aerodynamic design approach was based on permutation of:

1. Vector diagram selections/optimizations
2. Variations of some turbine basic geometric parameters and their effect on performance
3. Detailed flowpath design analyses
4. Blade designs for achievement of design velocity diagrams.

Before proceeding with a final design, the expendable gasifier turbine performance potential was examined to assure that the turbine base vector diagram selection was appropriate. Figure 191 shows results of such an investigation. It is seen from this plot that the turbine design point is nearly optimum and also is in a region where gradients in efficiency are the least. This feature ensures maximum turbine adaptability and least sensitivity to various other possible changes as imposed by different gasifier applications. Figure 192 shows the sensitivity of the gasifier turbine stage nozzle and rotor trailing edge thickness and rotor tip clearance. Consideration was also given to parasitic losses, leakages and tolerances to assure that performance goals will be met. Figure 193 provides a summary substantiating that a conservative gasifier turbine performance goal of 82.5 percent will be met. This takes into consideration various additional performance penalties and decrements, that have been imposed on production hardware, as may be expected in a real engine environment.

The final expendable gasifier turbine flow data for cold static conditions are given in Figure 194. An analysis was performed using a computerized version of radial equilibrium calculations between blade rows, which accounts for radial variations in total temperature, entropy and the effects of streamline curvature. The final cold flow path dimensions are based on brining the hot flow path solution to 70°F. Assumptions used in calculating the thermal contraction were:

| All shrouds | --- | MAR-M-509 | --- | Hot Temp. 1730°F |
| Disk | --- | IN-100 | --- | Hot Temp. 1300°F |

The turbine stage consists of a 13-vane constant section nozzle and a 29-bladed rotor. The constant section nozzle was finalized during the Phase I design effort. Once the nozzle hardware was fixed, the radial equilibrium streamline solution was then matched to the aerodynamic requirements of the constant section nozzle. The matching solution (Table 30) was the basis for the final flow path and the rotor blading design. The vector triangles corresponding to this streamline
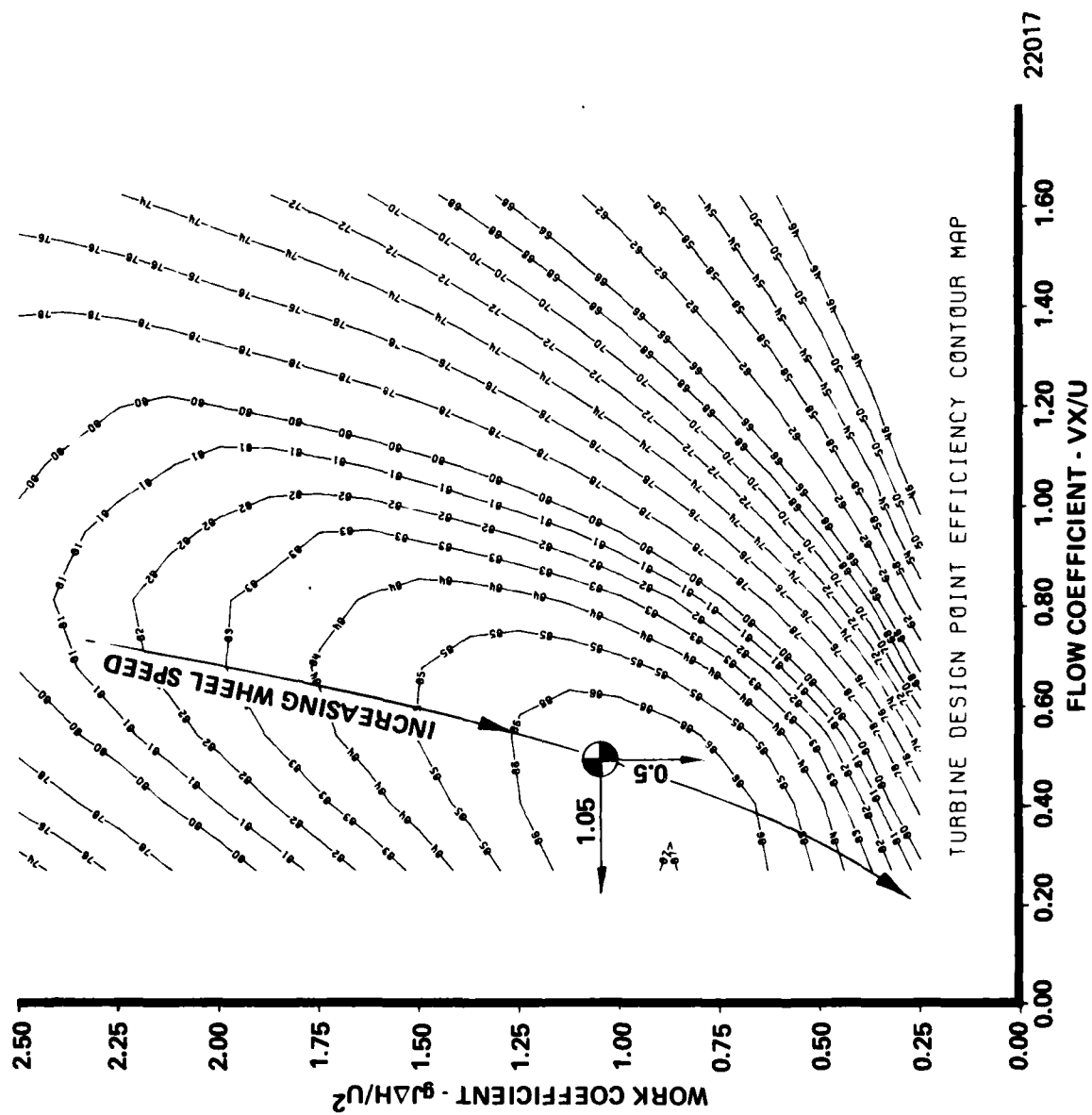
Figure 191. Expendable Gasifier Vector Diagram Potential.
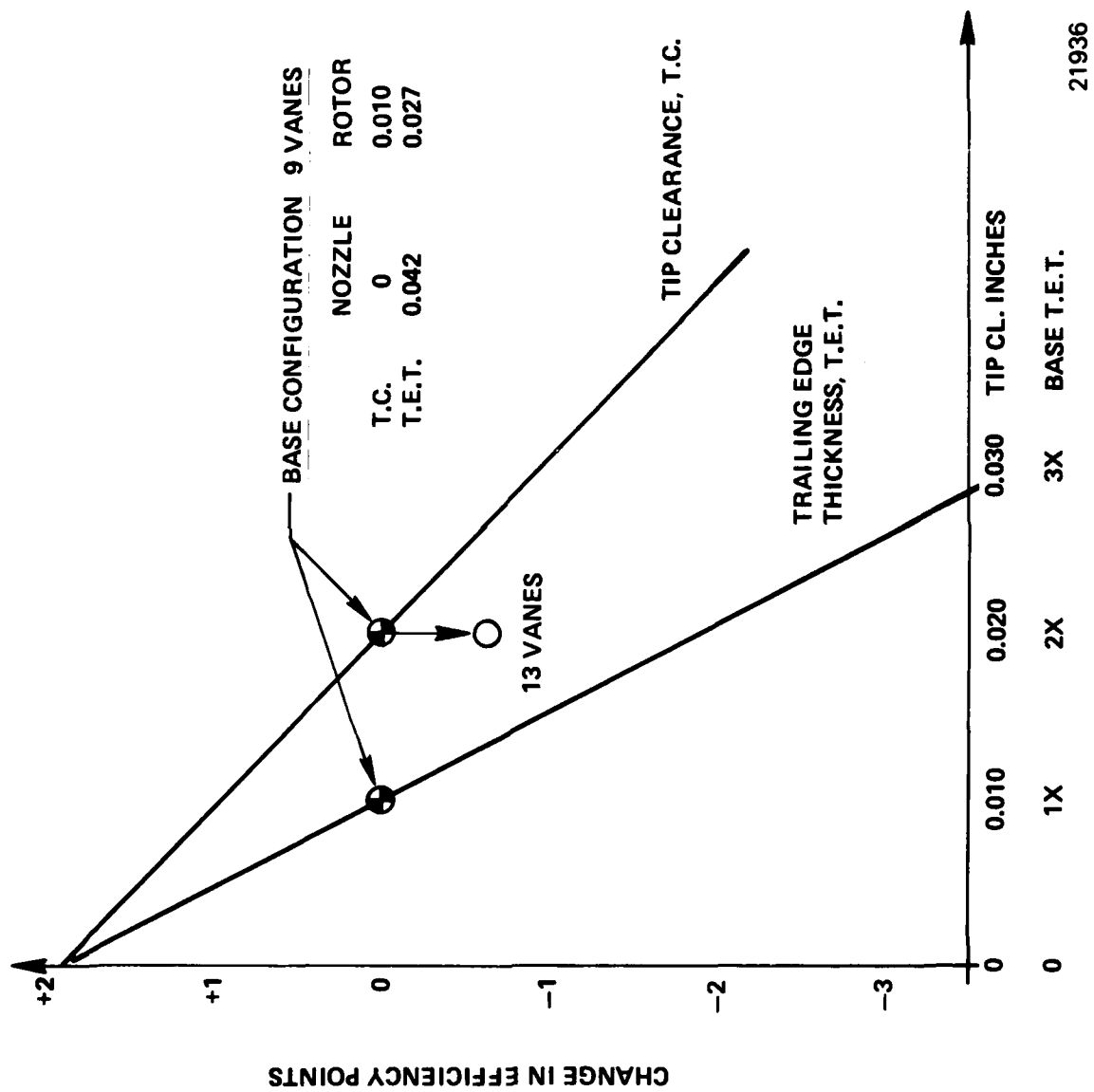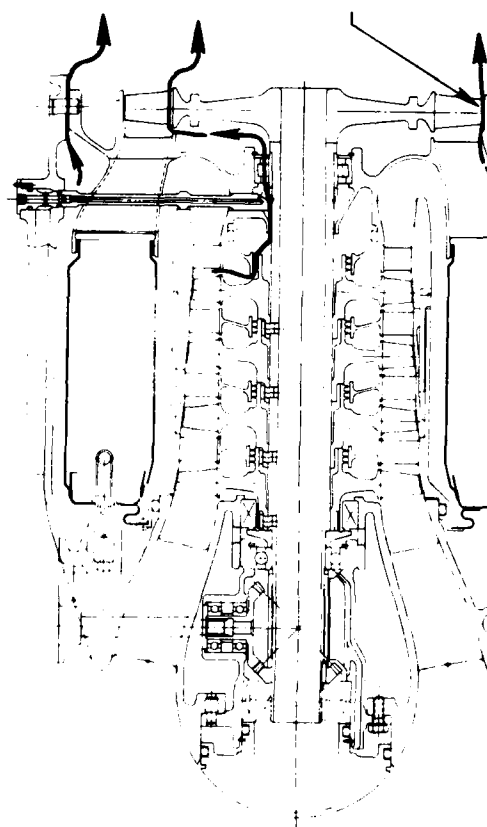
Figure 192. Turbine Sensitivity To Some Basic Geometric Parameters.

267

	BASE	PRODUCTION
FLANGE LEAKAGE	0	0.5%
LAB. SEAL TOLERANCE	0	±0.003 IN.
LAB. SEAL CLEARANCE	0	0.003 - 0.009
INTER-ROW LEAKAGE	0	0.18 - 0.54%
WINDAGE & BEARINGS	0	(1.7%)
ROTOR RADIAL TOL.	0	±0.002 IN.
ROTOR CLEARANCE	0.010	0.024 ± 0.003
CLEARANCE LOSS		1.94 - 2.99%
EFFICIENCY	87.8%	8.2 - 83.8%
AVERAGE		84.5%
OBJECTIVE MIN.		82.5%

26041

Figure 193. Expendable Gasifier Meets Minimum Performance Requirements.
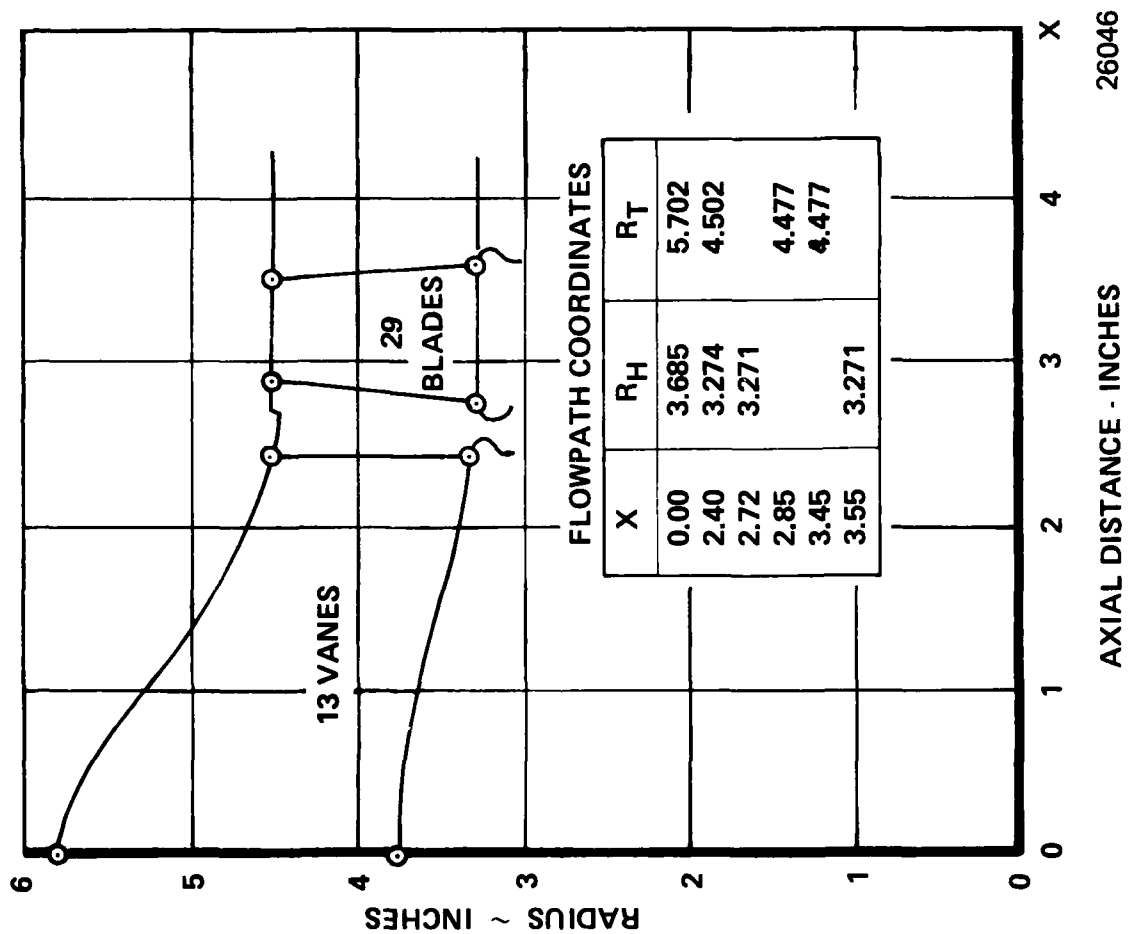
Figure 194. Cold Turbine Flowpath.

TABLE 30

COMPUTER PRINTOUT

* * * STATION 5 * * *

THE STAGE EFFICIENCY PRINTED BELOW REFERS TO THE TWO PRECEDING BLADE ROWS
THE RELATIVE VELOCITIES AND MACHNUMBERS REFER TO THE BLADE-ROW FOLLOWING THIS STATION

PRECEDING STAGE EFFICIENCY=	0.0	CUMULATIVE ISENTROPIC EFFICIENCY= 0.0
CUMULATIVE POLYTROPIC EFFICIENCY=	0.0	MASS-AVERAGE TOTAL TEMPERATURE= 2240.40
MASS-AVERAGE TOTAL PRESSURE=	5513.8	CUMULATIVE TOTAL PRESSURE RATIO= 1.0000

LOCA-TION	RADIUS	MERIDNAL VELOCITY	AXIAL VELOCITY	ABSOLUTE VELOCITY	VEL REL TO NEXT BLADE	VEL REL TO THIS BLADE	ABSOLUTE MACH NUMBER	MACH NO REL NEXT BLADE	MACH NO REL THIS BLADE	RAD OF CURVTRE	STRMLNE SLOPE ANGLE	AXIAL BLADE LDING	TANGEN BLADE LDING
1	0.3125	273.99	274.08	274.08	274.19	274.08	0.13058	0.13064	0.13058	-0.659	-1.4552	10.0	0.0
2	0.3380	270.77	270.27	270.27	270.14	270.27	0.12280	0.12274	0.12280	-0.446	-3.1779	7.3	0.0
3	0.3619	255.63	256.50	256.50	256.16	256.50	0.11385	0.11370	0.11385	-0.347	-4.7421	4.1	0.0
4	0.3843	235.00	236.36	236.36	235.92	236.36	0.10354	0.10334	0.10354	-0.289	-6.1654	1.6	0.0
5	0.4056	211.42	213.23	213.23	212.79	213.23	0.09285	0.09265	0.09285	-0.251	-7.4578	0.4	0.0
6	0.4260	186.93	189.07	189.07	188.70	189.07	0.08245	0.08229	0.08245	-0.222	-8.6243	0.8	0.0
7	0.4457	163.01	165.35	165.35	165.09	165.35	0.07272	0.07261	0.07272	-0.201	-9.6545	2.6	0.0
8	0.4648	140.67	143.08	143.08	142.90	143.08	0.06398	0.06391	0.06398	-0.183	-10.5322	5.5	0.0
9	0.4833	120.73	123.05	123.05	123.00	123.05	0.05675	0.05673	0.05675	-0.169	-11.1519	9.0	0.0

LOCA-TION	STAGN PRESSRE	STAGN TEMPTRE	STATIC PRESSRE	STATIC TEMPTRE	STATIC DENSITY	DELTA P UPON Q	DE HALL NUMBER	LOSS COEFF	DIFFUS FACTOR	RELATIVE EXIT ANG	ABSOLUTE FLOW ANG	NEXT-INL-ANGLE ACTUAL
1	5513.76	1961.90	5452.78	1956.72	0.05223	-1.10210	1.45436	0.0	-0.46436	0.0	0.0	0.0
2	5513.76	2166.21	5460.03	2161.24	0.04735	-0.86976	1.37129	0.0	-0.37129	0.0	0.0	0.0
3	5513.76	2274.49	5467.64	2270.05	0.04515	-0.60668	1.27081	0.0	-0.27081	0.0	0.0	0.0
4	5513.76	2337.49	5475.63	2333.74	0.04398	-0.33942	1.15998	0.0	-0.15998	0.0	0.0	0.0
5	5513.76	2366.35	5483.10	2363.30	0.04349	-0.09107	1.04664	0.0	-0.04664	0.0	0.0	0.0
6	5513.76	2358.29	5489.56	2355.89	0.04368	0.12630	0.93636	0.0	0.06364	0.0	0.0	0.0
7	5513.76	2315.90	5494.30	2314.06	0.04451	0.30775	0.83329	0.0	0.16671	0.0	0.0	0.0
8	5513.76	2235.90	5499.13	2234.52	0.04613	0.45221	0.74112	0.0	0.25898	0.0	0.0	0.0
9	5513.76	2095.30	5502.21	2094.27	0.04925	0.56288	0.66192	0.0	0.33808	0.0	0.0	0.0

TOTAL AXIAL FORCE ON BLADES = 0.69   TOTAL TANGENTIAL FORCE ON BLADES = 0.0   27401

TABLE 30 — CONTINUED

* * * STATION 8 * * *

THE STAGE EFFICIENCY PRINTED BELOW REFERS TO THE TWO PRECEDING BLADE ROWS
THE RELATIVE VELOCITIES AND MACHNUMBERS REFER TO THE BLADE-ROW FOLLOWING THIS STATION

PRECEDING STAGE EFFICIENCY= 0.0	CUMULATIVE ISENTROPIC EFFICIENCY=	0.0
CUMULATIVE POLYTROPIC EFFICIENCY= 0.0	MASS-AVERAGE TOTAL TEMPERATURE=	2260.42
MASS-AVERAGE TOTAL PRESSURE= 5388.9	CUMULATIVE TOTAL PRESSURE RATIO=	0.9773

LOCA-TION	RADIUS	MERIDONAL VELOCITY	AXIAL VELOCITY	ABSOLUTE VELOCITY	VEL REL TO NEXT BLADE	VEL REL TO THIS BLADE	ABSOLUTE MACH NUMBER	MACH NO REL NEXT BLADE	MACH NO REL THIS BLADE	RAD OF CURVTRE	STRMLNE SLOPE ANGLE	AXIAL BLADE LDING	TANGEN BLADE LDING
1	0.2775	463.45	461.15	1331.06	546.45	1331.06	0.65340	0.26826	0.65340	0.379	-5.3295	-261.4	162.2
2	0.2926	483.47	480.07	1373.01	555.81	1373.01	0.64177	0.25980	0.64177	0.322	-6.8000	-258.4	167.4
3	0.3062	499.85	495.27	1395.29	555.08	1395.29	0.63673	0.25331	0.63673	0.283	-7.7614	-255.2	173.3
4	0.3206	510.49	504.71	1392.90	543.51	1392.90	0.62677	0.24457	0.62677	0.253	-8.6211	-253.2	177.2
5	0.3338	517.77	510.12	1368.40	528.95	1368.40	0.61131	0.23630	0.61131	0.230	-9.4062	-219.8	177.1
6	0.3454	521.08	512.95	1334.11	521.73	1334.11	0.59622	0.23316	0.59622	0.211	-10.1397	-200.5	180.1
7	0.3586	521.52	512.23	1296.92	525.30	1296.92	0.57937	0.23649	0.57937	0.196	-10.8365	-198.9	183.1
8	0.3703	521.89	507.49	1228.33	544.30	1228.33	0.56166	0.24886	0.56166	0.183	-11.5229	-206.1	187.3
9	0.3817	512.12	500.70	1166.21	583.53	1166.21	0.54964	0.27360	0.54964	0.172	-12.1276	-203.3	198.7

LOCA-TION	STAGN PRESSURE	STAGN TEMPTRE	STATIC PRESSURE	STATIC TEMPTRE	STATIC DENSITY	DELTA P UPON Q	PF HALL NUMBER	LOSS COEFF	DIFFUS FACTOR	RELATIVE EXIT ANG	ABSOLUTE FLOW ANG	NEXT-INL-ANGLE ACTUAL
1	5229.64	1961.90	3985.64	1838.26	0.04064	-0.17625	1.09381	0.0	-0.16394	69.6292	69.6292	31.890
2	5227.43	2166.21	4079.11	2036.51	0.03754	-0.16925	1.08994	0.0	-0.15885	69.3870	69.3870	29.477
3	5393.61	2274.40	4171.94	2141.55	0.03651	-0.15751	1.08384	0.0	-0.15014	69.0130	69.0130	25.730
4	5478.54	2337.40	4232.78	2205.50	0.03557	-0.15111	1.08034	0.0	-0.14487	68.5061	68.5061	23.064
5	5439.32	2366.35	4292.16	2239.37	0.03593	-0.14600	1.07739	0.0	-0.13964	67.8035	67.8035	12.103
6	5437.84	2359.29	4339.53	2237.58	0.03635	-0.14889	1.07851	0.0	-0.14008	67.0140	67.0140	3.192
7	5474.10	2315.90	4381.45	2203.41	0.03727	-0.15667	1.08208	0.0	-0.14353	66.0981	66.0981	-7.112
8	5380.91	2235.90	4407.54	2172.83	0.03973	-0.17171	1.08917	0.0	-0.15158	65.0689	65.0689	-19.034
9	5370.60	2095.30	4426.22	2001.50	0.04145	-0.16517	1.10044	0.0	-0.16525	63.9561	63.9561	-29.159

TOTAL AXIAL FORCE ON BLADES = -25.74   TOTAL TANGENTIAL FORCE ON BLADES = -12.70

27401

TABLE 30 - CONTINUED

• • • STATION G F F •

THE STAGE EFFICIENCY PRINTED BELOW REFERS TO THE TWO PRECEDING BLADE ROWS
THE RELATIVE VELOCITIES AND MACHNUMBERS REFER TO THE BLADE-ROW FOLLOWING THIS STATION

PRECEDING STAGE EFFICIENCY=   0.9562   CUMULATIVE ISENTROPIC EFFICIENCY=   572.1456
CUMULATIVE POLYTROPIC EFFICIENCY=   573.6777   MASS-AVERAGE TOTAL TEMPERATURE=   2262.39
MASS-AVERAGE TOTAL PRESSURE=   5289.7   CUMULATIVE TOTAL PRESSURE RATIO=   0.9773

LOCA-TION	RADIUS	MERIDNAL VELOCITY	AXIAL VELOCITY	ABSOLUTE VELOCITY	VEL REL TO NEXT BLADE	VEL REL TO THIS BLADE	ABSOLUTE MACH NUMBER	MACH NO REL NEXT BLADE	MACH NO REL THIS BLADE	RAD OF CURVTRE	STRMLNE SLOPE ANGLE	AXIAL BLADE LDING	TANGEN BLADE LDING
1	0.2759	513.94	513.52	1356.01	506.50	505.13	0.66648	0.29320	0.29260	0.695	-2.3012	1.3	7.8
2	0.2976	522.62	522.07	1306.24	509.06	597.43	0.65332	0.27985	0.27963	0.495	-2.6217	3.4	10.5
3	0.3146	527.85	527.73	1413.23	587.27	587.30	0.64547	0.26822	0.26832	0.429	-2.7944	2.6	9.3
4	0.3177	528.23	527.58	1410.03	567.22	567.60	0.63495	0.25542	0.25567	0.382	-2.8457	-1.0	13.1
5	0.3305	525.89	525.26	1393.29	542.62	543.05	0.61833	0.24255	0.24282	0.347	-2.8023	-0.2	14.9
6	0.3423	522.31	521.74	1346.47	527.83	525.13	0.60203	0.23466	0.23487	0.319	-2.6704	0.2	16.1
7	0.3547	516.26	515.78	1296.60	517.64	517.67	0.58408	0.23312	0.23321	0.286	-2.4840	-1.2	17.3
8	0.3662	526.77	506.39	1236.36	526.19	525.71	0.56544	0.24064	0.24051	0.277	-2.3744	-3.7	19.2
9	0.3773	465.16	404.71	1170.13	551.00	552.89	0.55167	0.26109	0.26068	0.261	-1.9214	-2.9	18.6

LOCA-TION	STAGN PRESSURE	STAGN TEMPTRE	STATIC PRESSURE	STATIC TEMPTRE	STATIC DENSITY	DELTA P UPON Q	DE HALL NUMBER	LOSS COEFF	DIFFUS FACTOR	RELATIVE EXIT ANG, FLOW AVG	RELATIVE EXIT ANG, BLADE AVG	ABSOLUTE FLOW ANG	NEXT-INL-ANGLE ACTUAL
1	5223.64	1061.91	3942.74	1932.45	0.09031	-2.22444	1.09150	0.0	0.44708	30.2519		67.7327	30.353
2	5297.09	2166.26	4041.90	2032.07	0.03728	-2.20369	1.07663	0.0	0.42963	28.9848		68.0239	29.044
3	5389.64	2274.09	4140.19	2117.69	0.03639	-0.17845	1.05893	0.0	0.38983	26.0230		68.1728	26.041
4	5427.46	2337.38	4205.33	2202.22	0.03578	-0.16391	1.04460	0.0	0.31783	21.4855		68.0030	21.481
5	5430.10	2366.33	4269.32	2236.56	0.03574	-0.14421	1.0265	0.0	0.26406	14.4423		67.6616	14.440
6	5437.95	2358.20	4321.32	2235.33	0.03623	-0.11867	1.00621	0.0	0.17977	5.0418		67.1422	5.919
7	5434.81	2315.07	4367.10	2201.61	0.03714	-0.08784	0.98507	0.0	0.24013	-4.2244		66.5471	-4.272
8	5392.16	2236.12	4347.84	2131.60	0.03867	-0.15354	0.96545	0.0	0.06009	-15.4932		65.8064	-15.490
9	5370.60	2095.30	4420.94	2090.43	0.04161	-0.32396	0.95243	0.0	0.07121	-26.4129		64.9688	-26.432

TOTAL AXIAL FORCE ON BLADES =   3.21   TOTAL TANGENTIAL FORCE ON BLADES =   1.41

27401

272

TABLE 30 – CONTINUED

* * * STATION 19 * * *

THE STAGE EFFICIENCY PRINTED BELOW REFERS TO THE TWO PRECEDING BLADE ROWS
THE RELATIVE VELOCITIES AND MACHNUMBERS REFER TO THE BLADE-ROW FOLLOWING THIS STATION

PRECEDING STAGE EFFICIENCY=	1.1047	CUMULATIVE ISENTROPIC EFFICIENCY=	1.1585
CUMULATIVE POLYTROPIC EFFICIENCY=	1.1668	MASS-AVERAGE TOTAL TEMPERATURE=	2071.38
MASS-AVERAGE TOTAL PRESSURE=	3569.3	CUMULATIVE TOTAL PRESSURE RATIO=	0.6473

LOCA-TION	RADIUS	MERIDNAL VELOCITY	AXIAL VELOCITY	ABSOLUTE VELOCITY	VEL REL TO NEXT BLADE	VEL REL TO THIS BLADE	ABSOLUTE MACH NUMBER	MACH NO REL NEXT BLADE	MACH NO REL THIS BLADE	RAD OF CURVTRE	STRMLNE SLOPE ANGLE	AXIAL BLADE LDING	TANGEN BLADE LDING
1	0.2744	582.76	582.75	591.54	1074.95	1029.13	0.29457	0.51040	0.51239	10.771	-0.2393	-882.3	-1300.9
2	0.2495	620.21	620.21	621.06	1148.29	1151.08	0.29527	0.54592	0.54716	-47.135	0.0791	-1083.7	-1450.9
3	0.3030	640.27	640.25	641.57	1265.56	1266.64	0.29881	0.58944	0.58982	-8.216	0.3707	-1301.6	-1613.5
4	0.3177	642.66	642.62	646.43	1334.12	1334.40	0.29753	0.61405	0.61404	-4.661	0.6679	-1495.4	-1680.8
5	0.3300	632.61	632.53	635.98	1366.01	1366.00	0.29094	0.62490	0.62479	-3.291	0.9186	-1494.6	-1664.3
6	0.3436	609.35	609.22	617.39	1367.94	1368.17	0.27741	0.62617	0.62612	-2.541	1.1959	-1930.7	-1583.8
7	0.3561	576.81	574.61	575.97	1326.42	1327.93	0.26522	0.61106	0.61142	-2.054	1.4917	-2112.6	-1419.5
8	0.3670	542.17	541.30	553.12	1280.25	1284.01	0.25841	0.59809	0.59970	-1.713	1.8175	-2286.8	-1258.5
9	0.3705	517.61	517.23	542.17	1243.44	1245.61	0.26381	0.59695	0.59928	-1.490	2.1897	-2414.9	-1144.2

LOCA-TION	STATIC PRESSURE	STATIC TEMP OR	STATIC PRESSURE	STATIC TEMTOR	STATIC DENSITY	DELTA P UPON Q	DE HALL NUMBER	LOSS COEFF	DIFFUS FACTOR	RELATIVE EXIT ANG, FLOW ANG	ABSOLUTE NEXT-IM-ANGLE FLOW ANG, ACTUAL
1	3577.60	1809.50	3300.73	1784.12	0.03552	2.64796	1.72925	0.73242	-1.18679	-55.5142	9.8874	-55.340
2	3574.91	1892.05	3291.61	1865.41	0.03225	-3.12110	1.92671	0.75793	-1.49600	-57.4016	2.0075	-57.305
3	3549.72	2090.00	3426.64	2051.83	0.03004	-3.80364	2.15673	0.58829	-1.86799	-59.6429	-3.5534	-59.619
4	3545.31	2131.00	3425.39	2103.43	0.03017	-4.50147	2.35094	0.57745	-2.10817	-61.2139	-6.1363	-61.222
5	3581.61	2159.10	3399.49	2159.51	0.02983	-5.52035	2.51560	0.62040	-2.50572	-62.4197	-5.4911	-62.435
6	3556.73	2153.14	3550.65	2127.70	0.02947	-5.50072	2.60537	0.91294	-2.71097	-63.5572	-2.3163	-63.567
7	3544.59	2123.36	3530.11	2102.55	0.03075	-6.22475	2.56572	1.51511	-2.68447	-64.3556	3.4965	-64.335
8	3512.40	2052.67	3529.10	2038.62	0.03116	-5.98566	2.64434	1.48084	-2.41625	-64.941	11.9174	-64.935
9	3552.64	1924.71	3565.62	1915.54	0.03421	-5.12404	2.35477	1.61741	-2.05510	-65.4612	19.2747	-65.312

TOTAL AXIAL FORCE ON BLADES = -170.65   TOTAL TANGENTIAL FORCE ON BLADES = -154.61   27401

solution are shown in Figure 195. The moderate turbine design requirements translate into conservative Mach number levels and modest turning angles. The turbine inlet temperature distribution is given in Figure 196 and is consistent with Teledyne CAE design experience for shaping combustor exit temperature profiles. The total pressure profile at inlet to the turbine was assumed to be uniform. Nozzle and rotor radial loss distributions are given in Figure 197 and are consistent with the type and size of the blading under consideration. A near uniform total pressure at the rotor exit was specified to minimize entrance losses to following components. The radial work distribution of the turbine is given in Figure 198. The work extraction is biased to be low in the low efficiency regions, i.e., at the hub where low rim speed reaction, fillets and secondary flows predominate and at the tip where clearance and wall effects impair performance. The vane and blade Zweifel loading parameter distributions with respect to the prescribed nozzle/rotor axial chords are given in Figure 199. A list of various aerothermodynamic parameters is given in Table 30 for reference.

The basic vane design approach was to provide a low cost component that could be integrally cast as a nozzle assembly (Figure 200). The vane section itself is of simple shape which is hollow on the inside and supplies 64 percent of compressor flow to the combustor. A trailing edge view of the nozzle ring assembly is given in Figure 201.

Aerothermodynamically, the expendable gasifier turbine inlet nozzle (P/N 722102), is a 13-vane constant section, moderately loaded nozzle (Zweifel coefficient = 0.4). Figure 202 shows the general nozzle definition. The airfoil has a 2.37 inch axial chord, 0.048 inch nominal trailing edge thickness and tolerance band of ± 0.010 inch from nominal. The design cold throat area is 9.997 square inches; the hot throat area is 10.706 square inches. Compressible flow loading diagrams for the hub, mean and tip nozzle sections are shown in Figures 203, 204 and 205. A boundary layer analysis was applied to the tip section suction surface. The resultant displacement thickness, momentum thickness and form factor development along the surface are given in Figure 206. The solution started as laminar and at a stagnation point and it was assumed to trip to a turbulent solution at the point of instability. The vane geometric properties are given in Figure 207.

The rotor blade design approach is similar to that of the vanes. The rotor blades and disk are integrally cast and together with simple blading assure low cost.

The selection of a reasonable chord for castability and a Zweifel loading coefficient of 1.0 results in a rotor with 29 blades. Three airfoil sections were aerodynamically designed (0, 50, and 100 percent mass flow streamlines) and are given in Figures 208, 209, and 210. The cross-sectional areas were set to

274
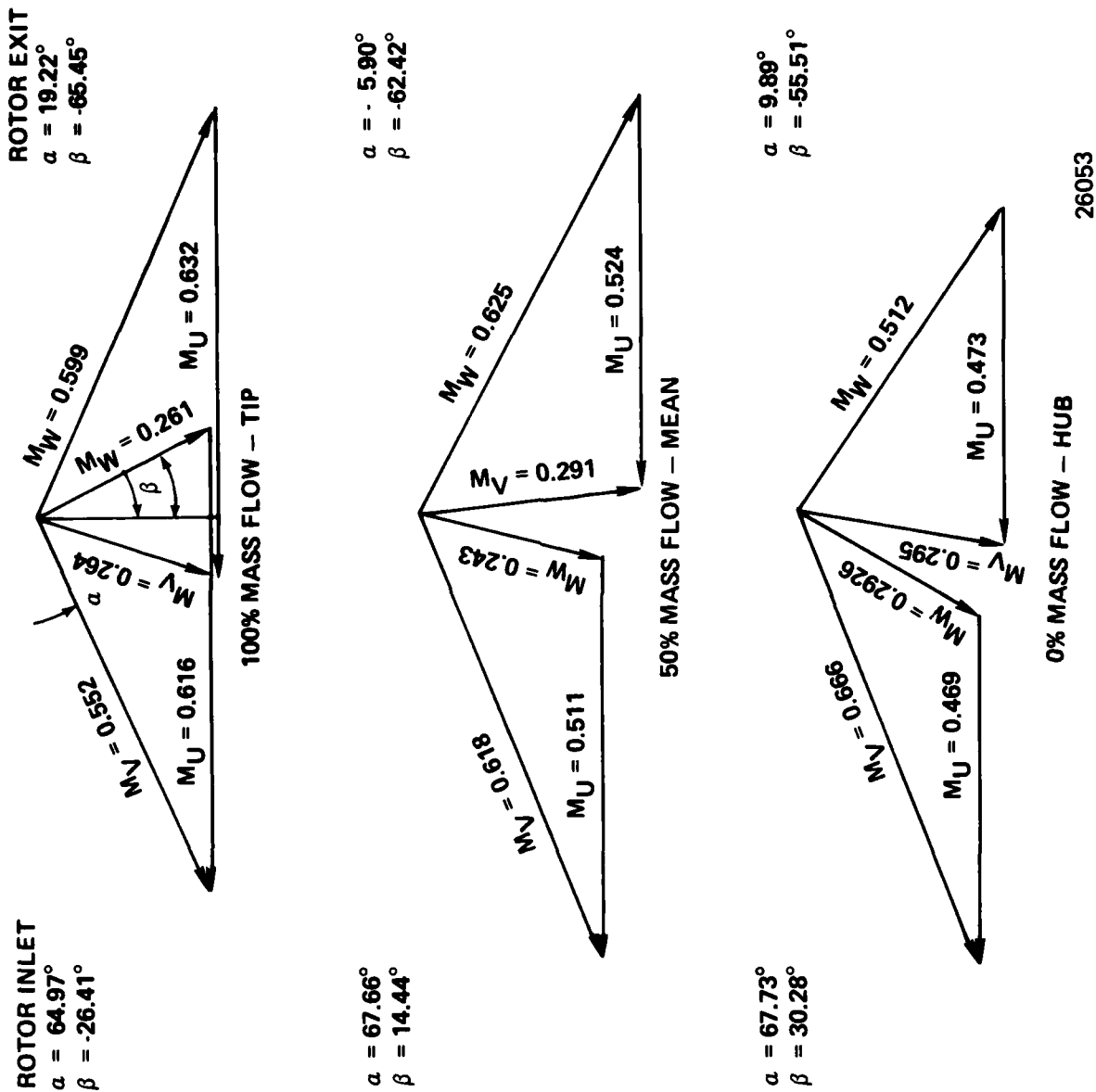
Figure 195. Expendable Gasifier HP Turbine Design Velocity Diagrams.

275
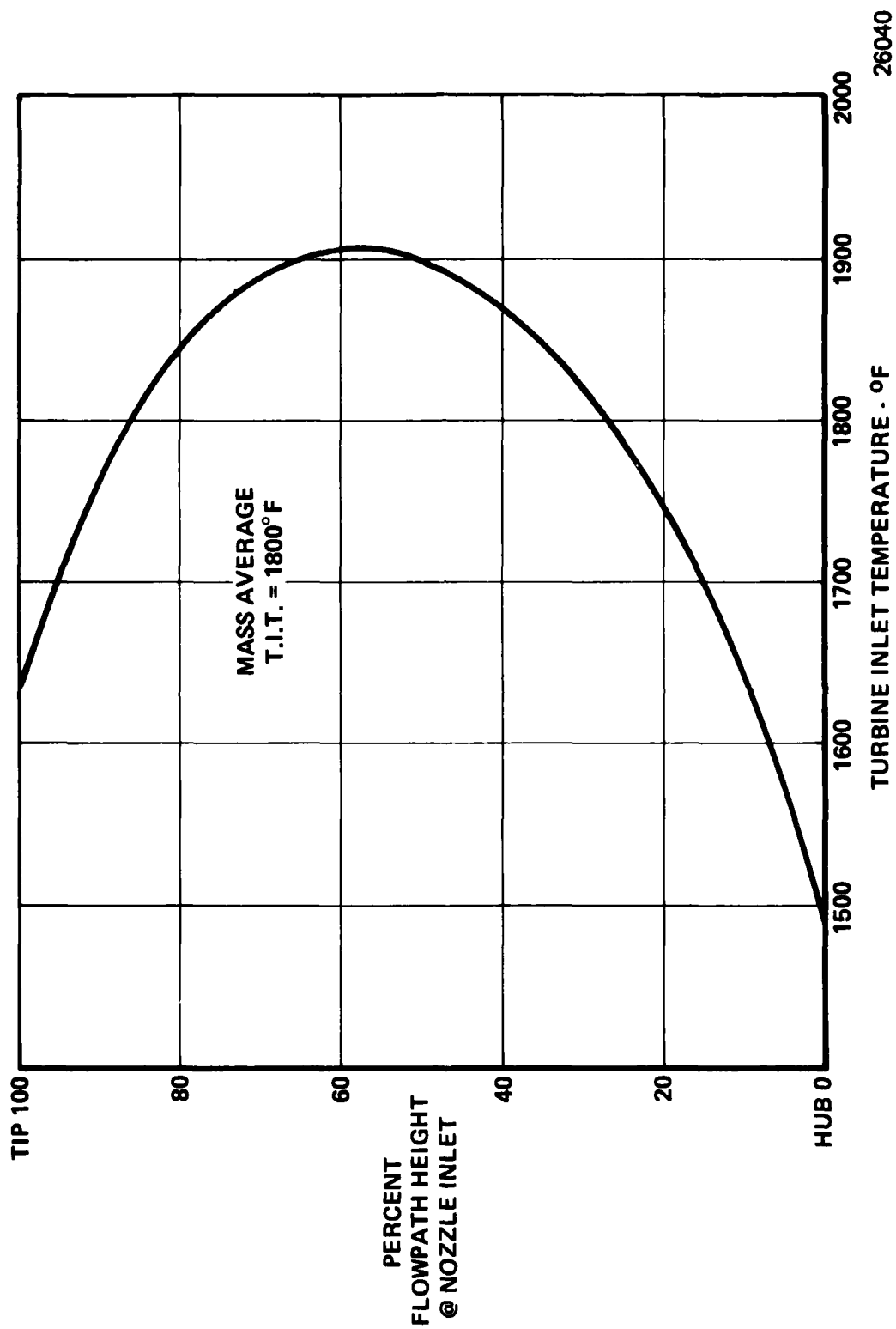
Figure 196. Turbine Design Inlet Temperature Profile.

276
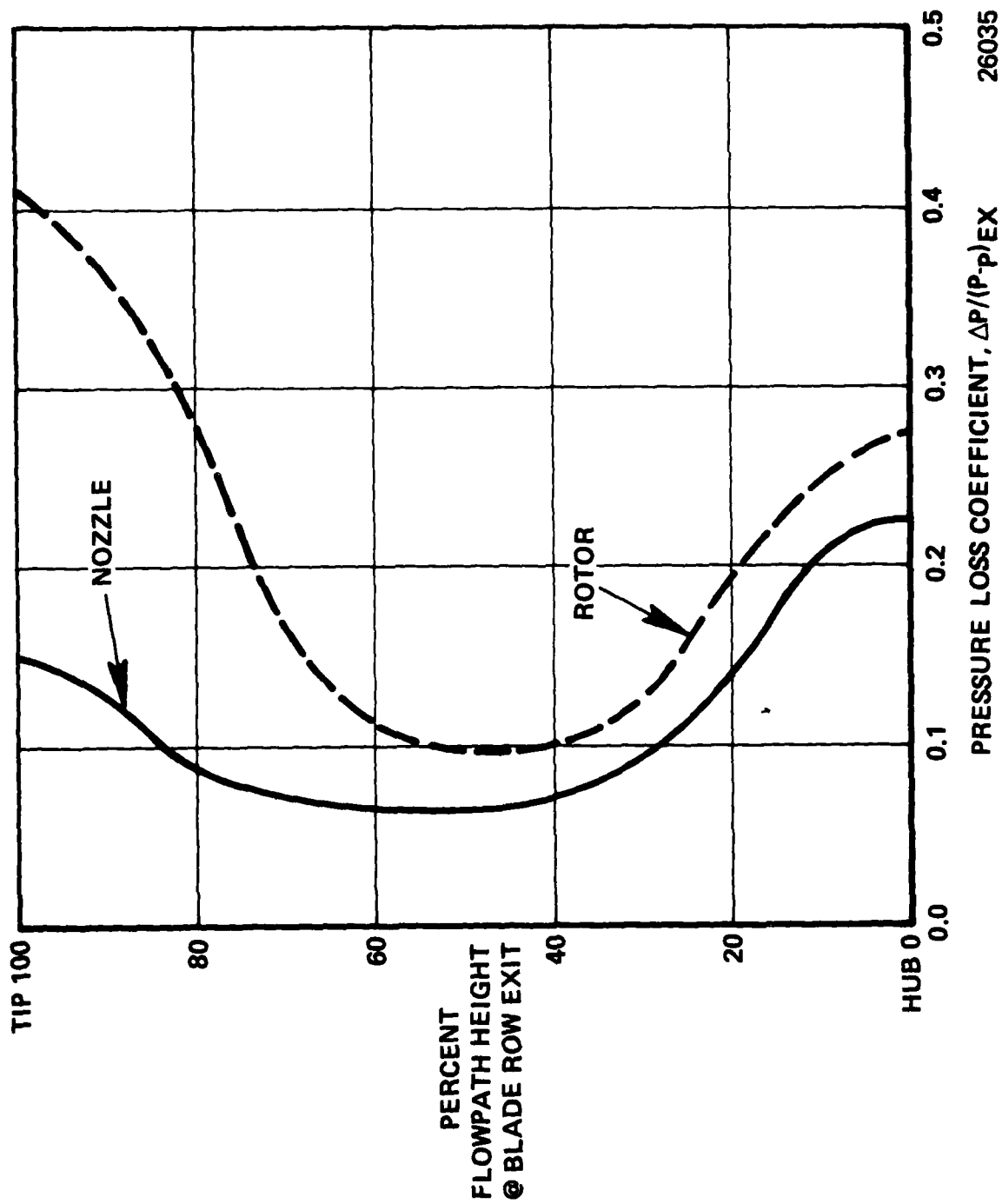
Figure 197. Design Vane and Rotor Loss Distribution.

277
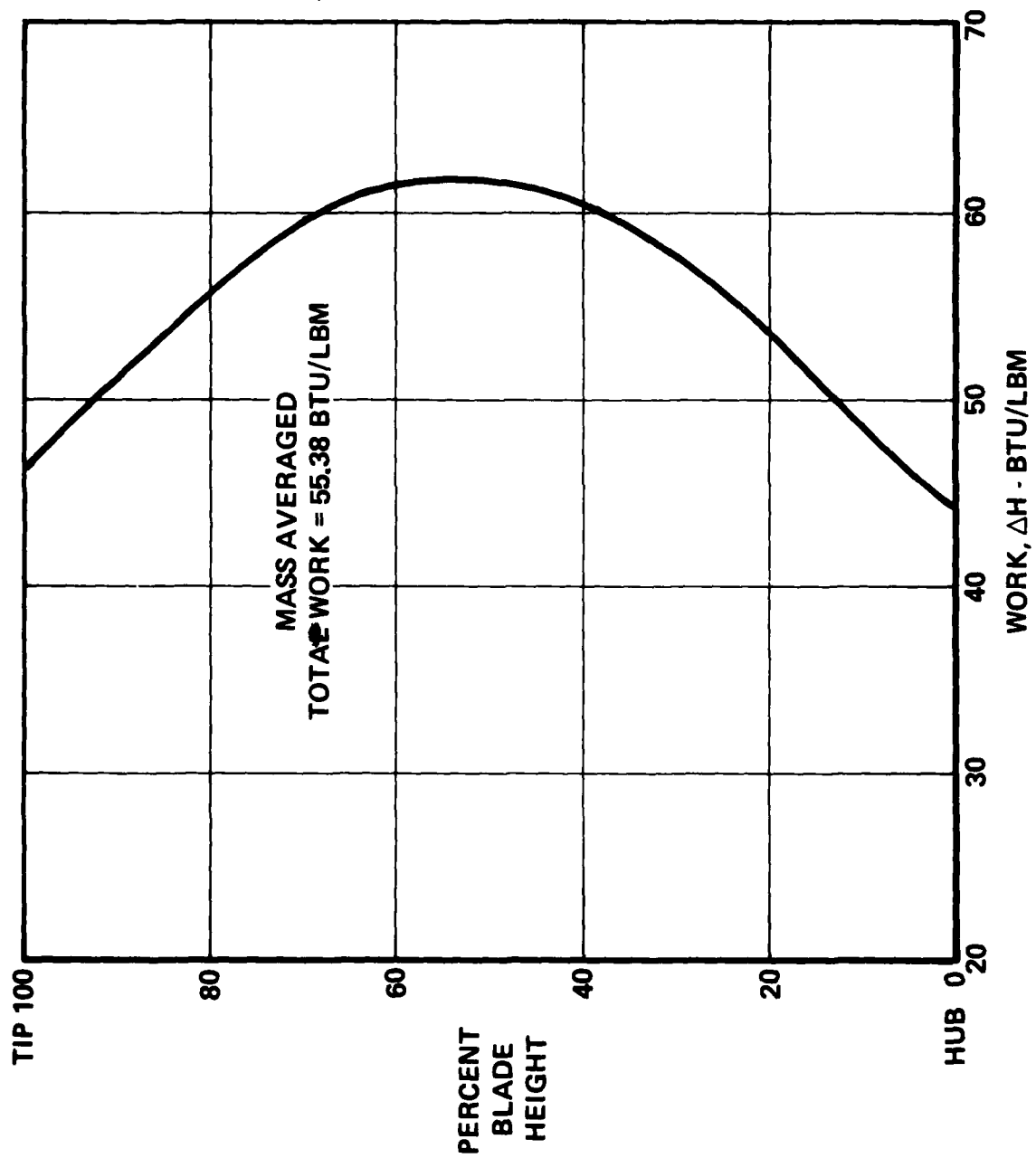
Figure 198. Turbine Radial Work Distribution.

26039

278
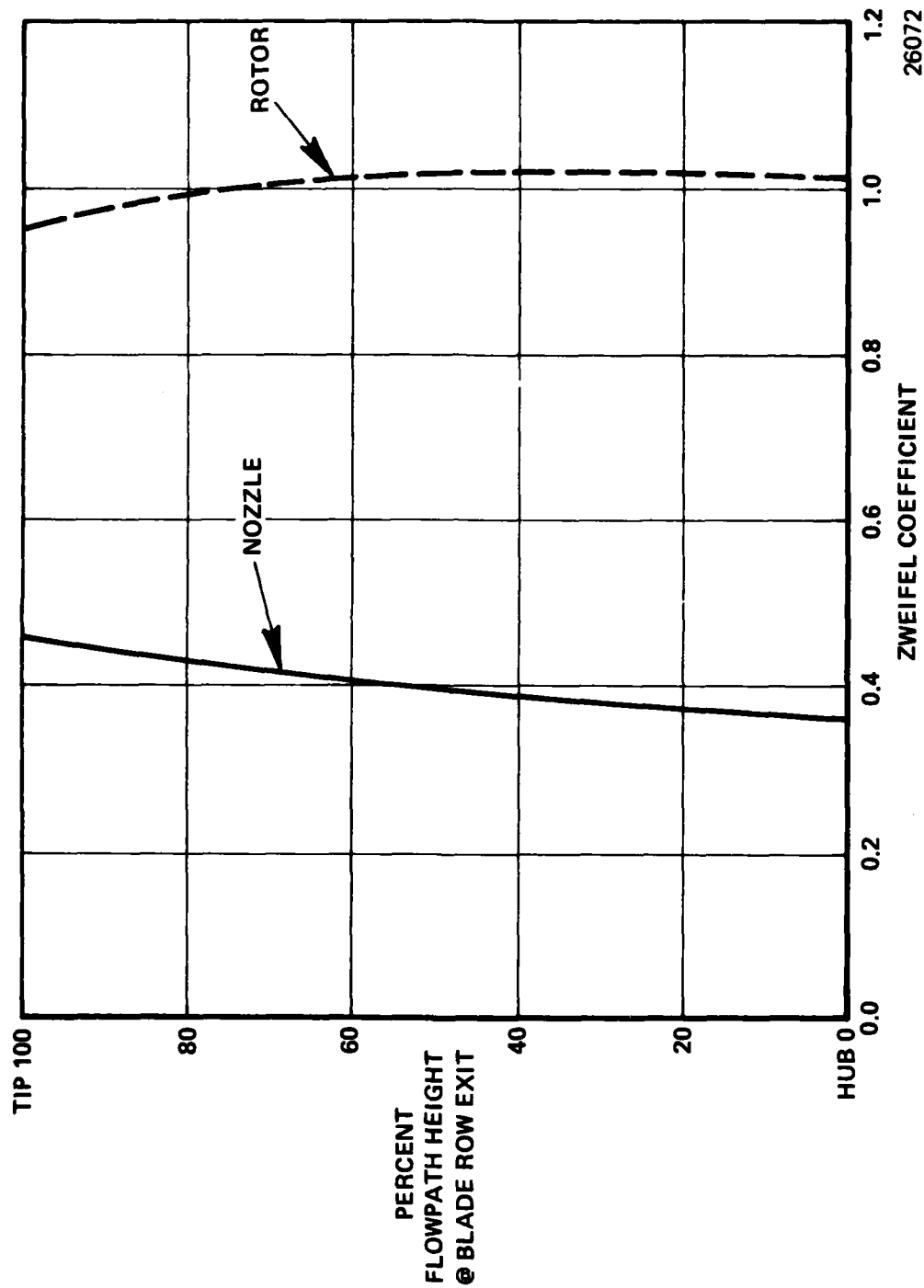
Figure 199. Turbine Vane/Blade Zweifel Loading Coefficient Distribution.

279
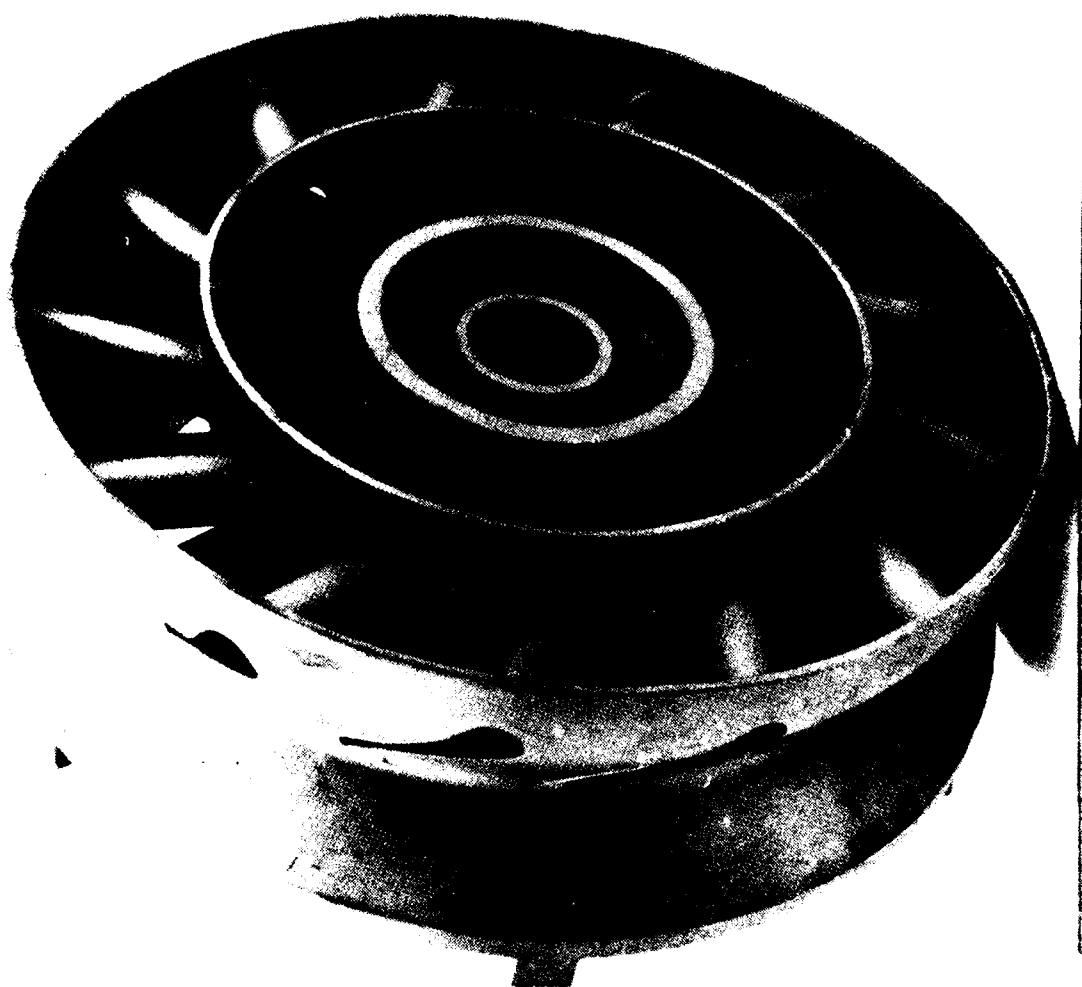
26122

Figure 200. Integrally Cast Nozzle Ring Assembly.
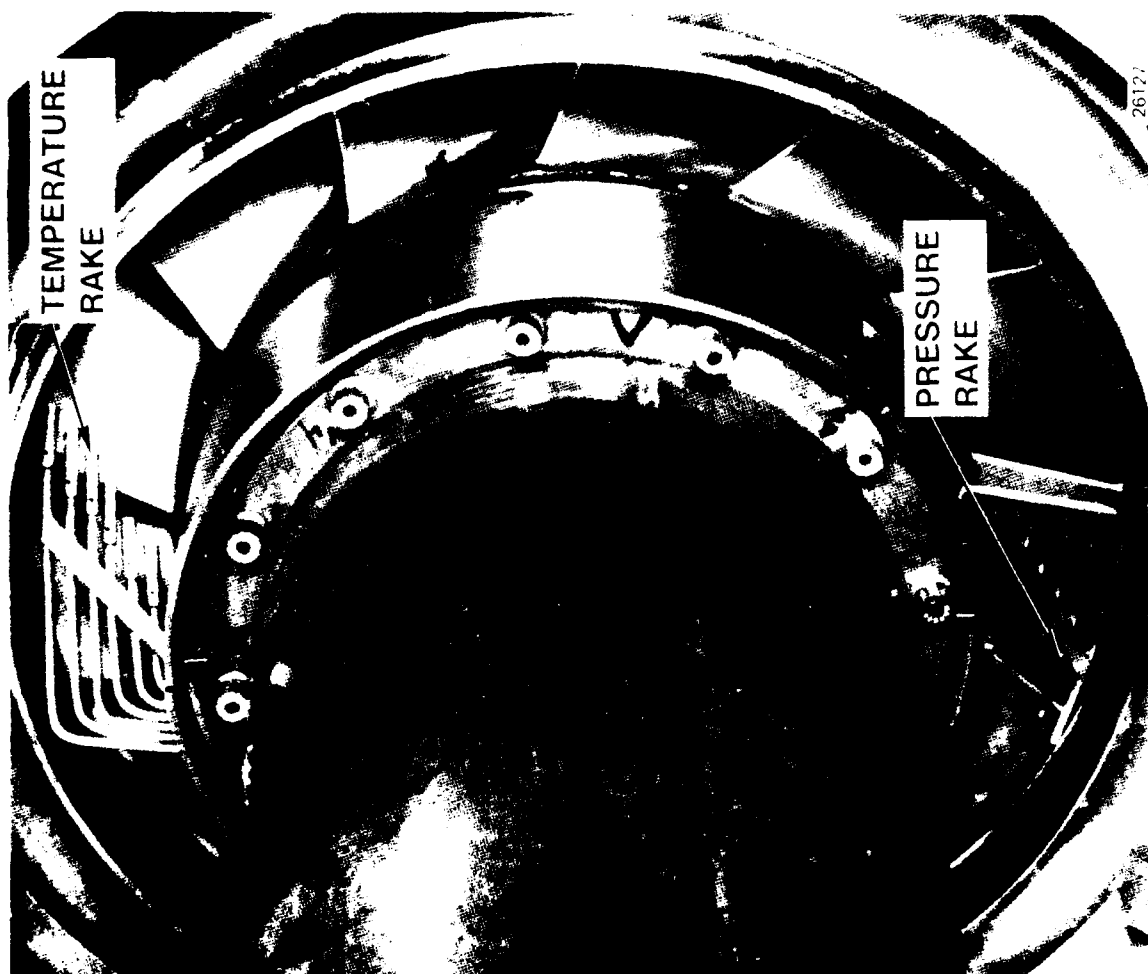
Figure 201. Nozzle Ring Assembly - Trailing Edge View.

281

WALL THICKNESS
0.030 - 0.050 IN.

PROFILE
TOLERANCE
± 0.010 IN.

27394

52°30'

OPEN AREA
1.02 IN² PER VANE

NOMINAL T.E.T. = 0.048 IN

13 VANES

64% OF
TOTAL FLOW
FOR COMBUSTOR

282
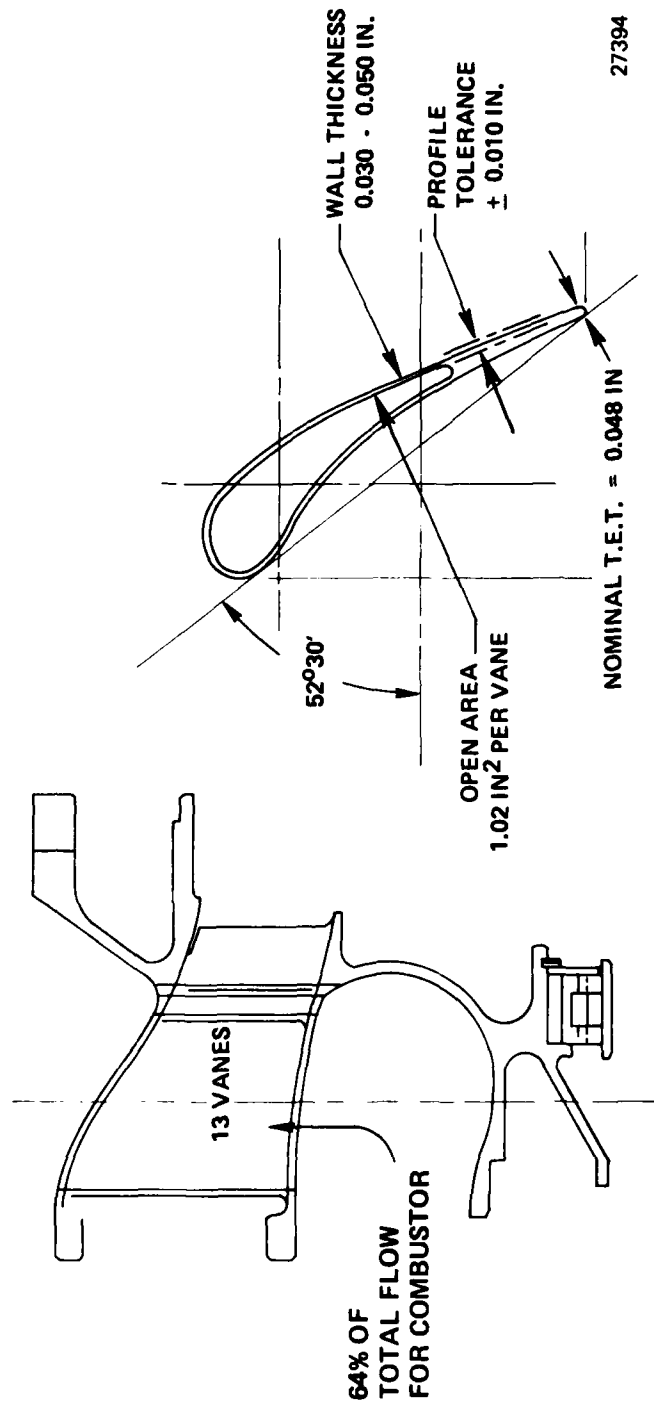
Figure 202 . General Nozzle Definition.
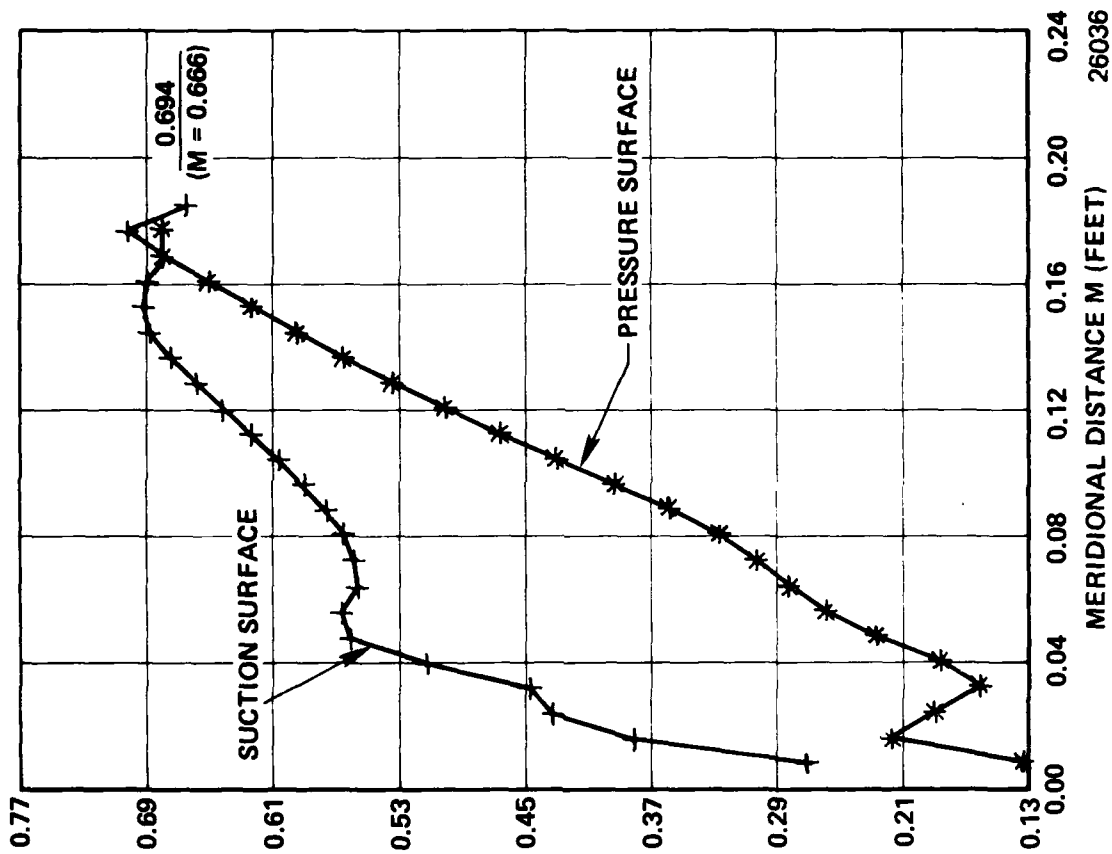
Figure 203. Vane Hub Velocity Distribution.

283
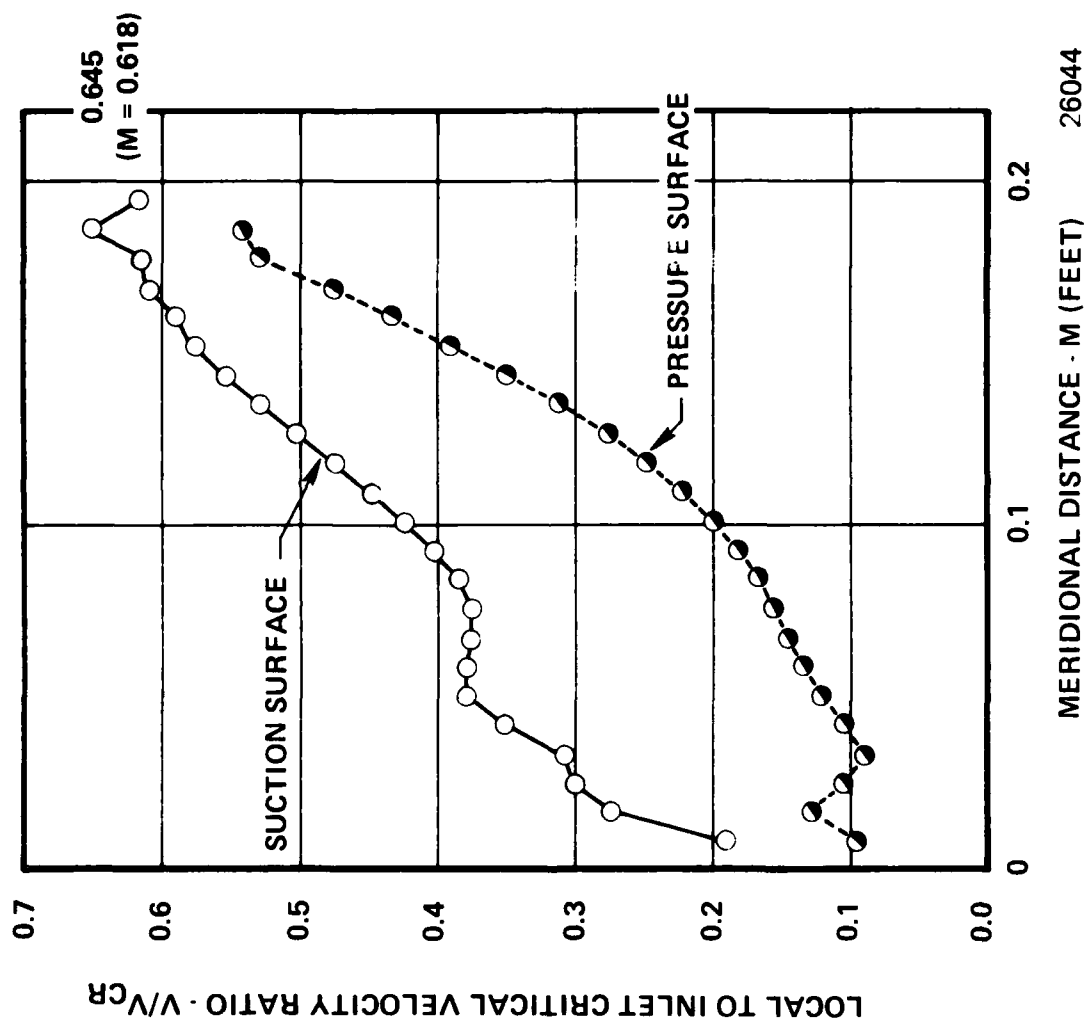
Figure 204. Vane Mean Velocity Distribution.

284
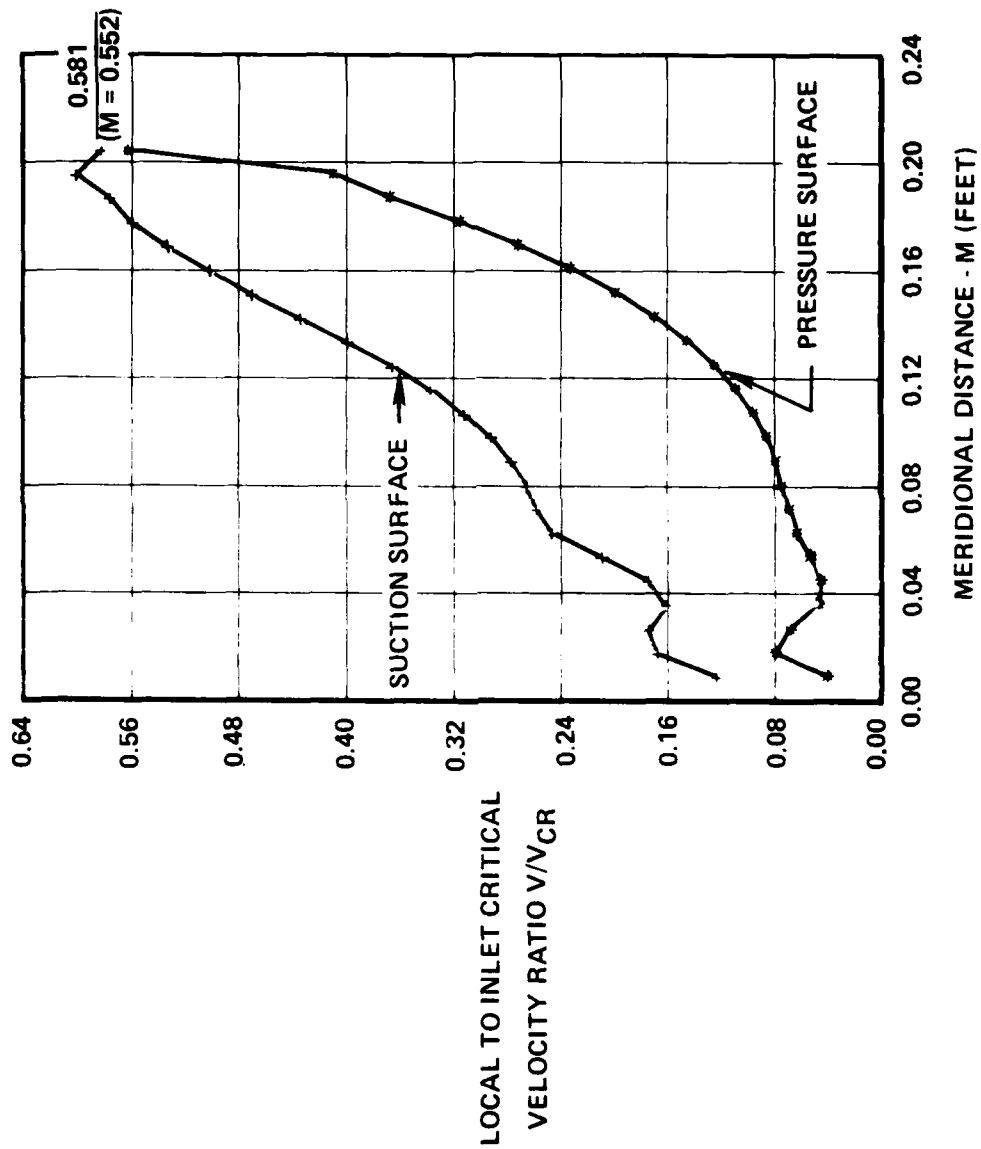
Figure 205. Vane Tip Velocity Distribution.

285
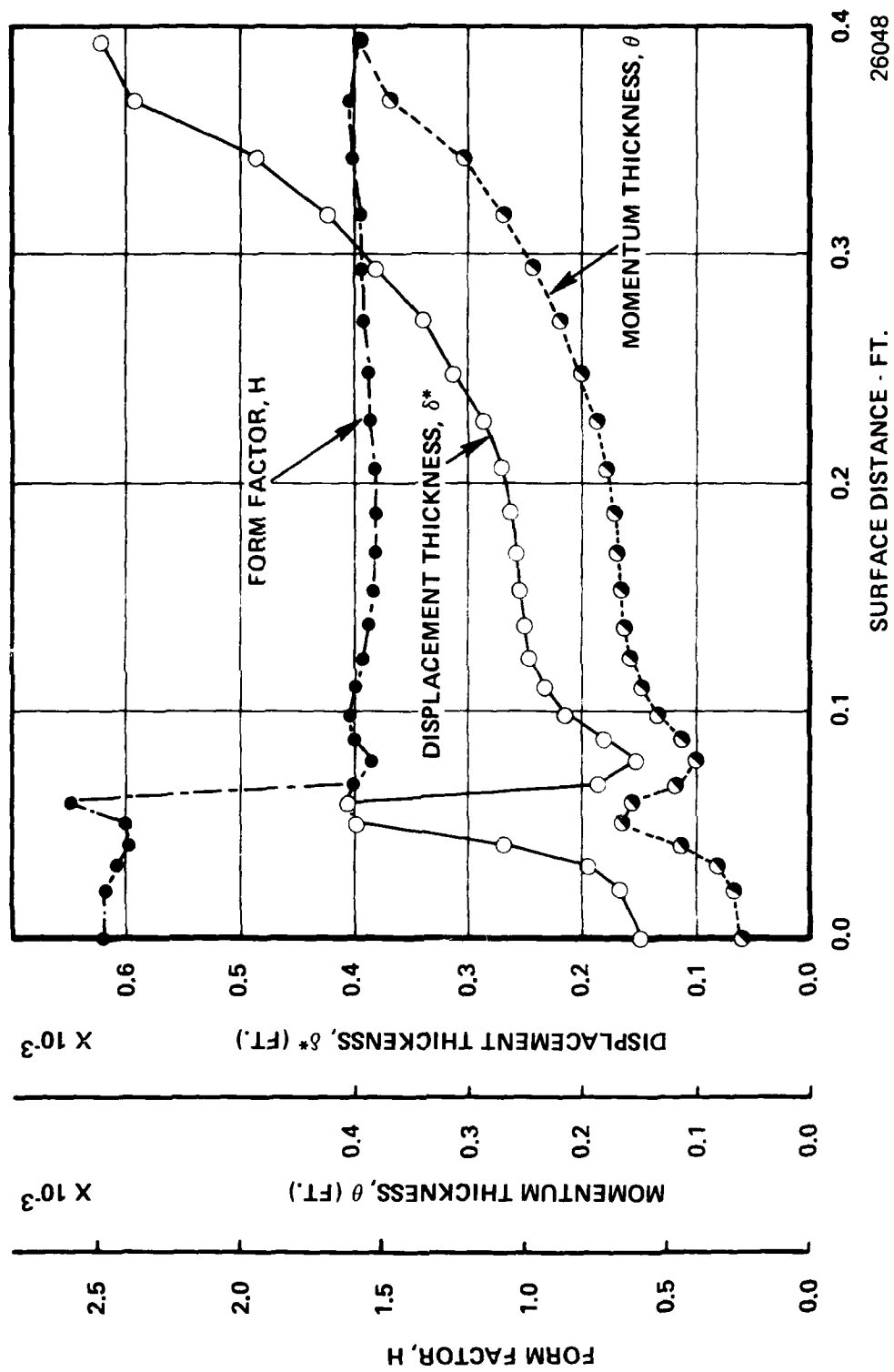
Figure 206. Vane Tip Section Suction Surface Boundary Layer Development.

286
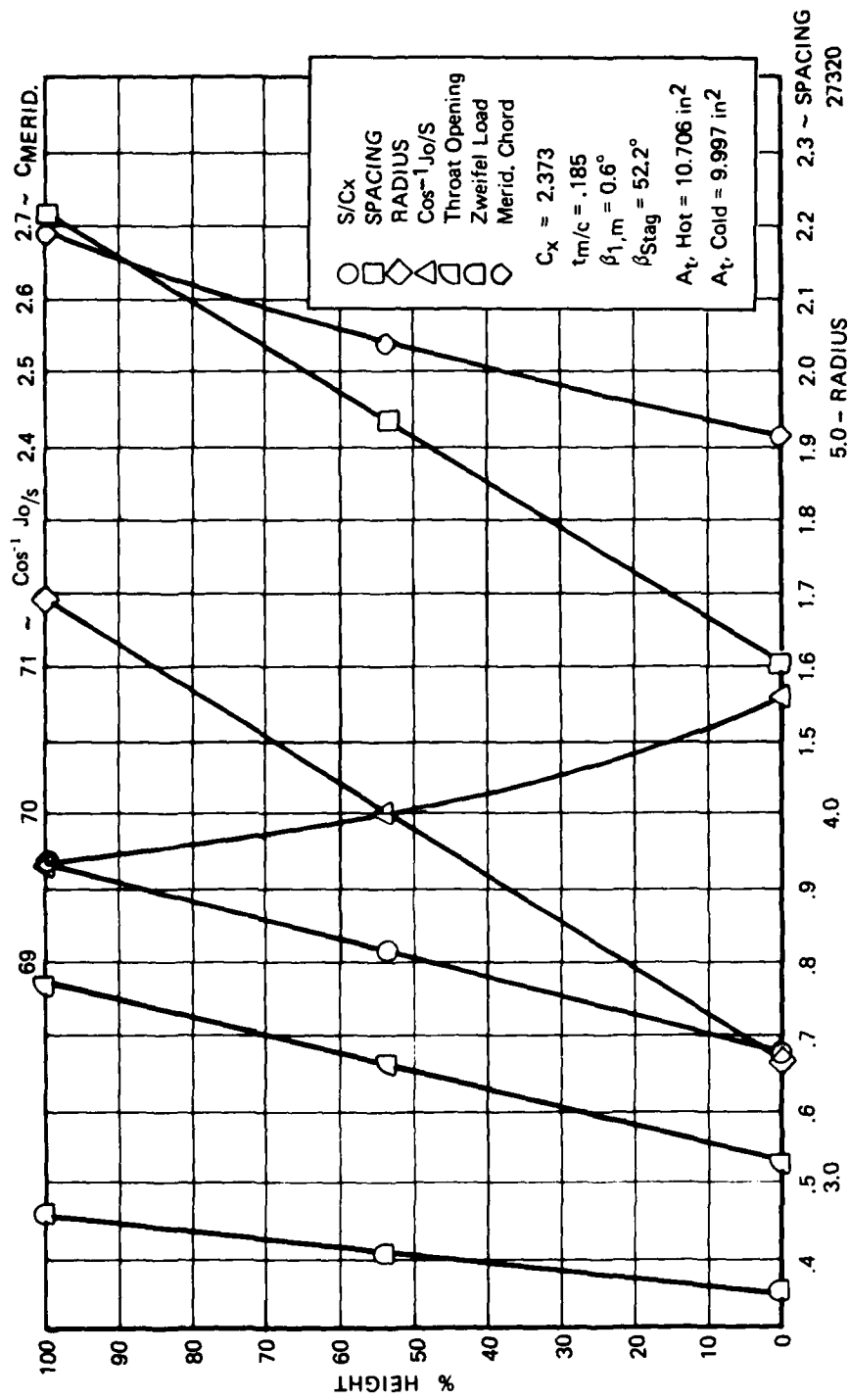
Figure 207. Expendable Gasifier Vane Geometric Properties.

287
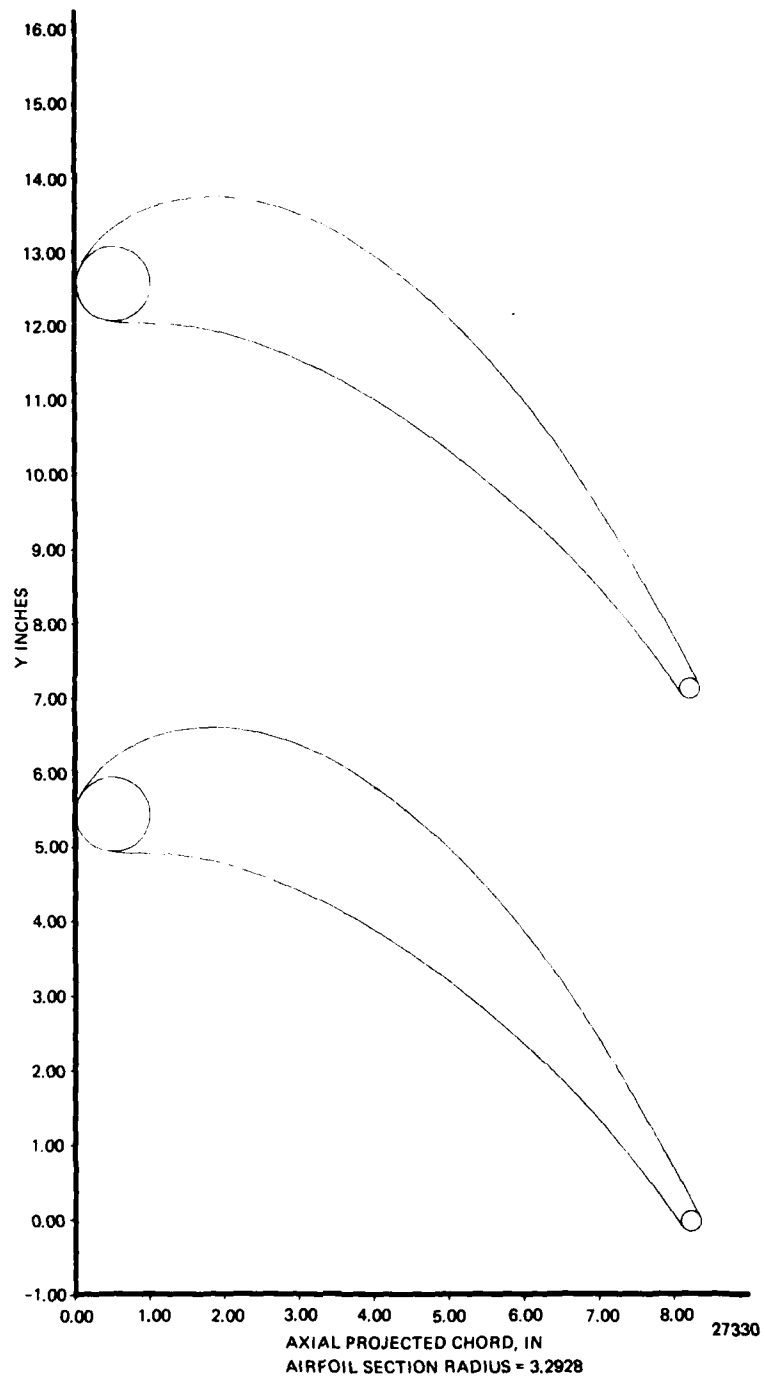
Figure 208. Turbine Rotor Hub Defining Section.
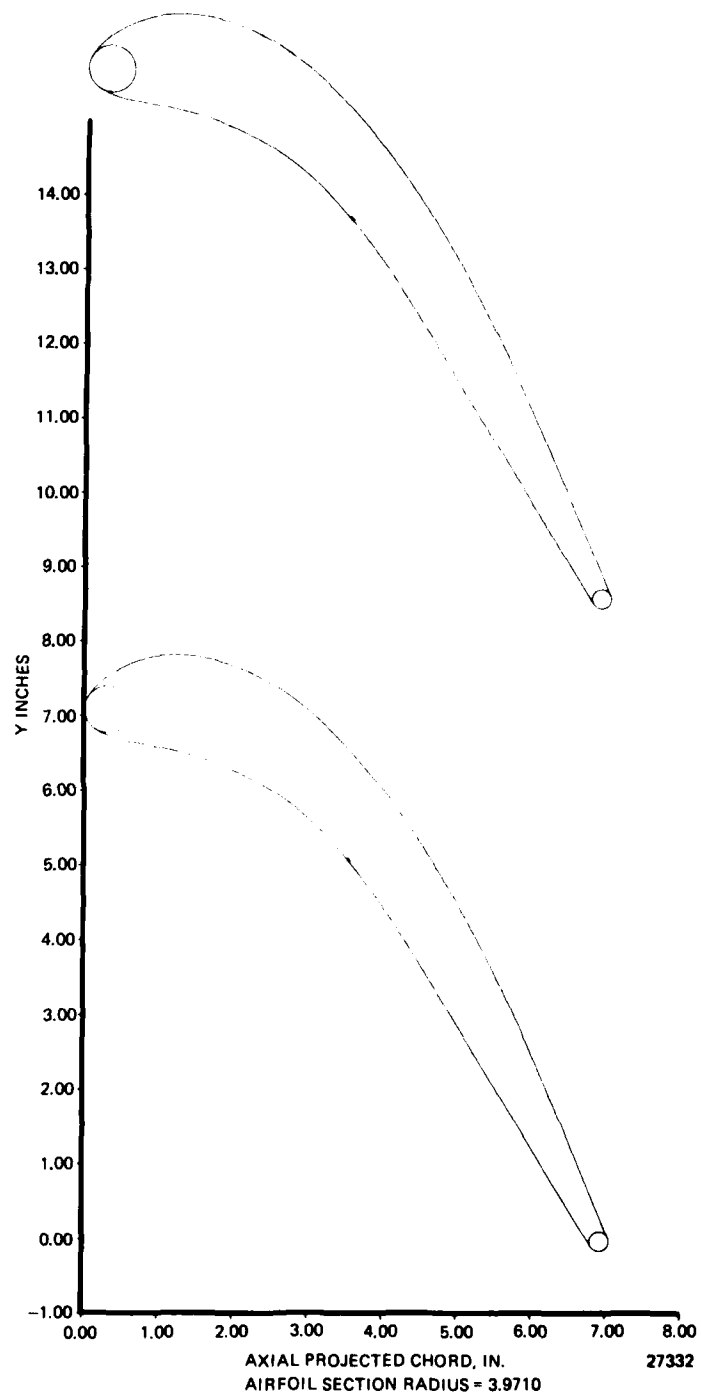
Figure 209. Turbine Rotor Mean Defining Section.

289
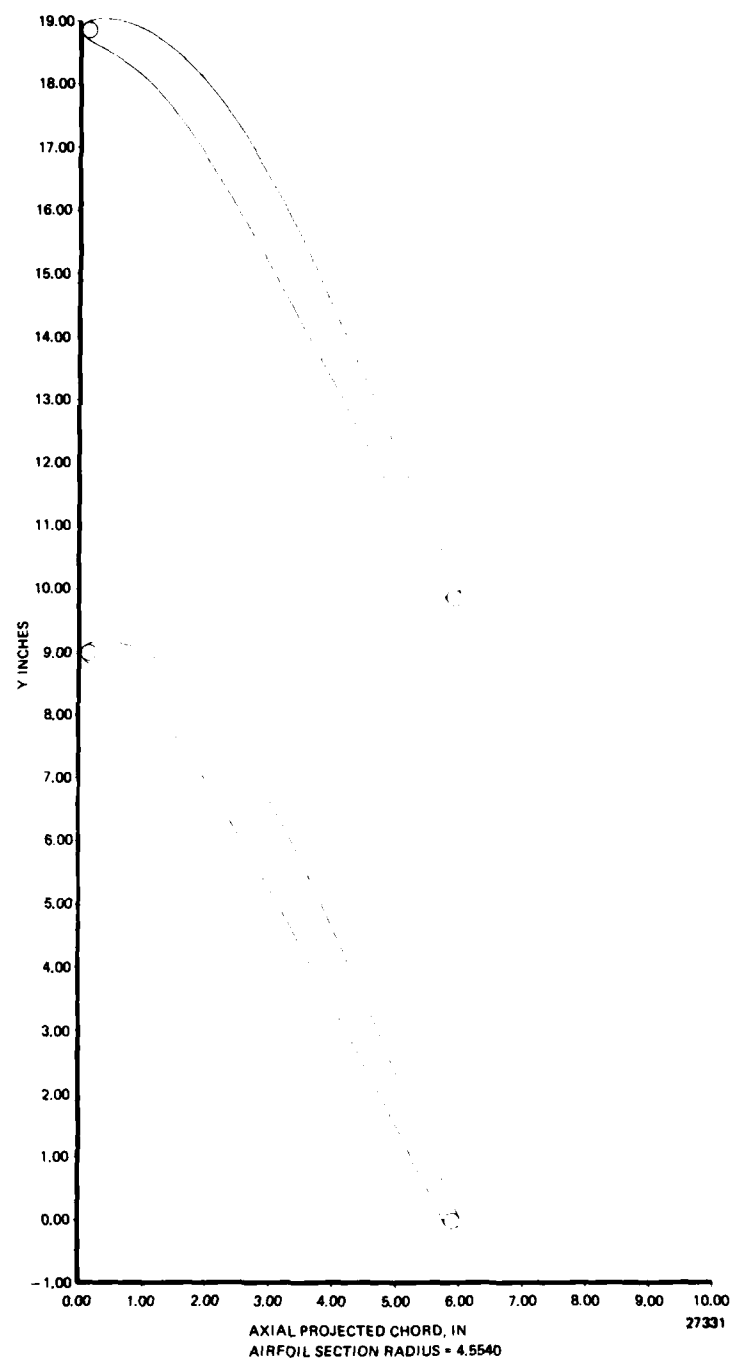
Figure 210 . Turbine Rotor Tip Defining Section.

290

best match the preliminary stress requirements at hot conditions, see Figure 211. The final blading has since been subjected to mechanical/stress analysis and is considered acceptable. Figure 212 shows the radial location of the mylar defining sections of the blade. A nested section view of the blade is given in Figure 213. At the mean, the blading has a 0.7 inch axial chord, 0.026 inch trailing edge thickness and tolerance band of ± 0.003 inch. The designed cold throat area is 12.94 square inches and the hot throat area is 13.75 square inches.

The hub, mean and tip sections were designed using incompressible flow solutions at nominal inlet relative gas angles and at ± 10 degrees from nominal. The airfoil shapes were adjusted to keep diffusion at a minimum. Figures 214, 215, and 216 are the final nominal incompressible flow loading diagrams. These sections were also checked for compressible flow and the resultant loading diagrams are given in Figures 217, 218 and 219. Boundary layer solutions corresponding to the compressible flow solutions on the suction surface of each section are given in Figures 220 through 222. The solutions were allowed to trip from laminar to turbulent near points of instability. The critical velocity ratios along the surfaces are moderate, less than 0.8, it is therefore unlikely that separation would occur because of high speed effects. The boundary layer solutions indicate that flow is stable over the entire blade. Additional rotor blade geometric properties are given in Figures 223 through 225.

The expendable gasifier map was estimated using the well known NASA, axial flow, turbine off-design deck (NASA - CR-710). In this procedure, the cascade losses are defined by cascade design efficiency levels plus an incidence loss. The turbine outer and inner annulus are specified together with blade-row throat openings. Off-design performance is then obtained by dropping the static pressure behind the blade rows in a systematic fashion until successive choking limit-loading occurs down through the exhaust annulus. Figure 226 gives the expendable gasifier estimate performance map obtained from this NASA program. The prediction shows that the turbine has a high tolerance to limit-load and provides optimum efficiency region along the estimated engine operating line.

Extensive combustor test rig activity served as an excellent vehicle to check expendable gasifier nozzle flow characteristics. Figure 227 provides results of a nozzle blow down test. These data show that the flow appears to be low by about 4.6 percent. However, test experience with earlier fan turbine tests (Figure 228) shows similar behavior in a low pressure region, depending on whether the rotor is present or not. Hence it is concluded that on an over-all basis, the nozzle characteristic is close to design. It was also possible to approximate the nozzle loss coefficient level from the combustor rig test. Results of these calculations are presented and compared with design loss level in Figure 229. The general level of agreement with the design objective is considered to be good.
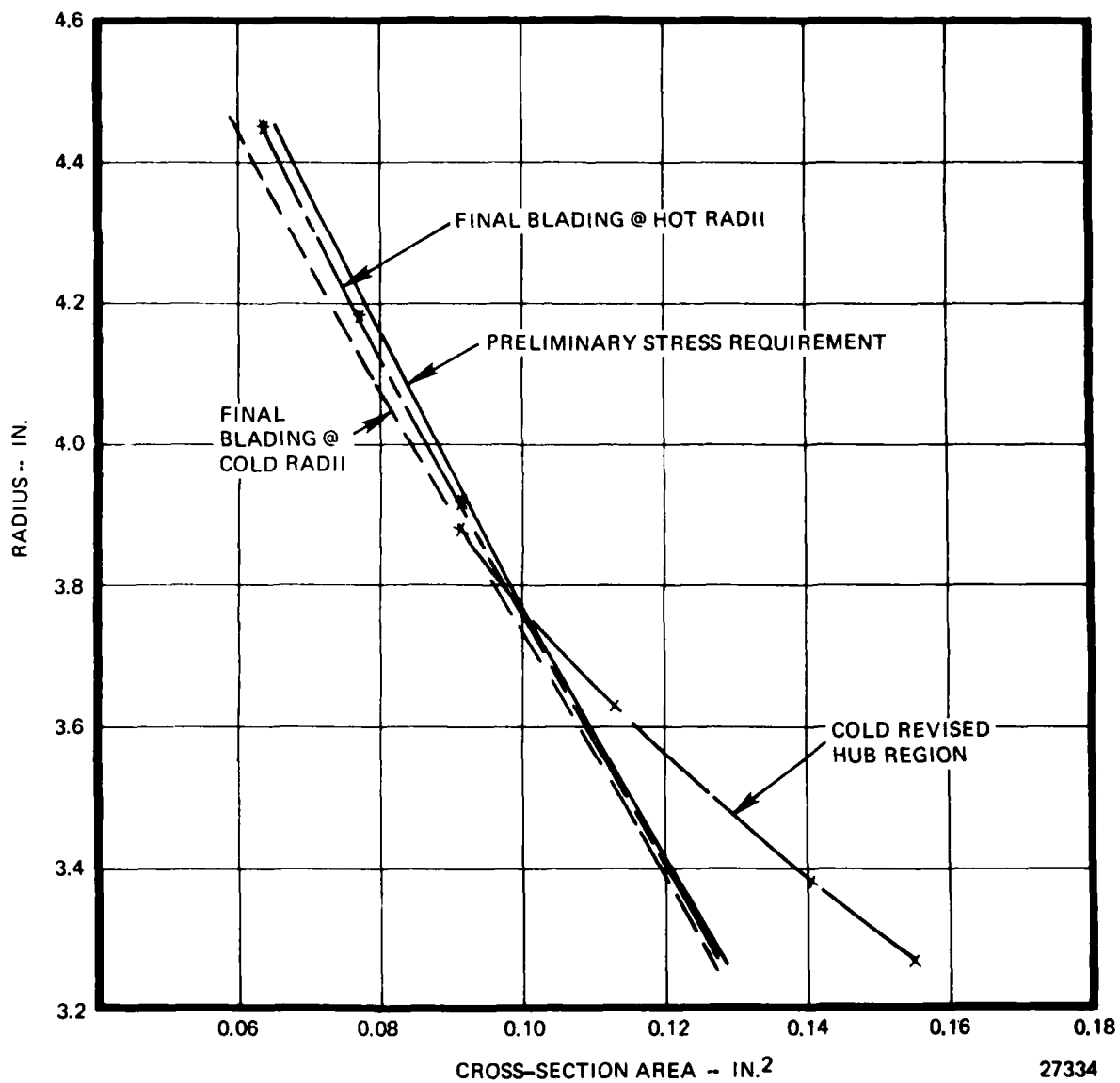
Figure 211. Comparison of Final Rotor Blading Area Distribution with Preliminary Stress Requirement.

292

SECTION HEIGHT

4.55 Inches

G — TIP CLEARANCE = 0.028 In. — G

SHROUD RADIUS = 4.477 INCHES

0.069 In.   4.38 Inches

F — F

4.13 Inches

E — E

3.88 Inches

D — D

3.63 Inches

C — C

3.38 Inches

B — B

0.109 In.   3.271 Inches

A — A
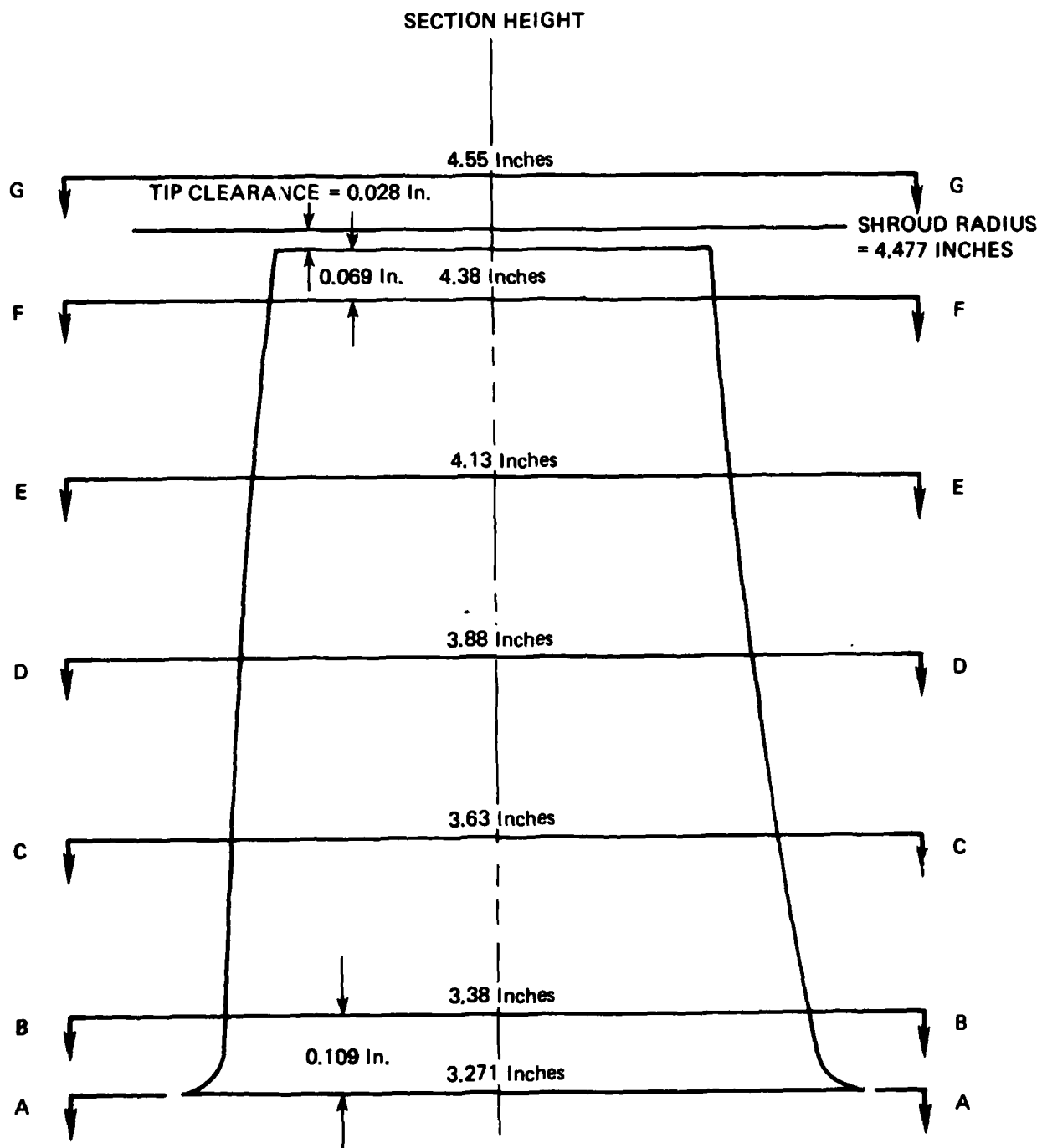
27324

Figure 212. Rotor Defining Sections.

293
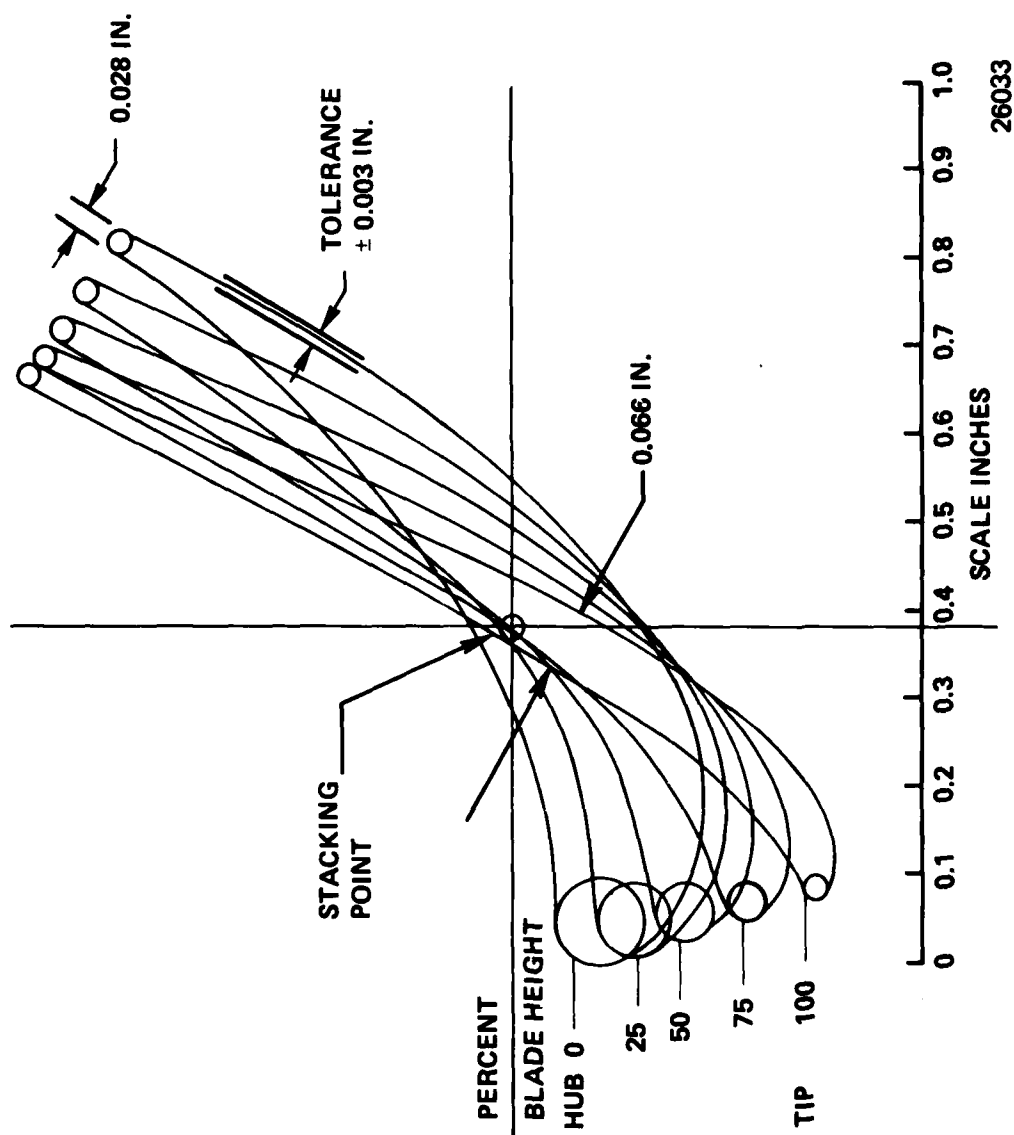
Figure 213 . Turbine Rotor Blade Sections Stacked Set.
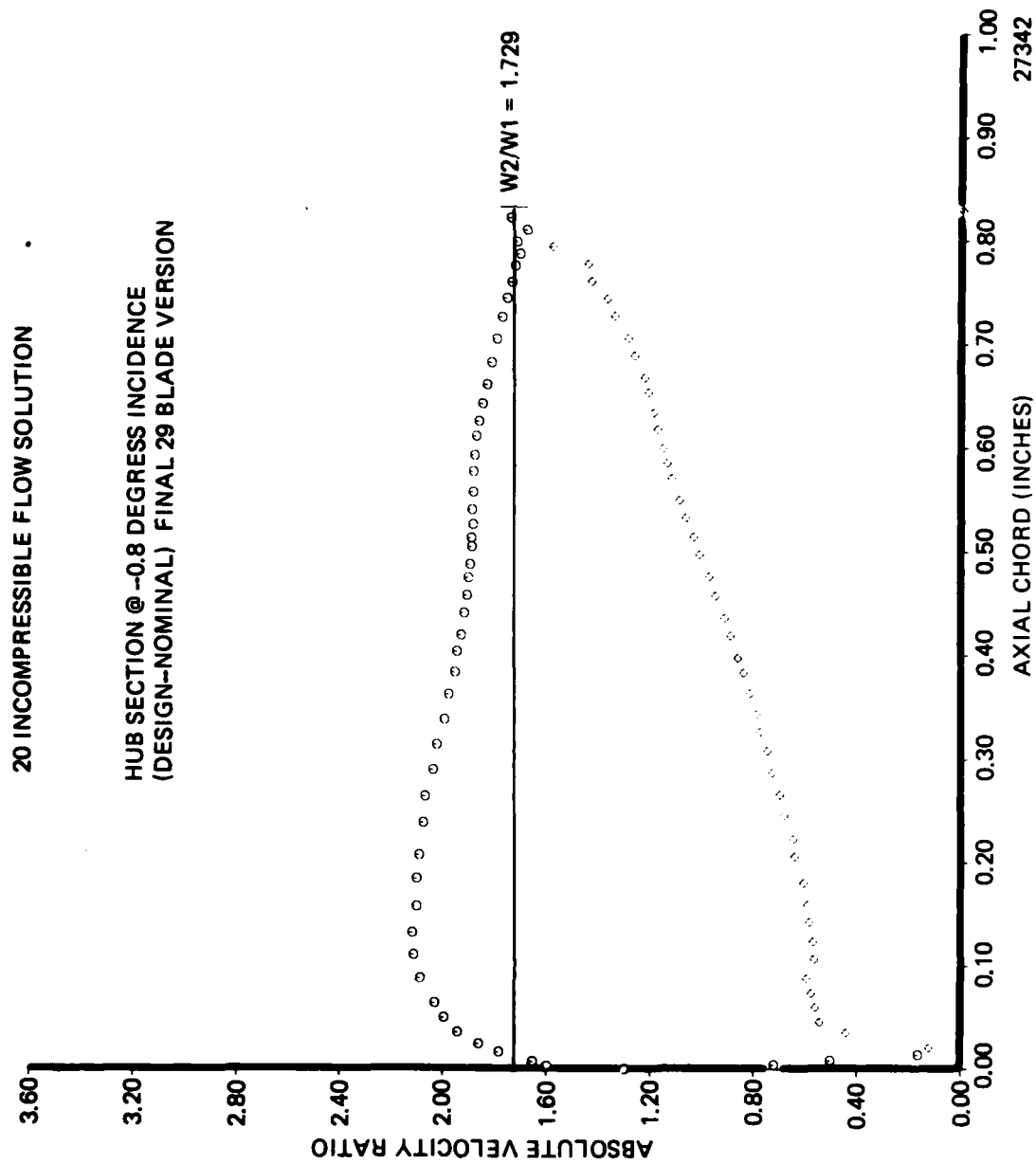
Figure 214. Rotor Hub Section Incompressible Velocity Distribution.
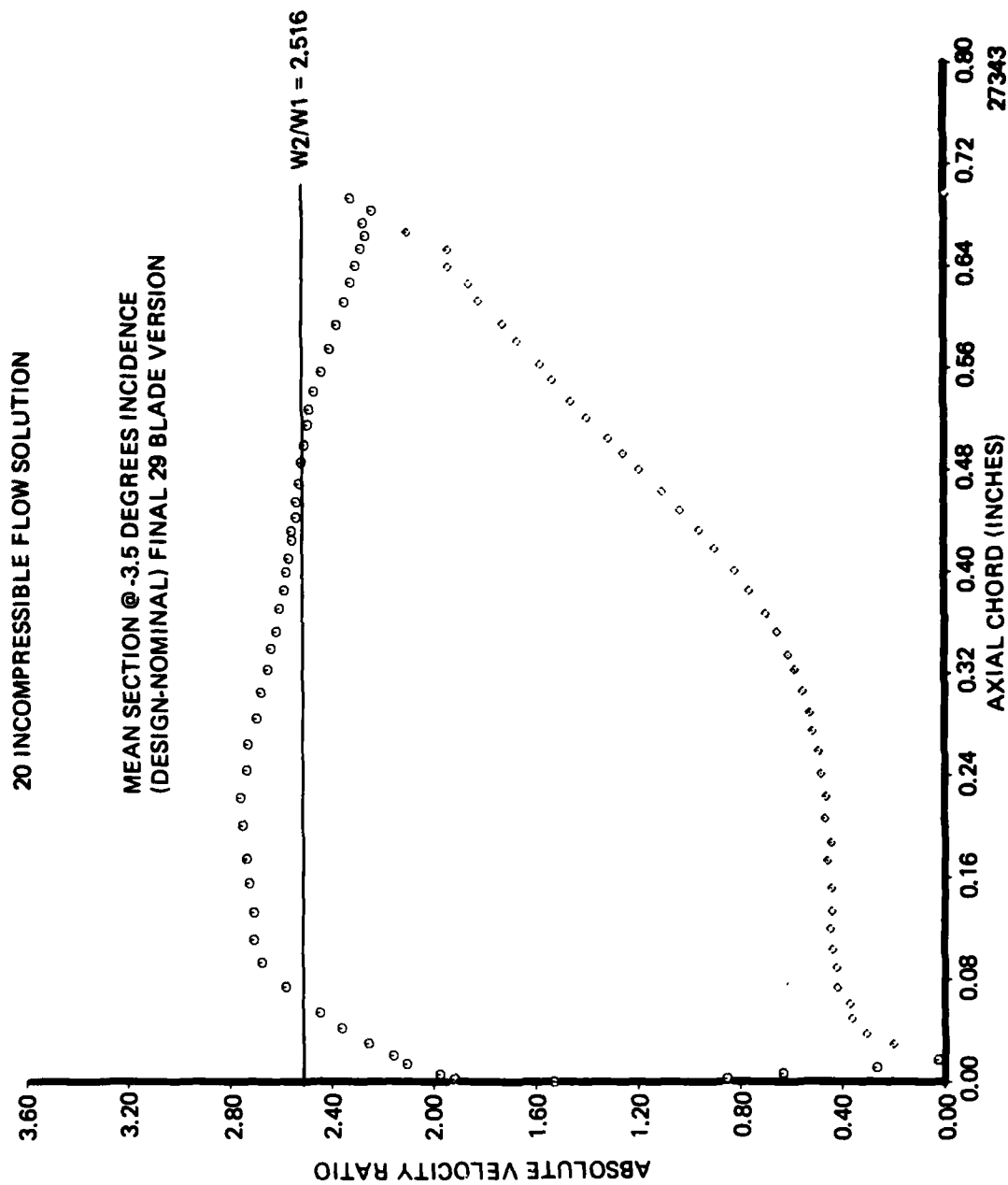
Figure 21.5. Rotor Mean Section Incompressible Velocity Distribution.
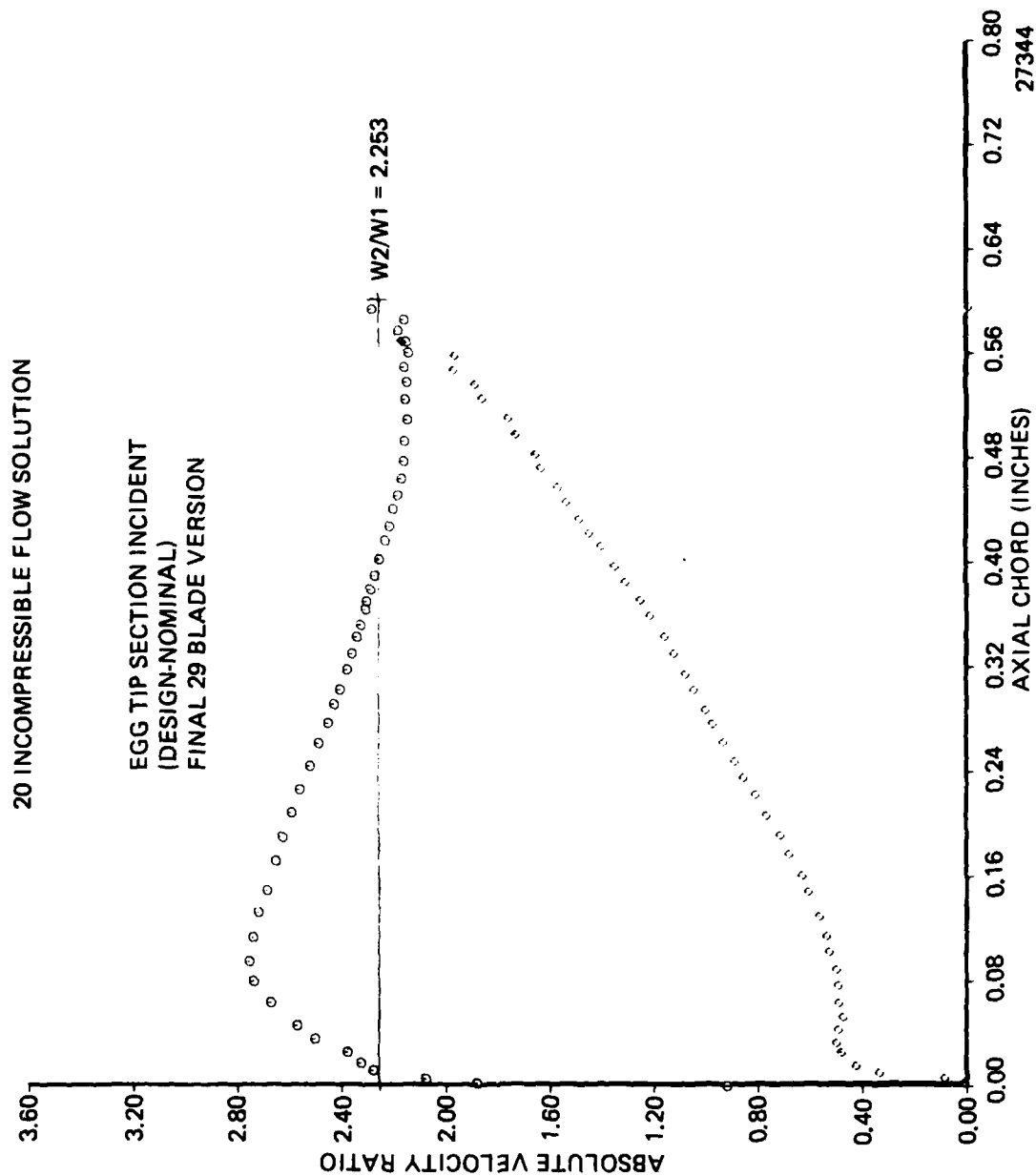
Figure 216. Rotor Tip Section Incompressible Velocity Distribution.
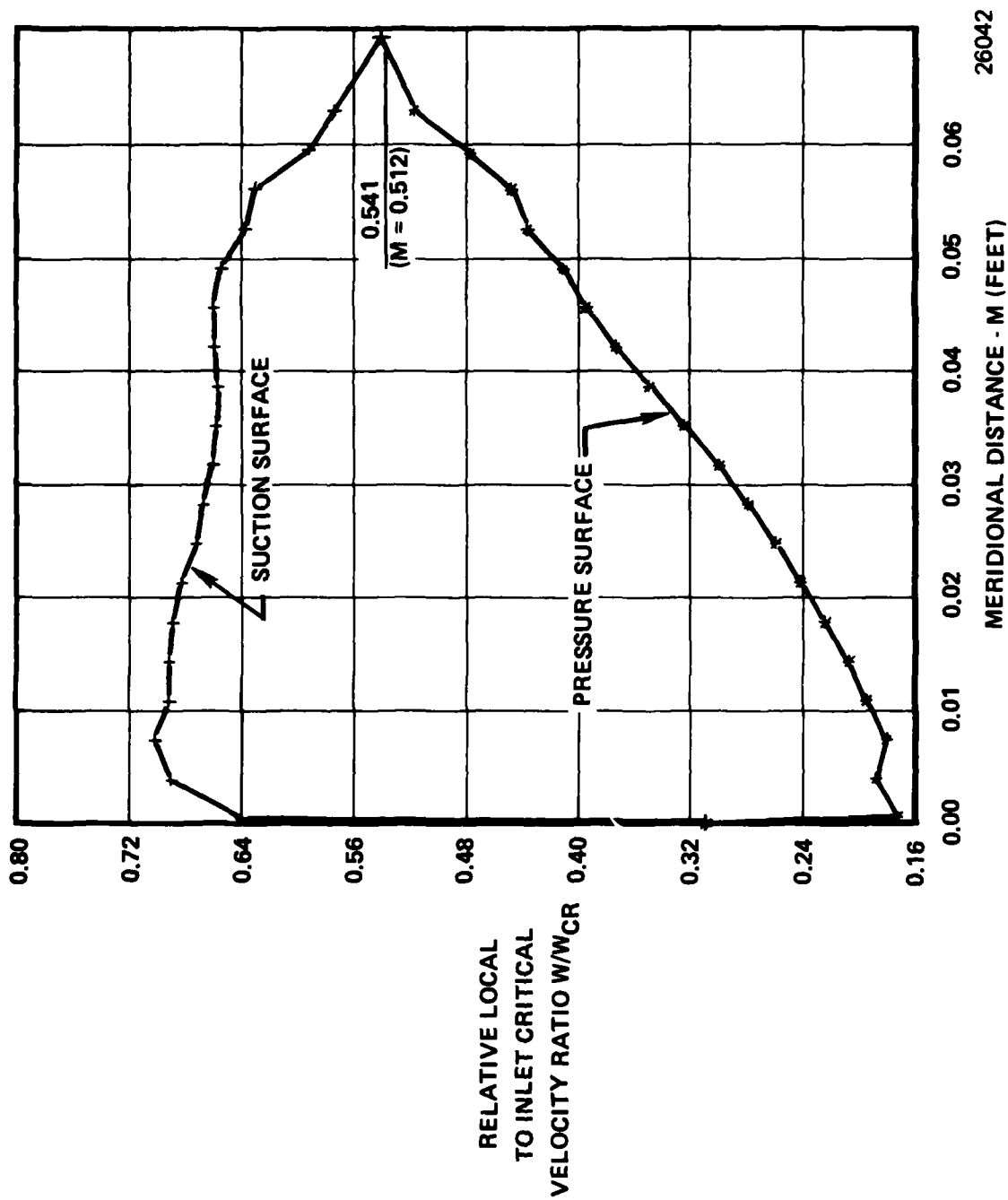
Figure 217. Rotor Hub Compressible Velocity Distribution.
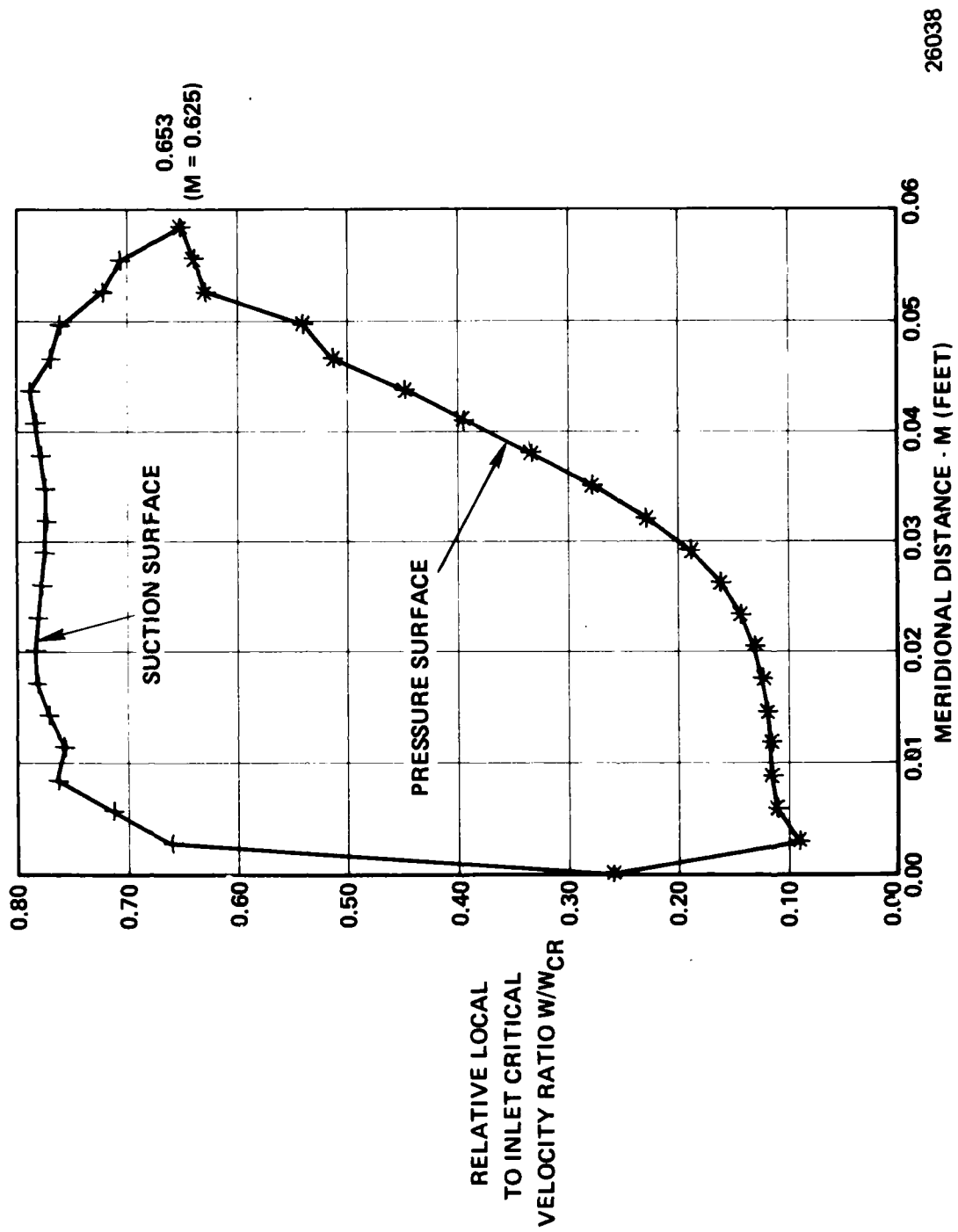
Figure 218. Rotor Mean Compressible Velocity Distribution.
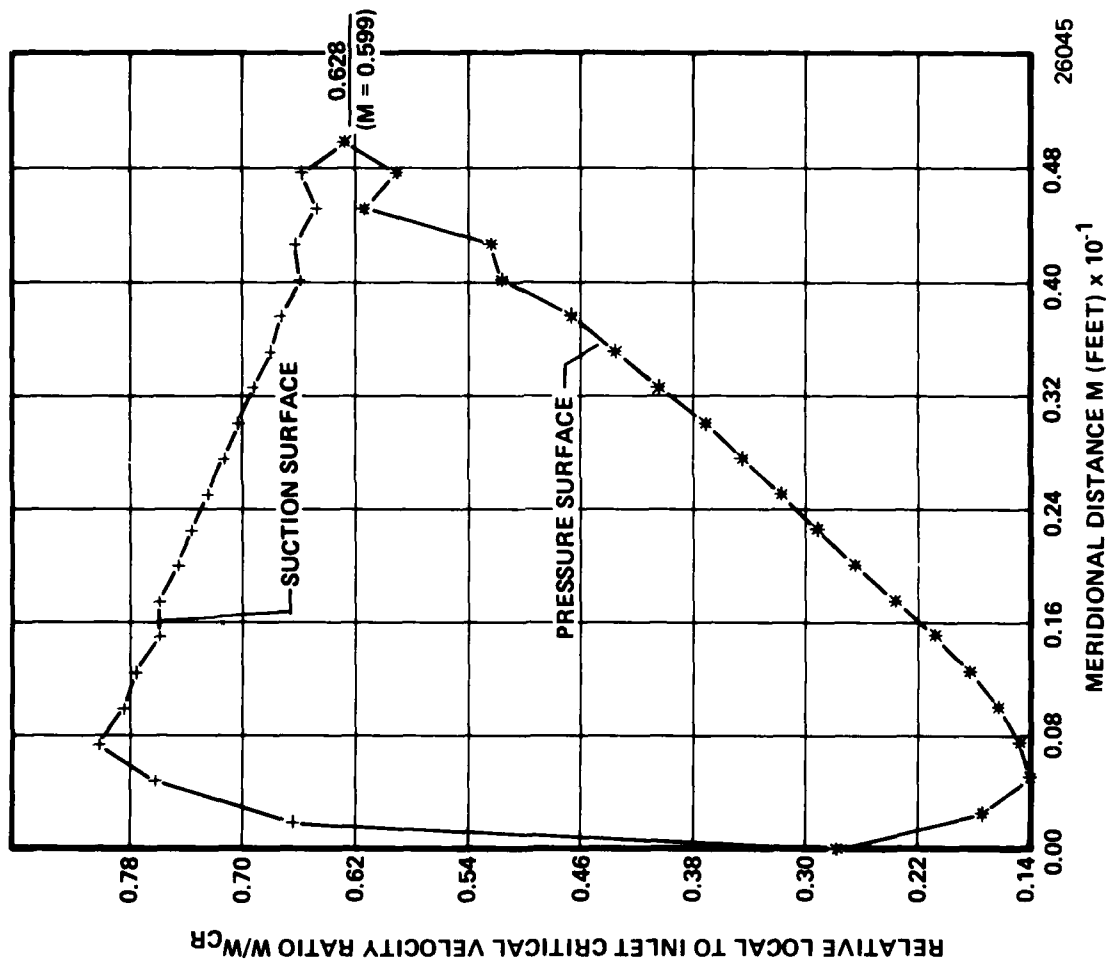
Figure 219. Rotor Tip Compressible Velocity Distribution.

300
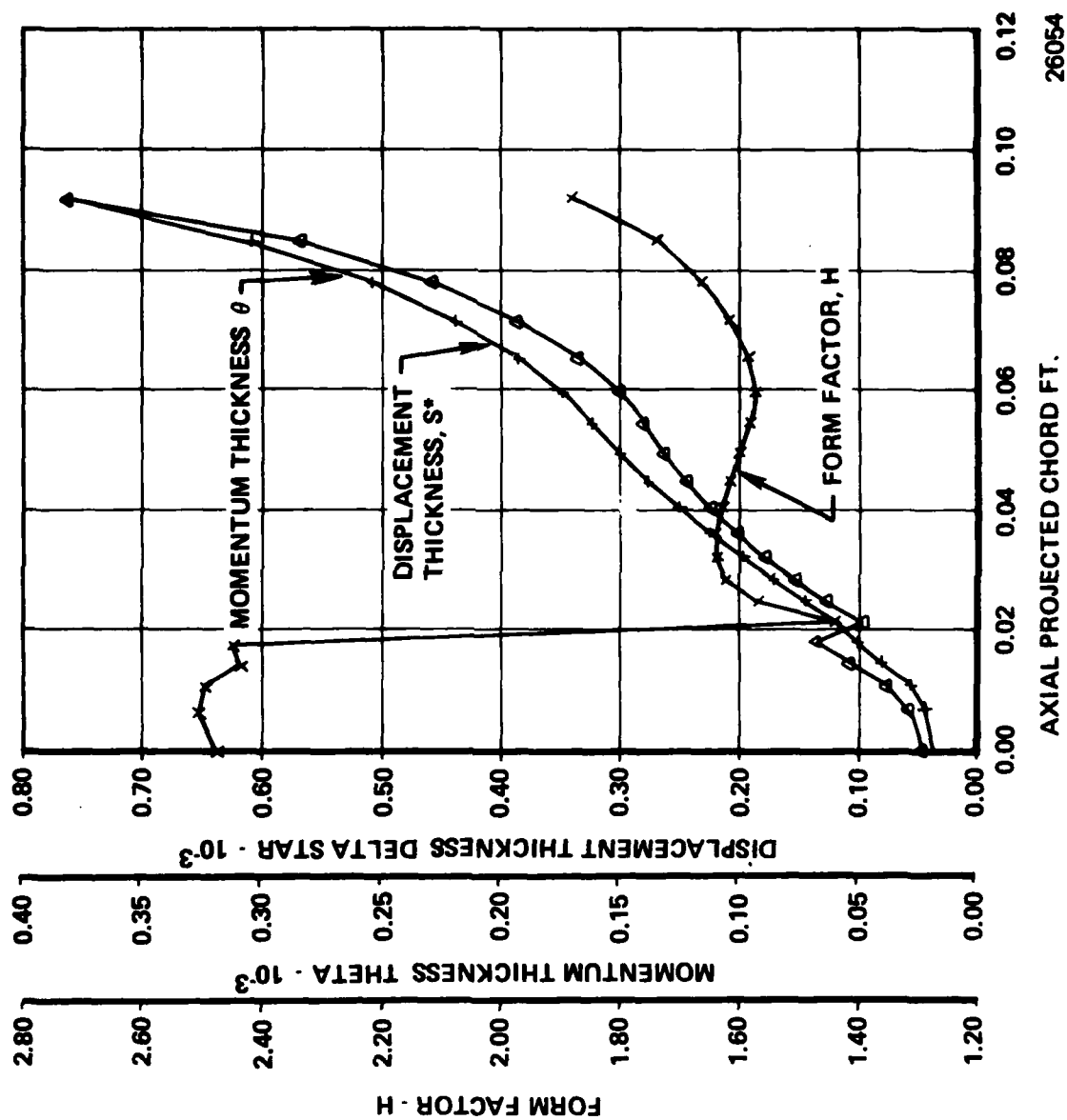
Figure 220. Turbine Rotor Hub Suction Surface Boundary Layer Development.

301
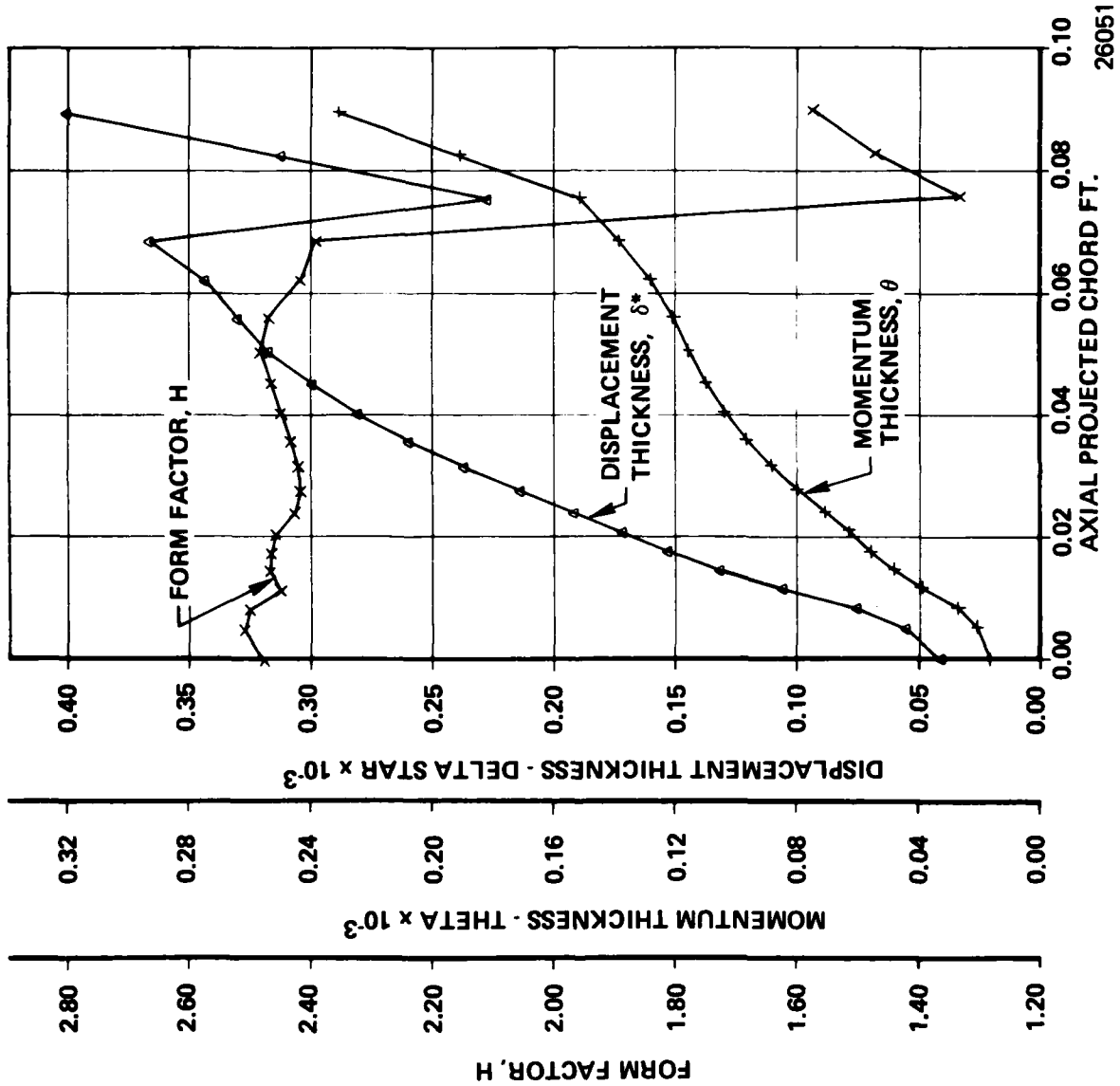
Figure 221. Turbine Rotor Mean Section Boundary Layer Development.
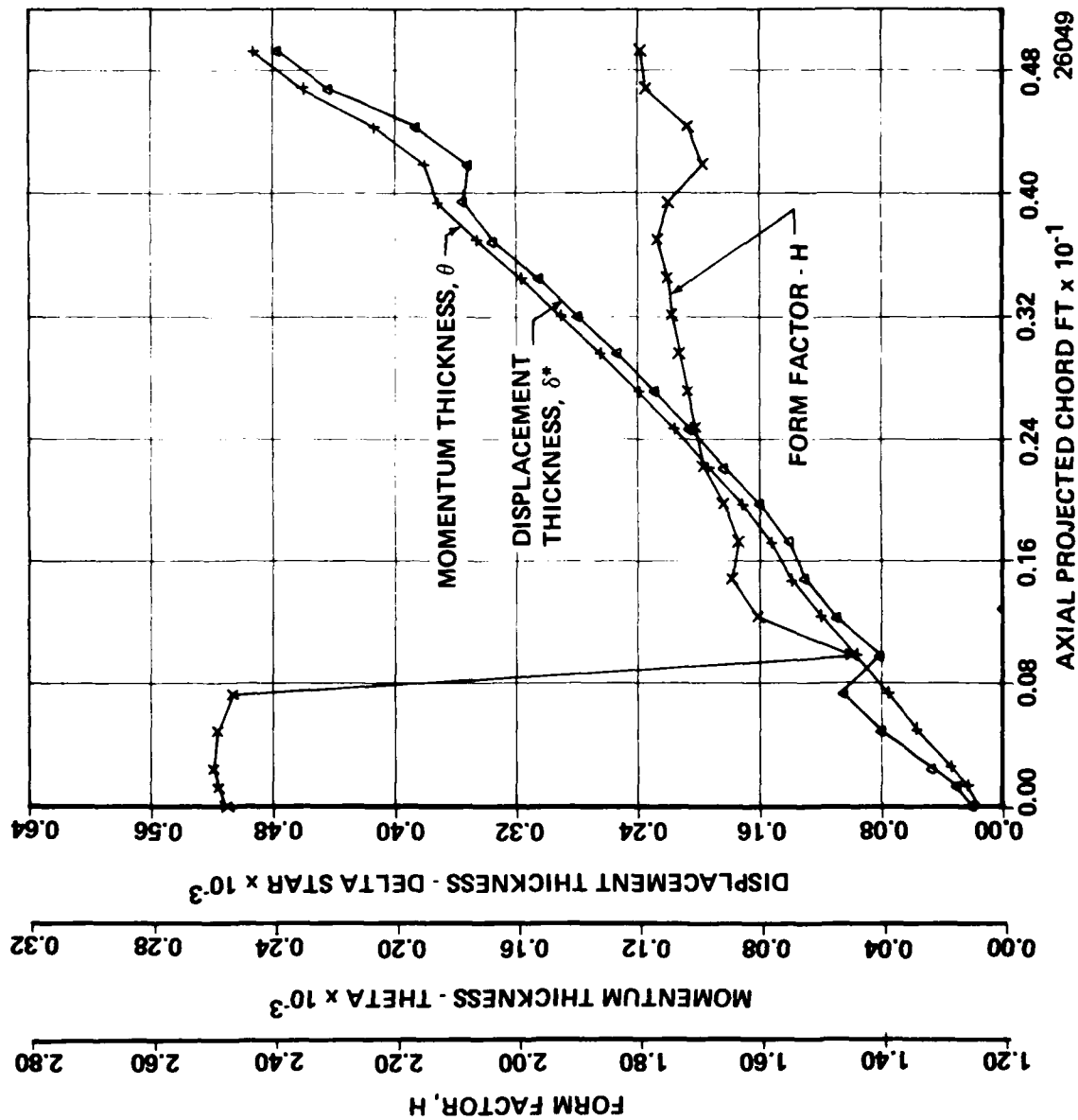
Figure 222. Turbine Rotor Tip Section Boundary Layer Development.

COLD
dσ̄ = 0.370 in.
h = 1.206 in.
At_{cold} = 12.94 in.^{2}

HOT
dσ̄ = 0.376 in.
h = 1.261 in.
At_{hot} ≈ 13.75 in.^{2}

dσ̄ = 0.370, Cold

Hot, dσ̄ = 0.376

% FLOWPATH HEIGHT

TIP 100

HUB 0

THROAT OPENING - dσ̄ - in

27335
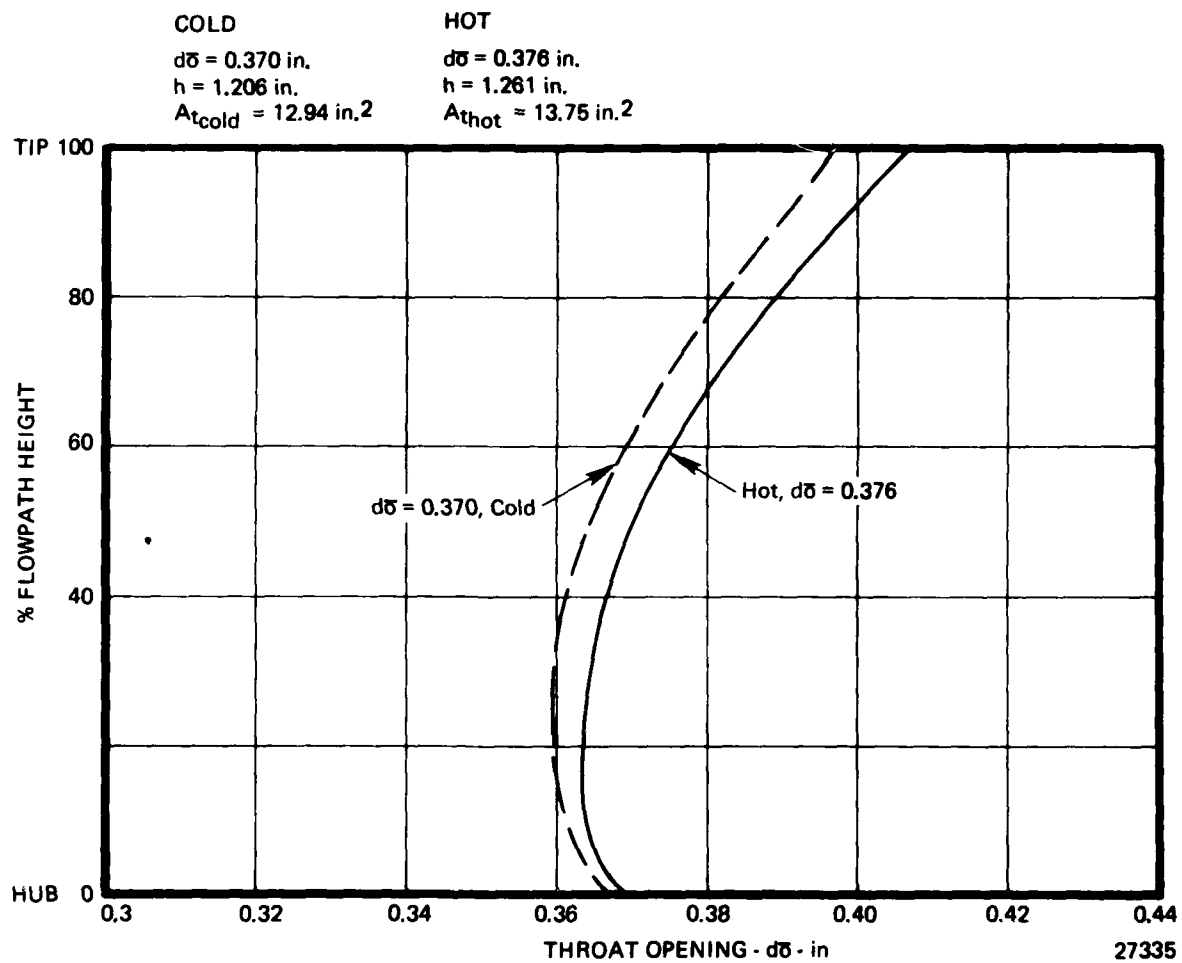
Figure 223. Turbine Rotor Final Design Radial Throat Opening Profiles, Hot and Cold Conditions.

304
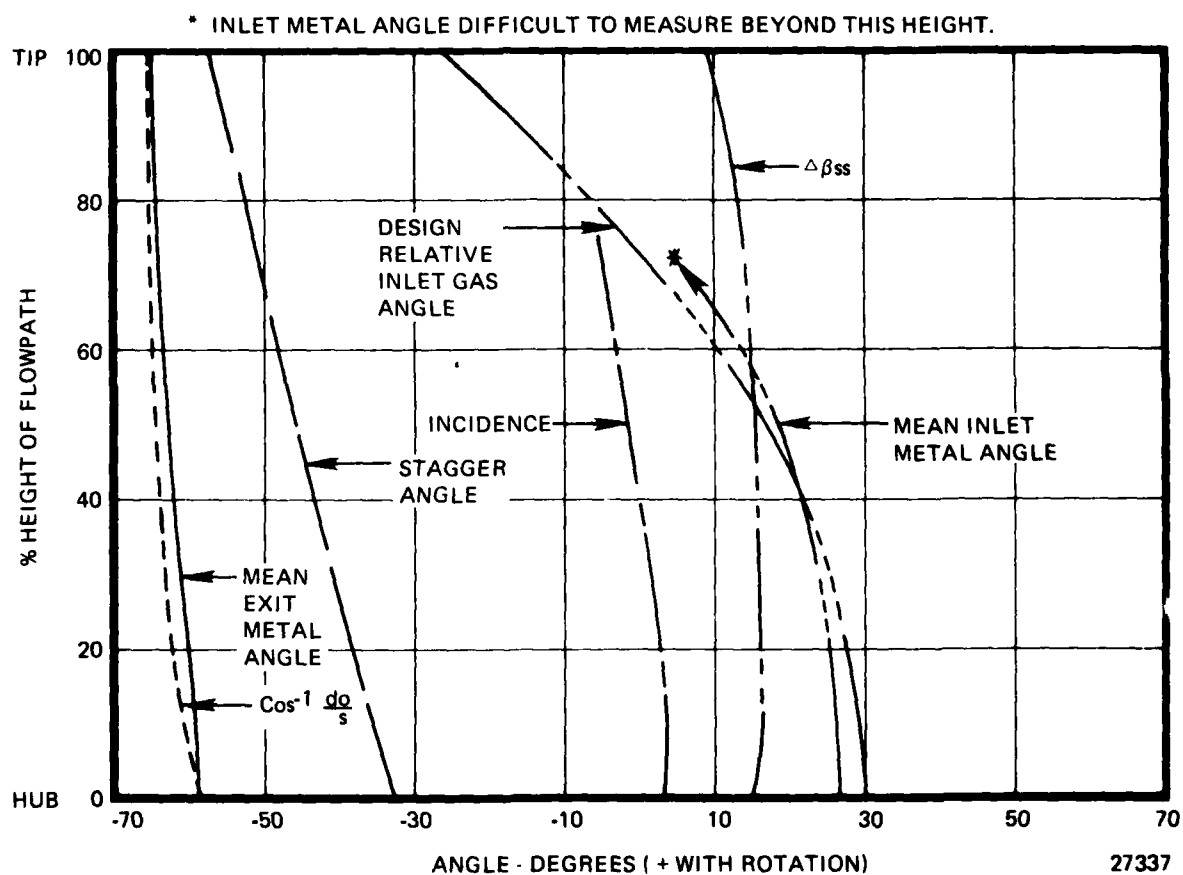
Figure 224. Turbine Rotor Final Design: Radial Profiles of Various Bladino Angle Parameters.
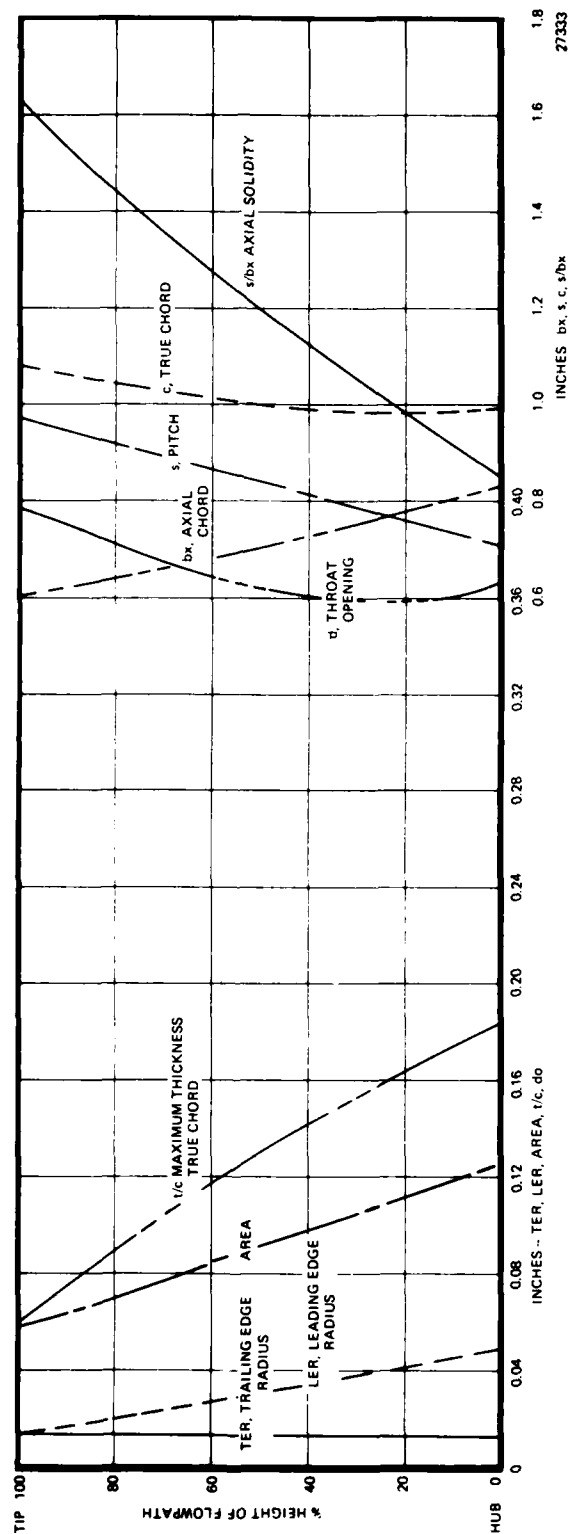
Figure 225. Turbine Rotor Final Design: Radial Profiles of Various Blading Parameters.
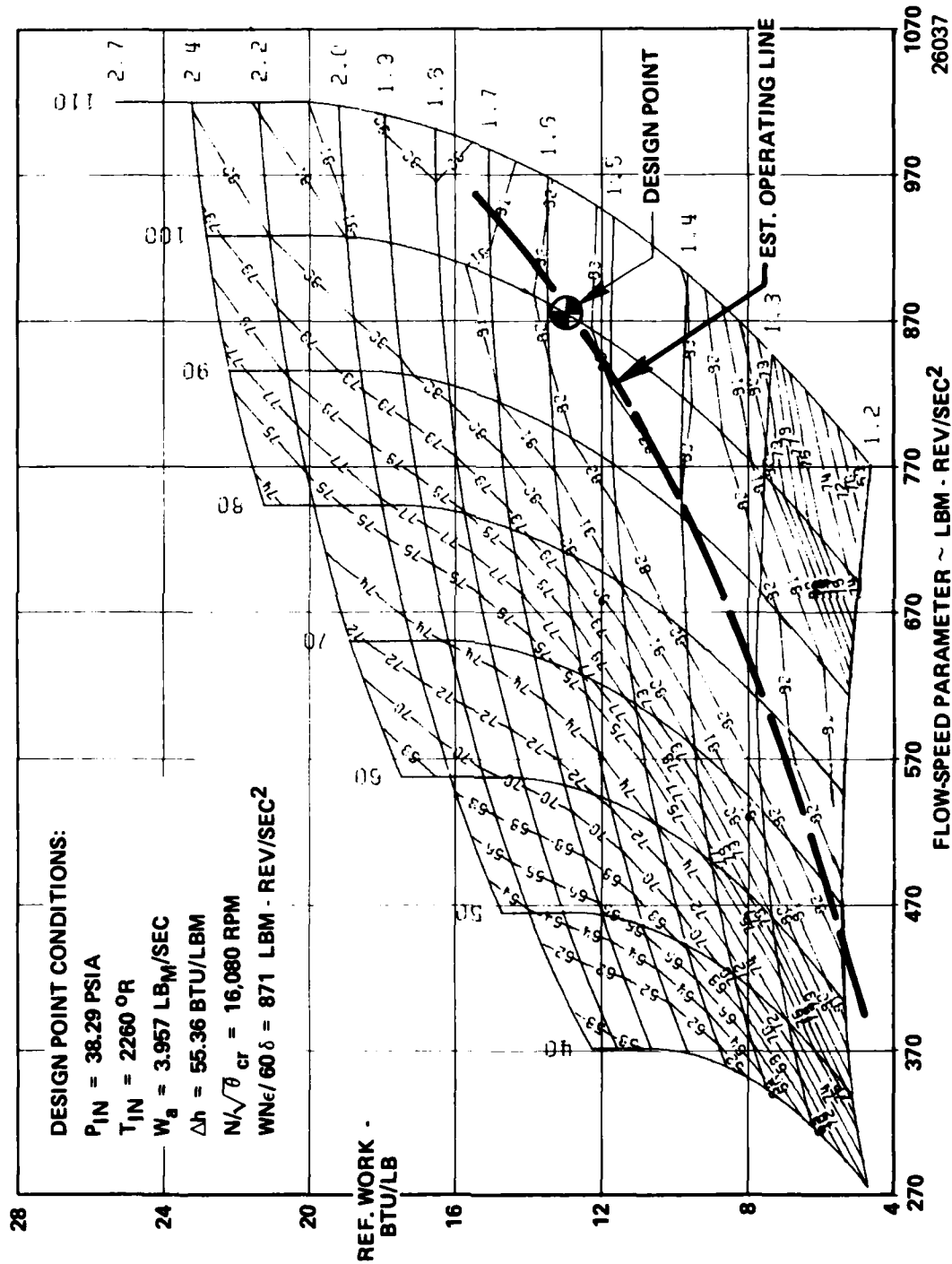
Figure 226. Turbine Estimated Performance Map.
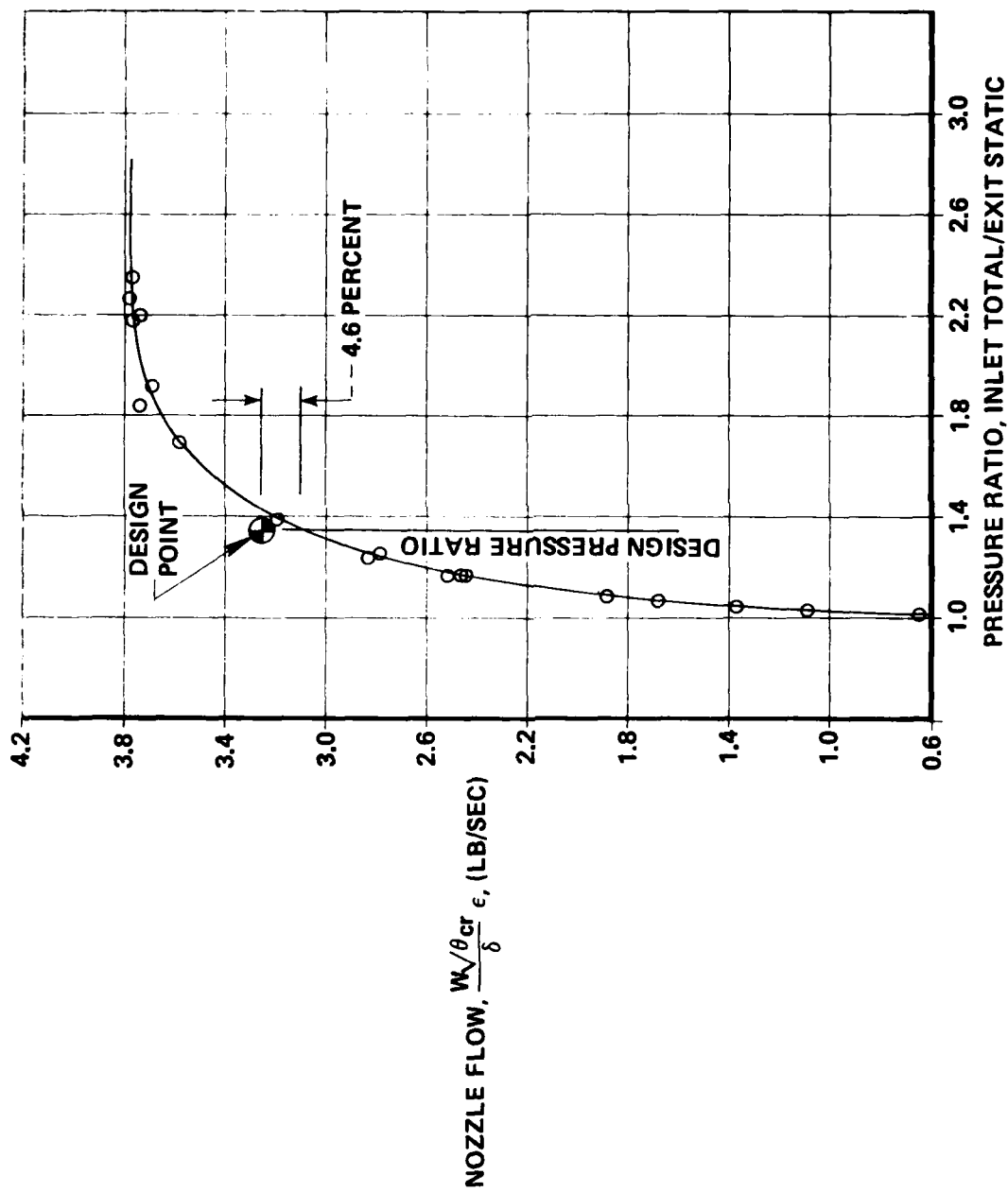
Figure 227. Nozzle Blow Down Test.

26161

308
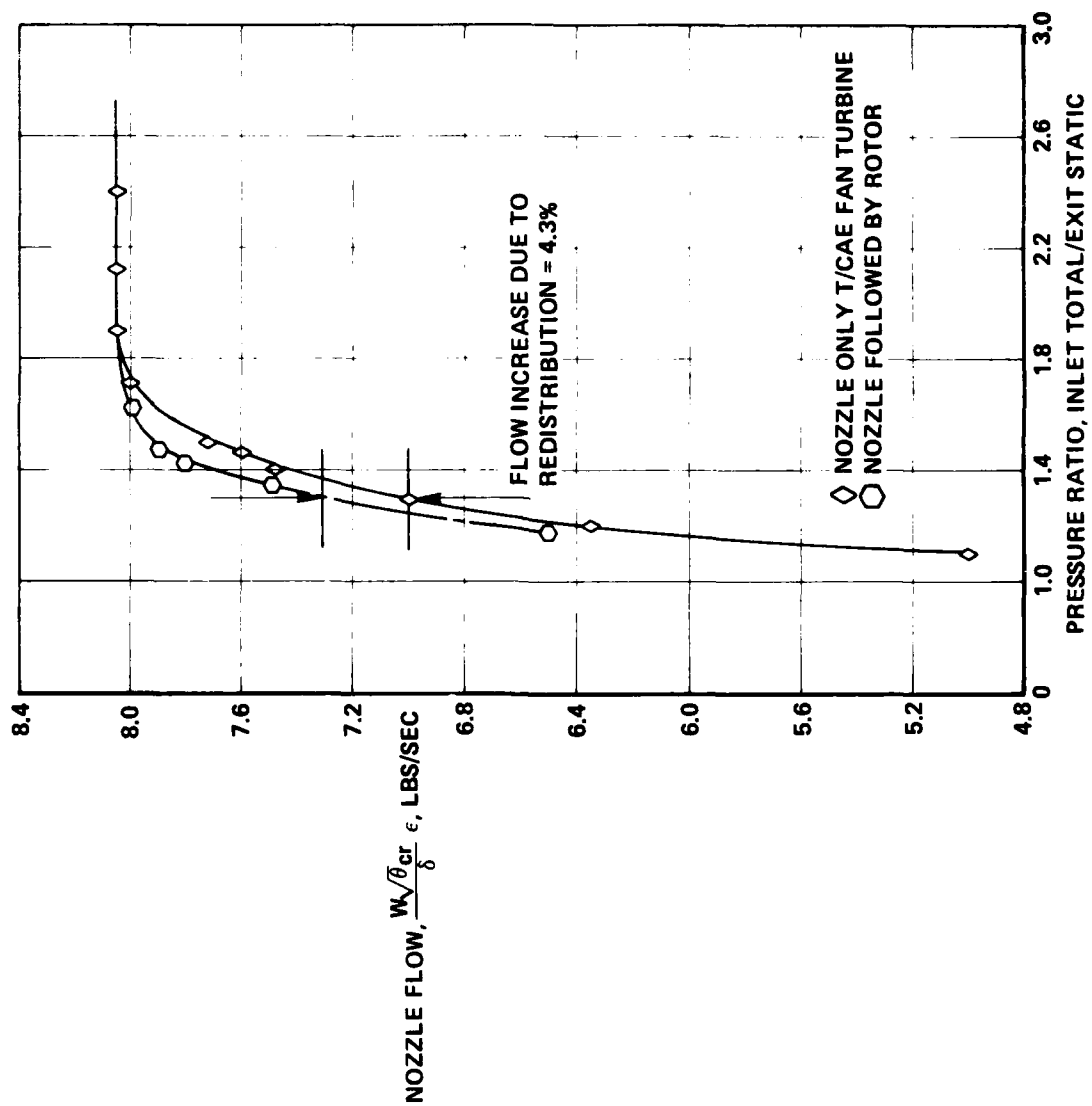
26137

Figure 228. Teledyne CAE Fan Turbine Nozzle Blow Down Test.
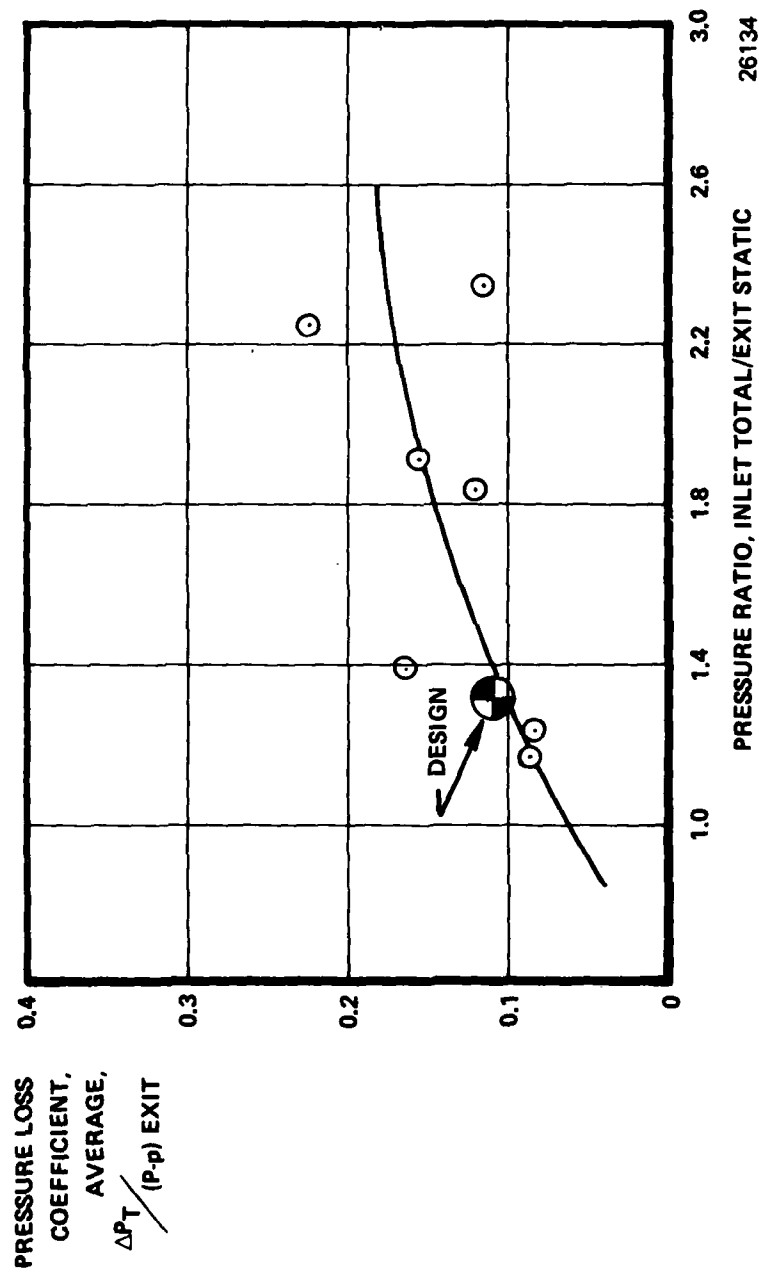
Figure 229. Turbine - Comparison of Design to Rig Determined Nozzle Loss Coefficients.

With respect to final engine cycle demands, the combustor rig development has demonstrated that the base turbine flow capacity needs to be increased by approximately 6 percent. Figure 230 tabulates the requirements and effects on pertinent variables. Figure 231 shows the amount of nozzle cut-back required to obtain proper flow match. Since the flow capacity of the first compressor build will not be known until test, the nozzle modification will be deferred until it is known that a modification is required.

	PRESENT CONFIGURATION	NOZZLE OPEN	CHANGE
NOZZLE THROAT AREA	10 IN^2	10.6 IN^2	6%
REFERRED FLOW $\frac{WN}{\delta 60} \epsilon$	864.65	900.36	4.1%
NOZZLE EXIT MACH NO.	0.618	0.598	-3.2%
ROTOR EXIT MACH NO.	0.583	0.612	5%
ROTOR REACTION	0.451	0.492	9%
EXIT SWIRL	3°	-2.2	5.2^o
TOTAL TO TOTAL, ηT-T	84.5	84.0	-0.5 POINTS
TOTAL TO STATIC, η	76.5	75.3	-1.2 POINTS
TOTAL TO AXIAL, η	84.5	83.9	-0.6 POINTS

27380

Figure 230. Turbine - Effect of Nozzle Cut-Back.

311

NOMINAL VANE STAGGER

52°

.040"

0.45"

.048"

CUT BACK FOR NOZZLE
OPENING = 6½%

EGG TURBINE VANE CASCADE
AT APPROXIMATELY MEAN EXIT
RADIUS

27323
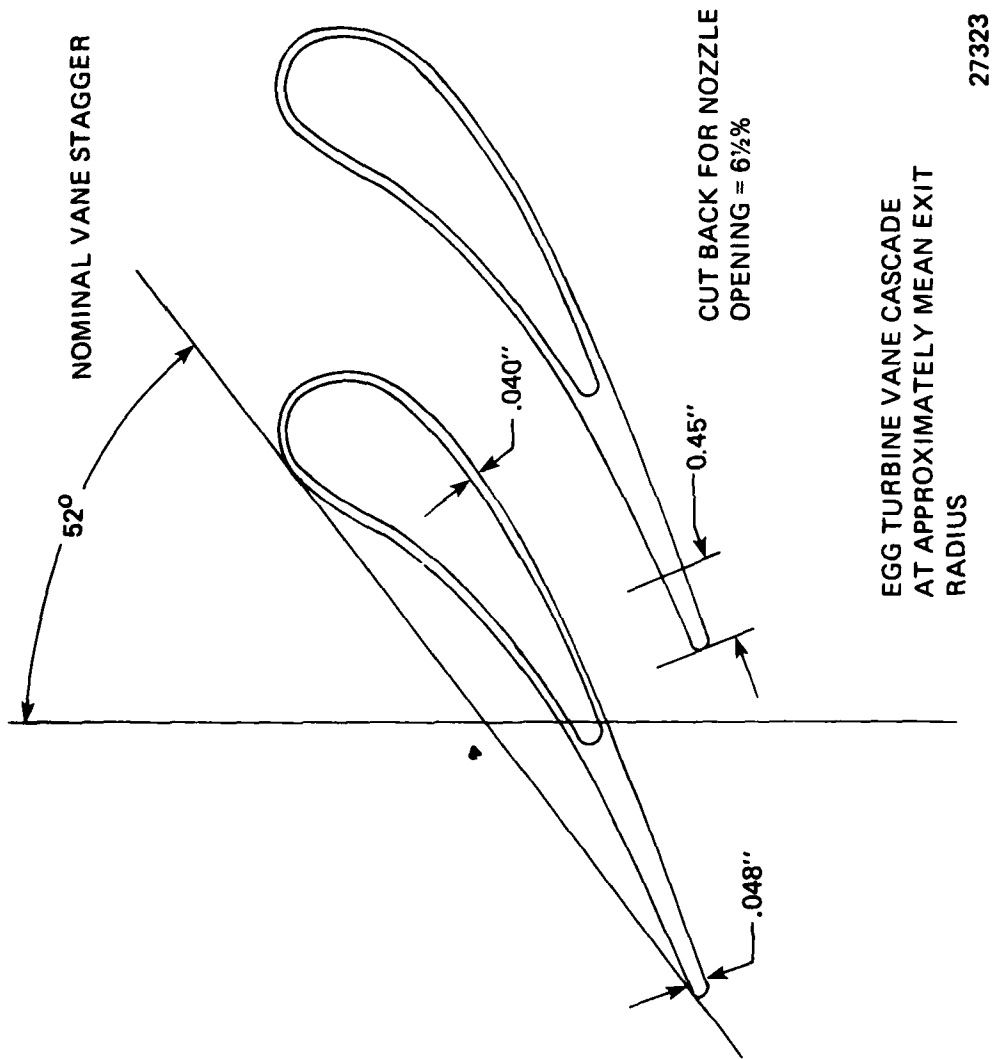
Figure 231. Turbine - Nozzle Cut-Back Requirements.

5.3.4 Mechanical Design

The selected material for the turbine rotor is IN 100, a nickel alloy chosen for high strength to 1900°F; this alloy has attained considerable industry usage for both individual blades and integral bladed rotors. Teledyne CAE experience with this material derives from the production J402 turbine rotors; the latter's comparable size to the E.G. rotor (within 1/2 inch at OD) and same material influenced the decision to select the same foundry to produce the E.G. rotor.

Recognizing the need to reduce machining operations (especially on nickel base alloys) in order to reduce procurement costs, the E.G. rotor is cast to net shape, needing only to have the blade tips cropped and the hub faced for the electron beam weld joint with the shaft.

The turbine clearances are shown in Figure 232

TURBINE
TIP

0.050
±0.003

0.125 ± 0.06

TURBINE
TO NOZZLE
AXIAL GAP
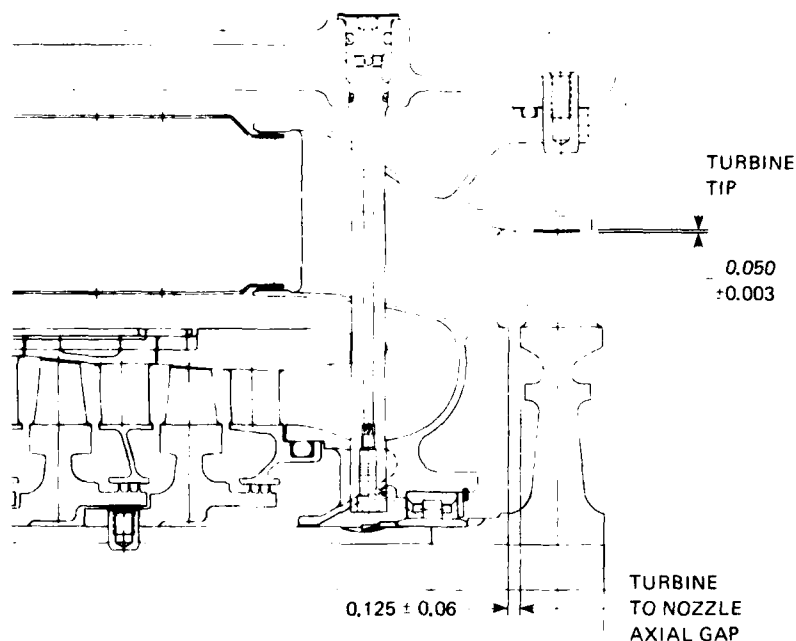
AT 100% SHAFT SPEED, STEADY STATE CONDITIONS, THE TURBINE TIP RADIAL
CLEARANCE IS CALCULATED AS FOLLOWS:
      0.050 MEAN BUILD CLEARANCE
     +0.027 TURBINE SHROUD THERMAL GROWTH
     -0.053 TURBINE TOTAL GROWTH
      0.024 MEAN OPERATING TIP CLEARANCE   27373

Figure **232**. Expendable Gasifier Turbine Clearances (at Cold, Static Conditions).

313

5.3.5 Structural Design

The turbine blade was modeled with four-node quadrilateral plate elements to determine natural frequencies using the NASTRAN finite element computer program. The original blade design was analyzed at zero speed using the normal modes rigid format of NASTRAN, and at maximum speed using the normal modes with differential stiffness rigid format. Sixty-four elements were used, and the blade was fixed at the hub. The blade model is presented in Figure 236. Results of the analysis are presented on a resonance diagram in Figure 233. The primary source of excitation to the turbine blades is the turbine inlet nozzle blockage (13E). The margin between the 13E excitation and the first torsion mode of 10 percent was believed to be too low. Therefore, an effort was made to increase the blade torsional frequency.

The blade redesign involved increasing the blade thickness at the hub and fairing it into the original blade at 50 percent span. The resulting change in blade cross sectional area distribution is presented in Figure 234. Blade frequencies calculated for this thickened blade are shown on the interference diagram, Figure 235. The 13E frequency margin for the first torsion mode was increased to 19 percent which was considered adequate. Resonance of the complex plate type modes (modes 3 through 7) with multiples of the vane passing frequency is not considered a problem. Mode shapes from the NASTRAN analysis are shown for the final turbine blade design in Figures 236 through 242 for the first through seventh modes respectively.

The blade centrifugal and restored gas bending stresses were calculated using a conventional tapered, twisted beam model. A summary of the blade stresses at the hub (maximum stress point) and at 50 percent span (minimum stress margin point) is presented in Figure 243. A minimum safety factor of 1.5 on the 20-hour stress rupture strength is indicated. This was determined by comparing the direct tensile stresses (centrifugal P/A) with the minimum 20-hour stress rupture strength, based on the adiabatic wall temperatures predicted for the blade at maximum speed and a turbine rotor inlet temperature of 1800°F. The predicted temperatures, centrifugal stresses and 20 hour stress rupture strengths are presented in Figure 244 for the complete blade span.

The design goal for the turbine disk is a low cycle fatigue (LCF) life of 2,000 start-stop cycles. A disk was designed, with a solid bore, for an assumed starting thermal gradient of 1000°F from rim to bore, based on the transient thermal analysis of similar IN-100 turbine disks. The stress analysis indicated that the bore stresses were below the yield strength of the material while the rim tangential stresses were in compression, near the yield strength. For a reverse thermal gradient of 500°F upon shutdown, a total strain range of less than 0.005 in/ in. was estimated for the rim, which results in an LCF life greater than 2000 cycles, according to the curve of Figure 245. The analysis is based upon a pseudo-plastic analysis by assuming elastic strain invariance from an elastic analysis which is

314
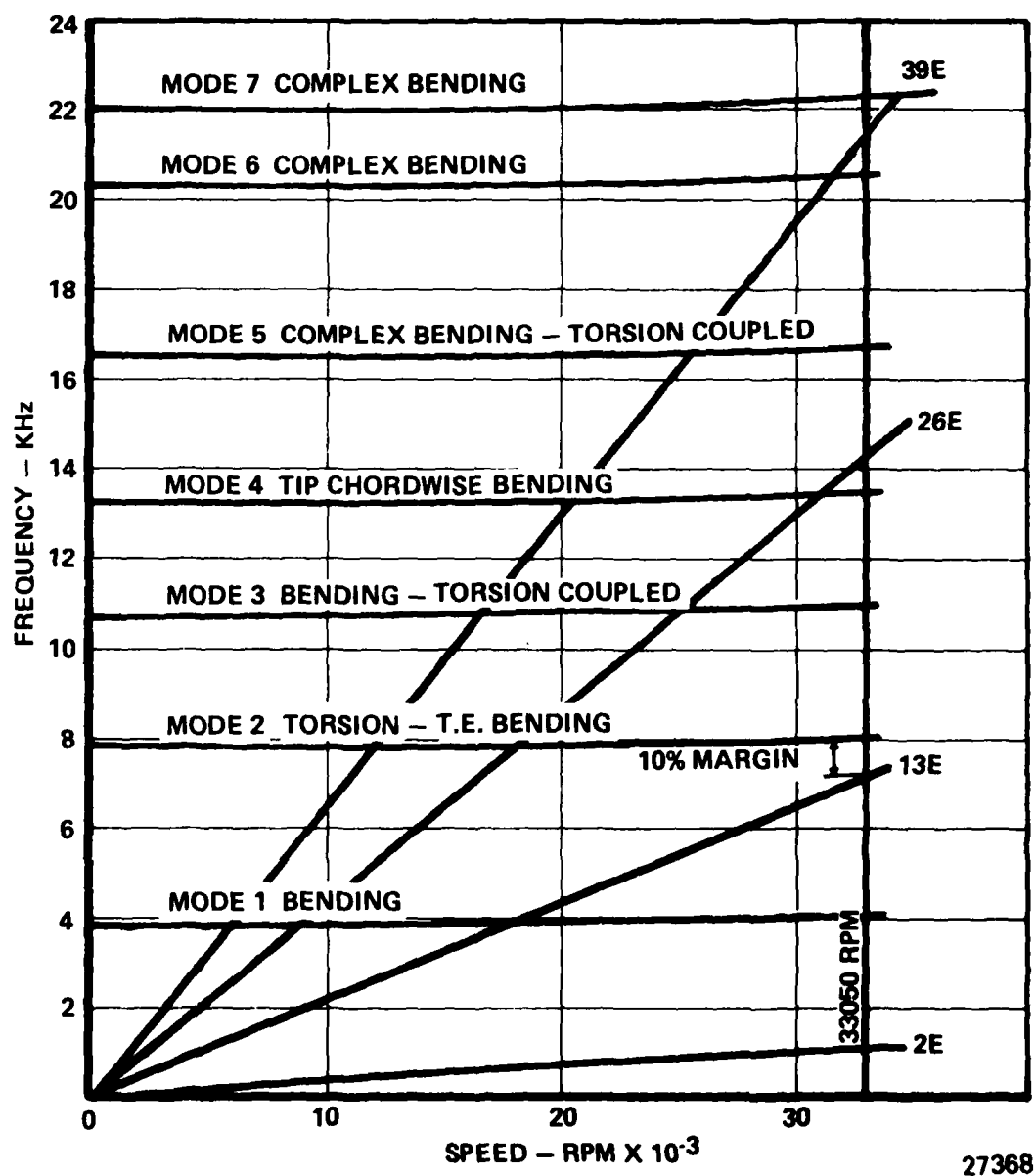
Figure 233. Turbine Blade (Design #1) Intereference Diagram.

315
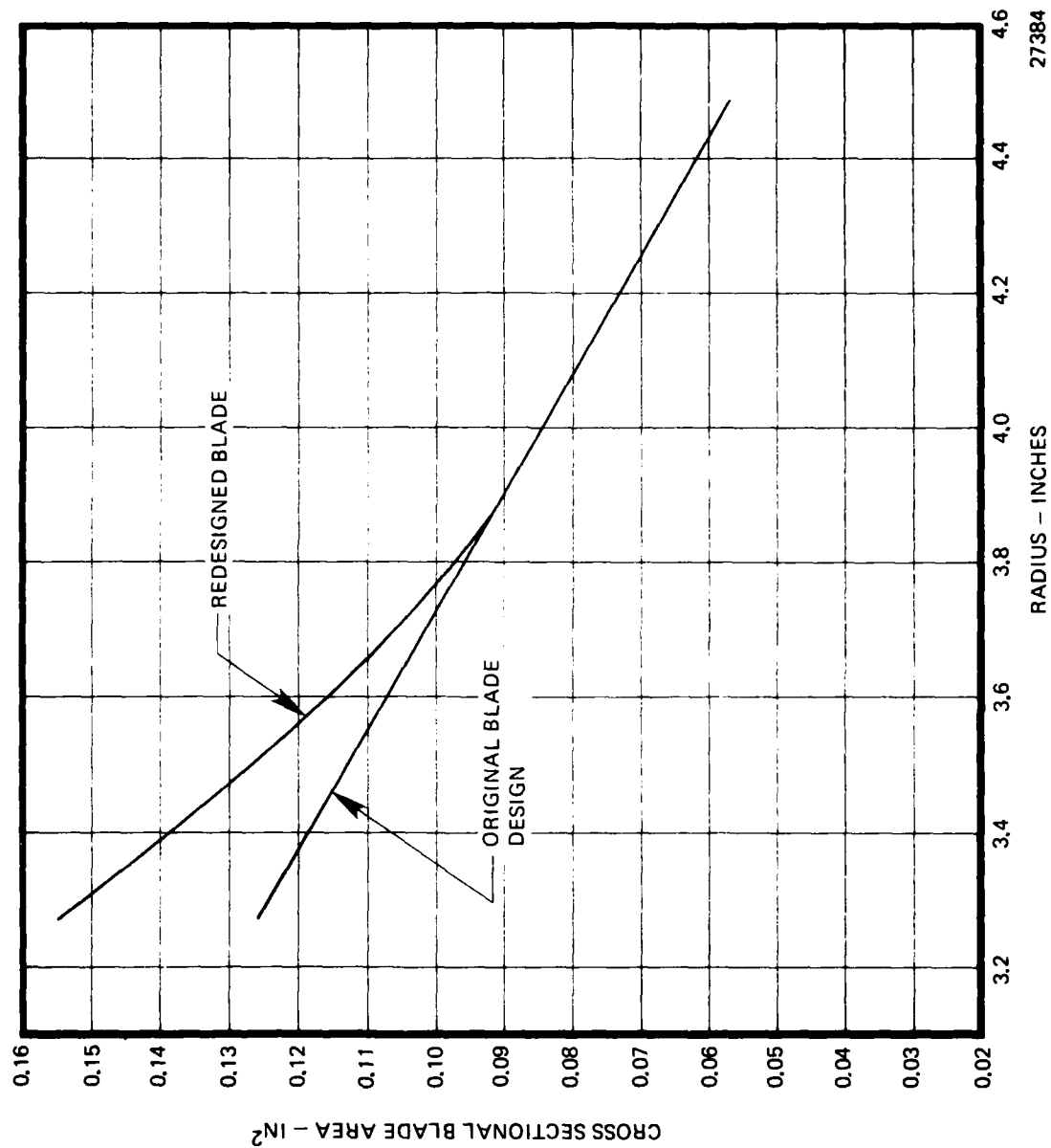
Figure 234. Turbine Blade Comparison of Original and Redesigned Blade Area Distributions.

27384

316
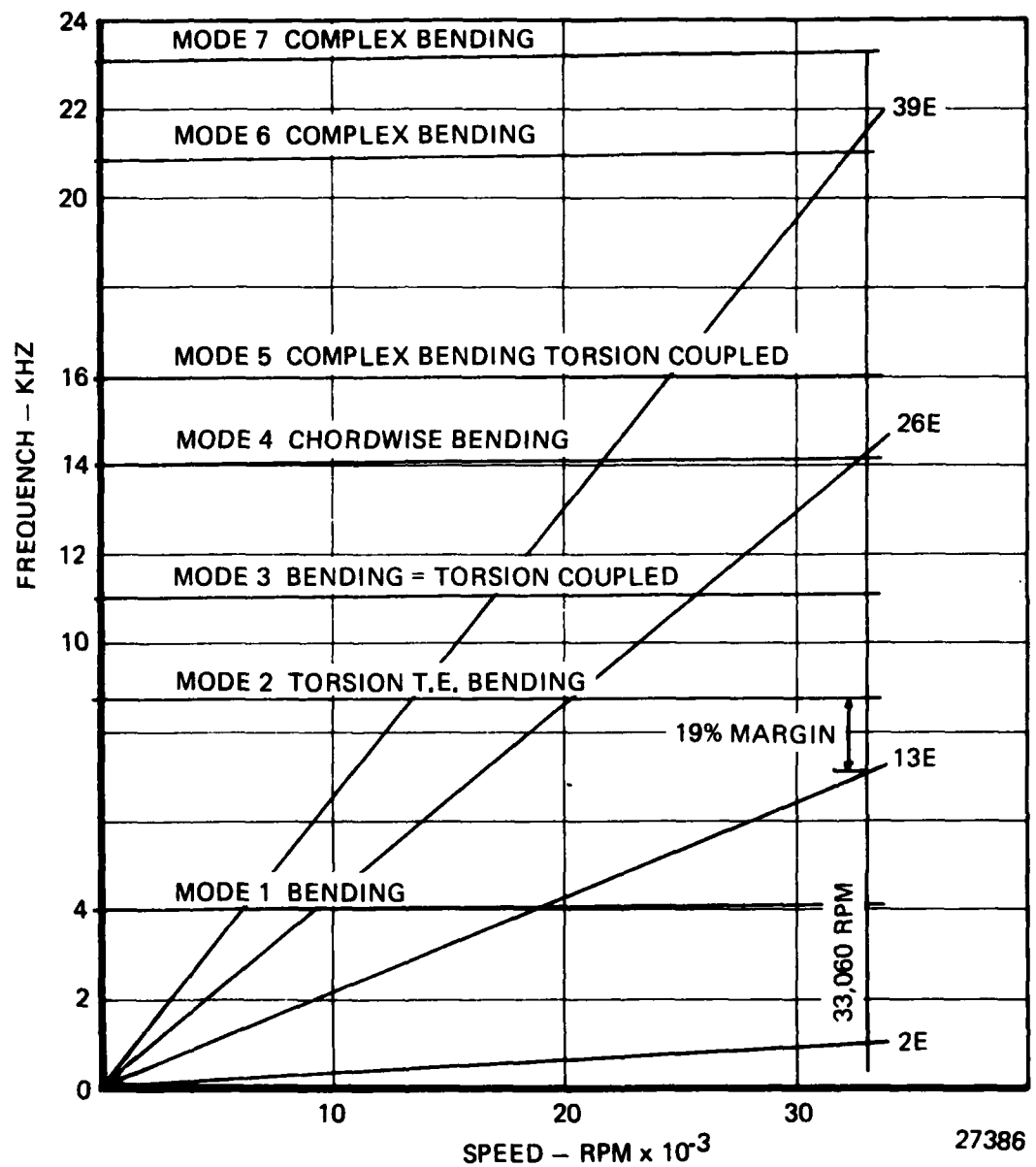
Figure 235. Turbine Blade (Design #2) Intereference Diagram.

317
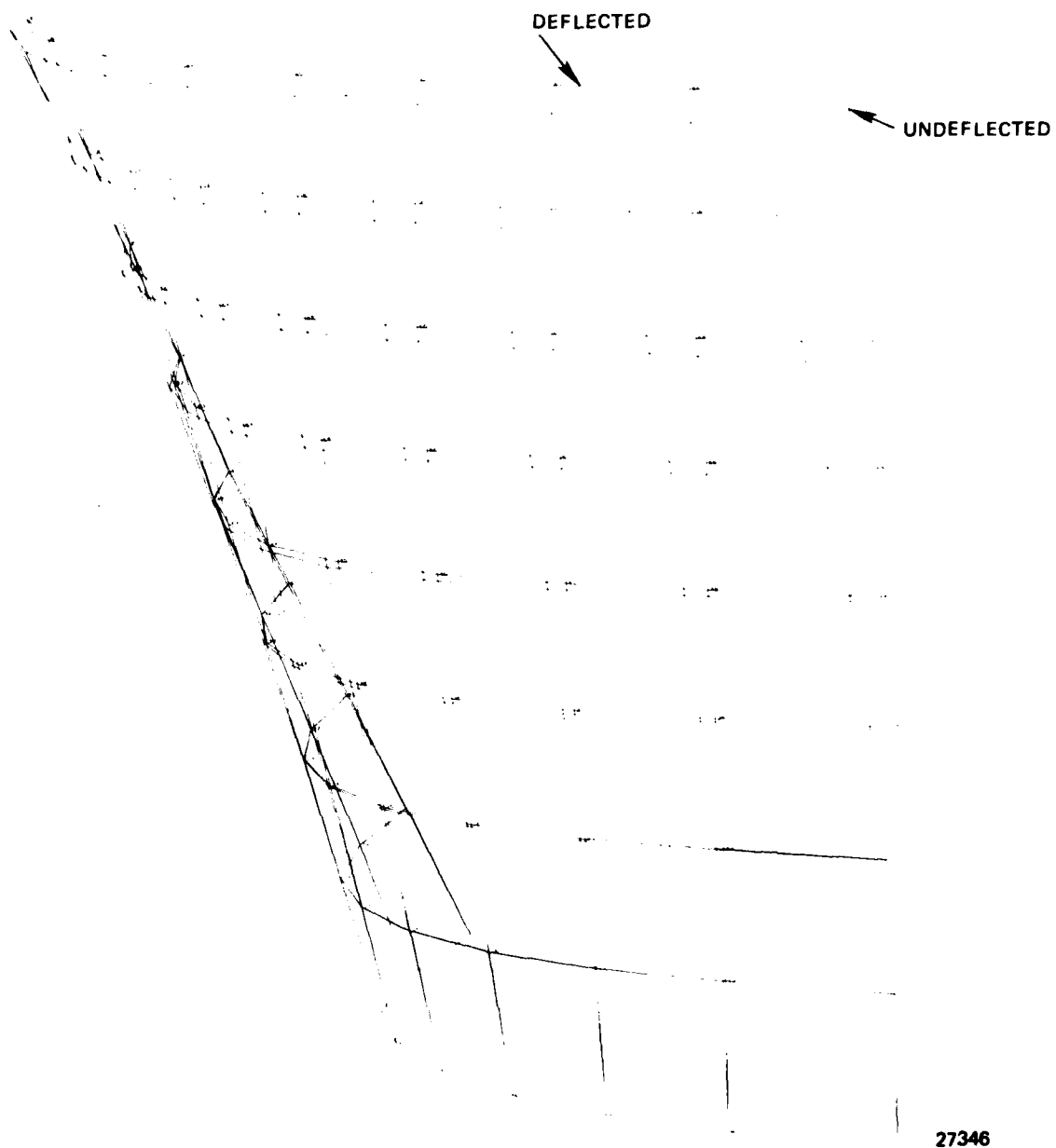
Figure 236. Turbine Blade NASTRAN Analysis 100 Percent Speed, Mode 1, 4217 Hz.

DEFLECTED

UNDEFLECTED

27353
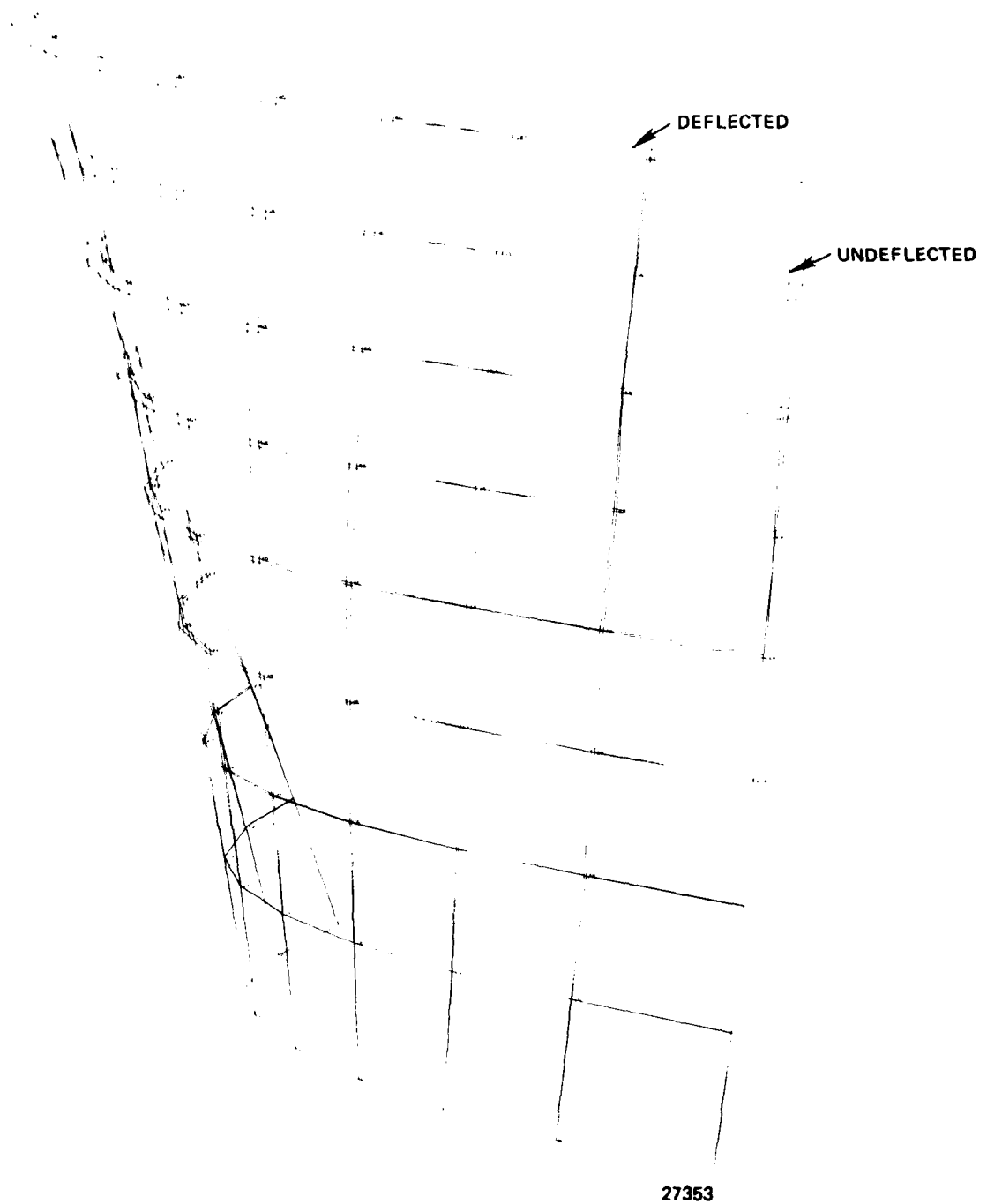
Figure 237. Turbine Blade NASTRAN Analysis 100 Percent Speed, Mode 2, 8862 Hz.

319

DEFLECTED

UNDEFLECTED

27354
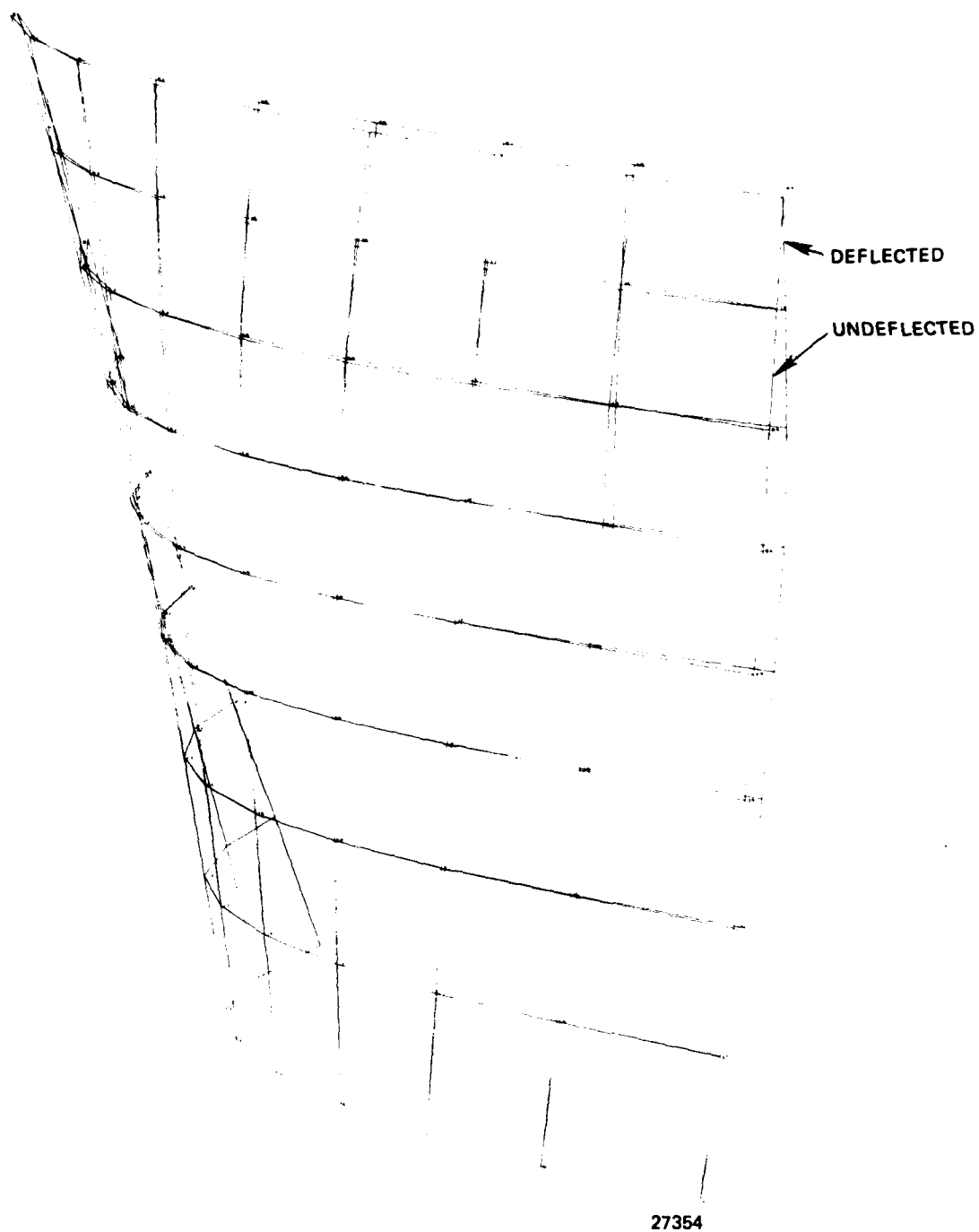
Figure 238. Turbine Blade NASTRAN Analysis 100 Percent Speed, Mode 3, 11188 Hz.

DEFLECTED

UNDEFLECTED

27351
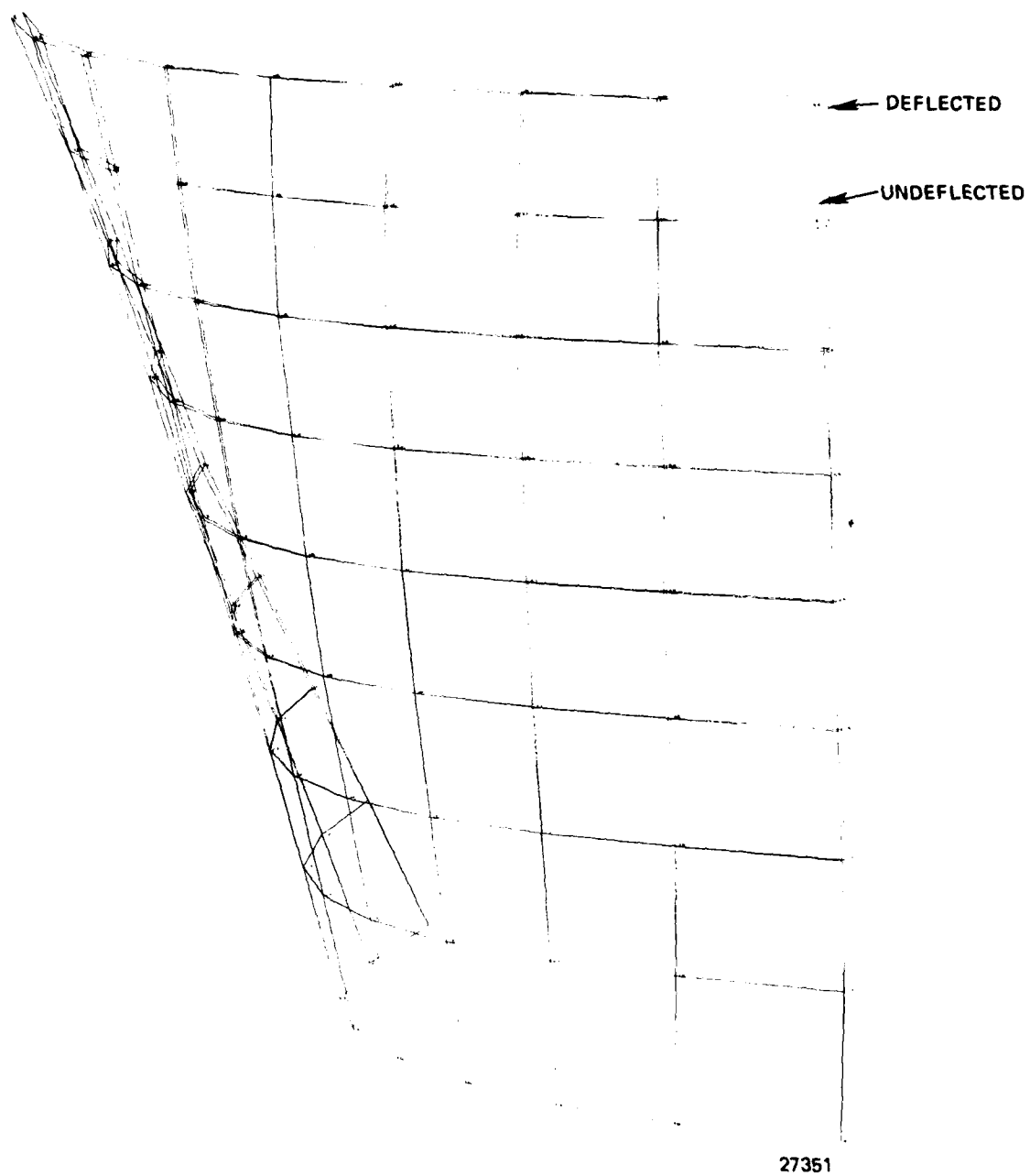
Figure 239. Turbine Blade NASTRAN Analysis, 100 Percent Speed, Mode 4, 14192 Hz.

DEFLECTED

UNDEFLECTED

27355
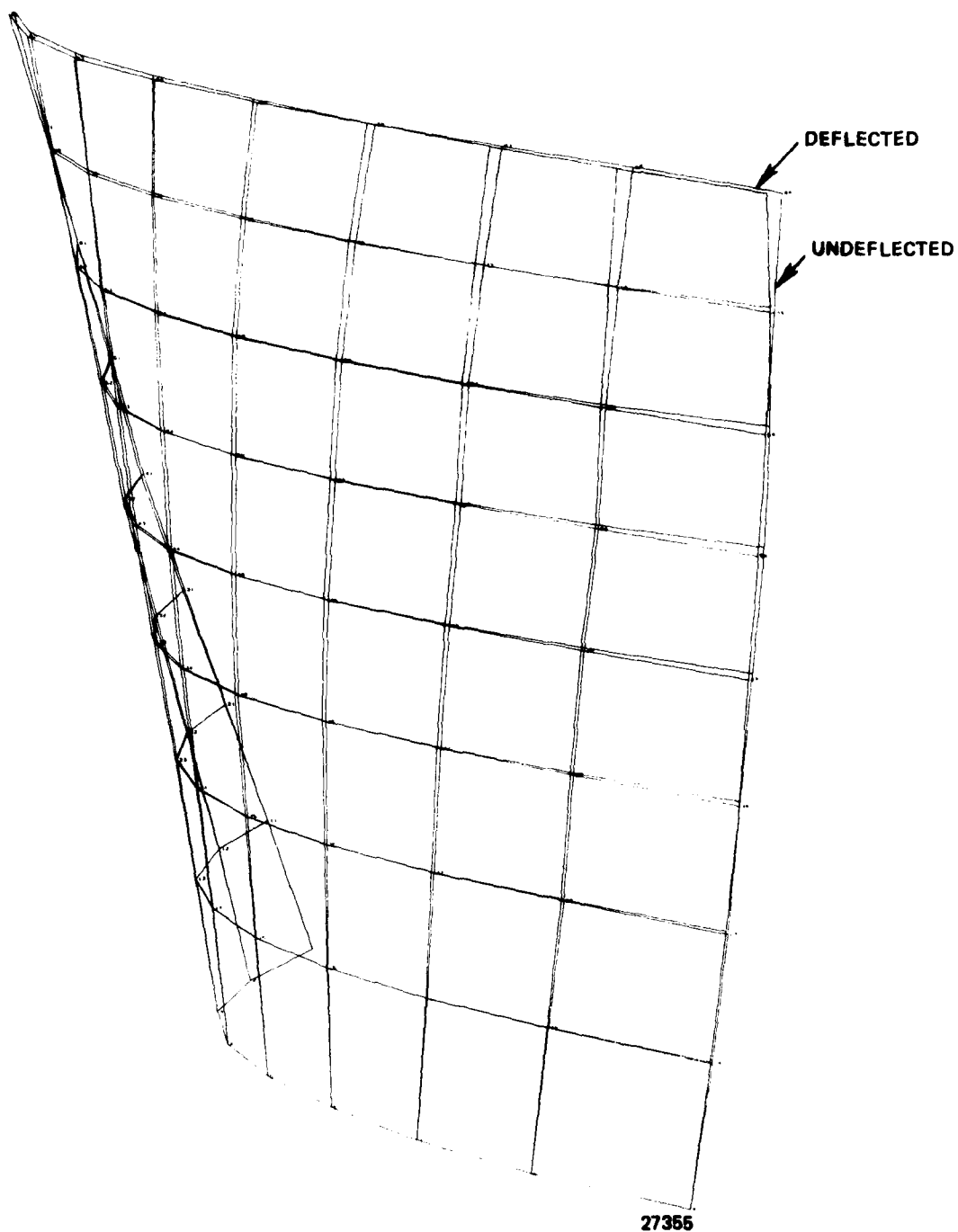
Figure 240. Turbine Blade NASTRAN Analysis, 100 Percent Speed, Mode 5, 16877 Hz.

322

DEFLECTED

UNDEFLECTED

27356
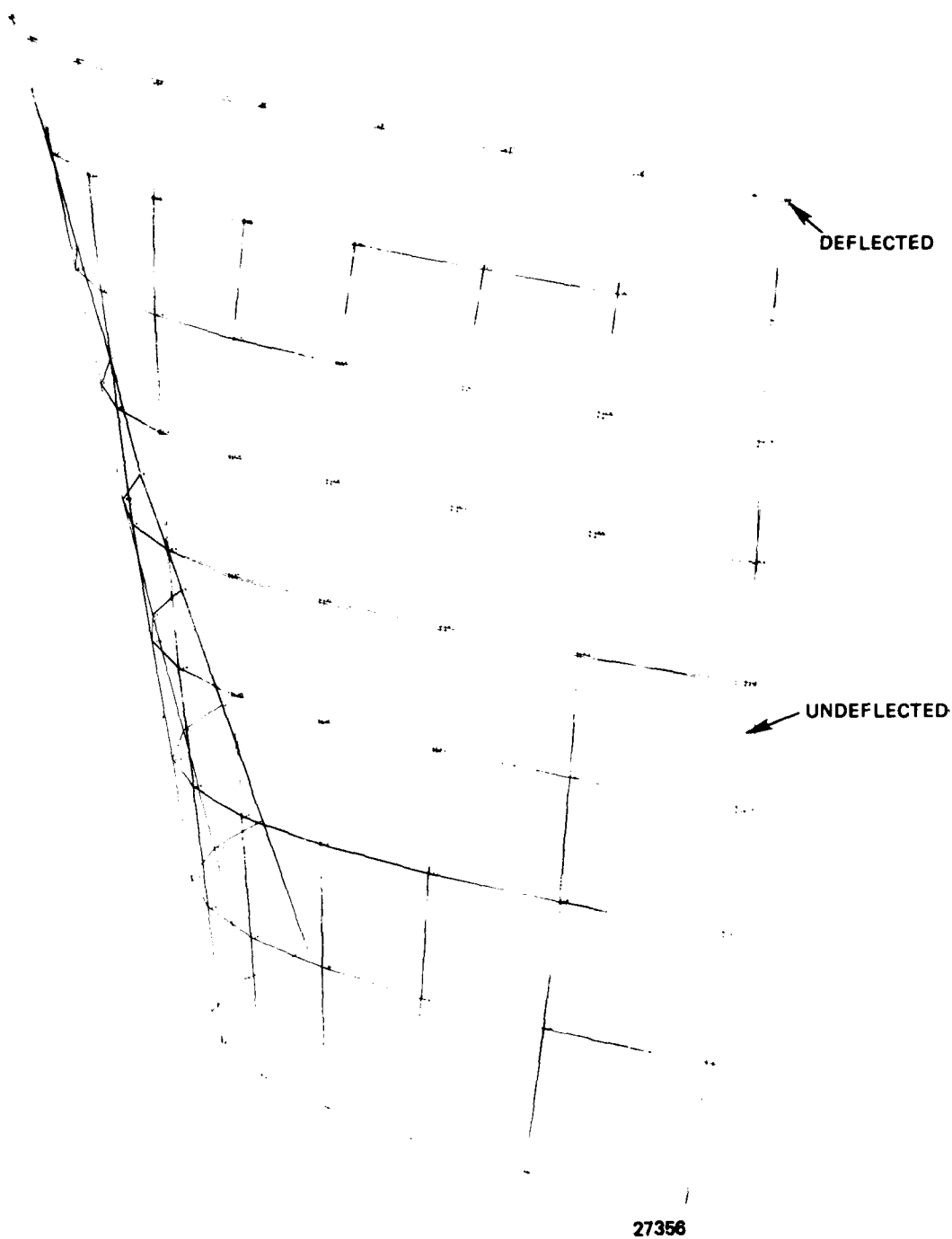
Figure 241. Turbine Blade NASTRAN Analysis, 100 Percent Speed, Mode 6, 21055 Hz.

DEFLECTED

UNDEFLECTED

27352
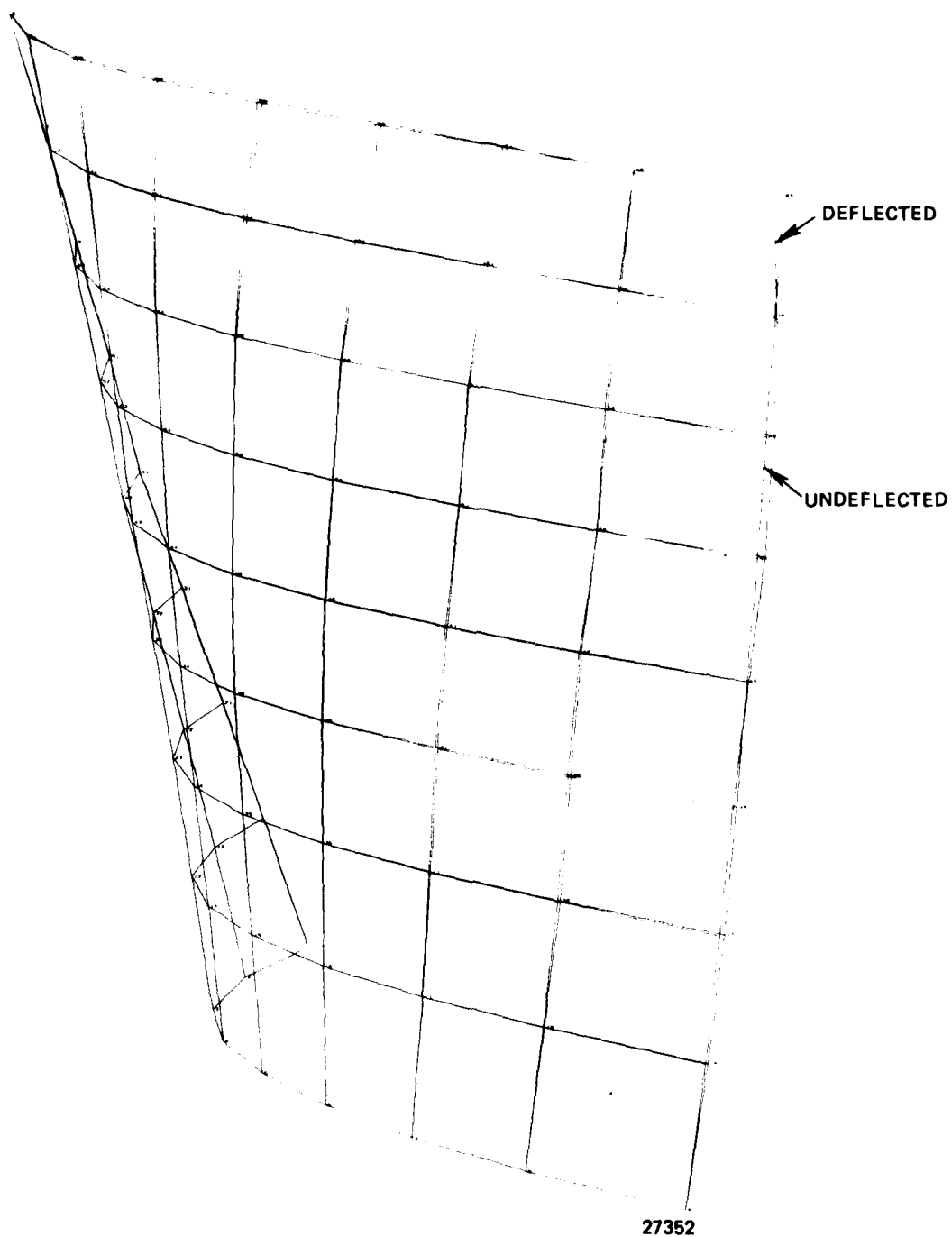
Figure 242. Turbine Blade NASTRAN Analysis, 100 Percent Speed, Mode 7, 23316 Hz.

ROTOR MATERIAL: IN-100
SHAFT SPEED 33,500 RPM (MAX)
T.I.T.: 1800°F

*BASED ON PRIMARY STRESSES
(CENTRIFUGAL P/A) ONLY

SUMMARY OF BLADE STRESSES

Blade Location	Temp. °F	Min. Material Properties, KSI			Applied Stresses, KSI				Safety Factors		
		.2% Yield	Ult.	20 Hrs. S.R.	Cent. P/A	Cent. Untwist	Restored Gas Bend	Max Comb'd.	Ult.*	Yield	St.* Rupt.
Root (Hub)	1390	90	100	76.	24.9	7.7	-0.7	31.9	4.0	2.8	3.1
50% Span	1775	50	62	26.5	17.4	6.5	-0.5	23.4	3.6	2.1	1.5

SUMMARY OF DISK STRESSES

Operating Condition	Temp. °F	Minimum Material Properties, KSI		Bore Tangential Stress - KSI	Average Tangential Stress, KSI	Burst Speed Margin %	Burst Speed RPM
		Ultimate	.2% Yield				
Design Point Bore	1275	100	90	78.4	42.4	37	46000
Steady State Rim	1390						

27357

Figure 243. Model 506-2X Turbine Rotor.
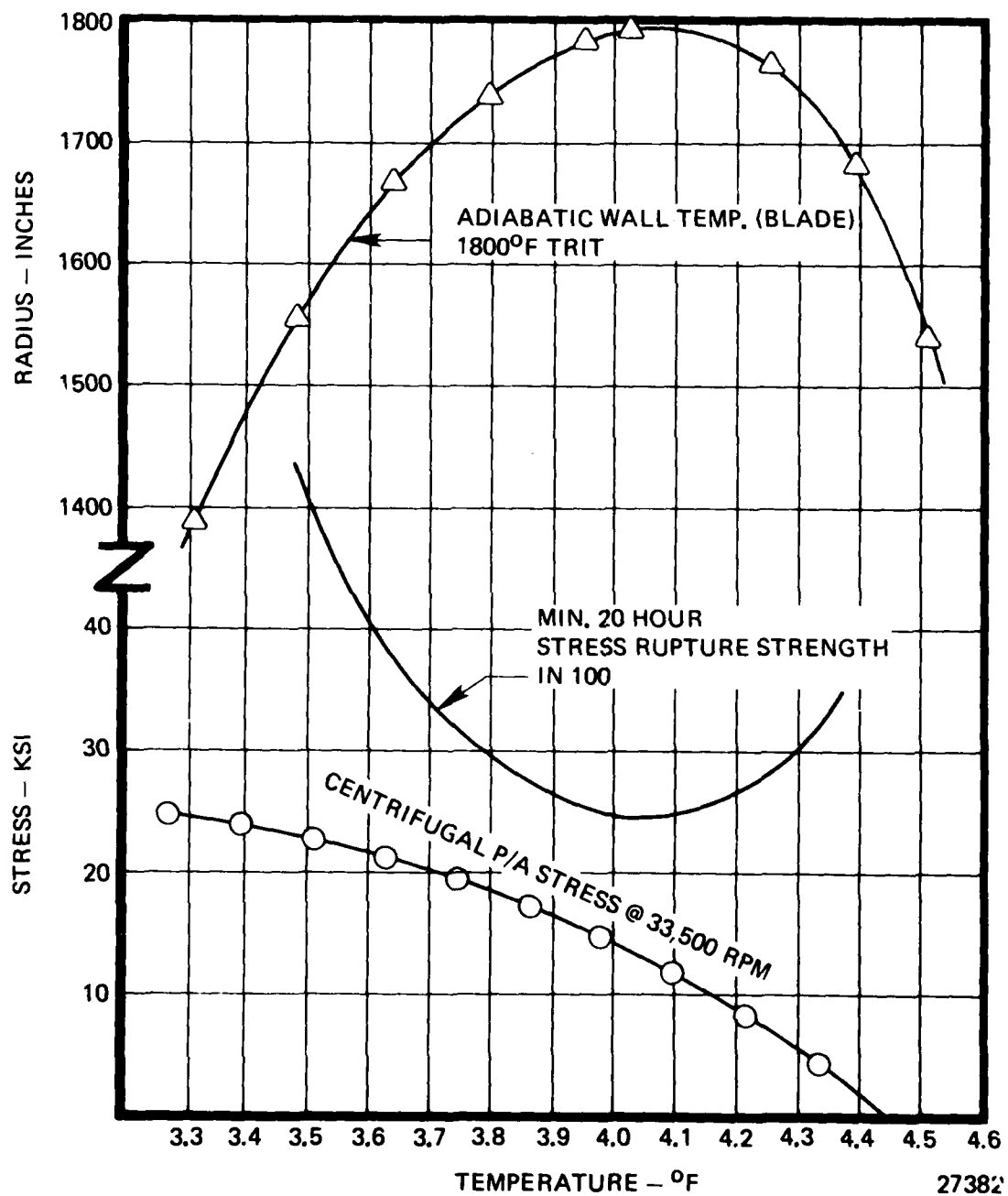
Figure 244. Final Turbine Blade Stresses Compared to Stress Rupture Strength.
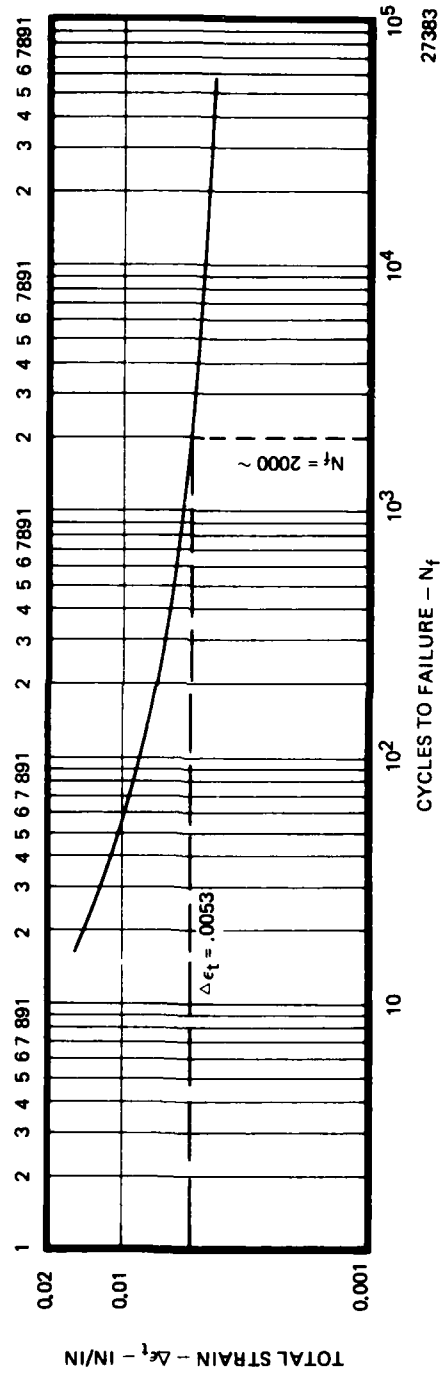
Figure 245 . Cast IN-100 LCF Curve - 1000°F to 1400°F Range From Axial Fatigue Data.

327

valid for thermal loads. This serves as a good approximation for rim strains since the rim loads are predominantly thermal.

A thermal analysis of the disk was performed from start-up to full speed, assuming a step increase in turbine rotor inlet temperature from ambient to 1800°F. The analysis indicated a thermal rim-to-bore gradient of 1290°F. The analysis did not predict the shutdown transient, so a reverse gradient of 50 percent of the start-up gradient was assumed. Using these gradients, the stress analysis of the rotor disk predicted the strain range of the disk rim of approximately one percent which produces a LCF life of less than 2000 start-stop cycles (Figure 245). The disk was not redesigned since there was a lack of IN-100 cyclic materials data in the temperature range of interest, and the program schedule would have been adversely impacted. Development of a turbine rotor with the capability to withstand 2000 rapid start-stop cycles will be accomplished in the next program phase. Currently the disk design is structurally sound for normal gasifier operation, but more accurate information concerning the rapid start-stop operation is required to more precisely predict the disk LCF life for a jet fuel starter application.

The disk was originally designed with a solid bore. However, a hollow bore was required for the gasifier application to allow for a through-shaft. This change was made, and the latter thermal/centrifugal stress analysis mentioned above is for a hollow bore. The combined centrifugal and thermal stresses at 100 percent speed and 1800°F turbine rotor inlet temperature are summarized in Figure 243. A 37 percent burst speed margin is indicated at 33,500 rpm.

5.4.   GASIFIER OVERALL MECHANICAL DESIGN

5.4.1   Basic Configuration

The Model 506-2X Expendable Gasifier (Figure 246) consists of an axial flow compressor, annular combustor, axial turbine and support structure. The annular, reverse-flow combustor overlaps the axial compressor to provide a compact unit 12.9 inches in diameter, 18.6 inches in length, and weighing approximately 73 lbs.

Basic design features of the expendable gasifier are as follows:

1. Lube System - Self-contained, having no oil pumps, filters, coolers, etc. and requiring no maintenance. These systems are based on those of proven production engine technology.

2. Compressor - Uses four identical aluminum precision castings, including stators which require a minimum of machining.

3. Compressor Drive - Uses radial pins that assure rotor bore uniform radial growth and eliminate splines.

4. Main Shaft - Investment cast to net shape turbine, permanently electron beam welded to tubular shaft; assures shaft dynamics stability.

328

QAD FLANGE

T.I.N/MAIN FRAME
RADIAL PIN DESIGN

FUEL LUBED
REAR BEARING

WEIGHT: 78 LBS.

TURBINE SHAFT:
TUBULAR CONSTRUCTION

12.9 DIA.

TURBINE ROTOR:
PRECISION CAST
TO NEAR NET-SHAPE

27095 A

T.I.N.: MONOLITHIC PRECISION
CASTING WITH HOLLOW
AIR COOLED VANES

27395

RADIAL PIN
COMPRESSOR
DRIVE

18.6 LENGTH

ACCESSORY UNIT
MOUNT FLANGE

MAIN FRAME
MULTI-FUNCTION
DESIGN

SELF-CONTAINED
SUMP LUBE SYSTEM

COMPRESSOR ROTORS:
IDENTICAL PRECISION
CASTINGS

COMBUSTOR:
PRE-PERFORATED
SHEET METAL
CONSTRUCTION

Figure 246 . Model 506-2X Expendable Gasifier.

329

5. <u>Combustor</u> - Pre-perforated sheet metal construction; spring leaf support accommodates thermal expansion.

6. <u>Turbine Inlet Nozzle</u> - Monolithic precision casting with hollow, air-cooled vanes.

7. <u>Quick Attach/Detatch Flanges</u> - Permits quick assembly of gear box and derivative modules.

8. <u>Main Frame</u> - Multi-purpose; incorporates many functions in one relatively low cost component.

5.4.2 Material Selection and Fabrication Methods

In selecting materials and manufacturing processes for the gasifier, emphasis was placed on the use of readily available alloys and the use of low cost fabrication methods such as sand and investment castings to reduce machining costs. In general, the materials selected have inherent corrosion resistance by virtue of their chemical composition. This pre-empts having to use cost impacting protective coatings.

Figure 247 shows the material selected, for the major engine components, and their fabrication method. Extensive use is made of castings for the main frame, compressor rotor and stators, turbine nozzle and rotor.

The cast aluminum alloy, C-355, selected for the compressor and stators, is currently used at Teledyne CAE for the cold end housings on the J402 series production engines. The alloy is easily cast and can be heat treated to a strength level of 40,000 psi. This alloy was also used in the initial procurement of the main frame combustor rig. However, test results indicated a possible temperature problem at the frame rear flange; the problem has been addressed by substituting a higher strength-at-temperature alloy (RR 350) for the frames presently on order.

For the combustor, pre-perforated sheet of Haynes 556 alloy has been selected for its good high temperature strength and corrosion resistance to 2000°F. It is readily formed and easily welded.

The turbine inlet nozzle is an investment casting of N-155 alloy. This alloy was selected for its good castability along with good oxidation and strength characteristics to 1800°F, and can easily be weld repaired.

The turbine rotor, cast virtually to net shape, is of IN-100, a nickel base alloy characterized by its high strength to 1900°F and its common use in gas turbines.

The following is the step-by-step procedure for assembling the gasifier, (refer to Figure 248).

330

RR-350 SAND CAST ALUMINUM MAIN FRAME CONTAINS
FUEL PASSAGES FOR PRIMER, MAIN FUEL NOZZLES,
REAR BEARING LUBRICATION

INVESTMENT CAST N-155 VAPORIZER TUBE

INVESTMENT CAST N-155
TURBINE INLET NOZZLE

INVESTMENT CAST IN-100
TURBINE ROTOR

17-4PH STEEL SHAFT (TUBING)
EB WELDED TO ROTOR

PERFORATED SHEET METAL COMBUSTOR
MATERIAL: HAYNES 656

C355 SAND OR PLASTER
MOLD CAST ALUMINUM FRONT
BEARING HOUSING

8617
CARBURIZING
STEEL GEARS

INJECTION MOLDED
POLYETHERSULFONE
TRANSLUCENT PLASTIC
FRONT HUB

C355 PRECISION CAST
ALUMINUM ROTORS AND
STATORS

27385

27084 A

331

Figure 247. Model 506-2X E.G. Material Selection and Fabrication Methods.
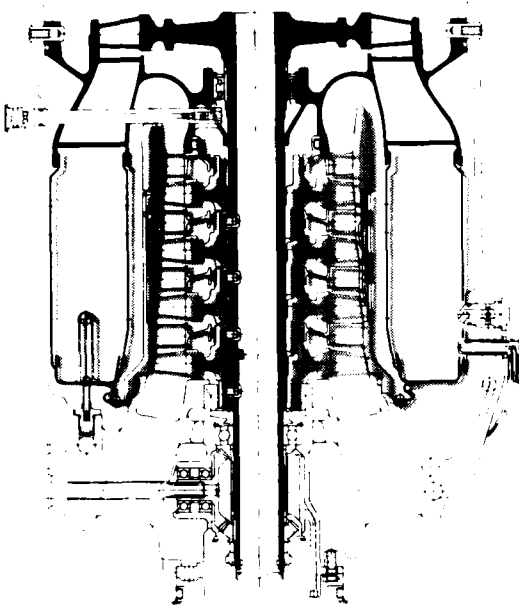
27392

STEP II: ADD COMPRESSOR, STATORS & COMBUSTOR
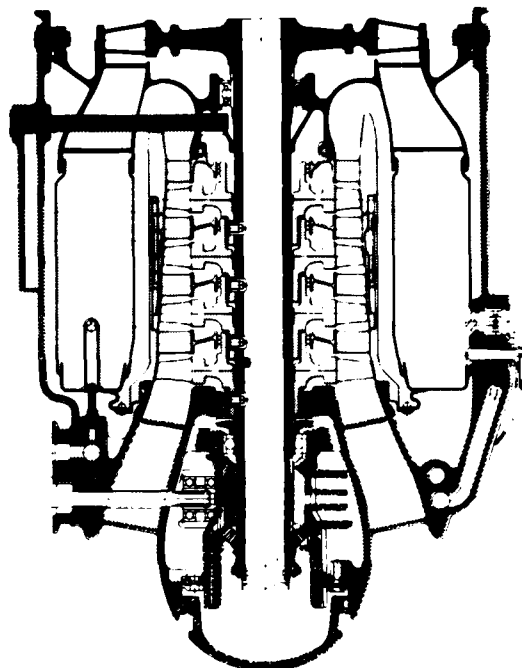
STEP IV: ADD BEVEL GEAR HOUSING, BEVEL
GEARS & NOSE CONE
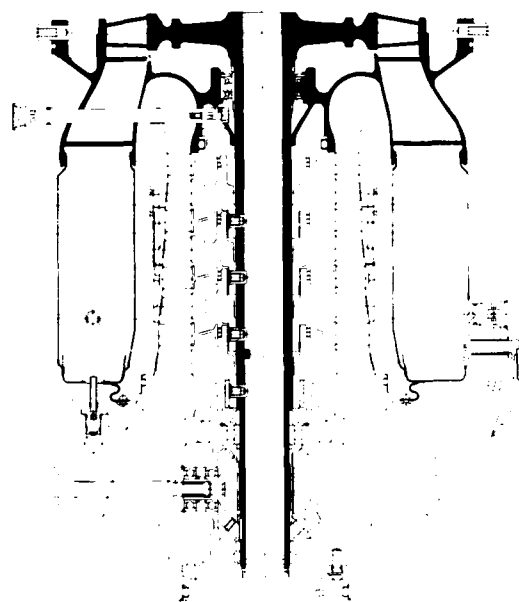
STEP I: BEGIN WITH TURBINE INLET NOZZLE
AND TURBINE SHAFT
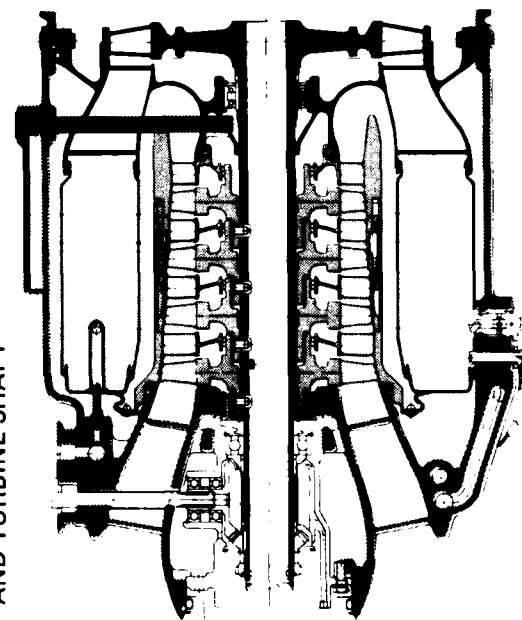
STEP III: ADD MAIN FRAME, FUEL LUBE TUBE,
& T.I.N. RADIAL PINS

Figure 248 . Model 506-2X Expendable Gasifier Assembly Procedure.

332

STEP 1.

      a.   Install rear bearing outer race and roller complement in turbine inlet nozzle.

      b.   Press rear bearing inner race in turbine shaft and secure with lock ring.

      c.   Introduce turbine shaft into inlet nozzle, engaging the rear bearing.

STEP 2.

      a.   Install fourth stage stator.

      b.   Install fourth stage compressor rotor engaging the three radial drive pins with the turbine shaft.

      c.   Repeat with the remaining stators and rotors. The combustor, being permanently riveted to the first stage stator, will assemble with the latter, mating with the turbine inlet nozzle.

STEP 3.

      a.   Pre-assemble the 14 fuel nozzles and the bearing sump seal into the main frame.

      b.   Install the main frame, engaging the rear bearing fuel lube tube and the six frame-to-turbine inlet nozzle radial pins.

STEP 4.

      a.   Pre-assemble the driven bevel and supportive bearings and the turbine shaft thrust bearing into the bevel gear set housing.

      b.   Introduce the bevel gear set housing into the main frame lube sump cavity and bolt in place, pressing the thrust bearing into the shaft.

      c.   Press the drive bevel and spacers onto the turbine shaft and torque the shaft nut.

      c.   Install the nose cone.

      e.   Fill front bearing lube sump, introducing lubricant through the accessory drive shaft hole, observing the lubricant level through the transparent plastic nose cone.

      f.   Install the accessory drive shaft.

      g.   Mount the accessory drive unit on the main frame pad and secure with QAD clamp.

5.4.3 Shaft Dynamics Suspension System

The principal source of mechanical vibration in the gas turbine engine is an unbalance in the rotating shaft system. This unbalance may excite critical speeds of the shaft itself and/or induce resonance in any combination of structural elements that may be tuned to the running frequency of the shaft. The expendable gasifier has been designed to minimize the effect of rotor unbalance and critical speeds through the proper combination of rotor and supporting structure compliances.

The E G shaft critical speeds curves (Figure 249) indicate that the third critical speed margin (first shaft bearing mode) is in excess of 28 percent for any combination of bearing/support springrates (based on a maximum operating speed of 33,500 rpm). This is an adequate margin for this shaft configuration.

To prevent the first and/or second critical speeds (primarily rigid body modes) from occurring within a 20 percent range of the normal operating speed (33,060 rpm), the front bearing/support springrate must be less than 60,000 lbs/in, and the rear bearing/support springrate must be less than 200,000 lbs/in. A rear bearing/support springrate of 1,000,000 lbs/in will place the second critical 28 percent beyond the maximum operating speed. It is doubtful that the combined rear bearing and support housing structure springrate will be this high.

The bearing support structural springrates, with bearings installed, will be determined experimentally, on the first engine hardware, to ascertain the necessity for a modification to provide additional flexibility for critical speed control. A radially-stepped flexible spring ring has been designed for the rear bearing support and a high temperature elastomeric "O" ring and adapter ring have been designed for the front bearing support to provide the necessary flexibility (Figure 250) in the event the measured structural compliance indicates a possible critical speed problem. The bearing support housings have been designed for easy modification to accept the flexible members, if necessary. The critical speed summary is presented in Figure 251. Shaft balancing procedure is illustrated in Figure 252.

5.4.4   Bearings and Lubrication Systems

Conventional lubrication systems require oil pumps, filters, cooler tanks, etc. The Model 506-2X uses production-engines-proven, self-contained systems whose reliability is enhanced by the elimination of rotating components.

The main shaft front thrust bearing lubrication system (Figure 253) is of the recirculating pot lube type; its technology has been amply demonstrated in both the VSTT and Harpoon engines. In the latter engine, successful bearing lubrication is accomplished at stringent starting conditions: -65°F, while accelerating the shaft from 0 to 41,000 rpm in less than 10 seconds.

The drive bevel (Figure 253) rotating at shaft speed, entraps oil and centrifugally slings it through the bevel gear housing cored passages that lead to the thrust bearing. Large holes in the cylindrical portion of the gear housing assure oil circulation to the driven bevel, vertical accessory, drive shaft spline and the supportive bearings. Oil drains by gravity to the sump and a conventional carbon face seal prevents leakage. Bearings and gear mesh friction heats are transferred to the oil which, in turn, rejects it to the inlet air flow, scrubbing the aluminum main frame oil sump walls. Oil level is readily discerned through the translucent plastic nose cone.
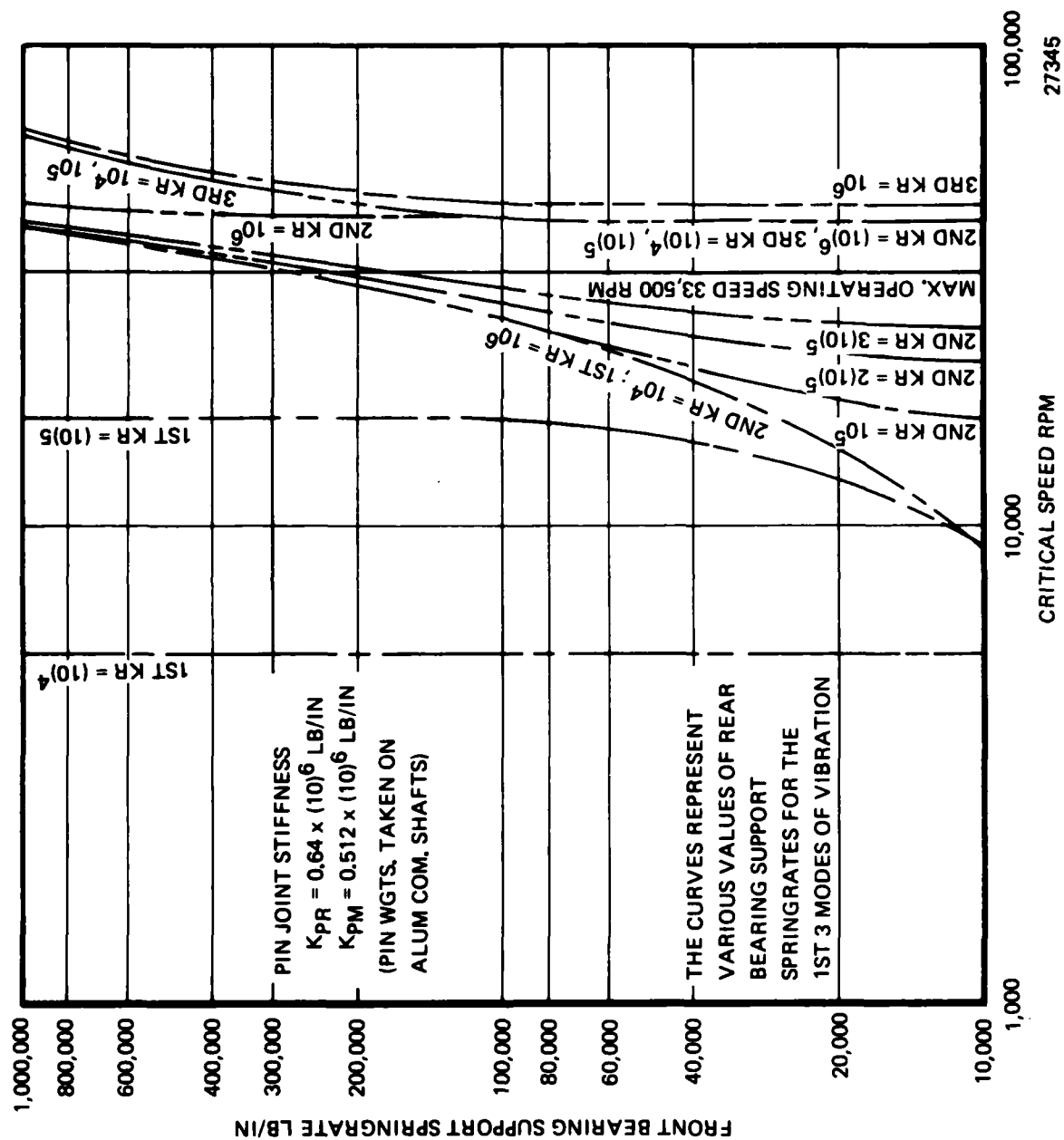
Figure 249. Expendable Gasifier Critical Speeds.

335
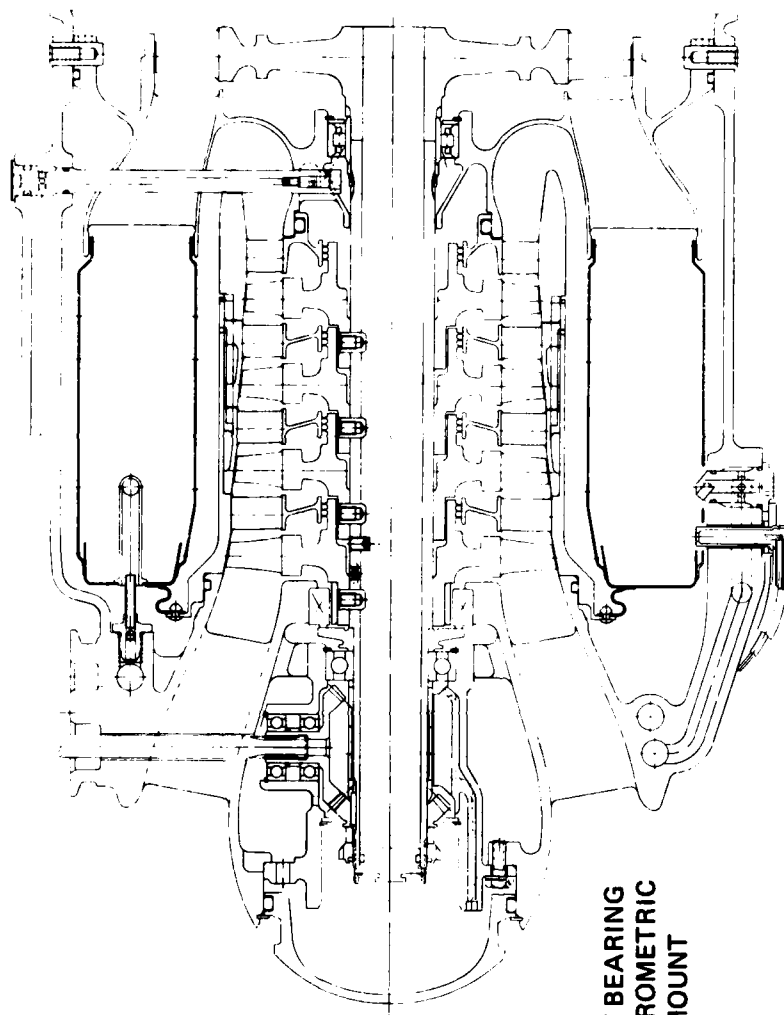
*REAR BEARING
LOWER SPRING
RATE FLEXIBLE
RING

27094 A

27399

*FRONT BEARING
ELASTROMETRIC
SOFT MOUNT

*BOTH SUPPORTS CAN ACCOMODATE SPRING RINGS IN EVENT THEY ARE
NEEDED TO CONTROL BEARING SUPPORT STRUCTURAL SPRING RATE.

Figure 250. Alternate Lower Spring Rate Shaft Supports.

336

	DESIGN AS SHOWN (HARD MOUNTS)	ALTERNATE CONFIGURATION (SOFT MOUNTS)
FRONT SPRINGRATE	60,000 TO 75,000 LBS/IN. (ESTIMATED)	3,700 LBS/IN. (DESIGN VALUE)
REAR SPRINGRATE	100,000 TO 200,000 LBS/IN. (ESTIMATED)	10,000 LBS/IN. (DESIGN VALUE)
1ST CRITICAL	16,000 TO 20,000 RPM	BELOW 9,000 RPM
MARGIN, UNDER 33,060 RPM NORMAL OPERATING SPEED	40% TO 52%	OVER 73%
2ND CRITICAL	23,000 TO 27,000 RPM	BELOW 9,000 RPM
MARGIN, UNDER 33,060 RPM NORMAL OPERATING SPEED	18% TO 30%	OVER 73%
3RD CRITICAL	43,000 RPM	43,000 RPM
MARGIN, OVER 33,500 RPM MAXIMUM OPERATING SPEED	28%	28%

27363

THE CRITICAL SPEEDS ARE BASED ON THE FOLLOWING VALUES OF CALCULATED ROTOR-SHAFT PIN JOINT STIFFNESS: K_{RADIAL} = 640,000 LBS/IN., K_{MOMENT} = 512,000 LBS/IN.

Figure 251 . 506-2X Critical Speed Summary.

TURBINE ROTOR
BALANCE RING

SHAFT SUPPORTED AT
BEARINGS JOURNALS

27084 A

BALANCING SET SCREWS

AXIAL COMPRESSOR
BALANCING STOCK
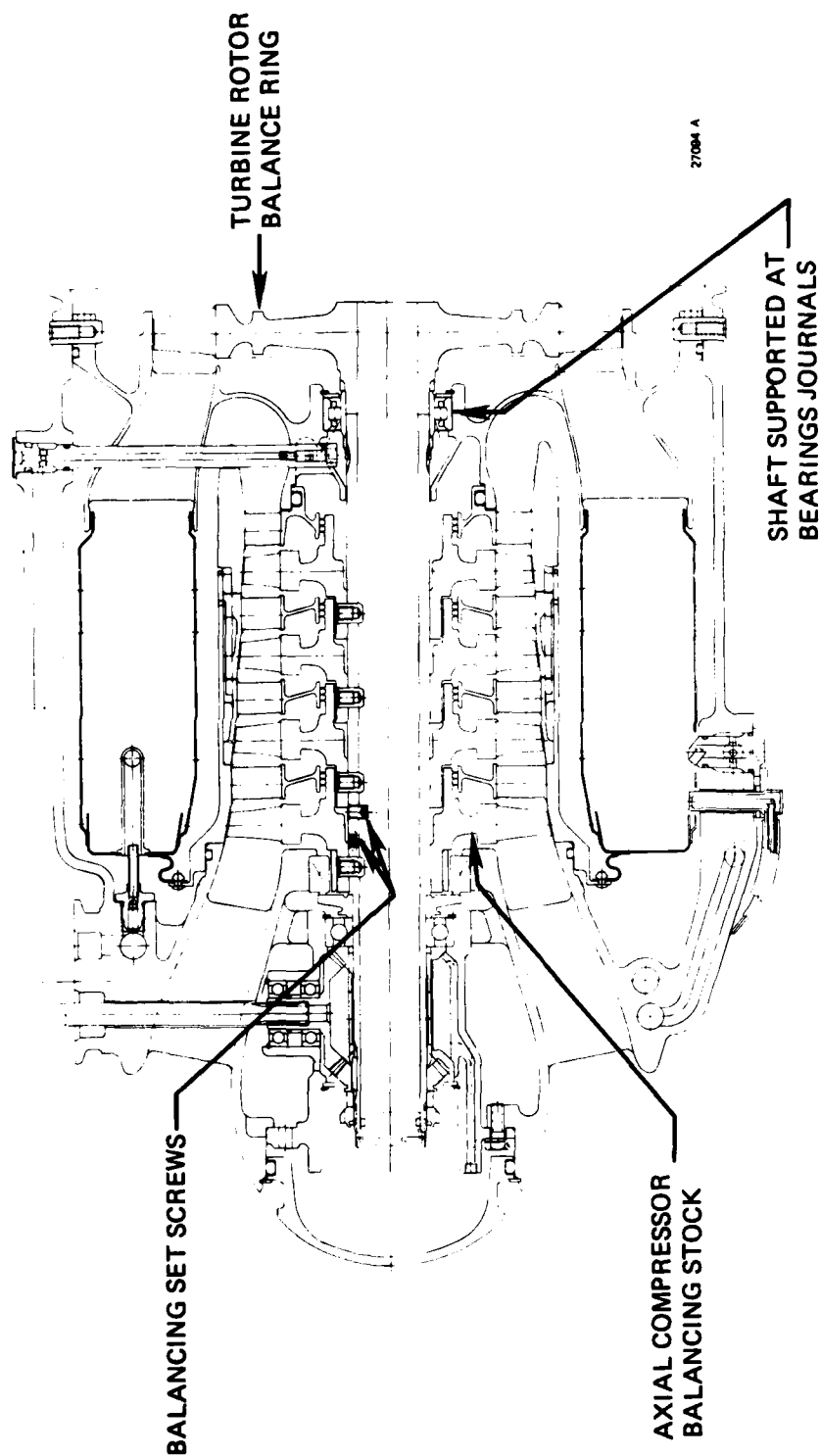
TURBINE SHAFT: BALANCED BY STOCK REMOVAL AT TURBINE ROTOR AND BY
RADIAL POSITION OF SET SCREWS. BALANCING LIMITS: 0.005 OZ. IN.

TURBINE & COMPRESSOR: BALANCED BY STOCK REMOVAL ON AXIAL COMPRESSOR.
SHAFT ASSY.   BALANCING LIMITS: 0.007 OZ.   27397

Figure 252.   E.G. Main Shaft Balancing Procedure.
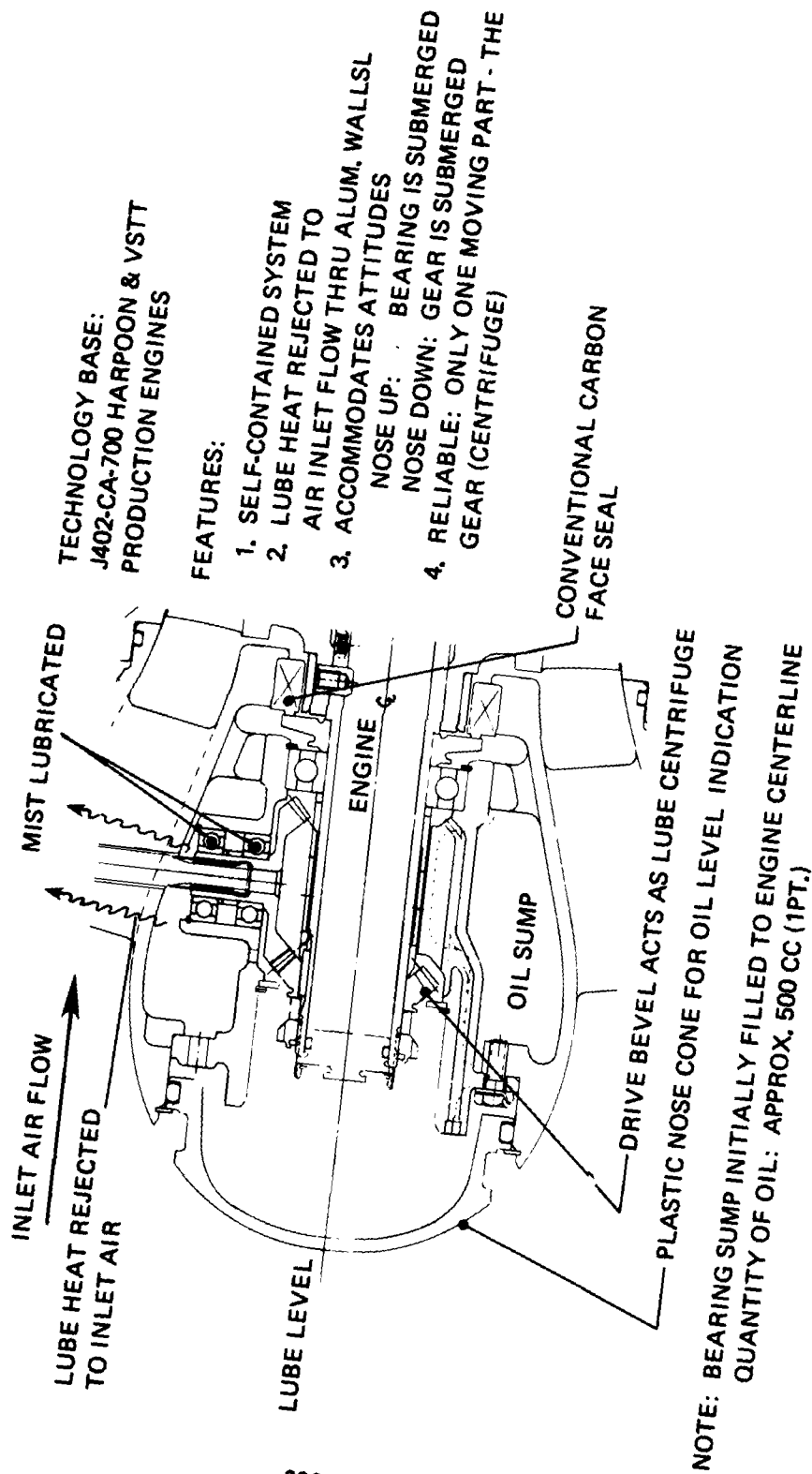
TECHNOLOGY BASE:
J402-CA-700 HARPOON & VSTT
PRODUCTION ENGINES

FEATURES:

1. SELF-CONTAINED SYSTEM
2. LUBE HEAT REJECTED TO AIR INLET FLOW THRU ALUM. WALLSL
3. ACCOMMODATES ATTITUDES
   NOSE UP: BEARING IS SUBMERGED
   NOSE DOWN: GEAR IS SUBMERGED
4. RELIABLE: ONLY ONE MOVING PART - THE GEAR (CENTRIFUGE)

INLET AIR FLOW

LUBE HEAT REJECTED TO INLET AIR

MIST LUBRICATED

ENGINE ₵

CONVENTIONAL CARBON FACE SEAL

LUBE LEVEL

OIL SUMP

DRIVE BEVEL ACTS AS LUBE CENTRIFUGE

PLASTIC NOSE CONE FOR OIL LEVEL INDICATION

NOTE: BEARING SUMP INITIALLY FILLED TO ENGINE CENTERLINE
QUANTITY OF OIL: APPROX. 500 CC (1PT.)

27400.

Figure 253 . Gasifier Thrust Bearing Lubrication System.

339

The front bearing absorbs the shaft thrust; its unique fractured outer ring feature was selected to provide a higher capacity ball complement than the conventional Conrad type of the same size while avoiding the inherent high cost of the split inner race design normally employed in turbine main shafts applications. The fractured outer rings permit the use of a single-piece machined ball retainer (not riveted) made of high strength steel plated silver; the retainer is outer-ring-guided for optimum lubrication characteristics. Salient features of the bearings are shown in Figure 254.

The rear bearing fuel lubrication system (Figure 255) derives its technology from the J402 VSTT engine. Fuel at pump discharge pressure flows through the main frame cored passages to the fuel lube tube. A high ΔP flow restrictor reduces the fuel pressure at the fuel jet inlet. The low pressure differential across the jet permits control of fuel lube flow in the range of 140-160 cc per minute. Low values of ΔP also allow use of a relatively large jet diameter (0.02 in), reducing the chance of jet plugging through fuel carbonization at shut down.

Fuel is injected in the bearing, aided by the fourth stage axial compressor labyrinth seal air leakage. The expended fuel/air mixture then flows radially outward to mix with the main gas stream. Approximately two-thirds of the above quoted fuel flow is required to lube the bearing. The other one third is necessary to maintain a rich fuel/air mixture to preclude self ignition.

The rear shaft roller bearing design is patterned after its VSTT counterpart. It features a wide, shoulderless inner race, lengthened to accommodate axial tolerance stack-ups and differential thermal expansion between shaft and structure. The roller complement and retainer construction are designed primarily to enhance high speed capability rather than load capacity, since the radial loading imposed by maximum shaft unbalance (and maneuvering forces) is a small fraction of the basic bearing capacity. Salient features of this bearing are summarized in Figure 256.

5.4.5 Accessory Drive

The accessory drive originating bevel gear set and vertical drive shaft are designed to the following requirements:

1.	Starter Output Torque - in/lbs	84
2.	Starter-to-Engine Speed Ratio	0.625
3.	Starter Cut-Out Speed - rpm	10,000
	at Engine Speed - rpm	16,000
4.	Continuous Accessory Drive Load - hp	3
	Fuel Pump Drive - hp	1
	Alternator Drive - hp	2
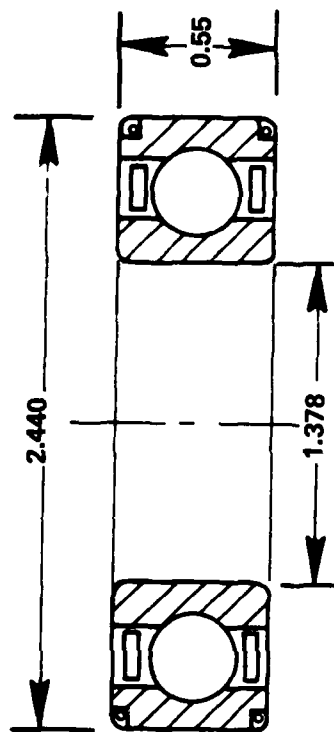
TYPE: BALL

BASE SIZE: 107

SPECIAL FEATURES: FRACTURED OUTER RING, OUTER RING RIDING RETAINER

MATERIALS: INNER AND OUTER RINGS
 SAE 52100 SIL (VACUUM DEGASSED)
 HARDNESS: RC 60 MIN.

 BALLS
 SAE 52100 STL (VACUUM DEGASSED)
 HARDNESS: RC 60 MIN.

 RETAINER
 AMS 6415 STL, ONE PIECE MACHINED, SILVER PLATED

DN: 1.17×10^6

BIO LIFE: +10,000 HRS. BASED ON 150 LB. THRUST LOAD AND
 100 LB. RADIAL UNBALANCE

TOLERANCE CLASSIFICATION: ABEC-5

25552

Figure 254. Expendable Gasifier Shaft Thrust Bearing Specifications.

341

TECHNOLOGY BASE:
J402-CA-700 (VSTT)
PRODUCTION ENGINE

FUEL LUBE TUBE

FEATURES:
1. SELF-CONTAINED SYSTEM
2. UNLIMITED LUBE SUPPLY
3. INSENSITIVE TO ENGINE ATTITUDES
4. RELIABLE: NO MOVING PARTS

EXPENDED FUEL

REAR BEARING

FUEL FROM
PUMP DISCHARGE

AIR FLOW

FLOW RESTRICTOR

FUEL JET

25569
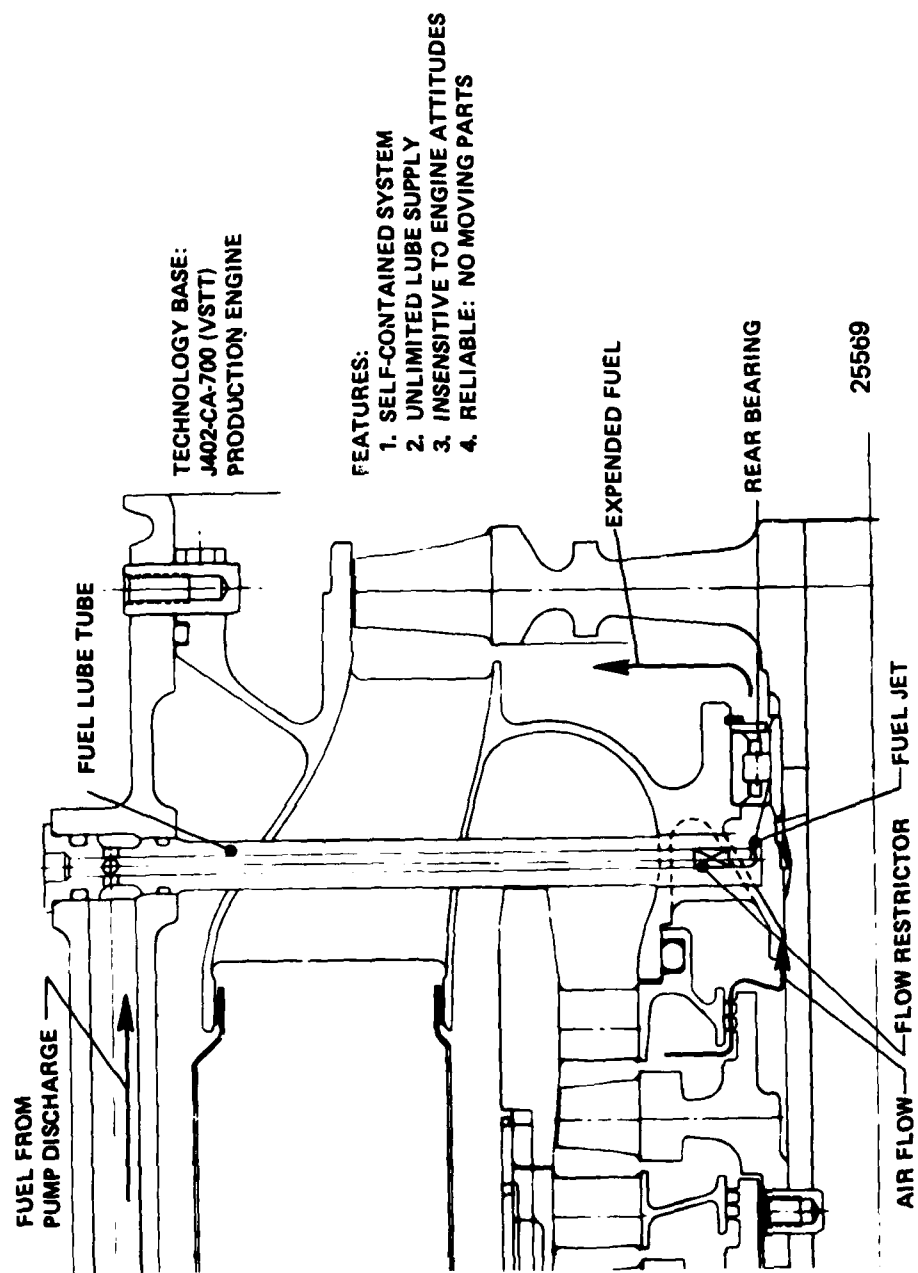
Figure 255. Gasifier Rear Bearing Lubrication System.

342
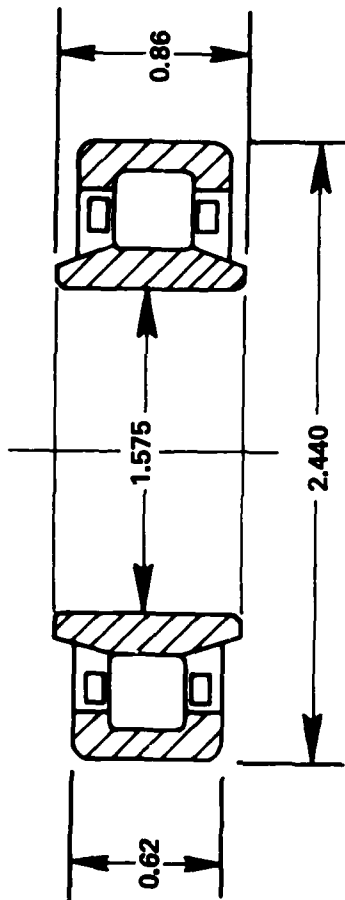
TYPE: ROLLER

BASIC SIZE: R1908

SPECIAL FEATURES: OUTER RING RIDING RETAINER, EXTENDED INNER RING

MATERIALS:

INNER AND OUTER RINGS
CEVM M-50 TOOL STEEL
HARDNESS: RC 60 MIN.

ROLLERS
CEVM M-50 TOOL STEEL
HARDNESS: RC 60 MIN.

RETAINER
AMS 6414 STL, RC 30-38, ONE PIECE MACHINED,
SILVER PLATE

DN: 1.34×10^6

BIO LIFE: +10,000 HRS. BASED ON A 100 LB. RADIAL UNBALANCE

TOLERANCE CLASSIFICATION: RBEC-5

25553

Figure 256. Gasifier Shaft Rear Bearing Specifications.

343

Both bevels are supported by bearings located in a single housing assuring gear tooth alignment (Figure 257). The gears are designed for unlimited life; a misalignment derating factor of 1.5 has been imposed to account for the overhung mounting of the gear set, i.e., the calculated applied tooth lead is increased by 50 percent to account for the overhung mounting. Notwithstanding, the derating factor, the bevel gear set with the specified material, processing and tolerances will exceed all life requirements (Figure 258).

The gears were originally designed to be the coneflex type: straight tooth, carburized, but not ground. In the procuring process, however, it was found that the normally higher cost Zerol type (ground carburized tooth) was cost competitive when the higher coneflex tooling was factored in. A decision was reached to select the higher reliability Zerols for the demonstrator phase. These higher precision gears will be capable of withstanding the protracted starting mode that may be encountered in the process of developing the gasifier starting cycle at initial assembly. The lower cost (when produced in quantities) coneflex gears can be re-introduced in the engineering development phase.

The accessories anticipated for the Model 206 Jet Fuel Starter are shown in Figure 259 .

5.4.6 Structural Components

The unique annular folded combustor design surrounding the compressor permits extending the main frame rearward, reducing the number of principal structural components to two: the main frame and the turbine inlet nozzle.

The mainframe aluminum sand casting is the expendable gasifier principal structural component. Its unitized construction is designed to perform a multitude of functions (Figure 260) reducing overall cost by eliminating separate, bolted-together parts. External lines prone to leakage and damage through handling are supplanted by internal cored passages. QAD flanges are used to permit quick attachment of the accessory gear unit and power modules.

RR350 (AMS 4225) aluminum has been selected for the frames slated for the compressor rig and the demonstrator. RR350 exhibits higher creep strength than the original choice C 355 aluminum at temperatures above 400°F (Figure 261). RR350 will also provide a higher yield strength safety factors (Figure 262) at the higher temperatures that may be encountered at the frame-to-turbine inlet nozzle joint. The foundry has stated that they are pouring RR350 aluminum and do not anticipate any difficulties casting it with the existing pattern equipment.

The single-piece, turbine inlet nozzle precision casting (Figure 263) is made from N155, an alloy easily cast and capable of being weld repaired (increasing foundry yield). The nozzle, like the main frame, is designed to perform a number

344

N = 31,993 RPM

31 TEETH

30 TEETH

N = 33,060 RPM
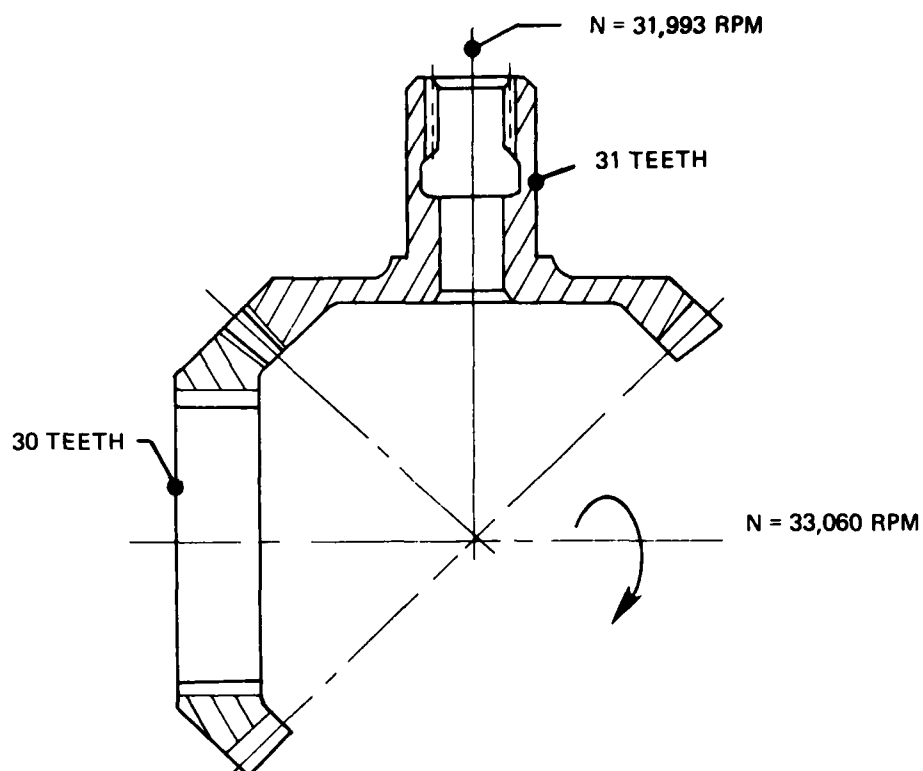
TYPE: ZEROL - CARBURIZED GROUND TEETH
MATERIAL: AMS 6272 STL
DIAMETRAL PITCH: 14

*STRESS:

MAX. TOOTH ROOT BENDING STRESS	12,240 PSI
ALLOW STRESS FOR UNLIMITED LIFE (400°F)	21,000 PSI
MAXIMUM HERTZ CONTACT STRESS	145,900 PSI
ALLOW STRESS FOR UNLIMITED LIFE (400°F)	180,000 PSI
SCORING INDEX	
MAX. STARTING LOAD	273°
MAX. CONT. OPERATING LOAD	451°
ALLOW SCORING INDEX	
MIL-L-7808	500°
MIL-L-23699	550°

27391

*NOTE: THE GEAR STRESSES ARE CALCULATED UNDER WORST LOAD
CONDITIONS (STARTING CYCLE); - NORMAL ACCESSORY
OPERATING STRESSES ARE APPROX. 25% OF THESE VALUES.

Figure 257. Accessory Drive Bevel Gear Set.

27396

FULL FLOATING
DRIVE SHAFT

DRIVE BEVEL
GEAR SET

DRIVE GEAR ACTS
AS LUBE PUMP

GEAR SET SUPPORT
(HOUSES BOTH GEARS,
BEARINGS, ASSURING
ALIGNMENT)

Figure 258. Accessory Drive Bevel Gears.

346

IGNITION EXCITER

FUEL SYSTEM MANAGEMENT
CONTROL (FSMC)

ALTERNATOR

27370

FUEL
PUMP

HYDRAULIC MOTOR

ELECTRICAL
INTERFACE
CONNECTOR

Figure 259. Model 206 Jet Fuel Starter Accessories.

347

FUEL LUBE TO REAR BEARING

QAD REAR FLANGE

TIN FLANGE SUPPORT

MAIN FUEL MANIFOLD
AND NOZZLE BOSS

ACCESSORY DRIVE
QAD FLANGE

COMBUSTOR CASING

BEVEL GEAR
HOUSING FLANGE

FRONT BEARING LUBE
SUMP SEAL BORE

AIR INLET FLOWPATH

E.G. MOUNT BOSSES

IGNITOR BOSS

STARTING FUEL
NOZZLE BOSS

23333

348
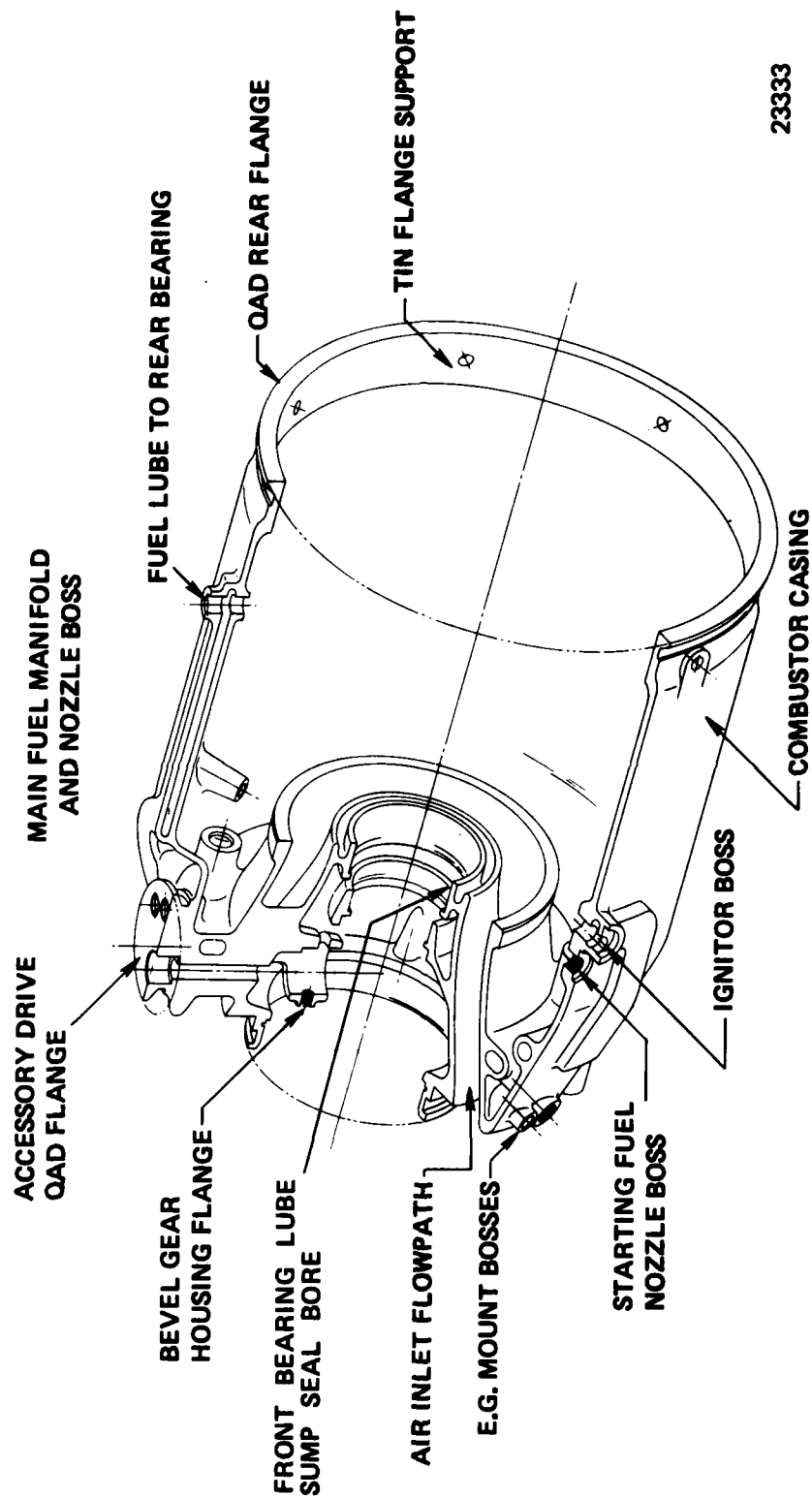
Figure 260 . Expendable Gasifier Main Frame.

STRESS TO PRODUCE 0.2% CREEP IN 100 HOURS FOR C-365 AND
RR-350 ALUMINUM ALLOYS
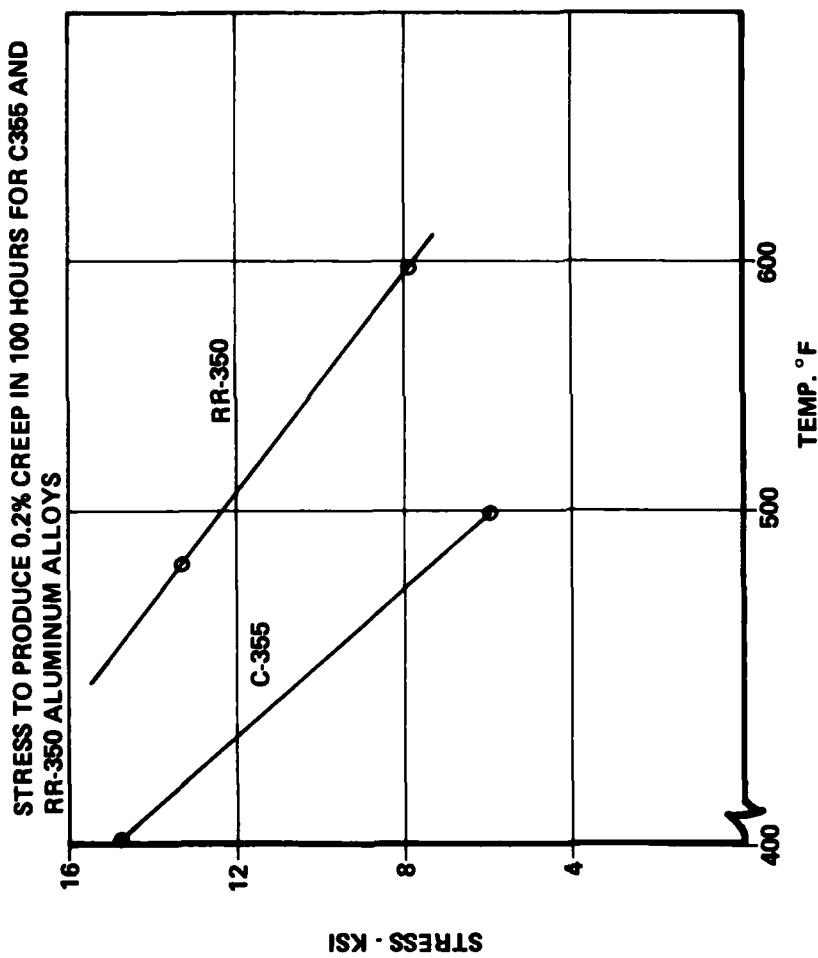
CREEP STRESS SAFETY FACTOR @ 500°F
& 1000 PSI APPLIED HOOP STRESS

MATERIAL	CREEP STRENGTH		SAFETY FACTOR	DATA SOURCE	
C-365 ALUM (AMS 4215)	6,000 PSI	1	6:1	1	AEROSPACE STRUCTURAL METALS HANDBOOK
RR-350 ALUM (AMS 4225)	12,000 PSI	2	12:1	2	HITCHCOCK IND. (HIGH DUTY ALLOYS LTD)

26095

Figure 261. Gasifier Main Frame Operating Creep Stress.

349

1. AS A PRESSURE VESSEL: $S = \dfrac{PR}{T} = \dfrac{30 \times 6.3}{0.20} = <1000$ PSI

YIELD STRENGTH SAFETY FACTOR AT 500°F

MATERIAL	YIELD STRENGTH 100 HRS @ 500°F	SAFETY FACTOR	DATA SOURCE
C355 ALUM (AMS 4215)	8,000 PSI (TYP)	8:1	AEROSPACE STRUCTURAL METALS HANDBOOK
RR350 ALUM (AMS 4225)	20,000 PSI (TYP)	20:1	HITCHCOCK INDUST. (HIGH DUTY ALLOYS LTD)

26083
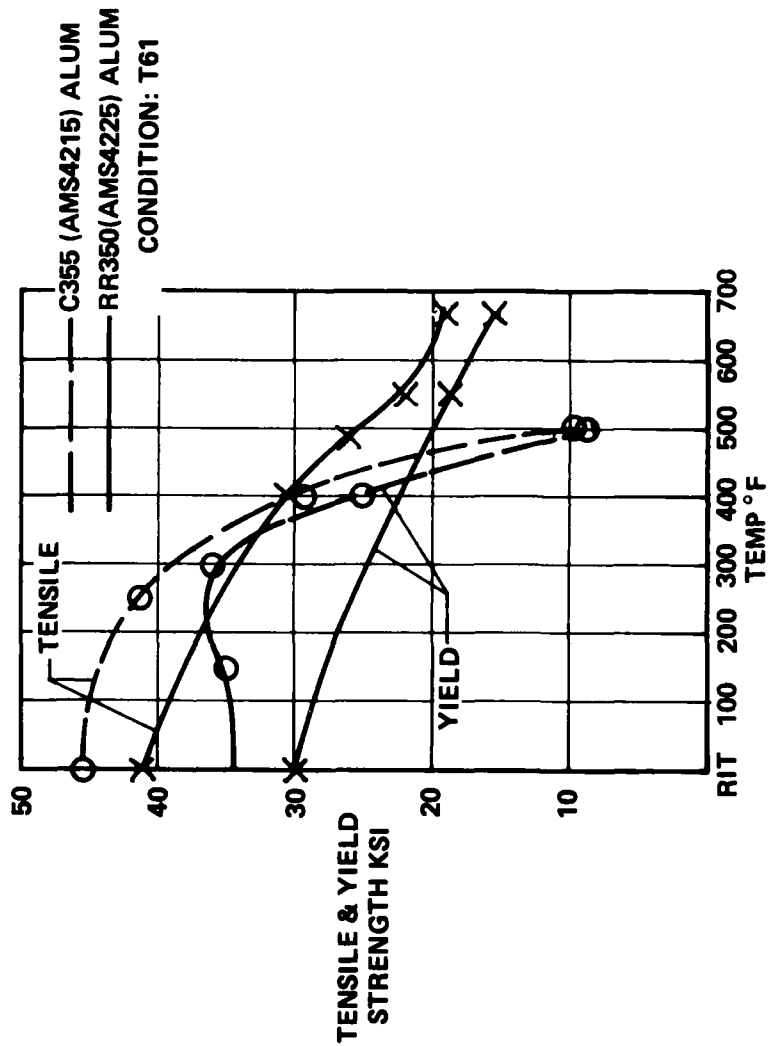
Figure 262 . Gasifier Main Frame Operating Stress Level.

350

NOZZLE MATERIAL: INVESTMENT CAST N-155

T.I.T.: 1800°F

13 VANES
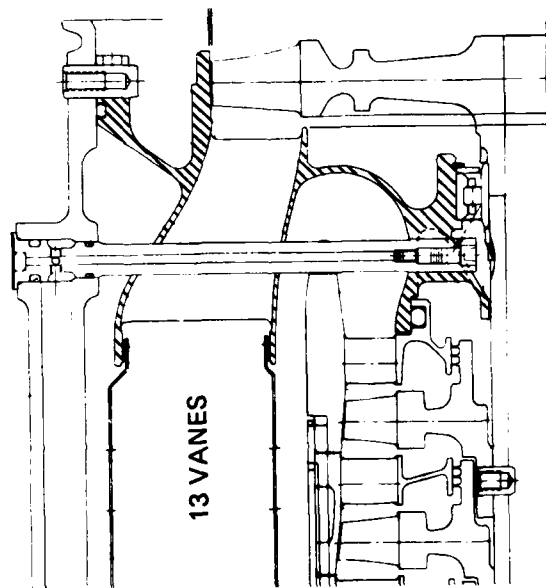
LOCATION	MAX. ESTIMATED TEMP. - °F	MAT'L PROPERTIES, KSI		COMMENTS
		ULTIMATE	0.2% YIELD	
VANE T.E.	1800	20	10	POST INSPECTION OF NOZZLE USED IN COMBUSTOR RIG HAS DISCLOSED NO STRUCTURAL PROBLEMS.
INNER SHROUD	1800	20	10	
OUTER SHROUD	1780	21	11	

27381

Figure 263. Gasifier Turbine Inlet Nozzle.

351

of functions. Besides its basic function of impinging combustion gas into the turbine blades, the nozzle houses the shaft rear bearing, supports the combustor, shrouds the turbine and transfers the bearing loads to the main frame through six radial pins. The latter accommodate the differential thermal expansion between the nozzle and the aluminum frame while maintaining shaft centrality. The thirteen hollow vanes provide the air path for the combustor outer shell, improving nozzle life by lowering vane wall temperature. No structural defects were detected in the nozzle used in the combustor development rig program. Rig testing subjected the nozzle to relatively stringent conditions imposed by the large temperature gradients encountered in combustor development.

5.4.7 Structural Verification

To assure material physical properties compliance, one casting from each master heat is sectioned and test bars are extracted by the foundry from one half of the casting (Figure 264). Test results are then corroborated by Teledyne CAE's metallurgical laboratory on the remaining sectioned casting. In the specific case of the aluminum axial compressor where the blade material physical properties are of paramount concern, each lot pour must be accompanied by flat test specimens that simulate blade thickness. These flat specimens are heat treated along with the casting lot and tested. The turbine rotor is subjected to room and elevated temperature tensile tests. In addition, time-at-load and temperature stress rupture tests are conducted (Figure 265).

Both the axial compressor and turbine rotors tensile centrifugal structural integrity will be verified in Teledyne CAE's spin pit test facilities (Figures 266 and 267). Both rotors will be spun to 120 percent speed.

The Teledyne CAE evacuated spin chamber will accept rotors up to 30 inches in diameter and provide for spinning components to speeds in excess of 65,000 rpm. The spin chamber is housed in an environmentally controlled room which provides ambient temperature control when conducting rotating brittle lacquer tests. The spin pit can achieve a vacuum of 0.05 in. of Hg (Abs) within a period of 15 minutes.

The rotating component is attached to a spin arbor that hangs vertically from the air-turbine drive motor mounted externally on the top of the spin pit cover lid. An upper and lower catcher arrangement restrains the rotor-arbor system if unbalance forces exceed the load-carrying capability of the air turbine motor's quill. This system provides for a coast-down of the rotor-arbor system, preventing damage to the test piece. Figure 268 (left picture) shows a test rotor installed on the spin chamber lid prior to being lowered into the spin chamber.
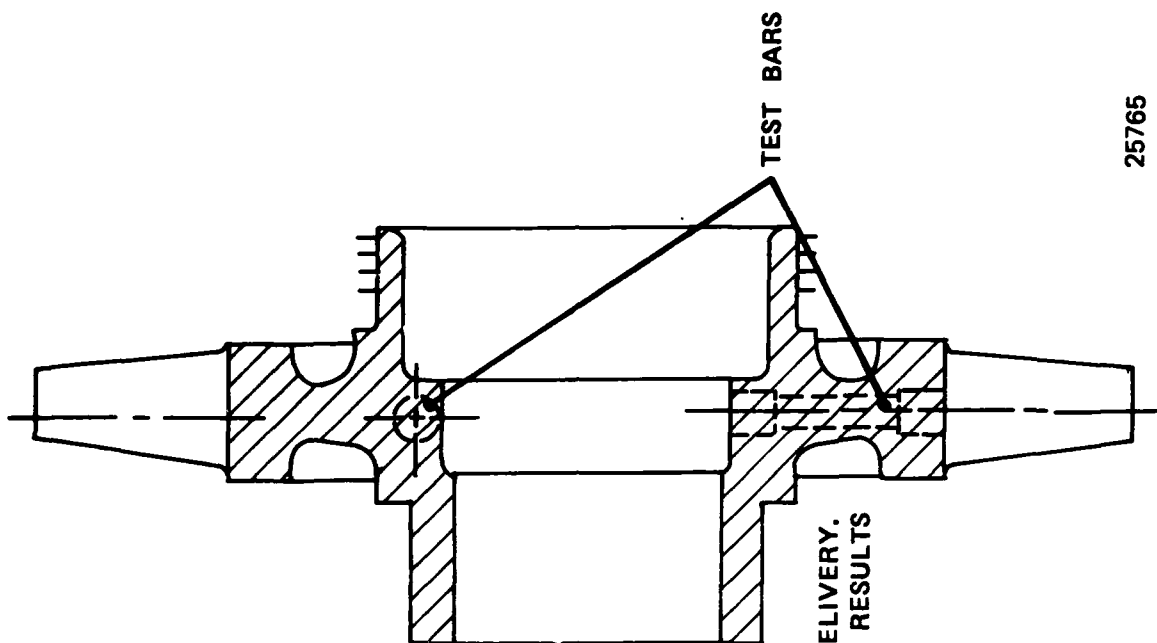
TEST BARS

FOUNDRY VERIFIES MATERIAL PRIOR TO CASTING DELIVERY.
TCAE METALLURICICAL LAB SUBSTANTIATES SOURCE RESULTS
ON REMAINING HALF OF SAME SAMPLE CASTING.

25765

Figure 264. Gasifier Compressor Material Properties Verification.

353

TELEDYNE CAE METALLURGICAL LAB TESTS CORROBORATES
ROTOR FOUNDRY TEST RESULTS

TEST BARS ARE MACHINED FROM
SECTIONED SAMPLE CASTING

TENSILE TEST AT ROOM AND ELEVATED
TEMPERATURES
(LAB FACILITIES CAPABILITY TO 1800°F)
STRESS RUPTURE (TIME AT LOAD & TEMP)
UP TO 1800°F

1800° STRESS
RUPTURE

25766

ROOM TEMP TENSILE
TEST SPECIMEN
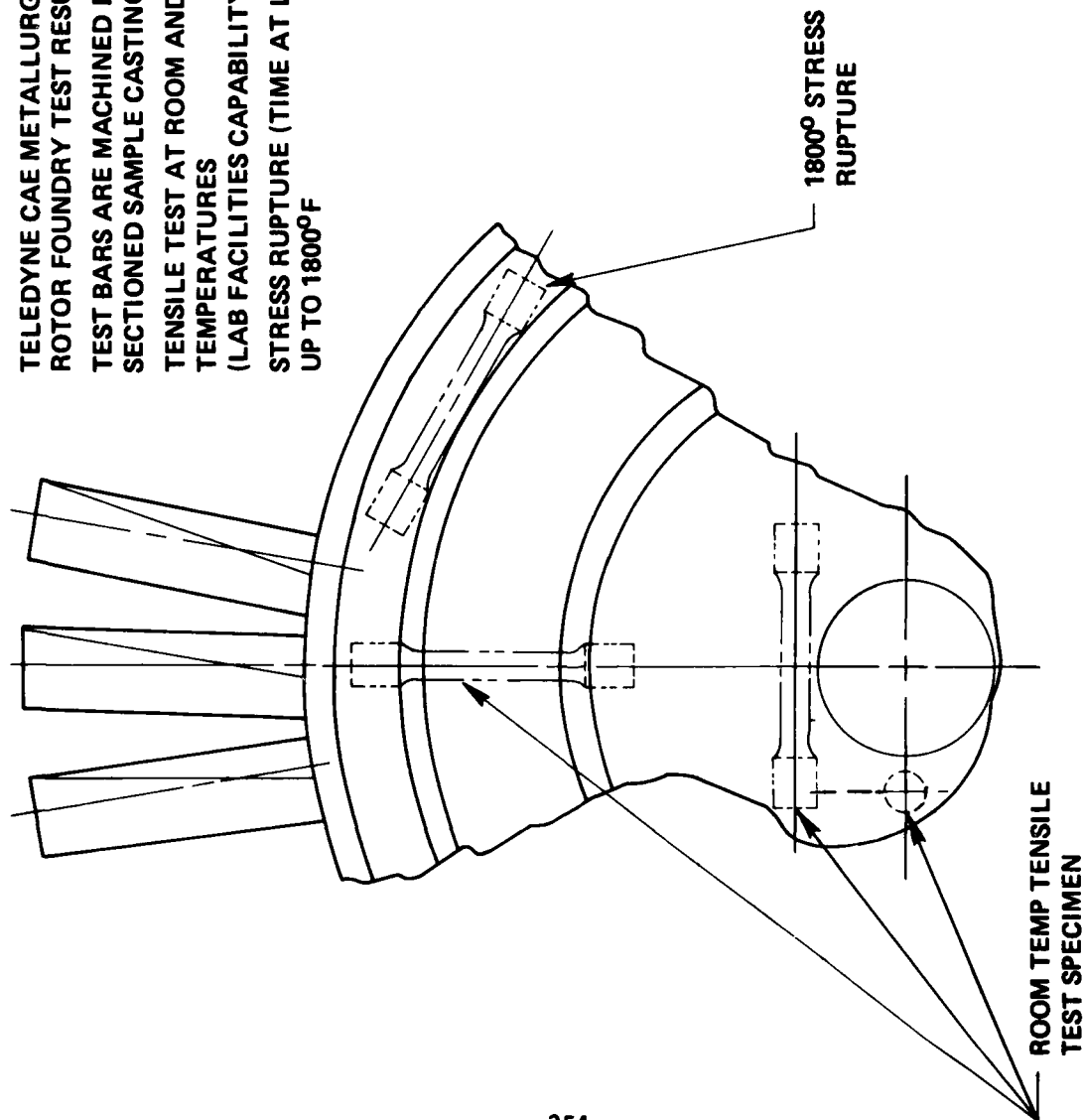
Figure 265. Gasifier Turbine Rotor Structural Testing.

354

SPIN ARBOR "CATCHER"

SPIN ARBOR

FIRST STAGE AXIAL COMPRESSOR

COMPRESSOR DRIVE PIN

SPIN ARBOR DRIVE END

25768
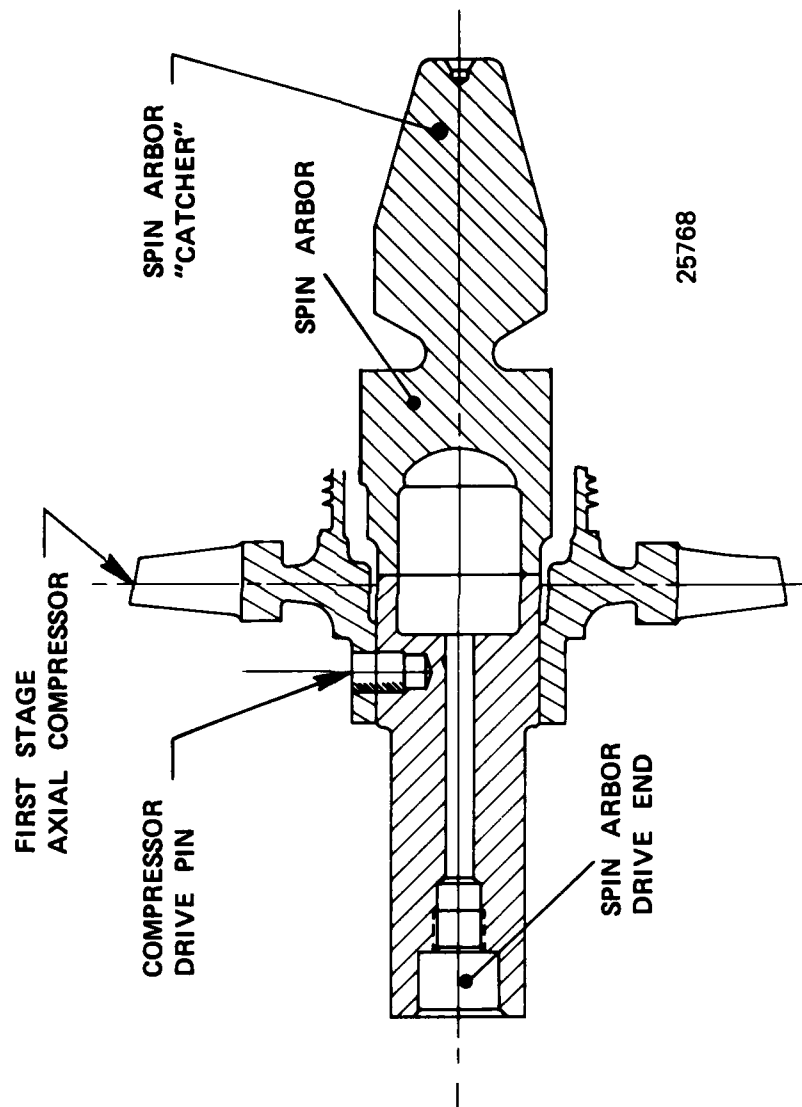
Figure 266. Gasifier Compressor Spin Test.

355

26075

SPIN ARBOR ELECTRON BEAM
WELDED TO ROTOR (JOINT
IDENTICAL TO E.G. SHAFT)

SPIN ARBOR
DRIVE END
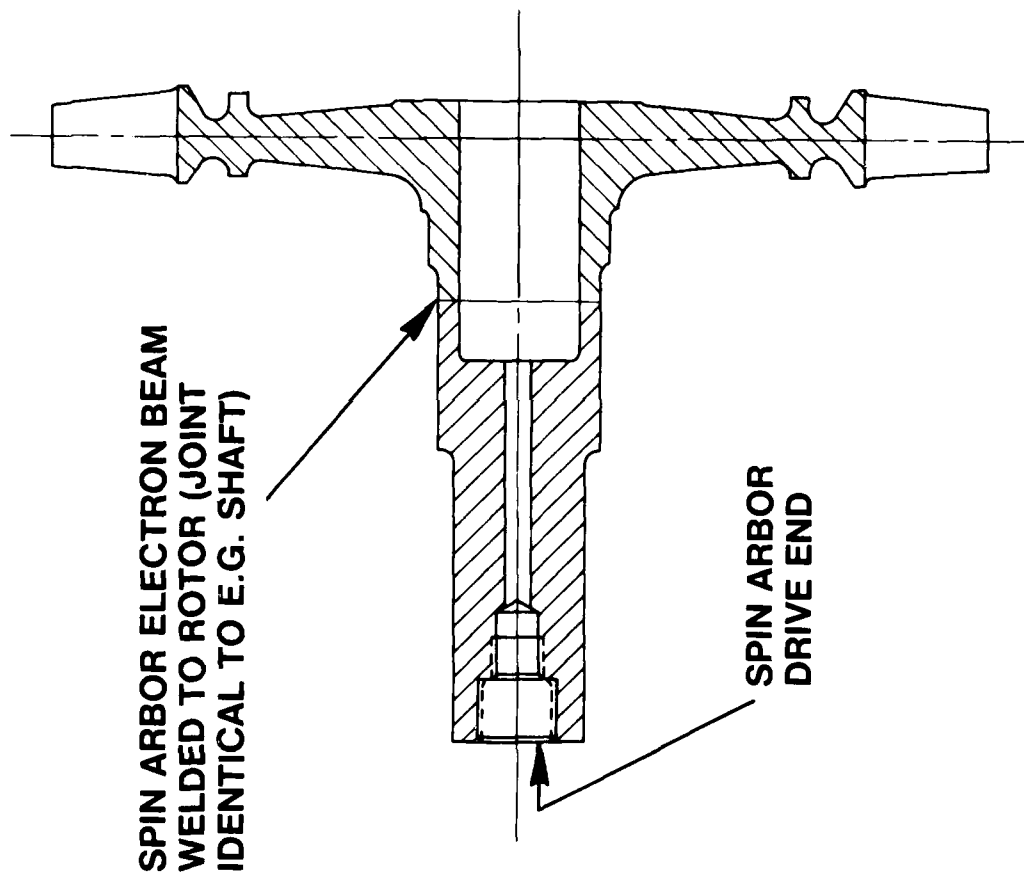
Figure 267. E.G. Turbine Rotor Spin Test.

356

COLD SPIN TEST FACILITY
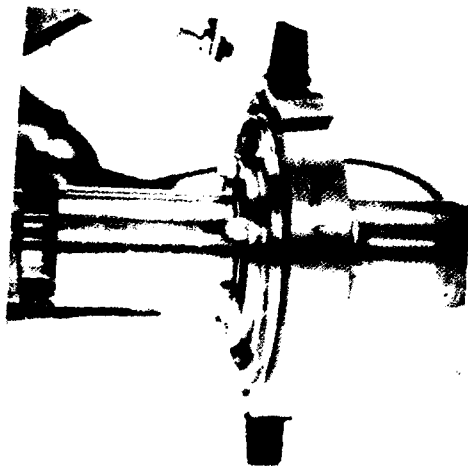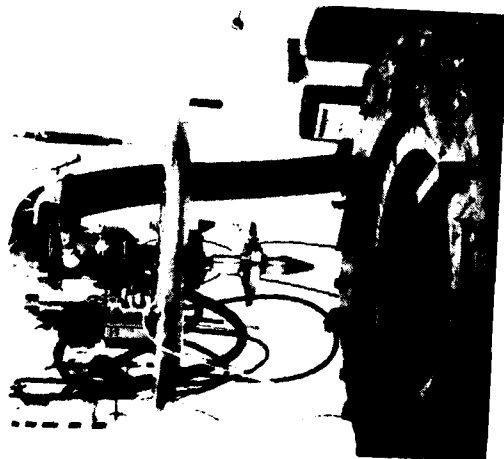
ACCOMMODATES ROTORS UP TO 30 INCHES IN DIAMETER

SPINS ROTORS TO SPEEDS IN EXCESS OF 65,000 RPM

ENVIRONMENTALLY CONTROLLED FOR CONDUCTING BRITTLE LACQUER TESTS

PROVISIONS FOR MOUNTING SLIP RINGS TO TRANSMIT STRAIN GAGE SIGNALS FROM ROTATING COMPONENTS AT SPEEDS UP TO 60,000 RPM

25771

Figure 268. Gasifier Rotors Testing.

Holographic interferometry has become a valuable tool in determining the natural frequencies and mode shapes of gas turbine blades. Both axial compressor and turbine rotor blades will be subjected to holographic interferometry to substantiate the blades analytically predicted vibratory modes. Teledyne CAE currently has on order a holographic system. In the event this system is not available in time, it is anticipated that holographic testing will be performed at WPAFB.

In the event that compressor blade vibration problems are encountered in the compressor rig development program, the basic rig hardware has been designed to accommodate a 40-channel slip ring (Figure 269). This device, a proven liquid cooled design, is on hand.

BASIC RIG HARDWARE WILL ACCOMMODATE SLIP RING

SLIP RING UNIT (ON HAND)   SLIP RING DRIVE SHAFT

25767
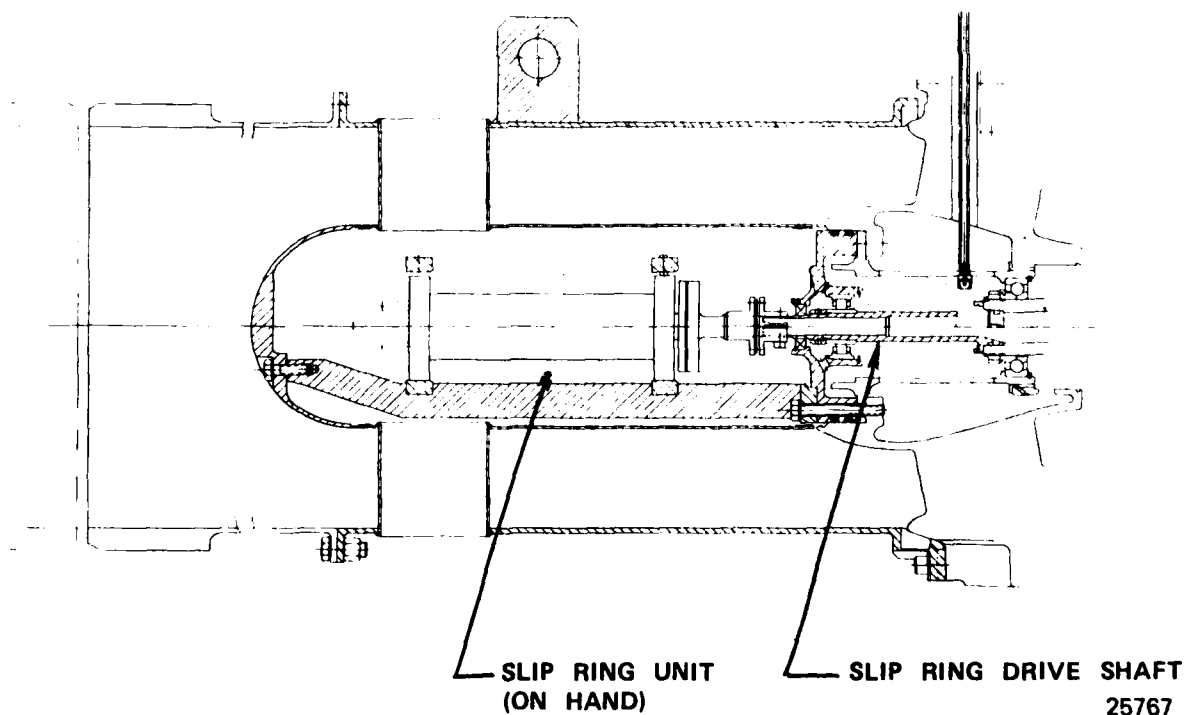
Figure 269 . Gasifier Compressor Rig Slip Ring Design.

5.5   CONTROL SYSTEM DESIGN

5.5.1   System Overview

The expendable gasifier subsystems have been functionally integrated to produce a system which is self-sufficient; operates automatically; is inherently simple; requires a minimum of aircraft/starter interfaces; and incorporates system safety features.

The EG starter/JFS operation is initiated by actuating the airframe hydraulic accumulator shut-off-valve which allows the JFS hydraulic motor to drive the gasifier shaft and its associated gearing. This action provides four key functions: AC power for the ignition excitor; DC power for system management (P & D valve actuation); fuel flow and gasifier shaft rotation. Hence, one interface with the airframe is needed to initiate and sustain EG operation. (The fuel tank shut-off-valve is normally open and is closed for EG removal from the aircraft.)   Figure 270 shows a system schematic.
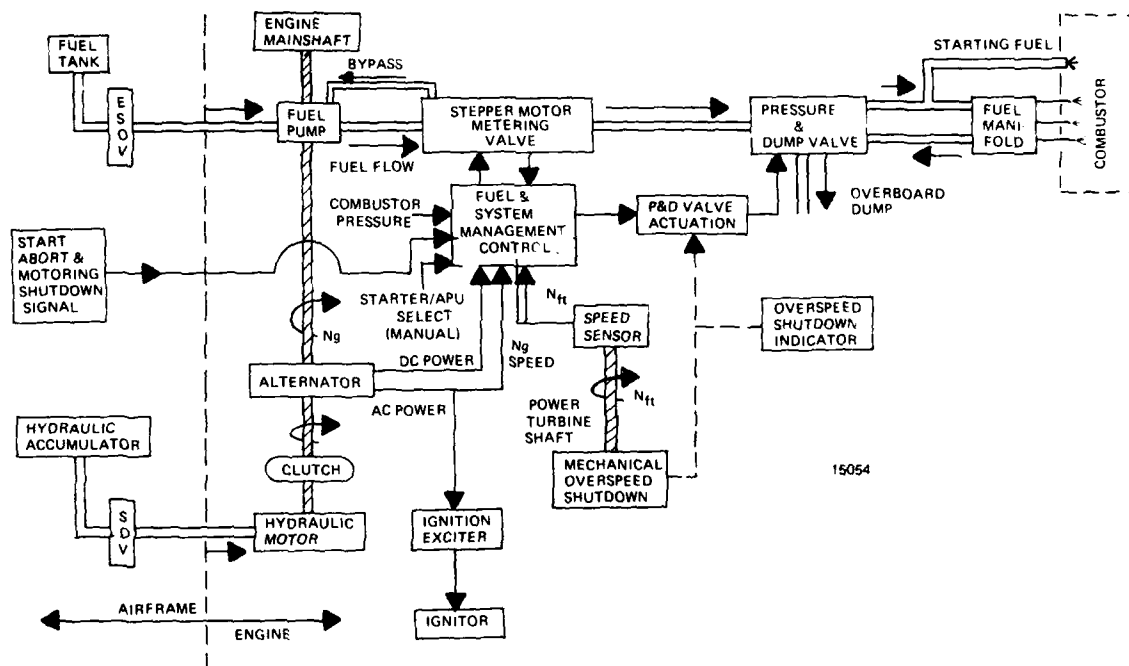
Figure 270.   Control and Subsystem Operation.

359

The EG is started and accelerated automatically by the fuel metering and control logic in combination with the continuously supplied starting fuel and ignition energy.

The system management control (SMC) is a simple logic network which actuates the pressurizing and dump (P & D) valve. The P & D valve is energized (using alternator DC power) to allow fuel to flow to the engine and to close the fuel manifold drain when the gas generator has reached 10 percent speed. The P & D valve remains energized for all engine operation. The system management control also receives signals which cause the EG to be shut-down.

The EG may be shut-down by four methods, two of which enhance the system safety. In normal operation the SMC monitors power turbine speed and de-energizes the P & D valve when the power turbine reaches 100 percent speed; a mechanical overspeed switch will de-energize the P & D valve should the SMC speed monitor become inoperative; start abort and motoring (no main engine light-off) shut-off may be commanded from the aircraft cockpit by means of an electrical logic signal to the SMC which will override all other inputs. The P & D valve will be de-energized in the event of alternator power loss.

All shutdown commands are reset automatically so that no specific action is required prior to initiating another start. If the EG was shut-down due to a power turbine overspeed, a mechanical indicator is set so that diagnostic action may be initiated.

The system management control function will be expanded to include all fuel scheduling and actuation functions for both the starting mode and the APU mode. The operational mode will be selected by a manual input (switch) on the EG control system. All internal control functions will automatically be selected by this action.

No additional aircraft control interfaces are required to implement the APU option and no starter system features such as self-sufficiency and shut-down control are lost.

5.5.2 Fuel and System Management Control

A system trade study was conducted to determine the most cost effective system (electronic or hydromechanical) which can be utilized as the SMC. Because of the many functions required of the SMC in an F15/F16 type of application, the digital electronic control is a clear-cut choice for a system controller.

The electronic fuel and System Management Control (SMC) is an all digital unit with an 8 bit microprocessor as the central processing unit (CPU). This approach yields high flexibility, since system operation can be altered by software rather than hardware changes. The system can be easily expanded by adding new software, with no effect on the existing hardware.

EG operation is controlled by accepting inputs from the engine and cockpit and providing properly sequenced discrete outputs and fuel flow regulation. The basic functions performed by the controller are described below.

Start Sequencing The SMC logic computes the required start sequence as a function of gasifier speed and time. A typical sequence is as follows:

1.   0% Ngg - Starter On
2.   2% Ngg - Ignition Excitor On
3.   6% Ngg - Ignition Fuel On
4.   12% Ngg - Main Fuel Valve On
5.   30% Ngg - Ignition Fuel Off, Starter Off
6.   35% Ngg - Ignition Excitor Off

The SMC also monitors engine parameters to verify that a successful start has been accomplished; if not, the functions will be reset and another attempt made. If the EG is in the APU mode of operation, the sequence portion will pass authority to the appropriate power turbine control mode (constant speed or load control). If the EG is in the main engine start mode, power turbine speed monitoring will be accomplished to shutdown the gasifier when the correct power turbine speed has been obtained to ensure that the main engine has attained self-sustaining speed. If the EG is to be operated as an APU after main engine start, control authority will be switched to the APU mode after the main engine is decoupled.

Acceleration Fuel Scheduling Acceleration limiting is provided by a Wf/Pa schedule obtained by generation of the function Wf/P2 versus corrected gasifier speed (Figure 271). Steady state fuel flow is generated by the integral plus proportional compensated speed governor and is reset by the power turbine internal or external speed reference. Inter-turbine temperature limiting is provided by scheduling of ITTc, which is obtained by generation of the function ITTc versus corrected gasifier speed, and then comparing the actual ITTc to the computer value. The summation of these three signals results in a desired Wf/P2 θ which is compared against a minimum schedule to prevent combustor flame-out. The Wf/P2 θ is then conditioned by P2 at 0 to yield the desired fuel flow. This signal is amplified and used to position fuel metering valve.

Limiting The gasifier operation will be limited by mechanical speed (Ng), corrected speed (Ngc), and inter-turbine temperature (ITT). This limiting allows the gasifier to be operated at peak power output for all inlet conditions around the flight envelope. Typically, the Ngc limits will have authority at cold T2 inlet conditions and ITT at hot T2 inlet conditions.

Power Turbine Governing The power turbine is governed isochronously in response to an internal speed reference, an external speed reference or an external load error signal. Power is delivered up to the point at which any gasifier limit is reached. The power turbine governor, when referenced to a speed command input, will hold the commanded speed with $\pm$ 0.25 percent.

361
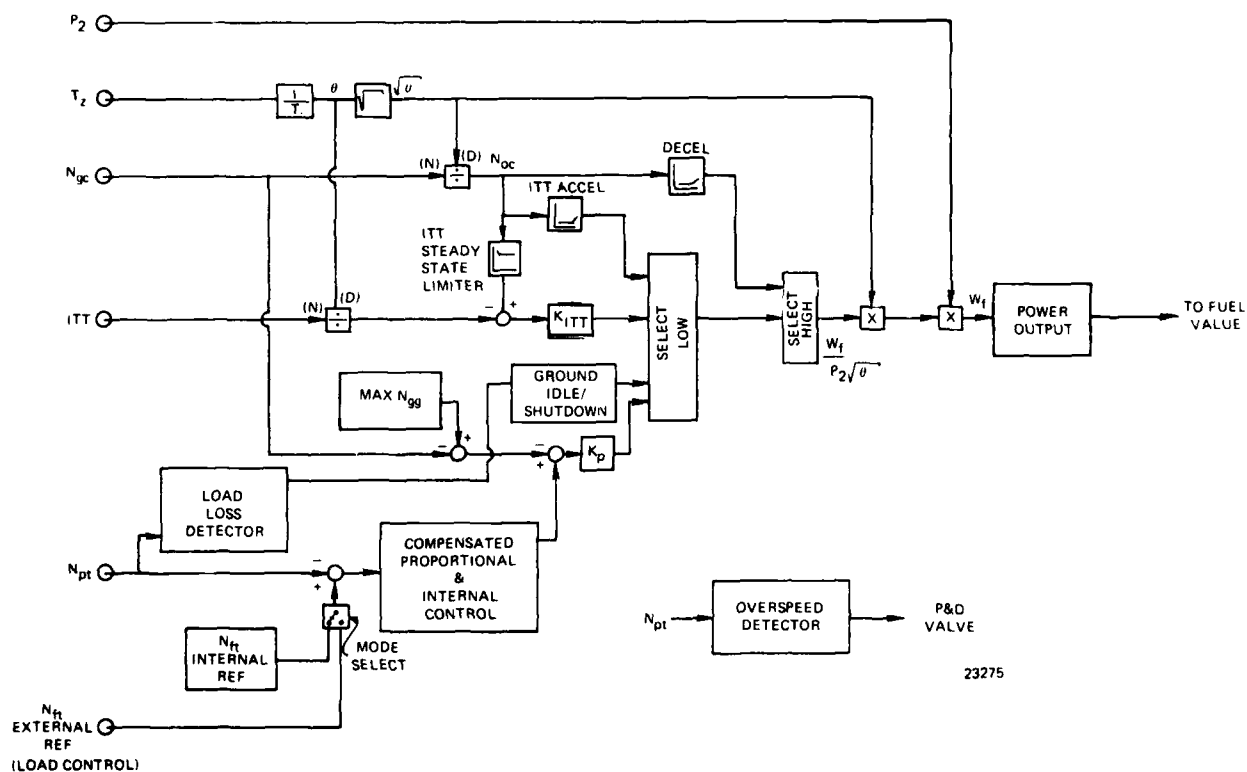
Figure 271. FUEL CONTROL ALGORITHM: The expendable gasifier's SMC provides all engine control and limiting functions as well as APU/JFS supervisory, test, and interface functions.

362

Power Turbine Overspeed Protection Power turbine overspeed is handled in a number of ways. The basic isochronous governor maintains power turbine speed (Np) over all normal operating loads. Npt as well as the rate of change of Npt is measured and a logic matrix load loss detector (generated based on these parameters) will either decelerate the gasifier to ground idle (no load speed) or rapidly shutdown the engine by actuating the P & D valve, thereby protecting the APU system while still allowing return to normal operation without, in many cases, a restart.

Self Test and Failure Reversion The software provides protection and failure reversion ability to the controller. Through the self-test, all engine sensors and certain key sections of the software program are continuously tested. If failure of a non-critical sensor (e.g. ITT) or program section is detected, the fuel metering valve is commanded to a safe condition (in the case of ITT failure, a gasifier speed that ensures the engine will not go over temperature). In the case of overspeed detection, the engine is shutdown or returned to ground idle. Two Npt magnetic pickups provide two Npt signals. If either pickup fails, the failure is annunciated and isochronous Npt governing and overspeed operate off the remaining Npt signal. If both Npt signals are lost, the engine is immediately shutdown. In addition to the continuous self-test, a test command from the cockpit will cause a check of the complete controller, including sensors and software. The test function may also be exercised from a ground test set which would have the capability to fault isolate within the control system.

SECTION 6.0

EXPENDABLE GASIFIER PHASE IV FABRICATION PLAN

6.1 Introduction

The ultimate objective of the expendable gasifier (EG) program was to provide the Air Force with a source of gas turbine power which achieves low cost by being discarded after its useful life and avoids the high costs associated with overhaul, iventory, parts accountability and other related costs. To achieve the low cost objective, considerable attention was given to the factors which effect low cost during design and system analysis. For example, multi-use capability for turbojets, turbofans and jet fuel starts was incorporated to exploit maximum production rate. A low pressure/temperature cycle was chosen to make maximum use of castings and inexpensive materials. Innovative design techniques were employed to achieve simplicity, reduce the number of components and relax the requirements for machining to small tolerances.

In order to realistically demonstrate the low cost features of the expendable gasifier considerable effort was expended with manufacturing engineering and subcontract vendors to produce demonstrator hardware using the actual manufacturing processes which would be used during full-scale production. Several items such as the cast aluminum main frame (Figure 272, the cast turbine inlet nozzle (Figure 273 and the perforated sheet metal combustor (Figure 274 were fabricated during Phases II and III and tested in the combustor rig in Phase III. The fabrication results were successful and the combustor rig tests demonstrated the durability of those components by accumulating over fifty hours of test time under simulated engine operating conditions.

The fabrication plan for the Phase IV hardware procurement consisted of producing the remainder of the gasifier hardware in sufficient quantities to provide two complete gasifier units and spare parts. The hardware was produced using the production manufacturing processes whenever possible.

6.2 Hardware Delivery Plan

The expendable gasifier hardware procurement flow chart (Figure 275) graphically depicts the flow of hardware from initial procurement during Phase II to completion in Phase IV. The hardware groups shown constitute the major items which make up the gasifier. An adequate number of castings were procured for all cast components to satisfy the requirements of mechanical properties, spin testing, rig tests and two gasifier units. The release of the remainder of the gasifier components for procurement in November of 1977 was intended to make all of the hardware available by May 1978 as shown in the original Phase IV Schedue (Figure 276).

23772

Figure 272 Main Frame, As-Cast C355 Aluminum Sand Casting.
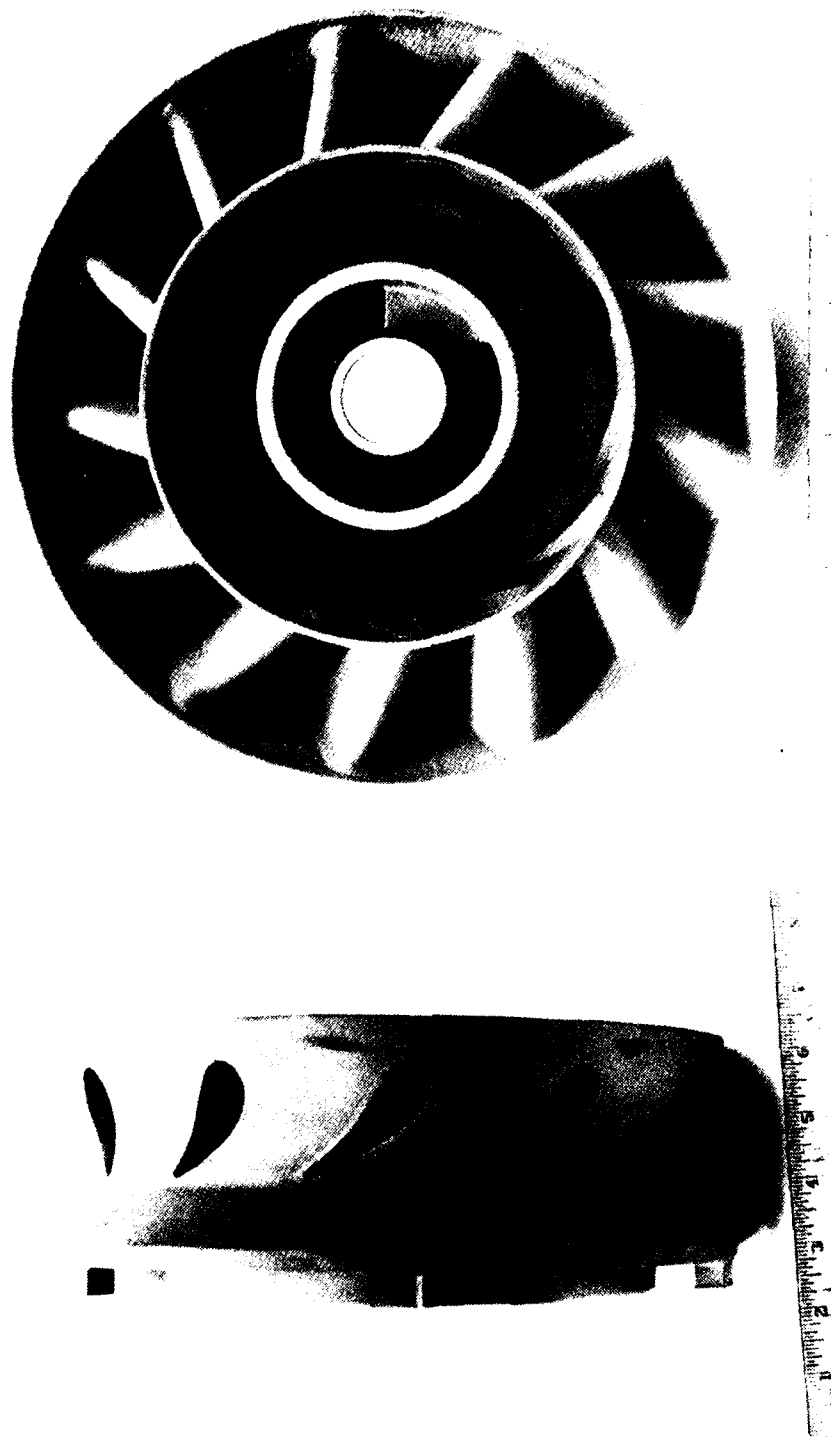
27447

Figure 273 Turbine Inlet Nozzle, As-Cast N-155 Nickel Base Alloy Investment Casting.
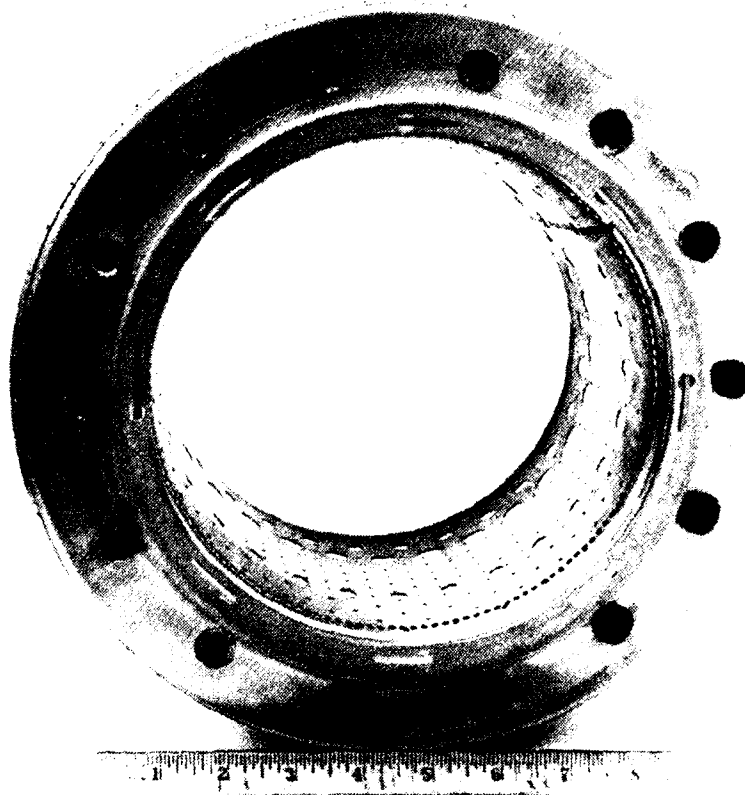
27446

Figure 274   Sheet Metal Combustor - Haynes 556 Perforated Sheet.
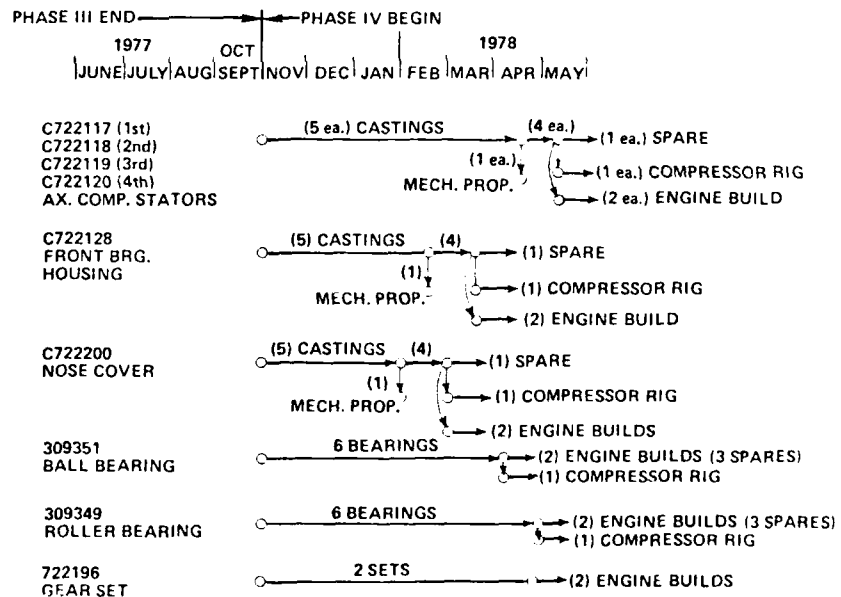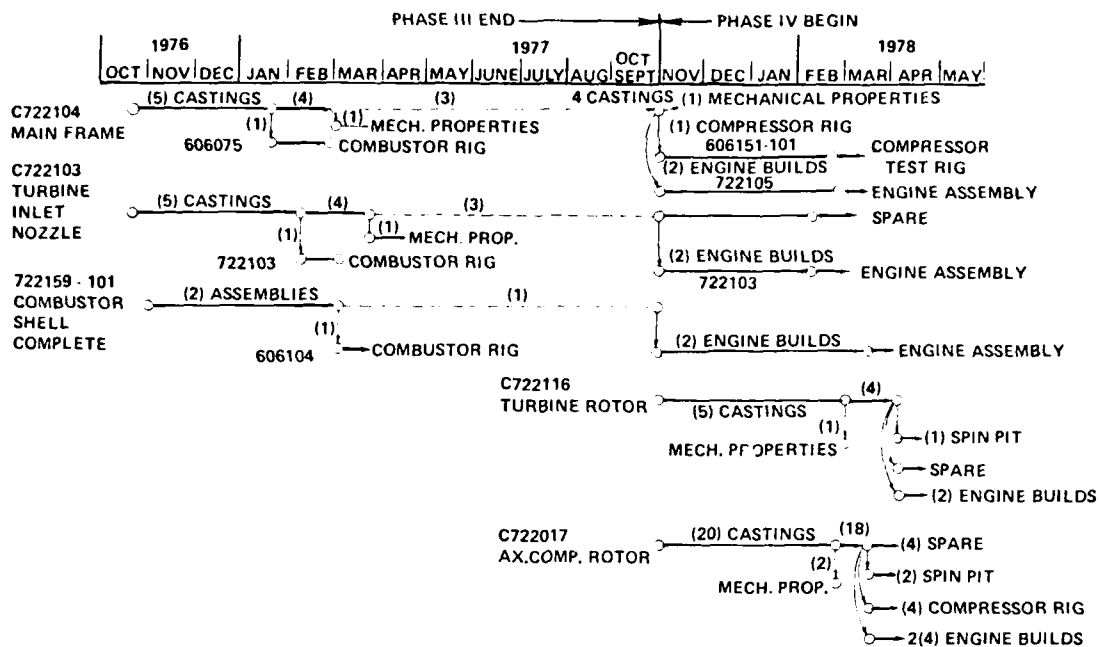
Figure 275. Expendable Gasifier Hardware Delivery Flow Chart.
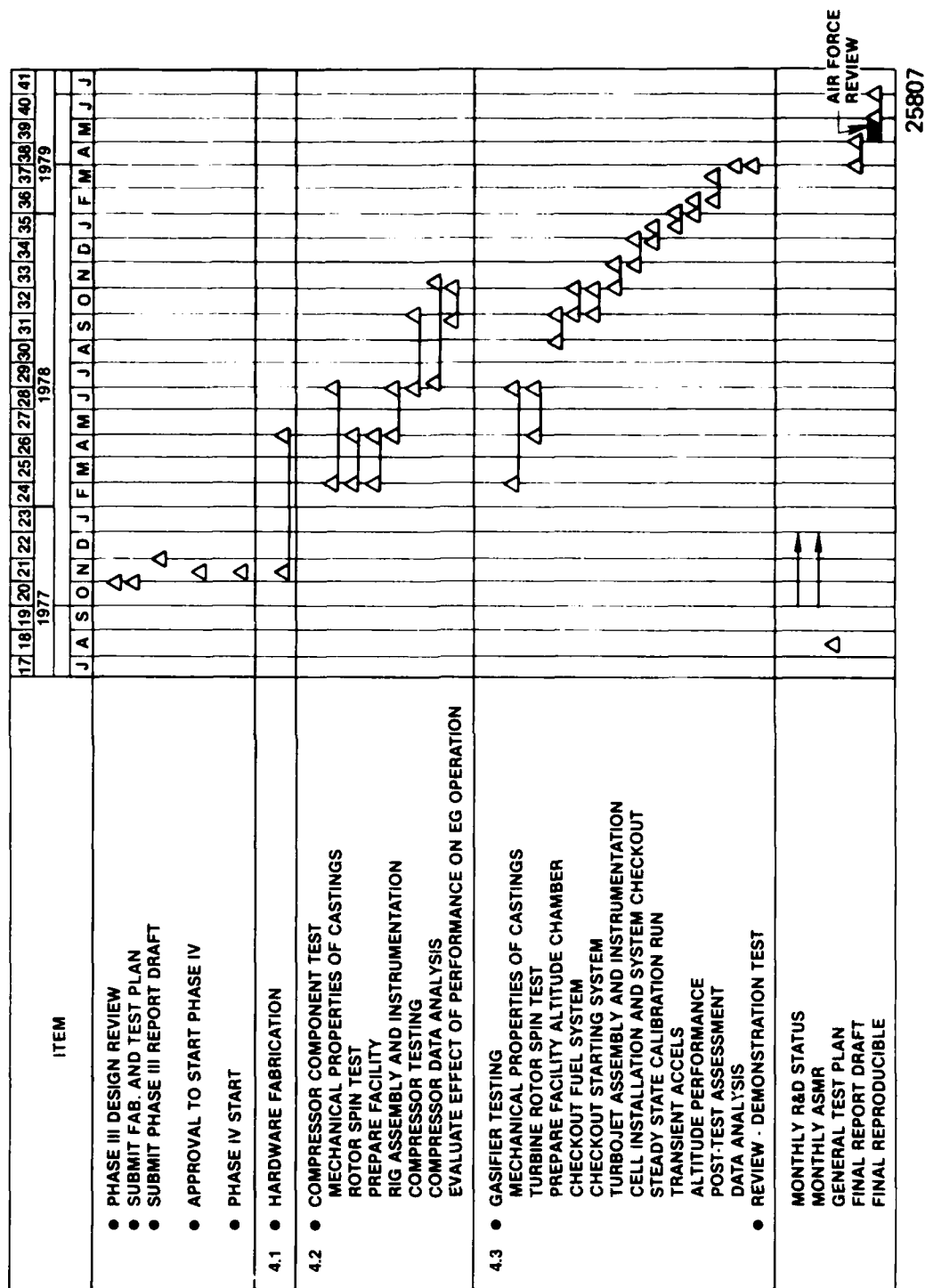
Figure 276. Original Phase IV Schedule Developed in Phase III.

370

A listing of the major hardware items which were procured during Phase IV for the expendable gasifier is shown in Table 31. The table is keyed by find number to the gasifier cross-section shown in Figure 277. The Table gives part number and name, vendor and location (state), estimated delivery date, unit cost, quantity (to cover rig tests, material properties, two gasifiers and spare parts), tooling cost, total cost and a line chart to chart the fabrication progress.

Table 32 presents a list of the adaptive hardware items required for the compressor rig to adapt the engine hardware to the compressor test facility. The instrumentation planned for the compressor test is also listed.

6.3   Hardware Delivery Impact on Program

The hardware delivery plan developed during Phase II held close to the predicted delivery dates with the exception of delivery of castings. Some castings were delivered more than five months after their scheduled delivery. The aluminum compressor rotor castings were being procured from Hitchiner Mfg. who was attempting to use their low cost "CLA" casting process to make these castings. This process uses a type of ceramic mold to allow a vacuum to draw the molten aluminum into the mold. Removal of this ceramic mold after casting proved an insurmountable problem. The rotor blades were invariably deviant in both angle setting and spacing due to the handling. The casting source indicated that they would not be able to make the rotor to print without additional development and tooling.

By the end of July 1978, it was decided to develop a plan to complete Phase IV with the minimum impact to the total program. The plan, shown in Figure 278, provided machined rotors (from forgings) for the compressor rig testing. The rotors were machined to the same dimensions and airfoil contours required for the castings. This check on the compressor performance was available prior to ordering the compressor rotor castings from an alternate casting vendor. The machined rotors were then used in the turbojet engine configuration for initial gasifier testing. The conventional precision cast aluminum rotors were procured and used to determine mechanical properties of the castings, for spin pit testing, and for additional gasifier testing.

The procurement of test castings did not occur as originally scheduled. The alternate casting vendor had difficulties similar to those experienced by the original vendor causing schedule delays as shown in Figure 279. The blade angle setting and blade spacing continued to be the cause for the rejection of the castings. After many attempts to produce satisfactory castings proved fruitless, the casting problems were carefully analyzed. The rough handling required for removal of the mold and movement of the blades during heat treatment of the castings were determined to be the cause of the deviatons to the

371

TABLE 31

EG HARDWARE, RIG AND ENGINE

	EG DEMO ENGINE PARTS	VENDOR/LOCATION	DELIVERY DATE	UNIT COST	QUAN.	TOOLING COST	TOTAL COST
1	722277 NOSE COVER / C72227? (CSTG UNFILLED PES)	CYLECTRON MI / KEITHLEY OH	4 WKS / 8 WKS	120 / 20	3 / 6	8,500	380 / 8,800
2	308467 SEAL, OIL	SEALOL R I	8 WKS	70	8		560
3	308363 NUT, LOCK (LH)	ESNA, N J	16 WKS	74	6		444
4	MS 9388-332 "O" RING		2 WKS	6	6		36
5	UR 4875 RING, RETAINING		2 WKS	1	6		6
6	MS 9388-348 "O" RING		2 WKS	4	6		32
7	722129 HOUSING FR BRG / C722128 (CSTG C356T6)	MORIC MI / HITCHCOCK MINN	5 WKS / 9 WKS	410 / 160	5 / 5	5,800	820 / 6,800
8	308350 WIPER SEAL	SEALOL R I	8 WKS	85	6		510
9	722198 OIL DAM	APOGEE MI	8 WKS	36	3		108
10	722198 GEAR BEVEL (ZEROLI SET = 722197	ARROW ILL	20 WKS	2,320	2		4,640
11	RR 1255 RING, RETAINER		3 WKS	2	6		12
12	308834 BRG BALL (15x32x9mm)	TELEDYNE CAE BOND RM	AVAIL	23	4		92
13	808076 104 NOZZLE, FUEL INLET	TELEDYNE CAE	AVAIL	20	28		560
14	MS 9388-442 O' RING		2 WKS	10	6		60
15	722131 1 ROTOR AX CPRSR 1ST / C722107 (CSTG)	HITCHINER, N.H	4 WKS / 14 WKS	220 / 150	3 / 20	11,800	660 / 14,800
16	808104 101 SHELL COMPL CMBSTH	SLOCOMB CONN	8 WKS	1,450	2	1,350*	4,250
17	722131 2 ROTOR AX CPRSR 2ND (722107)		4 WKS	220	3		660
18	722170 PIN AX CPRSR 3RD	DRAKE IND MI	8 WKS	3.50	100		350
19	722131 3 ROTOR AX CPRSR 4TH		4 WKS	220	3		660
20	722131 4 ROTOR AX CPRSR 4TH		4 WKS	220	3		660
21	722423 SHAFT HP TURBINE	TRIGON MI	4 WKS	215	3		845
22	722192 101 TUBE ASSY FUEL LUBE / C722193 (CSTG)	CADMET N J	9 WKS	25	5	850	975
23	308355 PIN	DRAKE IND MI	2 WKS	6.65	30		200
24	308348 BRG, ROLLER (40x62x18mm)	MPB N H	42 WKS	1,560	6		9,300
25	722664 SHIELD REAR BRG	U S GASKET OH	7 WKS	13	5		65
26	722116 ROTOR TURBINE / C722116 (CSTG)	HOWMET IND	16/28 WKS	478	5	22,248	24,638
27	RR 2445 RING, RETAINING		2 WKS	1	6		6
28	722103 NOZZLE, TURBINE INLET / C722103 (CSTG)	HOWMET IND	IN HOUSE	871	3	19,320	21,933*
29	MS 9388-340 "O" RING		2 WKS	5	6		30
30	722120 STATOR, AX CPRSR 4TH / C722119 (CSTG)	MORIC, MI / UNIVERSAL, ILL	4 WKS / 15 WKS	300 / 150	3 / 5	12,000	900 / 12,750
31	722107 KEY, AX CPRSR STATORS	DELTA, MI	3 WKS	16	10		160
32	722119 STATOR, AX CPRSR 3RD / C722119 (CSTG)	MORIC, MI / UNIVERSAL, ILL	4 WKS / 16 WKS	250 / 150	3 / 5	10,000	750 / 10,750
33	722105 101 MAIN FRAME / C722104 (CSTG)	WEST MILTON OH / HITCHCOCK, MINN	6 WKS / 16 WKS	2,800 / 785	2 / 4	19,500*	5,600 / 22,560
34	722118 STATOR, AX CPRSR 2ND / C722118 (CSTG)	MORIC, MI / UNIVERSAL, ILL	4 WKS / 16 WKS	250 / 150	3 / 5	13,500	750 / 14,250
35	722189 101 PRIMER, FUEL	CYLECTRON, MI	8 WKS	386	2		772
36	722117 STATOR, AX CPRSR 1ST / C722117 (CSTG)	MORIC, MI / UNIVERSAL, ILL	4 WKS / 20 WKS	290 / 235	3 / 5	13,800	870 / 14,975
37	722191 IGNITOR	CHAMPION, OH	14 WKS	90	2		180
38	308456 SEAL, OIL	SEALOL, R I	8 WKS	60	8		480
39	308356 WIPER, OIL SEAL	SEALOL, R I	22 WKS	89	4		356
40	RR 2445 RING, RETAINING		2 WKS	1	6		6
41	308351 BRG, BALL (35x62x14mm)	MPB, N H	36 WKS	125	6		750
42	308356 SHIM	U.S. GASKET, OH	4 WKS	25	4		100
43	308360 SPACER		4 WKS	21	4		84
44	722197 GEAR, BEVEL (see 10)						
45	MS 20034-1 BOLT		2 WKS	9	12		108
46	UR 2758 RING, RETAINING		2 WKS	1	66		6

57,701	EG	BUDGET
13,620	RIG	67,039
71,321		153,061
135,468	TOOLING	220,080
207,788		

136,468 | 194,188

25914

Figure 277. Expendable Gasifier (Model 506) Cross-Section, Find Numbers Keyed to Table 3.

21858

373

TABLE 32

EG COMPRESSOR RIG ADAPTIVE HARDWARE AND INSTRUMENTATION

FIND NO.	PART NO.	PART NAME	VENDOR/ LOCATION	DELIVERY WKS	UNIT COST	QUAN.	TOOLING COST	TOTA COST
①	606153	DUCT. AIR INLET	VALLEY, MI.	12	1800	1		1800
②	722462	RETAINER, FR. BRG	MORIC, MI.	6	690			690
③	722482-101 606151	MAIN FRAME WELDED STRUTS MAIN FRAME MOD.	MORIC, MI. GENTZ, MI.	6 14	1400 3750	1		1400 3750
④	606150-101	FAIRING, CPRSR, OUTER	CYLECTRON, MI.	8	1890	1		1890
⑤	606149	FAIRING, CPRSR, INNER	TRIGON, MI.	4	375	1		375
⑥	722175	SHAFT, CPRSR	MORIC, MI.	6	740	1		740
⑦	606146-101	ADAPTER, OIL INLET	APOGEE, MI.	4	175	1		175
⑧	308637	BRG. BALL	TELEDYNE CAE					

INSTRUMENTATION

	PART NO.	PART NAME	VENDOR/ LOCATION	DELIVERY WKS	UNIT COST	QUAN.	TOOLING COST	TOTA COST
	606154-101	INLET PRESS. RAKE	THERM PROD. ILL	8	223	2		446
	606158-101	INLET TEMP. RAKE	THERM PROD. ILL.	88	300	3		600
	606311-101	EXIT TEMP. RAKE	THERM PROD. ILL	8	143	3		429
	606155-101	EXIT PRESS. RAKE	MARLIN. OH.	8	180	3		540
	606312-101	EXIT P_T & A SURVEY PROBE	MARLIN, OH.	8	285	1		285
		MISC. BOLTS, GASKETS FITTINGS O RINGS		4				500
								13,620

25913

374
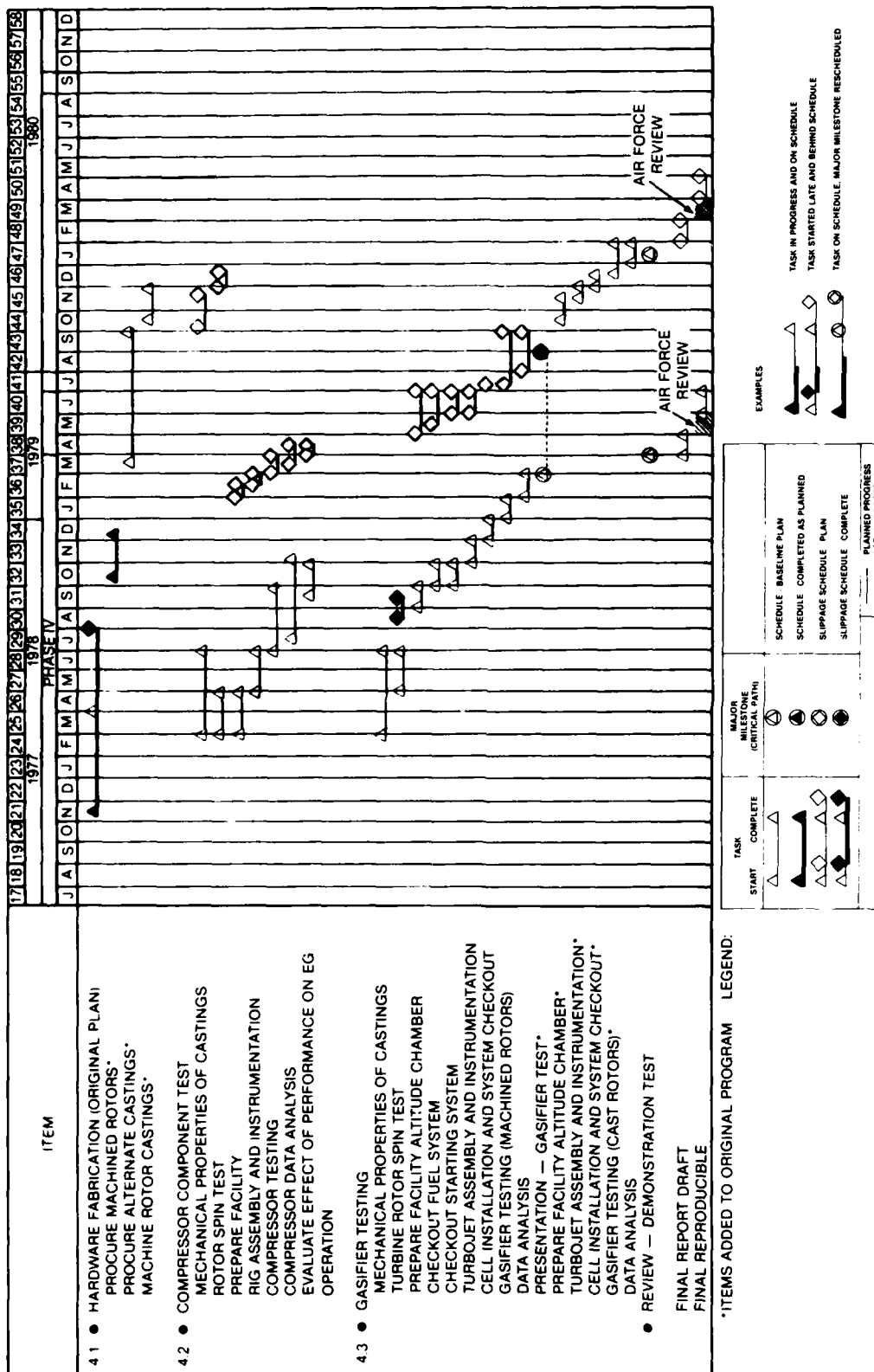
Figure 278. Phase IV Program Schedule.

41275

375
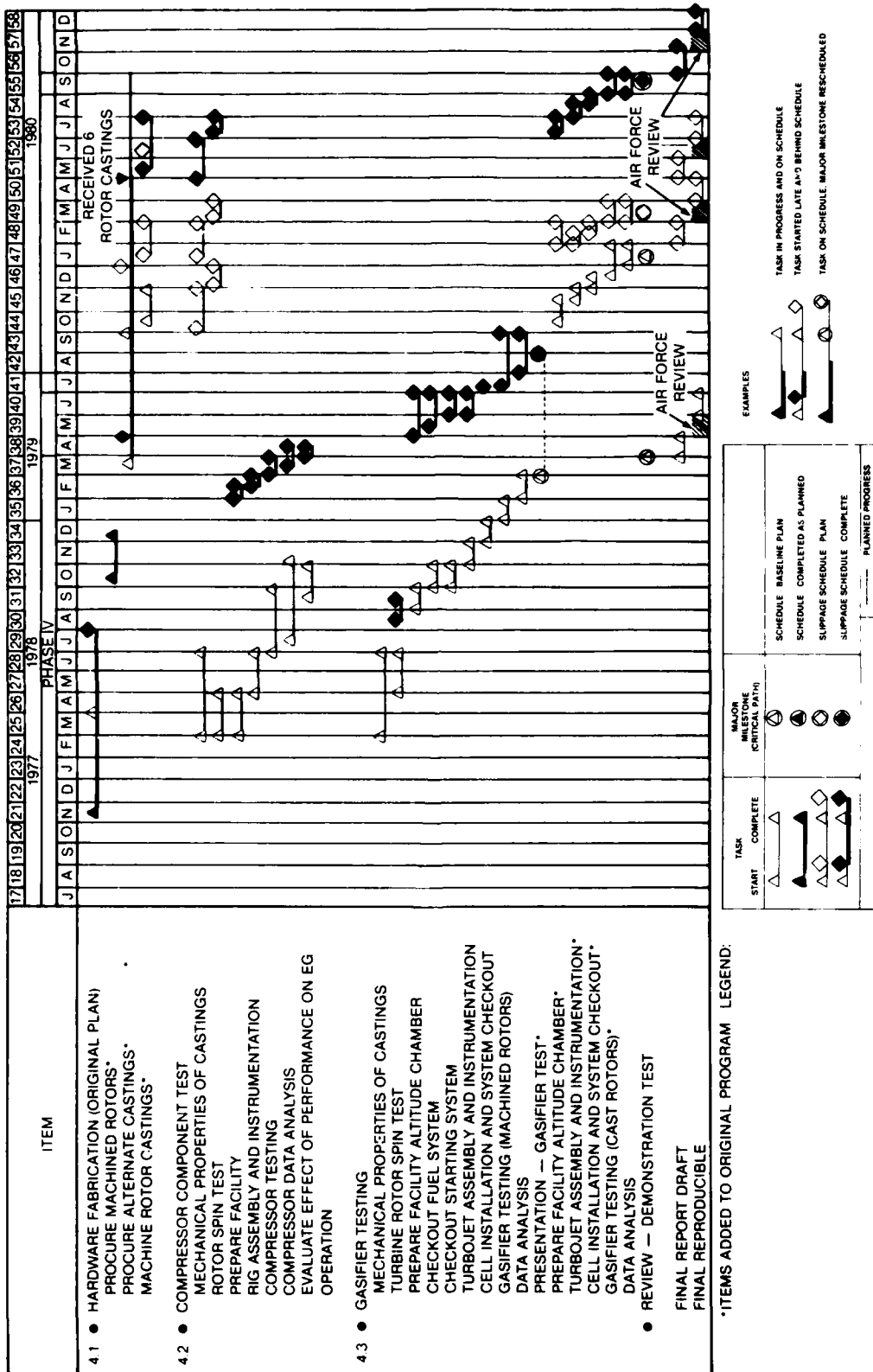
Figure 279. Phase IV Program Schedule.

casting dimensions. Since the remainder of the rotor dimensions
and the airfoil contours were to print, it was decided to accept
castings with deviant angle settings and blade spacings provided
they were metallurgically sound. This allowed testing of the
turbojet cast rotor configuration of the expendable gasifier to be
accomplished in a reasonable time frame. The comparison of the
performance using the machined rotors versus these cast rotors
represented the worst possible degradation of performance. In the
meantime, the casting vendor agreed to modify the tooling to cast
the rotor with a ring on the outer diameter (Figure 280) similar to
many stator castings. This provided the rigidity for mold removal
and acted as a fixture to hold the blades during heat treatment.
Since all rotors are machined at the tip diameter, machining off
the cast ring had a minimal impact on cost.
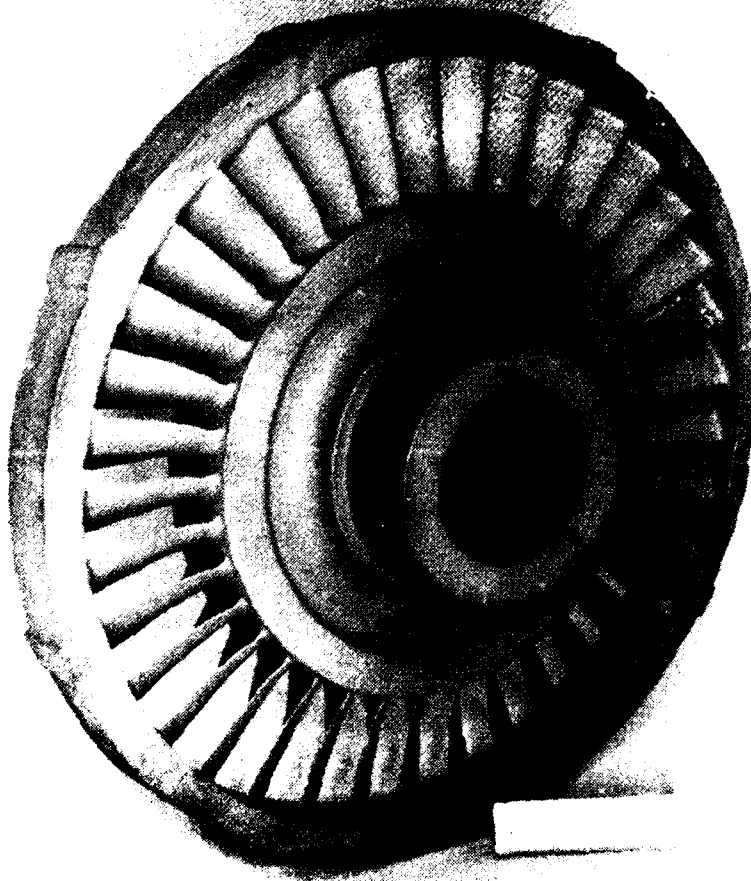
41283

Figure 280.   Compressor Rotor Casting With Ring Cast on Outside
                Diameter.

SECTION 7.0

TESTING (PHASE IV)

7.1   Compressor Testing

7.1.1   Compressor Design Goals and Features

The design point of the Expendable Gasifier (E.G.) four stage compressor is based on the sea level static jet fuel starter configuration performance objectives established in Phase I. The design goals as established in Phase I are shown in Table 33. The predicted performance of the final design hardware is also shown on this table. The compressor is predicted to achieve its flow goal and be within one percent of the pressure ratio and efficiency goals. The progression of the predicted performance from loop to loop in the iterative design procedure indicated that the design goals could be achieved with several more passes through the design process. However, due to the complexity of the design process, the time and effort required, and since the design was within one percent of all of its design goals it was frozen at this point. The deviation from the performance goals is probably within the tolerance of the design system.

TABLE 33

EXPENDABLE GASIFIER COMPRESSOR
AERODYNAMIC DESIGN PERFORMANCE

	Design Goal	Design Prediction After Phase III
Corrected Speed ($N/\sqrt{\theta}$) - RPM	33,060	33,060
Corrected Flow ($W\sqrt{\theta}/\delta$) - LBM/SEC	4.023	4.023
Pressure Ratio	2.86:1	2.83:1
Adiabatic Efficiency - %	80.0	79.2
Corrected Tip Speed - FT/SEC	900	900

The compressor is a subsonic, highly loaded, four-stage axial machine derived from an upscale of the Teledyne CAE Model 469 compressor. The compressor has a very low tip speed (900 ft/sec), for its pressure ratio, such that stresses are minimized and the blading can be cast in aluminum. The high loading minimizes the number of stages and thus minimize parts and cost.

The most notable of the low cost features is the use of a common rotor casting for all four stages. The casting is just machined to different outer diameters for each stage. This feature has been used by Teledyne CAE in the past very successfully on the Model 471 axial compressor (SCAD). Teledyne CAE also holds a patent on the common blading compressor design. The stators were used to tailor the incidence angles to the following rotors as shown schematically in Figure 281 to improve performance.
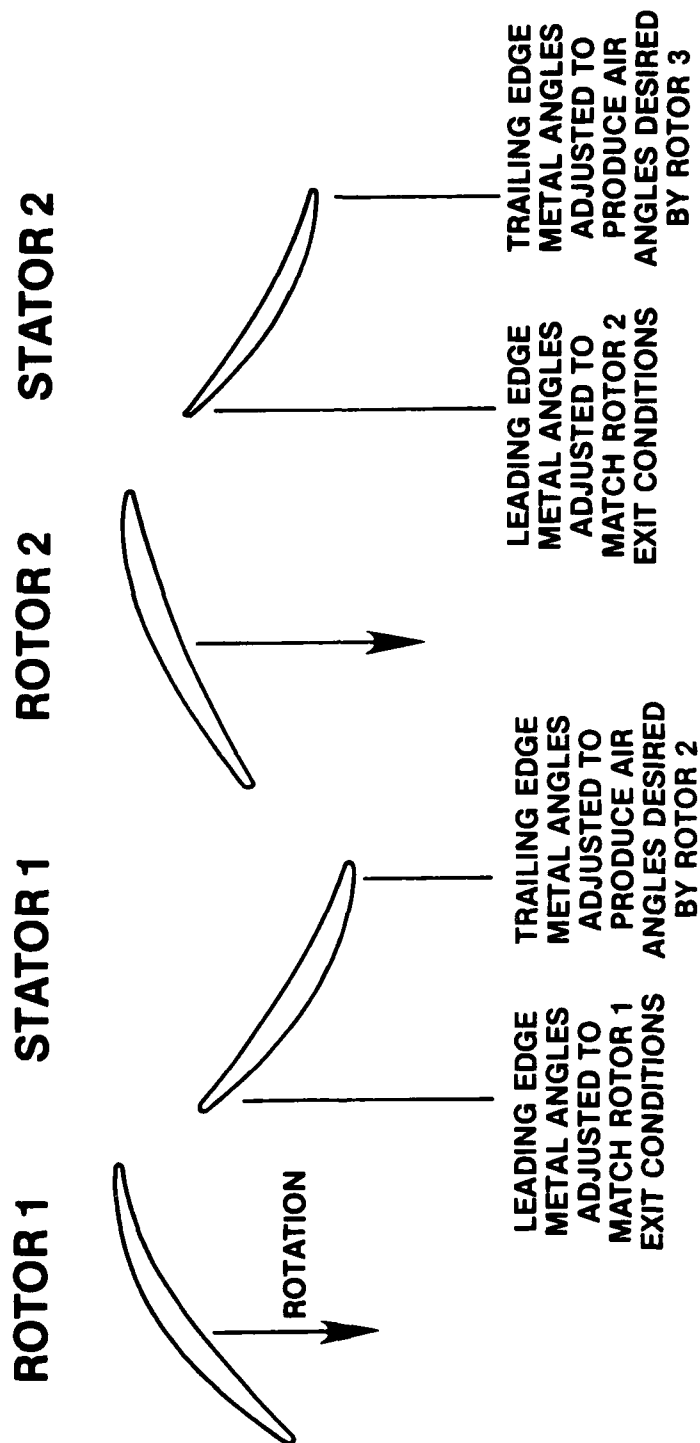
Figure 281. Individual Stator Stages Provide Desired Air Entry for Common Rotors.

The final E G compressor flowpath is shown in Figure 282. This flowpath was established in the Phase I preliminary design portion of this program and was unchanged in the final design. The radial dimensions are upscaled directly from the Model 469 compressor using a linear scale factor of 1.3166. The axial dimensions were modified to equalize the rotor and stator aspect ratios in each stage.

The common rotor blading design requirement altered the aero design procedure from that normally used for subsonic axial compressors. The E.G. design method is compared to the normal design procedure in Figure 283. The usual procedure is to specify an RPM flowpath geometry and pressure ratio requirements. The design program then calculates the resulting losses and velocity diagrams. The flowpath and specified pressure ratio distributions are then altered to achieve the desired efficiency and blade aerodyanmic loading levels. When satisfactory velocity diagrams have been obtained, blading is designed to match those velocity diagrams.

To achieve a single rotor design for all four stages required the compressor to be designed with an off-design compressor performance program such that the blading could be specified first. In the method employed, the RPM, flowpath geometry and blading geometry were specified. The blading geometry definition included the number of airfoils in each blade row plus specifications of chords and inlet and exit blade metal angle distributions versus radius for each blade and vane row. The off-design computer program then predicted the blade element losses and pressure ratios plus the velocity diagrams produced by that blading. The resulting pressure ratio, efficiency, and exit velocity profile are compared to the goals and the flowpath and/or blading geometry altered to achieve the desired results because a change in geometry in one of the front stages affects the performance of all the downstream blade rows. A detailed final design procedure logic path is shown in Figure 284.

An aerodynamic design summary is shown in Figure 285. The diffusion factor or aerodynamic loading levels should be noted as they are quite high for both rotors and stators. Diffusion factors of 0.6 are normally considered to be quite high; because of the very low tip speeds and minimum number of stages, this design has rotor D-factors as high as 0.674 and stators 0.756.

RADIAL
DISTANCE, R
INCHES

AXIAL DISTANCE, Z — INCHES
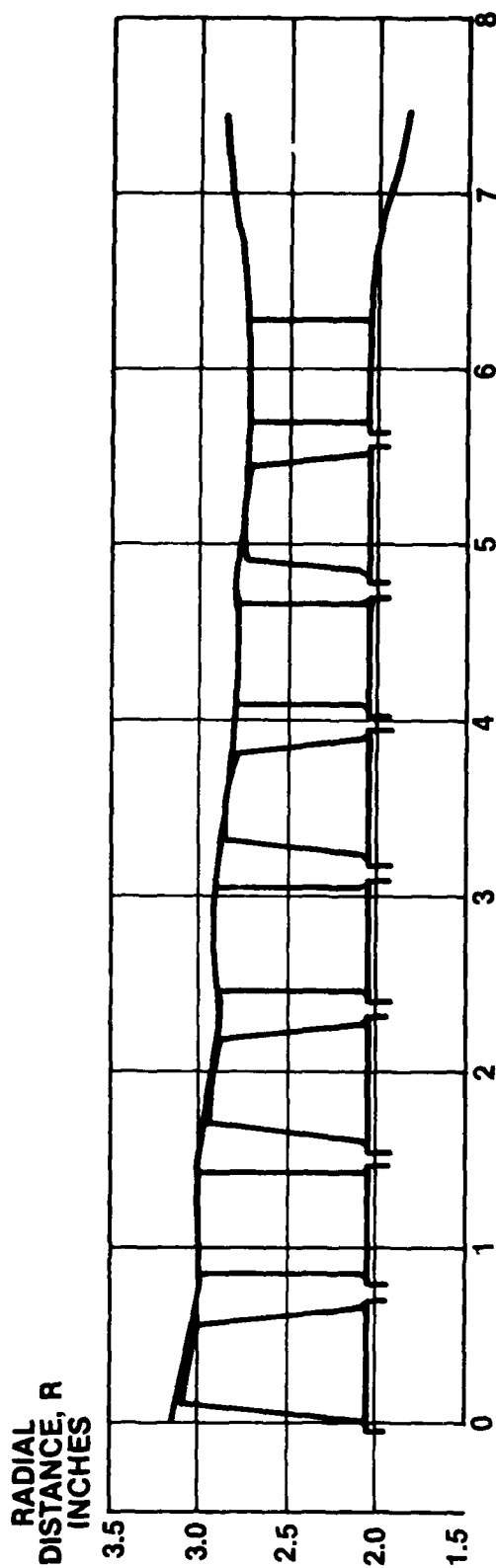
LOCATION	RH	RT	ZH	ZT	LOCATION	RH	RT	ZH	ZT
R1 IN	2.043	3.118	0.000	0.113	R3 OUT	2.043	2.820	3.893	3.810
OUT	2.043	3.033	0.671	0.567	S3 IN	2.043	2.802	4.073	4.073
S1 IN	2.043	2.997	0.851	0.851	OUT	2.043	2.802	4.653	4.653
OUT	2.043	2.997	1.431	1.431	R4 IN	2.043	2.788	4.833	4.911
R2 IN	2.043	2.969	1.611	1.708	OUT	2.043	2.742	5.504	5.431
OUT	2.043	2.914	2.282	2.192	S4 IN	2.043	2.731	5.684	5.684
S2 IN	2.043	2.889	2.462	2.462	OUT	2.043	2.731	6.264	6.264
OUT	2.043	2.889	3.042	3.042	—	1.980	2.790	6.850	6.850
R3 IN	2.043	2.870	3.222	3.310	—	1.860	2.846	7.465	7.465

40452

Figure 282. Expendable Gasifier Compressor Flowpath.
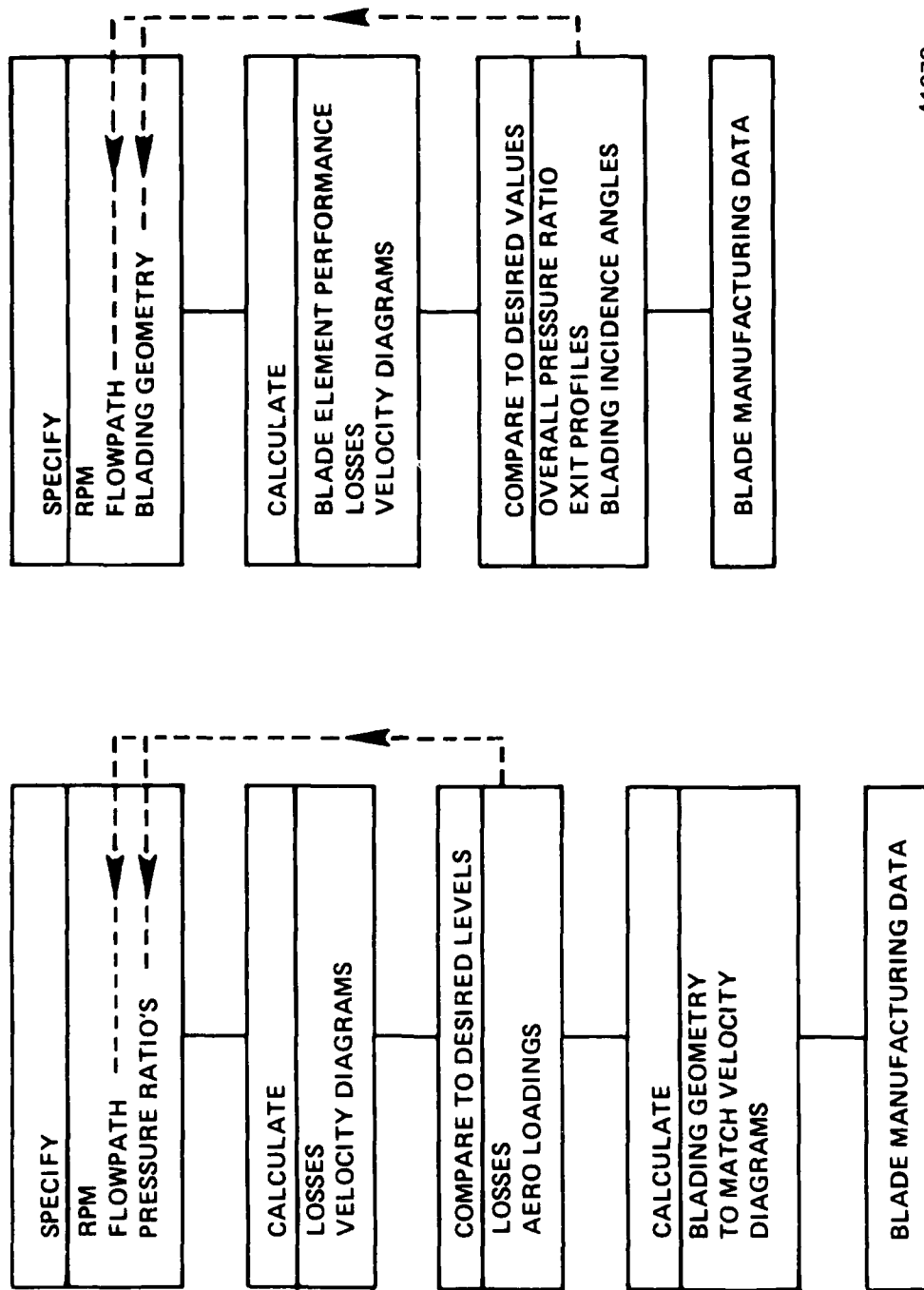
Figure 283. Subsonic Axial Compressor Design Procedure.

383

```
┌─────────────────────────┐
│ FLOWPATH ESTABLISHED    │
│ DURING PRELIMINARY      │
│ DESIGN PHASE            │
└─────────────────────────┘
            │
            ▼
┌─────────────────────────┐
│ ESTABLISH ROTOR METAL   │
│ ANGLES BASED ON         │
│ PRELIMINARY DESIGN:     │              ┌──────────────────────┐
│   *  ROTOR INLET METAL  │              │ INCIDENCE MODEL      │
│      ANGLE DETERMINED   │              │ LOSS MODEL           │
│      BY COMPUTER SOLN.  │              │ DEVIATION MODEL      │
│      FOR INLET DUCT     │              │ BLOCKAGE ASSUMPTION  │
│      AND REFERENCE      │              └──────────────────────┘
│      INCIDENCE ANGLE    │
└─────────────────────────┘
            │
            ▼
┌─────────────────────────────────────┐
│ COMPUTER PROGRAM  08.116            │
├─────────────────────────────────────┤
│ SUCCESSIVELY ADJUST STATOR          │
│ METAL ANGLES:                       │
│   * SATISFY STATOR REFERENCE        │
│     INCIDENCE BY VARIATION          │
│     OF INLET METAL ANGLE            │
│   * SATISFY DOWNSTREAM ROTOR        │
│     REFERENCE INCIDENCE BY          │
│     VARIATION OF EXIT METAL         │
│     ANGLE                           │
└─────────────────────────────────────┘
            │
            ▼
        ╱PRESSURE╲
       ╱  RATIO   ╲    NO      ┌──────────────────────────┐
      ╱ SATISFIED  ╲──────────▶│ REFINE ROTOR EXIT METAL  │
       ╲    ?     ╱            │ ANGLE TO SATISFY PRESSURE │
        ╲        ╱             │ RATIO AND/OR EXIT         │
         YES                   │ PROFILE REQUIREMENTS      │
          │                    └──────────────────────────┘
          ▼
        ╱ EXIT  ╲
       ╱ PROFILE ╲   NO
      ╱ SATISFIED ╲──────
       ╲         ╱
        ╲       ╱           ┌──────────────────────────┐
         YES                │ COMPUTER PROGRAM  08.130 │
          │                 ├──────────────────────────┤
          └────────────────▶│ GENERATE FINAL BLADING   │  21930
                            └──────────────────────────┘
```

Figure 284.   Expendable Gasifier Compressor - Detail Design Procedure
              Logic Path.

CORRECTED SPEED, RPM 33055
CORRECTED FLOW, LBM/SEC 4.023
PRESSURE RATIO 2.827
ADIABATIC EFFICIENCY, PERCENT 79.2
FIRST ROTOR INLET TIP SPEED, FT/SEC 899.1
FIRST ROTOR INLET TIP RADIUS, IN. ... 3.117

		STAGE		
	1	2	3	4
MASS AVERAGED STAGE PRESSURE RATIO	1.361	1.308	1.273	1.247
MASS AVERAGED STAGE ADIABATIC EFFICIENCY	81.6	81.6	81.5	80.6
ROTOR ASPECT RATIO (AVERAGE HEIGHT/CHORD)	1.512	1.315	1.175	1.059
STATOR ASPECT RATIO	1.514	1.341	1.201	1.097
ROTOR INLET HUB-TIP RATIO	0.655	0.688	0.711	0.733
STATOR INLET HUB-TIP RATIO	0.682	0.707	0.729	0.748
ROTOR DIFFUSION FACTOR HUB	0.665	0.656	0.656	0.674
MEAN	0.527	0.528	0.535	0.532
TIP	0.566	0.558	0.590	0.648
STATOR DIFFUSION FACTOR HUB	0.625	0.664	0.743	0.756
MEAN	0.530	0.577	0.635	0.621
TIP	0.555	0.578	0.661	0.672

40451

Figure 285. Expendable Gasifier Compressor Aerodynamic Design Summary.

385

7.1.2 Compressor Rig Testing

The purpose of the aerodynamic rig testing was to achieve the following objectives:

- Determine the compressor aero performance

- Investigate problem areas

- Verify structural integrity to 110% speed

- Measure exit profiles for combustor inlet evaluations

- Modify blading if necessary, to provide adequate performance for engine operation.

The test rig is shown in Figure 286. The rig makes maximum use of engine hardware. The cross hatched hardware shown in the figure is adaptive facility hardware.

The rig instrumentation (Figure 286) consists of inlet and exit pressure and temperature rakes for overall performance calculations, plus wall static pressures to assist in inter-compressor performance analysis. The pressure and temperature rakes are the same as those used in the demonstrator engine testing. Therefore, compressor performance from both tests can be compared directly. A cobra probe was used at the compressor exit to measure the total pressure and flow angle profiles for combustor studies. An ASME nozzle was used upstream of the rig to measure airflow and an electronic counter was used to measure rotational speed. The temperature rakes were calibrated for Mach number effects before testing.

7.1.3 Compressor Rig Test Results

Rig testing was performed on the Expendable Gasifier Compressor during March 1979. The compressor performance map obtained is shown in Figure 287. As can be seen from the map, the design performance goals for this machine have not been realized. Design goals and test results are shown in Table 34 below:

TABLE 34

E.G. COMPRESSOR AERODYNAMIC DESIGN PERFORMANCE

	Design Goals	Test Results
Corrected Airflow Rate - lbm/sec	4.023	4.023
Pressure Ratio - Total/Total	2.83	2.72
Isentropic Efficiency - Percent	79.2	77.0

386

3 - TOTAL PRESSURE RAKES
3 - TOTAL TEMPERATURE RAKES
1 - P_T, Y_{AW} SURVEY PROBE

2 - TOTAL PRESSURE RAKES
2 - TOTAL TEMPERATURE RAKES

● - WALL STATIC PRESSURE TAPS
▨ - COMPONENTS UNIQUE TO THIS TEST RIG
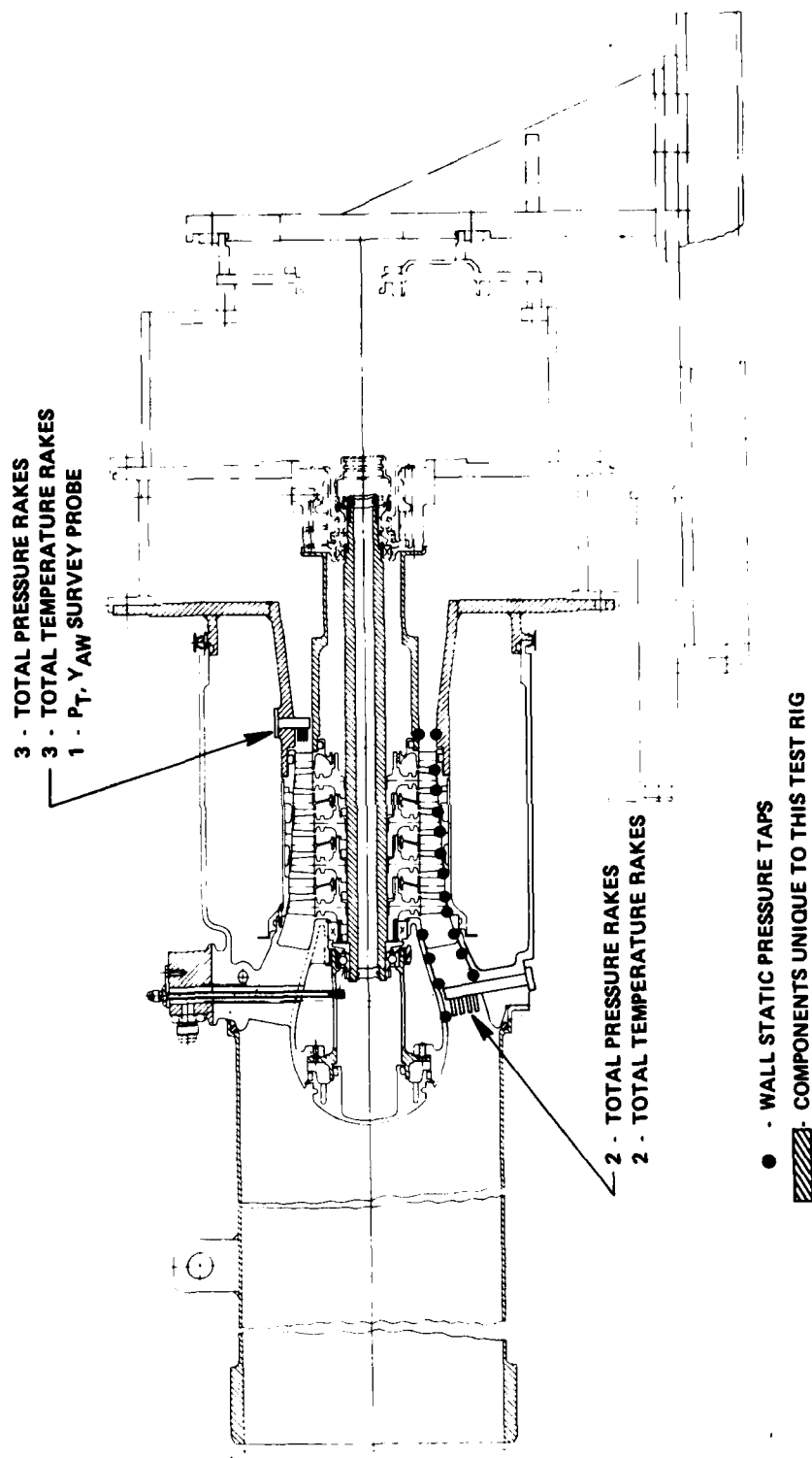
25976

Figure 286.   Expendable Gasifier Compressor Test Rig.

387
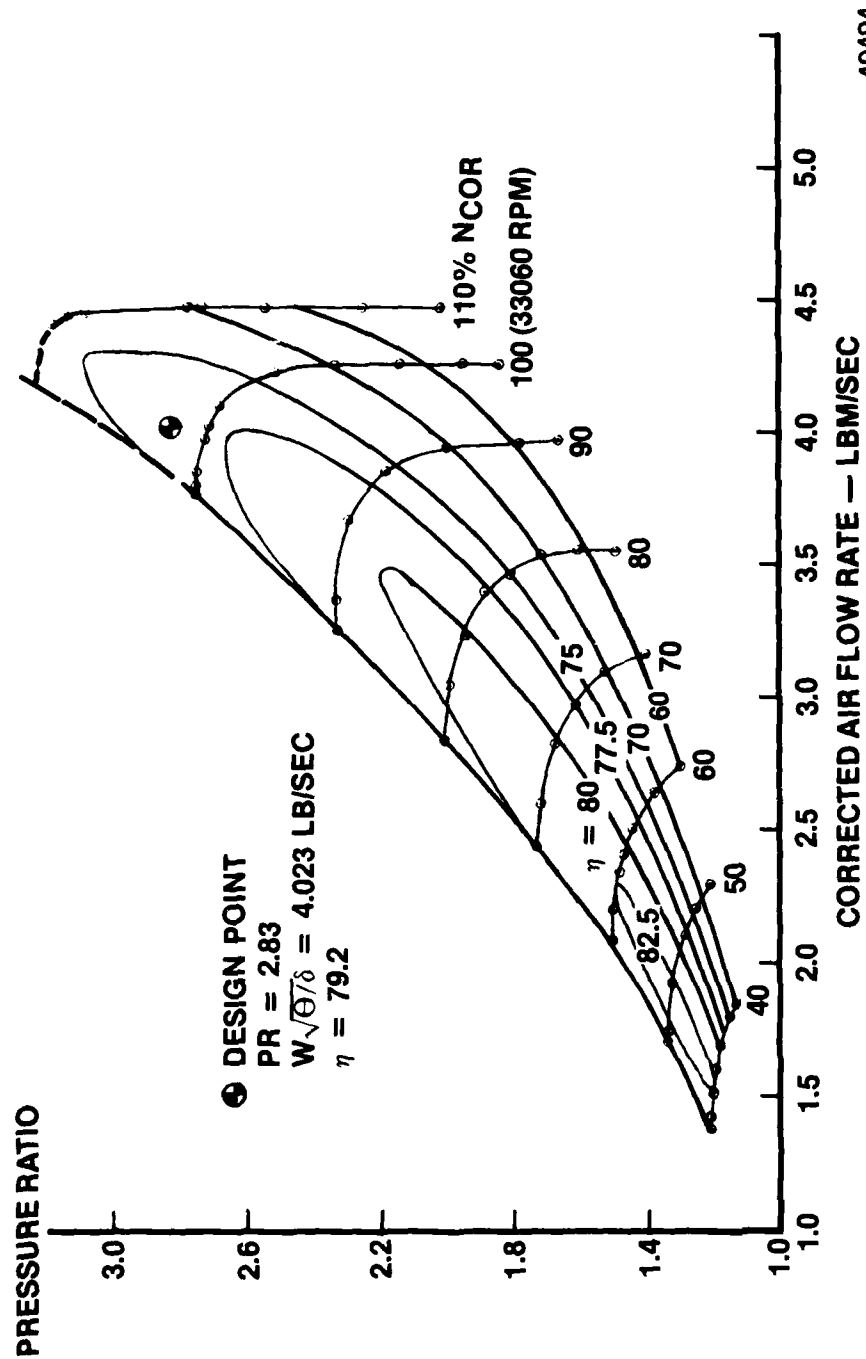
Figure 287. Expendable Gasifier Compressor Performance Map.

To determine the cause of the lower than predicted performance, the data available were used in conjunction with TCAE's compressor off-design performance prediction program (08.116). This program, which was also used to design this compressor, predicts detailed blade element performance based on built in loss correlations and blade turning correlations. The blade element losses are a function of diffusion factor, solidity, exit angle and incidence angle. Blade element turning is a function of incidence, blade camber, solidity and percent blade height.

The blade turning or deviation angle correlation used in the program has been developed over a period of years with all sizes and types of compressors. Therefore, its accuracy is not being questioned in this case. The items which are suspect are the blade element loss correlations and the boundary layer blockage assumptions made for this design.

The original loss assumptions are questionable because: (1) the loading levels used in this compressor design are very high and (2) due to the small size of this compressor, the higher end wall losses may influence a greater portion of the span (or the whole span) than originally assumed.

The blockage assumptions are open to question because previous TCAE small compressors have exhibited very high blockage values. The blockages used in the original design reflected some of this high blockage finding but not all of it. The original design used a blockage increase of 2-3 percent across rotors and a drop of 1 percent across stators. Large compressor designs often use a 1 percent increase across each blade row. Data from a TCAE development program on a 3.5 lbm/sec compressor showed blockage increases of 10-15 percent across rotors with decreases of almost the same magnitudes across the stators. The effects of high unaccounted for rotor exit blockages are low work and lower efficiency due to mismatched airfoils.

The test efficiency versus span is shown in Figure 288. The test data indicate that the losses used in the design were too high at the end walls and too low at the mean span height. Thus, confirming that the small size of this compressor is resulting in some "end wall" loss in the middle of the blade. The design loss parameter versus diffusion factor for the 10, 50 and 90% span heights of the rotors is shown in Figure 289. Changing the 50% span loss curve to that shown on the figure gives an efficiency curve, shown in Figure 288, which is close to the measured test data.

The measured values of tip wall static pressure are compared to the design values in Figure 290. The measured values being lower than design is due partially to the pressure ratio being lower than design, but also confirms the suspicion that the design blockages were somewhat optimistic (low). Blockage factors

389
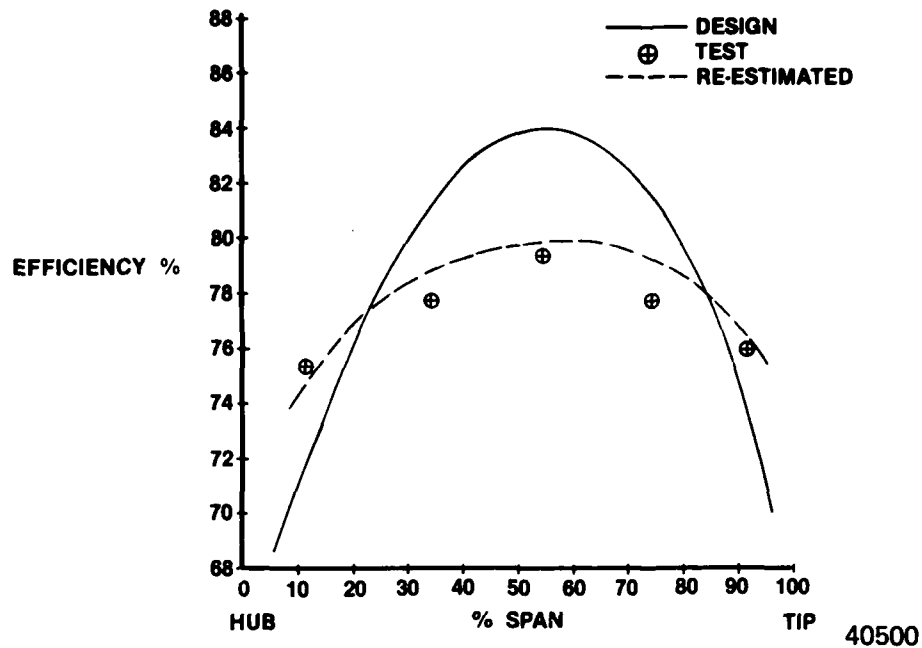
Figure 288. Expendable Gasifier Compressor Efficiency Versus Flow-path Span.
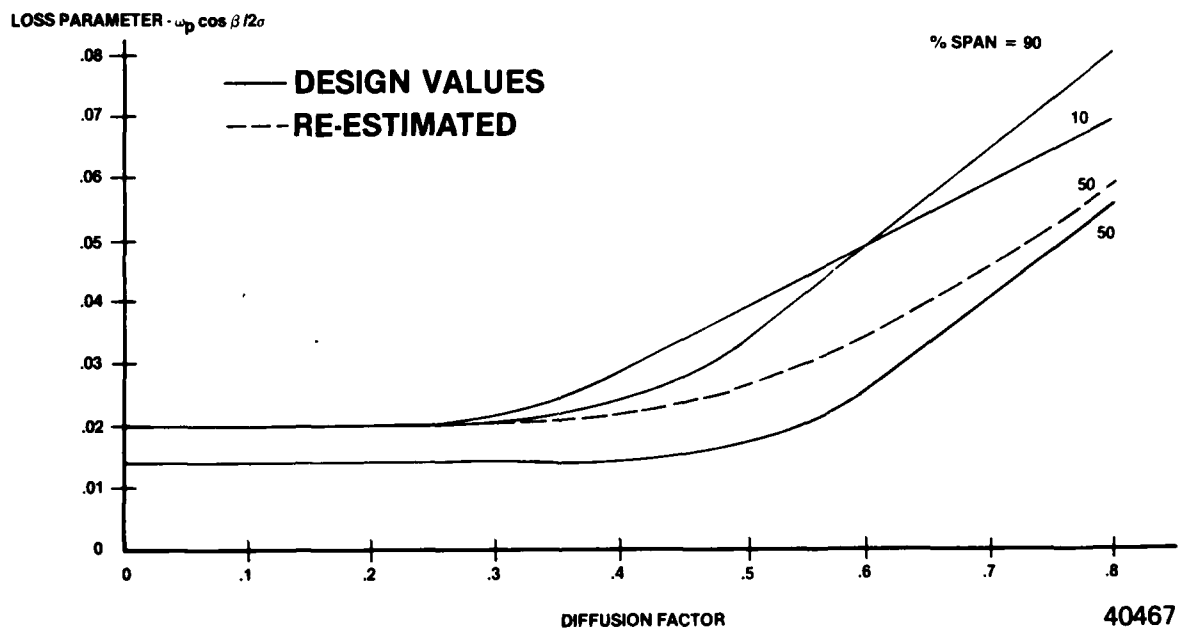
Figure 289. Compressor Loss Parameter Versus Diffusion Factor for Various Span Heights.

390
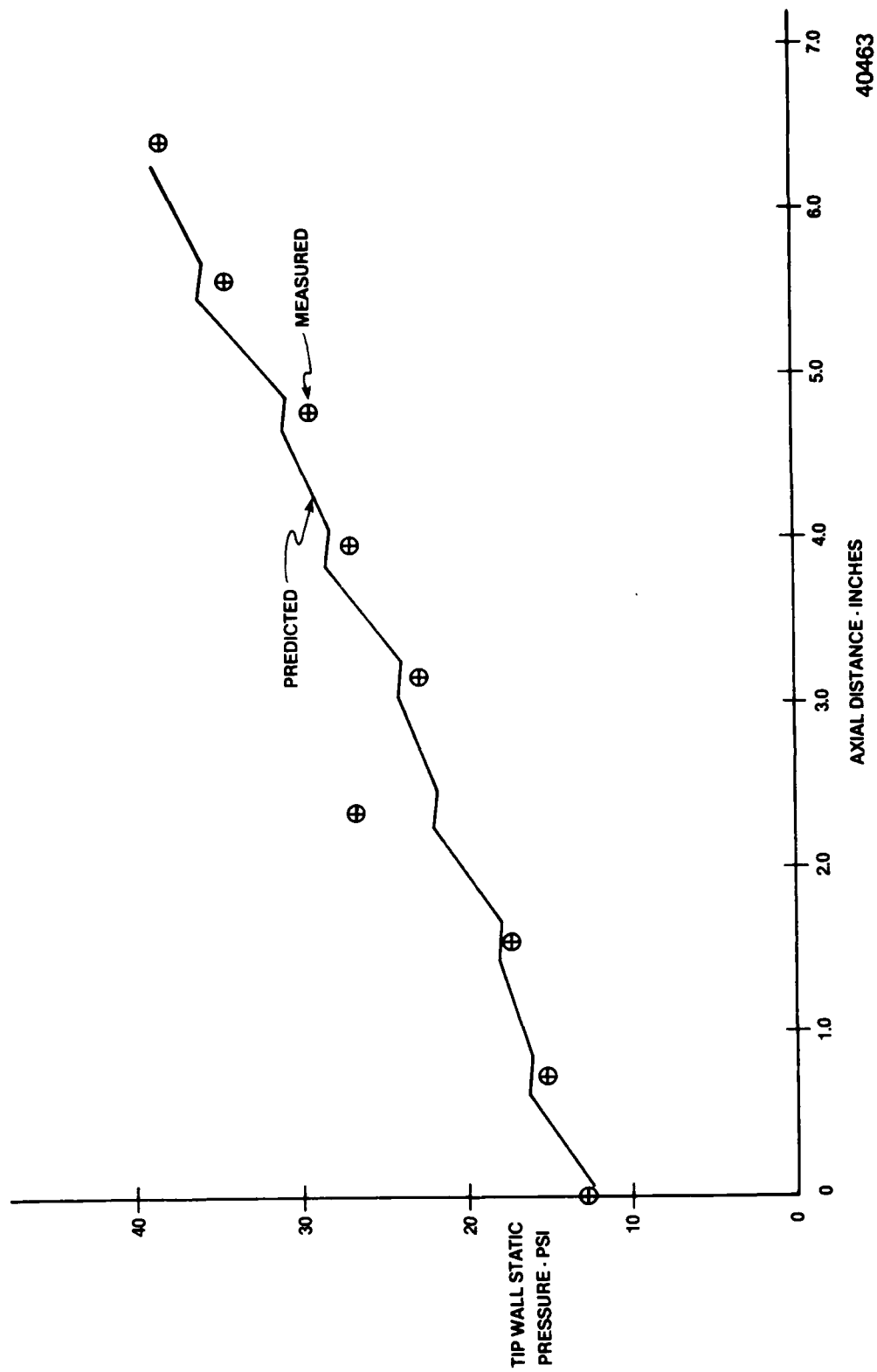
Figure 290. Compressor Outer Wall Static Pressure Distribution.

391

were calculated from test data at the compressor inlet and exit. The blockage was lower than design at the inlet and higher at the exit. Figure 291 shows the design blockage factor, as well as the test data values and the re-estimated values used in the computer simulation of the test data.

The results of the computer simulated performance are shown in Figure 292. The rotor blades of the simulated design were than twisted linearly from zero degrees at the rotor hubs to five degrees at the rotor tips. The resulting performance predicted is shown in Figure 292. Analysis of the engine shows that the original engine performance goals, except for efficiency, can be met with the twisted rotors at the design rated speed. The compessor efficiency would remain about two percent low.

Engine performance analysis also showed that the predicted goals could be met with no compressor modification by a slight engine overspeed to 33,900 rpm. Since this appeared to be a lower risk approach (no rotor blade breakage), no further compressor development work was required. The precision castings for the compressor rotors were subsequently procured to this configuration. The machined rotors were inspected and used in the turbojet engine configuration of the Expendable Gasifier.

7.1.4   Cast Rotor Structural Verification

To insure the structural integrity of the cast aluminum axial compressor rotors, material physical properties were obtained from one rotor while another was used for spin testing. To obtain material properties, one casting was sectioned and test bars were extracted from the casting as shown in Figure 293. These tensile specimens were found to exceed the minimum stress levels required per AMS4215.

The remainder of the compressor rotor structural verification was accomplished by spin pit testing. The compressor rotor casting was machined to the first stage rotor configuration and assembled on the spin pit arbor as shown in Figure 294. The rotor assembly was balanced, inspected and installed in the spin pit (Figure 295) and the rotor was spun to 110% of design speed (36,400 rpm). The rotor was subsequently removed from the spin pit and reinspected. The original dimensions were rechecked and recorded, and no measurable change was detected. The rotor assembly was then reinstalled in the spin pit and spun to 110% of the overspeed required to develop full power (38,930 rpm). The original dimensions were again rechecked and recorded with no measurable change detected. Zyglo inspection also revealed no signs of distress to the rotor. The arbor assembly was reinstalled in the spin pit and the rotor casting was spun to burst (Figure 296) which occured at 66,400 rpm. This speed is more than twice the 100% design speed and in excess of the predicted burst speed of 57,300 rpm which was conservatively estimated on the basis of minimum material properties and a .55 burst factor.

BLOCKAGE FACTOR
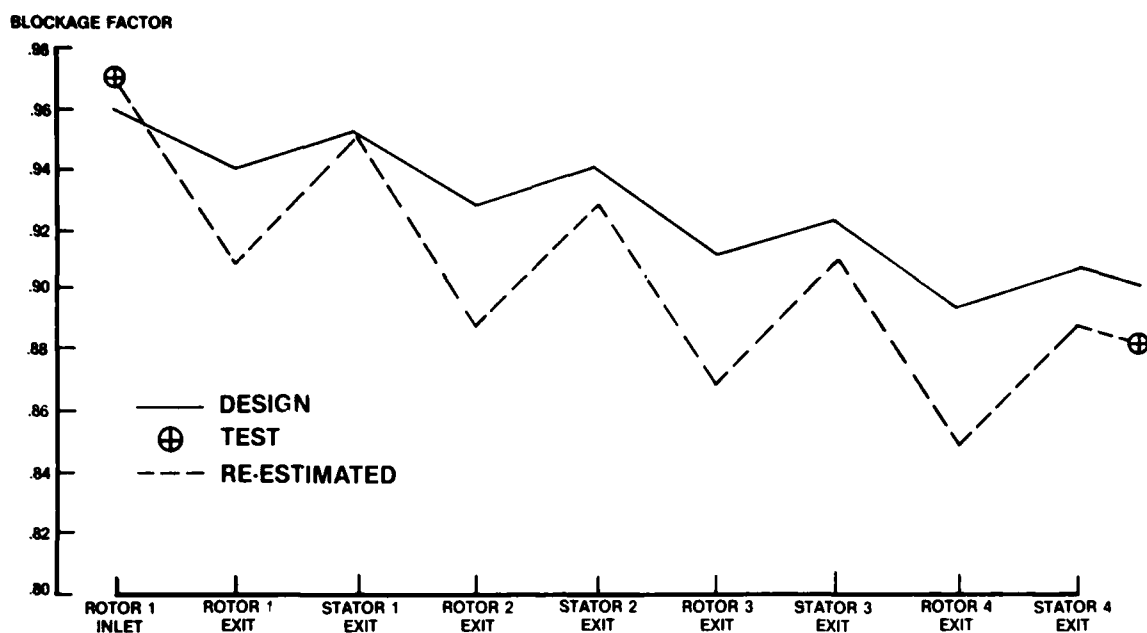
40488

Figure 291. Compressor Blockage Factor Distribution.

40489
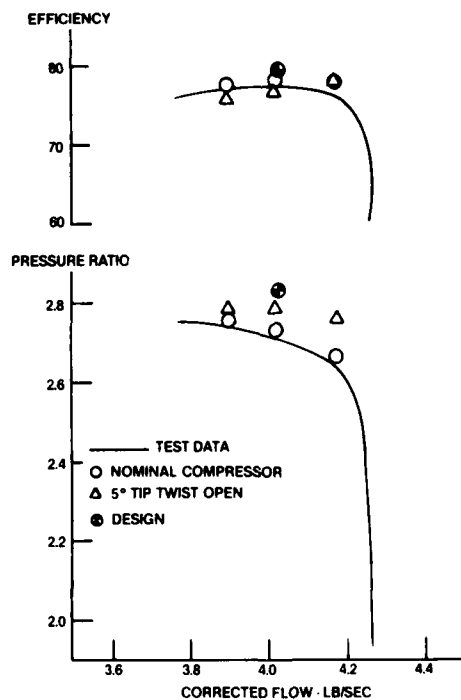
Figure 292. Compressor Predicted Efficiency and Pressure Ratio Versus Flow.

393

FIRST STAGE
AXIAL COMPRESSOR

COMPRESSOR
DRIVE PIN

SPIN ARBOR
"CATCHER"

SPIN ARBOR

SPIN ARBOR
DRIVE END

25768
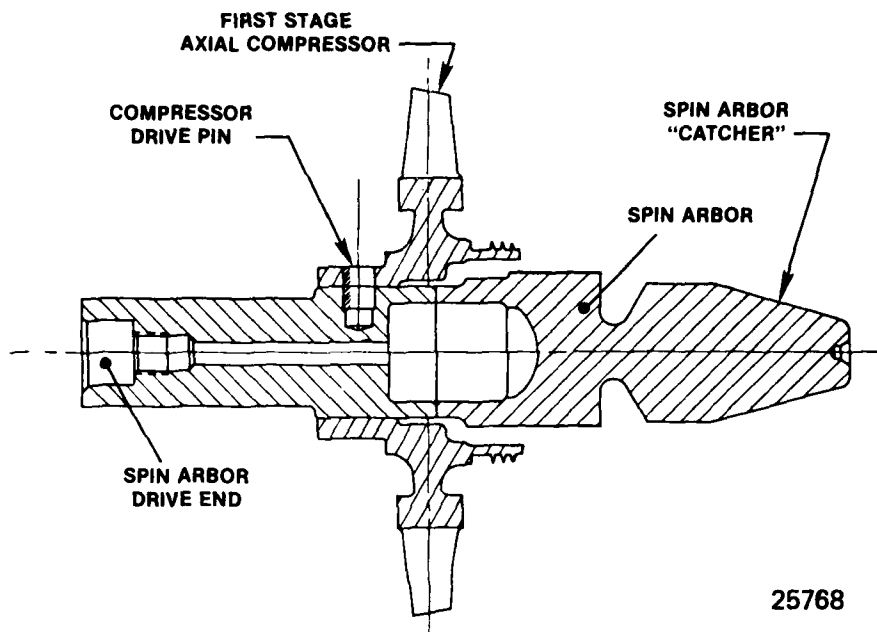
Figure 293.   Gasifier Compressor Material Properties Verification.

TEST BARS

FOUNDRY VERIFIES MATERIAL PRIOR TO CASTING DELIVERY.
TCAE METALLURICICAL LAB SUBSTANTIATES SOURCE RESULTS
ON REMAINING HALF OF SAME SAMPLE CASTING.

25765
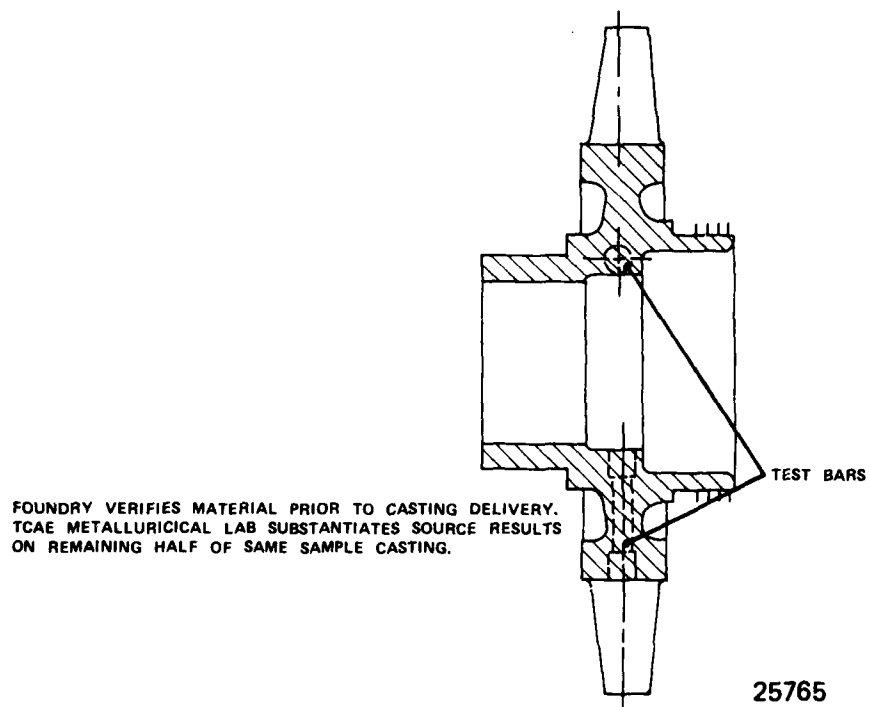
Figure 294.   Gasifier Compressor Rotor Spin Test.

394

41279

Figure 296. Expendable Gasifier Rotor Casting After Burst at 66,400 rpm.
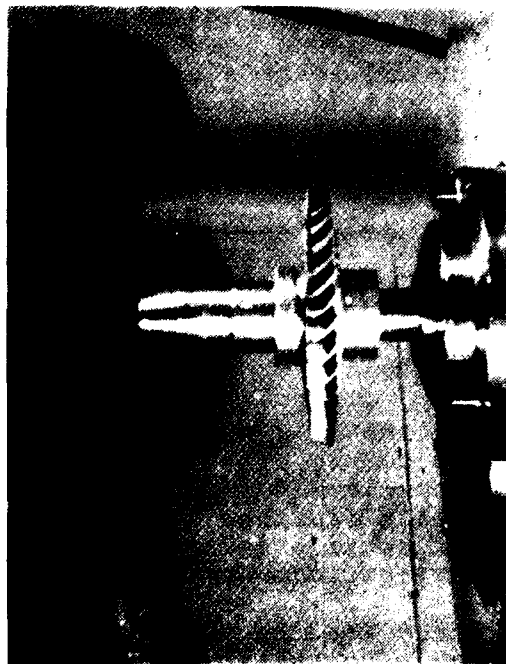
Figure 295. Arbor Assembly Installed in Spin Pit Prior to Test.

7.2   Turbine Testing

7.2.1   Turbine Design Goals and Features

       The expendable gasifier turbine design objectives were to
provide the following:

       -     Low Cost
       -     Good Performance and Flexibility
       -     Ease of Development

       Design requirements for the expendable gasifier turbine
were established to provide low cost, as exemplified by casting
techniques, simple blading design and moderate performance
requirements, providing for a wide variety of operating conditions
as demanded by various engine development considerations.

       The gasifier turbine inlet conditions at design point are:

Inlet Temperature - $^\circ$R	=	2260
Inlet Pressure - psia	=	38.29
Inlet Swirl - degrees	=	0
Mass Flow - lb_m/sec	=	3.957

       The turbine design requirements at these conditions are
given in Table 35.

       During the design, the expendable gasifier turbine
performance potential was examined to assure that the turbine base
vector diagram selection was appropriate. Figure 297 shows results
of such an investigation. It is seen from this plot that the
turbine design point is nearly optimum and also is in a region
where gradients in efficiency are the least. This feature ensures
maximum turbine adaptability and least sensitivity to various other
possible changes as imposed by different gasifier applications.
Consideration was also given to parasitic losses, leakages and
tolerances to assure that performance goals will be met. Figure 298
provides a summary substantiating that a conservative gasifier
turbine performance goal of 82.5 percent will be met. This takes
into consideration various additional performance penalties and
decrements, that have been imposed on production hardware, as may
be expected in a real engine environment.

       The final expendable gasifier turbine flowpath coordinates
for cold static conditions are given in Figure 299. The turbine
stage consists of a 13-vane constant section nozzle and a 29-bladed
rotor. The constant section nozzle was finalized during the phase
I design effort. Once the nozzle hardware was fixed, the radial
equilibrium streamline solution was then matched to the aerodynamic
requirements of the constant section nozzle. The matching solution
was the basis for the final flow path and the rotor blading design.

       The material selected for the turbine rotor is IN 100, a
nickel alloy chosen for high strength to 1900°F; this alloy has

396

TABLE 35

EXPENDABLE GASIFIER TURBINE DESIGN REQUIREMENTS

REFERRED WORK — BTU/LB$_M$ $\dfrac{\Delta H}{\Theta cr} = 12.9$

ABSOLUTE WORK — BTU/LB$_M$ $\Delta H = 55.4$

REFERRED SPEED — RPM $\dfrac{N}{\sqrt{\Theta cr}} = 16080$

REFERRED FLOW — SPEED PARAMETER —
LB. REV/SEC2 $\dfrac{WN}{60\delta}\ \epsilon = 871$

REFERRED FLOW — LB$_M$/SEC $\dfrac{W\sqrt{\Theta cr}}{\delta} = 3.25$

TOTAL-TO-TOTAL EFFICIENCY
(MINIMUM) — PERCENT $\eta = 82.5$

41262

Figure 297. Expendable Gasifier Vector Diagram Potential.

398

	BASE	PRODUCTION
FLANGE LEAKAGE	0	0.5%
LAB. SEAL TOLERANCE	0	± 0.003 IN.
LAB. SEAL CLEARANCE	0	0.003 - 0.009
INTER-ROW LEAKAGE	0	0.18 - 0.54%
WINDAGE & BEARINGS	0	(1.7%)
ROTOR RADIAL TOL.	0	± 0.002 IN.
ROTOR CLEARANCE	0.010	0.024 ± 0.003
CLEARANCE LOSS		1.94 - 2.99%
EFFICIENCY	87.8%	85.2 - 83.8%
AVERAGE		84.5%
OBJECTIVE MIN.		82.5%

26041
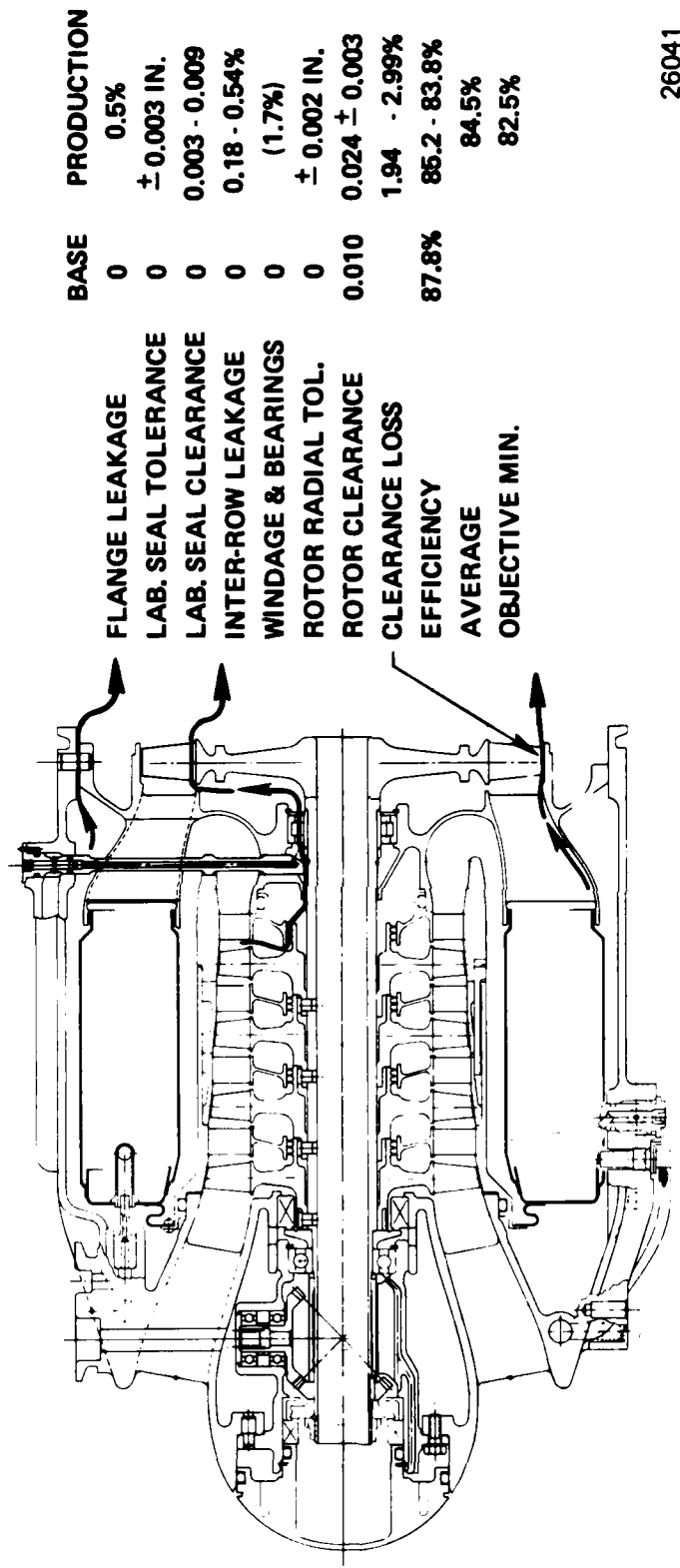
Figure 298. Expendable Gasifier Meets Minimum Performance
Requirements.

399

FLOWPATH COORDINATES

X	R_H	R_T
0.00	3.685	5.702
2.40	3.274	4.502
2.72	3.271	
2.85		4.477
3.45		4.477
3.55	3.271	

13 VANES

29 BLADES

RADIUS ~ INCHES

AXIAL DISTANCE - INCHES

26046
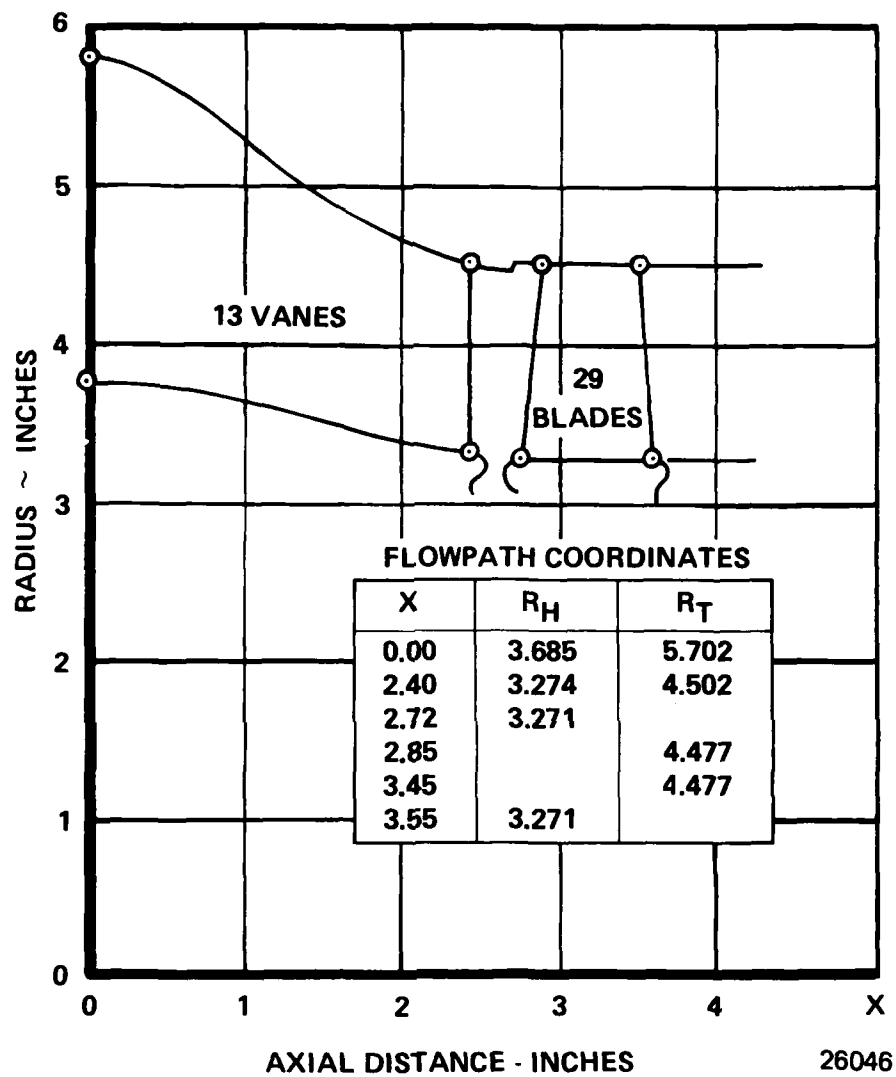
Figure 299. Cold Turbine Flowpath.

attained considerable industry usage for both individual blades and integral bladed rotors. Teledyne CAE experience with this material derives from the production J402 turbine rotors; the latter's comparable size to the E.G. rotor (within 1/2 inch at OD) and same material influenced the decision to select the same foundry to produce the E.G. rotor.

Recognizing the need to reduce machining operations (especially on nickel base alloys) in order to reduce procurement costs, the E.G. rotor is cast to net shape, needing only to have the blade tips cropped and the hub faced for the electron beam weld joint with the shaft.

The blade centrifugal and restored gas bending stresses were calculated using a conventional tapered, twisted beam model. A summary of the blade stresses at the hub (maximum stress point) and at 50 percent span (minimum stress margin point) is presented in Figure 300. A minimum safety factor 1.5 on the 20-hour stress rupture strength is indicated. This was determined by comparing the direct tensile stresses (centrifugal P/A) with the minimum 20-hour stress rupture strength, based on the adiabatic wall temperatures predicted for the blade at maximum speed and a turbine rotor inlet temperature of 1800°F. The predicted temperatures, centrifugal stresses and 20 hour stress rupture strengths are presented in Figure 301 for the complete blade span.

The design goal for the turbine disk is a low cycle fatigue (LCF) life of 2,000 start-stop cycles. A disk was designed for an assumed starting thermal gradient of 1000°F from rim to bore, based on the transient thermal analysis of similar IN-100 turbine disks. The stress analysis indicated that the bore stresses were below the yield strength of the material while the rim tangential stresses were in compression, near the yield strength. For a reverse thermal gradient of 500°F upon shutdown, a total strain range of less than 0.005 in/in. was estimated for the rim, which results in an LCF life greater than 2000 cycles. The analysis is based upon a pseudo-plastic analysis by assuming elastic strain invariance from an elastic analysis which is valid for thermal loads. This serves as a good approximation for rim strains since the rim loads are predominately thermal. The combined centrifugal and thermal stresses at 100 percent speed and 1800°F turbine rotor inlet temperature are summarized in Figure 300. A 37 percent burst speed margin is indicated at 33,500 rpm.

The conservative performance requirements of the turbine did not warrant aerodynamic rig testing before application in the engine.

7.2.2   Cast Rotor Structural Verification

The mechanical testing of the cast turbine rotor prior to its use in the engine consisted of mechanical properties evaluation of test specimens from the casting and spin pit testing of the turbine rotor. The test specimens were machined from one of the
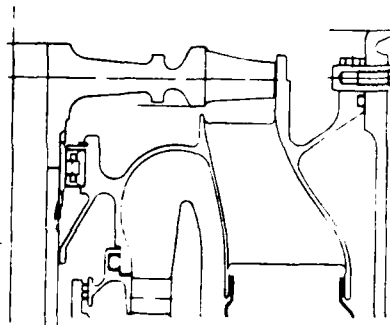
401

ROTOR MATERIAL: IN-100
SHAFT SPEED 33,500 RPM (MAX)
T.I.T.: 1800°F

*BASED ON PRIMARY STRESSES (CENTRIFUGAL P/A) ONLY

SUMMARY OF BLADE STRESSES

Blade Location	Temp. °F	Min. Material Properties, KSI			Applied Stresses, KSI				Safety Factors		
		Ult.	.2% Yield	20 Hrs. S.R.	Cent. P/A	Cent. Untwist	Restored Gas Bend	Max Comb'd.	Ult.*	Yield	St.* Rupt.
Root (Hub)	1350	100	90	76.	24.9	7.7	-0.7	31.9	4.0	2.8	3.1
50% Span	1775	62	50	26.5	17.4	6.5	-0.5	23.4	3.6	2.1	1.5

SUMMARY OF DISK STRESSES

Operating Condition	Temp. °F	Minimum Material Properties, KSI		Bore Tangential Stress – KSI	Average Tangential Stress, KSI	Burst Speed Margin %	Burst Speed RPM
		Ultimate	.2% Yield				
Design Point Bore 1275 Steady State Rim 1390		100	90	78.4	42.4	37	46000

27353

Figure 300. Model 506-2X Turbine Rotor.

Figure 301. Final Turbine Blade Stresses Compared to Stress Rupture Strength.

403

castings as shown in Figure 302. The mechanical properties were determined for three test bars and the results are presented in Table 36. As is readily apparent, all three specimens exceeded the specification strength requirements.

TABLE 36

TENSILE TEST RESULTS

	TEST SPECIMENS			TCAE MS-100 SPEC MIN
	BAR #1	BAR #2	BAR #3	
Ultimate Tensile Strength, psi	128,000	117,000	118,000	102,000
.2% Yield Strength, psi	112,000	108,000	108,000	90,000
% Elongation	9.8	4.3	6.3	4.0

One of the cast turbine rotors was machined as it would be for the engine shaft assembly and was welded in the spin arbor as shown in Figure 303. The arbor assembly was then balanced, inspected and installed in the spin pit. The rotor was then spun to a 15% overspeed of 38,525 rpm. The dimensional inspection made prior to and after the spin test showed the dimensions remained unchanged within the accuracies of the measuring devices. Zyglo inspection of the rotor also failed to show signed of distress, thus demonstrating that the spin test goals were achieved.

7.3   Demonstrator Engine Testing

7.3.1   Engine Test Procedures and Objectives

The compressor rotor casting procurement problem caused the scheduling of two expendable gasifier tests. Two turbojet engines using different compressors were tested. The first configuration tested was built with the machined compressor rotors used for the compressor rig testing, and the second configuration tested used the cast compressor rotors to verify the low cost manufacturing concept. The overall objectives of both engine tests were to achieve the following:

o   To demonstrate the feasibility of the overall design concept.

o   To establish the mechanical integrity of the turbojet engine.

o   To attain a target SLS thrust of 230 LBF in the turbojet configuration.

o   To achieve and demonstrate the desired performance goals for each individual component.

404

TELEDYNE CAE METALLURGICAL LAB TESTS CORROBORATES
ROTOR FOUNDRY TEST RESULTS

TEST BARS ARE MACHINED FROM
SECTIONED SAMPLE CASTING

STRESS
RUPTURE SPECIMEN

TENSILE
TEST SPECIMEN
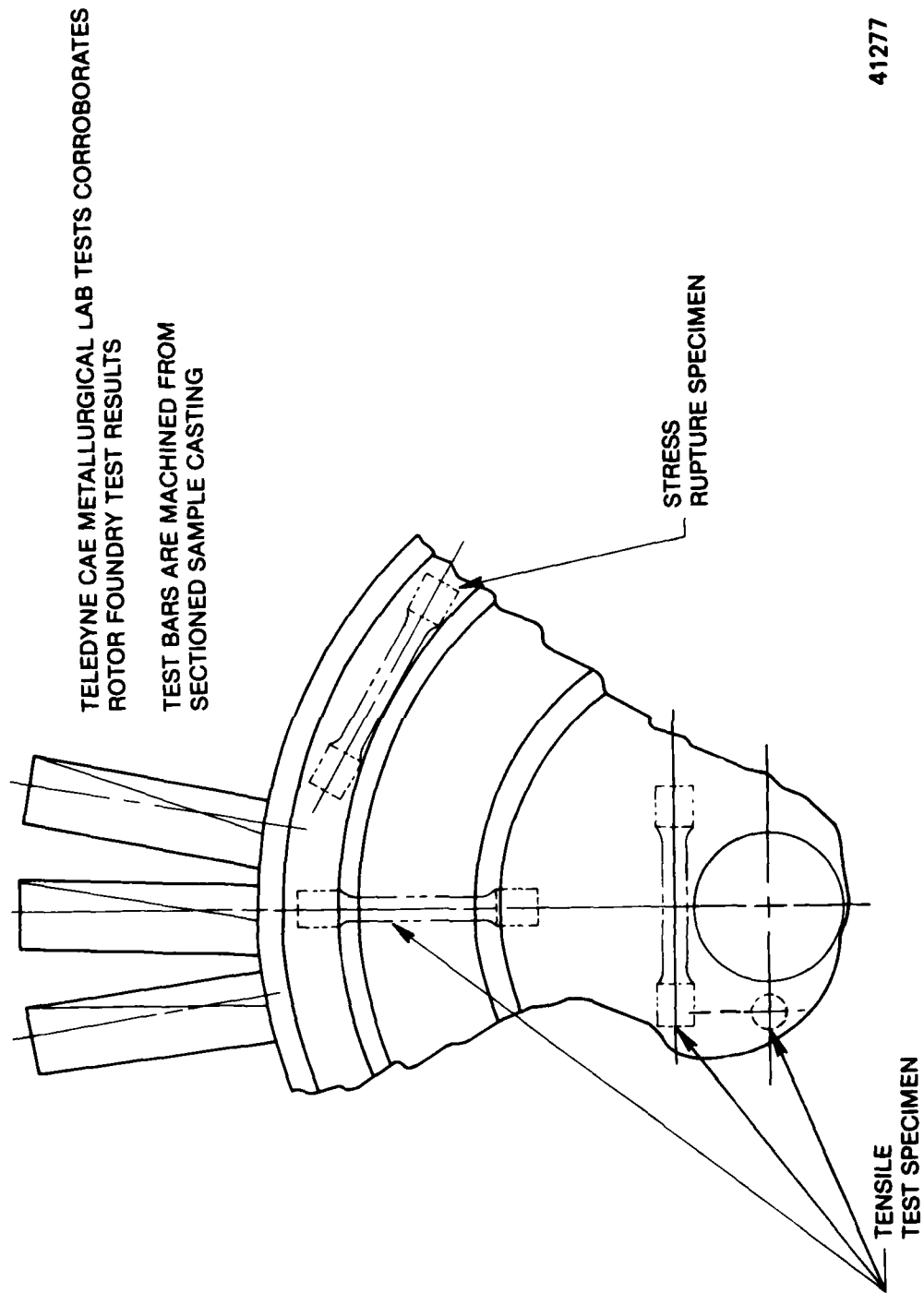
41277

Figure 302. Gasifier Turbine Rotor Structural Testing.

405

SPIN ARBOR ELECTRON BEAM
WELDED TO ROTOR (JOINT
IDENTICAL TO E.G. SHAFT)

SPIN ARBOR
DRIVE END
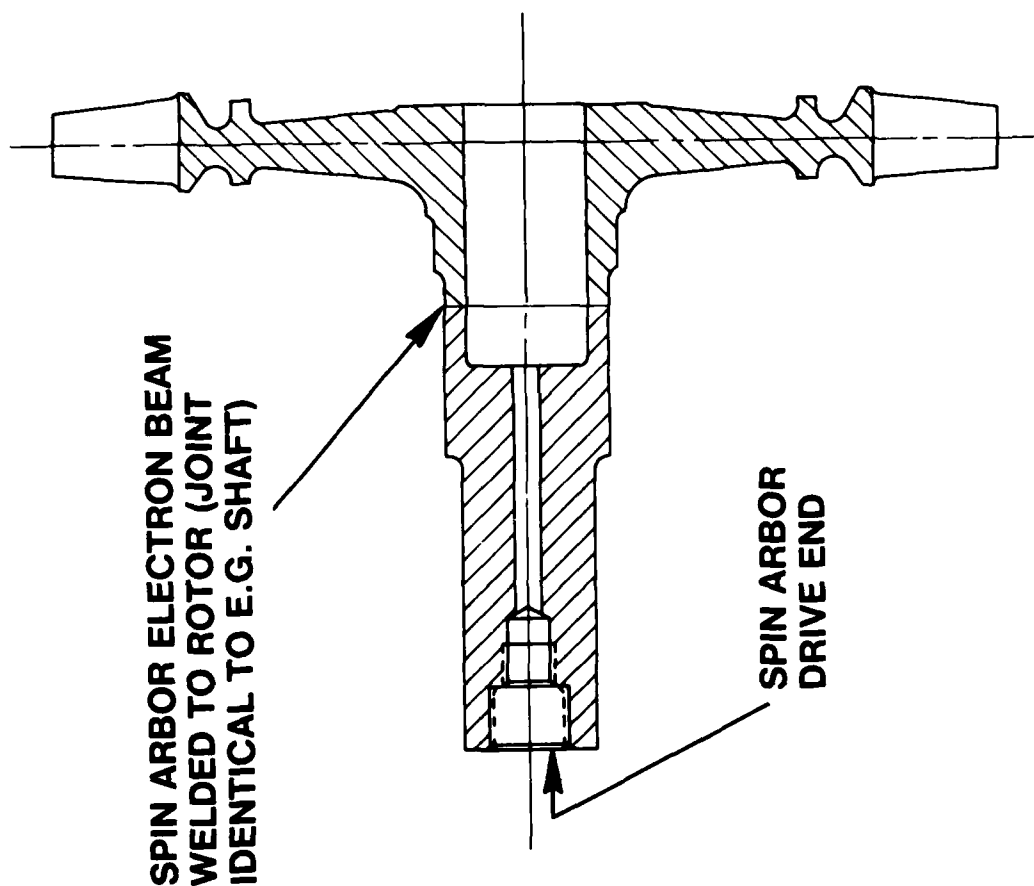
26075

Figure 303. E.G. Turbine Rotor Spin Test.

406

o   To test the operational capability of the engine over
        its flight envelope.

o   To test the engine starting capabilities

        To achieve these objectives, a comprehensive test plan
outlined the combinations of engine speeds, Mach numbers and alti-
tudes which were to be tested. The engine test plan incorporated
the following procedures:

o   Installation/windmill speed check (SLS)

o   Start attempt at SLS conditions

o   Accelerate to idle speed - mechanical check

o   Record engine data from idle to maximum speed

o   Performance calibration as per flight envelope for
        optimum jet nozzle area, speed - 80%, 90%, 100%, 102.5%

o   Define engine starting envelope

        In addition to the listed procedures, the test plan also
called out the location and the instrumentation to be used for
gathering the required data for performance analysis. This instrum-
entation and its location are shown in Figure 304 and described in
Table 37.

7.3.2   Machined Rotor Configuration Engine Tests

        Intial testing was performed to check the mechanical
operaticn of the Expendable Gasifier. Windmill operation of the
engine showed no indications of undesired rubbing, oil leakage or
vibratory problems. During this initial running, primer ignition at
various engine speeds was attempted and the upper and lower limits
of engine rpm's consistent with repeatable primer ignition was
established. First tests were run with the jet nozzle removed to
provide a jet nozzle area (JNA) of 29.6 square inches. This
conservative approach allowed preliminary data points to be taken at
a low TRIT which were then used to calculate the required JNA.
Subsequent incremental changes in the jet nozzle area were made to
"zero in" on the desired JNA. Since the turbine nozzle was
predicted to be unchoked, and turbine characteristics were untested,
it was not certain what the match characteristics of the engine
were. Therefore, it was considered prudent to match as low on the
compressor characteristics as possible on the initial calibration.
The purpose of testing the engine with the jet nozzle area equal to
20 sq. in. and 16.7 sq. in. was two-fold. The first objective was
to map out engine performance. The second was to optimize engine
performance consistent with adequate surge margin throughout the
speed range.

2T_{t2} RAKES
(4 ELEMENT)

2P_s 4T_t5
       P_t5

SKIN
TEMPERATURE
THERMOCOUPLES ✕

4P_t4

1P_t3 RAKES

1T_t3 RAKES
(4 ELEMENT)

4 (4) ELEMENT T/C
HARNESS

40449

2P_{t2} RAKES
(4 ELEMENT)

OTHER:

2 FUEL FLOW METERS
1 THRUST MEASUREMENT
1 SHAFT RPM
BAROMETRIC PRESSURE
2 T/C's BRG. FRONT & REAR
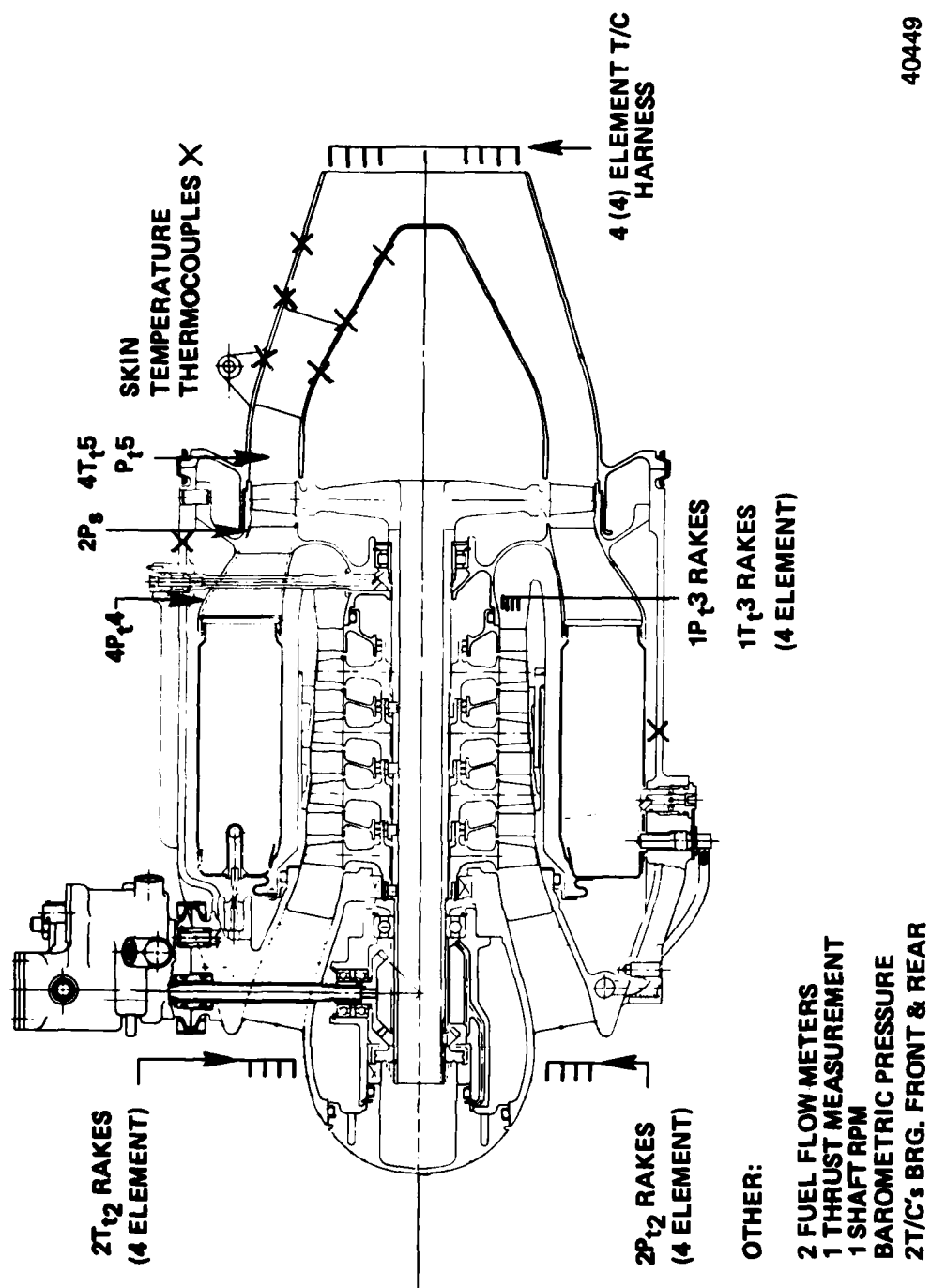
Figure 304.   Expendable Gasifier Turbojet Engine Instrumentation
              Placement.

408

TABLE 37

EXPENDABLE GASIFIER INSTRUMENTATION REQUIREMENTS

LOCATION/ITEM	INSTRUMENTATION
Inlet adapter	Total pressure Static pressure
Compressor inlet	Total pressure Pressure differential Total temperature
Compressor discharge	Total pressure Total temperature
Turbine nozzle (inlet)	Total pressure
Turbine nozzle (exit)	Static pressure
Turbine rotor (exit)	Total temperature Total pressure
Primary exhaust	Total temperature
Exhaust lip	Static pressure
Fuel	Total temperature Fuel flow
Thrust	Load cell
Speed	Electronic speed pick-up

An optimized jet nozzle area of 17.77 square inches was used during the test to demonstrate the operational capability of the engine over its projected flight envelope. A matrix of steady state data points was taken using engine speeds of 80%, 90%, 100% (33,060 rpm) and 102.5%, flight mach numbers of 0, .2, .4, and .8, and altitudes of 0, 10K, 20K, 30K and 40K in sufficient combinations to define the anticipated flight envelope shown in Figure 305. The data points taken to define performance of the engine throughout the flight envelope have been tabulated in Table 38. Some steady state data points (high altitude - low engine speeds) were not achievable due to an inability to manually control the low fuel flows required which resulted in instability of operation. Other steady state data points (high mach number - high engine speeds) were not obtainable due to a rise in the rear bearing temperature. The fuel coolant system must be upgraded for testing at these data points by reducing the heat input into the fuel and/or by increasing the fuel supply pressure. After all data points for mapping the performance were tested, a final test run was made to attain the targeted thrust of 230 pounds. The expendable gasifier achieved this thrust at a 107% overspeed condition. At this speed, a rear bearing temperature rise precluded maintained operation to be able to record data.

The expendable gasifier turbojet was disassembled and thoroughly inspected before being reassembled and installed in the test cell for starting tests. The completion of these tests ran the engine total operating time to 13 hours and 53 minutes with a total of 23 successful starts. A number of start attempts were made using the hydraulic starter alone at various altitude conditions and also using the hydraulic starter with ram air assist at various altitude conditions. The gasifier started successfully using the hydraulic starter at conditions from 0 to 20,000 feet altitude and ram air simulating 0.0 to 0.5 mach number. Although starts were not successful outside the range of conditions given, development of proper fuel scheduling as would be done for development of a fuel control would undoubtedly enlarge the starting envelope.

7.3.3   Machined Rotor Configuration Test Results

The initial testing was performed with various jet nozzle areas, each of which determined its own operating line. The operating line for each of these jet nozzle areas is plotted on the cmpressor map shown in Figure 306. The plot of thrust and turbine rotor inlet temperature (TRIT) versus engine speed for these jet nozzle areas (Figure 307) was also used to arrive at the optimum jet nozzle area. The 16.7 square inch jet nozzle area would operate with less surge margin and would need to be run over temperature to achieve the targeted thrust. The two larger jet nozzle areas of 29.62 square inches and 20.0 square inches would need to be run greatly over speed to reach the desired thrust. Based on the results of the acquired data from running with these jet nozzle areas used in an analytical model, the optimum jet nozzle area was determined to be 17.8 square inches.
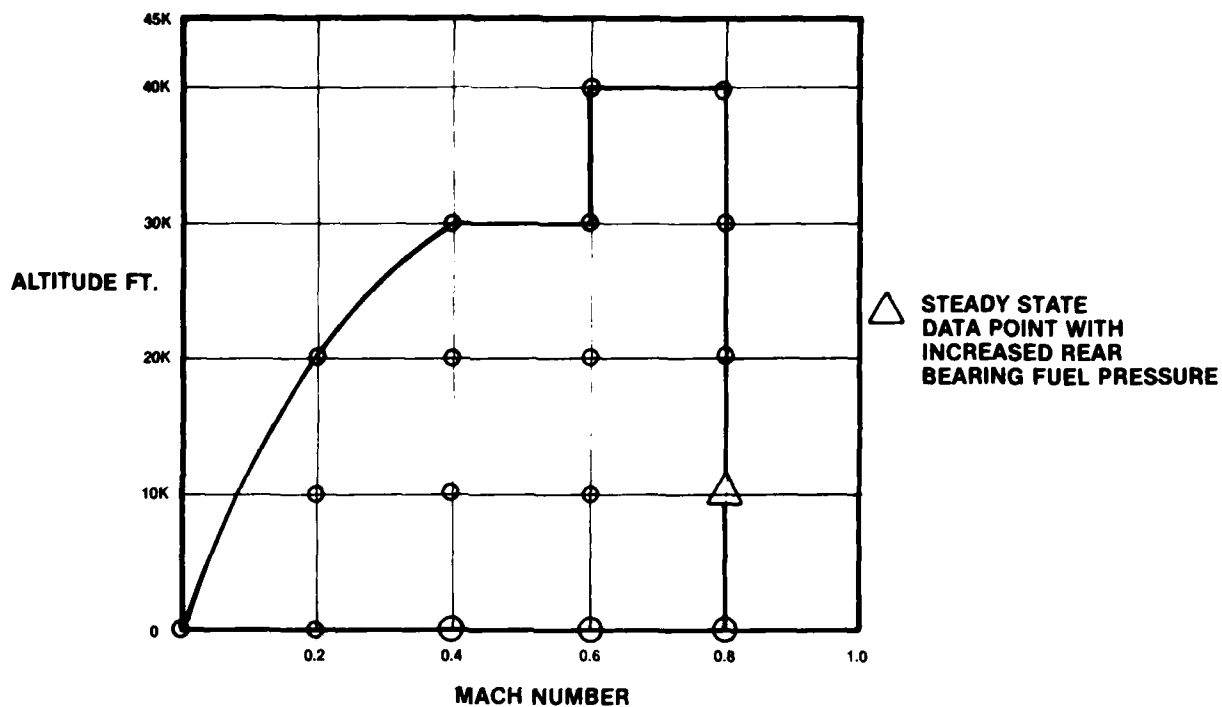
Figure 305. Expendable Gasifier Turbojet Flight Envelope.

TABLE 38

EXPENDABLE GASIFIER ALTITUDE TEST POINTS

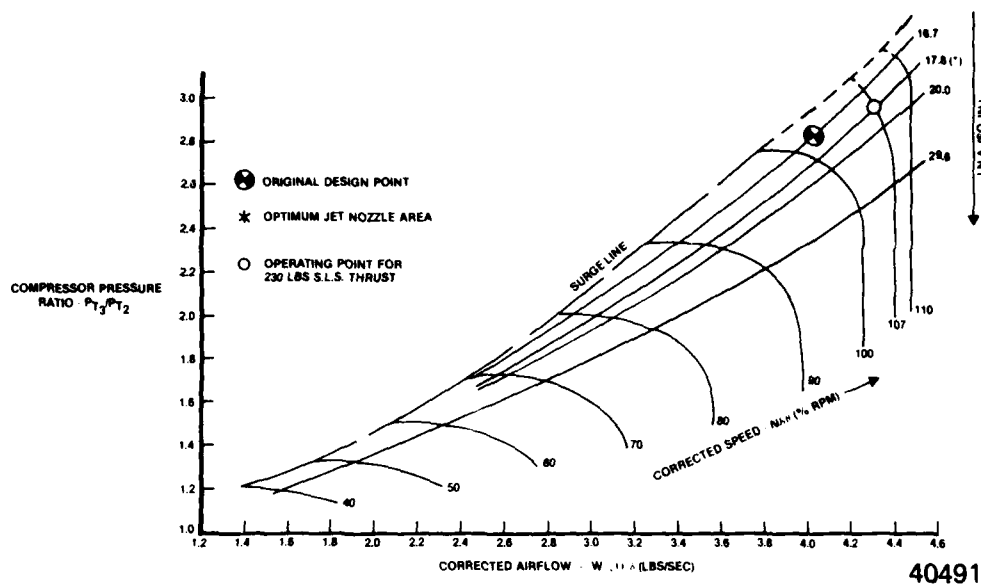| CONDITION		MECHANICAL SPEED			
ALTITUDE	MACH NO.	80%	90%	100%	102.5%
S.L.	0.0	●	●	●	●
	0.2, 0.4				●
	0.6	●	●	●	
10 K	0.2			●	●
	0.4				●
	0.6	●	●	●	●
	0.8				●
20 K	0.2, 0.4, 0.8			●	●
	0.6	●	●	●	●
30 K	0.4, 0.6	●	●	●	●
	0.8				●
40 K	0.6			●	●
	0.8		●	●	●

● TEST POINTS

41167

411

Figure 306. Compressor Map With Operating Lines for Tested Jet Nozzle Area Configurations.
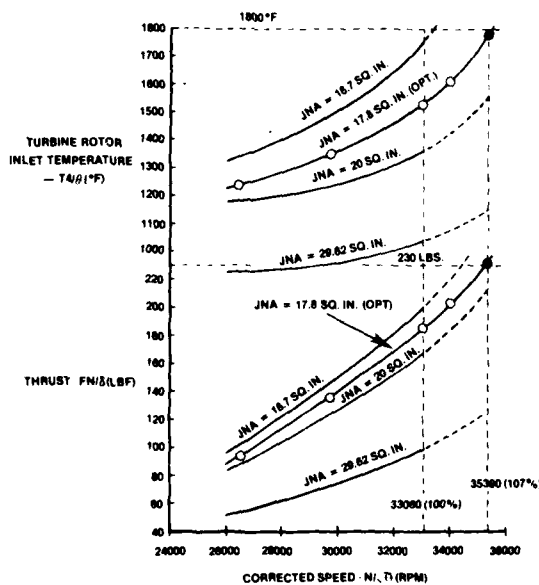
S.L.S. STD. DAY PERFORMANCE

Figure 307. Turbine Rotor Inlet Temperature and Thrust Versus Engine Speed for Tested JNA Configurations.

412

The targeted thrust of 230 LBF at 107% overspeed condition is shown on Figure 306. The turbine rotor inlet temperature (TRIT) @ 107% operating point was 20°F lower than the design TRIT of 1800°F. See Figure 307. Table 39 shows an overall turbojet performance for SLS STD day conditions @ 100%, 102.5% and 107% speeds. At 107% speed, the airflow increased by 7% and pressure ratio by 8.8% as compared to the design point.

The component compressor demonstrated an equivalent rig performance @ 100% speed in terms of flow and pressure ratio. Compressor efficiency improved by 0.3 percentage points as compared with rig efficiency @ 100% speed. Compressor results are presented in Table 40 for SLS STD day conditions. Although the compressor in the engine was tested at 107% speed, its actual overspeed capability was demonstrated at 110% during rig testing, which implies that the compressor can withstand higher aerodynamic loadings.

The combustor showed 10.1% loss, compared with the design value of 10.0%. Efficiency was 99% at 100% speed. Combustor loss for SLS STD day conditions is shown in Figure 308. Figure 309 shows the exhaust gas temperature (EGT) and turbine rotor inlet temperature (TRIT) profiles. The TRIT profile was estimated by taking into account variable turbine work along the span of the blade. A trend similarity between engine and rig measured TRIT profiles indicates a consistency between combustor design intent and combustor operation in an engine environment.

Turbine performance exceeded its design goals. Turbine efficiency @ 100% speed increased by 1.8 percentage points and absolute work (Δ H) decreased by 7.8% as compared with design values. Extrapolated turbine efficiency @ 107% speed was reduced by only .6 percentage points, compared with 100% demonstrated efficiency of 84.3%. Turbine design and demonstrated performance is shown in Table 41.

A block diagram illustrating the method for reducing the performance parameters such as efficiencies, air flow and TRIT etc. from the measured data is shown in Figure 310. Turbine rotor inlet temperature was derived from compressor turbine work balance and combustor efficiency from heat balance. Compressor efficiency was calculated from pressure and temperature measurements. Turbine efficiency was derived from measured and calculated values.

An error analysis on the compressor and turbine efficiencies and TRIT was carried out by using bias and precision indices. A sample calculation to determine the uncertainty (error) on TRIT is shown in Figure 311. This is consistent with industry practices as defined by ADEC TR 73-5 "Uncertainty in Gas Turbine Measurements Handbook" by R. B. Abernathy. Table 42 shows the accuracy analysis in absolute level at 100% speed.

413

TABLE 39

OVERALL TURBOJET PERFORMANCE AT
S.L.S. STD. DAY CONDITIONS

	TARGET		ACHIEVED	
N/√θ (RPM)	33060 (100%)	33060 (100%)	33900 (102.5%)	35390 (107%)
THRUST (LBS)	230	186	203	230
TRIT (°F)	1800	1527	1598	1780E
COMPRESSOR EFFICIENCY (%)	77.0*	77.3	76.5	74E
TURBINE EFFICIENCY (%)	82.5	84.3	84.2	83.7E
COMBUSTOR PRESSURE LOSS (%)	10.0	10.1	10.25	—
COMBUSTOR EFFICIENCY (%)	99.0	99.0	99.0	—
JET NOZZLE AREA (IN²)	—	17.8	17.8	17.8
AIR FLOW LBS/SEC	4.02	4.02	4.12	4.3E
COMP. PRESSURE RATIO	2.72	2.72	2.79	2.96E

E — EXTRAPOLATED PERFORMANCE
* RIG TESTED COMPRESSOR EFFICIENCY

40438

TABLE 40

COMPRESSOR AERODYNAMIC PERFORMANCE
AT S.L.S. STD. DAY

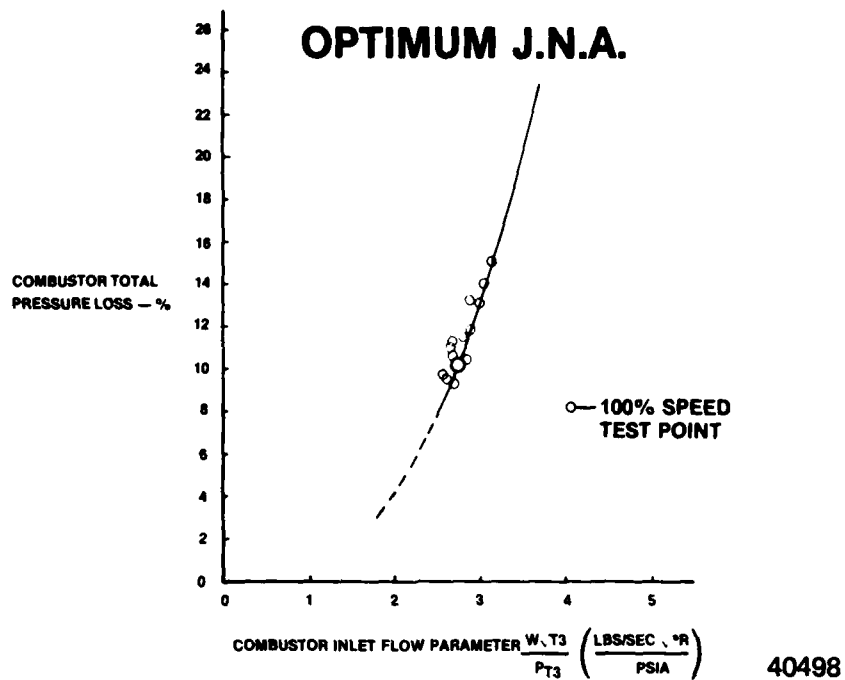|	DESIGN GOAL	RIG TEST RESULTS	DEMONSTRATED PERFORMANCE		
CORRECTED SPEED, N/√θ RPM	33060 (100%)	33060 (100%)	33060 (100%)	33900 (102.5%)	35390 (107%)
CORRECTED FLOW, W √θ/δ LBM/SEC	4.02	4.02	4.02	4.12	4.3E
PRESSURE RATIO, P_{T_3}/P_{T_2}	2.83	2.72	2.72	2.79	2.96E
ADIABATIC EFFICIENCY, %	79.2	77.0	77.3	76.5	74.0E
CORRECTED TIP SPEED, FT/SEC	900	900	900	923	963

E — EXTRAPOLATED PERFORMANCE

40437

415

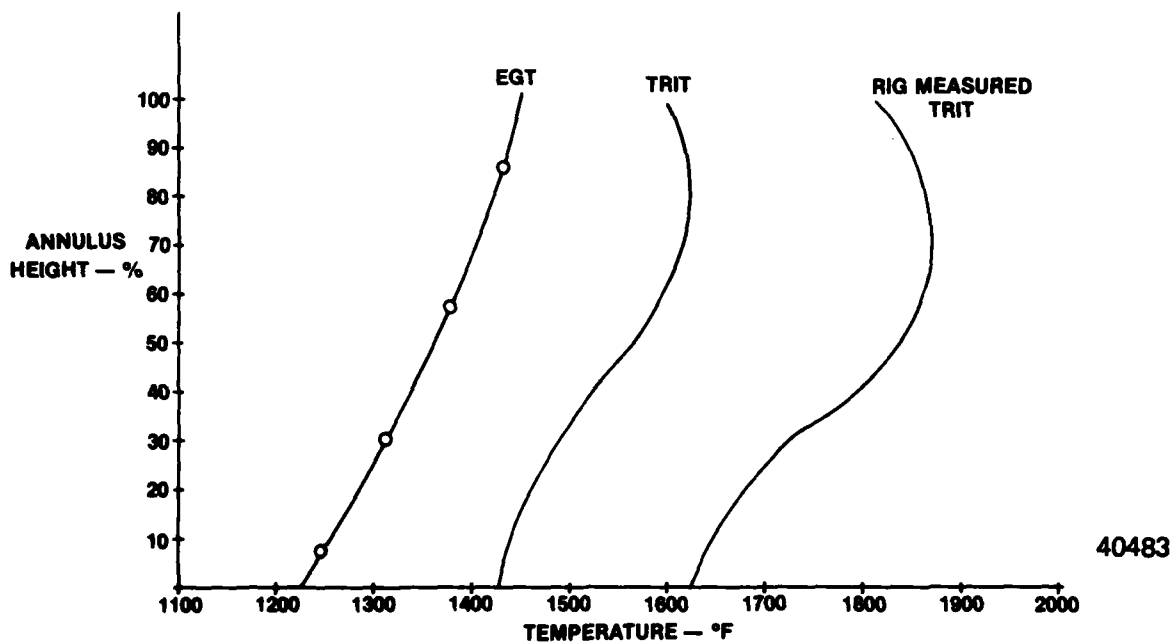Figure 308. Combustor Performance for S.L.S. STD. Day Conditions.

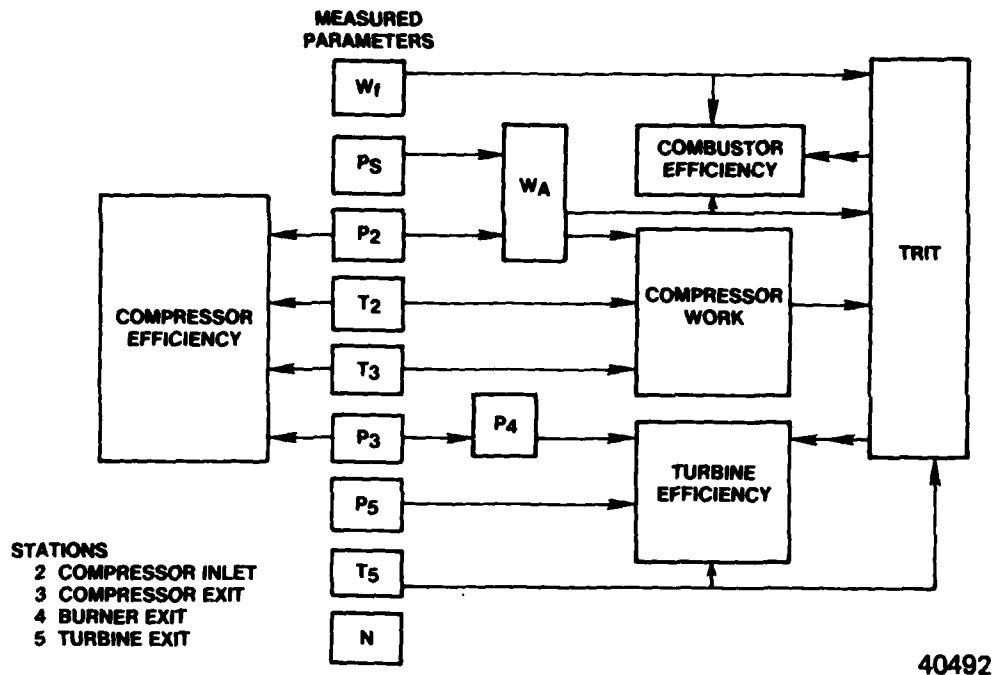Figure 309. Exhaust Gas Temperature and TRIT Profiles at 100% Speed.

416

MEASURED
PARAMETERS

STATIONS
2 COMPRESSOR INLET
3 COMPRESSOR EXIT
4 BURNER EXIT
5 TURBINE EXIT

40492

Figure 310. Expendable Gasifier Data Reduction Procedures.

TURBINE INLET TEMPERATURE:

FROM COMPRESSOR TURBINE WORK BALANCE — SEE FLOW CHARTS I & II —

$$\Delta T_{4R,5} = \frac{Cp_{23}}{Cp_{4R,5}} \cdot \frac{\Delta T_{23}}{(W_f/W_a + 1)} = K \cdot \frac{\Delta T_{23}}{(W_f/W_a + 1)}$$

BIAS IN $\Delta T_{4R,5}$

$$B_{T_{4R,5}} = \pm K \left\{ \left(\frac{\partial \Delta T_{4R,5}}{\partial T_2} \cdot B_{T_2} \right)^2 + \left(\frac{\partial \Delta T_{4R,5}}{\partial T_3} \cdot B_{T_3} \right)^2 + \left(\frac{\partial \Delta T_{4R,5}}{\partial W_f} \cdot B_{W_f} \right)^2 + \left(\frac{\partial \Delta T_{4R,5}}{\partial W_a} \cdot B_{W_a} \right)^2 \right\}^{1/2}$$

PRECISION IN $\Delta T_{4R,5}$

$$S_{T_{4R,5}} = \pm K \left\{ \left(\frac{\partial \Delta T_{4R,5}}{\partial T_2} \cdot S_{T_2} \right)^2 + \left(\frac{\partial \Delta T_{4R,5}}{\partial T_3} \cdot S_{T_3} \right)^2 + \left(\frac{\partial \Delta T_{4R,5}}{\partial W_f} \cdot S_{W_f} \right)^2 + \left(\frac{\partial \Delta T_{4R,5}}{\partial W_a} \cdot S_{W_a} \right)^2 \right\}^{1/2}$$

$$\pm B_{T_5} \pm B_{T_{4R,5}} \quad \pm S_{T_5} \pm S_{T_{4R,5}}$$

$$T_{4R} = T_5 + \Delta T_{4R,5} \; ; \; T_{4R} = T_5 + \Delta T_{4R,5}$$

BIAS IN T_{4R}

$$B_{T_{4R}} = \pm \left\{ B_{T_5}^2 + B_{T_{4R,5}}^2 \right\}^{1/2}$$

PRECISION IN T_{4R}

$$S_{T_{4R}} = \pm \left\{ S_{T_5}^2 + S_{T_{4R,5}}^2 \right\}^{1/2}$$

UNCERTAINTY IN T_{4R}

$$U_{T_{4R}} = \pm \left(B_{T_{4R}} + 2 S_{T_{4R}} \right)$$

NB — B AND S ARE BIAS AND PRECISION INDEX ASSOCIATED WITH THE MEASURED PARAMETERS.   40479

Figure 311. Sample Calculation to Determine the Uncertainty
on TRIT.

417

TABLE 41

TURBINE AERODYNAMIC PERFORMANCE
AT S.L.S. STD. DAY

	DESIGN GOAL	DEMONSTRATED PERFORMANCE	
REFERRED SPEED, $N/\sqrt{\Theta_{cr}}$ (RPM)	16080	17090	17305
TURBINE INLET TEMPERATURE, (°F)	1800	1527	1598
REFERRED WORK, $\Delta H/\Theta_{cr}$ (BTU/LB)	12.9	13.7	14.2
ABSOLUTE WORK, ΔH (BTU/LB)	55.4	51.1	54.7
REFERRED FLOW SPEED PARAMETER $WN/\delta 60 \cdot \epsilon$ (LB-REV/SEC^2)	871	962	983
EFFICIENCY (%)	82.5	84.3	84.2
COMPRESSOR CORRECTED SPEED, $N/\sqrt{\Theta}$ (RPM)	33060 (100%)	33060 (100%)	33900 (102.5%)

40436

TABLE 42

ACCURACY ANALYSIS AT 100% DESIGN SPEED

PARAMETER	MEASURED VALUE	ABSOLUTE LEVEL
Turbine Inlet Temperature, °F	1800	± 9.8
Compressor Efficiency (N_C)	.773	$\pm .01$
Turbine Efficiency (N_T)	.843	$\pm .01$

Pretest predicted performance was compared over a range of altitudes and Mach numbers to actual test results. These results, shown on Figure 312, indicate very good agreement between the analytical model and actual engine test results.

7.3.4   Cast Rotor Configuration Engine Tests

The cast compressor rotors configuration of the expendable gasifier was built up for testing immediately after completion of the spin pit tests. The cast rotors used did not conform to the drawing requirements as was discussed in Section 6.3 of this report. These deviant rotors provided the worst case possible for performance degradation from the previously run machined rotor configuration. The cast compressor rotor configuration of the turbojet engine was installed in the altitude chamber test facility for testing per the original objectives and procedures. The previously optimized jet nozzle area of 17.8 square inches was used for this engine testing also. The tests were conducted similar to the machined rotor configuration engine tests. Sea level static performance data was obtained first, and then the altitude performance was run. The performance testing used the same data points previously run for the machined rotor configuration to facilitate comparisons. A history of the engine testing for this build is summarized in Table 43.

7.3.5   Cast Rotor Configuration Test Results and Comparisons

The data was analyzed and the cast compressor rotor configuration performance data was compared to the performance data of the previously run machined compressor rotor configuration. The performance results indicated that the cast rotors have reduced flow capacity and efficiency compared to the machined rotors. Figure 313 shows the compressor performance and operating line for the jet nozzle area (JNA) = 17.8 square inches. There was no shift in the operating line from the machined rotor configuration; however, the cast compressor flow capacity was reduced by 5.7% at 100% speed. This resulted in a 9.8% thrust reduction as shown in Figure 314. Presented in Figure 315 is a comparison of efficiency and airflows versus rotor speed for the two configurations. The 2.3 percentage points efficiency reduction for the cast configuration at 100% speed resulted in a TRIT increase of 45°F as shown in Figure 316. The specific fuel consumption comparison presented in Figure 317 shows that the cast rotor configuration increased fuel consumption by 6% at the 184 pounds of thrust achieved at 100% speed for the machined rotor. This sfc is within .01 lbs/hr/lbf of the initial predictions. A full comparison of the performance of the cast and machined compressor rotor configurations is presented in Table 44. Although the cast compressor rotor configuration shows some degradation of performance compared to the machined rotor configuration, the Expendable Gasifier still has adequate performance to fulfill the requirements for the desired applications.
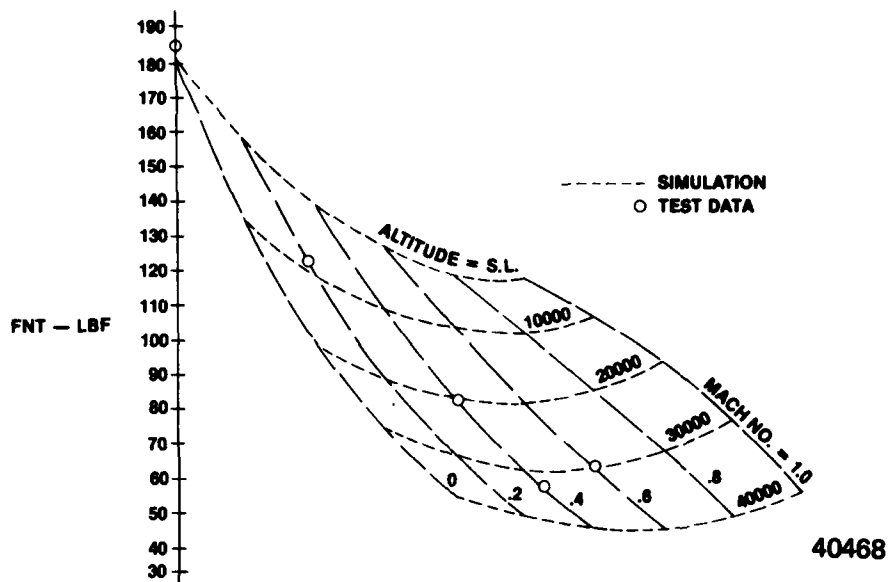
40468

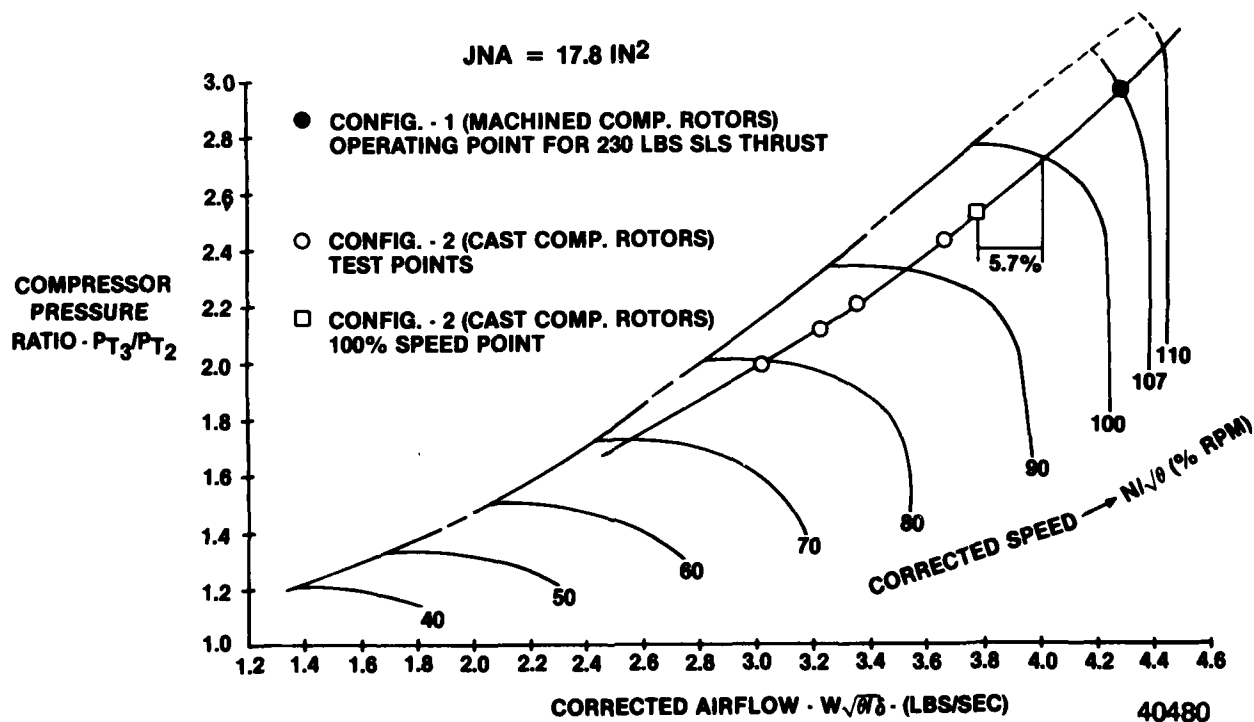Figure 312. Turbojet Altitude Performance at 100% Speed.

40480

Figure 313. Expendable Gasifier Machined Rotor Compressor Map With Cast Rotor Configuration Test Points for Comparison.

420

TABLE 43

CHRONOLOGICAL HISTORY OF ENGINE TEST UNDER BUILD 506-003

| TEST DATE	START NO.	TEST TIME	ACC. TIME	REMARKS
8/29/80	44	1:13	1:13	ENGINE PERFORMANCE @ SEA-LEVEL CONDITIONS
9/4/80	45	0:51	2:04	MAX T.R.I.T. PERFORMANCE POINT ABORTED
9/15/80	46	0:50	2:54	ENGINE PERFORMANCE @ SEA-LEVEL STATIC CONDITIONS
9/15/80	47	1:25	4:19	ENGINE PERFORMANCE @ 20,000 FEET ALTUDE, MACH 0.60
9/15/80	48	0:29	4:48	MAX T.R.I.T. PERFORMANCE POINT ABORTED
9/16/80	49	0:20	4:50	HYDRAULIC ENGINE START EVALUATION
9/17/80	50	0:01	4:51	PERSONNEL INDOCTRINATION FOR START SEQUENCING
9/17/80	51	0:01	4:52	PERSONNEL INDOCTRINATION FOR START SEQUENCING
9/17/80	52	0:12	5:04	DEMONSTRATION TEST RUN

41272
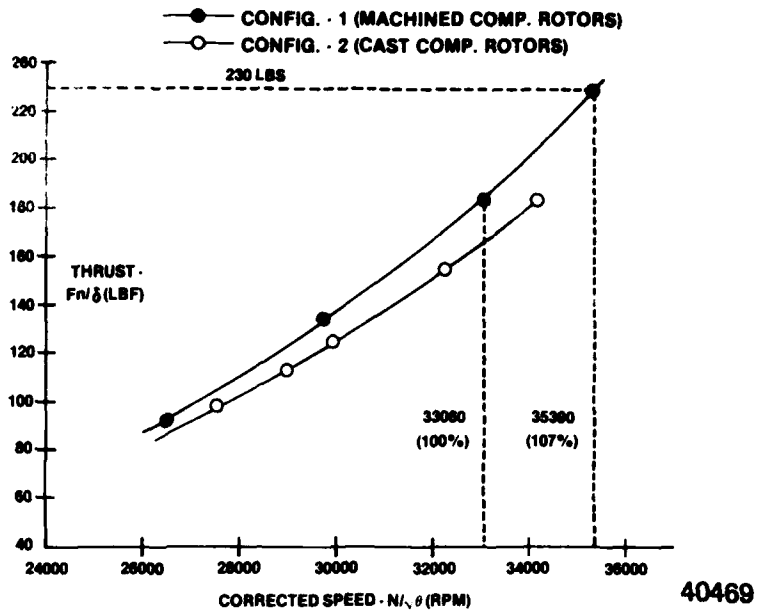
Figure 314. Expendable Gasifier Thrust Comparison for Machined Versus Cast Rotor Configurations.
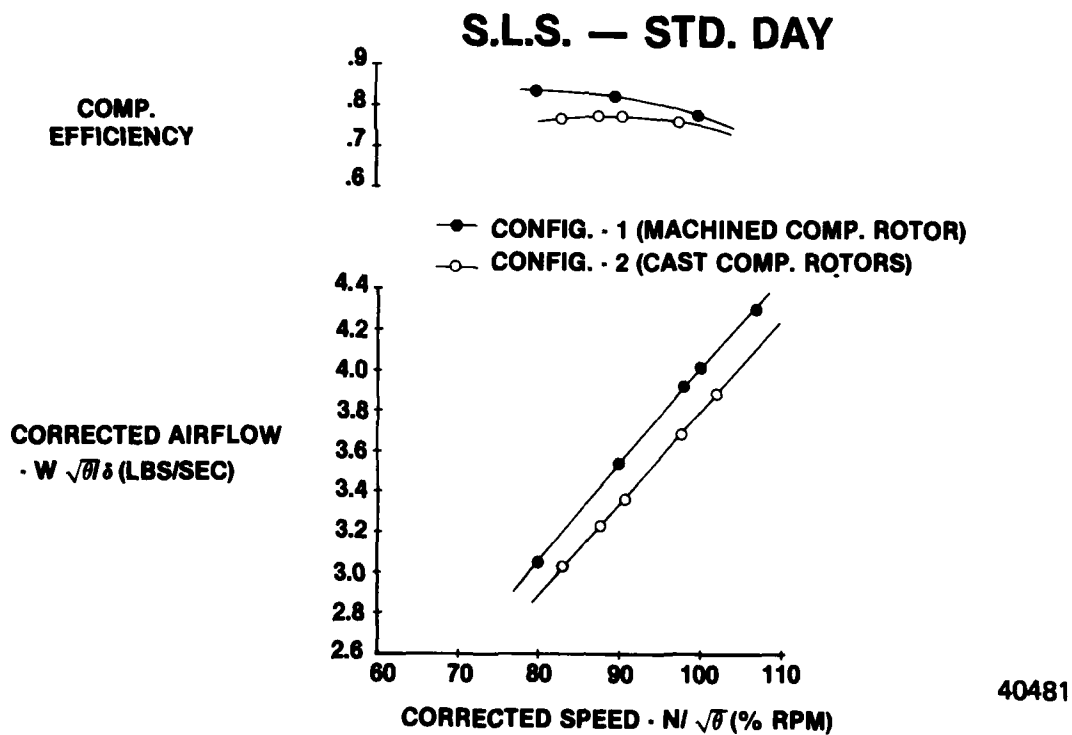

Figure 315. Expendable Gasifier Compressor Efficiency and Airflow Versus Rotor Speed for Two Configurations.
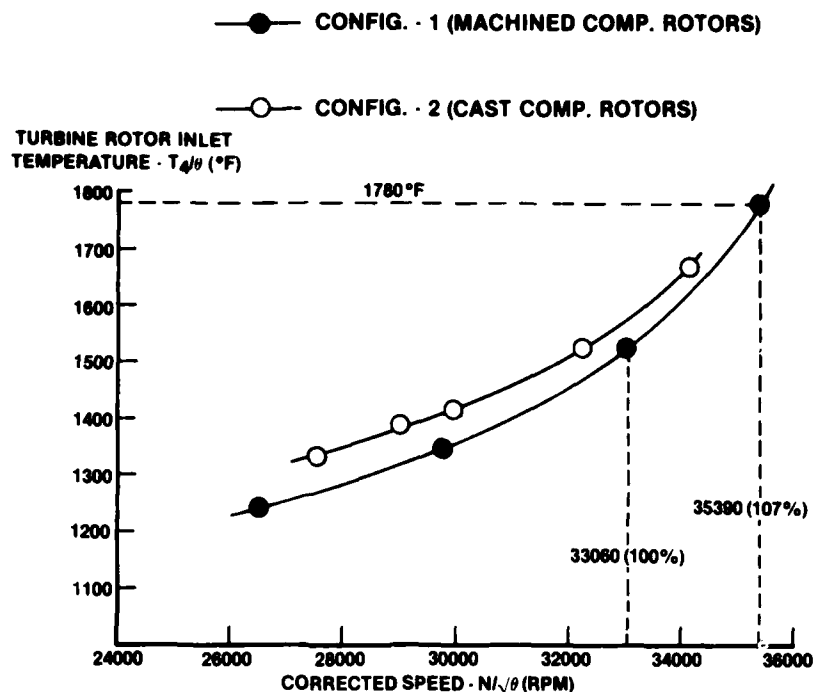
422

Figure 316. Expendable Gasifier Turbine Rotor Inlet Temperature
(TRIT) Comparison for Machined and Cast Rotor
Configurations.
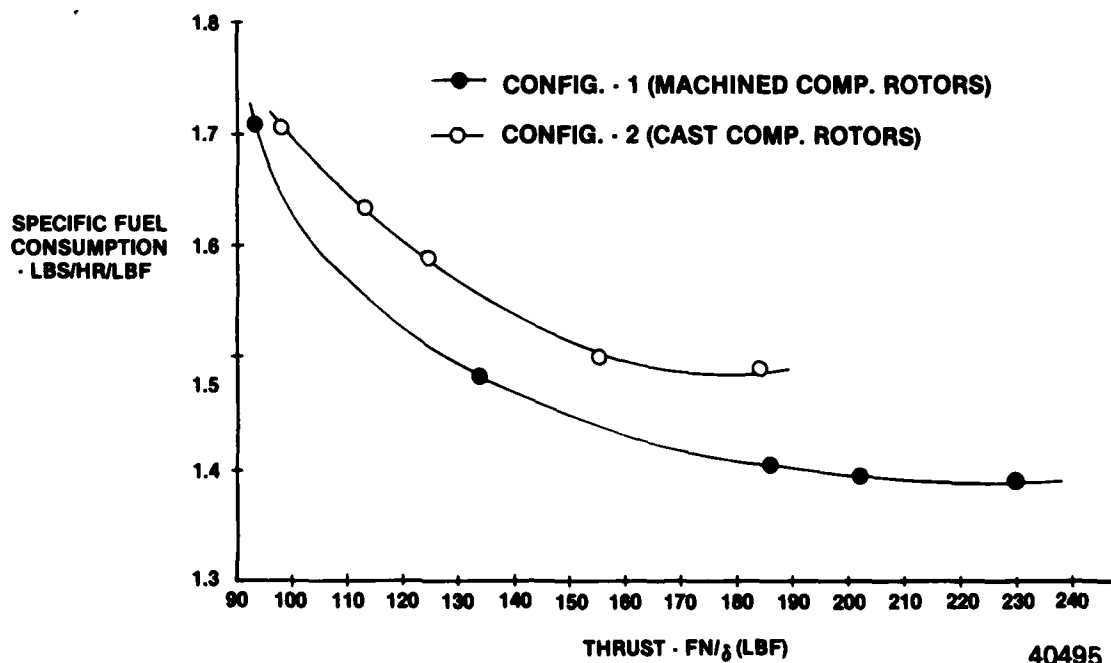
Figure 317. Expendable Gasifier Turbojet Engine Specific Fuel
Consumption Versus Thrust Comparison for Both
Configurations.

423

TABLE 44

EXPENDABLE GASIFIER OVERALL
PERFORMANCE COMPARISON

		MACHINED COMPRESSOR	CAST COMPRESSOR	Δ
CORRECTED SPEED	% RPM	100%	100%	+0
THRUST	LBF	184	166	-9.8%
TRIT	°F	1530	1575	+45
COMPRESSOR EFFICIENCY	%	77.3	75.0	-2.3 PTS.
AIR FLOW	LBS/SEC	4.02	3.79	-5.7%
JET NOZZLE AREA	IN²	17.8	17.8	+0

41276

424

SECTION 8.0

CONCLUSIONS AND RECOMMENDATIONS

8.1 Conclusions

The completion of the four phases of the Expendable Gasifier Program has resulted in the following conclusions:

1. The program has achieved its goals by providing the following results:

    o   The concept of a common expendable gasifier configuration matched with a nozzle or fan to produce thrust or with a power turbine to produce shaft horsepower is viable when applied early in the program. Application of this concept at the beginning of the System Design Phase meant that there was a minimum impact to accommodate the three applications.

    o   When acquisition cost is used as the prime objective (a necessity for expendable hardware), volume and specific fuel consumption are penalized slightly. The tradeoff between acquisition costs and performance must be accomplished on the basis of life cycle costs done early in the System Design and Preliminary Design Phases.

    o   During the preliminary and detail design, component aerodynamic and mechanical design goals were conservatively selected to achieve adequate performance at high reliability levels. The selection of these conservative goals was made to optimize performance versus cost for the engine applications.

    o   During preliminary design, cost and manu-facturing studies were performed which showed the expendable gasifier could be procured for under $8000 (FY 1977$). Subsequent detail designs incorporating design changes for functional, structural and/or producibility requirements, had no impact on cost where cost had been the driving objective.

    o   Component and engine testing verified that the hardware performance exceeded some design objectives and came sufficiently close to the remaining design objectives to provide adequate performance for all expendable gasifier applications.

2. The performance of the cast rotor configured EG can be raised to the level obtained with the machined rotor configuration by providing cast rotors to the print dimensions. These castings appear to be obtainable by casting the rotor with a ring on its outside diameter as was described in Section 6.3 and shown in Figure 280.

3. The major element contributing to the life cycle cost for a jet fuel starter or an auxiliary power unit has traditionally been the overhaul costs. This is vividly demonstrated by a comparison of life cycle costs for the expendable gasifier versus a conventional operational unit, shown in Figure 318. Calculation of the overhaul costs was done by determining replacement costs of the expendable gasifier portion of the jet fuel starter after every 2000 starts while actual overhaul rates being experienced by the user were applied for the operational unit.

8.2 Recommendations

Based on the results of the EG program, further development of the expendable gasifier concept is warranted and should include the following efforts:

1. Use the rotor castings with the cast shroud to obtain dimensionally accurate hardware, and test this hardware to demonstrate the predicted performance gains.

2. An analysis should be made to determine the testing required to simulate the equivalent of 2000 starts on the expendable gasifier portion of a jet fuel starter application. The performance of this testing will demonstrate the capability to achieve the predicted overhaul costs.

3. The expendable gasifier should be demonstrated in the jet fuel starter configuration, including design of the power turbine module and JFS control system, and demonstration of the EG/JFS under simulated operating conditions.

426

10 YEAR WEAPON SYSTEM LIFE

EXPENDABLE GASIFIER JFS/APU
EXISTING OPERATIONAL JFS/APU

FUEL (APU)
FUEL (JFS)
MAINTENANCE
OVERHAUL
ACQUISITION

DOLLARS (THOUSANDS)

0   50   100   150   200   250   300

EG CONCEPT SAVINGS FOR A FLEET OF 1000 AIRCRAFT
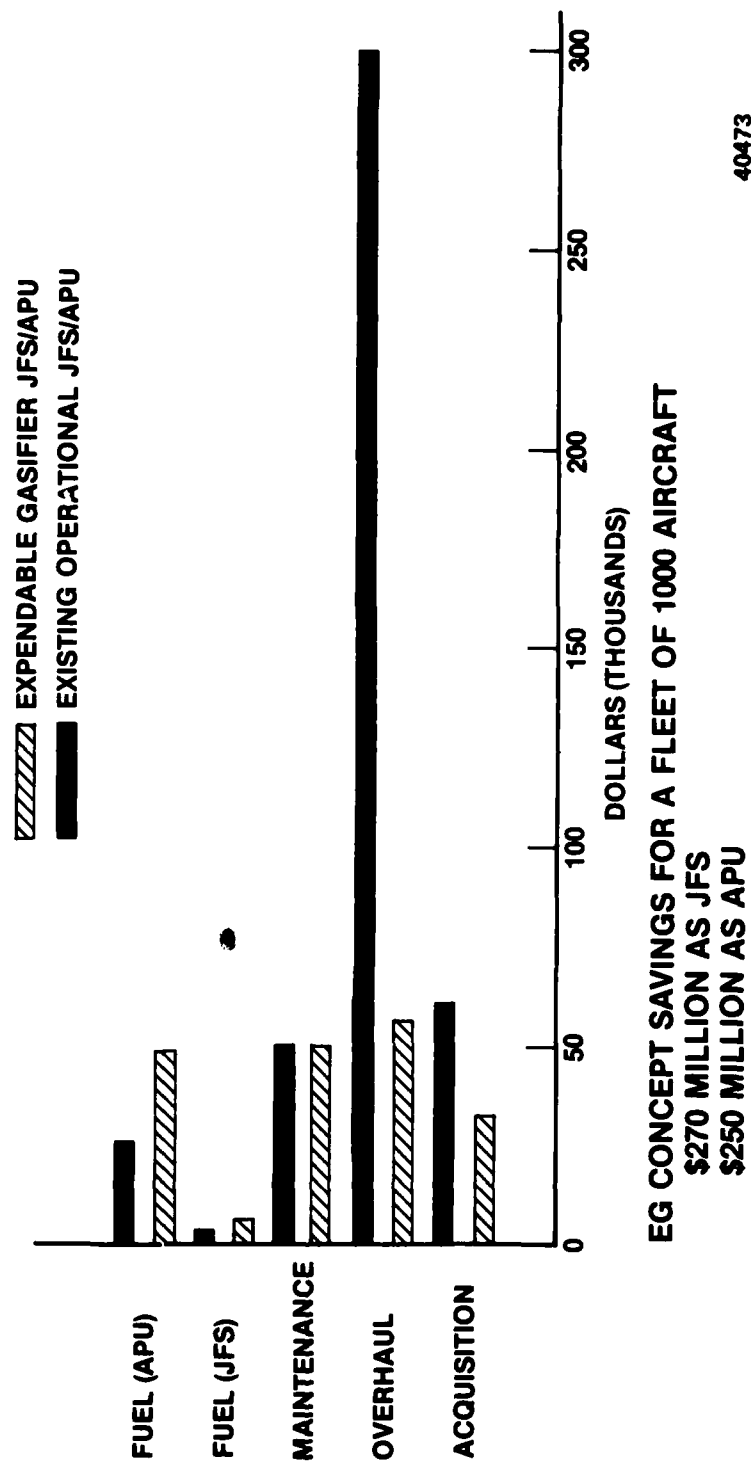$270 MILLION AS JFS
$250 MILLION AS APU

40473

Figure 318.   Expendable Gasifier Life Cycle Cost Comparison in
FY 1980 $.

427

REFERENCES

1. Smith, R., "Low Cost Jet Fuel Starter", SAE Paper 751117, November 1975.

2. Cook, M.H., "Computer Managed Parts for Manufacturing", Scientific American, February 1975.

3. Engine Systems Ownership Cost Reduction in Aircraft Propulsion Subsystem Integration (APSI), Interim Report No. 1467, AFAPL-TR-100, Vol. II, August, 1975.

4. Creveling, H.F. and Carmody, R.H.; "Axial Flow Compressor Computer Program for Calculating Off-Design Performance (Program IV)", NASA CR-72427, August 1968.

5. Clemmons, D.R., "Single Stage Experimental Evaluation of Tandem-Airfoil Rotor and Stator Blading of Compressors, Part VI - Data and Performance for Stage D", NASA CR-134511, November, 1973.

6. Cheatham, J.G., et al, "Single Stage Experimental Evaluation of Low Aspect Ratio, Highly Loaded Blading for Compressors, Part IX - Final Report, Stage F and Stage G, Volume I", NASA CR-134993, May, 1976.

7. Aerodynamic Design of Axial Flow Compressors (Revised), NASA SP-36, 1965.

8. Crouse, James E., "Computer Program for Definition of Transonic Axial-Flow Compressor Blade Rows", NASA TN D-7345, February, 1974.